



ADVANCES IN POSTHARVEST PATHOLOGY OF FRUITS AND VEGETABLES

EDITED BY: Boqiang Li, Chao-an Long, Hongyin Zhang and Nengguo Tao
PUBLISHED IN: Frontiers in Microbiology



frontiers

Frontiers eBook Copyright Statement

The copyright in the text of individual articles in this eBook is the property of their respective authors or their respective institutions or funders. The copyright in graphics and images within each article may be subject to copyright of other parties. In both cases this is subject to a license granted to Frontiers.

The compilation of articles constituting this eBook is the property of Frontiers.

Each article within this eBook, and the eBook itself, are published under the most recent version of the Creative Commons CC-BY licence.

The version current at the date of publication of this eBook is CC-BY 4.0. If the CC-BY licence is updated, the licence granted by Frontiers is automatically updated to the new version.

When exercising any right under the CC-BY licence, Frontiers must be attributed as the original publisher of the article or eBook, as applicable.

Authors have the responsibility of ensuring that any graphics or other materials which are the property of others may be included in the CC-BY licence, but this should be checked before relying on the CC-BY licence to reproduce those materials. Any copyright notices relating to those materials must be complied with.

Copyright and source acknowledgement notices may not be removed and must be displayed in any copy, derivative work or partial copy which includes the elements in question.

All copyright, and all rights therein, are protected by national and international copyright laws. The above represents a summary only. For further information please read Frontiers' Conditions for Website Use and Copyright Statement, and the applicable CC-BY licence.

ISSN 1664-8714

ISBN 978-2-88963-322-7

DOI 10.3389/978-2-88963-322-7

About Frontiers

Frontiers is more than just an open-access publisher of scholarly articles: it is a pioneering approach to the world of academia, radically improving the way scholarly research is managed. The grand vision of Frontiers is a world where all people have an equal opportunity to seek, share and generate knowledge. Frontiers provides immediate and permanent online open access to all its publications, but this alone is not enough to realize our grand goals.

Frontiers Journal Series

The Frontiers Journal Series is a multi-tier and interdisciplinary set of open-access, online journals, promising a paradigm shift from the current review, selection and dissemination processes in academic publishing. All Frontiers journals are driven by researchers for researchers; therefore, they constitute a service to the scholarly community. At the same time, the Frontiers Journal Series operates on a revolutionary invention, the tiered publishing system, initially addressing specific communities of scholars, and gradually climbing up to broader public understanding, thus serving the interests of the lay society, too.

Dedication to Quality

Each Frontiers article is a landmark of the highest quality, thanks to genuinely collaborative interactions between authors and review editors, who include some of the world's best academicians. Research must be certified by peers before entering a stream of knowledge that may eventually reach the public - and shape society; therefore, Frontiers only applies the most rigorous and unbiased reviews.

Frontiers revolutionizes research publishing by freely delivering the most outstanding research, evaluated with no bias from both the academic and social point of view. By applying the most advanced information technologies, Frontiers is catapulting scholarly publishing into a new generation.

What are Frontiers Research Topics?

Frontiers Research Topics are very popular trademarks of the Frontiers Journals Series: they are collections of at least ten articles, all centered on a particular subject. With their unique mix of varied contributions from Original Research to Review Articles, Frontiers Research Topics unify the most influential researchers, the latest key findings and historical advances in a hot research area! Find out more on how to host your own Frontiers Research Topic or contribute to one as an author by contacting the Frontiers Editorial Office: researchtopics@frontiersin.org

ADVANCES IN POSTHARVEST PATHOLOGY OF FRUITS AND VEGETABLES

Topic Editors:

Boqiang Li, Institute of Botany, Chinese Academy of Sciences, China

Chao-an Long, Huazhong Agricultural University, China

Hongyin Zhang, Jiangsu University, China

Nengguo Tao, Xiangtan University, China

Fruits and vegetables are an important part of a healthy diet. However, one third of fruit and vegetables are lost after harvest every year. Most losses are caused by pathogen (mostly fungi) infections, which lead to postharvest decay. In addition, some postharvest fungal pathogens can produce toxic secondary metabolites (i.e. mycotoxins) during their infecting periods. Mycotoxin contamination may cause serious food safety issues. At present, the use of synthetic fungicides is still the main means to control postharvest diseases. However, the development of resistance in fungal pathogens to fungicides and the growing public concern over the health and environmental risks associated with high levels of pesticides in fruits and vegetables have urged researchers to develop alternative methods of disease control. A deeper understanding of the infecting mechanisms of postharvest pathogens will provide great insight into developing new controlling strategies.

Citation: Li, B., Long, C.-a., Zhang, H., Tao, N., eds. (2019). Advances in Postharvest Pathology of Fruits and Vegetables. Lausanne: Frontiers Media SA.
doi: 10.3389/978-2-88963-322-7

Table of Contents

- 05** *iTRAQ Proteomic Analysis Reveals That Metabolic Pathways Involving Energy Metabolism are Affected by Tea Tree Oil in Botrytis cinerea*
Jiayu Xu, Xingfeng Shao, Yingying Wei, Feng Xu and Hongfei Wang
- 19** *Application of Proteomics for the Investigation of the Effect of Initial pH on Pathogenic Mechanisms of Fusarium proliferatum on Banana Fruit*
Taotao Li, Qixian Wu, Yong Wang, Afiya John, Hongxia Qu, Liang Gong, Xuewu Duan, Hong Zhu, Ze Yun and Yueming Jiang
- 31** *A Damaged Oxidative Phosphorylation Mechanism is Involved in the Antifungal Activity of Citral against Penicillium digitatum*
Qiuli OuYang, Nengguo Tao and Miaoling Zhang
- 44** *Genome Sequence, Assembly and Characterization of Two Metschnikowia fructicola Strains Used as Biocontrol Agents of Postharvest Diseases*
Edoardo Piombo, Noa Sela, Michael Wisniewski, Maria Hoffmann, Maria L. Gullino, Marc W. Allard, Elena Levin, Davide Spadaro and Samir Droby
- 61** *Effective Biodegradation of Mycotoxin Patulin by Porcine Pancreatic Lipase*
Bingjie Liu, Xiaoning Peng and Xianghong Meng
- 68** *Phomopsis longanae Chi-Induced Changes in Activities of Cell Wall-Degrading Enzymes and Contents of Cell Wall Components in Pericarp of Harvested Longan Fruit and its Relation to Disease Development*
Yihui Chen, Shen Zhang, Hetong Lin, Junzheng Sun, Yifen Lin, Hui Wang, Mengshi Lin and John Shi
- 76** *Perillaldehyde Controls Postharvest Black Rot Caused by Ceratocystis fimbriata in Sweet Potatoes*
Man Zhang, Man Liu, Shenyuan Pan, Chao Pan, Yongxin Li and Jun Tian
- 85** *Fungal Gene Mutation Analysis Elucidating Photoselective Enhancement of UV-C Disinfection Efficiency Toward Spoilage Agents on Fruit Surface*
Pinkuan Zhu, Qianwen Li, Sepideh M. Azad, Yu Qi, Yiwen Wang, Yina Jiang and Ling Xu
- 96** *Efficacy and Mechanism of Cinnamon Essential Oil on Inhibition of Colletotrichum acutatum Isolated From 'Hongyang' Kiwifruit*
Jingliu He, Dingtao Wu, Qing Zhang, Hong Chen, Hongyi Li, Qiaohong Han, Xingyue Lai, Hong Wang, Yingxue Wu, Jiagen Yuan, Hongming Dong and Wen Qin
- 108** *Phomopsis longanae Chi-Induced Disease Development and Pericarp Browning of Harvested Longan Fruit in Association With Energy Metabolism*
Yihui Chen, Hetong Lin, Shen Zhang, Junzheng Sun, Yifen Lin, Hui Wang, Mengshi Lin and John Shi
- 117** *Effect of β -Aminobutyric Acid on Disease Resistance Against Rhizopus Rot in Harvested Peaches*
Jing Wang, Shifeng Cao, Lei Wang, Xiaoli Wang, Peng Jin and Yonghua Zheng
- 127** *Control of Citrus Post-harvest Green Molds, Blue Molds, and Sour Rot by the Cecropin A-Melittin Hybrid Peptide BP21*
Wenjun Wang, Sha Liu, Lili Deng, Jian Ming, Shixiang Yao and Kaifang Zeng

- 136 ***Phomopsis longanae* Chi-Induced Change in ROS Metabolism and Its Relation to Pericarp Browning and Disease Development of Harvested Longan Fruit**
Hui Wang, Yihui Chen, Hetong Lin, Junzheng Sun, Yifen Lin and Mengshi Lin
- 144 ***Antifungal Activity and Action Mechanism of Ginger Oleoresin Against Pestalotiopsis microspora* Isolated From Chinese Olive Fruits**
Tuanwei Chen, Ju Lu, Binbin Kang, Mengshi Lin, Lijie Ding, Lingyan Zhang, Guoying Chen, Shaojun Chen and Hetong Lin
- 153 ***Selection Pressure Pathways and Mechanisms of Resistance to the Demethylation Inhibitor-Difenoconazole in Penicillium expansum***
Emran Md Ali and Achour Amiri
- 166 ***Assessment of Detoxification Efficacy of Irradiation on Zearalenone Mycotoxin in Various Fruit Juices by Response Surface Methodology and Elucidation of its in-vitro Toxicity***
Naveen Kumar Kalagatur, Jalarama Reddy Kamasani and Venkataramana Mudili
- 179 ***Chitosan, a Biopolymer With Triple Action on Postharvest Decay of Fruit and Vegetables: Eliciting, Antimicrobial and Film-Forming Properties***
Gianfranco Romanazzi, Erica Feliziani and Dharini Sivakumar



iTRAQ Proteomic Analysis Reveals That Metabolic Pathways Involving Energy Metabolism Are Affected by Tea Tree Oil in *Botrytis cinerea*

Jiayu Xu, Xingfeng Shao*, Yingying Wei, Feng Xu and Hongfei Wang

Department of Food Science and Engineering, Ningbo University, Ningbo, China

OPEN ACCESS

Edited by:

Boqiang Li,
Institute of Botany (CAS), China

Reviewed by:

Jun Tian,
Jiangsu Normal University, China
Soner Soylu,
Mustafa Kemal University, Turkey

*Correspondence:

Xingfeng Shao
shaoxingfeng@nbu.edu.cn

Specialty section:

This article was submitted to
Food Microbiology,
a section of the journal
Frontiers in Microbiology

Received: 06 September 2017

Accepted: 27 September 2017

Published: 12 October 2017

Citation:

Xu J, Shao X, Wei Y, Xu F and Wang H
(2017) iTRAQ Proteomic Analysis
Reveals That Metabolic Pathways
Involving Energy Metabolism Are
Affected by Tea Tree Oil in *Botrytis*
cinerea. *Front. Microbiol.* 8:1989.
doi: 10.3389/fmicb.2017.01989

Tea tree oil (TTO) is a volatile essential oil obtained from the leaves of the Australian tree *Melaleuca alternifolia* by vapor distillation. Previously, we demonstrated that TTO has a strong inhibitory effect on *Botrytis cinerea*. This study investigates the underlying antifungal mechanisms at the molecular level. A proteomics approach using isobaric tags for relative and absolute quantification (iTRAQ) was adopted to investigate the effects of TTO on *B. cinerea*. A total of 718 differentially expression proteins (DEPs) were identified in TTO-treated samples, 17 were markedly up-regulated and 701 were significantly down-regulated. Among the 718 DEPs, 562 were annotated and classified into 30 functional groups by GO (gene ontology) analysis. KEGG (Kyoto Encyclopedia of Genes and Genomes) enrichment analysis linked 562 DEPs to 133 different biochemical pathways, involving glycolysis, the tricarboxylic acid cycle (TCA cycle), and purine metabolism. Additional experiments indicated that TTO destroys cell membranes and decreases the activities of three enzymes related to the TCA cycle. Our results suggest that TTO treatment inhibits glycolysis, disrupts the TCA cycle, and induces mitochondrial dysfunction, thereby disrupting energy metabolism. This study provides new insights into the mechanisms underlying the antifungal activity of essential oils.

Keywords: iTRAQ, proteomics, essential oil, *Botrytis cinerea*, antifungal

INTRODUCTION

Botrytis cinerea, one of the most destructive fungal pathogens, causing gray mold rot in a wide range of fresh fruits and vegetables. The resulting reduction in shelf life is responsible for enormous economic losses in the produce industry. Although chemical fungicides are widely used to control the incidence of the disease, this practice potentially introduces harmful substances into the food chain, and also selects for *B. cinerea* strains with increased drug resistance (Brul and Coote, 1999; Leroux et al., 2002). These limitations provide a strong stimulus to explore safer and more effective antifungal agents. Essential oils are promising natural substitutes that offer disease control by inhibiting pathogen growth (Prakash et al., 2012). For example, the essential oils of *Angelica archangelica* L. (*Apiaceae*) roots and *Solidago canadensis* L. have been characterized and tested *in vitro* as antifungal agents against *B. cinerea* (Fraternali et al., 2014; Liu et al., 2016). Lemongrass essential oil significantly reduces the incidence of *B. cinerea* and prolongs the shelf-life and sensory properties of frozen mussels and vegetables (Abdulazeez et al., 2016). Essential oils of aromatic plants, which belong to the Lamiaceae family such as origanum (*Origanum syriacum* L. var. *bevanii*),

lavender (*Lavandula stoechas* L. var. *stoechas*) and rosemary (*Rosmarinus officinalis* L.), have been reported to cause considerable morphological degenerations of the fungal hyphae of *B. cinerea* and suppress *in vivo* disease development on tomato against *B. cinerea* (Soylu et al., 2010).

Tea tree oil (TTO) is a volatile natural plant essential oil obtained from the leaves of the Australian tree *Melaleuca alternifolia* by vapor distillation (Homer et al., 2000). The oil exhibits a broad spectrum of antimicrobial activities against a variety of bacteria, fungi, and virus (Carson et al., 2006; Miao et al., 2016). Growth and metabolic activity of *Escherichia coli* and *Candida albicans* are inhibited after treatment with TTO (Gustafson et al., 1998; Bona et al., 2016). Our previous studies showed that TTO treatment effectively inhibits spore germination and mycelial growth of *B. cinerea*, modifies its morphology and cellular ultrastructure, and controls gray mold on strawberry and cherry fruits (Shao et al., 2013a; Li et al., 2017a). TTO's antifungal mechanism in *B. cinerea* involves the loss of membrane integrity and the subsequent release of intracellular compounds, probably due in part to changes in membrane fatty acid and ergosterol composition (Shao et al., 2013b; Li et al., 2017a). TTO also causes mitochondrial damage in *B. cinerea*, disrupting the tricarboxylic acid (TCA) cycle and leading to the accumulation of reactive oxygen species (ROS) (Li et al., 2017b). Metabolomic analysis by quadrupole time-of-flight mass spectrometer was consistent with these results (Xu et al., 2017). However, the molecular mechanisms underlying the effects of TTO against *B. cinerea* have not yet been associated with specific proteins.

Proteomics can be used to study the changes in protein levels under stress conditions in great detail (Franco et al., 2013), and has been applied to investigate the mode of action of the antimicrobial agent apidaecin IB against membrane proteins in *E. coli* cells (Zhou and Chen, 2011). Other studies have revealed that proteins related to energy and DNA metabolism, and amino acid biosynthesis are down-regulated in *E. coli* JK-17 in the presence of rose flower extract (Cho and Oh, 2011). *Syzygium aromaticum* essential oil perturbs the expression of virulence-related genes involved in the synthesis of serine protease, flagella, and lipopolysaccharide in *Campylobacter jejuni* (Kovács et al., 2016). In this study, we conducted a proteomics analysis using isobaric tags for relative and absolute quantification (iTRAQ) to study *B. cinerea* to identify proteins and potential mechanisms underlying the antifungal activity of TTO.

MATERIALS AND METHODS

B. cinerea Growth and Exposure to TTO

Highly virulent *B. cinerea* (ACCC 36028) was purchased from the Agricultural Culture Collection of China and grown at 25°C on potato dextrose agar (PDA, containing 1 L potato liquid, 20 g/L glucose, and 15 g/L agar) before use. TTO was purchased from Fuzhou Merlot Lotus Biological Technology Company (Fujian Province, China). The primary components of TTO are terpinen-4-ol (37.11%), γ -terpinene (20.65%), α -terpinene (10.05%), 1, 8-cineole (4.97%), terpinolene (3.55%), p -cymene (2.14%), and α -terpineol (3.82%), as specified by the supplier. *B. cinerea* cultures

were maintained on PDA at 25°C for 3 days. Spore suspensions were harvested by adding 10 mL sterile 0.9% NaCl solution to each petri dish and then gently scraping the mycelial surface three times with a sterile L-shaped spreader to free the spores. The spore suspension was adjusted using a hemocytometer to 5×10^6 spores/mL. One milliliter suspension was inoculated into 250 mL flasks containing 150 mL sterile potato dextrose broth medium and cultured at 25°C on a rotary shaker at 150 revolutions per minute for 3 days. Before mycelia were harvested, TTO was added to the medium to a final concentration of 5 mL/L, and cultures incubated for another 2 h (Xu et al., 2017). Mycelia were collected and rinsed three times with 0.1 M phosphate buffered saline (PBS) (pH 7.4). Samples were stored at -80°C . Cultures without TTO were used as a control. Three samples were prepared in parallel for each condition.

Protein Extraction

Approximately 200 mg of frozen mixed mycelium from control or TTO treated cultures was ground into powder in liquid nitrogen and suspended in 25 mL 10% (v/v) trichloroacetic acid in acetone containing 65 mM dithiothreitol (DTT). The suspension was vortexed and incubated at -20°C for 2 h, centrifuged at $12,000 \times g$ for 45 min at 4°C , and the supernatant discarded. The precipitate was rinsed three times with chilled acetone. The pellet was vacuum dried and dissolved in lysis buffer (4% SDS, 100 mM Tris-HCl, 100 mM DTT, pH 8.0). After incubation for 5 min in boiling water, the suspension was sonicated on ice at 50 W for 5 min. The crude extract was incubated in boiling water again for 5 min, and clarified by centrifugation at $14,000 \times g$ for 40 min at 20°C . To digest protein in the supernatant, 200 μL UA buffer (8 M urea, 150 mM Tris-HCl, pH 8.5) was added and the mixture was centrifuged at $14,000 \times g$ for 30 min at room temperature. This step was repeated three times. Subsequently, 100 μL 50 mM iodoacetamide (IAM) was added, the samples were incubated for 30 min in darkness, and then centrifuged at $14,000 \times g$ for 30 min at room temperature. The precipitate was resuspended in 100 μL UA buffer and samples were centrifuged at $14,000 \times g$ for 30 min at room temperature. 100 μL dissolution buffer was added, followed by centrifugation at $14,000 \times g$ for 30 min at room temperature. This step was repeated three times. The supernatant was removed, the pellet was dissolved in 40 μL trypsin buffer, incubated at 37°C for 18 h, and clarified by centrifugation at $14,000 \times g$ for 30 min at room temperature. Finally, 40 μL 25 mM dissolution buffer was added and samples were centrifuged at $14,000 \times g$ for 30 min at room temperature. The supernatant was transferred to a new tube and quantified with the Bradford assay using BSA as the standard, and SDS-PAGE was performed to verify protein quality.

iTRAQ Labeling and Strong Cation Exchange (SCX) Fractionation

iTRAQ labeling was performed according to the manufacturer's instructions. Peptides were prepared using the 8-plex iTRAQ labeling kit (AB Sciex, CA, USA). Control replicates were labeled with reagents 113, 114, and 115, and the TTO treatment

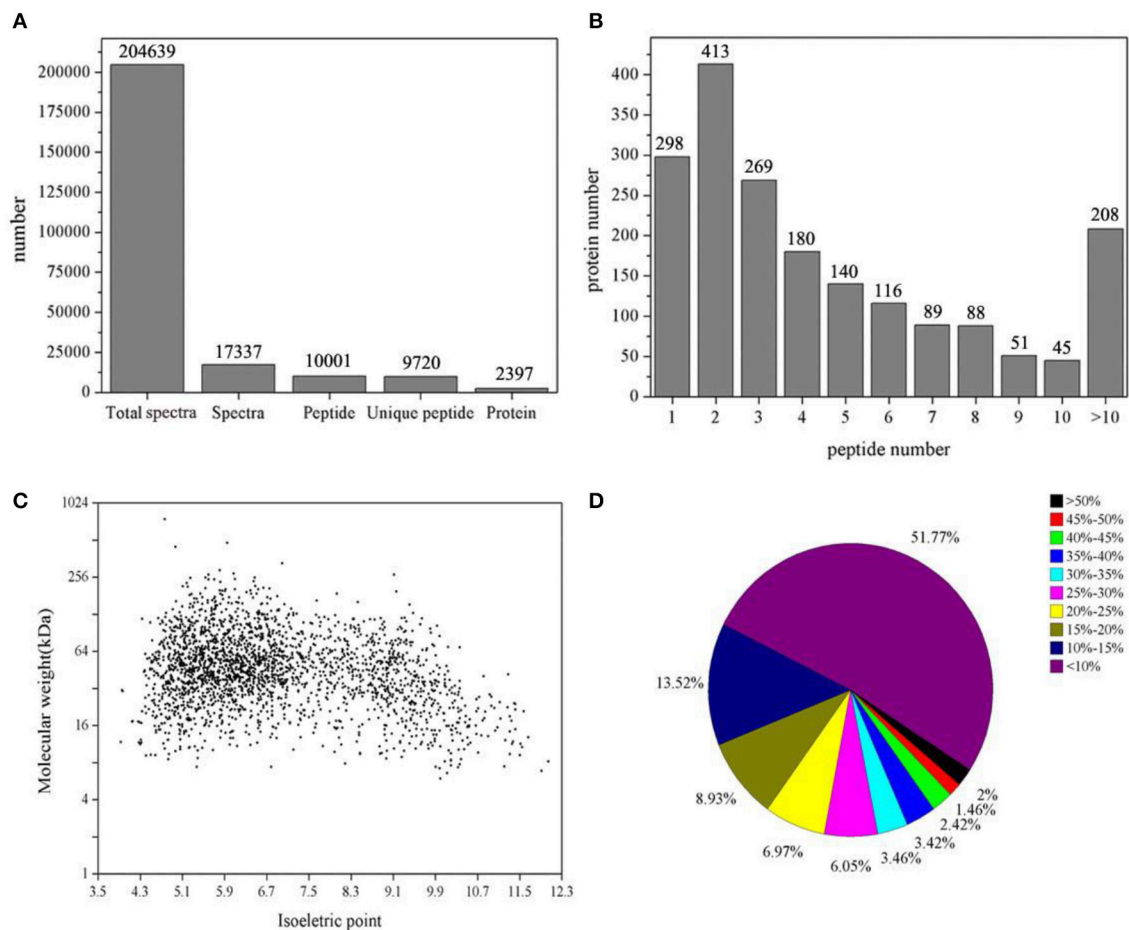


FIGURE 1 | Summary of iTRAQ results. **(A)**, total spectra, matched spectra, matched peptides, unique peptides, and identified proteins. **(B)**, number of peptides associated with identified proteins. **(C)**, molecular weights vs. isoelectric points, as calculated from protein sequences. **(D)**, sequence coverage for identified proteins.

replicates were labeled with reagents 116, 117, and 118. The labeled peptide mixtures were pooled and dried by vacuum centrifugation.

The labeled peptide mixtures were dissolved in 3 mL buffer A (10 mM KH_2PO_4 in 25% acetonitrile, pH 3.0) and loaded onto a polysulfoethyl 4.6 \times 100 mm column (5 μm , 200 Å, PolyLC, Inc., Maryland, USA). The peptides were eluted at a flow rate of 1 mL/min with a gradient of buffer A for 30 min, 5–70% buffer B (10 mM KH_2PO_4 , 500 mM KCl in 25% acetonitrile, pH 3.0) for 65 min, and 70–100% buffer B for 80 min. The eluted peptides were pooled into 10 fractions, desalted on C18 cartridges (Sigma), and vacuum-dried.

LC-MS/MS Analysis

For nano LC-MS/MS analysis, 10 μL of supernatant from each fraction was injected into an Orbitrap-Elite (ThermoFinnigan) equipped with an Easy nLC (Proxeon Biosystems, now Thermo Fisher Scientific). The mobile phase was a mixture of water containing 0.1% formic acid and acetonitrile with 0.1% formic acid isocratically delivered by a pump at a flowrate of 250 nL/min.

The elution gradient was: 0–105 min, 0–50% B; 105–110 min, 50–100% B; 110–120 min, 100% B. The MS scanning range was 300–1,800 m/z, MS resolution was 70,000, the number of scans range was 1, and the dynamic exclusion time was 40 s. The MS/MS activation type was HCD, the isolation window was 2 m/z, the MS/MS resolution was 17,500, the normalized collision energy was 30 eV, and the underfill ratio was 0.1%.

Analysis of Differentially Expression Proteins

For protein quantitation, one protein was required to contain at least two unique peptides. The quantitative protein ratios were weighted and normalized by the median ratio in Mascot (<http://www.matrixscience.com>). When differences in protein expression between TTO-treated and control groups were >1.5-fold or <0.67-fold, with $p < 0.05$, the protein was considered to be differentially expressed.

Bioinformatic Analysis

Gene Ontology (GO) is a standardized gene function classification system that describes the properties of proteins

TABLE 1 | The main differentially expressed proteins in *B. cinerea* after treatment with TTO.

Accession	Protein name	Score	Sequence coverage (%)	Fold ^a	p-value
gi 154691848	cytochrome c	96.3	37.9	0.328	0.007
gi 347441783	citrate synthase	133.1	8.0	1.819	0.028
gi 472236008	malate dehydrogenase protein	957.7	55.4	2.120	0.017
gi 472241505	oxoglutarate dehydrogenase protein	698.3	27.2	1.611	0.037
gi 347827327	pyruvate carboxylase	2,263.6	38.7	1.751	0.027
gi 347833674	phosphoenolpyruvate carboxykinase	548.7	30.2	1.625	0.044
gi 347839725	succinyl-CoA ligase subunit alpha	420.3	24.3	1.612	0.040
gi 347826865	fructose-1,6-bisphosphatase	308.1	39.1	1.640	0.031
gi 154323902	enolase	2,009.9	46.6	1.621	0.008
gi 472238209	glucose-6-phosphate isomerase protein	574.2	29.9	1.980	0.032
gi 472246374	phosphoglycerate mutase protein	54.3	2.6	1.576	0.021
gi 472240435	6-phosphofructokinase protein	539.9	28.1	1.775	0.022
gi 472237248	bisphosphoglycerate-independent phosphoglycerate mutase protein	823.0	44.1	2.164	0.018
gi 347841748	fructose-bisphosphate aldolase	1,045.2	42.2	1.725	0.027
gi 536718572	phosphoglycerate kinase 1	587.5	40.2	1.723	0.040
gi 347833674	phospho-2-dehydro-3-deoxyheptonate aldolase	548.7	30.2	1.870	0.029
gi 347835540	phosphoglycerate mutase family protein	36.0	4.7	1.792	0.015
gi 472240974	6-phosphofructo-2-kinase fructose bisphosphatase protein	98.8	9.4	1.851	0.037
gi 347441437	inosine 5-monophosphate dehydrogenase	581.8	19.9	1.606	0.020
gi 347841600	adenine phosphoribosyltransferase	182.4	37.8	1.777	0.022
gi 347829189	adenosine kinase	465.9	31.3	1.956	0.016
gi 347441679	adenosylhomocysteinease	1,287.4	61.7	1.881	0.027
gi 347837737	S-adenosylmethionine synthetase	423.1	30.1	2.004	0.008
gi 347831618	AMP deaminase 3	111.1	4.5	1.673	0.029
gi 347828730	adenylosuccinate synthetase	333.0	30.9	1.602	0.036
gi 347837737	S-adenosylmethionine synthetase	423.1	30.1	2.004	0.008
gi 347837845	adenylyl cyclase-associated protein	417.9	20.7	1.810	0.022
gi 472242224	guanyl-nucleotide exchange factor protein	65.4	1.5	1.674	0.004
gi 154691052	uracil phosphoribosyltransferase	90.6	9.4	1.796	0.046
gi 154697015	nucleoside diphosphate kinase	522.4	42.8	1.935	0.010
gi 347840376	UTP-glucose-1-phosphate uridylyltransferase	1,333.6	45.7	1.623	0.038
gi 347832865	ribulose-phosphate 3-epimerase	38.6	7.9	2.204	0.031
gi 154300519	alcohol dehydrogenase protein	167.7	16.5	1.960	0.026
gi 347836330	alcohol dehydrogenase (NADP dependent)	281.1	24.4	2.019	0.020
gi 347441899	zinc-containing alcohol dehydrogenase	636.5	44.8	1.656	0.032
gi 347440923	aldehyde dehydrogenase	1,070.9	48.0	1.865	0.021
gi 154703069	ATP synthase D chain, mitochondrial	252.1	26.4	1.924	0.050
gi 563298521	ATP synthase subunit e, mitochondrial	60.2	9.9	1.757	0.033
gi 347839842	ATP citrate lyase subunit	549.0	37.5	1.589	0.023
gi 154703371	vacuolar ATP synthase subunit E	93.3	12.7	2.382	0.013
gi 154692979	vacuolar ATP synthase subunit D	74.8	19.5	1.715	0.024
gi 347441643	vacuolar ATP synthase subunit H	307.6	22.3	1.761	0.028
gi 472245494	vacuolar ATP synthase catalytic subunit a protein	577.7	27.8	1.580	0.012
gi 347835157	v-type proton ATPase subunit B	274.1	17.6	2.041	0.019
gi 507414597	mitochondrial import protein 1	31.1	8.6	1.872	0.043
gi 472243251	mitochondrial pyruvate dehydrogenase kinase protein	61.4	3.4	2.632	0.009
gi 229891130	amino-acid acetyltransferase, mitochondrial	44.2	2.1	2.115	0.022
gi 3282211	isocitrate lyase 1, partial	27.8	2.5	1.874	0.029
gi 347832197	malate synthase	46.4	5.7	1.875	0.048
gi 347840647	acetyl-CoA carboxylase	2,370.7	33.8	1.622	0.039
gi 347842358	acetyl-CoA acetyltransferase	449.4	46.3	1.982	0.018

(Continued)

TABLE 1 | Continued

Accession	Protein name	Score	Sequence coverage (%)	Fold ^a	p-value
gi 347841050	fatty acid synthase	1,414.5	25.2	1.693	0.042
gi 472245418	fatty acid synthase beta subunit dehydratase protein	1,668.6	24.8	1.567	0.045
gi 347841364	NADP-specific glutamate dehydrogenase	1,138.8	46.9	1.840	0.021
gi 347827914	homocitrate synthase	454.5	39.0	1.501	0.031
gi 347837008	homoserine kinase	190.1	28.7	1.920	0.042
gi 347836521	GABA transaminase	483.9	27.7	1.544	0.018
gi 472242205	aspartate aminotransferase protein	385.8	26.1	1.837	0.048
gi 347841990	tryptophan synthase	611.0	28.3	1.542	0.024
gi 347832506	threonine synthase	348.4	16.4	1.560	0.047
gi 154692095	cysteine synthase	292.8	25.0	1.589	0.028
gi 347833148	glutamine synthetase	484.0	26.9	1.778	0.015
gi 347839014	histidine biosynthesis protein	184.6	9.3	1.840	0.027
gi 347828253	dihydropyridine synthetase family protein	518.7	28.0	1.869	0.013
gi 347836881	D-3-phosphoglycerate dehydrogenase	656.4	25.5	1.758	0.018
gi 472242394	saccharopine dehydrogenase protein	338.7	36.2	1.743	0.039
gi 347441047	glycine dehydrogenase	286.9	12.3	1.708	0.029
gi 507414630	C-1-tetrahydrofolate synthase	905.4	31.2	1.737	0.031
gi 347831191	glutamate carboxypeptidase protein	298.0	23.2	1.977	0.020
gi 347841903	methionine aminopeptidase 1	221.2	20.3	2.040	0.021
gi 332313356	methionine aminopeptidase 2	73.1	10.3	2.044	0.027
gi 347829817	serine/threonine protein kinase	32.6	4.4	1.693	0.037
gi 472244536	glutamate-cysteine ligase protein	61.6	3.6	1.698	0.037
gi 347829487	5-methyltetrahydropteroyltriglutamate-homocysteine methyltransferase	2,013.2	41.1	2.505	0.004
gi 347836712	glycine cleavage system H protein	116.0	22.0	1.982	0.025
gi 472236211	amino acid permease protein	39.7	4.0	1.999	0.031
gi 347830997	peptide methionine sulfoxide reductase	82.8	20.5	1.919	0.029
gi 472243795	aromatic-L-amino-acid decarboxylase protein	287.6	12.1	1.936	0.015
gi 347833024	lysine decarboxylase-like protein	79.7	8.6	1.585	0.033
gi 472246546	glutathione-dependent formaldehyde dehydrogenase	587.5	48.7	1.666	0.043
gi 347840830	NADH-cytochrome b5 reductase	305.5	23.0	1.545	0.029
gi 347827019	cytochrome P450 monooxygenase	31.4	2.4	1.722	0.042
gi 125949746	calcineurin	194.3	12.4	1.777	0.023
gi 154289817	chitin synthase	129.2	4.7	1.555	0.023
gi 347840218	sorbitol dehydrogenase	28.3	2.9	1.706	0.028
gi 347440923	aldehyde dehydrogenase	1,070.9	48.0	1.865	0.021
gi 347833737	mitochondrial peroxiredoxin Prx1	42.8	7.6	1.856	0.044
gi 347828993	antioxidant	129.5	33.1	2.127	0.028
gi 347839043	superoxide dismutase	163.1	17.0	1.717	0.012
gi 166408944	flavo-hemoglobin	294.7	35.7	1.994	0.009
gi 347828340	oxidoreductase	305.1	14.93	2.119	0.045
gi 347841065	nuclear control of ATPase protein	84.7	4.7	0.219	0.001
gi 347836808	heat shock protein 70	3,060.8	53.2	1.750	0.014
gi 472242753	30 kDa heat shock protein	296.7	47.5	1.959	0.019
gi 347827157	heat shock protein 90	1,603.7	37.7	1.650	0.032
gi 347830903	heat shock protein ST11	689.1	35.8	2.451	0.011
gi 347830415	heat shock protein Hsp88	1,199.5	34.3	1.817	0.020
gi 347833633	heat shock protein	748.3	34.3	1.999	0.020
gi 154288804	short chain dehydrogenase	105.9	20.7	2.142	0.005
gi 347840162	translation initiation factor 3	284.6	46.8	1.905	0.031
gi 472245156	eukaryotic translation initiation factor 3 subunit	749.4	18.9	1.890	0.015
gi 229463757	eukaryotic translation initiation factor 3 subunit H	195.8	20.7	1.851	0.013

(Continued)

TABLE 1 | Continued

Accession	Protein name	Score	Sequence coverage (%)	Fold ^a	p-value
gi 229501208	eukaryotic translation initiation factor 3 subunit K	232.7	33.5	1.751	0.044
gi 347841080	eukaryotic translation initiation factor 2 subunit alpha	193.5	17.1	1.574	0.030
gi 347830243	eukaryotic translation initiation factor 4e	151.7	12.0	1.798	0.044
gi 347840917	actin-depolymerizing factor 1	519.9	53.6	1.959	0.018
gi 3182891	actin	1,055.4	52.8	1.555	0.035
gi 347831507	actin binding protein	276.9	16.6	1.942	0.003
gi 347840551	actin related protein 2/3 complex	217.4	21.9	1.835	0.013
gi 347838304	F-actin capping protein beta subunit isoforms 1 and 2	156.0	27.7	1.595	0.044
gi 205716451	actin cytoskeleton-regulatory complex protein end 3	109.4	10.4	1.827	0.022
gi 347827283	actin lateral binding protein	691.2	50.3	2.621	0.002
gi 347441258	myosin regulatory light chain cdc4	327.6	43.9	1.775	0.049
gi 347838471	survival factor 1	321.9	28.4	1.608	0.038
gi 347441690	transcription factor HMG	78.8	21.8	3.565	0.004
gi 347838526	transcription factor CCAAT	39.1	3.5	4.970	0.001
gi 374093884	transcription regulator PAC1, partial	42.1	3.2	2.501	0.023
gi 472235708	cp2 transcription factor protein	92.2	6.2	1.748	0.040
gi 347826783	transcription initiation factor subunit	28.9	7.4	2.083	0.024
gi 347837746	transcription factor CBF/NF-Y	46.1	6.1	1.869	0.021
gi 347840266	transcription factor Zn, C ₂ H ₂	50.5	1.7	3.407	0.003
gi 347837101	EF-hand calcium-binding domain protein	42.8	3.7	0.031	0.001
gi 472246130	cell division control protein cdc48 protein	1,298.4	40.7	1.654	0.021
gi 472235945	cell lysis protein	103.7	20.5	1.930	0.025
gi 206558271	cell division cycle protein 123	38.6	3.9	1.809	0.050
gi 347828695	apoptosis-inducing factor 3	267.7	17.2	2.290	0.003
gi 472242094	thioredoxin protein	388.6	51.4	2.634	0.003
gi 472244889	sulfate adenylyltransferase protein	328.9	25.8	1.858	0.011
gi 347839319	protein disulfide-isomerase	542.3	39.1	1.862	0.031
gi 347442007	transaldolase	1,216.6	50.2	1.984	0.022
gi 154703303	elongation factor 1-alpha	2,637.4	50.0	1.831	0.034
gi 347830450	elongation factor 2	1,896.6	44.6	1.688	0.020
gi 472244387	elongation factor 1-beta protein	597.2	40.0	2.006	0.024
gi 347841449	NAD-dependent formate dehydrogenase	1,663.0	50.1	1.931	0.042
gi 347835785	26S protease regulatory subunit 6A	355.1	27.6	1.848	0.017
gi 472242788	proteasome component pre3 protein	101.7	23.9	1.942	0.023
gi 347841691	arp2/3 complex subunit Arc16	249.2	41.7	1.729	0.020
gi 154319207	26S protease regulatory subunit 7	221.9	19.4	2.009	0.026
gi 347833025	proteasome subunit alpha type 1	133.2	16.9	1.706	0.025
gi 347441407	protein kinase C substrate	282.5	18.1	1.703	0.028
gi 347827686	sec14 cytosolic factor	240.1	41.4	1.711	0.030
gi 347840528	peptidyl-prolyl cis-trans isomerase D	431.3	39.9	2.070	0.019
gi 563298153	inorganic pyrophosphatase	317.8	29.7	1.714	0.015
gi 347830035	aldose 1-epimerase	338.4	29.6	2.114	0.040
gi 347831189	carbohydrate-Binding Module family 48 protein	330.4	27.1	3.744	0.014
gi 347839149	carbohydrate-Binding Module family 50 protein	196.5	25.3	2.276	0.047
gi 347841295	cystathionine beta-synthase	416.0	26.0	1.790	0.031
gi 347842143	diphosphomevalonate decarboxylase	303.6	25.9	1.788	0.022
gi 347836348	protein phosphatase PP2A regulatory subunit A	414.1	21.1	1.576	0.045
gi 347838932	class I/II aminotransferase	340.3	23.9	1.844	0.015
gi 347831623	amidophosphoribosyltransferase	1,467.6	20.8	1.573	0.025
gi 472236449	enoyl- hydratase isomerase protein	101.1	19.1	1.849	0.026
gi 472237246	tubulin-specific chaperone c protein	222.7	20.7	1.621	0.044

(Continued)

TABLE 1 | Continued

Accession	Protein name	Score	Sequence coverage (%)	Fold ^a	p-value
gi 347826898	trans-2-enoyl-CoA reductase	31.9	1.9	0.031	0.001
gi 347837864	1,3,8-naphthalenetriol reductase	89.0	19.6	2.213	0.029
gi 472243905	casein kinase i protein	148.3	19.8	1.591	0.043
gi 347831955	acetate kinase	193.1	18.9	1.726	0.015
gi 347839614	aspartyl aminopeptidase	293.3	18.8	1.564	0.036
gi 472238538	3-hydroxybutyryl-dehydrogenase protein	133.3	17.2	1.645	0.025
gi 347441025	arf gtpase-activating protein	249.9	17.2	2.074	0.008
gi 347828551	phosphatidyl synthase	72.6	9.4	1.967	0.029
gi 154294387	mitogen-activated protein kinase	101.9	17.1	1.664	0.039
gi 472240101	alpha beta hydrolase fold-3 domain protein	45.3	9.0	1.812	0.020
gi 347827703	BAR domain protein	271.6	43.4	1.751	0.037
gi 347830570	ThiJ/Pfpl family protein	645.5	37.0	1.703	0.016
gi 347832713	DUF1688 domain-containing protein	437.7	27.6	1.726	0.034
gi 472245392	DUF718 domain-containing protein	75.6	27.3	1.803	0.019
gi 347836108	C2 domain-containing protein	286.0	23.6	1.947	0.021
gi 347833490	DUF757 domain-containing protein	74.8	22.4	1.840	0.045
gi 472245612	c6 finger domain protein	248.4	22.4	1.782	0.029
gi 347838618	UBX domain-containing protein	101.1	16.2	2.252	0.036
gi 472236354	yip1 domain-containing protein	66.0	11.1	2.052	0.033
gi 347836200	FAD binding domain-containing protein	117.4	10.7	2.072	0.015
gi 347836441	DUF89 domain-containing protein	69.4	6.0	1.638	0.027
gi 472240877	bar domain-containing protein	69.2	5.9	1.784	0.040
gi 347832303	acyl-CoA dehydrogenase domain protein	202.2	19.9	2.010	0.042
gi 472237107	saff domain-containing protein	94.8	8.5	1.933	0.015
gi 347828586	CUE domain-containing protein	53.8	3.1	3.833	0.008
gi 472244807	calponin domain protein	79.3	2.9	2.067	0.033
gi 563296966	KH domain protein	31.2	1.7	1.900	0.011
gi 347829378	R ₃ H domain-containing protein	32.3	1.6	1.938	0.001
gi 347836748	pumilio domain-containing protein	37.9	1.4	2.313	0.007
gi 347836261	methyltransferase domain-containing protein	27.9	2.9	0.031	0.001
gi 154691472	eukaryotic peptide chain release factor subunit 1	426.9	30.8	1.912	0.036
gi 347837479	glia maturation factor gamma	102.7	30.6	1.703	0.028
gi 347837628	CORD and CS domain-containing protein	134.3	29.8	1.787	0.013
gi 347828828	ruvB-like helicase 1	417.5	30.4	1.502	0.035
gi 347442085	CND8	99.4	6.3	0.405	0.001
gi 156051430	40S ribosomal protein S3	1,591.3	60.8	1.638	0.040
gi 347827805	40S ribosomal protein S5	418.3	38.5	1.531	0.044
gi 347835120	40S ribosomal protein S6	332.8	34.3	1.763	0.046
gi 347836429	40S ribosomal protein S7	276.1	30.4	1.857	0.007
gi 156043471	40S ribosomal protein S8	688.8	40.2	1.584	0.026
gi 154291145	40S ribosomal protein S10	106.2	25.4	1.891	0.016
gi 156061679	40S ribosomal protein S13	404.4	33.8	1.867	0.035
gi 472237384	40S ribosomal protein S18	546.8	42.3	1.902	0.018
gi 347837250	40S ribosomal protein S19	363.8	51.0	2.715	0.025
gi 347441467	40S ribosomal protein S21	157.1	63.6	2.762	0.018
gi 347829326	40S ribosomal protein S23	190.6	20.0	1.898	0.048
gi 156065881	40S ribosomal protein S24	348.1	32.6	1.861	0.040
gi 156065633	40S ribosomal protein S25	174.3	26.8	2.073	0.037
gi 347832333	40S ribosomal protein S27	322.4	37.8	1.823	0.028
gi 347828118	40S ribosomal protein S29	126.9	42.9	2.508	0.013
gi 347827513	40S ribosomal protein S30	63.1	16.1	0.199	0.002

(Continued)

TABLE 1 | Continued

Accession	Protein name	Score	Sequence coverage (%)	Fold ^a	p-value
gi 347828771	60S ribosomal protein L44	97.8	13.2	2.919	0.014
gi 156062084	60S ribosomal protein L9	1,053.6	63.4	1.571	0.031
gi 229891536	54S ribosomal protein L4, mitochondrial	54.3	6.8	0.375	0.024
gi 156037530	60S ribosomal protein L12	608.9	40.0	1.562	0.010
gi 347832401	60S ribosomal protein L13	444.7	33.0	1.662	0.032
gi 347835805	60S ribosomal protein L6	611.8	33.0	1.670	0.023
gi 347836248	60S ribosomal protein L10	126.5	11.3	2.336	0.030
gi 347839766	60S ribosomal protein L16	271.7	29.7	2.055	0.039
gi 154316257	60S ribosomal protein L17	563.9	30.5	2.136	0.011
gi 154310248	60S ribosomal protein L19	409.8	29.4	2.652	0.009
gi 347840178	60S ribosomal protein L21	247.9	35.6	1.977	0.029
gi 347830985	60S ribosomal protein L23	425.6	48.9	1.936	0.030
gi 347835534	60S ribosomal protein L24	274.0	29.0	2.291	0.015
gi 347831348	60S ribosomal protein L26	236.5	36.8	2.174	0.030
gi 347441549	60S ribosomal protein L27a	708.8	48.3	1.603	0.018
gi 347841474	60S ribosomal protein L28	236.9	52.7	3.593	0.010
gi 472245831	60S ribosomal protein L31	295.4	48.0	2.230	0.019
gi 347826648	60S ribosomal protein L33	274.2	37.6	1.909	0.034
gi 154315039	60S ribosomal protein L35	140.2	18.9	2.744	0.024
gi 156036474	60S ribosomal protein L36	166.0	35.9	1.648	0.038
gi 154297648	60S acidic ribosomal protein P0	1,277.7	41.7	1.896	0.029
gi 347835237	60S acidic ribosomal protein P1	553.2	41.2	2.379	0.011
gi 347838558	60S acidic ribosomal protein P2	500.4	55.9	2.178	0.012
gi 347441053	ribosome associated DnaJ chaperone Zuotin	635.2	25.3	1.863	0.029
gi 156044830	ribosome biogenesis protein Nhp2	106.9	9.8	1.594	0.024
gi 229485392	ribosome biogenesis protein erb1	56.1	4.2	1.636	0.045
gi 347837666	nuclear transport factor 2	236.2	28.2	2.249	0.020
gi 472246396	nuclear segregation protein	466.5	27.0	3.04	0.013
gi 347835094	leucyl-tRNA synthetase	722.1	25.9	1.809	0.016
gi 347835240	methionyl-tRNA synthetase	183.7	18.9	1.931	0.029
gi 347828755	tryptophanyl-tRNA synthetase	283.9	23.4	1.864	0.037
gi 563295297	histidyl-tRNA synthetase	286.9	21.9	1.691	0.027
gi 347835339	glutamyl-tRNA synthetase	353.0	21.5	1.783	0.032
gi 347841257	threonyl-tRNA synthetase	522.0	18.2	1.918	0.013
gi 347840344	valyl-trna synthetase	535.3	13.7	1.681	0.046
gi 347833265	aspartyl-tRNA synthetase	271.9	15.1	1.861	0.017
gi 347836347	phenylalanyl-tRNA synthetase beta chain	159.9	13.5	2.148	0.003
gi 347842507	tRNA methyltransferase	31.7	2.9	1.735	0.006
gi 347837080	polyadenylate-binding protein	621.1	19.8	1.755	0.039
gi 563292520	histone H1-binding protein	84.1	7.0	1.894	0.025
gi 472237673	oxysterol-binding protein	154.5	6.5	3.378	0.014
gi 154692219	glycogen synthase	204.9	11.1	1.884	0.038
gi 154308576	glucose-6-phosphate 1-dehydrogenase	365.5	25.1	1.986	0.023
gi 347833053	1,3-beta-glucan biosynthesis protein	131.7	10.6	2.131	0.033
gi 347841047	plasma membrane stress response protein	34.6	2.0	3.195	0.009
gi 347830640	methylenetetrahydrofolate reductase	196.2	13.4	1.552	0.019
gi 154309515	ca/CaM-dependent kinase-1	141.7	18.4	1.566	0.036
gi 347829911	GTP-binding nuclear protein Ran	301.8	38.1	1.732	0.025
gi 472236275	tRNA splicing endonuclease subunit protein	96.8	14.5	2.013	0.007
gi 347831289	RNA binding effector protein Scp160	853.4	22.1	1.568	0.050
gi 347839263	DNA-directed RNA polymerase I subunit	49.6	14.1	2.662	0.041

(Continued)

TABLE 1 | Continued

Accession	Protein name	Score	Sequence coverage (%)	Fold ^a	p-value
gi 347441996	HAD superfamily hydrolase	203.1	32.5	1.599	0.041
gi 347840552	ubiquitin carboxyl-terminal hydrolase	362.9	27.1	1.976	0.026
gi 347837756	ubiquitin-like protein SMT3	34.9	18.8	2.301	0.030
gi 472238757	ubiquitin-activating enzyme e1 1 protein	489.3	17.3	1.665	0.016
gi 154695558	ubiquitin-conjugating enzyme E2	36.3	7.5	1.579	0.042
gi 472241717	ubiquitin thioesterase protein	56.4	8.3	1.749	0.027
gi 347440894	translocon beta subunit Sbh1	225.3	44.6	1.753	0.042
gi 472236180	minor allergen alt a 7 protein	282.3	47.8	2.844	0.005
gi 472235513	anthranilate synthase component 2 protein	392.7	20.7	1.590	0.029
gi 347833273	nipsnap family protein	154.3	19.9	1.633	0.026
gi 347832071	phosphoglucomutase	1,936.2	53.1	1.896	0.017
gi 347829895	phosphomannomutase	182.7	21.5	1.854	0.028
gi 347832016	N-acetylglucosamine-phosphate mutase	436.9	26.4	1.853	0.011
gi 347841616	UDP-galactopyranose mutase	549.0	33.1	2.149	0.020
gi 347841593	UDP-N-acetylglucosamine pyrophosphorylase	519.9	35.0	1.922	0.008
gi 472237006	UDP-glucose 4-epimerase gal10 protein	191.1	20.5	1.867	0.009
gi 347441001	mannose-1-phosphate guanylttransferase alpha-a	584.1	36.3	1.631	0.033
gi 472241485	nad h-dependent d-xylose reductase xyl1 protein	247.9	28.6	1.541	0.046
gi 347828612	transketolase	1,284.8	41.2	2.020	0.013
gi 154321267	phosphoketolase	883.5	24.4	1.836	0.042
gi 347842358	acetyl-CoA acetyltransferase	449.4	46.3	1.982	0.018
gi 347830285	phospho-2-dehydro-3-deoxyheptonate aldolase	460.2	36.1	1.950	0.027
gi 347840715	3-isopropylmalate dehydratase	593.0	29.8	1.519	0.019
gi 347440697	cyanide hydratase/nitrilase	353.7	17.0	2.551	0.012
gi 347832595	aldo/keto reductase family oxidoreductase	497.6	42.5	1.999	0.018
gi 154322845	aldo/keto reductase	327.8	28.9	1.724	0.044
gi 347838695	nitroreductase family protein	228.3	32.7	1.893	0.018
gi 154293270	glucose 1-dehydrogenase	263.4	27.8	1.636	0.043

^aFold: the average ratio (control/TTO-treated) of protein levels from three biological replicates as determined by iTRAQ approach. A protein was considered a differential expression protein as it exhibited a >1.5-fold or <0.67-fold change and *P* < 0.05.

using three attributes: biological process, molecular function, and cellular components (Ashburner et al., 2000). A GO analysis (<http://www.geneontology.org>) was conducted to assign functional annotations for differentially expression proteins (DEPs), and the Kyoto Encyclopedia of Genes and Genomes (KEGG) (<http://www.genome.jp/kegg>) was used to predict the primary metabolic and signal transduction pathways in which the identified DEPs are involved.

Confocal Laser Scanning Microscopy

To assess the effects of TTO on the cytoplasmic membranes of *B. cinerea*, confocal laser scanning microscopy (LSM 880, Carl Zeiss, Germany) was performed, using the fluorescent indicator propidium iodide (PI) (Sigma-Aldrich, USA) and a modified protocol (Lee and Kim, 2017). *B. cinerea* cells containing 4×10^6 spores/ml were added to each glass tube and incubated with TTO (final concentration 5 mL/L) with shaking at 200 rpm at 25°C for 2 h. The cells were washed and resuspended in 0.5 mL PBS (pH 7.4), stained with PI (10 μM final concentration) for 30 min at room temperature in the dark, and then washed twice with PBS.

Images were acquired using confocal laser scanning microscopy. The experiment was repeated three times.

Measurement of Enzyme Activities Related to TCA Cycle

Using the protocol described above (see Protein Extraction), ground mycelium was suspended in PBS (pH 7.4) and centrifuged at $10,000 \times g$ for 10 min at 4°C. Enzyme activities were measured in the supernatant for malate dehydrogenase (MDH), citrate synthase (CS), and oxoglutarate dehydrogenase (OGDH), using kits purchased from Nanjing Jiancheng Bioengineering Institute (Nanjing, Jiangsu, China), following the manufacturer's instructions. Protein concentration was determined using a method based on the (Bradford, 1976) assay. MDH activity was calculated as μmol of NAD reduced per minute per mg of protein (U/mg protein). One unit of CS activity was defined as the amount of enzyme that produces 1 μmol of citric acid per minute (U/mg protein). OGDH activity was defined as the amount of enzyme that produces 1 nmol of NADH per minute (U/mg protein). Measurements were performed at 595 nm using three replicates for each sample.

Statistical Analysis

All experiments were repeated three times. Mean values and standard deviations were calculated using Excel 2010 (Microsoft Inc., Seattle, WA, USA). Statistical analyses were performed using one-way ANOVA with SPSS Statistics 17.0 (SPSS Inc., Chicago, USA).

RESULTS

Identification of *B. cinerea* Proteins by iTRAQ

A total of 204,639 spectra were generated by iTRAQ proteomic analysis using control and TTO-treated *B. cinerea* and were analyzed using the Mascot search engine. As shown in **Figure 1A**, 17,337 spectra matched known spectra, comprising 10,001 peptides, 9,720 unique peptides, and 2,397 proteins from control and TTO-treated samples. The distribution of the number of peptides, predicted molecular weights, and isoelectric points, and peptide sequence coverage are shown in **Figures 1B–D**, respectively. Over 87% of the proteins were represented by at least two peptides. Molecular weights ranged from 20 to 200 kDa, and isoelectric points ranged from 5.0 and 7.0. Approximately 51% of identified proteins had more than 10% peptide sequence coverage.

Identification of Differentially Expressed Proteins Using iTRAQ

The threshold for differential expression (TTO-treated vs. control) was a protein level difference >1.5 or <0.67 , with a $p < 0.05$. 718 differentially expressed proteins were identified in the TTO sample, of which 17 were up-regulated and 701 were down-regulated. Details for each protein are provided in **Table 1**.

GO Analysis of DEPs

GO analysis was conducted to identify significantly enriched GO functional groups. DEPs were categorized by biological process, cellular component, and molecular function. Of the 718 DEPs, 562 were annotated and classified into 30 functional groups (**Figure 2**). Biological processes accounted for 12 GO terms (with “metabolic process” accounting for 44.11% of these, and “cellular process” 34.32%). Cellular components accounted for 7 GO terms, dominated by “cell” (31.60%) and “cell part” (31.60%). Molecular functions accounted for 11 GO terms, the most abundant being “catalytic” (44.72%) and “binding” (43.61%).

The agriGO analysis tool was used to detect and visualize significantly enriched GO terms associated with the 562 annotated proteins, with an adjusted p -value cutoff of 0.05. Significant functions included “regulation of biological quality” (GO:0065008, $p = 0.033$) and “primary metabolic process” (GO:0044238, $p = 0.016$). There are 5 DEPs, accounting for about 45.45% of the total protein in regulation of biological quality. And 189 DEPs, accounting for about 73.82% of the total protein in primary metabolic process.

KEGG Analysis of DEPs

Proteins typically do not exercise their functions independently, but coordinate with each other to complete a series of biochemical reactions. Pathway analysis can help reveal cellular processes involved in disease mechanisms or drug action. Using the KEGG database as a reference, 562 DEPs were linked to 133 different pathways. Glycolysis, the TCA cycle, and purine metabolism were among the pathways most significantly altered by exposure to TTO.

Confocal Microscopy

Confocal laser scanning microscopy was used to investigate *B. cinerea* cell membrane integrity after TTO treatment. PI easily penetrates a membrane-damaged cell and binds to DNA, resulting in red fluorescence. *B. cinerea* cells were examined by both bright-field microscopy (**Figures 3A,C**) and fluorescence microscopy (**Figures 3B,D**). Control cells have no detectable red fluorescence (**Figure 3B**), indicating that they have intact cell membranes. In contrast, red fluorescence was observed after cells were treated for 2 h with TTO at 5 mL/L (**Figure 3D**). These results suggest that TTO compromises the integrity of the *B. cinerea* cell membrane, potentially causing cell death.

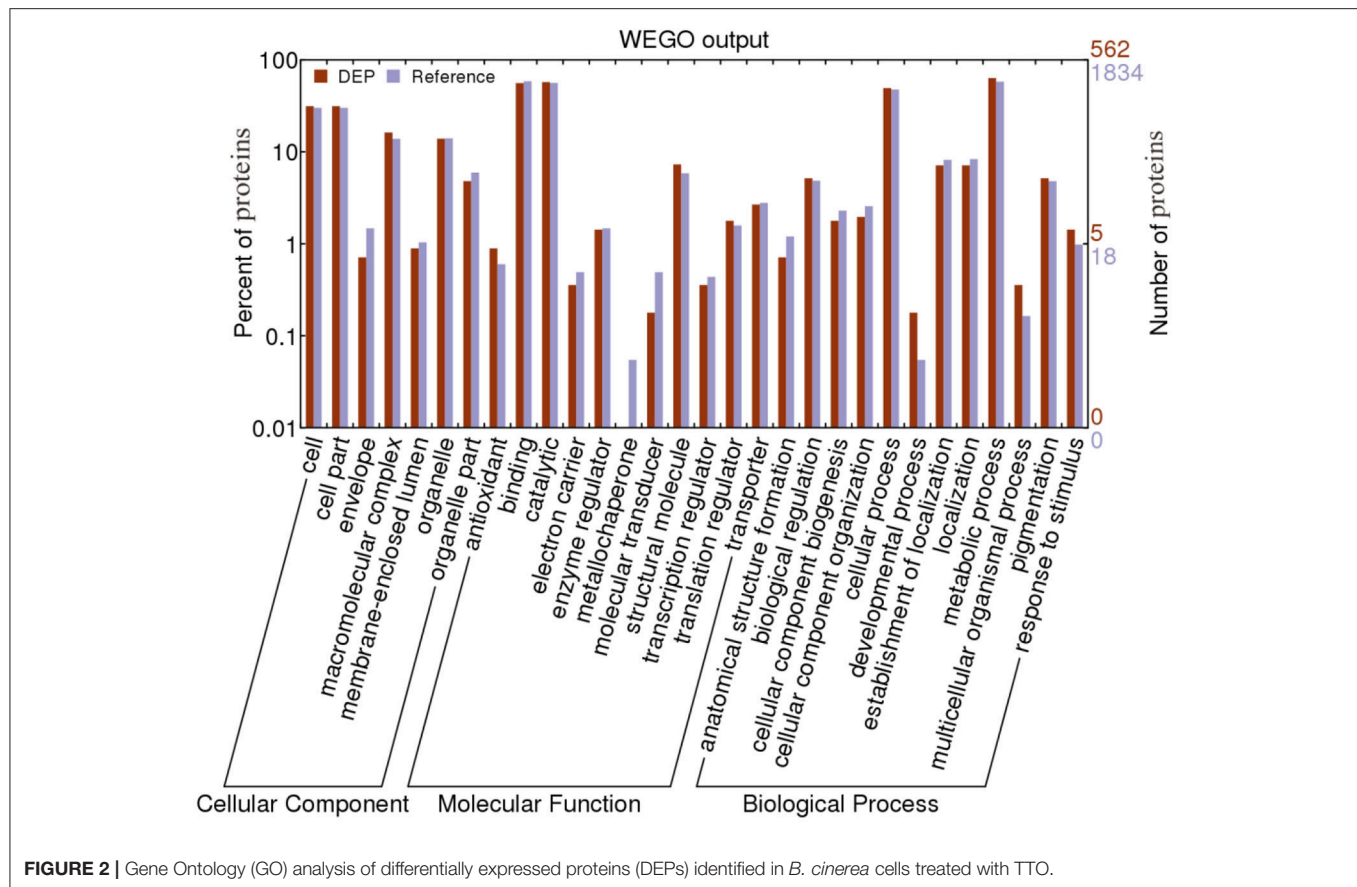
Enzyme Activities Related to TCA Cycle

Because the iTRAQ analysis clearly implicated the TCA cycle as a possible TTO target, we investigated the activities of MDH, CS, and OGDH, three key enzymes related to the TCA cycle (**Figure 4**). The results indicate that activities for these enzymes decreased significantly in TTO-treated cells (87.4, 53.3, and 40.3%, respectively), consistent with our observation that the MDH, CS, and OGDH proteins are significantly down-regulated in TTO-treated cells.

DISCUSSION

The antifungal activity of essential oils is probably based on their ability to significantly reduce total lipid and ergosterol content, thereby disrupting membrane permeability and resulting in leakage of cell components such as ATP, DNA, and potassium ions (Tian et al., 2011; Tao et al., 2014; Cui et al., 2015). Our previous study demonstrated that TTO considerably increases membrane permeability, causing extrusion of abundant material (Shao et al., 2013b; Yu et al., 2015) and decreasing intracellular ATP in *B. cinerea* (Li et al., 2017b). In this study, observations using confocal laser scanning microscopy indicate that TTO damages the *B. cinerea* cell membrane, potentially causing the release of internal material such as ATP.

Levels for many DEPs related to glycolysis metabolism, such as glucose-6-phosphate isomerase, 6-phosphofructokinase, phosphoenolpyruvate carboxykinase, fructose-1, 6-bisphosphatase, and enolase, are decreased by TTO treatment (**Table 1**). Glucose-6-phosphate isomerase catalyzes the conversion of glucose-6-phosphate into fructose 6-phosphate

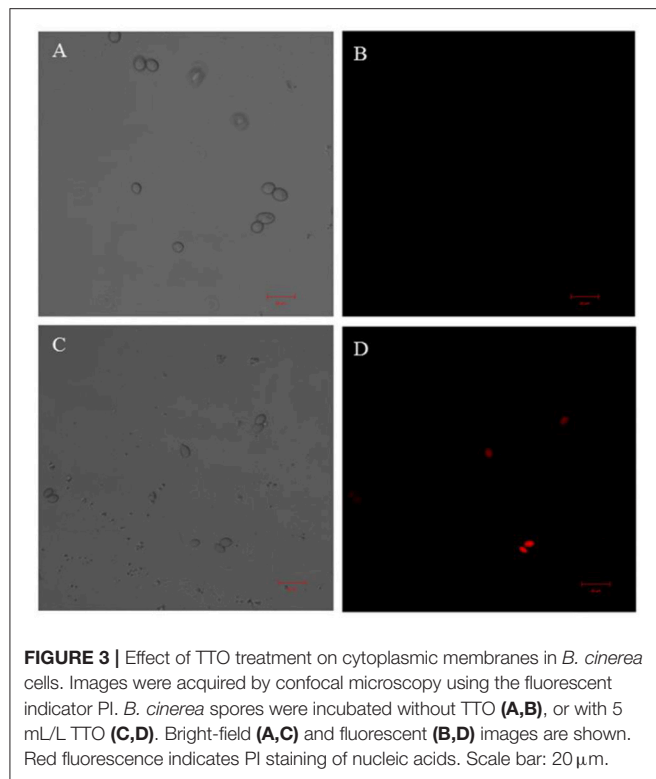


in the second step of glycolysis (Achari et al., 1981). 6-phosphofructokinase is a key enzyme in the control of the glycolytic pathway in nearly all cells (Wang et al., 2016). The activity of this enzyme is controlled by several metabolites, most notably its two substrates, fructose 6-phosphate and ATP. Glycolysis is also an important pathway for energy production in the cytosol of plant cells. Our results suggest that TTO inhibits glycolysis and may affect energy supply in *B. cinerea*.

Mitochondria are the primary sites of aerobic respiration in eukaryotic cells. They generate energy for cellular functions through oxidative phosphorylation and the TCA cycle, and also play a crucial role in regulating the apoptosis (Shaughnessy et al., 2014). In this study, several proteins associated with the mitochondrial respiratory chain and TCA cycle, such as ATP synthase D chain, ATP synthase subunit e, MDH, CS, and OGDH, were significantly down-regulated in cells treated with TTO (Table 1). ATP synthase D chain and ATP synthase subunit e are involved in the biosynthesis of ATP. Dill oil inhibits mitochondrial ATPase activity and dehydrogenase activities, and affects mitochondrial function in *Aspergillus flavus* (Tian et al., 2012). Mustard essential oils decrease intracellular ATP and increase extracellular ATP in *E. coli* O157:H7 and *Salmonella typhi* (Turgis et al., 2009). Citral decreases intracellular ATP content, increases extracellular ATP content, inhibits the TCA pathway, and decreases the activities of

CS and α -ketoglutarate dehydrogenase in *Penicillium digitatum* (Zheng et al., 2015). Our additional study demonstrates that TTO treatment significantly inhibits the activities of MDH, CS, and OGDH (Figure 4). In our previous study, we found that TTO decreases intracellular ATP and the activities of MDH, succinate dehydrogenase, ATPase, CS, isocitrate dehydrogenase, and α -ketoglutarate dehydrogenase, disrupting the TCA cycle in *B. cinerea* (Li et al., 2017b). The down-regulation of two MDHs suggests that the Krebs cycle is not completely functional in *Paracoccidioides lutzii* upon exposure to argentinolactone (Prado et al., 2014). Together, these results imply that TTO affects proteins in *B. cinerea* involved in glycolysis, the TCA cycle, and ATP synthesis, thereby disrupting the TCA cycle, interrupting energy metabolism, and inducing mitochondrial dysfunction.

Cytochrome c (cyt c) is a hemoglobin located in the inner mitochondrial membrane, and is responsible for transferring electrons between mitochondrial electron transport chain complexes III and IV (Reed, 1997; Lo et al., 2017). ATP is produced by the aerobic mitochondrial respiratory chain. Abnormal cyt c disrupts the mitochondrial respiratory chain and impacts ATP production (Zhou et al., 2015). Our study shows that cyt c is up-regulated in *B. cinerea* after TTO treatment at 5 mL/L (Table 1). The increase in cyt c levels may improve the performance of the oxidative

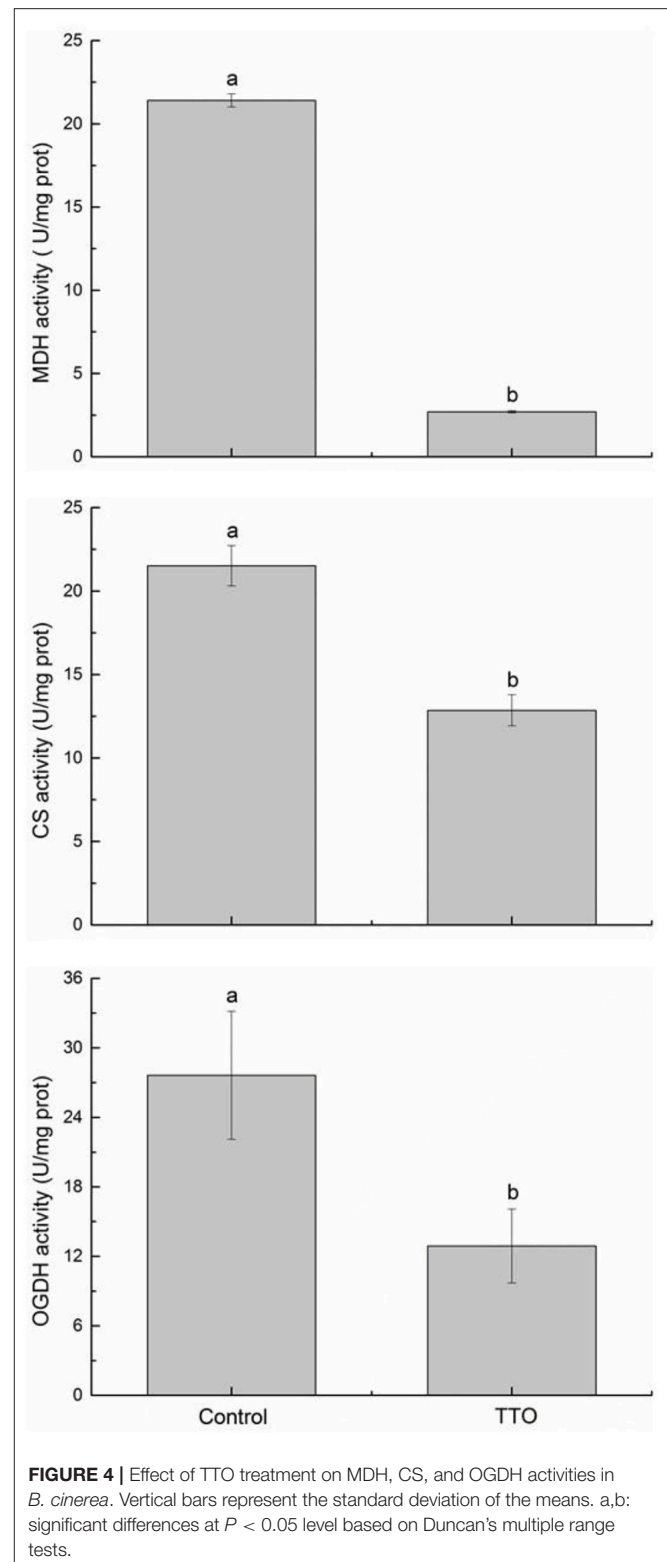


respiratory chain, perhaps as a protective response to TTO toxicity.

Purines are one of the building blocks for nucleic acids. Their synthesis pathways generate many kinds of energy molecules (Qian et al., 2014). Inosine 5'-monophosphate dehydrogenase (IMPDH) is a rate-controlling enzyme in the *de novo* synthesis of the guanine nucleotide, and plays crucial roles in cell growth and proliferation (Fotie, 2016). IMPDH inhibition reduces guanine nucleotide pools and interrupts cellular functions such as DNA replication, RNA synthesis, and signal transduction (Weber, 1983; Weber et al., 1996). These effects are associated with cell cycle disruption, cellular differentiation, and apoptosis (Vitale et al., 1997; Yalowitz and Jayaram, 2000). Nucleoside diphosphate kinases (NDPK) are critical enzymes related to the maintenance of intracellular nucleotide levels, and catalyze the conversion of nucleoside triphosphates to nucleoside diphosphates in all living organisms (Véron et al., 1994). Both NDPK and AK can mediate the conversion of adenosine into ATP by ADP and AMP (Senft and Crabtree, 1983). In our study, TTO treatment decreased IMPDH levels (**Table 1**). Furthermore, levels of adenosine kinase AK and NDPK were also reduced after TTO treatment (**Table 1**). From these results, we can conclude that TTO may block the accumulation of energy and disrupt the cell cycle, ultimately inducing apoptosis.

CONCLUSION

The effect of TTO treatment on proteins in *B. cinerea* is summarized in **Figure 5**. We found that important metabolic



pathways, including glycolysis, the TCA cycle, and purine metabolism, were compromised by TTO treatment, while cyt c increased. We conclude that the disruption of energy

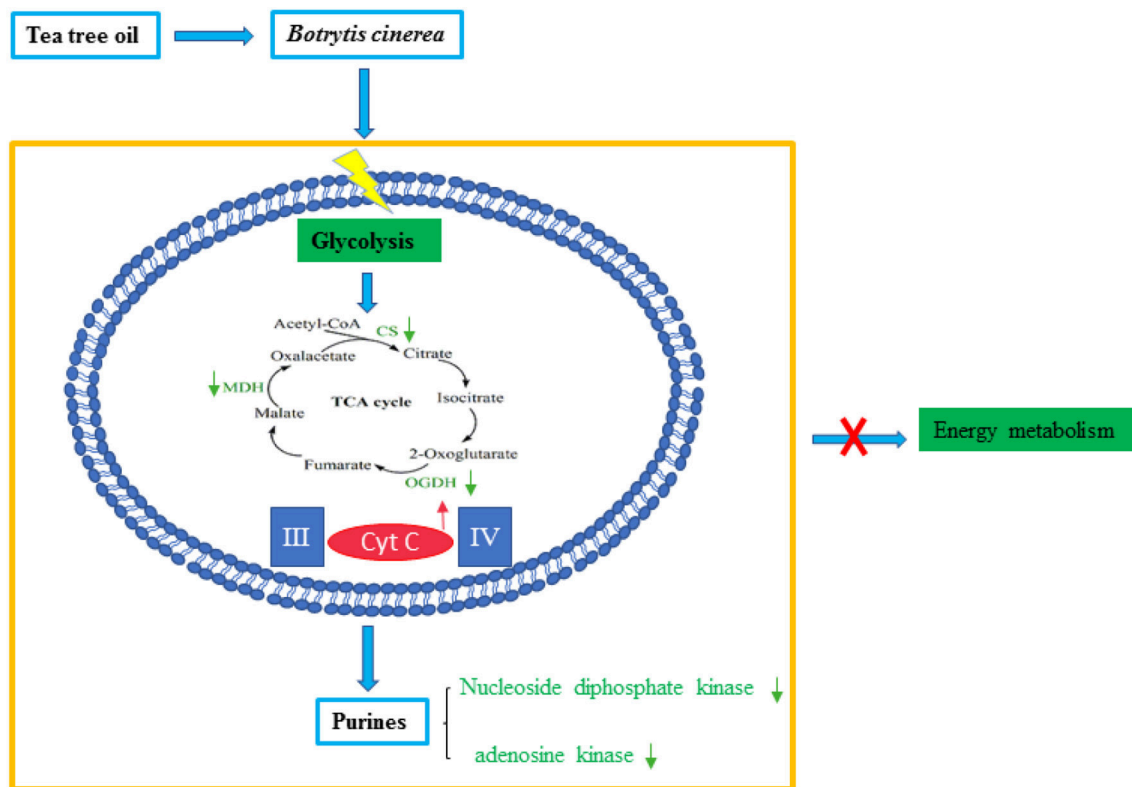


FIGURE 5 | Model summarizing antifungal effects of TTO in *B. cinerea*. Green arrows indicate down-regulation and red arrows indicate up-regulation.

metabolism by TTO contributes to its antifungal activity against *B. cinerea*.

AUTHOR CONTRIBUTIONS

JX and XS designed the experiments. JX and YW performed the experiments. FX and HW analyzed the data. JX, XS, and HW drafted the manuscript. All authors read and approved the final manuscript.

REFERENCES

- Abdulazeez, M. A., Abdullahi, A. S., and James, B. D. (2016). "Chapter 58 – Lemongrass (*Cymbopogon* spp.) Oils," in *Essential Oils in Food Preservation Flavor and Safet* (London, UK: Academic Press Books-Elsevier), 509–516.
- Achari, A., Marshall, S. E., Muirhead, H., Palmieri, R. H., and Noltmann, E. A. (1981). Glucose-6-phosphate isomerase. *Philos. Trans. R. Soc. London*. 293, 145–157. doi: 10.1098/rstb.1981.0068
- Ashburner, M., Ball, C. A., Blake, J. A., Botstein, D., Butler, H., Cherry, J. M., et al. (2000). Gene Ontology: tool for the unification of biology. *Nat. Genet.* 25, 25–29. doi: 10.1038/75556
- Bona, E., Cantamessa, S., Pavan, M., Novello, G., Massa, N., Rocchetti, A., et al. (2016). Sensitivity of *Candida albicans* to essential oils: are they an alternative to antifungal agents? *J. Appl. Microbiol.* 121, 1530–1545. doi: 10.1111/jam.13282
- Bradford, M. (1976). A rapid and sensitive method for the quantitation of microgram quantities of protein utilizing the principle of protein–dye binding. *Anal. Biochem.* 6, 3171–3188. doi: 10.1016/0003-2697(76)90527-3

ACKNOWLEDGMENTS

This study was funded by the National Science Foundation of China (No. 31371860), the Public Welfare Applied Research Project of Zhejiang Province (No. 2017C32010), the Science and Technology Program of Ningbo City (2017C10065), the School Research Project (XYL17014), and the K.C. Wong Magna Fund in Ningbo University.

- Brul, S., and Coote, P. (1999). Preservative agents in foods: mode of action and microbial resistance mechanisms. *Int. J. Food Microbiol.* 50, 1–17. doi: 10.1016/S0168-1605(99)00072-0
- Carson, C. F., Hammer, K. A., and Riley, T. V. (2006). *Melaleuca alternifolia* (Tea Tree) oil: a review of antimicrobial and other medicinal properties. *Clin. Microbiol. Rev.* 19, 50–62. doi: 10.1128/CMR.19.1.50-62.2006
- Cho, Y. S., and Oh, K. H. (2011). Cellular and proteomic responses of *Escherichia coli* JK-17 exposed to the Rosa hybrida flower extract. *Biotechnol. Bioprocess Eng.* 16, 885–893. doi: 10.1007/s12257-011-0051-5
- Cui, H., Zhang, X., Zhou, H., Zhao, C., and Lin, L. (2015). Antimicrobial activity and mechanisms of *Salvia sclarea* essential oil. *Bot. Stud.* 56, 16. doi: 10.1186/s40529-015-0096-4
- Fotie, J. (2016). Inosine 5'-Monophosphate Dehydrogenase (IMPDH) as a potential target for the development of a new generation of antiprotozoan agents. *Mini Rev. Med. Chem.* doi: 10.2174/1389557516666160620065558. [Epub ahead of print].

- Franco, C., Soares, R., Pires, E., Koci, K., Almeida, A. M., Santos, R., et al. (2013). Understanding regeneration through proteomics. *Proteomics* 13, 686–709. doi: 10.1002/pmic.201200397
- Fraternal, D., Flamini, G., and Ricci, D. (2014). Essential oil composition of *Angelica archangelica* L. (Apiaceae) roots and its antifungal activity against plant pathogenic fungi. *Plant Biosyst.* 150, 558–563. doi: 10.1080/11263504.2014.988190
- Gustafson, J., Liew, Y., Chew, S., Markham, J., Bell, H., Wyllie, S., et al. (1998). Effects of tea tree oil on *Escherichia coli*. *Lett. Appl. Microbiol.* 26, 194–198. doi: 10.1046/j.1472-765X.1998.00317.x
- Homer, L. E., Leach, D. N., Lea, D., Lee, L. S., Henry, R. J., and Baverstock, P. R. (2000). Natural variation in the essential oil content of *Melaleuca alternifolia* Cheel (Myrtaceae). *Biochem. Syst. Ecol.* 28, 367–382. doi: 10.1016/S0305-1978(99)00071-X
- Kovács, J. K., Felso, P., Makszin, L., Pápai, Z., Horváth, G. Á. H., et al. (2016). Antimicrobial and virulence modulating effect of clove essential oil on the food-borne pathogen *Campylobacter jejuni*. *Appl. Environ. Microbiol.* 82, 6158–6166. doi: 10.1128/AEM.01221-16
- Lee, H. S., and Kim, Y. (2017). *Paeonia lactiflora* inhibits cell wall synthesis and triggers membrane depolarization in *Candida albicans*. *J. Microbiol. Biotechnol.* 27, 395–404. doi: 10.4014/jmb.1611.11064
- Leroux, P., Fritz, R., Debieu, D., Albertini, C., Lanen, C., Bach, J., et al. (2002). Mechanisms of resistance to fungicides in field strains of *Botrytis cinerea*. *Pest Manag. Sci.* 58, 876–888. doi: 10.1002/ps.566
- Li, Y., Shao, X., Xu, J., Wei, Y., Xu, F., and Wang, H. (2017a). Effects and possible mechanism of tea tree oil against *Botrytis cinerea* and *Penicillium expansum* *in vitro* and *in vivo* test. *Can. J. Microbiol.* 63, 219–227. doi: 10.1139/cjm-2016-0553
- Li, Y., Shao, X., Xu, J., Wei, Y., Xu, F., and Wang, H. (2017b). Tea tree oil exhibits antifungal activity against *Botrytis cinerea* by affecting mitochondria. *Food Chem.* 234, 62–67. doi: 10.1016/j.foodchem.2017.04.172
- Liu, S., Shao, X., Wei, Y., Li, Y., Xu, F., and Wang, H. (2016). *Solidago canadensis* L. essential oil vapor effectively inhibits *Botrytis cinerea* growth and preserves postharvest quality of strawberry as a food model system. *Front. Microbiol.* 7:1179. doi: 10.3389/fmicb.2016.01179
- Lo, Y. T., Huang, H., W., Huang, Y. C., Chan, J. F., and Hsu, Y. H. (2017). Elucidation of tRNA-cytochrome c interactions through hydrogen/deuterium exchange mass spectrometry. *BBA Proteins Proteom.* 1865, 539–546. doi: 10.1016/j.bbapap.2017.02.015
- Miao, L., Zhu, L., Liu, B., Du, L., Jia, X., Li, H., et al. (2016). Tea tree oil nanoemulsions for inhalation therapies of bacterial and fungal pneumonia. *Colloids. Surface. B. Biointerfaces* 141, 408–416. doi: 10.1016/j.colsurfb.2016.02.017
- Prado, R. S., Bailão, A., M., Silva, L. C., Oliveira, C. M. A. D., and Marques, M. F., Silva, L. P., et al. (2014). Proteomic profile response of *Paracoccidioides lutzii* to the antifungal argentilactone. *Front. Microbiol.* 6:616. doi: 10.3389/fmicb.2015.00616
- Prakash, B., Singh, P., Kedia, A., and Dubey, N. K. (2012). Assessment of some essential oils as food preservatives based on antifungal, antiaflatoxin, antioxidant activities and *in vivo* efficacy in food system. *Food Res. Int.* 49, 201–208. doi: 10.1016/j.foodres.2012.08.020
- Qian, Z., Liu, Z. L., Kang, N., Wang, A., Zeng, X., and Jian, X. (2014). Genomic and transcriptome analyses reveal that MAPK- and phosphatidylinositol-signaling pathways mediate tolerance to 5-hydroxymethyl-2-furaldehyde for industrial yeast *Saccharomyces cerevisiae*. *Sci. Rep.* 4:6556. doi: 10.1038/srep06556
- Reed, J. C. (1997). Cytochrome c: can't live with it—can't live without it. *Cell* 91, 559–562. doi: 10.1016/S0092-8674(00)80442-0
- Senft, A. W., and Crabtree, G. W. (1983). Purine metabolism in the schistosomes: potential targets for chemotherapy. *Pharmacol. Ther.* 20, 341–356. doi: 10.1016/0163-7258(83)90031-1
- Shao, X., Cheng, S., Wang, H., Yu, D., and Mungai, C. (2013b). The possible mechanism of antifungal action of tea tree oil on *Botrytis cinerea*. *J. Appl. Microbiol.* 114, 1642–1649. doi: 10.1111/jam.12193
- Shao, X., Wang, H., Xu, F., and Cheng, S. (2013a). Effects and possible mechanisms of tea tree oil vapor treatment on the main disease in postharvest strawberry fruit. *Postharvest Biol. Tec.* 77, 94–101. doi: 10.1016/j.postharvbio.2012.11.010
- Shaughnessy, D. T., McAllister, K., Worth, L., Haugen, A. C., Meyer, J. N., Domann, F. E., et al. (2014). Mitochondria, energetics, epigenetics, and cellular responses to stress. *Environ. Health Perspect.* 122, 1271–1278. doi: 10.1289/ehp.1408418
- Soylu, E. M., Kurt, S., and Soyly, S. (2010). *In vitro* and *in vivo* antifungal activities of the essential oils of various plants against tomato grey mould disease agent *Botrytis cinerea*. *Int. J. Food Microbiol.* 143, 183–189. doi: 10.1016/j.ijfoodmicro.2010.08.015
- Tao, N., OuYang, Q., and Jia, L. (2014). Citral inhibits mycelial growth of *Penicillium italicum* by a membrane damage mechanism. *Food Control* 41, 116–121. doi: 10.1016/j.foodcont.2014.01.010
- Tian, J., Ban, X., Zeng, H., He, J., Chen, Y., and Wang, Y. (2012). The mechanism of antifungal action of essential oil from dill (*Anethum graveolens* L.) on *Aspergillus flavus*. *PLoS ONE* 7:e30147. doi: 10.1371/journal.pone.0030147
- Tian, J., Ban, X., Zeng, H., Huang, B., He, J., and Wang, Y. (2011). *In vitro* and *in vivo* activity of essential oil from dill (*Anethum graveolens* L.) against fungal spoilage of cherry tomatoes. *Food Control* 22, 1992–1999. doi: 10.1016/j.foodcont.2011.05.018
- Turgis, M., Han, J. J., Cailliet, S., and Lacroix, M. (2009). Antimicrobial activity of mustard essential oil against *Escherichia coli* O157:H7 and *Salmonella typhi*. *Food Control* 20, 1073–1079. doi: 10.1016/j.foodcont.2009.02.001
- Véron, M., Tepper, A., Hildebrandt, M., Lascu, I., Lacombe, M. L., Janin, J., et al. (1994). Nucleoside diphosphate kinase: an old enzyme with new functions? *Adv. Exp. Med. Biol.* 370, 607–611. doi: 10.1007/978-1-4615-2584-4_126
- Vitale, M., Zama, L., Falcieri, E., Zauli, G., Gobbi, P., Santi, S., et al. (1997). IMP dehydrogenase inhibitor, tiagofurin, induces apoptosis in K562 human erythroleukemia cells. *Cytometry* 30, 61–66. doi: 10.1002/(SICI)1097-0320(19970215)30:1<61::AID-CYTO9>3.0.CO;2-I
- Wang, J., Zhang, P., Zhong, J., Tan, M., Ge, J., Tao, L., et al. (2016). The platelet isoform of phosphofructokinase contributes to metabolic reprogramming and maintains cell proliferation in clear cell renal cell carcinoma. *Oncotarget* 7, 27142–27157. doi: 10.18632/oncotarget.8382
- Weber, G. (1983). Enzymes of purine metabolism in cancer. *Clin. Biochem.* 16, 57–63. doi: 10.1016/S0009-9120(83)94432-6
- Weber, G., Prajda, N., Yang, H., Yeh, Y. A., Shen, F., Singhal, R. L., et al. (1996). Current issues in the regulation of signal transduction. *Adv. Enzyme Regul.* 36, 33–55. doi: 10.1016/0065-2571(96)00003-9
- Xu, J., Shao, X., Li, Y., Wei, Y., Xu, F., and Wang, H. (2017). Metabolomic analysis and mode of action of metabolites of tea tree oil involved in the suppression of *Botrytis cinerea*. *Front. Microbiol.* 8:1017. doi: 10.3389/fmicb.2017.01017
- Yalowitz, J. A., and Jayaram, H. N. (2000). Molecular targets of guanine nucleotides in differentiation, proliferation and apoptosis. *Anticancer Res.* 20, 2329–2338.
- Yu, D., Wang, J., Shao, X., Xu, F., and Wang, H. (2015). Antifungal modes of action of tea tree oil and its two characteristic components against *Botrytis cinerea*. *J. Appl. Microbiol.* 119, 1253–1262. doi: 10.1111/jam.12939
- Zheng, S., Jing, G., Wang, X., Ouyang, Q., Jia, L., and Tao, N. (2015). Citral exerts its antifungal activity against *Penicillium digitatum* by affecting the mitochondrial morphology and function. *Food Chem.* 178, 76–81. doi: 10.1016/j.foodchem.2015.01.077
- Zhou, M., Li, Y., Hu, Q., Bai, X. C., Huang, W., Yan, C., et al. (2015). Atomic structure of the apoptosome: mechanism of cytochrome c- and dATP-mediated activation of Apaf-1. *Genes Dev.* 29, 2349–2361. doi: 10.1101/gad.272278.115
- Zhou, Y., and Chen, W. N. (2011). iTRAQ-coupled 2-D LC-MS/MS analysis of membrane protein profile in *Escherichia coli* incubated with apidaecin IB. *PLoS ONE* 7:e20442. doi: 10.1371/journal.pone.0020442

Conflict of Interest Statement: The authors declare that the research was conducted in the absence of any commercial or financial relationships that could be construed as a potential conflict of interest.

Copyright © 2017 Xu, Shao, Wei, Xu and Wang. This is an open-access article distributed under the terms of the Creative Commons Attribution License (CC BY). The use, distribution or reproduction in other forums is permitted, provided the original author(s) or licensor are credited and that the original publication in this journal is cited, in accordance with accepted academic practice. No use, distribution or reproduction is permitted which does not comply with these terms.



Application of Proteomics for the Investigation of the Effect of Initial pH on Pathogenic Mechanisms of *Fusarium proliferatum* on Banana Fruit

Taotao Li^{1,2}, Qixian Wu^{1,2}, Yong Wang³, Afiya John^{1,2}, Hongxia Qu¹, Liang Gong¹, Xuewu Duan¹, Hong Zhu¹, Ze Yun^{1*} and Yueming Jiang¹

¹ Key Laboratory of Plant Resource Conservation and Sustainable Utilization, South China Botanical Garden, Chinese Academy of Sciences, Guangzhou, China, ² College of Life Science, University of Chinese Academy of Sciences, Beijing, China, ³ Zhong Shan Entry-Exit Inspection and Quarantine Bureau, Zhong Shan, China

OPEN ACCESS

Edited by:

Nengguo Tao,
Xiangtan University, China

Reviewed by:

Xingfeng Shao,
Ningbo University, China
Qingping Zhong,
South China Agricultural University,
China

*Correspondence:

Ze Yun
yunze@scbg.ac.cn

Specialty section:

This article was submitted to
Food Microbiology,
a section of the journal
Frontiers in Microbiology

Received: 22 August 2017

Accepted: 13 November 2017

Published: 29 November 2017

Citation:

Li T, Wu Q, Wang Y, John A, Qu H,
Gong L, Duan X, Zhu H, Yun Z and
Jiang Y (2017) Application of
Proteomics for the Investigation of the
Effect of Initial pH on Pathogenic
Mechanisms of *Fusarium proliferatum*
on Banana Fruit.
Front. Microbiol. 8:2327.
doi: 10.3389/fmicb.2017.02327

Fusarium proliferatum is an important pathogen and causes a great economic loss to fruit industry. Environmental pH-value plays a regulatory role in fungi pathogenicity, however, the mechanism needs further exploration. In this study, *F. proliferatum* was cultured under two initial pH conditions of 5 and 10. No obvious difference was observed in the growth rate of *F. proliferatum* between two pH-values. *F. proliferatum* cultured under both pH conditions infected banana fruit successfully, and smaller lesion diameter was presented on banana fruit inoculated with pH 10-cultured fungi. Proteomic approach based on two-dimensional electrophoresis (2-DE) was used to investigate the changes in secretome of this fungus between pH 5 and 10. A total of 39 differential spots were identified using matrix-assisted laser desorption/ionization tandem time-of-flight mass spectrometry (MALDI-TOF/TOF-MS) and liquid chromatography electrospray ionization tandem mass spectrometry (LC-ESI-MS/MS). Compared to pH 5 condition, proteins related to cell wall degrading enzymes (CWDEs) and proteolysis were significantly down-regulated at pH 10, while proteins related to oxidation-reduction process and transport were significantly up-regulated under pH 10 condition. Our results suggested that the downregulation of CWDEs and other virulence proteins in the pH 10-cultured *F. proliferatum* severely decreased its pathogenicity, compared to pH 5-cultured fungi. However, the alkaline environment did not cause a complete loss of the pathogenic ability of *F. proliferatum*, probably due to the upregulation of the oxidation-reduction related proteins at pH 10, which may partially compensate its pathogenic ability.

Keywords: environmental pH-value, *Fusarium proliferatum*, secretome, cell wall degrading enzymes, oxidation-reduction process

INTRODUCTION

Fusarium proliferatum is a polyphagous fungus with a broad host range and is often isolated from several agriculturally important crops, including wheat (Palacios et al., 2015), banana (Li et al., 2012), citrus (Amby et al., 2015), etc. Various mycotoxins produced by *F. proliferatum* are harmful to human and animal health. Therefore, controlling its infection is important for food safety.

Ambient pH is an important environmental factor, which could influence the survival, proliferation, and pathogenicity of microorganism. Weak alkaline environment can significantly inhibit the growth of fungi and their infection to plants (Prusky and Yakoby, 2003). Meanwhile, the ambient pH has the critical role in determining the transcriptional levels of many genes, affecting growth, physiology, and differentiation processes (Lamb et al., 2001). Pathogens also boost some proteins to resist harsh environment and increase adaptability (Bi et al., 2016). Numerous researches were conducted to investigate the pH signal transduction and relationship between the pH regulation and fungal pathogenicity (Penalva et al., 2008). Transcription factor *PacC* appears to be necessary for the appropriate regulation of physiological processes *Sclerotinia sclerotiorum* (Rollins, 2003). *Pac1* is reported to regulate *Tri* gene expression and trichothecene production in *Fusarium graminearum* (Merhej et al., 2011). However, the regulatory mechanism is still not clearly understood, and little information was available on the effect of pH on the secretome of *Fusarium*.

Some pathogenic microorganisms usually secret proteins to facilitate their infection and host colonization (Zhang et al., 2014). Fruit pathogens can contribute to the acidification or alkalization of the host environment, and the capability has been used to divide fungal pathogens into acidifying and/or alkalizing classes (Bi et al., 2016). To comprehensively unravel how pathogens manipulate the infection process, the investigation of secretome changes under different ambient pH conditions will be useful to explore the pathogenic mechanism of fungal pathogens. The secreted pathogenicity factors are well known for their ability to help the pathogen successfully colonize and invade the targeted host (Zong et al., 2015). In recent years, proteomic approach has been widely used to explore the secretome change and infection mechanism of several fungal pathogens (Li et al., 2012; Meijer et al., 2014; Lakshman et al., 2016). Additionally, proteomics analyses were used to comprehensively characterize infection-specific protein expression pattern of early defense-related signaling in *Medicago truncatula* (Trapphoff et al., 2009). However, little information is available for *F. proliferatum*, especially for the secretome. Therefore, understanding secretomics can provide vital information for advances in the identification of extracellular proteins with a potential role in pathogenicity of *F. proliferatum*.

In previous research of our lab, we investigated the effect of different initial pH values (ranging from 3 to 10) on the growth of *F. proliferatum*, and the results showed that pH 5 and 10 had no influence on the growth but affected fusic acid (FA) production (Li et al., 2012). Additionally, our previous research also showed that the initial pH 5 and 10 showed no significant effect on the growth rate of *F. proliferatum* (Li et al., 2017). Based on these results, the effect of pH 5 and 10 on the pathogenic ability of *F. proliferatum* needs further analysis, especially at secreted proteins. In the present study, the effect of initial pH values on the growth of *F. proliferatum* was further verified on PDA plate culture media, and inoculation experiment on banana fruit was performed to verify the effect of these two pH values on the pathogenicity of *F. proliferatum*. Additionally,

the secretome change was comparatively analyzed at pH 5 and 10, using a gel based proteomic approach. The objective of this study was to investigate the molecular mechanism of different starting environmental pH values in regulating the pathogenicity of *F. proliferatum*. This study will be helpful in providing insightful knowledge of the pathogenic mechanism of *F. proliferatum*, which will also facilitate the development of new antifungals/fungicides.

MATERIALS AND METHODS

Fungal Strains and Growth Conditions

Fusarium proliferatum was isolated from carambola and then stored in 50% glycerol at -80°C . *Fusarium proliferatum* was grown for 7 days at 28°C on PDA (Oxoid, Basingstoke, Hampshire, England) plates. Then six small plates (5 mm) was cut and transferred to Czapek's broth medium (CB) modified with NaOH or HCl to maintain their starting pH with the range of 5.0 ± 0.2 and 10.0 ± 0.2 , respectively. The pH value was measured by Ultrabasic pH Meters, UB-7 (Denver Instrument, Arvada, USA). The conical flask containing 150 mL above cultures was incubated at 28°C for 10 days in an orbital shaker (200 rpm). Mycelium and medium were separated by filtering with a vacuum pump. Three independent biological replicates were conducted.

Ripe Banana Inoculation with *F. proliferatum*

Yellow ripe banana (*Musa acuminata* L. AAA group, cv. Brazilian) fruit were bought from a commercial orchard in Guangzhou, China. Fruit fingers with uniform shape, color, and size were selected for further experiment. The culture of *F. proliferatum* under different initial pH conditions was filtered using two layers of gauze, and the spore solution was diluted to 1×10^6 spores/mL. Fruit fingers were washed by sterile water, then wounded with a nail (1 mm wide, 2 mm deep) and inoculated with 15 μL aqueous conidia suspension. The inoculated fruits were stored at 22°C and 85% relative humidity for 3 days. Three biological replicates with 12 fruit fingers for each were conducted.

Secreted Protein Isolation, Two-Dimensional Gel Electrophoresis, in-Gel Digestion, Mass Spectrometry (MS), and Database Searching

Fusarium proliferatum was cultured in CB and used for secreted proteins extraction. After removing the residual mycelia and other debris from the media by filtrating, the secreted proteins were isolated from the filtrate according to the methods described by Li et al. (2016). The protein concentration was measured using the Bio-Rad protein assay kit (Bio-Rad, USA). Two-dimensional electrophoresis (2-DE) was performed using 2 mg of protein sample to rehydrate gel strips (IPG strip, pH 4–7, 17 cm; Bio-Rad, USA). After stained with Coomassie Brilliant Blue R-250, PDQuest™ Version 8.0.1 (Bio-Rad) was used to analyze the gel images. At least three independent biological replicate gels were run. Spots with more than a three-fold differential accumulation

in three independent gels ($p < 0.05$) were excised and then used for protein identification.

In-gel tryptic digestion and MALDI-TOF/TOF analysis were performed according to mature research method (Li et al., 2015). Mascot software 2.3.02 (Matrix Science, London, UK) was used for database sequence searches against UniProt_Fusarium database (<http://www.uniprot.org/uniprot/?query=fusarium&offset=50&sort=score&columns=id%2centry+name%2creviewed%2cprotein+names%2cgenes%2corganism%2clength>) with 292990 sequences. Protein candidates provided by the combined PMF and MS/MS search were considered as valid when the global Mascot score was greater than Significance Score (58) with a significance level of e -value < 0.05 . For LC-ESI-MS/MS analysis, the method described by Li et al. (2016) was carried out. The same software and database described above were used for protein identification. To reduce the probability of false peptide identification, peptides with ion scores greater than “identity” score were counted as identified. Each reliably identified protein contained at least one unique peptide.

Prediction of Extracellular Location of Identified Proteins

Classical secreted proteins were identified by SignalP 4.0 (<http://www.cbs.dtu.dk/services/SignalP/>) and non-classical protein secretion was analyzed by SecretomeP 1.0b (<http://www.cbs.dtu.dk/services/SecretomeP/>).

Quantitative Real-Time PCR Validation

The mycelia of *F. proliferatum* cultured under different pH values for 10 days was used for RNA extraction. The total RNA extraction and qRT-PCR were conducted according to our previous methods (Li et al., 2017). The specific primers used for qRT-PCR analysis were shown in Supplementary Table S1. Three independent biological replicates were conducted.

RESULTS

Infection Ability of *F. proliferatum* under Acidic or Alkaline Environment

To verify the effect of pH value on the fungus growth rate, *F. proliferatum* was cultured on PDA plates under pH 10 for 10 days; pH 5 set as control. No significant difference of growth rate was shown in the two different pH values (Figure 1). After inoculated to the ripen banana peel, a smaller lesion diameter was found on the ripe banana peel inoculated with pH 10-cultured *F. proliferatum* than that with pH 5 (Figure 2). It seemed that weak alkaline environment decreased the pathogenicity slightly, small difference between pH 10 and pH 5 was observed in the pathogenicity of *F. proliferatum*.

2-DE and Protein Identification

Two milligrams of total proteins were separated using 2-DE, and more than 600 protein spots were detected in each gel (Figure 3). After comparative analysis, protein spots showing statistically significant ($p < 0.05$) changes and more than three-fold in relative abundance between pH 5 and 10 were selected for identification. Due to the lack of *F. proliferatum* genome information, only 17 protein spots were successfully identified

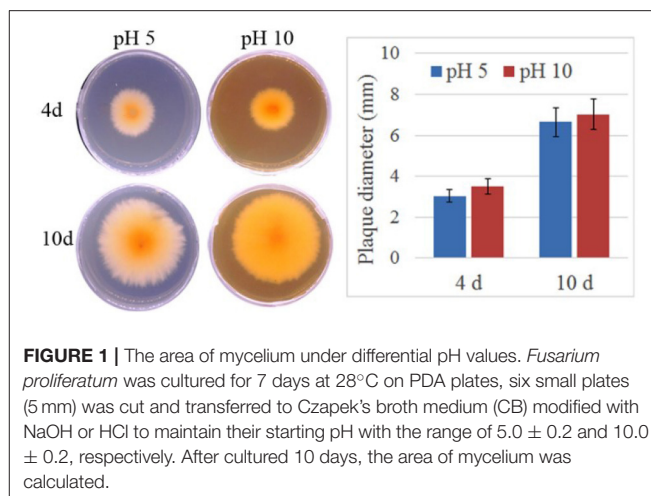


FIGURE 1 | The area of mycelium under differential pH values. *Fusarium proliferatum* was cultured for 7 days at 28°C on PDA plates, six small plates (5 mm) was cut and transferred to Czapek's broth medium (CB) modified with NaOH or HCl to maintain their starting pH with the range of 5.0 ± 0.2 and 10.0 ± 0.2 , respectively. After cultured 10 days, the area of mycelium was calculated.

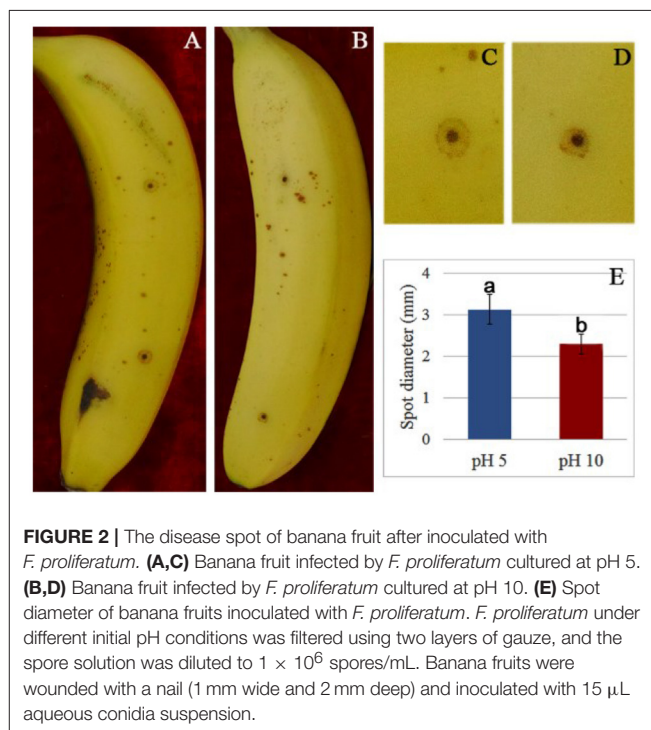
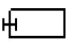

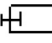
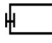
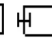
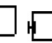
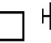
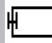
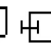
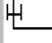
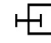
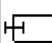


FIGURE 2 | The disease spot of banana fruit after inoculated with *F. proliferatum*. (A,C) Banana fruit infected by *F. proliferatum* cultured at pH 5. (B,D) Banana fruit infected by *F. proliferatum* cultured at pH 10. (E) Spot diameter of banana fruits inoculated with *F. proliferatum*. *F. proliferatum* under different initial pH conditions was filtered using two layers of gauze, and the spore solution was diluted to 1×10^6 spores/mL. Banana fruits were wounded with a nail (1 mm wide and 2 mm deep) and inoculated with 15 μ L aqueous conidia suspension.

by means of matrix-assisted laser desorption/ionization-time of flight mass spectrometry (MALDI-TOF MS). The unidentified protein spots were then analyzed using liquid chromatography-electronic spray ionization-tandem mass spectrometry (LC-ESI-MS/MS), 22 of them were successfully identified via searching NCBI nr database (Figure 3).

Compared to pH 5, 17 proteins were up-regulated at pH 10 (Table 1), and 22 protein spots were down-regulated (Table 2). The up-regulated proteins were also classified into five clusters using Blast2GO base on biological process, including carbohydrate metabolism (2 spots), oxidation-reduction process (7 spots), transport (3 spots), regulation of biological process (2 spots), and unknown function (3 spots) (Figure 4A, Table 1). Meanwhile, the down-regulated proteins were categorized into

TABLE 1 | Up-regulated secretory proteins in *F. proliferatum* under alkaline environment.

Sample name	SignalP	Changefold	Protein ID	Protein description	Theo Mr/PI	2D Mr/PI	Protein score
OXIDATION-REDUCTION PROCESS (7)							
SP1	P		tr S0E3Q1 S0E3Q1_GIBF5	Related to thioredoxin reductase	34.39/5.9	21.55/4.46	104.22
SP2	P		tr S0E3Q1 S0E3Q1_GIBF5	Related to thioredoxin reductase	34.39/5.9	20.62/6.41	50.34
SP3	P		tr S0EF18 S0EF18_GIBF5	Superoxide dismutase	25.07/8.03	26.25/5.06	45.91
SP4	+		tr S0EEC6 S0EEC6_GIBF5	Superoxide dismutase	28.38/6.23	29.08/5.68	221.98
SP5	+		tr S0EEC6 S0EEC6_GIBF5	Superoxide dismutase	28.38/6.23	26.51/6.53	115.28
SP6	+		tr S0EEC6 S0EEC6_GIBF5	Superoxide dismutase	28.38/6.23	26.56/6.0	518.16
SP7	P		tr S0EMH8 S0EMH8_GIBF5	Related to tyrosinase (Monophenol monooxygenase)	76.19/5.97	14.41/5.17	32.24
CARBOHYDRATE METABOLIC PROCESS (2)							
SP8	+		tr S0EJD2 S0EJD2_GIBF5	Related to covalently-linked cell wall protein	41.90/4.58	17.81/4.75	117.73
SP9	+		tr S0E9I4 S0E9I4_GIBF5	Related to SPR1-exo-1 3-beta-glucanase	49.00/6.19	45.73/5.79	115.39
REGULATION OF BIOLOGICAL PROCESS (2)							
SP10	-		tr A0A071M2G2 A0A071M2G2_9BURK	Elongation factor	41.76/4.92	48.74/6.3	765.52
SP11	-		tr W7MJH9 W7MJH9_GIBM7	30S ribosomal protein S13	13.32/12.08	20.56/4.96	71.9
TRANSPORT (3)							
SP12	+		tr A0A071M865 A0A071M865_9BURK	Porin	39.18/9.41	34.13/5.16	70.34

(Continued)

TABLE 1 | Continued

Sample name	SignalP	Changefold	Protein ID	Protein description	Theo Mr/PI	2D Mr/PI	Protein score
OTHERS (3)							
SP13	+		tr A0A071MG81 A0A071MG81_9BURK	Iron ABC transporter substrate-binding protein	39.87/9.7	39.58/6.21	72.02
SP14	+		tr A0A071MG81 A0A071MG81_9BURK	Iron ABC transporter substrate-binding protein	39.87/9.7	39.12/5.86	42.42
SP15	+		tr S0EHG0 S0EHG0_GIBF5	Uncharacterized protein	21.39/5.92	21.81/5.89	39.9
SP16	+		tr C7Z0J4 C7Z0J4_NECH7	Predicted protein	12.81/4.33	74.06/6.73	67.3
SP17	+		tr D2IKP5 D2IKP5_9HYPO	APS1	571.27/5.9	17.08/5.89	72.2

A total of 17 proteins were identified and up-regulated at pH 10 compared to pH 5. Protein accumulation is represented by the column configuration, and accumulation of pH 5 and pH 10 was shown from left to right. +, Proteins with positive result from SignalP; P, Proteins with positive result from SecretomeP; -, Proteins with negative result from both SignalP and SecretomeP. Theo Mr/PI: Theoretical molecular mass and isoelectric point based on amino acid sequence of the identified proteins. 2D Mr/PI: Experimental molecular mass and isoelectric point estimated from the 2D gels. The error bar represents the standard error of the average over three independent biological replicate gels. The same is for Table 2.

five groups, including carbohydrate metabolism (8 spots), nitrogen compound metabolic process (3 spots), proteolysis (3 spots), response to stress (2 spots), and unknown function (6 spots) (Figure 4B, Table 2). All the spots with unknown function were also searched against PROSITE database for more protein domain information and only spot SP25 was hit by acyl carrier protein phosphatetheine domain.

Up-Regulated Proteins at pH 10

Total of 17 protein spots were up-regulated at pH 10 compared to pH 5. Most of proteins were predicted as extracellular location by the results of SignalP or SecretomeP. Only spots SP10 and 11, predicted to “regulation of biological process,” were located intracellular. Different from that at pH 5, functions of most differently expressed proteins at pH 10 were mainly involved in oxidation-reduction process, including two thioredoxin reductases (SP1 and 2) and four superoxide dismutases (SOD, SP3-6). In addition, two iron ABC transporter substrate-binding proteins (SP13 and 14) were also up-regulated in the secretome of pH 10-cultured sample. A close-up view of the changes in abundance of these spots was shown in Figure 5A.

Down-Regulated Proteins at pH 10

Compared with proteins at pH 5, 22 spots were down-regulated at pH 10 (Table 2). Most of them have the putative functions of carbohydrate metabolism. Interestingly, four of them were involved in the cell wall degrading enzymes (CWDEs), including 1 3-beta-glucanosyltransferase (SP18), related to SPR1-exo-1,3-beta-glucanase (SP19), related to glucan 1 3-beta-glucosidase (SP20) and related to endo alpha-1,4 polygalactosaminidase precursor (SP21). Gluconolactonase (SP23) and probable cellulose (SP24) were also down-regulated at pH 10 compared to pH 5. All of them might play a vital role in the infection of fungi at pH 5. A close-up view of the changes in abundance of these spots was shown in Figure 5B. Three spots related to proteolysis and two spots related to response to stress were also down-regulated. Additionally, three proteins related to nitrogen compound metabolic process (Spots SP26-28) were down-regulated at pH 10, such as serine/threonine protein kinase. All spots were predicted as extracellular proteins according to the positive results from SignalP or SecretomeP except enolase (SP22).

Transcriptional Expression of Related Genes at pH 5 and 10

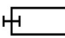
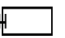
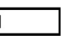
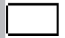
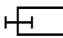
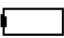
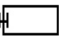
To verify the validity of proteomic data, we analyzed the expression level of related genes using qRT-PCR. A total of six genes were performed, which were related to cell wall degradation, proteolysis and redox reaction, including 1,3-beta glucanosyltransferase, alpha-1,4 polygalactosaminidase, cellulase, aspartic proteinase, gluconolactonase, and thioredoxin reductase (Figure 6). Result showed that all genes corresponding to CWDEs and proteolysis were down-regulated at pH 10 compared to pH 5 (Figure 6). On the contrary, redox related gene was up-regulated significantly at pH 10 compared to pH 5 (Figure 6). All those genes expression were correlated well with proteomic data. It suggested that the proteomic data was accurate and credible.

TABLE 2 | Down-regulated secretory proteins in *F. proliferatum* under alkaline environment.

Sample name	SignalP	Changefold	Protein ID	Protein description	Theo Mr/PI	2D Mr/PI	Protein score
CARBOHYDRATE METABOLIC PROCESS (8)							
SP18	+		tr S0E1L4 S0E1L4_GIBF5	1 3-beta-glucanosyltransferase	48.81/4.71	56.58/5.19	88.74
SP19	+		tr S0E9I4 S0E9I4_GIBF5	Related to SPR1-exo-1,3-beta-glucanase	49.00/6.19	45.94/5.92	274
SP20	+		tr S0DSA1 S0DSA1_GIBF5	Related to glucan 1 3-beta-glucosidase	42.49/4.51	80/5.3	41.65
SP21	P		tr S0E8F8 S0E8F8_GIBF5	Related to endo alpha-1 4 polygalactosaminidase precursor	38.24/9.6	32.21/5.41	104.13
SP22	-		tr A0A063XCK4 A0A063XCK4_BACIU	Endase	46.61/4.4	48.07/4.92	84.67
SP23	+		tr X0HDL4 X0HDL4_FUSOX	Gluconolactonase	43.25/5.18	64.84/5.39	144.47
SP24	+		tr S0DM93 S0DM93_GIBF5	Probable cellulase	37.12/7.71	38/6.9	23.84
SP25	+		tr S0DSR5 S0DSR5_GIBF5	Probable rAsp f 9 allergen	29.51/4.26	34.05/4.34	67.2
NITROGEN COMPOUND METABOLIC PROCESS (3)							
SP26	P		tr X0J1C7 X0J1C7_FUSOX	Adenosinetriphosphatase	190.16/4.99	35.00/4.50	67.2
SP27	P		tr Q05GS8 Q05GS8_GIBFU	Peptidyl-prolyl cis-trans isomerase	12.05/4.59	15.04/4.98	337
SP28	P		tr X0CL22 X0CL22_FUSOX	Serine/threonine protein kinase	50.9/7.29	27.6/5.22	24.52
RESPONSE TO STRESS (2)							
SP29	P		tr S0E8X5 S0E8X5_GIBF5	Probable peroxisomal membrane protein	18.14/4.96	19.84/4.88	154
SP30	+		tr W9ZB77 W9ZB77_FUSOX	Catalase-peroxidase	85.26/7.04	81.03/6.70	381

(Continued)

TABLE 2 | Continued

Sample name	SignalP	Changefold	Protein ID	Protein description	Theo Mr/PI	2D Mr/PI	Protein score
PROTEOLYSIS (3)							
SP31	+		tr N1RNP5 N1RNP5_FUSC4	Antigen	31.81/5.18	54.78/5.07	109
SP32	+		tr S0D1T6 S0D1T6_GIBF5	Probable PRC1-carboxypeptidase y, serine-type protease	60.95/4.93	54.08/4.81	116
SP33	+		tr S0E6V7 S0E6V7_GIBF5	Related to aspartic proteinase	41.80/4.4	53.65/4.89	65.67
OTHERS (6)							
SP34	+		tr C7Z1Q5 C7Z1Q5_NECH7	Predicted protein	27.52/4.79	32.59/4.44	118
SP35	P		tr A0A016PY6 A0A016PY6_GIBZA	Fusarium graminearum chromosome 1	60.95/10.23	26.79/5.91	72.1
SP36	+		tr S0EL20 S0EL20_GIBF5	Uncharacterized protein	27.83/4.48	32.39/4.52	278
SP37	+		tr S0EAM0 S0EAM0_GIBF5	Uncharacterized protein	18.11/9.69	57.88/5.34	88.7
SP38	+		tr W7MXEQ W7MXEQ_GIBM7	Uncharacterized protein	23.82/7.36	22.39/6.23	154
SP39	+		tr S0EL20 S0EL20_GIBF5	Uncharacterized protein	27.83/4.48	32.80/4.57	83.5

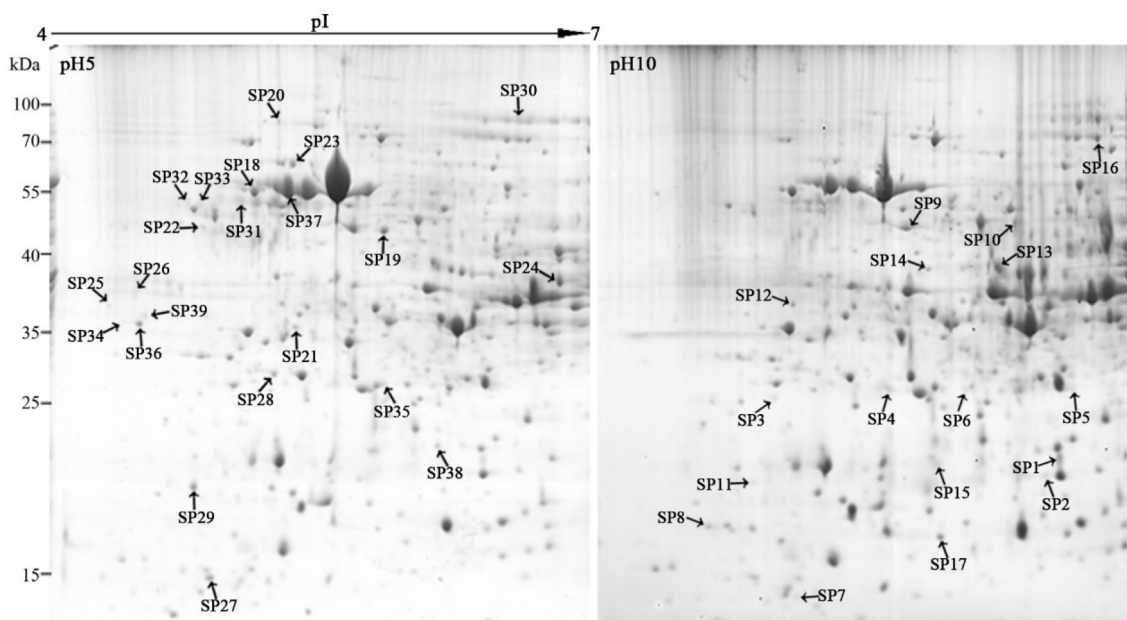


FIGURE 3 | Representative two-dimensional electrophoresis maps of *Fusarium proliferatum*. Total secreted proteins were extracted from *F. proliferatum* after 10 d culture under pH 5 or pH 10 condition. The location of differentially expressed proteins were identified successfully.

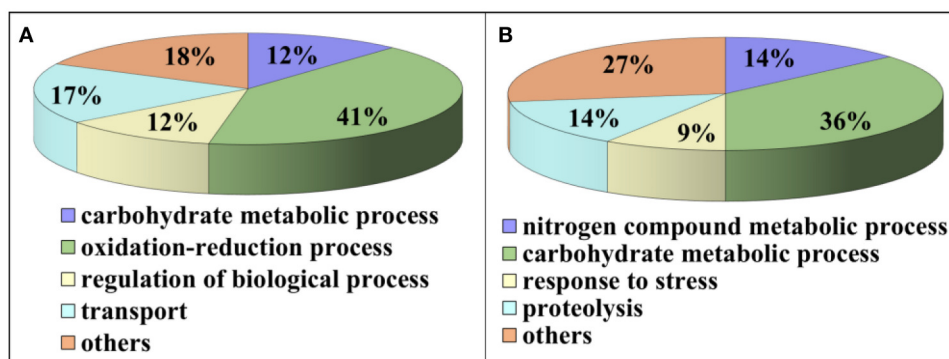


FIGURE 4 | Functional classification of differentially expressed proteins. Proteins were classified using Blast2Go base on biological process. **(A)** Up-regulated proteins at pH 10 compared to pH 5. **(B)** Down-regulated proteins at pH 10 compared to pH 5.

DISCUSSION

The Secreted Proteins in *F. proliferatum*

Classical secretory pathway is the most important mechanism to translocate proteins to externally cells with a signal peptide in eukaryotes while proteins without signal peptide can also be secreted out of cells by non-classical secretory pathway (Nickel and Rabouille, 2009). Among these 39 identified proteins, 36 proteins were predicted as the secreted proteins including 26 proteins in classical secretory pathways and 10 proteins in non-classical secretory pathways. Although enolase (SP22), elongation factor (SP10) and 30 S ribosomal protein S13 (SP11) were predicted with negative results from both SignalP and SecretomeP, they were previously reported as secreted proteins in other research (Hughes et al., 2002; Paper et al., 2007).

Moreover, enolase might act as virulence factors and be involved in a variety of extracellular functions (Oliveira et al., 2013).

Alkaline Environment Induced Proteins in *F. proliferatum*

Most up-regulated proteins at pH 10 were involved with oxidation-reduction process, such as thioredoxin reductase and superoxide dismutase. The critical roles of reactive oxygen species (ROS) in many plant pathogen interactions have been well-established (Williams et al., 2011). For pathogens, in response to oxidative stress generated by plant, antioxidant defenses were activated, such as up-regulated SOD (Xu and Chen, 2013). Moreover, SOD was reported to enhance

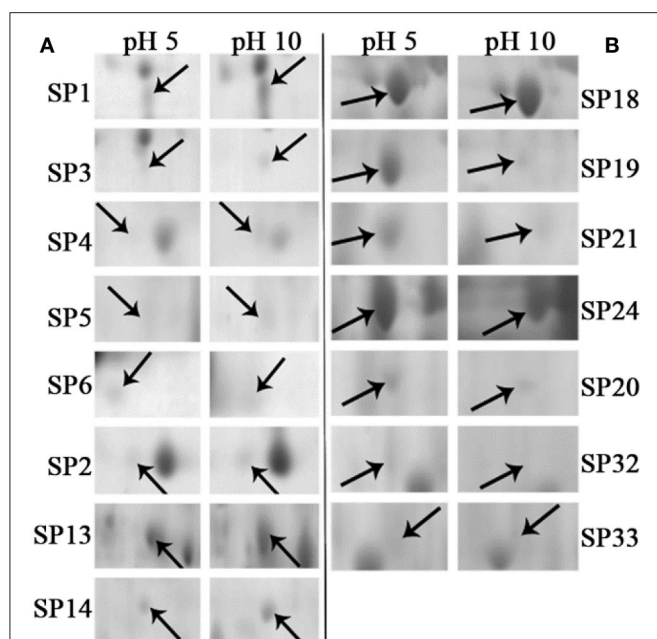


FIGURE 5 | Close-up views of some significant differentially expressed proteins. Some typical spots with significantly differential accumulation patterns were pointed by arrows. **(A)** Up-regulated secretory proteins in *F. proliferatum* under alkaline environment. **(B)** Down-regulated secretory proteins in *F. proliferatum* under alkaline environment. Detail information of proteins were shown in **Tables 1, 2**.

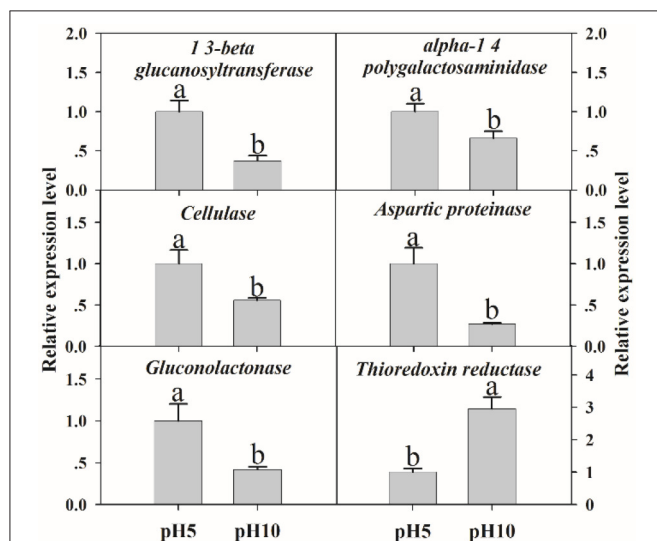


FIGURE 6 | The expression levels of selected genes. The relative expression levels of selected genes were analyzed using qRT-PCR. Each data point represents a mean \pm standard error ($n = 3$) and the values with different letters are significantly different ($p < 0.05$).

could not only enhance the defense ability of *F. proliferatum* against ROS stress but also increase the toxicity of fumonisin during infection process. The mycelium proteomics analysis of *F. proliferatum* also proved that pH 10 induced SOD accumulation (Li et al., 2017), which further confirmed the role of SOD in antioxidant defense.

Thioredoxin reductase is another important protein in the antioxidant defense system of fungi, and it is also important to the virulence of *Cryptococcus neoformans* (Missall and Lodge, 2005). Thioredoxin was thought to be important virulence factor induced during pathogens infection or might protect *Phytophthora* from plant counter defenses (Meijer et al., 2014). Moreover, it reported that thioredoxin reductase deletion strain of *Magnaporthe oryzae* was significantly reduced in conidiation and unable to produce expanded necrotic lesions on the leaf surface (Fernandez and Wilson, 2014). In this study, two thioredoxin reductases (Spots SP1 and 2) were significantly up-regulated at pH 10 compared to pH 5 (**Table 1**), which indicated that thioredoxin reductase might play a vital role in *F. proliferatum* infection process. Interestingly, *thioredoxin reductase* was also induced at pH 10 in gene expression of *F. proliferatum*, which further confirmed our inference.

Porin has been reported to have the function of adhering to host cells (Goo et al., 2006) and pathogen/symbiont recognition (Nyholm et al., 2009). Additionally, the mitochondrial porin was related to the function of SOD, which act as an important pathogenicity/virulence factor for fungi (Budzinska et al., 2007). Recently, it is reported that porin might act as virulence factors modulating host mitochondrial physiology for bacterial survival and immune evasion inside the host cells (Rana et al., 2015). In the present study, porin (Spot SP12) was up-regulated at pH 10 compared with pH 5 (**Figure 5A, Table 1**), which might also play a crucial role in fungal pathogens.

In this study, two iron ABC transporter substrate-binding proteins (SP13 and 14), were also up-regulated in the secretome of *F. proliferatum* at pH 10. ABC transporter substrate-binding proteins have been reported to participate in nutrient import and protection from stress (Vigonsky et al., 2013). It is reported that exclusive expression of ABC transporters genes is a basic fungal defense reaction when *F. graminearum* was growing on the living plant (Boedi et al., 2016). Our previous study also indicated that in response to BHA treatment, *F. proliferatum* could assemble different ABC transporter substrate-binding proteins to accelerate the nutrient uptake (Li et al., 2016). Collectively, in response to the stress caused by high pH, *F. proliferatum* might assemble different ABC transporter substrate-binding proteins to accelerate the nutrient uptake for the maintaining of growth.

In plants, the alkaline condition results in oxidative burst and alkalization is an essential factor in the induction of defense response (Wojtaszek et al., 1995; Clarke et al., 2005). Tomato fruit apoplastic alkalization activated oxidative burst and SA mediated defense response (Alkan et al., 2012). All these responses of plant under alkaline condition could greatly affect fungal pathogenicity. In response, the fungi adjusted the extracellular proteins in order to survive in the host. Therefore, the high accumulation of these antioxidant enzymes might contribute greatly to the normal growth and pathogenicity of fungus. These antioxidant enzymes involved in the virulence of

fungal pathogens may serve as excellent targets for antifungal therapy (Missall and Lodge, 2005). On the other hand, fumonisin content was significantly increased at pH 10 compared to pH 5 (Li et al., 2017), which effectively enhanced the infection ability of *F. proliferatum* and greatly recovered the negative effect of pathogen pathogenicity inhibited by host (Figure 2).

Alkaline Environment Inhibited Proteins in *F. proliferatum*

It is well known that extracellular proteins related to CWDEs or proteolysis are important for the pathogenicity of plant pathogens. The plant cell wall is an internal physical defensive barrier, and pathogens use extracellular enzymes to degrade the cell wall and invade host (Lakshman et al., 2016). Many researches have reported that CWDEs are involved in the direct degradation of plant tissue, and they have been suggested to be pathogenicity factors of several pathogens, such as pectate lyase (PL), polygalacturonase (PG), etc. (Zhang et al., 2014; Lakshman et al., 2016). In this study, alkaline environment significantly inhibited the accumulation of CWDEs (Table 2), including 1, 3-beta-glucanase (SP18), SPR1-exo-1, 3-beta-glucanase (SP19), glucan 1, 3-beta-glucosidase (SP20), endo alpha-1, 4 polygalactosaminidase precursor (SP21), gluconolactonase (SP23), and probable cellulose (SP24). Those results were also reported in *Thielavia reesei* (Adav et al., 2011). On the other hand, qRT-PCR results demonstrated that these proteins under different ambient pH values were also down-regulated at transcriptional level (Figure 6). Therefore, the lower accumulation of these CWDEs under pH 10 condition might result in the slower infection of *F. proliferatum* on banana fruit (Figure 2).

1, 3-beta-glucanase was essential for *Fusarium oxysporum* to infect tomato plants (Caracuel et al., 2005). For SPR1-exo-1, 3-beta-glucanase and glucan 1, 3-beta-glucosidase, the degradation of β -1,3-glucans may contribute to activating the induction of the programmed cell death in plant cells via generating elicitors in the form of β -(1,3)(1,6)-oligomers (Espino et al., 2010). Gluconolactonase may regulate oxidative stress tolerance and fitness of microorganism (Tarighi et al., 2011). The downregulation of those enzymes might contribute to decrease the infection and growth metabolism of *F. proliferatum* at pH 10. Therefore, our proteomic data indicated that these secreted proteins might have close connection to the biology of *F. proliferatum* during the interaction with its host especially under pH 5 condition.

Besides CWDEs, the proteinase has been also suggested to be involved in plant-pathogen interactions in many studies (Li et al., 2012). It was reported that proteolytic enzymes including aspartic proteases could contribute to the degradation of the host tissue for nutritional acquisition and invasion (Dagenais and Keller, 2009). In the present study, the down-regulation of serine-type protease and aspartic proteinase might contribute to harder infection of *F. proliferatum* at pH 10. Similarly, aspartic proteinase was also down-regulated at transcriptional level (Figure 6). Cell surface enolase of different pathogenic microorganisms could participate in the tissue invasion process and mediate degradation of host tissues and immune evasion (Avilán et al., 2011). The down-regulation of enolase at pH 10

might inhibit the adhesion and invasion of *F. proliferatum* to host tissues then decrease the infection ability of *F. proliferatum*. Enolase was also identified with downregulation in the mycelium proteomics (Li et al., 2017). Therefore, different pH can also cause the significant changes of mycelium proteomics, which might affect the pathogenicity of *F. proliferatum*.

Another protein in the group of "response to stress" is catalase-peroxidase (SP30), which plays a role in defense to oxidative stress. Similar to the upregulation of thioredoxin reductase at pH 10, the upregulation of catalase-peroxidase at pH 5 might also contribute to the normal growth of *F. proliferatum* in response to oxidative stress.

It was worthy to note that the expressions of protein related to nitrogen compound metabolic process (SP26, 27, and 28) were up-regulated under pH 5 condition. Of these proteins, serine/threonine protein kinase with positive results from SecretomeP attracted our attention. Manandhar et al. (2012) reported that the serine/threonine protein kinase could regulate the fusion at the lysosomal vacuole and maintained the fusion/fission dynamics of *Saccharomyces cerevisiae*. Moreover, mitogen-activated protein (MAP) kinases, one of the important type of serine/threonine protein kinases, was reported to be involved in multiple developmental processes related to sexual reproduction, plant infection and cell wall integrity of *F. graminearum* (Hou et al., 2002). Moreover, the virulence of *F. graminearum* was severely reduced in the MAPK mutants (Hou et al., 2002). Our previous study also indicated that serine/threonine protein kinases were greatly reduced by the BHA treatment which might disturbed trafficking and organelle biogenesis beyond the vacuole of *F. proliferatum* (Li et al., 2016). In this study, we observed that serine/threonine protein kinase (SP28) was up-regulated under pH 5 (Table 1), which consequently might contribute to the pathogenic ability of *F. proliferatum*.

CONCLUSIONS

In the present study, *F. proliferatum* cultured under initial pH 5 and 10 conditions both exhibited infection ability on banana fruit. However, pH 10 condition decreased the pathogenicity of the fungus, compared to pH 5. The effect of different pH values on the secretome of *F. proliferatum* was analyzed based on 2-DE. The proteomic data indicated that the secretome of *F. proliferatum* had distinct differences between pH 5 and 10 conditions. Under weak alkaline condition, a great number of CWDEs were down-regulated in *F. proliferatum*, which suggested that the pathogenicity might be significantly inhibited at pH 10 by the inability to degrade the host cell wall effectively. However, a larger number of antioxidant enzymes were up-regulated at pH 10 compared to pH 5, which might contribute greatly to recover the normal growth and pathogenicity of the fungus. We carefully concluded that under pH 5 condition, the *F. proliferatum* secreted more CWDEs for proteolysis, which are more urgently required to degrade the stiffer cell wall of the banana peel. In all, the present study provided a new clue to reveal the reason why banana is susceptible infected by *Fusarium* when pH is below 5.5. It is suggested that *F. proliferatum*

is capable of adapting itself with different pH conditions by changing a set of extracellular proteins that prepares itself for encountering stress and infection of the host plant. Further research *in vitro* and in planta is still needed to confirm the exact role of these proteins involved in the infection mechanisms of *F. proliferatum*.

AUTHOR CONTRIBUTIONS

TL and ZY conceived and designed the study. TL, QW, YW, AJ, HQ, LG, and XD performed the experiments and analyzed the data. TL, ZY, HZ, and YJ drafted and revised the manuscript. All authors participated in the interpretation of data of the manuscript. All authors approved the submission and publication for all aspects of the work.

REFERENCES

- Adav, S. S., Ravindran, A., Chao, L. T., Tan, L., Singh, S., and Sze, S. K. (2011). Proteomic analysis of pH and strains dependent protein secretion of *Trichoderma reesei*. *J. Proteome Res.* 10, 4579–4596. doi: 10.1021/pr200416t
- Alkan, N., Fluhr, R., and Prusky, D. (2012). Ammonium secretion during *Colletotrichum coccodes* infection modulates salicylic and jasmonic acid pathways of ripe and unripe tomato fruit. *Mol. Plant Microb. Interact.* 25, 85–96. doi: 10.1094/MPMI-01-11-0020
- Amby, D. B., Thuy, T. T. T., Ho, B. D., Kosawang, C., Son, T. B., and Jorgensen, H. J. L. (2015). First report of *Fusarium lichenicola* as a causal agent of fruit rot in pomelo (*Citrus maxima*). *Plant Dis.* 99, 1278–1279. doi: 10.1094/PDIS-10-14-1017-PDN
- Avilán, L., Gualdrón-López, M., Qui-ones, W., González-gonzález, L., Hannaert, V., Michels, P. A. M., et al. (2011). Enolase: a key player in the metabolism and a probable virulence factor of trypanosomatid parasites—perspectives for its use as a therapeutic target. *Enzym. Res.* 2011:932549. doi: 10.4061/2011/932549
- Bi, F. C., Barad, S., Ment, D., Luria, N., Dubey, A., Casado, V., et al. (2016). Carbon regulation of environmental pH by secreted small molecules that modulate pathogenicity in phytopathogenic fungi. *Mol. Plant Pathol.* 17, 1178–1195. doi: 10.1111/mpp.12355
- Boedi, S., Berger, H., Sieber, C., Münsterkötter, M., Maloku, I., Warth, B., et al. (2016). Comparison of *Fusarium graminearum* transcriptomes on living or dead wheat differentiates substrate-responsive and defense-responsive genes. *Front. Microbiol.* 7:1113. doi: 10.3389/fmicb.2016.01113
- Budzinska, M., Galganska, H., Wojtkowska, M., Stobienia, O., and Kmita, H. (2007). Effects of VDAC isoforms on CuZn-superoxide dismutase activity in the intermembrane space of *Saccharomyces cerevisiae* mitochondria. *Biochem. Biophys. Res.* 357, 1065–1070. doi: 10.1016/j.bbrc.2007.04.090
- Caracul, Z., Martinez-Rocha, A. L., Di Pietro, A., Madrid, M. P., and Roncero, M. I. G. (2005). *Fusarium oxysporum* gas1 encodes a putative beta-1,3-glucanotransferase required for virulence on tomato plants. *Mol. Plant Microb.* 18, 1140–1147. doi: 10.1094/MPMI-18-1140
- Clarke, A., Mur, L. A., Darby, R. M., and Kenton, P. (2005). Harpin modulates the accumulation of salicylic acid by Arabidopsis cells via apoplastic alkalization. *J. Exp. Bot.* 56, 3129–3136. doi: 10.1093/jxb/eri310
- Dagenais, T. R. T., and Keller, N. P. (2009). Pathogenesis of *Aspergillus fumigatus* in invasive aspergillosis. *Clin. Microbiol. Rev.* 22, 447–465. doi: 10.1128/CMR.00055-08
- Espino, J. J., Gutierrez-Sanchez, G., Brito, N., Shah, P., Orlando, R., and Gonzalez, C. (2010). The *Botrytis cinerea* early secretome. *Proteomics* 10, 3020–3034. doi: 10.1002/pmic.201000037
- Fernandez, J., and Wilson, R. A. (2014). Characterizing roles for the glutathione reductase, thioredoxin reductase and thioredoxin peroxidase-encoding genes of *Magnaporthe oryzae* during rice blast disease. *PLoS ONE* 9:87300. doi: 10.1371/journal.pone.0087300

ACKNOWLEDGMENTS

This work was supported by National Natural Science Foundation of China (grant nos. 31671911 and 31701657), National Postdoctoral Program for Innovative Talents (grant no. BX201600170), China Postdoctoral Science Foundation (grant no. 2017M610559), Science and Technology Planning Project of Guangdong Province, China (no. 2016A020210061), Pearl River S&T Nova Program of Guangzhou (no. 201610010041).

SUPPLEMENTARY MATERIAL

The Supplementary Material for this article can be found online at: <https://www.frontiersin.org/articles/10.3389/fmicb.2017.02327/full#supplementary-material>

- Goo, S. Y., Lee, H. J., Kim, W. H., Han, K. L., Park, D. K., Lee, H. J., et al. (2006). Identification of OmpU of *Vibrio vulnificus* as a fibronectin-binding protein and its role in bacterial pathogenesis. *Infect. Immun.* 74, 5586–5594. doi: 10.1128/IAI.00171-06
- Hou, Z. M., Xue, C. Y., Peng, Y. L., Katan, T., Kistler, H. C., and Xu, J. R. (2002). A mitogen-activated protein kinase gene (MGV1) in *Fusarium graminearum* is required for female fertility, heterokaryon formation, and plant infection. *Mol. Plant Microbe Interact.* 15, 1119–1127. doi: 10.1094/MPMI.2002.15.11.1119
- Hughes, M. J., Moore, J. C., Lane, J. D., Wilson, R., Pribul, P. K., Younes, Z. N., et al. (2002). Identification of major outer surface proteins of *Streptococcus agalactiae*. *Infect. Immun.* 70, 1254–1259. doi: 10.1128/IAI.70.3.1254-1259.2002
- Lakshman, D. K., Roberts, D. P., Garrett, W. M., Natarajan, S., Darwish, O., Alkharouf, N. W., et al. (2016). Proteomic investigation of *Rhizoctonia solani* AG 4 identifies secretome and mycelial proteins with roles in plant cell wall degradation and virulence. *J. Agric. Food Chem.* 64, 3101–3110. doi: 10.1021/acs.jafc.5b05735
- Lamb, T. M., Xu, W. J., Diamond, A., and Mitchell, A. P. (2001). Alkaline response genes of *Saccharomyces cerevisiae* and their relationship to the RIM101 pathway. *J. Biol. Chem.* 276, 12476–12476. doi: 10.1074/jbc.M008381200
- Li, B. Q., Wang, W. H., Zong, Y. Y., Qin, G. Z., and Tian, S. P. (2012). Exploring pathogenic mechanisms of *Botrytis cinerea* secretome under different ambient pH based on comparative proteomic analysis. *J. Proteome Res.* 11, 4249–4260. doi: 10.1021/pr300365f
- Li, J., Jiang, G. X., Yang, B., Dong, X. H., Feng, L. Y., Lin, S., et al. (2012). A luminescent bacterium assay of fusaric acid produced by *Fusarium proliferatum* from banana. *Anal. Bioanal. Chem.* 402, 1347–1354. doi: 10.1007/s00216-011-5546-6
- Li, T. T., Gong, L., Wang, Y., Chen, F., Gupta, V. K., Jian, Q. J., et al. (2017). Proteomics analysis of *Fusarium proliferatum* under various initial pH during fumonisin production. *J. Proteomics* 164, 59–72. doi: 10.1016/j.jpro.2017.05.008
- Li, T. T., Zhu, H., Wu, Q. X., Yang, C. W., Duan, X. W., Qu, H. X., et al. (2015). Comparative proteomic approaches to analysis of litchi pulp senescence after harvest. *Food Res. Int.* 78, 274–285. doi: 10.1016/j.foodres.2015.09.033
- Li, T., Jian, Q., Wang, Y., Chen, F., Yang, C., Gong, L., et al. (2016). Inhibitory mechanism of butylated hydroxyanisole against infection of *Fusarium proliferatum* based on comparative proteomic analysis. *J. Proteomics* 148, 1–11. doi: 10.1016/j.jpro.2016.04.051
- Manandhar, S. P., Ricarte, F., Cocca, S. M., and Gharakhanian, E. (2012). *Saccharomyces cerevisiae* Env7 is a novel serine/threonine kinase 16-Related protein kinase and negatively regulates organelle fusion at the lysosomal vacuole. *Mol. Cell. Biol.* 33, 526–542. doi: 10.1128/MCB.01303-12
- Meijer, H. J. G., Mancuso, F. M., Espadas, G., Seidl, M. F., Chiva, C., Govers, F., et al. (2014). Profiling the secretome and extracellular proteome of the potato late

- blight pathogen *Phytophthora infestans*. *Mol. Cell. Proteomics* 13, 2101–2113. doi: 10.1074/mcp.M113.035873
- Merhej, J., Richard-Forget, F., and Barreau, C. (2011). The pH regulatory factor Pad1 regulates Tri gene expression and trichothecene production in *Fusarium graminearum*. *Fungal Genet. Biol.* 48, 275–284. doi: 10.1016/j.fgb.2010.11.008
- Missall, T. A., and Lodge, J. K. (2005). Function of the thioredoxin proteins in *Cryptococcus neoformans* during stress or virulence and regulation by putative transcriptional modulators. *Mol. Microbiol.* 57, 847–858. doi: 10.1111/j.1365-2958.2005.04735.x
- Nickel, W., and Rabouille, C. (2009). Mechanisms of regulated unconventional protein secretion. *Nat. Rev. Mol. Cell Biol.* 10, 148–155. doi: 10.1038/nrm2617
- Nyholm, S. V., Stewart, J. J., Ruby, E. G., and McFall-Ngai, M. J. (2009). Recognition between symbiotic *Vibrio fischeri* and the haemocytes of *Euprymna scolopes*. *Environ. Microbiol.* 11, 483–493. doi: 10.1111/j.1462-2920.2008.01788.x
- Oliveira, D. L., Rizzo, J., Joffe, L. S., Godinho, R. M. C., and Rodrigues, M. L. (2013). Where do they come from and where do they go: candidates for regulating extracellular vesicle formation in fungi. *Int. J. Mol. Sci.* 14, 9581–9603. doi: 10.3390/ijms14059581
- Palacios, S. A., Susca, A., Haidukowski, M., Stea, G., Cendoya, E., Ramirez, M. L., et al. (2015). Genetic variability and fumonisin production by *Fusarium proliferatum* isolated from durum wheat grains in Argentina. *Int. J. Food Microbiol.* 201, 35–41. doi: 10.1016/j.ijfoodmicro.2015.02.011
- Paper, J. M., Scott-Craig, J. S., Adhikari, N. D., Cuom, C. A., and Walton, J. D. (2007). Comparative proteomics of extracellular proteins *in vitro* and in planta from the pathogenic fungus *Fusarium graminearum*. *Proteomics* 7, 3171–3183. doi: 10.1002/pmic.200700184
- Penalva, M. A., Tilburn, J., Bignell, E., and Arst, H. N. (2008). Ambient pH gene regulation in fungi: making connections. *Trends Microbiol.* 16, 291–300. doi: 10.1016/j.tim.2008.03.006
- Prusky, D., and Yakoby, N. (2003). Pathogenic fungi: leading or led by ambient pH? *Mol. Plant Pathol.* 4, 509–516. doi: 10.1046/j.1364-3703.2003.0196.x
- Rana, A., Kumar, D., Rub, A., and Akhter, Y. (2015). Proteome-scale identification and characterization of mitochondria targeting proteins of *Mycobacterium avium* subspecies paratuberculosis: potential virulence factors modulating host mitochondrial function. *Mitochondrion* 23, 42–54. doi: 10.1016/j.mito.2015.05.005
- Rollins, J. A. (2003). The *Sclerotinia sclerotiorum* pac1 gene is required for sclerotial development and virulence. *Mol. Plant Microb. Interact.* 16, 785–795. doi: 10.1094/MPMI.2003.16.9.785
- Tarighi, S., Wei, Q., Camara, M., Williams, P., Fletcher, M. P., Kajander, T., et al. (2011). The PA4204 gene encodes a periplasmic gluconolactonase (PpgL) which is important for fitness of *Pseudomonas aeruginosa*. *World J. Microbiol. Biotechnol.* 27:1303. doi: 10.1099/mic.0.2008/018465-0
- Trapphoff, T., Beutner, C., Niehaus, K., and Colditz, F. (2009). Induction of distinct defense-associated protein patterns in *Aphanomyces euteiches* (Oomycota)-elicited and -inoculated *Medicago truncatula* cell-suspension cultures: a proteome and phosphoproteome approach. *Mol. Plant. Microb. Interact.* 22, 421–436. doi: 10.1094/MPMI-22-4-0421
- Vigonsky, E., Ovcharenko, E., and Lewinson, O. (2013). Two molybdate/tungstate ABC transporters that interact very differently with their substrate binding proteins. *Proc. Natl. Acad. Sci. U.S.A.* 110, 5440–5445. doi: 10.1073/pnas.1213598110
- Williams, B., Kabbage, M., Kim, H. J., Britt, R., and Dickman, M. B. (2011). Tipping the balance: *Sclerotinia sclerotiorum* secreted oxalic acid suppresses host defenses by manipulating the host redox environment. *PLoS Pathog.* 7:1002107. doi: 10.1371/journal.ppat.1002107
- Wojtaszek, P., Trethowan, J., and Bolwell, G. P. (1995). Specificity in the immobilisation of cell wall proteins in response to different elicitor molecules in suspension-cultured cells of French bean (*Phaseolus vulgaris* L.). *Plant Mol. Biol.* 28, 1075–1087. doi: 10.1007/BF00032668
- Xie, X. Q., Wang, J., Huang, B. F., Ying, S. H., and Feng, M. G. (2010). A new manganese superoxide dismutase identified from *Beauveria bassiana* enhances virulence and stress tolerance when overexpressed in the fungal pathogen. *Appl. Microbiol. Biotechnol.* 86, 1543–1553. doi: 10.1007/s00253-010-2437-2
- Xu, L. S., and Chen, W. D. (2013). Random T-DNA mutagenesis identifies a Cu/Zn superoxide dismutase gene as a virulence factor of *Sclerotinia sclerotiorum*. *Mol. Plant Microb. Interact.* 26, 431–441. doi: 10.1094/MPMI-07-12-0177-R
- Zhang, J., Bruton, B. D., and Biles, C. L. (2014). Cell wall-degrading enzymes of *Didymella bryoniae* in relation to fungal growth and virulence in cantaloupe fruit. *Eur. J. Plant Pathol.* 139, 749–761. doi: 10.1007/s10658-014-0429-2
- Zhang, Z. Q., Qin, G. Z., Li, B. Q., and Tian, S. P. (2014). Knocking out Bcsa1 in *Botrytis cinerea* impacts growth, development, and secretion of extracellular proteins, which decreases virulence. *Mol. Plant Microb. Interact.* 27, 590–600. doi: 10.1094/MPMI-10-13-0314-R
- Zong, Y. Y., Li, B. Q., and Tian, S. P. (2015). Effects of carbon, nitrogen and ambient pH on patulin production and related gene expression in *Penicillium expansum*. *Int. J. Food Microbiol.* 206, 102–108. doi: 10.1016/j.ijfoodmicro.2015.05.007

Conflict of Interest Statement: The authors declare that the research was conducted in the absence of any commercial or financial relationships that could be construed as a potential conflict of interest.

Copyright © 2017 Li, Wu, Wang, John, Qu, Gong, Duan, Zhu, Yun and Jiang. This is an open-access article distributed under the terms of the Creative Commons Attribution License (CC BY). The use, distribution or reproduction in other forums is permitted, provided the original author(s) or licensor are credited and that the original publication in this journal is cited, in accordance with accepted academic practice. No use, distribution or reproduction is permitted which does not comply with these terms.



A Damaged Oxidative Phosphorylation Mechanism Is Involved in the Antifungal Activity of Citral against *Penicillium digitatum*

Qiuli OuYang, Nengguo Tao* and Miaoling Zhang

School of Chemical Engineering, Xiangtan University, Xiangtan, China

OPEN ACCESS

Edited by:

Juan Aguirre,
Universidad de Chile, Chile

Reviewed by:

María Serrano,
Universidad Miguel Hernández de
Elche, Spain
Cristobal Noe Aguilar,
Universidad Autónoma de Coahuila,
Mexico

*Correspondence:

Nengguo Tao
nengguotao@126.com

Specialty section:

This article was submitted to
Food Microbiology,
a section of the journal
Frontiers in Microbiology

Received: 20 December 2017

Accepted: 31 January 2018

Published: 16 February 2018

Citation:

OuYang Q, Tao N and Zhang M (2018)
A Damaged Oxidative
Phosphorylation Mechanism Is
Involved in the Antifungal Activity of
Citral against *Penicillium digitatum*.
Front. Microbiol. 9:239.
doi: 10.3389/fmicb.2018.00239

Citral exhibits strong antifungal activity against *Penicillium digitatum*. In this study, 41 over-expressed and 84 repressed proteins in *P. digitatum* after 1.0 μ L/mL of citral exposure for 30 min were identified by the iTRAQ technique. The proteins were closely related with oxidative phosphorylation, the TCA cycle and RNA transport. The mitochondrial complex I, complex II, complex III, complex IV and complex V, which are involved in oxidative phosphorylation were drastically affected. Among of them, the activities of mitochondrial complex I and complex IV were apparently suppressed, whereas those of mitochondrial complex II, complex III and complex V were significantly induced. Meanwhile, citral apparently triggered a reduction in the intracellular ATP, the mitochondrial membrane potential (MMP) and glutathione content, in contrast to an increase in the glutathione S-transferase activity and the accumulation of reactive oxygen species (ROS). Addition of exogenous cysteine decreased the antifungal activity. In addition, cysteine maintained the basal ROS level, deferred the decrease of MMP and the membrane damage. These results indicate that citral inhibited the growth of *P. digitatum* by damaging oxidative phosphorylation and cell membranes through the massive accumulation of ROS.

Keywords: *Penicillium digitatum*, citral, iTRAQ, oxidative phosphorylation, reactive oxygen species

INTRODUCTION

The green mold caused by *Penicillium digitatum* is a damaging disease in citrus fruits (Jing et al., 2014). Currently, this disease is mainly controlled by the intensive use of synthetic fungicides, but the application of chemical fungicides usually leads to the appearance of resistant strains and brings concerns about food and environmental safety. Plant essential oils and their volatile components are attracting considerable research efforts because of their potential use as food preservatives and additives in controlling postharvest diseases in fruits (Pérez-Alfonso et al., 2012; Shao et al., 2015; Tian et al., 2015; Boubaker et al., 2016; Li Y. H. et al., 2016).

Citral (3,7-dimethyl-2,6-octadienal) is mixture of two isomers, namely, geranial and neral, and is extracted from several lemon-scented herbal plants, most notably lemons, verbena, and lemongrass. Because of its particular aroma, substantial antibacterial, antifungal and insecticidal effects, as well as its low toxicity and low carcinogenicity, citral is classified as a substance that is “Generally Recognized as Safe” (GRAS) and has been widely used as a food additive and fragrance material in cosmetics. In recent years, citral has been illustrated to exhibit strong antifungal activities against *P. digitatum*, *P. italicum*, and *Geotrichum citri-aurantii* (Wuryatmo et al., 2003, 2014; Tao et al., 2014a; Zhou et al., 2014).

In our previous studies, citral was found to inhibit the mycelial growth of *P. digitatum* in a dose dependent manner with a minimum inhibitory concentration (MIC) of 2.0 $\mu\text{L/mL}$ and a minimum antifungal concentration (MFC) of 4.0 $\mu\text{L/mL}$, and the wax + citral ($10 \times \text{MFC}$) treatment significantly decreased the incidence of green mold in Ponkan mandarin fruit after 6 days of storage at $25 \pm 2^\circ\text{C}$, but did not influence the external and internal fruit qualities of citrus fruit (Fan et al., 2014). Therefore, citral is a promising substance that can be used in biological control of postharvest diseases in citrus fruit.

The potential mechanisms underlying the antifungal activity of citral are not fully understood, but several possible mechanisms have been proposed. The lipophilic nature of citral enables it to have the capacity to permeabilize the cell membrane, disrupt cell integrity, cause the leakage of cellular components, and finally lead to the cell death (Harris, 2002). Park et al. (2009) demonstrated that the cell membrane and organelles of *Trichophyton mentagrophytes* were irreversibly damaged by 0.2 mg/ml citral. Rajput and Karuppaiyil (2013) found that citral could exert their antifungal effect through inhibition of ergosterol biosynthesis. In a recent study, citral was able to alter the morphology of *Candida albicans*, but did not influence the cell wall or ergosterol (Leite et al., 2014). We previously reported that citral could inhibit the mycelial growth of *P. digitatum*, *P. italicum*, and *G. citri-aurantii* by a membrane damage mechanism (Tao et al., 2014b; Zhou et al., 2014; OuYang et al., 2016a). Meanwhile, citral evidently altered the mitochondrial morphology and repressed the citrate cycle (TCA cycle), respiratory metabolism and glycolysis of *P. digitatum* (Tao et al., 2015; Zheng et al., 2015). RNA-Seq data further showed that citral treatment greatly affected the expression levels of genes participating in ABC transport, steroid biosynthesis, the TCA cycle, oxidative phosphorylation, RNA degradation and ribosome biosynthesis (OuYang et al., 2016b).

It is well known that proteins serve an indispensable role in mediating the adaptability of pathogens to different stresses (Lackner et al., 2012), and proteins involved in the interaction of the pathogen with fungicides are crucial to understand the inhibition mechanism of fungicides on pathogens. In recent years, several techniques were developed aiming at understanding the complex biological systems and determining the relationships between proteins, their functions, and protein-protein interactions, such as isobaric tags for relative and absolute quantitation technique (iTRAQ), two-dimensional polyacrylamide gel electrophoresis and two-dimensional difference gel electrophoresis (Zieske, 2006). Among of them, iTRAQ is becoming one of the most powerful tools

to compare the protein expression patterns in microorganisms under different condition (Redding et al., 2006; Taylor et al., 2008; Yang et al., 2015; Zhang et al., 2015; Liu et al., 2017). To the best of our knowledge, however, the research considering the *P. digitatum* proteome in response to citral has not been conducted until now. Therefore, this research aims to identify differentially expressed proteins (DEPs) in *P. digitatum* upon exposure to citral by iTRAQ, in an effort to elucidate the antifungal mechanism of citral on *P. digitatum*.

MATERIALS AND METHODS

Fungal Strains

P. digitatum was isolated from infected citrus fruit and preserved on potato dextrose agar at $25 \pm 2^\circ\text{C}$. Two hundred micro liter fungal suspensions (5×10^5 cfu/mL) were added to the 40-mL potato dextrose broth (PDB) and incubated in a moist chamber at $25 \pm 2^\circ\text{C}$. The mycelia of *P. digitatum* grown for 48 h were collected and re-suspended in phosphate buffered saline (pH 7.0). The suspensions were then treated with 1/2MIC (1.0 $\mu\text{L/mL}$) of citral and incubated at $25 \pm 2^\circ\text{C}$ under agitation in an environmental incubator shaker for 30 min (OuYang et al., 2016b). The resulting samples were selected and named T30. The mycelia treated with phosphate buffered saline (pH 7.0) for 30 min were used as a negative control (CK30). All *P. digitatum* mycelia were immediately frozen in liquid nitrogen and stored at -80°C until further analysis.

Quantitative Proteomics by iTRAQ and LC-ESI-MS/MS

Total proteins were extracted from the mycelia as described by Zhang et al. (2015). The samples were solubilized with 500 mM triethylammonium bicarbonate (TEAB) and quantified by the Bradford assay (Bradford, 1976). One hundred micro grams of proteins were taken out of each sample solution and digested with Trypsin Gold (Promega, Madison, WI, USA) with a protein:trypsin ratio of 30:1 at 37°C for 16 h. After trypsin digestion, peptides were dried by vacuum centrifugation. Peptides were reconstituted in 0.5 M TEAB and processed according to the manufacture's protocol for 8-plex iTRAQ reagent (Applied Biosystems, Milan, Italy). Briefly, one unit of iTRAQ reagent was thawed and reconstituted in 24 μL isopropanol. Samples were labeled with the iTRAQ tags 117, 119, 114, and 115. The peptides were labeled with the isobaric tags, incubated at room temperature for 2 h. The labeled peptide mixtures were then pooled and dried by vacuum centrifugation. The labeled peptides were separated by SCX chromatography with a LC-20AB HPLC Pump system (Shimadzu, Kyoto, Japan) as described previously (Zhang et al., 2015).

After reconstituting dried fractions with solvent A (5% ACN and 0.1% FA) to a concentration of 0.5 $\mu\text{g}/\mu\text{L}$, 5 μL samples were analyzed on an LC-20AD nano-LC-ESI-MS/MS system (Shimadzu, Kyoto, Japan), and data acquisition was performed with a TripleTOF 5600 System (AB SCIEX, Concord, ON) fitted with a Nanospray III source (AB SCIEX, Concord, ON) and a pulled quartz tip as the emitter (New Objectives, Woburn, MA) (Zhang et al., 2015).

Abbreviations: DEPs, Differentially expressed proteins; iTRAQ, isobaric tags for relative and absolute quantization; MMP, mitochondrial membrane potential; ROS, reactive oxygen species; Cys, cysteine; GRAS, Generally Recognized as Safe; MFC, minimum antifungal concentration; MIC, minimum inhibitory concentration; TCA cycle, citrate cycle; PDB, potato dextrose broth; TEAB, triethylammonium bicarbonate; KEGG, Kyoto Encyclopedia of Genes and Genomes; GST, glutathione S-transferase; GSH, glutathione; DCFH-DA, redox-sensitive fluorescent probe dichloro-dihydro-fluorescein diacetate; PI, propidium iodide.

Data Analysis and Bioinformatics Analysis

For protein identification, a mass tolerance of 0.05 Da (ppm) was permitted for intact peptide masses and 0.1 Da for fragmented ions, allowing for one missed cleavage in the trypsin digests. Gln- > pyro-Glu (N-term Q), oxidation (M), deamidated (NQ) were treated as potential variable modifications, and carbamidomethyl (C), iTRAQ8plex (N-term), iTRAQ8plex (K) as fixed modifications. The charge states of the peptides were set to +2 and +3. Specifically, an automatic decoy database search was performed in Mascot by choosing the decoy checkbox in which a random sequence database is generated and tested for raw spectra as well as the real database. To reduce the probability of false peptide identification, only peptides with significance scores (≥ 20) at the 99% confidence interval by a Mascot probability analysis greater than the “identity” were counted as identified. Each confident protein identification involves at least one unique peptide.

For protein quantization, it was required that a protein contains at least two unique peptides. The quantitative protein ratios were weighted and normalized by the median ratio in Mascot. We only used ratios with $p < 0.05$, and only fold changes of > 1.5 were considered significant.

Functional annotations of the proteins was conducted using the Blast2GO program against the non-redundant protein database (NR; NCBI). The KEGG database (<http://www.genome.jp/kegg/>) and the COG database (<http://www.ncbi.nlm.nih.gov/COG/>) were used to classify and group these identified proteins, and then, the proteins were assigned to 108 known biological pathways in the Kyoto Encyclopedia of Genes and Genomes (KEGG) database (www.genome.jp/kegg/).

Enzymatic Activities of Mitochondrial Respiratory Complexes

The enzymatic activities of the mitochondrial complex I, complex II, complex III, complex IV, and complex V of the *P. digitatum* cells with citral at 0 and 1/2MIC for 0, 30, 60 and 120 min were determined by a UV2450 UV/Vis spectrophotometer [Shimadzu (Shanghai), Shanghai, China] using the commercially available kits (Solarbio Beijing, Beijing, China) following the manufacturer's instructions. Three independent replicates were performed for each treatment.

Glutathione S-Transferase (GST) Activities and Glutathione (GSH) Contents

The GST activities and GSH contents of *P. digitatum* cells with or without 1/2MIC of citral for 0, 30, 60, and 120 min were determined by a UV2450 UV/Vis spectrophotometer using a commercially available kit (Solarbio Beijing, Beijing, China) following the manufacturer's instructions. Three independent replicates were performed for each treatment.

ATP Contents

The intracellular and extracellular ATP contents of *P. digitatum* cells treated with 1/2MIC of citral or not were determined according to our previous method (Zheng et al., 2015).

Mitochondrial Membrane Potential (MMP)

P. digitatum hyphae incubated with 1/2MIC citral or without citral for 0, 30, 60, and 120 min were used to determine the MMP following the JC-10 Assay Kit (Solarbio, Shanghai, China). The treated cells were stained with JC-10 and analyzed

TABLE 1 | Enrichment pathway analysis of DEPs in *P. digitatum*.

	Pathway	Diff proteins with pathway annotation (82)	All proteins with pathway annotation (2,443)	P-value	Pathway ID
1	Oxidative phosphorylation	10 (12.2%)	86 (3.52%)	0.000461176	ko00190
2	Endocytosis	5 (6.1%)	47 (1.92%)	0.01912532	ko04144
3	Ribosome	7 (8.54%)	84 (3.44%)	0.02083807	ko03010
4	Caffeine metabolism	1 (1.22%)	1 (0.04%)	0.03356529	ko00232
5	SNARE interactions in vesicular transport	2 (2.44%)	13 (0.53%)	0.0683191	ko04130
6	Non-homologous end-joining	1 (1.22%)	4 (0.16%)	0.1277259	ko03450
7	Basal transcription factors	2 (2.44%)	22 (0.9%)	0.1671543	ko03022
8	Spliceosome	5 (6.1%)	90 (3.68%)	0.1821064	ko03040
9	Synthesis and degradation of ketone bodies	1 (1.22%)	6 (0.25%)	0.1854038	ko00072
10	Glyoxylate and dicarboxylate metabolism	2 (2.44%)	24 (0.98%)	0.1915471	ko00630
11	Nitrogen metabolism	2 (2.44%)	24 (0.98%)	0.1915471	ko00910
12	Pentose and glucuronate interconversions	2 (2.44%)	25 (1.02%)	0.2039195	ko00040
13	RNA degradation	3 (3.66%)	51 (2.09%)	0.243635	ko03018
14	Alanine, aspartate and glutamate metabolism	2 (2.44%)	31 (1.27%)	0.2793793	ko00250
15	Fatty acid metabolism	2 (2.44%)	31 (1.27%)	0.2793793	ko00071
16	Arginine and proline metabolism	2 (2.44%)	37 (1.51%)	0.3545094	ko00330
17	Ribosome biogenesis in eukaryotes	3 (3.66%)	64 (2.62%)	0.3644286	ko03008
18	Peroxisome	2 (2.44%)	38 (1.56%)	0.3668124	ko04146
19	Biosynthesis of unsaturated fatty acids	1 (1.22%)	14 (0.57%)	0.380771	ko01040
20	MAPK signaling pathway - yeast	2 (2.44%)	41 (1.68%)	0.4031635	ko04011

TABLE 2 | Translational-related DEPs and energy production and conversion-related DEPs in *P. digitatum*.

Proteins	NCBI nr accession	Change folds
60S ribosomal protein L35	gi 425779472 gb EKV17524.1	1.562
60S ribosomal protein L35Ae	gi 425783374 gb EKV21228.1	1.426
Ribosomal protein L44e	gi 425766420 gb EKV05032.1	-0.707
40S ribosomal protein S24	gi 425773071 gb EKV11444.1	1.469
40S ribosomal protein S26E	gi 425769642 gb EKV08131.1	-0.727
60S ribosomal protein L28	gi 425782319 gb EKV20238.1	-0.694
60S ribosomal protein L38	gi 425782646 gb EKV20545.1	-0.801
Transcription initiation factor TFIID subunit TSM1/127kD	gi 425783990 gb EKV21801.1	-0.747
Hypothetical protein PDIP_22250 TAF9	gi 425781794 gb EKV19739.1	1.427
Small nuclear ribonucleoprotein SmG	gi 425783989 gb EKV21800.1	1.395
Hypothetical protein PDIP_32220 SF3b	gi 425779117 gb EKV17206.1	1.958
Small nuclear ribonucleoprotein SmG Lsm	gi 425783989 gb EKV21800.1	1.395
Splicing factor u2af large subunit	gi 425773483 gb EKV11835.1	-0.649
U2 auxiliary factor small subunit	gi 425770129 gb EKV08603.1	-0.818
MRNA decapping hydrolase DCPs	gi 425765840 gb EKV04486.1	1.448
Hypothetical protein PDIP_50840 PABP1	gi 425774597 gb EKV12899.1	-0.574
Small nuclear ribonucleoprotein (LSM7)	gi 425770497 gb EKV08967.1	1.412
Casein kinase II beta subunit CKB1	gi 425781873 gb EKV19809.1	-0.731
Hypothetical protein PDIP_22250 Fap7	gi 425781794 gb EKV19739.1	1.427
Acyl carrier protein	gi 425769175 gb EKV07676.1	-0.565
LYR family protein	gi 425784140 gb EKV21934.1	-0.596
NADH-ubiquinone oxidoreductase	gi 425775152 gb EKV13435.1	-0.692
Hypothetical protein PDIP_56530	gi 425773011 gb EKV11388.1	-0.785
Hypothetical protein PDIP_64010	gi 425771150 gb EKV09603.1	2.338
Cytochrome b-c1 complex subunit 6	gi 425778715 gb EKV16822.1	-0.607
Cytochrome c oxidase polypeptide vib	gi 425778405 gb EKV16533.1	-0.698
Cytochrome c oxidase copper chaperone Cox17	gi 425783196 gb EKV21055.1	-0.673
ATP synthase delta chain	gi 425766735 gb EKV05334.1	1.626
Glutamine synthetase	gi 425776031 gb EKV14269.1	-0.661
Electron transfer flavoprotein alpha subunit putative	gi 425773543 gb EKV11891.1	-0.691
Delta-1-pyrroline-5-carboxylate dehydrogenase PrnC	gi 425778146 gb EKV16288.1	-0.757
Succinate dehydrogenase cytochrome b560 subunit	gi 425773767 gb EKV12100.1	2.250
Glutathione S-transferase	gi 425768826 gb EKV07338.1	1.444

with an ECLIPSE TS100 microscope (Nikon, Japan). The fluorescence values were measured by a F97 PRO fluorescence spectrophotometer (Lengguang Technology, Shanghai, China). Three replications for each treatment were performed. These experiments were also performed in samples supplied with antioxidant cysteine (Cys) at a concentration of 10 μ M.

Reactive Oxygen Species (ROS) Levels

The ROS levels in *P. digitatum* cells treated with citral at 1/2MIC or not for 0, 30, 60, and 120 min were determined by a redox-sensitive fluorescent probe dichloro-dihydro-fluorescein diacetate (DCFH-DA), according to the ROS assay kit (Solarbio Beijing, Beijing, China) instructions. The fluorescence values were measured by a F97 PRO fluorescence spectrophotometer (Lengguang Technology, Shanghai, China). Three independent replicates were performed for each treatment. The mycelia were observed with an ECLIPSE TS100 microscope (Nikon, Japan). These experiments were also conducted in samples supplied with the antioxidant Cys at a concentration of 10 μ M.

Effect of Exogenous Cys on the Antifungal Activity of Citral against *P. digitatum*

Cys at a final concentration of 10 μ M was added to the *P. digitatum* cultures supplied citral at the concentrations 0.0 μ L/mL, 1.0 μ L/mL (1/2MIC), and 2.0 μ L/mL (MIC). The antifungal activity was measured by the agar dilution method (Tao et al., 2014b). The cultures without Cys were used as the negative control.

Plasma Membrane Integrity

Plasma membrane integrity of the *P. digitatum* cells with citral (0 or 1/2MIC) were analyzed by propidium iodide (PI) staining coupled with fluorescence microscopy (Liu et al., 2010) with minor modifications. The 2-day-old mycelia from 50 mL PDB were collected and centrifuged at 4,000 g for 10 min. The collected mycelia were stained with 10 μ g/mL of PI for 15 min at 30°C. Residual dyes were removed by washing twice with PBS (pH 7.0). Samples were observed with an ECLIPSE TS100 microscope (Nikon, Japan), and the fluorescence value was determined by a F97 PRO fluorescence spectrophotometer (Lengguang Technology, Shanghai, China). These experiments were also performed with antioxidant Cys at a concentration of 10 μ M.

Statistical Analysis

All data were expressed as the mean \pm SD (standard deviation) by measuring three independent replicates and analyzed by one-way analysis of variance (ANOVA) followed by Duncan's multiple range test. A value of $P < 0.05$ was considered statistically significant, and data were analyzed using the SPSS statistical software package release 16.0 (SPSS Inc., Chicago, IL, USA).

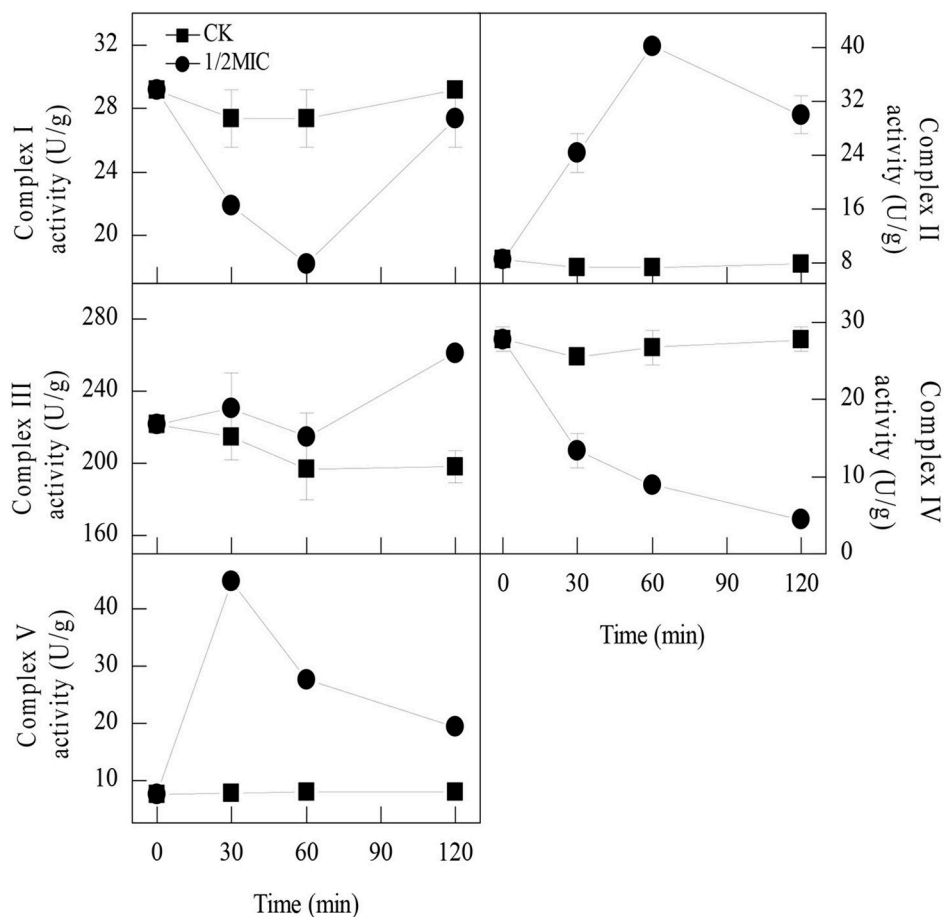


FIGURE 1 | Activities of the five enzymes involved in oxidative phosphorylation of *P. digitatum* mycelia. Data presented are the means of the pooled data. Error bars indicate the SDs of the means ($n = 3$).

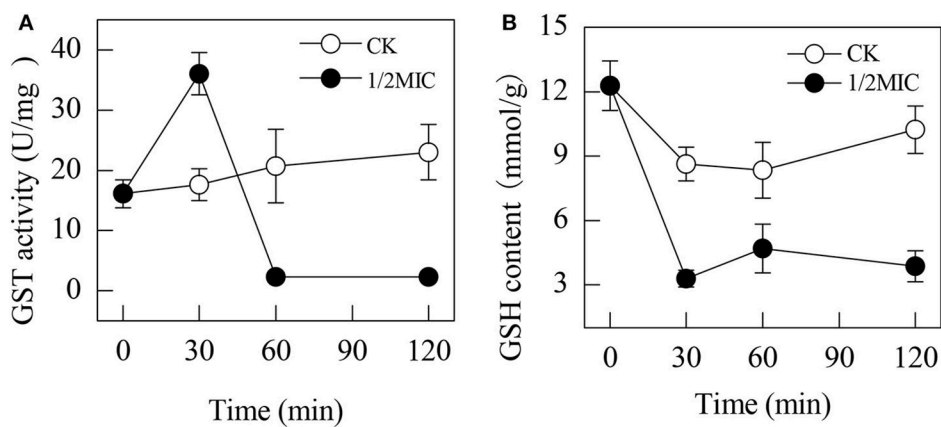


FIGURE 2 | Effects of citral on the GST activities (A) and GSH contents (B) of *P. digitatum* mycelia. Data presented are the means of the pooled data. Error bars indicate the SDs of the means ($n = 3$).

RESULTS

Proteins in *P. digitatum* Cells

Based on the iTRAQ-labeled peptides, a total of 3,251 proteins were isolated or identified. These proteins were further categorized into three GO ontologies, including biological processes, cellular components, and molecular functions. The most favored biological process was the “metabolic process” (29.34%), mainly consisting of the “cellular process” (27.35%) and “single-organism process” (10.70%) subcategories. A greater number of proteins were assigned to the cellular component category. The largest subclasses of proteins within this group were “cell” (24.69%) and “cell part” (24.69%). Categorization of the identified proteins on the basis of molecular function indicated that the most abundant proteins belonged to “catalytic activity” (47.28%) and “binding” classes (41.09%) (Table S1).

These proteins were further classified into 24 COG functional subcategories (Table S2). Most of these proteins were involved in “general function prediction only” (515 proteins), “translation, ribosomal structure and biogenesis” (298 proteins), and “posttranslational modification, protein turnover, chaperones”

(246 proteins). Only a few proteins were associated with “defense mechanisms” (17 proteins), “cell motility” (5 proteins), and “nuclear structure” (1 proteins). A total of 2,443 proteins were assigned to 107 KEGG pathways (Table S3). Among them, 708, 285, and 92 proteins were distributed to the metabolic pathway, biosynthesis of secondary metabolites, and purine metabolism, respectively. One protein that correlated with glycosaminoglycan degradation or caffeine metabolism was also found.

Differentially Expressed Proteins Induced by Citral

The difference in the protein expressions between CK30 and T30 was further analyzed. As a result, 125 proteins, including 41 up-regulated and 84 down-regulated proteins, were identified as DEPs. Among them, 82 DEPs were mapped to the KEGG database and assigned to 42 specific pathways, such as oxidative phosphorylation, endocytosis, ribosome, spliceosome, RNA degradation, ribosome biogenesis in eukaryotes, peroxisome, MAPK signaling pathway, glutathione metabolism, and cell cycle (Table 1 and Table S4).

Nineteen proteins related with the ribosome, RNA degradation, ribosome biogenesis in eukaryotes, spliceosome, basal transcription factors, RNA transport and mRNA surveillance pathway were affected by citral (Table 2, Tables S5, S6). Interestingly, the 60S ribosomal protein L35, the 60S ribosomal protein L35Ae, and the ribosomal protein S24 involved in ribosome were up-regulated after citral treatment, while the ribosomal protein L44e, 40S ribosomal protein S26E, 60S ribosomal protein L28, and 60S ribosomal protein L38 were down-regulated.

The expression pattern of the proteins related to energy and reactive oxygen species (ROS) were greatly influenced by the addition of citral (Table 2, Tables S5, S6). Approximately 12 mitochondrial proteins were found to be differentially expressed in response to 1/2MIC of citral. Among these DEPs, the succinate dehydrogenase (ubiquinone) flavoprotein subunit and GST, which were involved in the citrate cycle (TCA cycle) and glutathione metabolism, respectively, were both up-regulated. In addition, the rest of the enzymes that belong to oxidative phosphorylation that mainly participate in the electron transport chain and are located in the inner mitochondrial membrane were significantly affected by citral. For example, the following enzymes were down-regulated: acyl carrier protein (Ndufab1), LYR family protein (Ndubf9), NADH-ubiquinone oxidoreductase (Ndufs6) and hypothetical protein PDIP_56530 (Ndubf8), all of which constitute the mitochondrial complex I; cytochrome b-c1 complex subunit 6 (QCR6), which belongs to mitochondrial complex III; and cytochrome c oxidase polypeptide vib (COX6B) and cytochrome c oxidase copper chaperone Cox17 (COX17), which belong to mitochondrial complex IV. The following enzymes were up-regulated: succinate dehydrogenase cytochrome b560 subunit (SDHC), which belongs to mitochondrial complex II; hypothetical protein PDIP_64010 (QCR10), which belongs to mitochondrial complex III; and, ATP synthase delta chain, which belongs to mitochondrial complex V.

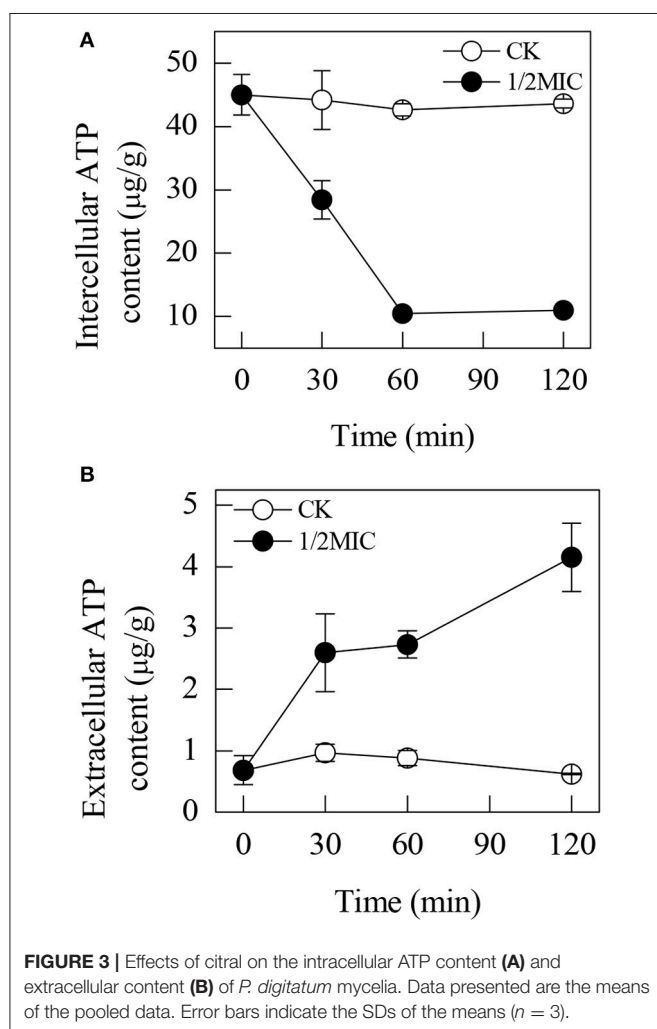


FIGURE 3 | Effects of citral on the intracellular ATP content (A) and extracellular ATP content (B) of *P. digitatum* mycelia. Data presented are the means of the pooled data. Error bars indicate the SDs of the means ($n = 3$).

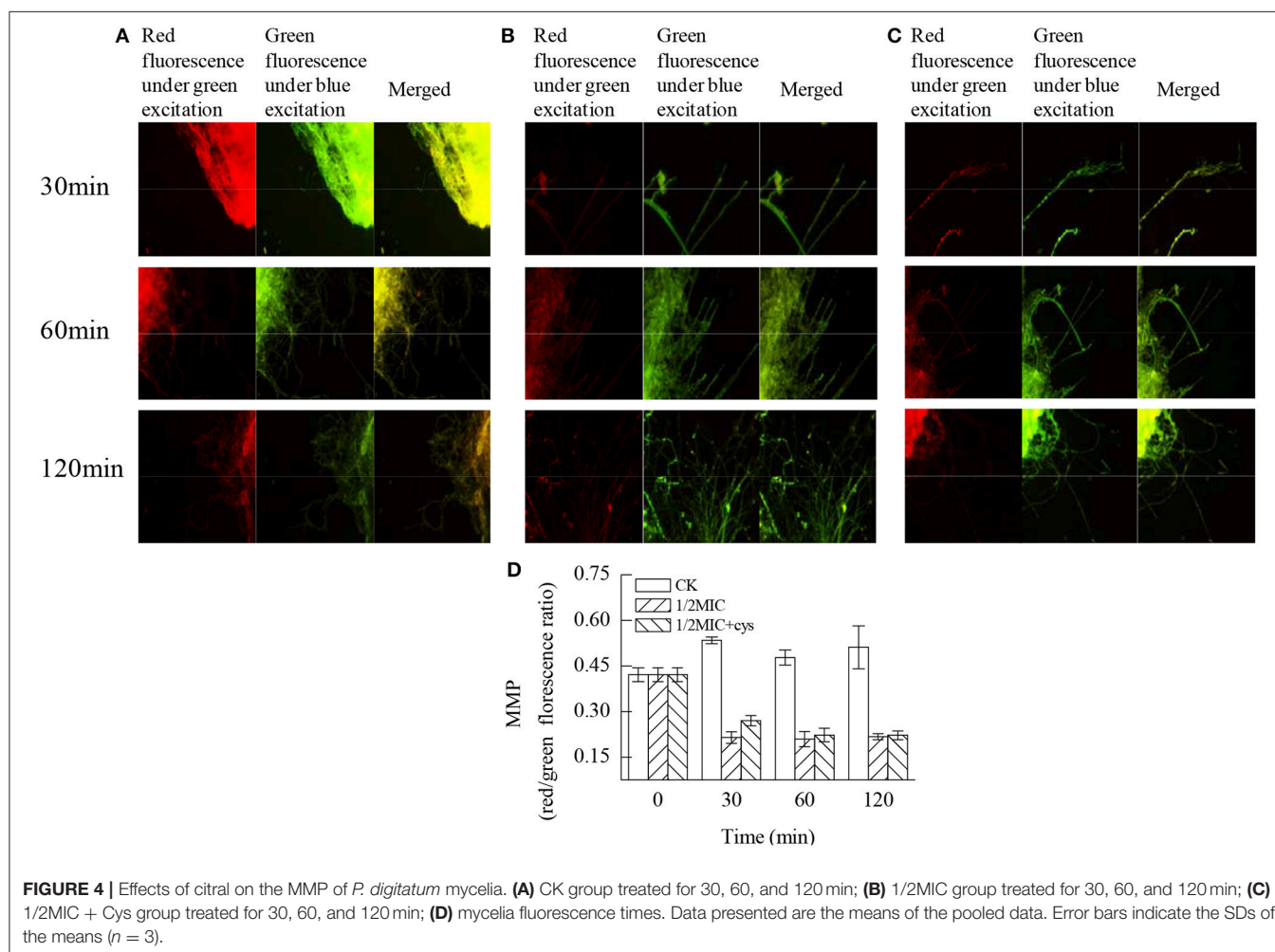
Mitochondrial Respiration Complexes Activities

The enzymatic activities of the mitochondrial respiration complexes were found to be consistent with those of the iTRAQ analysis. The mitochondrial complex I activity in the control samples remained relatively stable during the entire period. In contrast, the mitochondrial complex I activity in the samples treated with 1/2MIC of citral was sharply decreased at 60 min of exposure, with the values reaching 18.3 ± 0.0 U/g, which was significantly lower than that of the control sample (27.4 ± 1.8 U/g, $P < 0.05$; **Figure 1**). After 120 min of exposure, the mitochondrial complex I activity in the *P. digitatum* cells treated with 1/2MIC of citral was notably increased to 27.4 ± 1.8 U/g and no obvious difference between the treated and untreated cells was observed. The mitochondrial complex II and complex V activities in the citral treated samples were quite different from those of mitochondrial complex I. The mitochondrial complex II and complex V activities increased to peak values (40.1 ± 0.8 U/g, 44.9 ± 1.5 U/g) at 60 and 30 min of exposure, respectively, which were significantly higher than the control (7.3 ± 0.6 U/g, 7.7 ± 0.7 U/g). At 120 min, mitochondrial complex II and complex V activities in 1/2MIC of citral treated groups dropped to 29.9

± 2.8 U/g and 19.3 ± 0.4 U/g, respectively, which were still higher than the control sample (7.9 ± 0.0 U/g, 8.0 ± 1.1 U/g). In the case of the mitochondrial complex III, no difference in the activities between the 1/2MIC-treated samples and the control samples was observed before 60 min of exposure. After 120 min of exposure, the mitochondrial complex III activity in the control groups remained at a comparable level with the initial exposure, whereas its activity in 1/2MIC citral treated samples was induced and reached 261.0 ± 3.1 U/g. The mitochondrial complex IV activity was impaired by the addition of citral. Compared with the control samples, the mitochondrial complex IV activities in the 1/2MIC citral-treated samples decreased from 47.8 to 84.0% during citral exposure.

GST Activities and GSH Contents

The activity of GST was induced by the addition of citral during the initial 30 min (**Figure 2A**). At 30 min of exposure, the GST activity in the citral-treated sample was 36.03 ± 3.51 U/mg, which was higher than that of the control (17.63 ± 2.65 U/mg, $P < 0.05$). However, the activity of GST in *P. digitatum* cells with 1/2MIC of citral was suddenly decreased over the remaining period and



remained at a lower level compared to that of the control samples ($P < 0.05$).

The GSH content in the control samples was significantly higher than those of the citral treated samples (**Figure 2B**). In contrast, the GSH content in the citral-treated *P. digitatum* was significantly decreased ($P < 0.05$) from $12.3 \pm 1.2 \mu\text{mol/g}$ at the initial exposure to $3.2 \pm 0.4 \mu\text{mol/g}$ at 30 min of exposure, which was significantly lower than that in the control samples. After 30 min of exposure, the GSH contents in the 1/2MIC-treated *P. digitatum* cells maintained a relatively low level throughout the whole period.

ATP Contents

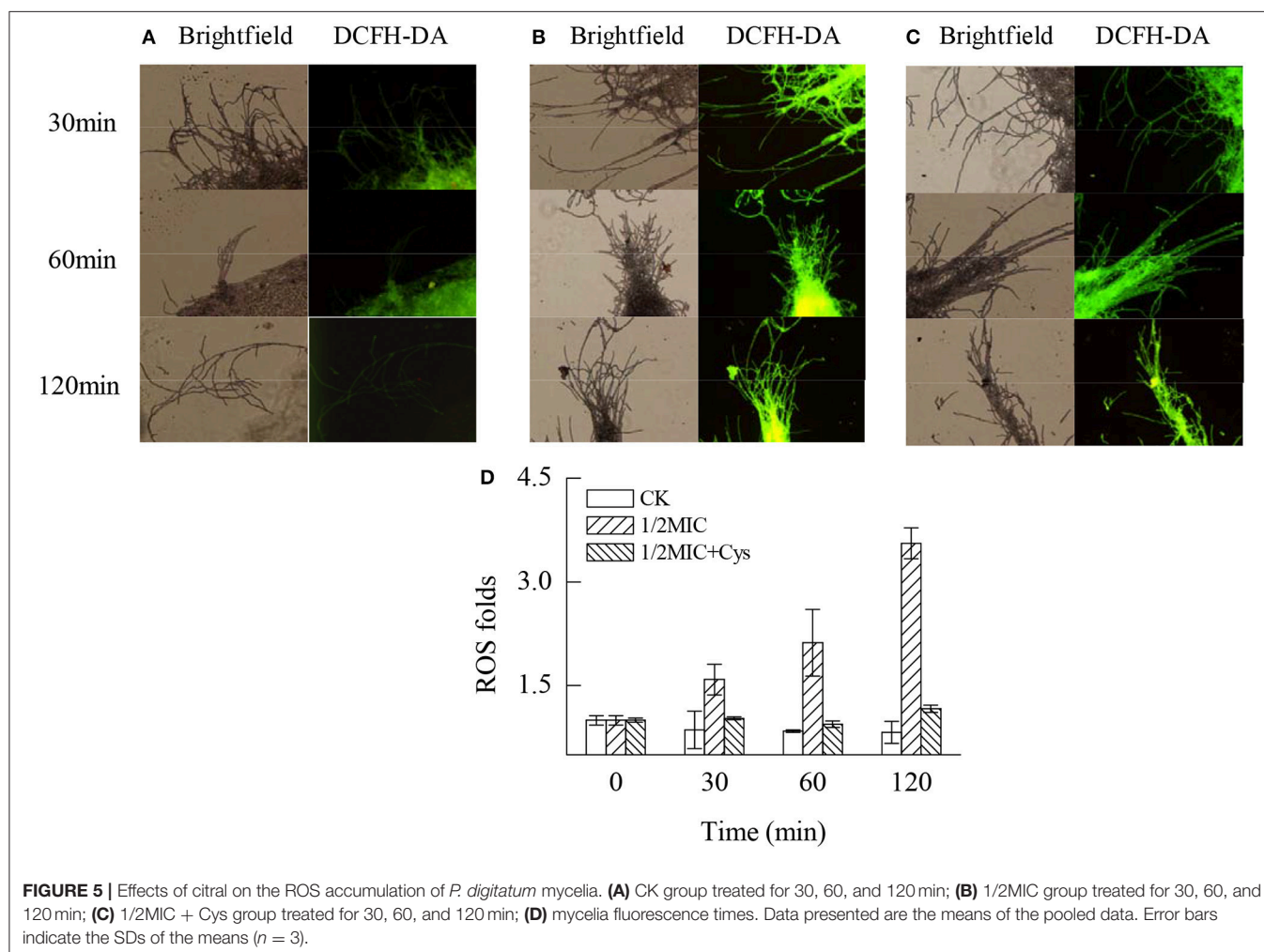
The intracellular ATP contents in the *P. digitatum* cells treated with citral continuously decreased during the entire period, whereas those in the untreated cells remained stable (**Figure 3A**). After incubation with 1/2MIC of citral for 30 min, the intracellular ATP content was $28.4 \pm 3.0 \mu\text{g/g}$, which was lower than that of the control ($44.2 \pm 4.6 \mu\text{g/g}$).

Citral exhibited an opposite effect on the extracellular ATP content (**Figure 3B**). After 30 min of exposure, the

extracellular ATP content in the control suspensions ($1.0 \pm 0.1 \mu\text{g/g}$) was lower than those treated with 1/2MIC treatments ($2.6 \pm 0.6 \mu\text{g/g}$). As the culture time increased, the extracellular ATP content sharply increased. At 120 min of exposure, the extracellular ATP content in the *P. digitatum* cells treated with 1/2MIC citral was $4.2 \pm 0.55 \mu\text{g/g}$, which was still much higher than that of the control samples ($0.6 \pm 0.0 \mu\text{g/g}$).

MMP

According to the data in **Figure 4**, citral induced an immediate decrease on the MMP ($P < 0.05$). In untreated cells, the red/green fluorescence ratio was 0.534 ± 0.011 at 30 min. However, the addition of citral caused an immediate loss of MMP, blocking JC-10 entry to the mitochondria, leaving the JC-10 monomers to fluoresce green within the cytoplasm. This finding was reflected in the red/green fluorescence ratio, which decreased to 0.214 ± 0.019 following citral treatment for 30 min and was significantly lower than that of the control sample ($P < 0.05$). Moreover, the addition of cysteine (Cys) could delay the reduction of MMP to a certain degree, with a red/green fluorescence ratio of $0.270 \pm$



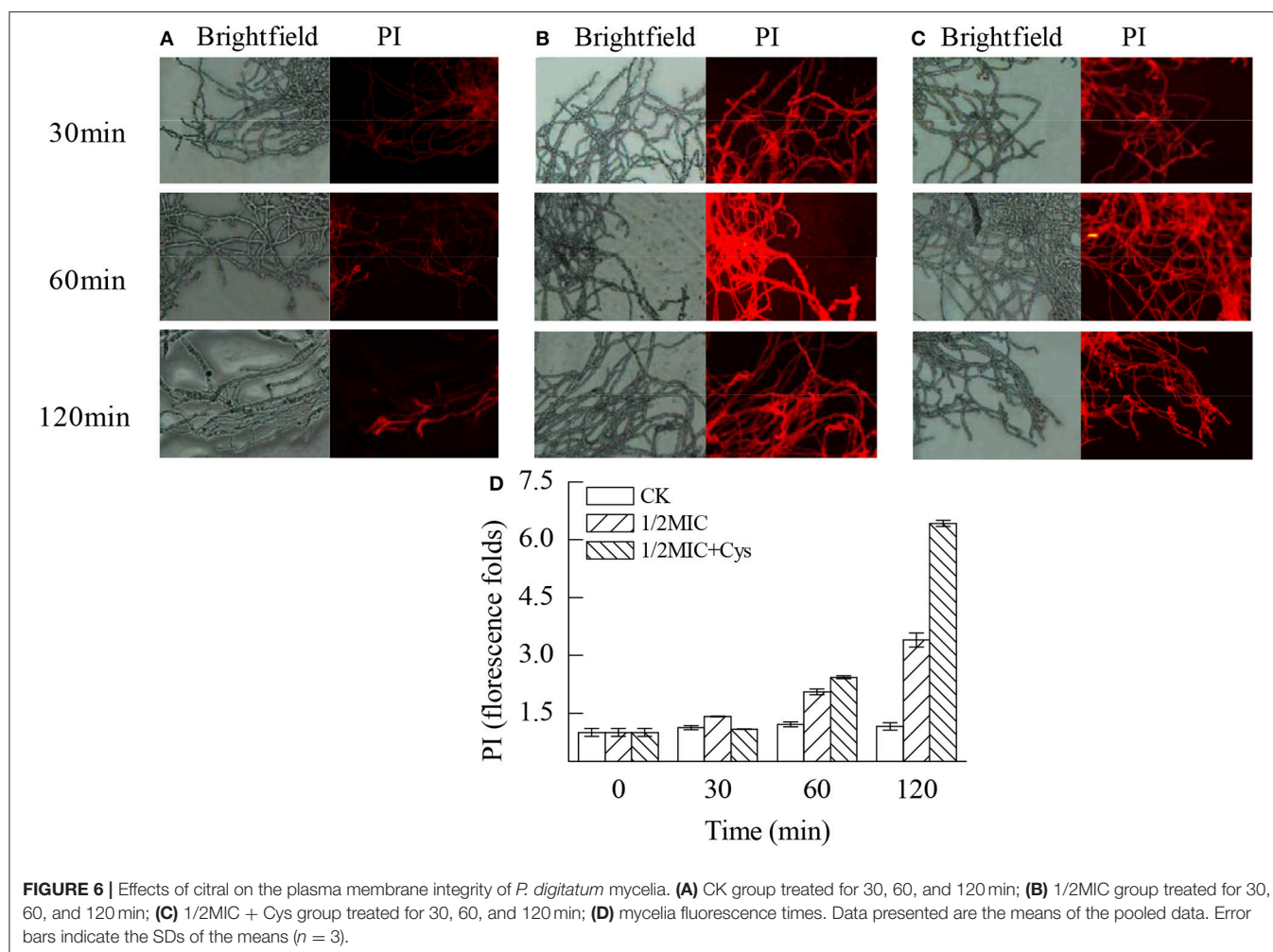


FIGURE 6 | Effects of citral on the plasma membrane integrity of *P. digitatum* mycelia. **(A)** CK group treated for 30, 60, and 120 min; **(B)** 1/2MIC group treated for 30, 60, and 120 min; **(C)** 1/2MIC + Cys group treated for 30, 60, and 120 min; **(D)** mycelia fluorescence times. Data presented are the means of the pooled data. Error bars indicate the SDs of the means ($n = 3$).

0.017 at 30 min, which was significantly higher ($P < 0.05$) than that in the citral treatment (Figure 4C).

ROS Levels

As illustrated by Figure 5, citral treatment significantly induced the massive accumulation of ROS in the *P. digitatum* mycelia ($P < 0.05$). After 120 min of exposure, the ROS levels in the *P. digitatum* mycelia treated with 1/2MIC of citral were 3.55-fold higher than that of the control (Figure 5D). In contrast, the ROS accumulation in *P. digitatum* cells induced by citral treatment was evidently repressed ($P < 0.05$) by the addition of Cys. These results were consistent with the results of the fluorescence microscopy (Figures 5A–C).

Plasma Membrane Integrity

The plasma membrane integrity of *P. digitatum* was markedly damaged by citral ($P < 0.05$; Figure 6). As revealed by Figure 6A, a slight red fluorescence was observed in the control hyphae. In contrast, the hyphae in Figure 6B had a strong red fluorescence. These results were consistent with the result of the fluorescence spectrophotometer that the fluorescence intensity of the 1/2MIC group was 3.4 times higher than the control groups after 120 min

treatment (Figure 6D, $P < 0.05$). Before treatment with 1/2MIC of citral + Cys for 30 min, hyphae exhibited relatively slight red fluorescence, indicating that the exposure to citral + Cys induced the permeation of PI in fewer cells (Figure 6C). After 60 min, the hyphae in the treatment group showed markedly higher ($P < 0.05$) staining intensity than that of the control group (Figure 6D).

Effect of Exogenous Cys on the Antifungal Activity of Citral against *P. digitatum*

The antifungal activity of citral against *P. digitatum* cells was alleviated by the addition of Cys (Table 3). After 2 days of culture with Cys, only 30.2 and 19.05% of the mycelial growths were inhibited by MIC and 1/2 MIC of citral, respectively. As similar phenomenon was also observed after 4 days of culture.

DISCUSSIONS

In the present study, a comprehensive proteome analysis was determined to study the antifungal mechanism of citral against

TABLE 3 | Effect of exogenous Cys on the antifungal activity of citral against *P. digitatum*.

Compound	Antifungal rate (%)			
	1d	2d	3d	4d
1.0 μ L/mL citral	37.5 \pm 0.0b	55.1 \pm 0.0b	16.1 \pm 2.0c	19.2 \pm 1.4b
1.0 μ L/mL citral + Cys	25.0 \pm 0.0c	19.05 \pm 0.0d	9.7 \pm 0.0d	8.4 \pm 1.0d
2.0 μ L/mL citral	100.0 \pm 0.0a	100.0 \pm 0.0a	32.2 \pm 2.0a	42.9 \pm 0.7a
2.0 μ L/mL citral + Cys	39.3 \pm 6.2b	30.2 \pm 3.6c	23.0 \pm 2.7b	10.5 \pm 0.0c

a–d Significant differences at $P < 0.05$ according to Duncan's multiple range test. Values are presented as the mean \pm SD.

P. digitatum. A total of 82 DEPs were identified in 1/2MIC citral-treated samples. These DEPs were mainly involved in oxidative phosphorylation, the TCA cycle, glycolysis and translationally related pathways, ribosome biogenesis in eukaryotes, the mRNA surveillance pathway, and RNA transport (Table 1), which were consistent with our previous results obtained by RNA-Seq analysis (OuYang et al., 2016b).

Oxidative phosphorylation is the primary source of the energy-producing pathway in eukaryotic cells, which is catalyzed by five mitochondrial complexes (I–V) (Chaban et al., 2014). A recent study has revealed that the antifungal activity of garlic oil against *C. albicans* was attributed to the severe disruption of oxidative phosphorylation (Li W. R. et al., 2016). In the current study, 10 DEPs involved in oxidative phosphorylation were obtained after citral treatment (Table 2). Among of these DEPs, three subunits of mitochondrial complex I (Ndufb9, Ndufs6, and Ndufb8), mitochondrial complex III (QCR6), and two subunits of mitochondrial complex IV (COX6B and COX17), were all down-regulated. In contrast, one subunit of mitochondrial complex II (SDHC) and QCR10 and the ATP synthase delta chain as well as the subunits belonging to the mitochondrial complex III and mitochondrial complex V, respectively, were all up-regulated. To confirm this finding, the enzymatic activities of the above five mitochondrial complex enzymes were further measured. After exposure to citral, the activities of mitochondrial complex I and complex IV were inhibited, whereas the activities of mitochondrial complex II, complex III and complex V were significantly induced ($P < 0.05$, Figure 1). These results were largely consistent with the iTRAQ results. It should be pointed out, however, that the DEPs comprising the mitochondrial complexes III exhibited an opposite expression pattern irrespective of the increased enzymatic activity of mitochondrial complexes III. This phenomenon could be explained by the fact that the enzymatic activities of proteins are generally determined by the coordination of different subunits (Buechler et al., 1991).

Mitochondrial oxidative phosphorylation constitutes the major cellular ATP-producing mechanism under aerobic conditions and hence plays an important role in maintaining the ATP levels in the cell. The function of oxidative phosphorylation is to synthesize ATP by generating a proton gradient within the inner mitochondrial membrane. Blocking or restraining oxidative phosphorylation can effectively decrease the ATP concentrations in the cell (Wang et al., 2015). In another study, the inhibitor of mitochondrial electron transport could

reduce MMP via inhibiting the proton-pumping function of the respiratory chain, leading to the reduction of ATP production and cell death (Kaim and Dimroth, 1999). In this study, a decrease in the content of intracellular ATP and an increase in the content of extracellular ATP were observed. Moreover, exposure to citral led to a significant decrease in the MMP (Figure 4). These observations indicated the existence of irreversible mitochondrial membrane damage, which would consequently lead to an efflux of ATP from the collapsed mitochondrial membrane and an increase in the extracellular ATP content. These results were also in agreement with our previous observations that citral treatment could lead to the morphological changes of mitochondria, the reduction of the ATP content and the inhibition of the TCA cycle in *P. digitatum* hyphae (Zheng et al., 2015). Similar results were reported in some earlier studies (Machado et al., 2012; Xia et al., 2013). It is worth noticing that the oxidative damage of mitochondrial proteins and the collapse of the MMP were generally supposed to be the result of undesirable accumulation of ROS, and the accumulation of ROS might affect the normal morphology and function of mitochondria (Genova et al., 2004; Fujita et al., 2014; Tian et al., 2016). Therefore, the above results indicated that the abnormal leakage of electrons from the mitochondrial respiratory chain might be caused by oxidative damage in fungal cells.

In fact, the mitochondrial respiratory chain is a major source of ROS (Tian et al., 2013). This process was highly regulated by mitochondrial complex I, complex II, and complex III (Finkel and Holbrook, 2000; Tian et al., 2013). In addition, the inhibition of mitochondrial complex IV could lead to the incompletely catalysis of oxygen, resulting in the generation of ROS through mitochondrial complex I or complex III (Semenza, 2007). Previous studies have demonstrated that the antifungal action of some essential oils, such as dill oil, *Curcuma longa* oil and thymol, were positively related with the accumulation of ROS (Tian et al., 2012; Kumar et al., 2016; Shen et al., 2016). Similarly, higher fluorescence values were exclusively observed in the 1/2MIC citral treated samples. This phenomenon was obvious with the increasing of the exposure time (Figure 5). This result is consistent with our previous study suggesting that citral could induce the massive accumulation of H_2O_2 in *P. digitatum* and lead to lipid peroxidation via oxidation burst (OuYang et al., 2016a).

Normally, the balance between ROS production and antioxidant defenses determines the degree of oxidative stress.

Our previous study found that the addition of citral resulted in oxidative stress by stimulating the activities of lipoxygenase and peroxidase in *P. digitatum* (OuYang et al., 2016a). In this study, the up-regulation of GST, a key enzyme involved in glutathione metabolism, also supported this point of view, whose activity was significantly increased after the addition of citral ($P < 0.05$; **Figure 2A**). The significant decrease in the GSH content ($P < 0.05$; **Figure 2B**) further confirmed this hypothesis. In a previous study, citral was illustrated to be able to stimulate the activity of GST in RL34 cells, whereas geraniol treatment could attenuate the intracellular GSH level, and this process was accompanied with the increasing ROS content (Nakamura et al., 2003). Similar results were also reported in some other investigations (Guha et al., 2011; Pramanik et al., 2011). These results again suggested that citral addition could lead to the oxidative damage of *P. digitatum* hyphae.

It is generally accepted that the accumulation of ROS will result in the breakdown of the normal cellular, membrane and reproductive functions by oxidizing lipids, proteins, nucleic acids, and carbohydrates (Qin et al., 2007; Tian et al., 2012, 2013). In this study, the plasma membrane integrity was also positively correlated with the accumulation of ROS. As revealed by **Figure 6**, exposure to 1/2MIC of citral apparently induced a severe plasma membrane lesion, as convinced by the results of PI staining. Accordingly, this process was accompanied by the massive accumulation of ROS (**Figure 5**).

Application of exogenous antioxidants could maintain ROS at the basal level and repair cellular damage caused by ROS (Lai et al., 2011; Tian et al., 2013). Liu et al. (2013) reported that the addition of antioxidant Cys could significantly reduce the detrimental effects of D-limonene on *S. cerevisiae*. To further confirm the oxidative damage of *P. digitatum* hyphae, Cys was added to the culture media. Cys is the rate-limiting precursor for the synthesis of GSH and is also the preeminent antioxidant of the cell (Tian et al., 2013). Cys could prevent the accumulation of ROS and alleviate the oxidative damage of cells. As shown in **Table 3**, addition of exogenous Cys significantly reduced the

antifungal activity of citral against *P. digitatum*. In addition, Cys maintained the basal ROS level (**Figure 5**), and deferred the decrease of MMP (**Figure 4**) and the membrane damage in citral treated samples (**Figure 6D**). These results indicated that ROS might serve as a mediator in regulating the antifungal activity of citral against *P. digitatum*.

Taken together, our present study suggests that the antifungal activity of citral against *P. digitatum* is caused by damaged oxidative phosphorylation through massive ROS accumulation. These findings not only provide a better understanding of antifungal mechanism of plant essential oils but also provide important theoretical guidance for the development of novel fungicides, reducing the postharvest decay of fruits in the future.

AUTHOR CONTRIBUTIONS

NT designed research; QO performed research; NT and QO analyzed data; QO, NT and MZ wrote the paper. All authors contributed to study design and provided input on the manuscript preparation. All authors have given approval to the final version of the manuscript.

FUNDING

This study was supported by the National Natural Science Foundation of China (Nos. 31772364 and 31271964), Collaborative Innovation Center of New Chemical Technologies for Environmental Benignity and Efficient Resource Utilization, Research Foundation of Education Bureau of Hunan Province (No. 15A181), Hunan Provincial Natural Science Foundation of China (No. 2017JJ2247) and Hunan Provincial Innovation Foundation for Postgraduate (No. CX2016B266).

SUPPLEMENTARY MATERIAL

The Supplementary Material for this article can be found online at: <https://www.frontiersin.org/articles/10.3389/fmicb.2018.00239/full#supplementary-material>

REFERENCES

- Boubaker, H., Karim, H., El Hamdaoui, A., Msanda, F., Leach, D., Bombarda, I., et al. (2016). Chemical characterization and antifungal activities of four *Thymus* species essential oils against postharvest fungal pathogens of citrus. *Ind. Crop. Prod.* 86, 95–101. doi: 10.1016/j.indcrop.2016.03.036
- Bradford, M. (1976). A rapid and sensitive method for the quantitation of microgram quantities of protein utilizing the principle of protein-dye binding. *Anal. Biochem.* 6, 3171–3188. doi: 10.1016/0003-2697(76)90527-3
- Buechler, W. A., Nakane, M., and Murad, F. (1991). Expression of soluble guanylate cyclase activity requires both enzyme subunits. *Biochem. Biophys. Res. Commun.* 174, 351–357. doi: 10.1016/0006-291X(91)90527-E
- Chaban, Y., Boekema, E. J., and Dudkina, N. V. (2014). Structures of mitochondrial oxidative phosphorylation supercomplexes and mechanisms for their stabilisation. *BBA-Bioenergetics*. 1837, 418–426. doi: 10.1016/j.bbabi.2013.10.004
- Fan, F., Tao, N. G., Jia, L., and He, X. L. (2014). Use of citral incorporated in postharvest wax of citrus fruit as a botanical fungicide against *Penicillium digitatum*. *Postharvest Biol. Technol.* 90, 52–55. doi: 10.1016/j.postharvbio.2013.12.005
- Finkel, T., and Holbrook, N. J. (2000). Oxidants, oxidative stress and the biology of ageing. *Nature* 408, 239–247. doi: 10.1038/35041687
- Fujita, K., Tatsumi, M., Ogita, A., Kubo, I., and Tanaka, T. (2014). Anethole induces apoptotic cell death accompanied by reactive oxygen species production and DNA fragmentation in *Aspergillus fumigatus* and *Saccharomyces cerevisiae*. *FEBS J.* 281, 1304–1313. doi: 10.1111/febs.12706
- Genova, M. L., Pich, M. M., and Bernacchia, A. (2004). The mitochondrial production of reactive oxygen species in relation to aging and pathology. *Ann. N.Y. Acad. Sci.* 4, 86–100. doi: 10.1196/annals.1293.010
- Guha, P., Dey, A., Sen, R., Chatterjee, M., Chattopadhyay, S., and Bandyopadhyay, S. K. (2011). Intracellular GSH depletion triggered mitochondrial Bax translocation to accomplish resveratrol-induced apoptosis in the U937 cell line. *J. Pharmacol. Exp. Ther.* 336, 206–214. doi: 10.1124/jpet.110.171983
- Harris, R. (2002). Progress with superficial mycoses using essential oils. *Int. J. Aromather.* 12, 83–91. doi: 10.1016/S0962-4562(02)00032-2
- Jing, L., Lei, Z., Li, L., Xie, R., Xi, W., Guan, Y., et al. (2014). Antifungal activity of citrus essential oils. *J. Agr. Food Chem.* 62, 3011–3033. doi: 10.1021/jf5006148

- Kaim, G., and Dimroth, P. (1999). ATP synthesis by F-type ATP synthase is obligatorily dependent on the transmembrane voltage. *EMBO J.* 18, 4118–4127. doi: 10.1093/emboj/18.15.4118
- Kumar, K. N., Venkataramana, M., Allen, J. A., Chandranayaka, S., Murali, H. S., and Batra, H. V. (2016). Role of *Curcuma longa* L. essential oil in controlling the growth and zearalenone production of *Fusarium graminearum*. *LWT-Food Sci. Technol.* 69, 522–528. doi: 10.1016/j.lwt.2016.02.005
- Lackner, D. H., Schmidt, M. W., Wu, S., Wolf, D. A., and Bähler, J. (2012). Regulation of transcriptome, translation, and proteome in response to environmental stress in fission yeast. *Genome Biol.* 13:R25. doi: 10.1186/gb-2012-13-4-r25
- Lai, T., Li, B., Qin, G., and Tian, S. (2011). Oxidative damage involves in the inhibitory effect of nitric oxide on spore germination of *Penicillium expansum*. *Curr. Microbiol.* 62, 229–234. doi: 10.1007/s00284-010-9695-1
- Leite, M. C. A., de Brito Bezerra, A. P., de Sousa, J. P., and de Oliveira Lima, E. (2014). Investigating the antifungal activity and mechanism(s) of geraniol against *Candida albicans* strains. *Med. Mycol.* 53, 275–284. doi: 10.1093/mmy/myu078
- Li, W. R., Shi, Q. S., Dai, H. Q., Liang, Q., Xie, X. B., Huang, X. M., et al. (2016). Antifungal activity, kinetics and molecular mechanism of action of garlic oil against *Candida albicans*. *Sci. Rep.* 6:22805. doi: 10.1038/srep22805
- Li, Y., Shao, X., Xu, J., Wei, Y., Xu, F., and Wang, H. (2016). Effects and possible mechanism of tea tree oil against *Botrytis cinerea* and *Penicillium expansum* in vitro and in vivo test. *Can. J. Microbiol.* 63, 219–227. doi: 10.1139/cjm-2016-0553
- Liu, J. D., Zhu, Y. B., Du, G. C., Zhou, J. W., and Cheng, J. (2013). Response of *Saccharomyces cerevisiae* to D-limonene-induced oxidative stress. *Appl. Microbiol. Biot.* 97, 6467–6475. doi: 10.1007/s00253-013-4931-9
- Liu, J. Y., Men, J. L., Chang, M. C., Feng, C. P., and Yuan, L. G. (2017). iTRAQ-based quantitative proteome revealed metabolic changes of *Flammulina velutipes* mycelia in response to cold stress. *J. Proteomics* 156, 75–84. doi: 10.1016/j.jprot.2017.01.009
- Liu, J., Zong, Y., Qin, G., Li, B., and Tian, S. (2010). Plasma membrane damage contributes to antifungal activity of silicon against *Penicillium digitatum*. *Curr. Microbiol.* 61, 274–279. doi: 10.1007/s00284-010-9607-4
- Machado, M., Pires, P., Dinis, A. M., Santos-Rosa, M., Alves, V., Salgueiro, L., et al. (2012). Monoterpenic aldehydes as potential anti-*Leishmania* agents: activity of *Cymbopogon citratus* and citral on *L. infantum*, *L. tropica* and *L. major*. *Exp. Parasitol.* 130, 223–231. doi: 10.1016/j.exppara.2011.12.012
- Nakamura, Y., Miyamoto, M., Murakami, A., Ohigashi, H., Osawa, T., and Uchida, K. (2003). A phase II detoxification enzyme inducer from lemongrass: identification of citral and involvement of electrophilic reaction in the enzyme induction. *Biochem. Bioph. Res. Co.* 302, 593–600. doi: 10.1016/S0006-291X(03)00219-5
- OuYang, Q. L., Jia, L., and Tao, N. G. (2016a). Citral inhibits mycelial growth of *Penicillium digitatum* involving membrane peroxidation. *Food Sci.* 37, 32–37. doi: 10.7506/spkx1002-6630-201623006
- OuYang, Q. L., Tao, N. G., and Jing, G. X. (2016b). Transcriptional profiling analysis of *Penicillium digitatum*, the causal agent of citrus green mold, unravels an inhibited ergosterol biosynthesis pathway in response to citral. *BMC Genomics* 17:599. doi: 10.1186/s12864-016-2943-4
- Park, M. J., Gwak, K. S., Yang, I., Kim, K. W., Jeung, E. B., Chang, J. W., et al. (2009). Effect of citral, eugenol, nerolidol and α -terpineol on the ultrastructural changes of *Trichophyton mentagrophytes*. *Fitoterapia* 80, 290–296. doi: 10.1016/j.fitote.2009.03.007
- Pérez-Alfonso, C. O., Martínez-Romero, D., Zapata, P. J., Serrano, M., Valero, D., and Castillo, S. (2012). The effects of essential oils carvacrol and thymol on growth of *Penicillium digitatum* and *P. italicum* involved in lemon decay. *Int. J. Food Microbiol.* 158, 101–106. doi: 10.1016/j.ijfoodmicro.2012.07.002
- Pramanik, K. C., Boreddy, S. R., and Srivastava, S. K. (2011). Role of mitochondrial electron transport chain complexes in capsaicin mediated oxidative stress leading to apoptosis in pancreatic cancer cells. *PLoS ONE* 6:e20151. doi: 10.1371/journal.pone.0020151
- Qin, G., Tian, S., Chan, Z., and Li, B. (2007). Crucial role of antioxidant proteins and hydrolytic enzymes in pathogenicity of *Penicillium expansum* analysis based on proteomics approach. *Mol. Cell Proteomic.* 6, 425–438. doi: 10.1074/mcp.M600179-MCP200
- Rajput, S. B., and Karuppayil, S. M. (2013). Small molecules inhibit growth, viability and ergosterol biosynthesis in *Candida albicans*. *Springerplus* 2:26. doi: 10.1186/2193-1801-2-26
- Redding, A. M., Mukhopadhyay, A., Joyner, D. C., Hazen, T. C., and Keasling, J. D. (2006). Study of nitrate stress in *Desulfovibrio vulgaris* Hildenborough using iTRAQ proteomics. *Brief. Funct. Genomics* 5, 133–143. doi: 10.1093/bfpg/ell025
- Semenza, G. L. (2007). Oxygen-dependent regulation of mitochondrial respiration by hypoxia-inducible factor 1. *Biochem. J.* 405, 1–9. doi: 10.1042/BJ20070389
- Shao, X. F., Cao, B. Y., Xu, F., Xie, S. H., Yu, D. D., and Wang, H. F. (2015). Effect of postharvest application of chitosan combined with clove oil against citrus green mold. *Postharvest Biol. Technol.* 99, 37–43. doi: 10.1016/j.postharvbio.2014.07.014
- Shen, Q., Zhou, W., Li, H., Hu, L., and Mo, H. (2016). ROS involves the fungicidal actions of thymol against spores of *Aspergillus flavus* via the induction of nitric oxide. *PLoS ONE* 11:e0155647. doi: 10.1371/journal.pone.0155647
- Tao, N. G., Jia, L., and Zhou, H. E. (2014a). Anti-fungal activity of *Citrus reticulata* Blanco essential oil against *Penicillium italicum* and *Penicillium digitatum*. *Food Chem.* 153, 265–271. doi: 10.1016/j.foodchem.2013.12.070
- Tao, N. G., OuYang, Q. L., and Jia, L. (2014b). Citral inhibits mycelial growth of *Penicillium italicum* by a membrane damage mechanism. *Food Control* 41, 116–121. doi: 10.1016/j.foodcont.2014.01.010
- Tao, N. G., Zheng, S. J., Jing, G. X., and Wang, X. (2015). Effects of citral on glycolysis of *Penicillium digitatum*. *Modern Food Sci. Technol.* 12:026. doi: 10.13982/j.mfst.1673-9078.2015.12.026
- Taylor, R. D., Saparno, A., Blackwell, B., Anoop, V., Gledie, S., and Tinker, N. A. (2008). Proteomic analyses of *Fusarium graminearum* grown under mycotoxin-inducing conditions. *Proteomics* 8, 2256–2265. doi: 10.1002/pmic.200700610
- Tian, J., Ban, X., Zeng, H., He, J., Chen, Y., and Wang, Y. (2012). The mechanism of antifungal action of essential oil from dill (*Anethum graveolens* L.) on *Aspergillus flavus*. *PLoS ONE* 7:e30147. doi: 10.1371/journal.pone.0030147
- Tian, J., Wang, Y., Lu, Z., Sun, C., Zhang, M., Zhu, A., et al. (2016). Perillaldehyde, a promising antifungal agent used in food preservation, triggers apoptosis through a metacaspase-dependent pathway in *Aspergillus flavus*. *J. Agr. Food Chem.* 64, 7404–7413. doi: 10.1021/acs.jafc.6b03546
- Tian, J., Wang, Y., Zeng, H., Li, Z., Zhang, P., Tessema, A., et al. (2015). Efficacy and possible mechanisms of perillaldehyde in control of *Aspergillus niger* causing grape decay. *Int. J. Food Microbiol.* 202, 27–34. doi: 10.1016/j.ijfoodmicro.2015.02.022
- Tian, S., Qin, G., and Li, B. (2013). Reactive oxygen species involved in regulating fruit senescence and fungal pathogenicity. *Plant Mol. Biol.* 82, 593–602. doi: 10.1007/s11103-013-0035-2
- Wang, L., Zhang, J. H., Cao, Z. L., Wang, Y. J., Gao, Q., Zhang, J., et al. (2015). Inhibition of oxidative phosphorylation for enhancing citric acid production by *Aspergillus niger*. *Microb. Cell Fact.* 14:7. doi: 10.1186/s12934-015-0190-z
- Wuryatmo, E., Able, A. J., Ford, C. M., and Scott, E. S. (2014). Effect of volatile citral on the development of blue mould, green mould and sour rot on navel orange. *Australas. Plant Path.* 43, 403–411. doi: 10.1007/s13313-014-0281-z
- Wuryatmo, E., Klieber, A., and Scott, E. S. (2003). Inhibition of citrus postharvest pathogens by vapor of citral and related compounds in culture. *J. Agr. Food Chem.* 51, 2637–2640. doi: 10.1021/jf026183l
- Xia, H., Liang, W., Song, Q., Chen, X., Chen, X., and Hong, J. (2013). The in vitro study of apoptosis in NB4 cell induced by citral. *Cytotechnology* 65, 49–57. doi: 10.1007/s10616-012-9453-2
- Yang, W., Ding, D., Zhang, C., Zhou, J., and Su, X. (2015). iTRAQ-based proteomic profiling of *Vibrio parahaemolyticus* under various culture conditions. *Proteome Sci.* 13:19. doi: 10.1186/s12953-015-0075-4
- Zhang, F., Zhong, H., Han, X., Guo, Z., Yang, W., Liu, Y., et al. (2015). Proteomic profile of *Aspergillus flavus* in response to water activity. *Fungal Biol.* 119, 114–124. doi: 10.1016/j.funbio.2014.11.005

- Zheng, S. J., Jing, G. X., Wang, X., Ouyang, Q. L., Jia, L., and Tao, N. G. (2015). Citral exerts its antifungal activity against *Penicillium digitatum* by affecting the mitochondrial morphology and function. *Food Chem.* 178, 76–81. doi: 10.1016/j.foodchem.2015.01.077
- Zhou, H. E., Tao, N. G., and Jia, L. (2014). Antifungal activity of citral, octanal and α -terpineol against *Geotrichum citri-aurantii*. *Food Control* 37, 277–283. doi: 10.1016/j.foodcont.2013.09.057
- Zieske, L. R. (2006). A perspective on the use of iTRAQTM reagent technology for protein complex and profiling studies. *J. Exp. Bot.* 57, 1501–1508. doi: 10.1093/jxb/erj168

Conflict of Interest Statement: The authors declare that the research was conducted in the absence of any commercial or financial relationships that could be construed as a potential conflict of interest.

Copyright © 2018 OuYang, Tao and Zhang. This is an open-access article distributed under the terms of the Creative Commons Attribution License (CC BY). The use, distribution or reproduction in other forums is permitted, provided the original author(s) and the copyright owner are credited and that the original publication in this journal is cited, in accordance with accepted academic practice. No use, distribution or reproduction is permitted which does not comply with these terms.



Genome Sequence, Assembly and Characterization of Two *Metschnikowia fructicola* Strains Used as Biocontrol Agents of Postharvest Diseases

Edoardo Piombo^{1,2†}, Noa Sela^{3†}, Michael Wisniewski⁴, Maria Hoffmann⁵, Maria L. Gullino^{1,2}, Marc W. Allard⁵, Elena Levin⁶, Davide Spadaro^{1,2} and Samir Drobby^{6*}

¹ Department of Agricultural, Forestry and Food Sciences, University of Torino, Turin, Italy, ² Centre of Competence for the Innovation in the Agro-environmental Sector, University of Torino, Turin, Italy, ³ Department of Plant Pathology and Weed Research, Agricultural Research Organization, Volcani Center, Rishon LeZion, Israel, ⁴ United States Department of Agriculture – Agricultural Research Service, Kenersville, WV, United States, ⁵ Division of Microbiology, United States Food and Drug Administration, College Park, MD, United States, ⁶ Department of Postharvest Science, Agricultural Research Organization, Volcani Center, Rishon LeZion, Israel

OPEN ACCESS

Edited by:

Boqiang Li,
Institute of Botany (CAS), China

Reviewed by:

Raffaello Castoria,
University of Molise, Italy
Xiaoyun Zhang,
Jiangsu University, China

*Correspondence:

Samir Drobby
samird@volcani.agri.gov.il

[†] These authors have contributed
equally to this work.

Specialty section:

This article was submitted to
Food Microbiology,
a section of the journal
Frontiers in Microbiology

Received: 06 January 2018

Accepted: 15 March 2018

Published: 03 April 2018

Citation:

Piombo E, Sela N, Wisniewski M, Hoffmann M, Gullino ML, Allard MW, Levin E, Spadaro D and Drobby S (2018) Genome Sequence, Assembly and Characterization of Two *Metschnikowia fructicola* Strains Used as Biocontrol Agents of Postharvest Diseases. *Front. Microbiol.* 9:593. doi: 10.3389/fmicb.2018.00593

The yeast *Metschnikowia fructicola* was reported as an efficient biological control agent of postharvest diseases of fruits and vegetables, and it is the bases of the commercial formulated product “Shemer.” Several mechanisms of action by which *M. fructicola* inhibits postharvest pathogens were suggested including iron-binding compounds, induction of defense signaling genes, production of fungal cell wall degrading enzymes and relatively high amounts of superoxide anions. We assembled the whole genome sequence of two strains of *M. fructicola* using PacBio and Illumina shotgun sequencing technologies. Using the PacBio, a high-quality draft genome consisting of 93 contigs, with an estimated genome size of approximately 26 Mb, was obtained. Comparative analysis of *M. fructicola* proteins with the other three available closely related genomes revealed a shared core of homologous proteins coded by 5,776 genes. Comparing the genomes of the two *M. fructicola* strains using a SNP calling approach resulted in the identification of 564,302 homologous SNPs with 2,004 predicted high impact mutations. The size of the genome is exceptionally high when compared with those of available closely related organisms, and the high rate of homology among *M. fructicola* genes points toward a recent whole-genome duplication event as the cause of this large genome. Based on the assembled genome, sequences were annotated with a gene description and gene ontology (GO term) and clustered in functional groups. Analysis of CAZymes family genes revealed 1,145 putative genes, and transcriptomic analysis of CAZyme expression levels in *M. fructicola* during its interaction with either grapefruit peel tissue or *Penicillium digitatum* revealed a high level of CAZyme gene expression when the yeast was placed in wounded fruit tissue.

Keywords: postharvest pathology, biocontrol agent, fungi, genome assembly, genome annotation, plant pathogen interactions

INTRODUCTION

The yeast *Metschnikowia fructicola* (type strain NRRL Y-27328, CBS 8853) was first isolated from grapes and identified as a new species by Kurtzman and Droby (2001). The identification was achieved by comparing its nucleotide sequence in the species-specific ca. 500–600-nucleotide D1/D2 domain of 26S ribosomal DNA (rDNA) with a database of D1/D2 sequences from all the recognized ascomycetous yeasts available at that time (Kurtzman and Robnett, 1998), and subsequent entries in GenBank.

Yeasts have been identified by many workers as potential biological control agents suitable for the prevention of postharvest diseases, especially since they are naturally occurring on fruits and vegetables, and exhibit a number of traits that favor their use as fungal antagonists. These traits include high tolerance to environmental stresses (low and high temperatures, desiccation, wide fluctuations in relative humidity, low oxygen levels, pH fluctuations, UV radiation) encountered during fruit and vegetable production before and after harvest, and their ability to adapt to the micro-environment present in wounded fruit tissues, characterized by high sugar concentration, high osmotic pressure, low pH and conditions that conducive to oxidative stress. These traits are especially beneficial for their use as biocontrol agents, since the majority of postharvest decay pathogens are necrotrophic and infect fruit through wounded tissues (Droby et al., 2016; Wisniewski et al., 2016). Additionally, many yeast species can grow rapidly on inexpensive substrates in fermenters, traits that are conducive to their large-scale commercial production and use (Spadaro and Droby, 2016). Moreover, in contrast to filamentous fungi, the vast majority of naturally occurring yeasts do not produce allergenic spores or mycotoxins, and have simple nutritional requirements that enable them to colonize dry surfaces for long periods of time (Spadaro et al., 2008).

Significant progress has been made in the development, registration and commercialization of postharvest biocontrol products (Droby et al., 2009, 2016) and a variety of different biocontrol agents have reached advanced stages of development and commercialization. “Shemer,” based on the yeast *M. fructicola* (Droby et al., 2009), is one of the commercial products that has reached the market.

Several studies have documented the biocontrol efficacy of *M. fructicola* and its ability to prevent or limit the infection of harvested products by postharvest pathogens (Karabulut et al., 2003, 2004; Spadaro et al., 2013). Similar to other postharvest biocontrol agents, *M. fructicola* exhibits several modes of action to achieve its ability to act as an antagonist. Like its sister species *M. pulcherrima*, *M. fructicola* produces the red pigment, pulcherrimin, which is formed non-enzymatically from pulcherriminic acid and ferric ions (Sipiczki, 2006). Pulcherrimin has been reported to play a role in the control of *Botrytis cinerea*, *Alternaria alternata*, and *Penicillium expansum* on apple (Saravanakumar et al., 2008). Enhanced expression of several genes involved in defense signaling, including PRP genes and MAPK cascade genes was demonstrated in grapefruit when surface wounds were treated with *M. fructicola* cells (Hershkovitz et al., 2012). The enhanced gene expression was consistent

with an induced resistance response suggesting that induced host resistance plays a role in the biocontrol of *M. fructicola* against postharvest pathogens such as *P. digitatum* (Hershkovitz et al., 2012). *M. fructicola* also exhibits chitinase activity and the chitinase gene, *MfChi*, was demonstrated to be highly induced in yeast cells when cell walls of *Monilinia fructicola*, the causal agent of brown rot in stone fruit, was added to the growth medium. These data suggest that *MfChi* may also play a role in the biocontrol activity exhibited by *Metschnikowia* species (Banani et al., 2015). Macarasin et al. (2010) demonstrated that yeast antagonists, including *M. fructicola*, used to control postharvest diseases have the ability to produce relatively high amounts of superoxide anions. They also demonstrated that yeast cells applied to surface wounds of fruits produce greater levels of superoxide anions than yeast grown *in vitro* in artificial media.

Several studies have examined differential gene expression during the interaction of the yeast *M. fructicola* with host fruit tissue or with the mycelium of the postharvest pathogen *P. digitatum* (Hershkovitz et al., 2012, 2013). Due to the lack of an assembled genome sequence, de-novo assembly of the transcriptome of *M. fructicola* was performed, which resulted in the identification of 9,674 unigenes, half of which could be annotated based on homology to genes in the NCBI database (Hershkovitz et al., 2013). Approximately, 69% of the unigene sequences identified in *M. fructicola* showed high homology to genes of the yeast *Clavispora lusitaniae*. Thus, the RNA-Seq-based transcriptome analysis generated a large number of newly identified *M. fructicola* yeast genes and significantly increased the number of sequences available for *Metschnikowia* species in the NCBI database. Shotgun sequencing data enabled to construct a draft genome of *M. fructicola* based on Illumina paired-end assembly with ~7000 contigs that was submitted to Genbank (Hershkovitz et al., 2013).

Details about the structure and annotation of the genomes of yeast biocontrol agents are lacking. Such information would be a valuable tool for analyzing the sequences of putative “biocontrol-related” genes among different species of yeast biocontrol agents, characterizing gene clusters with known and unknown functions, as well as studying global changes in gene transcription rather than just specific, targeted genes. Obtaining full genome sequences would also allow comparative genomic analyses to be conducted among closely related yeast species that do not exhibit antagonist properties (Massart et al., 2015).

In the present study, a whole genome sequence of the 277 type-strain of *M. fructicola* (NRRL Y-27328) was assembled using PacBio technology. Results indicate that the genome of *M. fructicola* (Mf genome) is approximately 26 Mbp and contains 8,629 gene coding sequences. The new assembly resulted in a high quality assembly consisting of 93 contigs – the longest one is 2,548,689 bp – with 439X average genome coverage.

In parallel, the genome of another biocontrol strain of *M. fructicola* (strain AP47) isolated in northern Italy from apple fruit surfaces and used to control brown rot of peaches (Zhang et al., 2010), was assembled by aligning Illumina shotgun sequences (with a genome coverage of 161.8 X), using the genome assembly of the strain 277 as a reference. The mutation rate

between the two biocontrol strains of *M. fructicola* was also determined.

RESULTS AND DISCUSSION

Assembly, Gene Prediction and Functional Annotation of the Genome of *Metschnikowia fructicola* Strain 277

A new assembly of the *M. fructicola* (type strain NRRL Y-27328, CBS 8853) genome (Genbank accession ANFW02000000) was constructed using sequence data obtained from the Pacific Biosciences (PacBio) RS II Sequencer. The PacBio genomic sequences were assembled with the HGAP3.0 program (Chin et al., 2013) and yielded a high-quality draft genome consisting of 93 contigs with an N50 of 957,836 bp. The estimated genome size is approximately 26 Mb. Total of 8,629 genes were predicted with MAKER, and 6,262 were successfully annotated with Blast2GO (Conesa et al., 2005) and InterProScan (Finn et al., 2016a,b). The results of assembly, gene prediction and annotation are presented in **Table 1**. In contrast to the previous assembly (Hershkovitz et al., 2013), where 9,674 transcripts were identified, the current high-quality assembly provided a more accurate estimate of the transcript number (8,629) and size of the *M. fructicola* genome. We believe that the current number is more accurate because it was estimated by using the MAKER gene predictor (Cantarel et al., 2008), trained with the transcript sequences obtained by mapping the RNA reads obtained by Hershkovitz et al. (2013) on a high-quality genomic sequence. On the other hand, the 9,674 predicted by Hershkovitz et al. (2013) were obtained by *de novo* assembly with the Trinity software (Grabherr et al., 2011), which can be prone to the overestimation of the number of transcripts (Cerveau and Jackson, 2016). The annotated transcripts are listed in **Supplementary Table S1**, and their sequences, CDSs and protein sequences are presented in **Supplementary Data Sheets S1–S3**. **Supplementary Data Sheet S4** contains the gene coordinates. The main characteristics of the current *M. fructicola* genome assembly and a comparison

to the previous assembly (Hershkovitz et al., 2013) are summarized in **Table 1**. Comparative analysis of *M. fructicola* proteins with the other three available closely related genomes of *Clavispora lusitaniae*, *Candida auris*, and *M. bicuspidata* revealed a shared core of homologous proteins coded by 5,776 genes (**Supplementary Data Sheet S5**). A recently published work describing the phylogeny of strains belonging to *Metschnikowia* species isolated from the guts of flower-visiting insects (Lachance et al., 2016) allowed us to construct a phylogenetic tree of *Metschnikowia* spp that is based on the fastq raw-data deposited in Genbank (**Figure 1**). The tree was constructed using an assembly and alignment-free method of phylogeny reconstruction (Fan et al., 2015). Interestingly, the phylogenetic analysis showed that the two *M. fructicola* strains described in our study were grouped together and were separate from other *Metschnikowia* species described by Lachance et al. (2016). This difference in phylogeny may be related to evolutionary history and niche colonization of fruit surfaces versus insect guts.

The GO analysis revealed that 6,262 of the 8,629 identified *M. fructicola* genes were characterized with 4,493 GO terms (**Supplementary Data Sheet S6**). The most common descriptors concerning the cellular component were “Cell” and “Cell Part,” followed by “Organelle,” while “Cellular process” and “Metabolic Process,” followed by “Localization,” “Establishment of Localization,” “Biological Regulation,” “Pigmentation” and “Response to stimulus” were the most common in the biological processes. Regarding the molecular function, the most common descriptors were “Binding” and “Catalytic,” followed by “Transporter.” The same descriptors in the three categories were the most common in the genes characterized in the paper of Hershkovitz et al. (2013).

Utilization of *M. fructicola* 277 Genome for Reference-Based Assembly of Strain AP47

The assembly of the genome of strain 277 presented here is the most comprehensive and complete assembly for *M. fructicola* to date. This assembly was used as a reference to assemble the genome of the AP47 strain of *M. fructicola*, obtained by Illumina MySeq (161.8 X) shotgun sequencing data (**Table 2**). The reference guided assembly resulted in an N50 of 957,045, which was much higher than the one obtained by *de novo* assembly (**Table 3**). The length of the AP47 genome was similar to the reference strain 277 (~26 Mb), but had a slightly higher GC content (46.3% compared to 45.8%).

The assembly presented here was also compared to the AP47 strain assembly using a SNP calling approach. Results of this analysis are presented in **Table 4**, and the complete vcf is found in **Supplementary Data Sheet S7**. Considering only homozygous polymorphisms, a total of 546,356 SNPs, 11,987 insertions and 5,959 deletions were identified. Among these mutations, 185,649 were in coding regions, and the vast majority of the variations (135,616) were silent. However, 50,822 were missense mutations, and 212 were nonsense mutations. The differences with strain AP47 were mapped on strain 277 and presented in **Figure 2**.

TABLE 1 | Summary of the main assembly and annotation features of the genome of the sequenced *Metschnikowia fructicola* strain 277.

	New sequence	Old sequence (Hershkovitz et al., 2013)
Sequencing technology	PacBio	Illumina
Genome size	~26 Mb	~23 Mb
Sequencing coverage	20X	700X
Number of contigs	93	8430
Number of large contigs (> 100 Kb)	84	2
N50 (base pairs)	957,836 bp	3,784 bp
GC content (%)	45.8%	45.5%
N50 of transcript length (nucleotides)	5033bp	589bp
Number of genes	8,629	15,803
Annotated genes	6,277	–

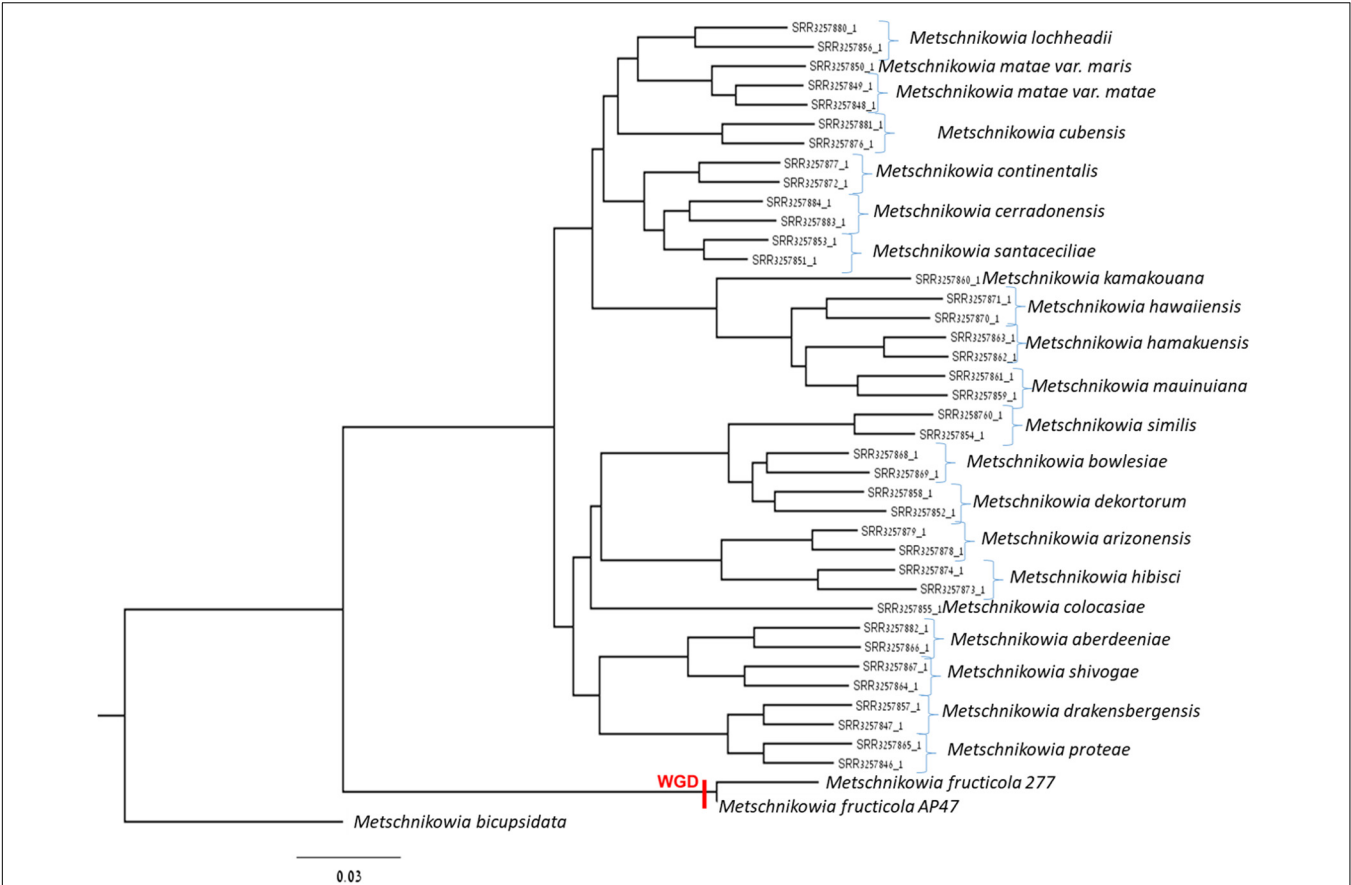


FIGURE 1 | Phylogenetic tree comprised of *Metschnikowia fructicola* 277, *Metschnikowia fructicola* AP47, and other *Metschnikowia* species. The tree was constructed using an assembly and alignment-free method of phylogeny reconstruction (Fan et al., 2015). The whole genome duplication event was indicated on the tree with “WGD.”

TABLE 2 | Sequencing data of the two pair end libraries used to sequence the genome of *Metschnikowia fructicola*, strain AP47.

Sequencing data	Library PE1	Library PE2	Library MP1
Number of raw reads	3717646	2599548	10188012
Number of clean reads	2545140	2546666	9126542
Total length (Mb)	301.257	927.79	2977.528
GC percentage	43% GC	45% GC	43% GC

The average mutation rate was one every 46 bases, which is exceptionally high in respect to the average reported for other yeast species. For example, the average mutation rate is approximately one SNP every 235 and 269 nucleotides, in *C. albicans* (Hirakawa et al., 2015) and *Saccharomyces cerevisiae*, respectively (Drozdova et al., 2016). The high number of observed mutations may be related to the different geographical origin and host species of the strains. The 277 type-strain of *M. fructicola* (NRRL Y-27328) was isolated in Israel from the surface of grapes, while the AP47 strain was isolated in Italy from the surface of apples.

The strain AP47 Whole Genome Shotgun project has been deposited at DDBJ/ENA/GenBank under the accession

TABLE 3 | *De novo* and reference guided assemblies of the genome of the sequenced *Metschnikowia fructicola*, strain AP47.

	<i>De novo</i> assembly*	Reference guided assembly**
Sequence length	~23.3 Mb	~26.2 Mb
Number of scaffolds	10,173	93
Number of scaffolds > 100 Kb	35	53
Number of scaffolds > 1 Kb	3156	93
N50 (base pairs)	63,477 bp	957,045 bp
G + C content (%)	46.3%	46.3%

*Obtained with SPAdes (Bankevich et al., 2012). **Obtained with IMR-DENOM (<http://mtweb.cs.ucl.ac.uk/mus/www/19genomes/IMR-DENOM/>).

MTJM00000000. The version described in this paper is version MTJM01000000.

The D1/D2 region ribosomal region was identified in strain 277 genome by blasting *M. pulcherrima* D1/D2 region on it. Since we observed that none of the identified SNPs were localized in that region, we can confirm with high confidence that both strains 277 and strain AP47 belong to the same species, which is different from *M. pulcherrima* (Kurtzman and Robnett, 1998).

TABLE 4 | Number of mutations in the genome sequence of *M. fructicola* strain AP47, compared to the reference genome of *M. fructicola* strain 277, and their predicted effect and impact on coding sequences.

Number of mutations	564,302
SNPs	546,356
Insertions	11,987
Deletions	5,959
Variant rate	1 variant every 46 bases
Predicted mutation effect	
Silent	135,884
Missense	49,794
Nonsense	212
Mutation impact	
High	2,023 (0.08%)
Moderate	50,032 (1.97%)
Low	136,810 (5.39%)
Negligible	2,348,195 (92.56%)

Stress-induced genomic instability has been studied in various yeast and bacteria, under a variety of stress conditions. Stresses were suggested to induce several genetic changes including small changes (one to few nucleotides), deletions and insertions, gross chromosomal rearrangements, copy-number variations and movement of mobile elements (Galhardo et al., 2007).

We suggest that *M. fructicola* as a species could undergo genomic changes in order to survive environmental stresses, in particular on the fruit surface. These changes may have led to evolve mechanisms not only to tolerate stresses, but also to generate large-scale genetic variation as a means of adaptation, giving both *M. fructicola* strains the genetic traits to be successful plant surface colonizers (intact and wounded surfaces) and, possibly, antagonists of fruit pathogens. A second reason of the high polymorphism-rate between *M. fructicola* strains may be the high-mutation rate in the promoters of genes putatively involved in the repair or mutation of the genomic sequences. A list of GO terms related to these processes (**Supplementary Data Sheet S8**) was used to identify 272 annotated genes, and in their promoter sequences the variant rate was of 1/35 bases, against the average of 1/40 in the promoters of the rest of the genomes. The variant rate in the actual transcribed sequence was, however, in line with the rest of the genome (1/66 against 1/67 bases). We also calculated the percentage of these genes showing a putative high impact polymorphism, and 21% of them (57 out of 272) did: this number was slightly higher than the percentage of total genes showing a similar polymorphism (16%, 1,379 out of 8,629).

Uncommonly Large Genome

The genome of *M. fructicola* was surprisingly large in size, being 26 Mb long. In fact, the most closely related available genomes (*M. bicuspidata*, *C. auris* and *C. lusitaniae*), are 16 Mb (BioProject PRJNA207846, Riley et al., 2016), 12.5 Mb (BioProjects PRJNA342691 and PRJNA267757, Chatterjee et al., 2015) and 11.9 Mb (BioProject PRJNA12753, Butler et al., 2009), respectively. The most probable explanation for such a genome

size seemed to be a whole genome duplication event. To have evidence of this, we searched the genome for homologs, finding 5,132 genes out of 8,629, all in pairs but for 228, which come in groups of three or more copies. This is a high degree of homology, since in the genomes of *M. bicuspidata*, *C. auris*, and *C. lusitaniae* we found only 71, 69, and 56 homologous genes, respectively.

Ordinarily, after a whole-genome duplication event in yeasts, most of the duplicates of genes situated in low mutation regions are lost, while the ones situated in rapidly evolving regions accumulate mutations and differentiate themselves from their homologs (Fares et al., 2017). We compared the average number of polymorphisms identified between strains 277 and AP47 on homologous and single-copy genes, finding that the first group of genes has a variant rate of 1/65 bases, while for the second group this value is of 1/68. Since divergence between gene copies can also happen at the expression level, so that each copy can be expressed in a different situation and accumulate mutations useful for a specific environmental condition (Fares et al., 2017), the variant rate in the promoters was also checked. Among the promoters of the homologous genes, the average variant rate is of 1/37 bases, while in the single-copy gene promoters it is of 1/45.

Despite the low difference in the mutation rate of single-copy and homologous genes, particularly in the proper gene sequence and not in the promoters, we believe that the available data strengthen the hypothesis of a whole-genome duplication event being responsible for the large genome of *M. fructicola*. This is due principally to the fact that nearly all the homologous genes come in pairs, with only 228 having more than one homolog. The sequencing of other *M. fructicola* strains will undoubtedly be critical to gain further insight on the reasons of this yeast's large genome.

It should be noted that the strain AP47 has SNPs spread along all the contigs of strain 277 (**Figure 2**). This seems to indicate that the whole genome duplication event occurred in AP47 as well, and that the strains share a common ancestor. This was observed despite the high mutation rate between the strains.

The genomes of the *Metschnikowia* spp. present in **Table 5** were downloaded from ncbi, to look for others whole-genome duplication events. Since *M. bicuspidata* is the only one of these species to have been fully annotated, it was impossible to look for the whole genome duplication event as has been done with *M. fructicola*. Therefore, we blasted both the transcriptomes of *M. fructicola* and *M. bicuspidata* on all the considered genomes, counting how many of these had matches on different contigs: even if not every transcript had a match, the result of the analysis gave us an idea of the level of homology inside the genomes of interest. In *M. fructicola*, 75% of the transcripts had matches on more than one contig. Furthermore, of the *M. bicuspidata* transcripts with a match on the *M. fructicola* genome, 58% had a match on more than one contig. On the contrary, none of the other analyzed genomes reached a percentage of transcripts mapping on different contigs of 10%. Based on this data, it seems that the whole-genome duplication event is unique to *M. fructicola*. This data correlates well with the high homology level found in the genome, because a high number of homologous genes is commonly associated with relatively recent whole genome duplication events (Lenassi et al., 2013).

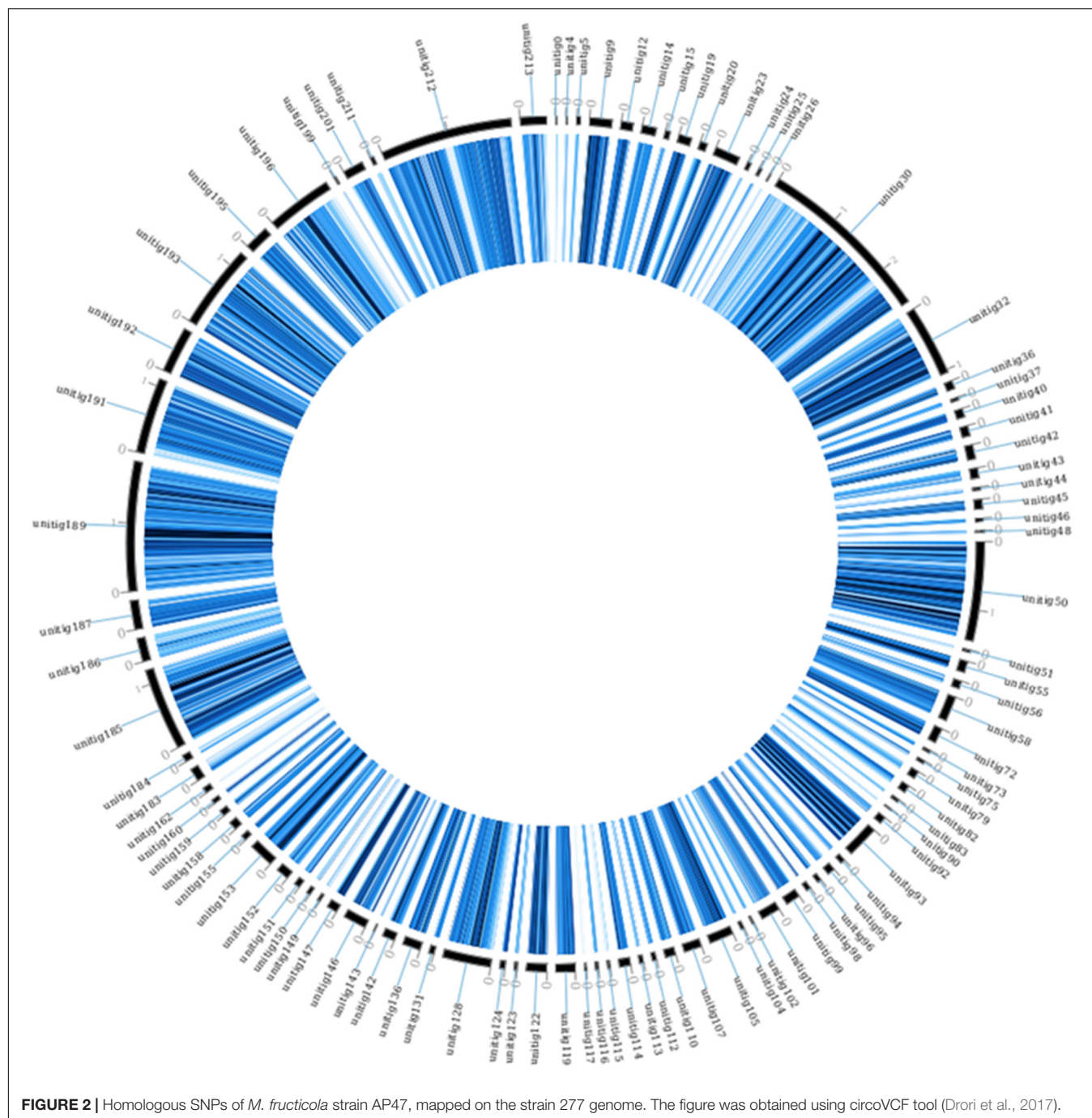


FIGURE 2 | Homologous SNPs of *M. fructicola* strain AP47, mapped on the strain 277 genome. The figure was obtained using circoVCF tool (Drori et al., 2017).

Carbohydrate Active Enzymes

Plant cell walls consist of a complex network of carbohydrate components, including cellulose, hemicellulose and pectin, as well as a variety of proteins and glycoproteins. These polysaccharides, and other analogous microbial related structural compounds, are targets of carbohydrate-active enzymes (CAZymes) that cleave them into oligomers and simple monomers, which can then be used as nutrients by microorganisms (Cantarel et al., 2009). Bacteria and fungi that are associated with and interact with plants have evolved

carbohydrate enzymes strongly linked to the plant environment that these microbes inhabit (Kolton et al., 2013). *M. fructicola* strain 277 MAKER predicted proteins were analyzed with CAT (Park et al., 2010) showing 1,145 putative CAZymes in *M. fructicola* (Figure 3). This represents one of the largest number of potential CAZyme genes that have been reported in Ascomycetes (Amselem et al., 2011). In comparison, the genomes of *Botrytis cinerea* and *Sclerotinia sclerotiorum*, two versatile necrotrophic plant pathogens, contain 367 and 346 putative CAZyme genes, respectively, including 106 and 118

TABLE 5 | Homology level in different *Metschnikowia* spp. genomes.

	Matched transcripts		Homology level	
	<i>M. fructicola</i> transcriptome	<i>M. bicuspidata</i> transcriptome	<i>M. fructicola</i> transcriptome	<i>M. bicuspidata</i> transcriptome
<i>M. aberdeeniae</i> (GCA_002370615.1)	39.16%	38.89%	3.64%	4.93%
<i>M. arizonensis</i> (GCA_002370875.1)	33.97%	33.3%	4.74%	7.15%
<i>M. bicuspidata</i> (PRJNA207846)	67.96%	100%	3.27%	9.23%
<i>M. bowlesiae</i> (GCA_002370295.1)	36.77%	38.02%	5.55%	7.26%
<i>M. cerradonensis</i> (GCA_002370635.1)	37.66%	38.51%	6.98%	8.1%
<i>M. colocasiae</i> (GCA_002370175.1)	39.89%	41.32%	4.71%	6.55%
<i>M. continentalis</i> (GCA_002370835.1)	37.46%	38.05%	8.42%	9.37%
<i>M. cubensis</i> (GCA_002374405.1)	38.3%	38.98%	6.51%	8.53%
<i>M. dekortorum</i> (GCA_002374455.1)	36.46%	38%	5.02%	6.99%
<i>M. drakensbergensis</i> (GCA_002370475.1)	39.02%	40.16%	4.1%	5.25%
<i>M. fructicola</i>	100%	66.52%	74.13%	58.23%
<i>M. hawaiiensis</i> (GCA_002370325.1)	40.06%	40.74%	7.52%	9.71%
<i>M. hibisci</i> (GCA_002374725.1)	31.71%	29.57%	3.4%	5.91%
<i>M. kamakouana</i> (GCA_002374535.1)	38.86%	39.3%	3.67%	5.58%
<i>M. lochheadii</i> (GCA_002370915.1)	36.49%	36.3%	7.21%	9.44%
<i>M. matae</i> (GCA_002370695.1)	35.07%	35.12%	7.93%	9.56%
<i>M. mauinuiana</i> (GCA_002374555.1)	38.63%	39.59%	7.47%	9.04%
<i>M. proteae</i> (GCA_002370515.1)	39.65%	40.57%	3.98%	5.83%
<i>M. santacecilliae</i> (GCA_002374485.1)	38.08%	38.74%	6.57%	8.4%
<i>M. shivogae</i> (GCA_002374645.1)	39.85%	40.19%	3.63%	5.33%
<i>M. similis</i> (GCA_002370765.1)	36.93%	38.15%	5.3%	7.5%

The table is divided in two sections. The left section (Matched transcripts) shows the percentage of *M. fructicola* or *M. bicuspidata* transcripts having a match when blasted on the genome of various *Metschnikowia* spp. The homology level on the right section shows the percentage of matched transcripts which also have a second match on another contig.

clearly related to cell wall degradation (Apweiler et al., 2001). The impressive repertoire of CAZymes in *M. fructicola* thus may play an important role in its nutritional status and ability to colonize plant surfaces as well as being an effective biocontrol control agent. This role becomes particularly important giving that injured fruit surfaces contain a wide variety of simple and complex carbohydrates that can be consumed by pathogens. Despite different studies characterizing the action of some of these genes (Iijakli and Lepoivre, 1998; Friel et al., 2007), the prospective role of CAZymes in the mechanism of action of microbial antagonists is yet to be fully explored. Among the identified CAZymes in *M. fructicola*, 463 have clear assignments to either glycoside hydrolases (GH) or carbohydrate esterases (CE), all involved in fungal cell wall degradation. Two of the aforementioned genes, unitig185_25 and unitig50_23, have a strong resemblance to MfChi (Genbank accession number: HQ113461.1), a *M. fructicola* chitinase which was shown to inhibit *Monilinia fructicola* and *M. laxa* *in vitro* and on fruit (Banani et al., 2015). A comparison of the number of CAZymes in each of the four annotated genomes belonging to the Metschnikowiaceae family (Mf – *Metschnikowia fructicola*, Mb – *Metschnikowia bicuspidata*, CL – *Clavispora lusitanae*, and CA – *Candida auris*) was conducted (Figure 3). Mb is a fresh-water fish pathogen, while CL and CA are both human pathogens. Results indicated that the *M. fructicola*

genome contained a significantly greater variation and number of CAZyme genes, including glycoside hydrolase (GH), glycosyl transferases (GT) and carbohydrate-binding modules (CBM) family genes (Figure 3 and Supplementary Table S2). The Mf genome contained several unique CAZymes involved in the metabolism of glucans, arabinose, and rhamnogalacturonan that are exclusively associated with terrestrial plant hemicellulose.

M. fructicola Response to *P. digitatum* and to Grapefruit Peel Tissue

The current assembly and genome annotation of Mf enabled us to examine the identification of genes associated with the interaction of Mf with either *P. digitatum* or grapefruit peel tissue and determine the genes that are specific to each interaction.

The transcriptomic RNAseq libraries of Mf, available from BioProject PRJNA168317 (Hershkovitz et al., 2013), were then analyzed. These libraries were constructed from Mf under four different conditions: (1) Mf growing in NYPD broth (control), (2) Mf in contact with *P. digitatum* (Pd) mycelium for 24 h, (3) Mf in contact with *P. digitatum* (Pd) mycelium for 48 h, and (4) Mf in contact with grapefruit peel for 24 h.

The analysis of DEGs indicated that gene expression in Mf cells that were in contact with fruit peel tissue or had no contact with fruit tissue (control), was more similar to each other than to gene expression in Mf cells that were in contact with *P. digitatum* mycelia. In total, 2,588 DEGs were identified among Mf cells in

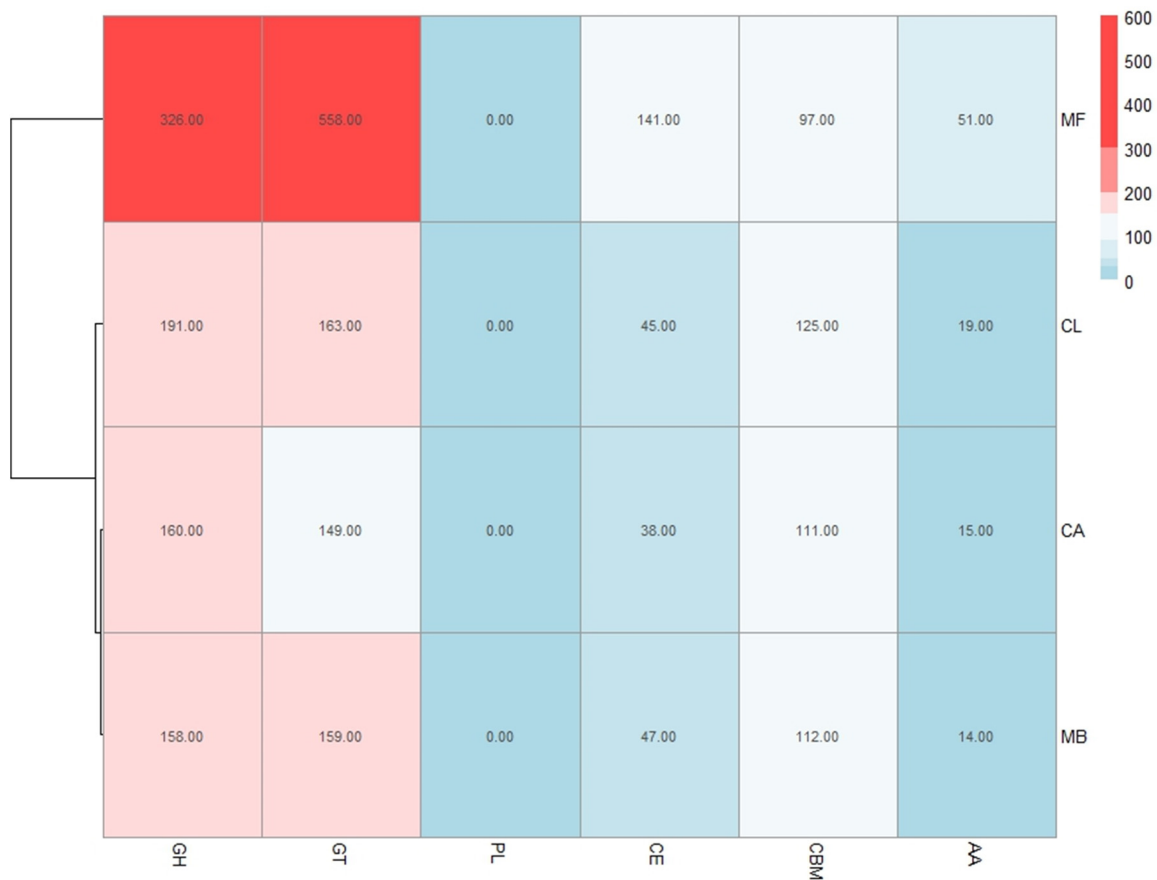


FIGURE 3 | The number of CAZYenzyme genes in each of the 4 sequenced genomes belonging to the Metschnikowiaceae family: Mf – *Metschnikowia fructicola*, Mb – *Metschnikowia bicuspidate*, CL – *Clavispora lusitanae*, and CA – *Candida auris*. Different classes of CAZYenzyme genes are designated as GH – Glycoside Hydrolases; GT – Glycosyl Transferases; PL – Polysaccharide Lyases; CE – Carbohydrate Esterases; CBM – Carbohydrate-Binding Modules and AA – Auxiliary Activities. The color reflects the relative number of genes in each of the four species as indicated by the scale in the upper right portion of the figure. 28 genes were included in 2 categories, and therefore the sum of the total of **Figure 3** for *M. fructicola* is slightly more than 1,145, which is the reported number of CAZymes.

contact or not in contact with citrus fruit, peel tissue, and Mf cells that were in contact with *P. digitatum* mycelium (**Supplementary Table S3**). The DEGs could be grouped into three different co-expressed clusters (**Figures 4A,B**).

Cluster1 genes were more highly expressed during contact with *P. digitatum* (Pd) mycelia, relative to cells grown in NYPD broth (control) or on grapefruit peel tissue. We have found 1353 such genes (while only 153 unigenes were found in the previous analysis when using de-novo transcriptome assembly). Cluster 2 genes were more highly expressed in Mf grown in NYPD broth (control) than they were when Mf was in contact with either grapefruit peel tissue or *P. digitatum* mycelium (total of 635 genes). Cluster 3 genes exhibited higher levels of expression when Mf cells were in contact with grapefruit peel tissue, rather than when grown in NYPD broth (control) or in contact with *P. digitatum* mycelium (600 genes).

Transcriptomic analysis of CAZyme expression levels in *M. fructicola* during its interaction with grapefruit peel tissue or *P. digitatum* mycelium when cultured in a PDB medium revealed a high level of CAZyme gene expression when the yeast was

placed in wounded fruit tissue (**Figure 5**). These results suggest that CAZyme genes may play an important role in the adaptation of *M. fructicola* to a fruit environment.

Secondary Metabolite Clusters Present in *M. fructicola*

The sequence of the *M. fructicola* genome revealed that this yeast possesses several secondary metabolite (SM) genes. SMs are known to play an important role in the virulence of many plant pathogens (Namdeo, 2007), but limited knowledge is available about the SM repertoire present in *M. fructicola*. Using antiSMASH (Weber et al., 2015) software, the *M. fructicola* genome was analyzed for the presence of secondary metabolite clusters or homologs of these genes present in related fungi. Twenty-six SM gene clusters were identified in *M. fructicola*, four of which are highly conserved in yeast and other fungi. The remaining 22 clusters could only be designated as putative clusters as similar clusters could not be identified in other fungal genomes using the ClusterFinder algorithm (Cimermanic et al., 2014). These 22

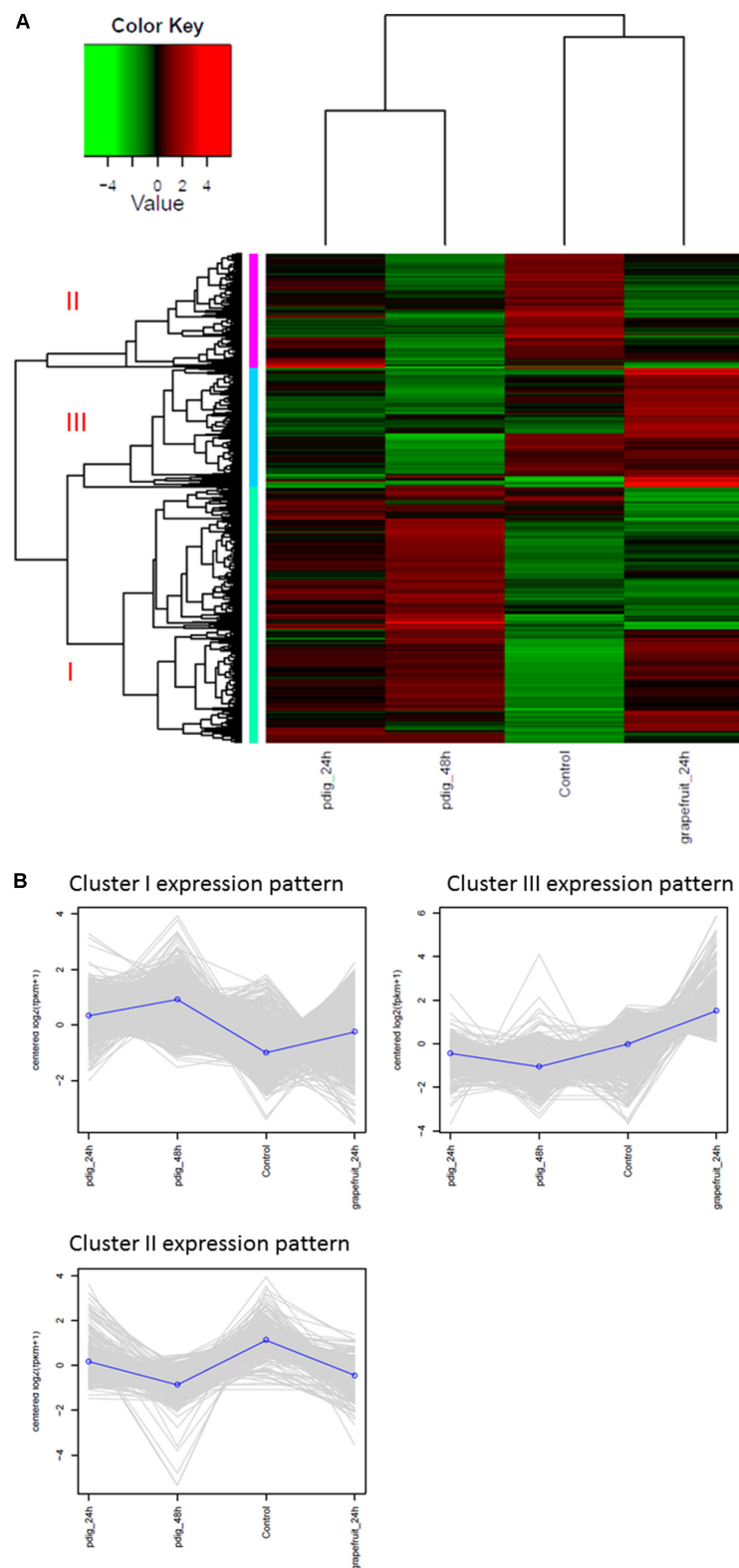
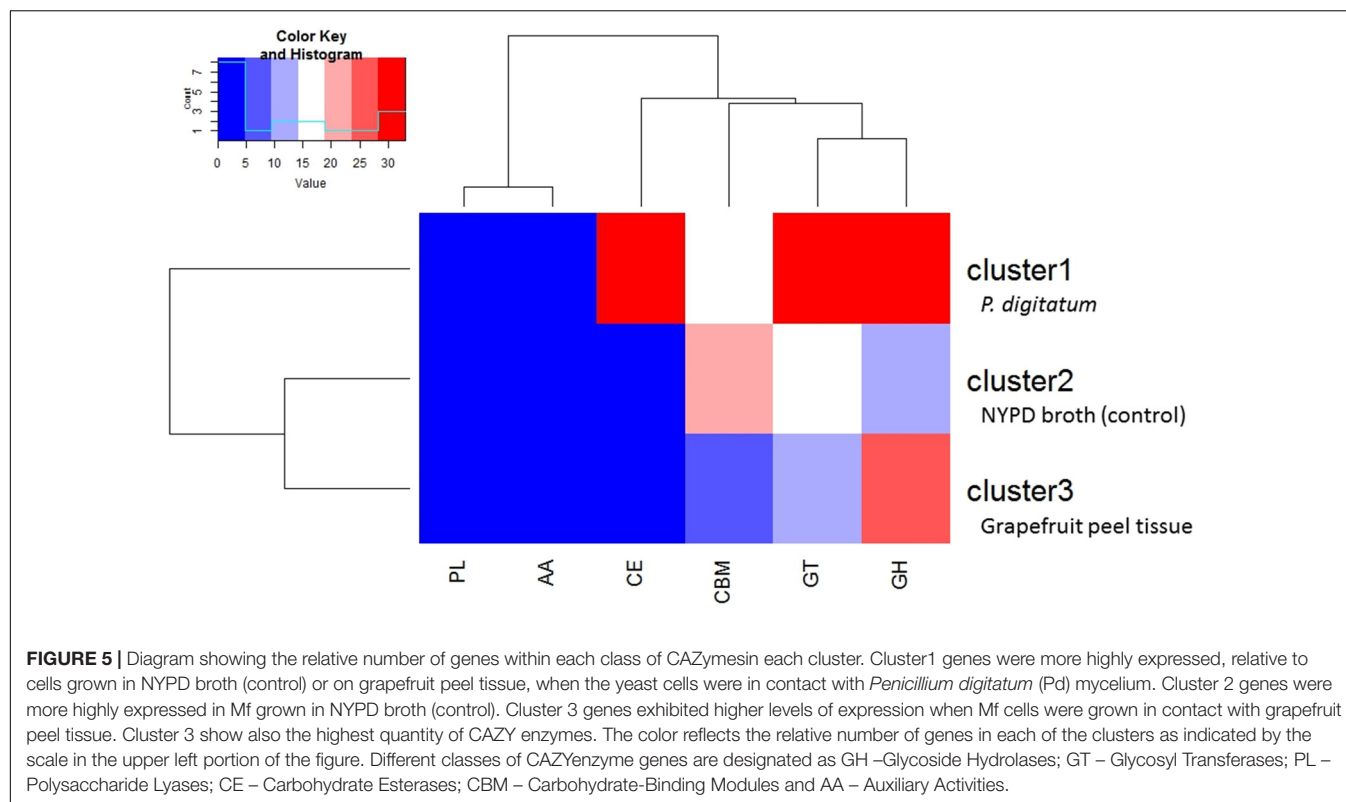


FIGURE 4 | (A) Heatmap and expression profile of differentially expressed genes in *Metschnikowia fructicola* (Mf) grown on different substrates. Three clusters were identified. Cluster 1 – genes with higher expression level when Mf was grown in contact with *Penicillium digitatum* (Pd). Cluster 2 – genes with higher expression level when Mf was grown in NYPD broth (control). Cluster 3 - genes with higher expression level when in Mf was grown in contact with grapefruit peel. **(B)** The expression profile of the three clusters in response to the different growth conditions.



potential clusters included putative saccharide and fatty acid biosynthetic clusters. The analysis of secondary metabolite genes indicated that *M. fructicola* is capable of producing small, potentially bioactive molecules. Two of the identified clusters (Figure 6 and Table 6) code for the production of a terpene that is conserved within *Candida* species. Terpenoid compounds are known to play a significant role in yeast antimicrobial defense mechanism (Hyldegard et al., 2012). The isoprenoid backbones of these compounds are synthesized by terpene synthases (TSs). The classification of various terpene synthases and their catalytic mechanisms have been recently reviewed (Gao et al., 2012). Although terpenoid SMs have not been previously reported in *M. fructicola*, the genome sequence clearly possesses two gene sequences that encode squalene/phytoene synthases: the transcripts unitig50_211 and unitig147_7.

YAP Gene Expression in *M. fructicola*

The Yap protein family plays a role in cellular response to oxidative stress (Rodrigues-Pousada et al., 2010) and *M. fructicola* has been demonstrated to have a high tolerance to oxidative stress (Macarasin et al., 2010). An analysis of YAP genes in the *M. fructicola* genome revealed the presence of 14 YAP genes (Table 7). In comparison, 7 YAP genes were found in *C. albicans* (BioProjects PRJNA14005 and PRJNA10701), *C. auris* (BioProjects PRJNA342691 and PRJNA267757) and *M. bicuspidata* (BioProject PRJNA207846), while *C. lusitanae* (BioProject PRJNA12753) had 6. YAP genes are important for resistant to oxidative stress

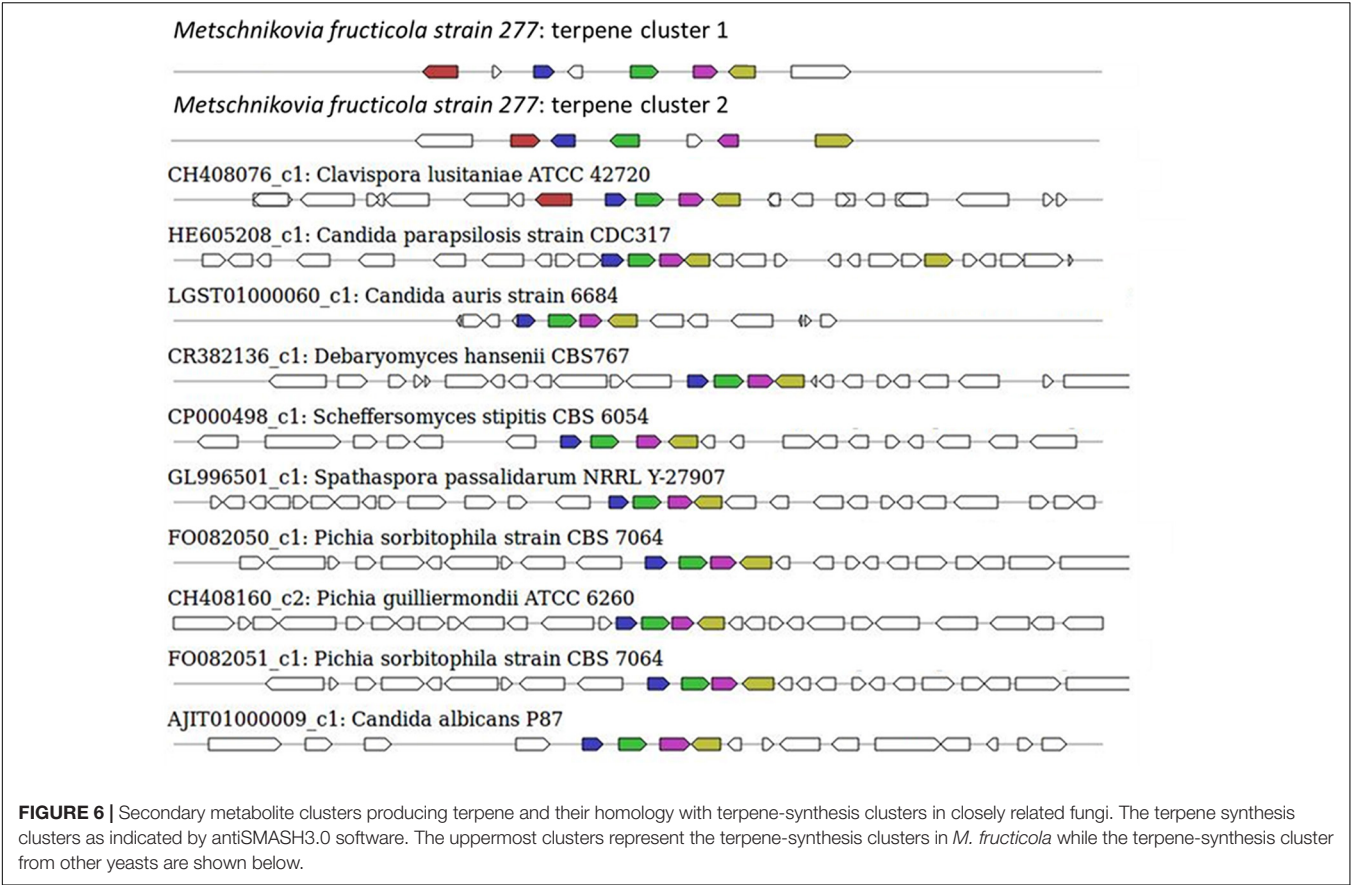
(Macarasin et al., 2010). a feature that could possibly play a role in the ecological fitness and antagonistic activity of *M. fructicola*.

Pulcherrimin Cluster Analysis

Pulcherrimin is a *M. fructicola* metabolite of major interest, since it is involved in the biocontrol action of this yeast (Saravanakumar et al., 2008) and of other biocontrol yeast strains (Castoria et al., 2003). The genes responsible for the biosynthesis of this siderophore were successfully identified only in *B. subtilis* (Randazzo et al., 2016), and an analysis of orthology with proteinortho and blast showed no homology between the *B. subtilis* pulcherrimin gene cluster and the proteins predicted in *M. fructicola*. It is probable that the *B. subtilis* and *M. fructicola* genes involved in pulcherrimin biosynthesis are the product of different evolutionary processes.

CONCLUSION

The genomes of two strains of *M. fructicola* (277 and AP47) were sequenced, assembled and compared. The comparison of the two genomes sequences indicated a very high rate of mutation, even though it will be necessary to sequence additional strains to establish if the average mutation rate in *M. fructicola* is intrinsically high, or if the mutation rate identified in the present study is related to the geographical origin and fruit host in which they evolved. The genome size (~26 Mb) of both *M. fructicola* strains, as well as the rate of mutation, may suggest



that *M. fructicola* could undergo genomic changes in order to adapt to plant surfaces, tolerate various environmental stresses and survive under restricted nutritional resources. Its adaptation to plant environment can also be explained by the presence of a relatively large number of secondary metabolites clusters, YAP and CAZymes related genes in the genome.

Another interesting result was the discovery of 1,145 putative CAZymes in the *M. fructicola* genome. These genes could be the target of studies aimed to identify enzymes able to control fungal diseases *in vivo*, to evaluate their potential use as treatments for fruits and plants.

MATERIALS AND METHODS

DNA Extraction

Metschnikowia fructicola, Strain 277, (Kurtzman and Droby, 2001) was grown in NYDP (nutrient broth (8 g l⁻¹), yeast extract (5 g l⁻¹), D-glucose (10 g l⁻¹) and chloramphenicol (250 mg l⁻¹). One ml of the yeast cell suspension was aseptically transferred from 24 h old starter culture to 250 ml Erlenmeyer flasks and place on an orbital shaker at 160 rpm for 24 h at 26°C. Yeast cells were pelleted by centrifugation at 6,000 rpm, washed twice with sterile distilled water, re-suspended in sterile water to initial volume and the cell suspension concentration was adjusted to 1 × 10⁸ cells ml⁻¹.

TABLE 6 | Secondary metabolites clusters identified with antiSMASH (Weber et al., 2015) software.

Secondary metabolite cluster type	Transcripts of Mf found in cluster	Location
Terpene cluster	unitig147_4	unitig147 15287 – 36642
	unitig147_5	
	unitig147_6	
	unitig147_7	
	unitig147_8	
	unitig147_9	
	unitig147_10	
Terpene cluster	unitig50_207	unitig50 578895 – 600250
	unitig50_208	
	unitig50_209	
	unitig50_210	
	unitig50_211	
	unitig50_212	
	unitig50_213	
	unitig50_214	

Metschnikowia fructicola strain AP47 was isolated from the carposphere of an apple grown in Piedmont, Northern Italy (Zhang et al., 2010). The strain was stored in tubes of Potato Dextrose Agar and 50 mg/L streptomycin at 4°C. Suspensions of *M. fructicola* AP47 (5 × 10⁵ cells/mL) were inoculated in

TABLE 7 | Yap family genes and homologs identified in the genome of *M. fructicola*.

Systematic name <i>Saccharomyces cerevisiae</i>	Homologue in Mf genome	Gene name	Alias(es)	Description
YDR259C	Not found	YAP6	HAL7	Basic leucine zipper (bZIP) transcription factor
YDR423C	Not found	CAD1	YAP2	AP-1-like basic leucine zipper (bZIP) transcriptional activator
YGR241C	unitig192_208	YAP1802		Protein of the AP180 family, involved in clathrin cage assembly
YHL009C	unitig142_42	YAP3		Basic leucine zipper (bZIP) transcription factor
	unitig187_66			
YHR161C	Not found	YAP1801		Protein of the AP180 family, involved in clathrin cage assembly
YIR018W	Not found	YAP5		Basic leucine zipper (bZIP) iron-sensing transcription factor
YJR005W	unitig146_71	APL1	YAP80	Beta-adaptin
	unitig192_37			
YJR058C	unitig122_58	APS2	YAP17	Small subunit of the clathrin-associated adaptor complex AP-2
	unitig50_345			
YLR120C	unitig104_2	YPS1	aspartyl protease,	Aspartic protease
	unitig150_6			
	unitig193_349			
	unitig32_12			
YLR170C	unitig196_234	APS1	YAP19	Small subunit of the clathrin-associated adaptor complex AP-1
YML007W	Not found	YAP1	PDR4, DNA-binding transcription factor YAP1, SNQ3, PAR1	Basic leucine zipper (bZIP) transcription factor
YOL028C	Not found	YAP7		Putative basic leucine zipper (bZIP) transcription factor
YOR028C	Not found	CIN5	YAP4, HAL6	Basic leucine zipper (bZIP) transcription factor of the yAP-1 family
YPL259C	unitig105_13	APM1	YAP54	Mu1-like medium subunit of the AP-1 complex
	unitig193_251			
YPR199C	Not found	ARR1	ACR1, YAP8	Transcriptional activator of the basic leucine zipper (bZIP) family

500 mL Potato Dextrose Broth (PDB, Difco) and incubated on a rotary shaker (180 rpm) at 24°C for 4 days. Yeast mass was filtered from the culture, frozen in liquid nitrogen and DNA was extracted from 1 g frozen tissue. The final DNA preparation was incubated overnight at room temperature in 490 µl of Tris-EDTA (TE) buffer and 10 µl of DNase-free RNase (10 µg/ml), followed by phenol-chloroform extraction and isopropanol precipitation. Finally, DNA was resuspended in 30 µl TE buffer. DNA concentration and purity were checked by a spectrophotometer (Nanodrop 2000, Thermo Scientific, Wilmington, DE, United States), and the DNA integrity was analyzed by agarose gel electrophoresis (data not shown).

Sequencing

Strain 277 was sequenced on the Pacific Biosciences (PacBio) RS II Sequencer, as previously described (Hoffmann et al., 2013; Pirone-Davies et al., 2015). Specifically, we prepared the library using 10 µg of genomic DNA, that was sheared

to a size of 20 kb fragments by g-tubes (Covaris, Inc., Woburn, MA, United States) according to the manufacturer's instruction. The SMRTbell 20-kb template library was constructed using DNA Template Prep Kit 1.0 with the 20-kb insert library protocol (Pacific Biosciences; Menlo Park, CA, United States). Size selection was performed with BluePippin (Sage Science, Beverly, MA, United States). The library was sequenced using the P6/C4 chemistry on 24 single-molecule real-time (SMRT) cells (8 with BluePippin and 16 without), with a 240-min collection protocol along with stage start.

The genome of *M. fructicola* AP47 was sequenced at the Genomics Platform of the Parco Tecnologico Padano using the Illumina MiSeq technology. Two paired-ends were prepared using Nextera XT DNA Sample Preparation Kit, following the manufacturer's instructions. Two paired-end (PE) libraries were prepared: PE1 with overlapping paired-end reads and PE2 with non-overlapping paired-end reads. One mate pair library was also prepared, using Nextera Mate Pair Sample Preparation Kit

and following the manufacturer's instructions. Libraries were purified by AMPure XP beads and normalized to ensure equal library representation in the pools. Equal volumes of libraries were diluted in the hybridization buffer, heat denatured and sequenced. Standard phi X control library (Illumina) was spiked into the denatured HCT 116 library. The libraries and phi X mixture were finally loaded into a MiSeq 250 and MiSeq 300-Cycle v2 Reagent Kit (Illumina). Base calling was performed using the Illumina pipeline software. PE1 was composed of 2,1 Gb (330 mean insert size, 43% GC, 35% duplication level). PE2 was composed of 846 Mb (132 mean insert size, 45% GC, 12/duplication level).

All the paired end sequences were trimmed with Trimmomatic v. 0.36 (Bolger et al., 2014) and cleaned with sickle v. 1.33 (Joshi and Fass, 2011) (Table 2). The mate pair sequences were trimmed and cleaned with TrimGalore v. 0.4.2¹.

The genome of *M. fructicola* AP47 was assembled at first with a *de novo* approach, using SPAdes (Bankevich et al., 2012), and then with a reference guided approach using IMR-DENOM², with the strain 277 as the reference.

Assembly

Analysis of the sequence reads was implemented by using SMRT Analysis 2.3.0. The best *de novo* assembly was established with the PacBio Hierarchical Genome Assembly Process HGAP3.0 program (Chin et al., 2013) using the continuous-long-reads from the four SMRT cells, which contained the longest subreads, with a minimum subread length cutoff of 5000 kb and target coverage of 20X. The resulting HGAP unique contigs (unitigs) were blasted against each other to identify smaller unitigs that show complete overlapping with other larger unitigs. These smaller unitigs were removed from the analysis. Afterward the improved consensus sequence was uploaded in SMRT Analysis 2.3.0. and polished with Quiver using all 24 SMRT cells (Chin et al., 2013).

In total 24 SMRT cells were used, resulting in 93 contigs with 439X average genome coverage. The longest contig comprised 2,548,689 bp.

Transcriptome Assembly, Gene Prediction and Functional Annotation

RNAseq from previous analysis (Hershkovitz et al., 2013) was used to assemble and predict transcribed regions in the *Mf* genome. Overall, 6,150 transcripts were identified based on tophat, cufflinks and bowtie2 pipeline as described in (Langmead and Salzberg, 2012).

The transcriptome data, together with the transcripts and proteins sequences available on NCBI for *M. fructicola*, *M. bicuspidata*, *C. auris* and *C. lusitaniae*, were used to train the gene predictor SNAP³, following the suggested procedure⁴. The

augustus gene predictor⁵ was trained with the WebAUGUSTUS web service (Stanke and Morgenstern, 2005), using as data the sequence of the 6,150 transcripts identified with the RNA seq.

SNAP and augustus were then used as a part of the MAKER software (Cantarel et al., 2008) to conduct the gene prediction in the genome. The evidence used were the 6,150 transcripts discovered with the RNA seq and the transcripts and proteins sequences available on NCBI for *M. fructicola*, *M. bicuspidata*, *C. auris* and *C. lusitaniae*. The transcripts not coming from *M. fructicola* were included in the MAKER control files as "altest" evidence, which is specifically used for data from species related to the target genome and not from the target itself. The repeat library was constructed following the Basic protocol⁶, and MAKER was launched using the option "correct_est_fusion" in the control files and "-fix-nucleotides" in the command line. MAKER produced a gene coordinates gff3 file, which was used to extract the CDSs from the genome in order to translate them with BioPython (Cock et al., 2009) using the Alternative Yeast Nuclear Code, obtaining the protein sequences. Some of the predicted genes had putative CDSs, which did not start with a start codon and/or did not end with a stop one, and were therefore discarded, with the following exceptions: (i) genes missing the stop codon, localized on the plus filament, which were the last gene of their contig; (ii) genes missing the stop codon, localized on the minus filament, which were the first gene of their contig; (iii) genes missing the start codon, localized on the plus filament, which were the first gene of their contig; (iv) genes missing the start codon, localized on the minus filament, which were the last gene of their contig. The genes of these categories were kept as partial genes.

The proteins were annotated with Blast2GO and Interproscan, using as blast database the fungal fraction of uniprot and swissprot databases (UniProt Consortium, 2017).

The CAT webservice was used to find Pfam modules (Finn et al., 2016b) in the proteins and assign them CAZy families.

Proteinortho v. 5.16 was used to look for homologous proteins in the proteomes of *M. fructicola* 277, *C. auris* (BioProjects PRJNA342691 and PRJNA267757), *M. bicuspidata* (BioProject PRJNA207846) and *C. lusitaniae* (BioProject PRJNA12753).

Gene Expression Analysis

RNAseq analysis was done using RNAseq data from previous research (Hershkovitz et al., 2013). The RNAseq data number SRA054245 was download from SRA database in NCBI. The RNAseq data was mapped using bowtie (Langmead et al., 2009). Expression quantification was estimated using RSEM software (Li and Dewey, 2011). Differential expression analysis was done using edgeR Bioconductor package (Robinson et al., 2010). Clustering was done using K-mean cluster analysis (Basu et al., 2002) differentially expressed genes threshold was FDR < 0.05 (Benjamini and Hochberg, 1995) and log fold changes greater than 1 or smaller than -1.

¹https://www.bioinformatics.babraham.ac.uk/projects/trim_galore/

²<http://mtweb.cs.ucl.ac.uk/mus/www/19genomes/IMR-DENOM/>

³<http://korflab.ucdavis.edu/software.html>

⁴http://weatherby.genetics.utah.edu/MAKER/wiki/index.php/MAKER_Tutorial_for_GMOD_Online_Training_2014

⁵<http://augustus.gobics.de/>

⁶http://weatherby.genetics.utah.edu/MAKER/wiki/index.php/Repeat_Library_Construction--Basic

Phylogenetic Tree

All raw-data sequences of *Metschnikowia* species (Lachance et al., 2016) were downloaded from NCBI using SRAtoolkit (Leinonen et al., 2011) from BioProject ID PRJNA312754. The phylogenetic tree was constructed with an assembly and alignment-free method of phylogeny reconstruction from next-generation sequencing data (Fan et al., 2015).

To place the whole-genome duplication event in the three, we downloaded the genomes of all the considered species, and we used them as databases to blast the full transcriptomes of *M. fructicola* and *M. bicuspidata* (Table 5), using blastall v. 2.2.26 with default parameters. We then calculated the percentage of transcripts having a match, and, inside this fraction, the percentage of transcripts having a match on at least 2 contigs.

Genome Comparison With *M. fructicola* Strain AP47

A SNP calling approach was followed, using bwa mem (Li and Durbin, 2009) to map Illumina reads of the strain AP47 of *M. fructicola* on the assembly of the strain 277. After using samtools view and samtools sort (Li et al., 2009) to obtain a sort.bam file, the following pipeline was used as described by Li (2011) for the SNP calling:

```
samtools mpileup -guf reference.fa AP47.sort.bam | bcftools view -cg -| vcfutils.pl varFilter -D 200 -Q 20 -> file.vcf
```

The file AP47.sort.bam was obtained by merging the data from the two Illumina libraries with samtools merge.

The genome of the strain 277 and the gff3 and protein fasta files obtained with MAKER, were used to build a SnpEff (Cingolani et al., 2012) database, and the tool “snpeff eff” was used to evaluate the effect of the homozygous SNPs of the strain AP47. Since *M. fructicola* is a haploid organism, heterozygous SNPs were probably mistakes. The Alternative Yeast Nuclear Code was used to evaluate the effect of missense SNPs on protein sequences.

Analysis of the Polymorphisms-Related Genes

The variant rate of the genes characterized by gene ontology terms present in **Supplementary Data Sheet S8** was calculated, and the same was done with their promoters. **Supplementary Data Sheet S8** was obtained by selecting all GO terms including the word “repair” or “mutation,” and then removing manually undesired terms (es: “cell wall repair”).

The promoter analysis was performed considering as promoter the 1000 bases preceding the genes in the genome, or the 1000 bases following the genes when these were on the antisense strand.

Analysis of the D1/D2 Region

The primers NL-1 (GCATATCAATAAGCGGAGGAAAAAG) and NL-4 (GGTCCGTGTTTCAAGACGG) (O'Donnell, 1993), used by Kurtzman and Robnett (1998) to amplify the D1/D2 region in *S. cerevisiae*, were blasted on the *M. pulcherrima* sequences available on NCBI, so to identify the D1/D2 region. The partial sequence of the large subunit ribosomal RNA

gene of *M. pulcherrima* culture-collection CBS:2256 (GenBank: KY108498.1) was therefore downloaded, and blasted on the *M. fructicola* strain 277 genome. We then proceeded to identify the SNPs present in that region in the strains 277 and AP47, looking at both the homozygous and heterozygous SNPs. The blast version used was blastall v. 2.2.26.

Whole-Genome Duplication Hypothesis

Proteinortho v. 5.16 was used to look for homologous proteins in the proteomes of *M. fructicola* 277, *C. auris* (BioProjects PRJNA342691 and PRJNA267757), *M. bicuspidata* (BioProject PRJNA207846) and *C. lusitaniae* (BioProject PRJNA12753). The variant rate in single-copy and homologous genes was calculated, and the same was done in their promoters.

The promoter analysis was performed considering as promoter the 1000 bases preceding the genes in the genome, or the 1000 bases following the genes when these were on the antisense strand.

YAP Genes Analysis

The protein sequence of various Yap genes was downloaded from www.yeastgenome.org, and analyzed with Proteinortho v. 5.16 (Lechner et al., 2011), looking for homologs in the proteins predicted for *M. fructicola* strain 277 and in the proteomes of *Candida albicans* (BioProjects PRJNA14005 and PRJNA10701), *C. auris* (BioProjects PRJNA342691 and PRJNA267757), *M. bicuspidata* (BioProject PRJNA207846) and *C. lusitaniae* (BioProject PRJNA12753).

Secondary Metabolites Cluster Prediction

Secondary metabolites clustering was predicted using antiSMASH website (Weber et al., 2015).

Pulcherrimin Gene Cluster Analysis

The proteins involved in pulcherrimin biosynthesis in *B. subtilis* (YVNB, YVNA, YVMC, YVMB, YVMA, CYPX; Randazzo et al., 2016) were downloaded from NCBI and used in a proteinortho v. 5.15 analysis with the MAKER predicted proteins of *M. fructicola*, with default parameters. The *B. subtilis* genes of interest were also blasted with blastp (blastall v. 2.2.26) against the predicted proteome of *M. fructicola*, using an *e*-value threshold of 10^{-5} .

AUTHOR CONTRIBUTIONS

EP and NS performed the bioinformatics analyses and contributed to writing the manuscript. MH and MA performed the PacBio sequencing and contigs assembly. EL contributed in DNA extraction and preparation samples for sequencing. MW, MG, DS, and SD designed the study and wrote the manuscript.

ACKNOWLEDGMENTS

Work carried out with a contribution of the LIFE Financial Instrument of the European Union for the Project “Low pesticide IPM in sustainable and safe fruit production”

(Contract No. LIFE13 ENV/HR/000580). The authors wish to thank Prof. Alberto Acquadro, University of Torino for his useful suggestion about bioinformatics analysis.

SUPPLEMENTARY MATERIAL

The Supplementary Material for this article can be found online at: <https://www.frontiersin.org/articles/10.3389/fmicb.2018.00593/full#supplementary-material>

DATA SHEET S1 | Fasta file of transcripts of MF.

DATA SHEET S2 | Fasta file of CDSs of MF.

DATA SHEET S3 | Fasta file of proteins of MF.

REFERENCES

- Amselem, J., Cuomo, C. A., van Kan, J. A., Viaud, M., Benito, E. P., Couloux, A., et al. (2011). Genomic analysis of the necrotrophic fungal pathogens *Sclerotinia sclerotiorum* and *Botrytis cinerea*. *PLoS Genet.* 7:e1002230. doi: 10.1371/journal.pgen.1002230
- Apweiler, R., Attwood, T. K., Bairoch, A., Bateman, A., Birney, E., Biswas, M., et al. (2001). The InterPro database, an integrated documentation resource for protein families, domains and functional sites. *Nucleic Acids Res.* 29, 37–40. doi: 10.1093/nar/29.1.37
- Banani, H., Spadaro, D., Zhang, D., Matic, S., Garibaldi, A., and Gullino, M. L. (2015). Postharvest application of a novel chitinase cloned from *Metschnikowia fructicola* and overexpressed in *Pichia pastoris* to control brown rot of peaches. *Int. J. Food Microbiol.* 199, 54–61. doi: 10.1016/j.ijfoodmicro.2015.01.002
- Bankevich, A., Nurk, S., Antipov, D., Gurevich, A. A., Dvorkin, M., Kulikov, A. S., et al. (2012). SPAdes: a new genome assembly algorithm and its applications to single-cell sequencing. *J. Comput. Biol.* 19, 455–477. doi: 10.1089/cmb.2012.0021
- Basu, S., Banerjee, A., and Mooney, R. J. (2002). “Semi-supervised clustering by seeding,” in *Proceedings of 19th International Conference on Machine Learning*, Stroudsburg, PA, 19–26.
- Benjamini, Y., and Hochberg, Y. (1995). Controlling the false discovery rate: a practical and powerful approach to multiple testing. *J. R. Stat. Soc. B* 57, 289–300. doi: 10.2307/2346101
- Bolger, A. M., Lohse, M., and Usadel, B. (2014). Trimmomatic: a flexible trimmer for Illumina sequence data. *Bioinformatics* 30, 2114–2120. doi: 10.1093/bioinformatics/btu170
- Butler, G., Rasmussen, M. D., Lin, M. F., Santos, M. A., Sakthikumar, S., Munro, C. A., et al. (2009). Evolution of pathogenicity and sexual reproduction in eight *Candida* genomes. *Nature* 459, 657–662. doi: 10.1038/nature08064
- Cantarel, B. L., Coutinho, P. M., Rancurel, C., Bernard, T., Lombard, V., and Henrissat, B. (2009). The carbohydrate-active EnZymes database (CAZy): an expert resource for glycogenomics. *Nucleic Acids Res.* 37, 233–238. doi: 10.1093/nar/gkn663
- Cantarel, B. L., Korf, I., Robb, S. M., Parra, G., Ross, E., Moore, B., et al. (2008). MAKER: an easy-to-use annotation pipeline designed for emerging model organism genomes. *Genome Res.* 18, 188–196. doi: 10.1101/gr.6743907
- Castoria, R., Caputo, L., De Curtis, F., and De Cicco, V. (2003). Resistance of postharvest biocontrol yeasts to oxidative stress: a possible new mechanism of action. *Phytopathology* 93, 564–572. doi: 10.1094/PHYTO.2003.93.5.564
- Cerveau, N., and Jackson, D. J. (2016). Combining independent de novo assemblies optimizes the coding transcriptome for nonconventional model eukaryotic organisms. *BMC Bioinformatics* 17:525. doi: 10.1186/s12859-016-1406-x
- Chatterjee, S., Alampalli, S. V., Nageshan, R. K., Chettiar, S. T., Joshi, S., and Tatu, U. S. (2015). Draft genome of a commonly misdiagnosed multidrug resistant pathogen *Candida auris*. *BMC Genomics* 16, 686. doi: 10.1186/s12864-015-1863-z
- DATA SHEET S4** | Gff file of MF.
- DATA SHEET S5** | Proteinortho analysis of *M. fructicola*, *M. bicuspidata*, *C. auris* and *C. lusitanae*.
- DATA SHEET S6** | Annotation file of MF, produced by Blast2GO.
- DATA SHEET S7** | Vcf file, obtained by mapping the *M. fructicola* strain AP47 reads on the genome of strain 277.
- DATA SHEET S8** | List of GO terms related to the mutation or repair of the DNA sequence.
- TABLE S1** | Annotation of Mf transcripts.
- TABLE S2** | CAZymes predicted in the *M. fructicola* 277 genome.
- TABLE S3** | fpkm expression data and statistical differences among conditions analyzed with RNAseq.
- Chin, C. S., Alexander, D. H., Marks, P., Klammer, A. A., Drake, J., Heiner, C., et al. (2013). Nonhybrid, finished microbial genome assemblies from long-read SMRT sequencing data. *Nat. Methods* 10, 563–569. doi: 10.1038/nmeth.2474
- Cimernancic, P., Medema, M. H., Claesen, J., Kurita, K., Brown, L. C. W., Mavrommatis, K., et al. (2014). Insights into secondary metabolism from a global analysis of prokaryotic biosynthetic gene clusters. *Cell* 158, 412–421. doi: 10.1016/j.cell.2014.06.034
- Cingolani, P., Platts, A., Wang, L. L., Coon, M., Nguyen, T., Wang, L., et al. (2012). A program for annotating and predicting the effects of single nucleotide polymorphisms, SnpEff: SNPs in the genome of *Drosophila melanogaster* strain w1118. *Fly* 6, 80–92. doi: 10.4161/fly.19695
- Cock, P. J., Antao, T., Chang, J. T., Chapman, B. A., Cox, C. J., Dalke, A., et al. (2009). Biopython: freely available Python tools for computational molecular biology and bioinformatics. *Bioinformatics* 25, 1422–1423. doi: 10.1093/bioinformatics/btp163
- Conesa, A., Götz, S., García-Gómez, J. M., Terol, J., Talón, M., and Robles, M. (2005). Blast2GO: a universal tool for annotation, visualization and analysis in functional genomics research. *Bioinformatics* 21, 3674–3676. doi: 10.1093/bioinformatics/bti610
- Droby, S., Wisniewski, M., Macarasin, D., and Wilson, C. (2009). Twenty years of postharvest biocontrol research: is it time for a new paradigm? *Postharvest Biol. Technol.* 52, 137–145. doi: 10.1016/j.postharvbio.2008.11.009
- Droby, S., Wisniewski, M., Teixidó, N., Spadaro, D., and Jijakli, M. H. (2016). The science, development, and commercialization of postharvest biocontrol products. *Postharvest Biol. Technol.* 122, 22–29. doi: 10.1016/j.postharvbio.2016.04.006
- Drori, E., Levy, D., Smirin-Yosef, P., Rahimi, O., and Salmon-Divon, M. (2017). CircosVCF: circos visualization of whole-genome sequence variations stored in VCF files. *Bioinformatics* 33, 1392–1393. doi: 10.1093/bioinformatics/btw834
- Drozdzova, P. B., Tarasov, O. V., Matveenko, A. G., Radchenko, E. A., Sopova, J. V., Polev, D. E., et al. (2016). Genome sequencing and comparative analysis of *Saccharomyces cerevisiae* strains of the petherhof genetic collection. *PLoS One* 11:e0154722. doi: 10.1371/journal.pone.0154722
- Fan, H., Ives, A. R., Surget-Groba, Y., and Cannon, C. H. (2015). An assembly and alignment-free method of phylogeny reconstruction from next-generation sequencing data. *BMC Genomics* 16:522. doi: 10.1186/s12864-015-1647-5
- Fares, M. A., Sabater-Muñoz, B., and Toft, C. (2017). Genome mutational and transcriptional hotspots are traps for duplicated genes and sources of adaptations. *Genome Biol. Evol.* 9, 1229–1240. doi: 10.1093/gbe/evx085
- Finn, R. D., Attwood, T. K., Babbitt, P. C., Bateman, A., Bork, P., Bridge, A. J., et al. (2016a). InterPro in 2017—beyond protein family and domain annotations. *Nucleic Acids Res.* 45, 190–199. doi: 10.1093/nar/gkw1107
- Finn, R. D., Coghill, P., Eberhardt, R. Y., Eddy, S. R., Mistry, J., Mitchell, A. L., et al. (2016b). The Pfam protein families database: towards a more sustainable future. *Nucleic Acids Res.* 44, D279–D285. doi: 10.1093/nar/gkv1344
- Friel, D., Pessoa, N. M. G., Vandenbol, M., and Jijakli, M. H. (2007). Separate and combined disruptions of two exo-beta-1,3-glucanase genes decrease the efficiency of *Pichia anomala* (strain K) biocontrol against *Botrytis cinerea* on apple. *Mol. Plant Microbe Int.* 20, 371–379. doi: 10.1094/MPMI-20-4-0371

- Galhardo, R. S., Hastings, P. J., and Rosenberg, S. M. (2007). Mutation as a stress response and the regulation of evolvability. *Crit. Rev. Biochem. Mol.* 42, 399–435. doi: 10.1080/10409230701648502
- Gao, Y., Honzatko, R. B., and Peters, R. J. (2012). Terpenoid synthase structures: a so far incomplete view of complex catalysis. *Nat. Prod. Rep.* 29, 1153–1175. doi: 10.1039/c2np20059g
- Grabherr, M. G., Haas, B. J., Yassour, M., Levin, J. Z., Thompson, D. A., Amit, I., et al. (2011). Full-length transcriptome assembly from RNA-Seq data without a reference genome. *Nat. Biotechnol.* 29, 644–652. doi: 10.1038/nbt.1883
- Hershkovitz, V., Ben-Dayana, C., Raphael, G., Pasmanik-Chor, M., Liu, J., Belasov, E., et al. (2012). Global changes in gene expression of grapefruit peel tissue in response to the yeast biocontrol agent *Metschnikowia fructicola*. *Mol. Plant Pathol.* 13, 338–349. doi: 10.1111/j.1364-3703.2011.00750.x
- Hershkovitz, V., Sela, N., Taha-Salaime, L., Liu, J., Rafael, G., Kessler, C., et al. (2013). De-novo assembly and characterization of the transcriptome of *Metschnikowia fructicola* reveals differences in gene expression following interaction with *Penicillium digitatum* and grapefruit peel. *BMC Genomics* 14:168. doi: 10.1186/1471-2164-14-168
- Hirakawa, M. P., Martinez, D. A., Sakthikumar, S., Anderson, M. Z., Berlin, A., Gujja, S., et al. (2015). Genetic and phenotypic intra-species variation in *Candida albicans*. *Genome Res.* 25, 413–425. doi: 10.1101/gr.174623.114
- Hoffmann, M., Muruvanda, T., Allard, M. W., Korlach, J., Roberts, R. J., Timme, R., et al. (2013). Complete genome sequence of a multidrug-resistant *Salmonella enterica* serovar Typhimurium var. 5- strain isolated from chicken breast. *Genome Announc.* 1:e1068-e13. doi: 10.1128/genomeA.01068-13
- Hyldgaard, M., Mygind, T., and Meyer, R. L. (2012). Essential oils in food preservation: mode of action, synergies, and interactions with food matrix components. *Front. Microbiol.* 25, 3–12. doi: 10.3389/fmicb.2012.00012
- Jijakli, M. H., and Lepoivre, P. (1998). Characterization of an exo-beta-1,3-glucanase produced by *Pichia anomala* strain K, antagonist of *Botrytis cinerea* on apples. *Phytopathology* 88, 335–343. doi: 10.1094/PHYTO.1998.88.4.335
- Joshi, N., and Fass, J. (2011). *Sickle: A Sliding-Window, Adaptive, Quality-Based Trimming Tool for FastQ Files*. Available at: github.com/najoshi/sickle
- Karabulut, O., Tezcan, H., Daus, A., Cohen, L., Wiess, B., and Droby, S. (2004). Control of preharvest and postharvest fruit rot in strawberry by *Metschnikowia fructicola*. *Biocontrol. Sci. Technol.* 14, 513–521. doi: 10.1080/09583150410001682287
- Karabulut, O. A., Smilanick, J. L., Gabler, F. M., Mansour, M., and Droby, S. (2003). Near-harvest applications of *Metschnikowia fructicola*, ethanol, and sodium bicarbonate to control postharvest diseases of grape in central California. *Plant Dis.* 87, 1384–1389. doi: 10.1094/PDIS.2003.87.11.1384
- Kolton, M., Sela, N., Elad, Y., and Cytryn, E. (2013). Comparative genomic analysis indicates that niche adaptation of terrestrial Flavobacteria is strongly linked to plant glycan metabolism. *PLoS One* 8:e76704. doi: 10.1371/journal.pone.0076704
- Kurtzman, C. P., and Droby, S. (2001). *Metschnikowia fructicola*, a new ascosporic yeast with potential for biocontrol of postharvest fruit rots. *Syst. Appl. Microbiol.* 24, 395–399. doi: 10.1371/journal.pone.0076704
- Kurtzman, C. P., and Robnett, C. J. (1998). Identification and phylogeny of ascomycetous yeasts from analysis of nuclear large subunit (26S). ribosomal DNA partial sequences. *Antonie Van Leeuwenhoek* 73, 331–371. doi: 10.1023/A:1001761008817
- Lachance, M. A., Hurtado, E., and Hsiang, T. (2016). A stable phylogeny of the large-spored *Metschnikowia* clade. *Yeast* 33, 261–275. doi: 10.1002/yea.3163
- Langmead, B., and Salzberg, S. L. (2012). Fast gapped-read alignment with Bowtie 2. *Nat. Methods* 9, 357–359. doi: 10.1038/nmeth.1923
- Langmead, B., Trapnell, C., Pop, M., and Salzberg, S. L. (2009). Ultrafast and memory-efficient alignment of short DNA sequences to the human genome. *Genome Biol.* 10:R25. doi: 10.1186/gb-2009-10-3-r25
- Lechner, M., Findeiß, S., Steiner, L., Marz, M., Stadler, P. F., and Prohaska, S. J. (2011). Proteinortho: detection of (Co-) orthologs in large-scale analysis. *BMC Bioinformatics* 12:124. doi: 10.1186/1471-2105-12-124
- Leinonen, R., Sugawara, H., and Shumway, M. (2011). The sequence read archive. *Nucleic Acids Res.* 39(Database issue), D19–D21. doi: 10.1093/nar/gkq1019
- Lenassi, M., Gostinčar, C., Jackman, S., Turk, M., Sadowski, I., Nislow, C., et al. (2013). Whole genome duplication and enrichment of metal cation transporters revealed by de novo genome sequencing of extremely halotolerant black yeast *Hortaea werneckii*. *PLoS One* 8:e71328. doi: 10.1371/journal.pone.0071328
- Li, B., and Dewey, C. N. (2011). RSEM: accurate transcript quantification from RNA-Seq data with or without a reference genome. *BMC Bioinformatics* 12:323. doi: 10.1186/1471-2105-12-323
- Li, H. (2011). A statistical framework for SNP calling, mutation discovery, association mapping and population genetic parameter estimation from sequencing data. *Bioinformatics* 27, 2987–2993. doi: 10.1093/bioinformatics/btr509
- Li, H., and Durbin, R. (2009). Fast and accurate short read alignment with Burrows–Wheeler transform. *Bioinformatics* 25, 1754–1760. doi: 10.1093/bioinformatics/btp324
- Li, H., Handsaker, B., Wysoker, A., Fennell, T., Ruan, J., Homer, N., et al. (2009). The sequence alignment/map format and SAMtools. *Bioinformatics* 25, 2078–2079. doi: 10.1093/bioinformatics/btp352
- Macarasin, D., Droby, S., Bauman, G., and Wisniewski, M. (2010). Superoxide anion and hydrogen peroxide in the yeast antagonist–fruit interaction: A new role for reactive oxygen species in postharvest biocontrol? *Postharvest Biol. Technol.* 58, 194–202. doi: 10.1016/j.postharvbio.2010.07.008
- Massart, S., Perazzoli, M., Höfte, M., Pertot, I., and Jijakli, M. H. (2015). Impact of the omic technologies for understanding the modes of action of Biological Control agents against plant pathogens. *BIOCONTROL* 60, 725–746. doi: 10.1007/s10526-015-9686-z
- Namdeo, A. (2007). Plant cell elicitation for production of secondary metabolites: a review. *Pharmacogn. Rev.* 1, 69–79.
- O'Donnell, K. (1993). “Fusarium and its near relatives,” in *The Fungal Holomorph: Mitotic, Meiotic and Pleomorphic Speciation in Fungal Systematics*, eds D. R. Reynolds and J. W. Taylor (Wallingford, CT: CAB International), 225–233.
- Park, B. H., Karpins, T. V., Syed, M. H., Leuze, M. R., and Uberbacher, E. C. (2010). CAZymes Analysis Toolkit (CAT): web service for searching and analyzing carbohydrate-active enzymes in a newly sequenced organism using CAZy database. *Glycobiology* 20, 1574–1584. doi: 10.1093/glycob/cwq106
- Pirone-Davies, C., Hoffmann, M., Roberts, R. J., Muruvanda, T., Timme, R. E., Strain, E., et al. (2015). Genome-wide methylation patterns in *Salmonella enterica* subsp. *enterica* serovars. *PLoS One* 10:e0123639. doi: 10.1371/journal.pone.0123639
- Randazzo, P., Aubert-Frambourg, A., Guillot, A., and Auger, S. (2016). The MarR-like protein PchR (YvmB) regulates expression of genes involved in pulcherriminic acid biosynthesis and in the initiation of sporulation in *Bacillus subtilis*. *BMC Microbiol.* 16:190. doi: 10.1186/s12866-016-0807-3
- Riley, R., Haridas, S., Wolfe, K. H., Lopes, M. R., Hittinger, C. T., Göker, M., et al. (2016). Comparative genomics of biotechnologically important yeasts. *Proc. Natl. Acad. Sci. U.S.A.* 113, 9882–9887. doi: 10.1073/pnas.1603941113
- Robinson, M. D., McCarthy, D. J., and Smyth, G. K. (2010). edgeR: a Bioconductor package for differential expression analysis of digital gene expression data. *Bioinformatics* 26, 139–140. doi: 10.1093/bioinformatics/btp616
- Rodrigues-Pousada, C., Menezes, R. A., and Pimentel, C. (2010). The Yap family and its role in stress response. *Yeast* 27, 245–258. doi: 10.1002/yea.1752
- Saravanakumar, D., Ciavarella, A., Spadaro, D., Garibaldi, A., and Gullino, M. L. (2008). *Metschnikowia pulcherrima* strain MACH1 outcompetes *Botrytis cinerea*, *Alternaria alternata* and *Penicillium expansum* in apples through iron depletion. *Postharvest Biol. Technol.* 49, 121–128. doi: 10.1016/j.postharvbio.2007.11.006
- Sipiczki, M. (2006). *Metschnikowia* strains isolated from botrytized grapes antagonize fungal and bacterial growth by iron depletion. *Appl. Environ. Microbiol.* 72, 6716–6724. doi: 10.1128/AEM.01275-06
- Spadaro, D., and Droby, S. (2016). Development of biocontrol products for postharvest diseases of fruit: the importance of elucidating the mechanisms of action of yeast antagonists. *Trends Food Sci. Technol.* 47, 39–49. doi: 10.1016/j.tifs.2015.11.003
- Spadaro, D., Loré, A., Garibaldi, A., and Gullino, M. L. (2013). A new strain of *Metschnikowia fructicola* for postharvest control of *Penicillium expansum* and patulin accumulation on four cultivars of apple. *Postharvest Biol. Technol.* 75, 1–8. doi: 10.1016/j.postharvbio.2012.08.001
- Spadaro, D., Sabetta, W., Acquadro, A., Portis, E., Garibaldi, A., and Gullino, M. L. (2008). Use of AFLP for differentiation of *Metschnikowia pulcherrima*

- strains for postharvest disease biological control. *Microbiol. Res.* 163, 523–530. doi: 10.1016/j.micres.2007.01.004
- Stanke, M., and Morgenstern, B. (2005). AUGUSTUS: a web server for gene prediction in eukaryotes that allows user-defined constraints. *Nucleic Acids Res.* 33, 465–467. doi: 10.1093/nar/gki458
- UniProt Consortium (2017). UniProt: the universal protein knowledgebase. *Nucleic Acids Res.* 45, 158–169. doi: 10.1093/nar/gkw1099
- Weber, T., Blin, K., Duddela, S., Krug, D., Kim, H. U., Brucoleri, R., et al. (2015). antiSMASH 3.0—a comprehensive resource for the genome mining of biosynthetic gene clusters. *Nucleic Acids Res.* 43, 237–243. doi: 10.1093/nar/gkv437
- Wisniewski, M., Droby, S., Norelli, J., Liu, J., and Schena, L. (2016). Alternative management technologies for postharvest disease control: the journey from simplicity to complexity. *Postharvest Biol. Technol.* 122, 3–10. doi: 10.1016/j.postharvbio.2016.05.012
- Zhang, D., Spadaro, D., Garibaldi, A., and Gullino, M. L. (2010). Selection and evaluation of new antagonists for their efficacy against postharvest brown rot of peaches. *Postharvest Biol. Technol.* 55, 174–181. doi: 10.1016/j.postharvbio.2009.09.007
- Conflict of Interest Statement:** The authors declare that the research was conducted in the absence of any commercial or financial relationships that could be construed as a potential conflict of interest.

Copyright © 2018 Piombo, Sela, Wisniewski, Hoffmann, Gullino, Allard, Levin, Spadaro and Droby. This is an open-access article distributed under the terms of the Creative Commons Attribution License (CC BY). The use, distribution or reproduction in other forums is permitted, provided the original author(s) and the copyright owner are credited and that the original publication in this journal is cited, in accordance with accepted academic practice. No use, distribution or reproduction is permitted which does not comply with these terms.



Effective Biodegradation of Mycotoxin Patulin by Porcine Pancreatic Lipase

Bingjie Liu, Xiaoning Peng and Xianghong Meng*

College of Food Science and Engineering, Ocean University of China, Qingdao, China

Patulin is a common contaminant in fruits and vegetables, which is difficult to remove. In this study, the biodegradation of patulin using porcine pancreatic lipase (PPL) was investigated. The method of HPLC was used to analyze the concentration of patulin. Batch degradation experiments were performed to illustrate the effect of PPL amount, pH, temperature, contact time, and initial concentration. Besides, the degradation product of patulin was characterized by full wavelength scanning and MS technologies. The results showed that the optimum degradation conditions of PPL for patulin was observed at pH 7.5, 40°C for 48 h. The percentage of degradation could reach above 90%. The structure of degradable product of patulin was inferred by the molecular weight 159.0594, named $C_7H_{11}O_4^+$. It indicated that PPL was effective for the degradation of patulin in fruits and vegetables juice.

Keywords: porcine pancreatic lipase, patulin, biodegradation, characterization, molecular structure

OPEN ACCESS

Edited by:

Nengguo Tao,
Xiangtan University, China

Reviewed by:

Jun Tian,
Jiangsu Normal University, China
Xingfeng Shao,
Ningbo University, China

*Correspondence:

Xianghong Meng
mengxh@ouc.edu.cn

Specialty section:

This article was submitted to
Food Microbiology,
a section of the journal
Frontiers in Microbiology

Received: 01 November 2017

Accepted: 16 March 2018

Published: 09 April 2018

Citation:

Liu B, Peng X and Meng X (2018)
Effective Biodegradation of Mycotoxin
Patulin by Porcine Pancreatic Lipase.
Front. Microbiol. 9:615.
doi: 10.3389/fmicb.2018.00615

INTRODUCTION

Patulin (4-hydroxy-4H-furo [3, 2c] pyran-2 [6H]-one), a mycotoxin contamination, is synthesized by various fungi, particularly *Penicillium*, *Aspergillus*, and *Byssoschlamys* species (Moake et al., 2005; Castoria et al., 2011; Zhu et al., 2015) (**Figure 1**). These fungi are important post-harvest pathogens of apples, pears, peaches, apricots as well as some vegetables (e.g., tomatoes) and caused the accumulation of patulin in infected products (Yuan et al., 2010; Castoria et al., 2011). Patulin poses a health risk to humans and livestock following acute and chronic effects, even at relatively low concentration (Moake et al., 2005; Zhu et al., 2015; Peng et al., 2016). Due to its toxicity, many countries and organizations, including China and WHO, have established the provisional maximum permitted level of patulin contamination for fruit- and vegetable-derived products (Food Agricultural Organization/World Health Organization [FAO/WHO], 1995; Castoria et al., 2005; Yuan et al., 2010). Therefore, it's necessary to remove patulin from foodstuffs.

The commonly used strategies for patulin removal include filtering and adsorption, electromagnetic irradiation, chemical addition, and biological degradation (Moake et al., 2005; Li et al., 2015). However, some problems still exist in the use of available physical and chemical methods for patulin detoxification, such as safety issues, possible losses in the nutritional quality, environmental damages, limited efficacy, and high cost (Kabak et al., 2006; Guo et al., 2013; Dong et al., 2015). So, the use of biological agents as an alternative strategy is considered as a powerful potential method (Dong et al., 2015). Besides, patulin was nearly degraded completely during the yeast *Saccharomyces cerevisiae* fermentation, this method was more useful than the other decontamination ones (Moake et al., 2005). It has been reported that the biocontrol Yeast *Rhodosporidium kratochvilovae* strain LS11 can reduce patulin contamination in the stored fruit (Castoria et al., 2011) and the complete degradation of patulin was observed within 48 and 72 h in the presence of 15 $\mu\text{g/mL}$ patulin (Reddy et al., 2011). A later study showed that a strain of marine

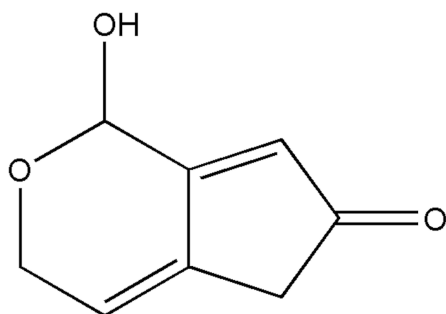


FIGURE 1 | Molecular structure of patulin.

yeast renamed *K. ohmeri* HYJM34 was screened, which has high patulin degradation ability, and the biodegradation of patulin by *K. ohmeri* might be an enzymatically driven process (Dong et al., 2015). However, biological control with yeast is limited to product that it could be fermented in the process (Moake et al., 2005).

The structure of patulin reveals the presence of a lactone bond. Therefore, reducing enzymes such as those involved in yeast fermentation, as well as lactone degrading enzymes such as lactamase, may well be able to degrade patulin alone (Moake et al., 2005). This paper was focus on investigating the effect of enzymes for patulin degradation.

Lipases (triacylglycerol ester hydrolases; E.C. 3.1.1.3) are found in microorganisms, plants and animal tissues. Among them, porcine pancreatic lipase (PPL) is one of the most widely used lipases in catalyzing a variety of reactions, such as esterification, interesterification and hydrolysis, which is cheaper than other commercial microbial and animal lipases (Kartal et al., 2009; Li et al., 2009; Mendes et al., 2012). The PPL investigated is composed of a single chain of 449 kinds of amino acids and 7 kinds of disulfide bonds (Giessauf and Gamse, 2000; Mendes et al., 2012). PPL had already been used as a biocatalyst for enantioselective esterification of glycidol (Martins et al., 1994) and enzymatic hydrolysis of triolein as well as its partial glycerides (Głowacz et al., 1996). In this study, PPL was chosen as a catalyzer that could be possibly used for patulin degradation.

So far, there are few studies about the direct enzymatic degradation of patulin. The aim of this work was to study the degradation of patulin using PPL, which can provide a kind of material to degrade patulin in fruits and vegetables product. And the purpose of this study reported here were to investigate the degradation rate of PPL for patulin at various conditions and characterize the action mechanism by full wavelength scanning and mass spectrometry analysis.

MATERIALS AND METHODS

Materials

The PPL (type II, E.C. 3.1.1.3, with a specific activity of 100–400 olive oil units per milligram of protein) was supplied by Sigma-Aldrich, Co., Ltd. (St. Louis, MO, United States);

acetic acid was of analytical purity and used as received without further purification. Acetonitrile and chloroform were of high performance liquid chromatography grade. Patulin was obtained from Sigma-Aldrich, Co., Ltd. Ultrapure water was used throughout all of the experiments.

Preparation of Patulin Solution

Working Solution A

Solid patulin was dissolved into 50 mL of chloroform to obtain 100 mg/L standard patulin solution, and stored at -18°C . The patulin standard solution could evaporated to dry, then dissolved in deionized water (adjusted to pH 4.0 with acetic acid) with the final concentration of 5 mg/L (Zhang et al., 2016). The working solution A was obtained.

Working Solution B

The *Penicillium expansum* strain M1 was obtained by our laboratory. Strains M1 was cultivated at 28°C for 14 days in PDA medium. The patulin extraction process was prepared according to the methodology described by MacDonald et al. (2000) with some modifications: the mixture of fungus and culture medium was separated, followed by extracting three times with ethyl acetate, cleaned up by extraction with 10 mL of a 1.5% (w/v) sodium bicarbonate aqueous solution. The ethyl acetate extract was passed over a shaker-incubator with 180 r/min, 25°C for 1 h and evaporated to dryness. Then, patulin was dissolved into 1 mL deionized water, adjusted to pH 4.0 with acetic acid. Thus, the working solution B was obtained.

Patulin Degradation by PPL

The degradation experiments of patulin in aqueous solution were carried out in 50 mL Erlenmeyer flasks. The powdered PPL was added to 5 mL working solution B constantly. The control was prepared without addition of PPL (Guo et al., 2013). They were placed on a shaker-incubator with 180 r/min, 30°C . The concentration of patulin in aqueous solution after the degradation could be measured by HPLC. Then, 0.45 μm microPES (Shimadzu, Japan) was used for purification before detection (Peng et al., 2016). The samples were detected by HPLC with UV detection (Li et al., 2007).

The effect of lipase amounts on degradation rate was investigated in the range of 0.3–2.4 mg. The effect of pH was investigated at the pH range from 3.5 to 8.5. The pH value was adjusted to the desired 1 mol/L phosphate buffer solution. The effect of temperature on degradation rate was investigated ranging from 20 to 60°C . The effect of contact time was conducted at nine different levels every 6 h for 54 h. The effect of initial patulin concentration was conducted in the range of 5–30 mg/L.

The degradation rate of PPL for patulin was calculated using Eq. (1):

$$\omega = \frac{C_0 - C_e}{C_0} \quad (1)$$

where, ω (%) is the degradation rate of PPL for patulin; C_0 and C_e (mg/L) are the initial and equilibrium concentrations of patulin in the solutions, respectively.

The degradation capacity of PPL for patulin was calculated using Eq. (2).

$$q_e = \frac{(C_0 - C_e) \times V}{m} \quad (2)$$

where, q_e (mg/mg) is the degradation capacity of PPL for patulin; C_0 and C_e (mg/L) are the initial and equilibrium concentrations of patulin in the solutions, respectively. V (mL) is the volume of patulin aqueous solutions and m (mg) is the mass of dry PPL.

Ultrafiltration and Determination

The Vivaspın centrifugal concentrators with a molecular weight cut off of 3000 were obtained from Millipore (Bedford, MA, United States). The samples were transferred to Vivaspın centrifugal filters spun at $4000 \times g$ in swing bucket rotor at 25°C for 10 min to deplete the high molecular weight proteins. Finally, 1 mL of patulin degradation was collected (Zheng et al., 2006).

Then, a 1260 HPLC system (Agilent, United States) equipped with UV detector was used to detect the concentration of patulin. The analytical column was Agilent ZORBAX SB-C18, $5 \mu\text{m} \times 4.6 \text{ mm} \times 250 \text{ mm}$; no guard column was used. The mobile phase, eluting at a flow rate of 1 mL/min, consisted of an isocratic mixture of acetonitrile/water (1:9, v:v). The chromatograms for calculations were extracted at 276 nm. The HPLC column was conditioned before analysis by running a background without injection. For regular analysis, 20 μL of sample or standard solution was injected. In addition to samples and calibration standards, control samples were analyzed for each matrix. The requirements for recovery of these samples were set to 60–115%. The limits of detection and quantification were 10.78 and 32.67 $\mu\text{g/L}$, respectively (Li et al., 2015).

Identification of the Degradation Products

The powdered PPL was added to 5 mL working solution A constantly.

The optical spectra of samples were recorded by using a Unico UV2102-PC UV-Visible spectrophotometer (Shanghai, China) (Zhu et al., 2016). The samples at 24 h were transferred to Vivaspın centrifugal filters spun at $4000 \times g$ for 10 min to deplete the PPL. Finally, 1 mL of patulin degradation product was collected. The preparation of patulin solutions was diluted by ultrapure water. And the UV-vis spectra were recorded from 190 to 700 nm.

Accurate-Mass Q-TOF LC/MS (Agilent, United States) was used. The molecular weight of patulin degradation products was identified by was determined by ESI-MS. The mobile phase eluting at a flow rate of 0.4 mL/min, consisted of an isocratic mixture of methanol/water (1:9, v:v). The sample injection volume was 20 μL . ESI-MS experiments were performed on positive ionization mode. The MS operation parameters were set as followed: capillary voltage 4000 V, drying gas flow 10 L/min, drying gas temperature 350°C , vaporizer temperature 450°C , and nebulizer pressure 40 psi. The optimal fragmentor voltage was 50 V, with a mass range of m/z 20–500 for MS/MS scan modes containing product and precursor ion

scans. The Agilent Mass Hunter software package (version 6.1) was used for data acquisition and analysis (Agilent, United States).

Statistical Analyses

All of the experiments were carried out in triplicate, and the results were expressed as means \pm standard deviation. The data was analyzed by one-way analysis of variance (ANOVA) using SPSS (version 19.0, SPSS, Inc.), and Duncan's multiple comparisons were adopted to assess the statistical significance ($P < 0.05$).

RESULTS AND DISCUSSION

Effect of PPL Amount on Degradation Rate and Degradation Capacity

The dosage of PPL added into 5 mL patulin solution varied between 0.3 and 2.4 mg. Experiments were performed at 30°C for 30 h. As can be seen from **Figure 2**, the degradation rate of patulin increased obviously with the increasing of PPL concentration in solution and approached equilibrium at 0.36 mg/mL. It is more likely to predict that PPL catalyzed the degradation of patulin, while the substrate-binding sites maybe have reached to the saturation point as the concentration of PPL was above 0.36 mg/mL. However, the degradation capacity of PPL was decreased drastically between 0.06 and 0.18 mg/mL, later, it kept invariability. This is probably because that the velocity of PPL promoting reaction was related with the concentration of patulin. Thus, the optimal addition of PPL was 1.8 mg/5 mL.

Effect of pH on Degradation Rate and Degradation Capacity

Experiments were performed at the controlled pH (3.5–8.5) and 30°C by shaking 1.8 mg of PPL with 5 mL of patulin solutions

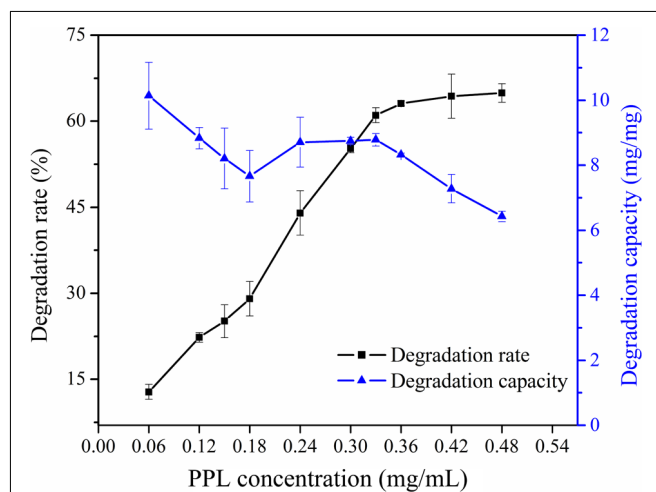


FIGURE 2 | Effect of enzyme concentration on degradation rate and degradation capacity of PPL for patulin.

for 30 h with 180 r/min. Results were shown in **Figure 3**. It indicated that the degradation rate was the highest at pH 7.5. The degradation rate changed insignificantly in the range of 3.5–5.5. This may be explained by the stability of patulin in acidic condition, and meanwhile, the activity of PPL was inhibited. As pH may not only affect the shape of an enzyme, but also it may change the shape or charge properties of the substrate. The data also demonstrated that the degradation rate increased between pH 5.5 and 7.5, later, it changed slightly at high pH. In general, the effect of pH probably results from the activity of enzyme. Therefore, the degradation capacity and degradation rate had the same change trend at early stage, which increased from pH 3.5 to 7.5. However, the degradation capacity declined quickly at pH 8.5. This was because that the activity of PPL was still high, but the patulin content of controlled group was declined significantly for the instability of patulin. Therefore, pH 7.5 was selected as the optimal pH in the following experiments.

Effect of Temperature on Degradation Rate and Degradation Capacity

The effect of temperature on degradation rate of PPL for patulin was studied at pH 7.5 and the results were shown in **Figure 4**. The degradation rate increased greatly with an increasing of temperature from 10 to 40°C and then onwards changes slightly. A possible explanation for the results was that the active site of an enzyme was the region that binds the substrates (Berg et al., 2002). The reaction rate would increase with the rising of temperature because the substrates would collide more frequently with PPL active site. And the heat of molecules in the system would increase. Thus, the degradation capacity increased as the temperature raised from 10 to 40°C. The increase of degradation capacity of PPL for patulin with increasing of temperature indicated that the nature of PPL hydrolysis process for patulin was endothermic (Kannamba et al., 2010). Besides, the reaction capacity then abruptly declined with further increase

of temperature. This is not only because PPL activity was low, but the patulin content of controlled group was also declined obviously at 60°C. Hence, the optimal temperature was set at 40°C for further studies.

Effect of Initial Patulin Concentration on Degradation Rate and Degradation Capacity

Effect of initial concentration of patulin was investigated. Taken into consideration need of practical application, experiments were conducted containing 5–30 mg/L patulin at 40°C for 30 h with 180 r/min (**Figure 5**). The results showed that the degradation rate declined evidently first and then remained steady in varying initial concentration from 15 to 30 mg/L. It was indicated that the degradation effect of patulin was favorable

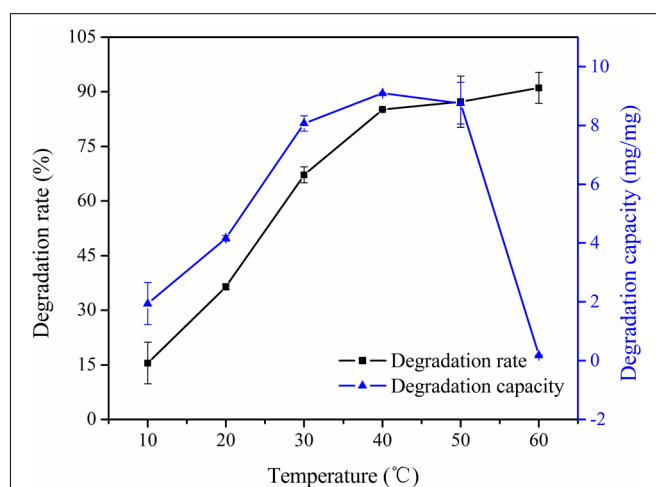


FIGURE 4 | Effect of temperature on degradation rate and degradation capacity of PPL for patulin.

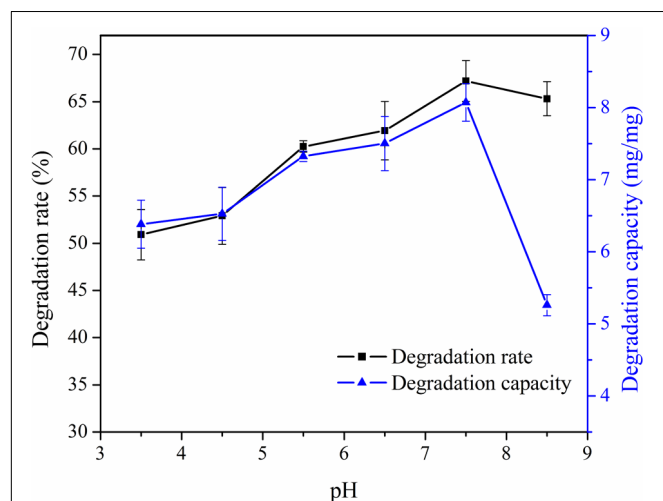


FIGURE 3 | Effect of pH on degradation rate and degradation capacity of PPL for patulin.

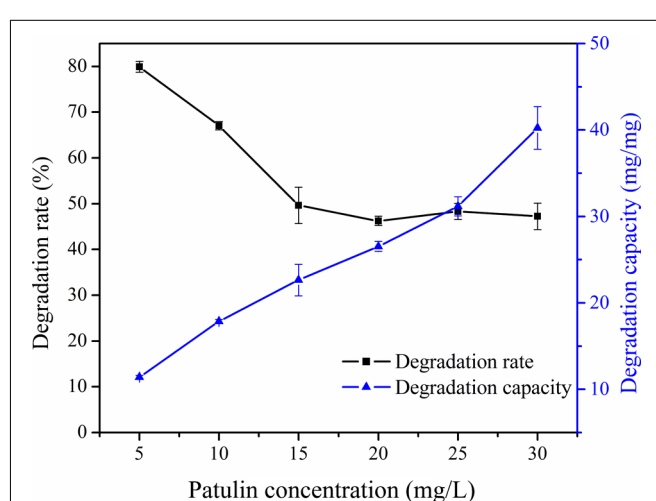
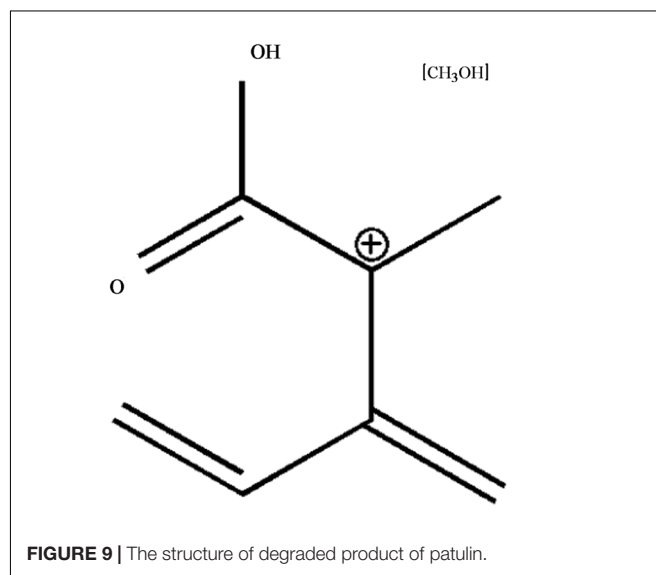
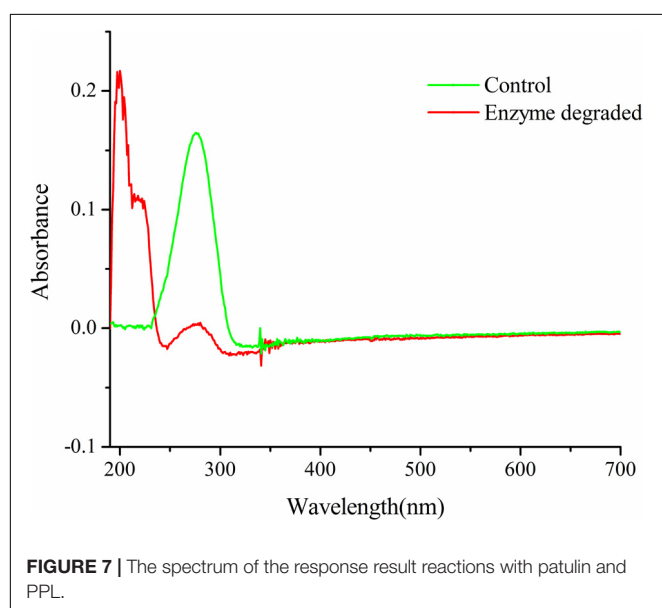
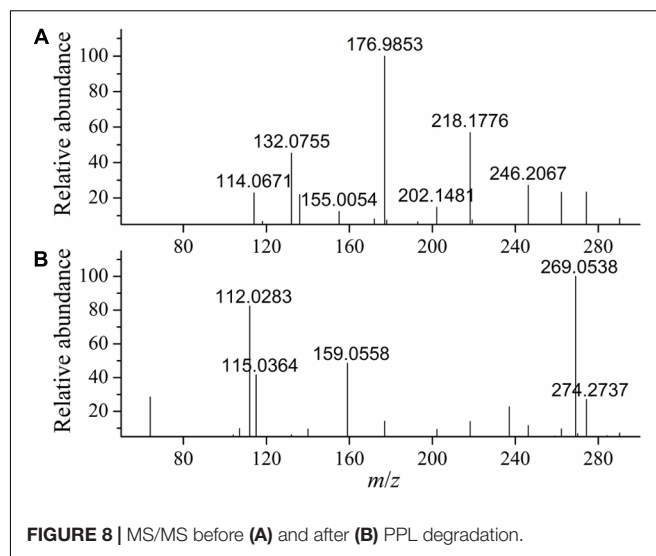
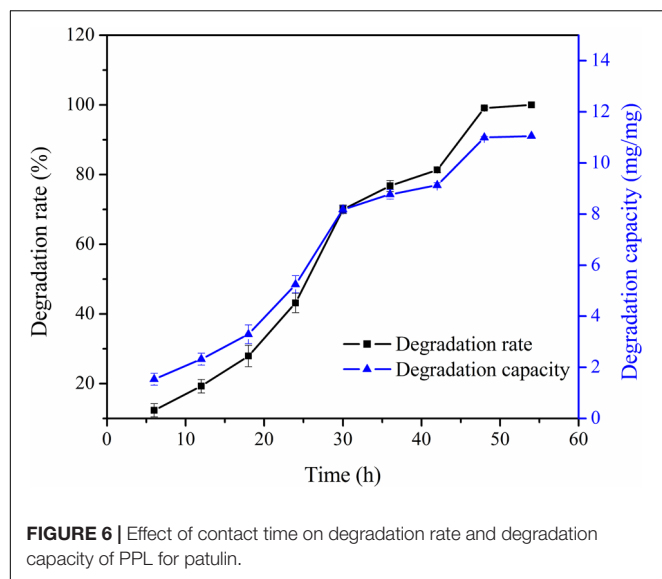


FIGURE 5 | Effect of initial concentration on degradation rate and degradation capacity of PPL for patulin.



at low substrate concentration. However, the results showed that the degradation capacity increased with the increasing of initial patulin concentration. A possible explanation for this was that PPL was unsaturated with substrate. It showed that the degradation capacity was going to be proportional to the concentration of substrate, according to the characteristic of enzymatic reaction (Berg et al., 2002).

Effect of Contact Time on Patulin Degradation Rate and Degradation Capacity

Degradation experiments with PPL were conducted at different times and the results were presented in **Figure 6**. The degradation rate increased with increasing of contact time and reached the maximum value at 48 h. The degradation capacity was following

the same trend. The results showed that the rate of degradation increased rapidly with contact time up to 30 h and then onwards was slow considerably. This was because that the active sites of PPL were more and concentration of patulin was higher during the initial stage of degradation (Kannamba et al., 2010; Peng et al., 2016). Similarly, then declining the active sites of PPL limited the reaction rate to the saturation condition.

Full Wavelength Scanning

Figure 7 showed the degradation spectrum of patulin at 24 h. The relationship between wavelength of the maximum absorption and structure was also explained (Ibarz et al., 2014). The results showed that the maximum absorption peaks of degradation product shifted to shorter wavelengths. And there was typical absorption of conjugated structures by UV scanning.

MS Scan of Degradation Products

MS analyses of patulin before and after PPL degradation were shown in **Figure 8**. As was shown in **Figure 8A**, the standard aqueous solution of patulin with Na^+ adducts $\text{C}_7\text{H}_6\text{NaO}_4$ ($\text{M}+\text{Na}^+$) calculated: 177.0158, the ESI-MS found: 176.9852. And patulin was identified at $m/z = 155.0054$ for protonated cation $[\text{M}+\text{H}]^+$. MS of patulin after degradation (**Figure 8B**) showed that the patulin in PPL treated samples was very less than untreated ones. The molecular weight of product might be 159.0558, according with the molecular weight 159.0594 for $\text{C}_7\text{H}_{11}\text{O}_4^+$ (**Figure 9**). It indicated that patulin was reacted with ring opening reaction with PPL. The fragment at m/z 159 can alternatively undergo successive losses of carbon dioxide (Malysheva et al., 2012). The speculation corresponds to the previous study by UV scanning. It was suggested that patulin was possibly metabolized to degradation product, which was chemically different from patulin.

CONCLUSION

In this study, PPL has been successfully used to degrade patulin in aqueous solution. It was conjectured that the process of patulin

degradation was enzymatic reaction. Batch studies showed that the degradation percentage of patulin was strongly dependent on reactive conditions such as pH, temperature, initial patulin concentration, and contact time. The complete degradation of patulin occurred at pH 7.0, 40°C for 48 h, the degradation capacity of PPL for patulin is 10.99 mg/mg PPL. The mechanism of degradation was discussed by using full spectrum scanning and MS analysis. Generally, PPL exhibited good degradation ability and it might have practical application for degradation of patulin in apple juice.

AUTHOR CONTRIBUTIONS

BL did the experiments and organized the manuscript. XP did the experiments. XM guided the analysis of the catabolite structure.

FUNDING

This work was financially supported by The National Key R&D Program of China (2016YFD0400902).

REFERENCES

- Berg, J. M., Tymoczko, J. L., and Stryer, L. (2002). *Biochemistry*, 5th Edn. New York, NY: W. H. Freeman and Company.
- Castoria, R., Mannina, L., Duránpatrón, R., Maffei, F., Sobolev, A. P., De Felice, D. V., et al. (2011). Conversion of the mycotoxin patulin to the less toxic desoxypatulinic acid by the biocontrol yeast *Rhodotorula glutinis* strain LS11 on patulin accumulation in stored apples. *Phytopathology* 95, 11571–11578. doi: 10.1021/jf203098v
- Castoria, R., Morena, V., Caputo, L., Panfili, G., De Curtis, F., and De Cicco, V. (2005). Effect of the biocontrol yeast *Rhodotorula glutinis* strain LS11 on patulin accumulation in stored apples. *Phytopathology* 95, 1271–1278. doi: 10.1094/PHYTO-95-1271
- Dong, X. Y., Jiang, W., Li, C. S., Ma, N., Xu, Y., and Meng, X. H. (2015). Patulin biodegradation by marine yeast *Kodameae ohmeri*. *Food Addit. Contam. Part A* 32, 352–360. doi: 10.1080/19440049.2015.1007090
- Food Agricultural Organization/World Health Organization [FAO/WHO] (1995). *44th Report of the Joint FAO/WHO Expert Committee on Food Additives*. Technical Report. WHO: Geneva.
- Giessauf, A., and Gamse, T. (2000). A simple process for increasing the specific activity of porcine pancreatic lipase by supercritical carbon dioxide treatment. *J. Mol. Catal. B Enzym.* 9, 57–64. doi: 10.1016/S1381-1177(99)00084-3
- Glowacz, G., Bariszlovich, M., Linke, M., Richter, P., Fuchs, C., and Mörsel, J. T. (1996). Stereoselectivity of lipases in supercritical carbon dioxide. Independence of the region and enantioselectivity of porcine pancreas lipase on the water content during the hydrolysis of triolein and its partial glycerides. *Chem. Phys. Lipids* 79, 101–106. doi: 10.1016/0009-3084(95)02513-8
- Guo, C. X., Yue, T. L., Yuan, Y. H., Wang, Z. L., Guo, Y. D., Wang, L., et al. (2013). Biosorption of patulin from apple juice by caustic treated waste cider yeast biomass. *Food Control* 32, 99–104. doi: 10.1016/j.foodcont.2012.11.009
- Ibarz, R., Garvin, A., Falguera, V., Pagán, J., Garza, S., and Ibarz, A. (2014). Modelling of patulin photo-degradation by a UV multi-wavelength emitting lamp. *Food Res. Int.* 66, 158–166. doi: 10.1016/j.foodres.2014.09.006
- Kabak, B., Dobson, A. D., and Var, I. (2006). Strategies to prevent mycotoxin contamination of food and animal feed: a review. *Crit. Rev. Food Sci. Nutr.* 46, 593–619. doi: 10.1080/10408390500436185
- Kannamba, B., Reddy, K. L., and Appa Rao, B. V. (2010). Removal of Cu(II) from aqueous solutions using chemically modified chitosan. *J. Hazard. Mater.* 175, 939–948. doi: 10.1016/j.jhazmat.2009.10.098
- Kartal, F., Akkaya, A., and Kilinc, A. (2009). Immobilization of porcine pancreatic lipase on glycidyl methacrylate grafted poly vinyl alcohol. *J. Mol. Catal. B Enzym.* 57, 55–61. doi: 10.1016/j.molcatb.2008.06.016
- Li, J.-k., Wu, R.-n., Hu, Q.-h., and Wang, J.-h. (2007). Solid-phase extraction and HPLC determination of patulin in apple juice concentrate. *Food Control* 18, 530–534. doi: 10.1016/j.foodcont.2005.12.014
- Li, Y., Wang, J. Y., Meng, X. H., and Liu, B. J. (2015). Removal of patulin from aqueous solution using cross-linked chitosan beads. *J. Food Saf.* 35, 248–256. doi: 10.1111/jfs.12173
- Li, Y. J., Zhou, G. W., Li, C. J., Qin, D. W., Qiao, W. T., and Chu, B. (2009). Adsorption and catalytic activity of Porcine pancreatic lipase on rod-like SBA-15 mesoporous material. *Colloids Surf. A Physicochem. Eng. Asp.* 341, 79–85. doi: 10.1016/j.colsurfa.2009.03.041
- MacDonald, S., Long, M., Gilbert, J., and Felgueiras, I. (2000). Liquid chromatographic method for determination of patulin in clear and cloudy apple juices and apple puree: collaborative study. *J. AOAC Int.* 83, 1387–1394.
- Malysheva, S. V., Diana Di Mavungu, J., Boonen, J., De Spiegeleer, B., Goryacheva, I. Y., Vanhaecke, L., et al. (2012). Improved positive electrospray ionization of patulin by adduct formation: usefulness in liquid chromatography-tandem mass spectrometry multi-mycotoxin analysis. *J. Chromatogr. A* 1270, 334–339. doi: 10.1016/j.chroma.2012.10.060
- Martins, J. F., de Carvalho, I. B., de Sampaio, T. C., and Barreiros, S. (1994). Lipase-catalyzed enantioselective esterification of glycidol in supercritical carbon dioxide. *Enzyme Microb. Technol.* 16, 785–790. doi: 10.1016/0141-0229(94)90036-1
- Mendes, A. A., Oliveira, P. C., and Castro, H. F. D. (2012). Properties and biotechnological applications of porcine pancreatic lipase. *J. Mol. Catal. B Enzym.* 78, 119–134. doi: 10.1016/j.molcatb.2012.03.004
- Moake, M. M., Padilla-Zakour, O. I., and Worobo, R. W. (2005). Comprehensive review of patulin control methods in foods. *Comp. Rev. Food Sci. Food Saf.* 4, 8–21. doi: 10.1111/j.1541-4337.2005.tb00068.x
- Peng, X. N., Liu, B. J., Chen, W., Li, X. H., Wang, Q. R., Meng, X. H., et al. (2016). Effective biosorption of patulin from apple juice by cross-linked xanthated chitosan resin. *Food Control* 63, 140–146. doi: 10.1016/j.foodcont.2015.11.039

- Reddy, K. R., Spadaro, D., Gullino, M. L., and Garibaldi, A. (2011). Potential of two *Metschnikowia pulcherrima* (yeast) strains for in vitro biodegradation of patulin. *J. Food Prot.* 74, 154–156. doi: 10.4315/0362-028X.JFP-10-331
- Yuan, Y., Zhuang, H., Zhang, T. H., and Liu, J. B. (2010). Patulin content in apple products marketed in Northeast China. *Food Control* 21, 1488–1491. doi: 10.1016/j.foodcont.2010.04.019
- Zhang, X. R., Guo, Y. R., Ma, Y., Chai, Y. H., and Li, Y. Y. (2016). Biodegradation of patulin by a *Byssochlamys nivea* strain. *Food Control* 64, 142–150. doi: 10.1016/j.foodcont.2015.12.016
- Zheng, X. Y., Baker, H., and Hancock, W. S. (2006). Analysis of the low molecular weight serum peptidome using ultrafiltration and a hybrid ion trap-Fourier transform mass spectrometer. *J. Chromatogr. A* 1120, 173–184. doi: 10.1016/j.chroma.2006.01.098
- Zhu, J. X., Sun, X. W., Chen, X. L., Wang, S. H., and Wang, D. F. (2016). Chemical cleavage of fucoxanthin from *Undaria pinnatifida* and formation of apo-fucoxanthinones and apo-fucoxanthinals identified using LC-DAD-APCI-MS/MS. *Food Chem.* 211, 365–373. doi: 10.1016/j.foodchem.2016.05.064
- Zhu, R. Y., Feussner, K., Wu, T., Yan, F. J., Karlovsky, P., and Zheng, X. D. (2015). Detoxification of mycotoxin patulin by the yeast *Rhodospiridium paludigenum*. *Food Chem.* 179, 1–5. doi: 10.1016/j.foodchem.2015.01.066
- Conflict of Interest Statement:** The authors declare that the research was conducted in the absence of any commercial or financial relationships that could be construed as a potential conflict of interest.
- Copyright © 2018 Liu, Peng and Meng. This is an open-access article distributed under the terms of the Creative Commons Attribution License (CC BY). The use, distribution or reproduction in other forums is permitted, provided the original author(s) and the copyright owner are credited and that the original publication in this journal is cited, in accordance with accepted academic practice. No use, distribution or reproduction is permitted which does not comply with these terms.



Phomopsis longanae Chi-Induced Changes in Activities of Cell Wall-Degrading Enzymes and Contents of Cell Wall Components in Pericarp of Harvested Longan Fruit and Its Relation to Disease Development

Yihui Chen¹, Shen Zhang¹, Hetong Lin^{1*}, Junzheng Sun¹, Yifen Lin¹, Hui Wang¹, Mengshi Lin² and John Shi³

OPEN ACCESS

Edited by:

Nengguo Tao,
Xiangtan University, China

Reviewed by:

Jia Liu,
Chongqing University of Arts
and Sciences, China
José Ascención Martínez-Álvarez,
University of Guanajuato, Mexico
Prashant Singh,
Florida State University, United States

*Correspondence:

Hetong Lin
hetonglin@126.com;
hetonglin@163.com

Specialty section:

This article was submitted to
Food Microbiology,
a section of the journal
Frontiers in Microbiology

Received: 31 March 2018

Accepted: 03 May 2018

Published: 23 May 2018

Citation:

Chen Y, Zhang S, Lin H, Sun J,
Lin Y, Wang H, Lin M and Shi J
(2018) *Phomopsis longanae*
Chi-Induced Changes in Activities
of Cell Wall-Degrading Enzymes
and Contents of Cell Wall
Components in Pericarp of Harvested
Longan Fruit and Its Relation
to Disease Development.
Front. Microbiol. 9:1051.
doi: 10.3389/fmicb.2018.01051

¹ Institute of Postharvest Technology of Agricultural Products, College of Food Science, Fujian Agriculture and Forestry University, Fuzhou, China, ² Food Science Program, Division of Food System & Bioengineering, University of Missouri, Columbia, MO, United States, ³ Guelph Food Research Center, Agriculture and Agri-Food Canada, Guelph, ON, Canada

The main goal of this study was to investigate the influences of *Phomopsis longanae* Chi infection on activities of cell wall-degrading enzymes (CWDEs), and contents of cell wall components in pericarp of harvested “Fuyan” longan (*Dimocarpus longan* Lour. cv. Fuyan) fruit and its relation to disease development. The results showed that, compared with the control samples, *P. longanae*-inoculated longans showed higher fruit disease index, lower content of pericarp cell wall materials (CWMs), as well as lower contents of pericarp cell wall components (cholate-soluble pectin (CSP), sodium carbonate-soluble pectin, hemicelluloses, and cellulose), but higher content of pericarp water-soluble pectin (WSP). In addition, the inoculation treatment with *P. longanae* significantly promoted the activities of CWDEs including pectinesterase, polygalacturonase, β -galactosidase, and cellulase. The results suggested that the *P. longanae* stimulated-disease development of harvested longans was due to increase in activities of pericarp CWDEs, which might accelerate the disassembly of pericarp cell wall components. In turn, resulting in the degradation of pericarp cell wall, reduction of pericarp mechanical strength, and subsequently leading to the breakdown of longan pericarp tissues. Eventually resulting in development of disease development and fruit decay in harvested longans during storage at 28°C.

Keywords: longan (*Dimocarpus longan* Lour.), *Phomopsis longanae* Chi, disease development, cell wall components, cell wall-degrading enzymes, cell wall disassembly

INTRODUCTION

In developed countries, fruit decay caused by pathogens affects 20–25% of the harvested fruits during post-harvest handling and storage. While in developing countries, the situation is even worse due to inadequate transportation, storage, and preservation facilities for fruits (Al-Hindi et al., 2011). Infection by pathogenic bacteria and fungi could take place in almost every step of fruit

production from pre-harvest to post-harvest storage and marketing (Yao and Tian, 2005; Aghdam and Fard, 2017; Li et al., 2017).

In botanic cells, the cell wall is the first barrier against the infection by fungal pathogens (Kubicek et al., 2014). Cell wall-degrading enzymes (CWDEs) secreted by pathogens play a key role in penetrating the cell wall to utilize the nutrients (Kang and Buchenauer, 2000; Lalaoui et al., 2000; Kikot et al., 2009; Tian et al., 2009; Gharbi et al., 2015; Ramos et al., 2016). There is a diverse array of CWDEs, including polygalacturonase (PG), pectin methylgalacturonase (PMG), pectinesterase (PE), pectin lyase (PL), pectate lyase (PNL), cellulase (C_X), β -glucosidase, and xylanases (Al-Hindi et al., 2011; Li et al., 2012; Kubicek et al., 2014). Ramos et al. (2016) found that *Macrophomina phaseolina* induced the cell wall degradation of maize and sunflower, which was initiated by the pectinase that was the first CWDE secreted by *M. phaseolina*. The activities of PG and PMG were higher than C_X that appeared in the later stage of the degradation process (Ramos et al., 2016). This sequence promoted the initial tissue maceration before the degradation of cell wall materials (CWMs). It was reported that *Fusarium culmorum* was able to secrete CWDEs including cellulases, xylanases, and pectinases. These CWDEs degraded the wheat spike plant tissues (cellulose, xylan, and pectin) and enabled the invasion to the tissues by *F. culmorum* (Kang and Buchenauer, 2000). Kang and Buchenauer (2000) also reported that in the cell wall, the degree of pectin degradation was higher compared with cellulose and xylan at the early stage of infection, which implied that there might be earlier secretion or higher activity of pectinases over cellulases or xylanases. Moreover, Li et al. (2012) showed that *Botryodiplodia theobromae* Pat. caused the stem-end rot of mangoes by producing PG, PMG, and C_X that disrupted the fruit tissues in the deterioration process. Therefore, it can be concluded that the secretion of CWDEs plays an important role in the degradation of plant cell wall during pathogenesis.

Longan is a well-known subtropical fruit with a short shelf life at room temperature due to its high susceptibility to pathogenic infections (Chen et al., 2014; Lin et al., 2017a,b,c, 2018; Zhang et al., 2017, 2018; Sun et al., 2018). Our previous studies demonstrated that *Phomopsis longanae* Chi (*P. longanae*) is one of the dominating pathogens that can cause postharvest decay of longans (Chen et al., 2011a,b, 2014; Lin et al., 2017a). To date, there has been no report on the types or activities of the CWDEs produced by *P. longanae*, and there is still a lack of research regarding the effect of these enzymes on infected longan fruits. The objective of this study was to investigate the changes of CWDEs activities during disease development in *P. longanae*-inoculated longan fruits and their effect on the degradation of cell wall. This study also aimed to elucidate the CWDEs' function during the infection of *P. longanae* on harvested longan fruits.

MATERIALS AND METHODS

Inoculation of Longan Fruits

Phomopsis longanae culturing and the preparation of spore suspension were performed as described in our previous

publication (Chen et al., 2014). The concentration of spore suspension was diluted to 1×10^4 spores mL^{-1} and used for inoculation.

"Fuyan" longan (*Dimocarpus longan* Lour. cv. Fuyan) fruit at commercial maturity were handpicked from a longan orchard (Quanzhou, Fujian, China). The harvested fruit were carefully packed and transported to a research laboratory in Fujian Agriculture and Forestry University (Fuzhou, Fujian, China) within 3 h and stored at 4°C. Fruit in uniform maturity and size were selected for the experiment and any rotten or damaged fruit were excluded.

The fruits were dipped in 0.5% sodium hypochlorite solution for 10 s to eliminate surface microorganisms, and then air-dried. A total of 150 fruits were employed to evaluate the properties of harvested fruits on day 0. The remaining 3000 fruits were randomly divided into two lots (1500 fruits per lot) for the control and *P. longanae*-inoculated treatment. The control group (1500 fruits) was dipped into the sterile deionized water for 5 min. The *P. longanae*-inoculated group (1500 fruits) was immersed into the *P. longanae* spore suspension (1×10^4 spores mL^{-1}) for 5 min. All fruits were then air dried and packed in a polyethylene bag with a thickness of 0.015 mm. Each bag contained 50 longan fruits and 30 bags were used for each treatment. The samples were then stored at 28°C with a relative humidity of 90%. For each treatment, three bags of fruit (total 150 longan fruits) were randomly selected on a daily basis during the storage period and used for the assessments of longan fruit. All the evaluations were conducted in triplicate.

Assessment of the Index of Fruit Disease

Longan fruit disease was assessed based on our previous study (Chen et al., 2014). The lesion proportion on fruit surface of 50 individual longan fruits was measured and defined to five disease scales. The calculations of fruit disease index were performed based on the method of Chen et al. (2014).

Preparation of CWM

Extraction of CWM was based on the modified procedures described in Duan et al. (2011) and Chen et al. (2017a,b). Ten grams of frozen longan pericarp were homogenized in 200 mL of 80 % ethanol. The mixture was boiled for 30 min with stirring. The solution was then cooled to room temperature, followed by filtration with filter papers ($\phi 11$ cm Medium-Speed, Whatman, Zhejiang, China). The residues were subsequently washed with 200 mL of 80% ethanol, immersed into 50 mL of 90 % dimethyl sulfoxide for 8 h to remove starches. It was subsequently washed with 200 mL of acetone, dried for 3 days at 40°C to report the final weight as CWM.

Fractionation and Analysis of Cell Wall Components

Cell wall components fractionation and analysis were followed the procedures reported in Rugkong et al. (2010) and Chen et al. (2017a,b) with some modifications. Water-soluble pectin (WSP) was extracted via dispersing CWM (300 mg) in sodium acetate buffer (50 mmol L^{-1} , pH 6.5) for 6 h with shaking (SKY-200B,

SUKUN, Shanghai, China). The mixture was then centrifuged ($10,000 \times g$, 4°C) for 10 min (Centrifuge 5810R, Eppendorf AG, Hamburg, Germany). The sediment was immersed in 20 mL of 50 mmol L^{-1} ethylene diamine tetraacetic acid (EDTA) with 1 mol L^{-1} NaCl (pH 6.8). After shaking and centrifugation, the supernatant containing chelate-soluble pectin (CSP) was collected. Residues were further immersed in 20 mL of 50 mmol L^{-1} Na_2CO_3 with 20 mmol L^{-1} NaBH_4 for another shaking and centrifugation. The supernatant containing Na_2CO_3 -soluble pectin (NSP) was collected. The remaining residue was further dipped in 10 mL of 4 mmol L^{-1} KOH solution with 100 mmol L^{-1} NaBH_4 for shaking and centrifugation, and the supernatant collected was considered as hemicellulose. A volume of 1% sodium sulfite and 50 mL of 8 mol L^{-1} KOH solution with 10 mmol L^{-1} NaBH_4 were then added to the remaining residue for shaking and centrifugation, and the supernatant containing cellulose was collected. The amounts of WSP, CSP, and NSP were determined via m-hydroxydiphenyl method (Wang et al., 2015; Chen et al., 2017a,b). The amount of hemicellulose and cellulose were determined based on the anthrone method (Wang et al., 2015; Chen et al., 2017a,b).

Extraction and Assay of CWDEs

Enzyme extraction was based on the procedures described by Andrews and Li (1995) and Chen et al. (2017a,b). Briefly, frozen longan pericarp (1 g) was ground with 8 mL of 40 mmol L^{-1} sodium acetate buffer (containing 100 mmol L^{-1} NaCl, 2% mercaptoethanol and 5% PVP, pH 5.2). The homogenous solution was centrifuged ($12,000 \times g$, 20 min) at 4°C . The collected supernatant was used to measure the activities of PE, PG, β -galactosidase and cellulase.

Pectinesterase activity was measured by combining 3 mL of crude enzyme with 10 mL of 1% pectin for the titration using 0.01 mol L^{-1} NaOH (pH 7.4 at 37°C for 30 min). The amount of enzyme that consumed 1 μmol NaOH solution per hour was used to define one unit of PE activity.

Polygalacturonase activity was determined by mixing 5 mL of 20 mmol L^{-1} sodium acetate (pH 4.0), 2 mL of 1% (w/v) polygalacturonic acid, and 1 mL of crude enzyme extract, followed by incubation at 37°C for the 30 min. A volume of 2 mL of 10 mmol L^{-1} $\text{Na}_2\text{B}_4\text{O}_7$ was then added to the reaction mixture before terminating the reaction with 0.1 mL of 1% (w/v) 2-cyanoacetamide and boiling for 5 min. The boiled reaction mixture without adding substrate was used as the blank. The concentrations of the reducing groups were measured at 276 nm with D-galacturonic acid as the standard. The amount of enzyme producing 1 μmol galacturonic acid per hour was considered as one unit of PG activity.

To determine the β -galactosidase activity, 5 mL of 20 mmol L^{-1} sodium acetate (pH 4.7), 2 mL of 3 mmol L^{-1} *p*-nitrophenyl- β -D-galactopyranoside, and 1 mL of crude enzyme were combined and incubated at 37°C for 30 min. A volume of 2 mL of 0.2 mmol L^{-1} Na_2CO_3 was then added to the mixture. The concentration of the reducing product was determined at 400 nm with *p*-nitrophenol (PNP) as a standard. One unit of β -galactosidase activity referred to the amount of enzyme that produced 1 μmol PNP per hour.

Cellulase activity was assayed by mixing 5 mL of 20 mmol L^{-1} sodium acetate (pH 4.0), 1 mL of 0.25% carboxymethyl cellulose, and 1 mL of crude enzyme extract. The mixture was incubated at 37°C for 30 min followed by addition of 2 mL of 10 mmol L^{-1} $\text{Na}_2\text{B}_4\text{O}_7$ and 0.1 mL of 1% (w/v) 2-cyanoacetamide. The reaction was stopped by heating in a boiling water bath for 5 min. A blank was prepared for each sample by boiling the reaction mixture before addition of substrate. One unit of cellulase activity referred to the amount of enzyme that produced 1 μg D-glucose per hour.

The activities of CWDEs were presented as U mg^{-1} protein. Protein content was measured following the method of Bradford (1976) using bovine serum as standard.

Statistical Analysis

All experiments were repeated three time and data were acquired. The values in figures were expressed in the format of the mean values and standard errors. Analysis of variance (ANOVA) was used to analyze the data using the software (SPSS version 17.0). Student's *t*-test was used to compare the mean values of the data set. A *P*-value of less than or equal to 0.05 or 0.01 was considered statistically significant.

RESULTS AND DISCUSSION

Changes in Fruit Disease Index

As indicated in Figure 1, control fruits were intact without lesion during the first two storage days, and then the fruit disease index gradually increased with further storage. But the disease index of *P. longanae*-inoculated fruit increased rapidly throughout the storage period. Statistical analysis reveals that *P. longanae*-inoculated fruit had consistently higher fruit disease index than the control fruit at the same storage time ($P < 0.01$). After 5 days of storage, the disease index of *P. longanae*-inoculated

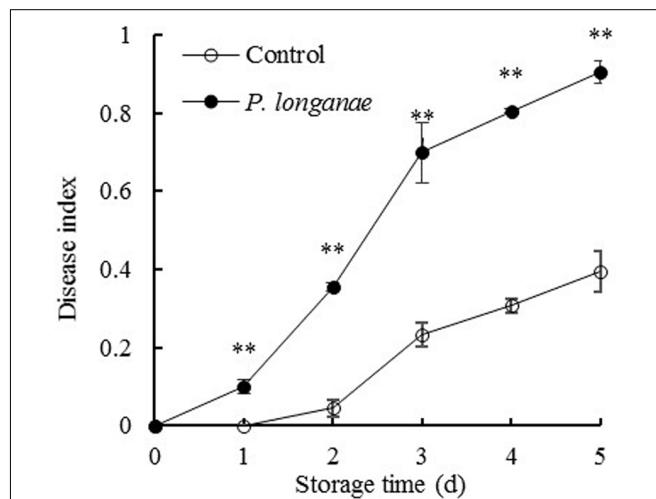


FIGURE 1 | Effects of *Phomopsis longanae* infection on fruit disease index of harvested longan fruit during storage at 28°C . The asterisks indicate significant difference between control and *P. longanae*-inoculated fruit (** $P < 0.01$). ○, control; ●, *P. longanae*-inoculation treatment.

longans was 0.9, which was almost twice as high as that of the control longans. This clearly demonstrates that inoculation treatment could significantly increase disease development of longans during storage.

Changes in CWM

As shown in **Figure 2**, the pericarp CWM content decreased rapidly during storage and CWM readings of *P. longanae*-inoculated longans was significantly ($P < 0.05$) lower than the control longans on each storage day. After 5 days of storage, the CWM in pericarp of control longans decreased from 12.18 to 6.23 mg g⁻¹, while *P. longanae*-inoculated longans has a pericarp CWM value of 5.08 mg g⁻¹ on storage day 5. Correlation analysis indicates that there was a significant negative correlation between disease index (y) and CWM content (x) ($y = 1.5173 - 0.1362x$, $r = -0.915$, $P < 0.05$) for the *P. longanae*-inoculated longans during storage. These findings indicate that the disease development or loss of disease resistance of longan fruits during storage could lead to cell wall disassembly.

Changes in Cell Wall Components

Cell wall components including pectic substances, hemicelluloses, and cellulose constitute the material basis for the mechanical properties of cell wall, and also for maintaining the mechanical strength of the pericarp (Huang et al., 1999; Vorwerk et al., 2004). Pectic substances like WSP, CSP, and NSP are located in the primary cell wall and the middle lamella. The degradation of pectic substances led to cellulose and hemicellulose disassembly, which caused pericarp tissue loosening or fruit softening (Duan et al., 2008; Zhou et al., 2011; Chen et al., 2017a,b). In a similar study performed on litchi fruit, higher levels of structural materials like insoluble pectin, hemicellulose, and cellulose were observed in the cell walls of 'Huaizhi' litchi fruit pericarp compared with 'Nuomici' litchis, which might

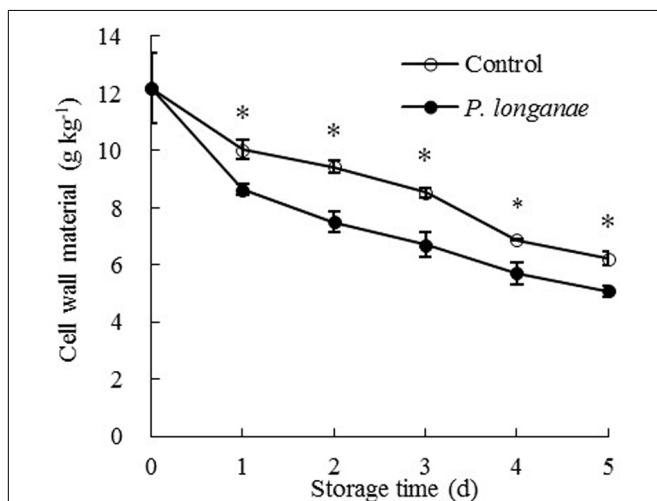


FIGURE 2 | Effects of *P. longanae* infection on cell wall material (CWM) in pericarp of harvested longan fruit during storage at 28°C. The asterisks indicate significant difference between control and *P. longanae*-inoculated fruit (* $P < 0.05$). ○, control; ●, *P. longanae*-inoculation treatment.

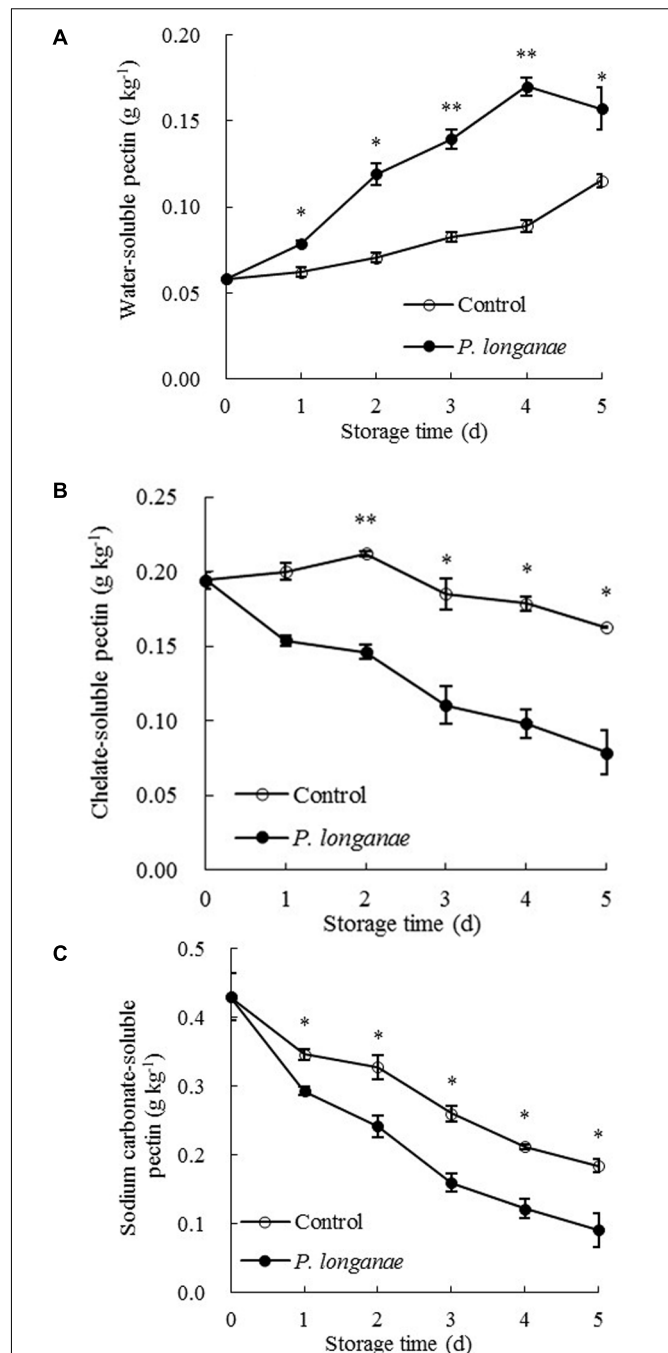


FIGURE 3 | Effects of *P. longanae* infection on water-soluble pectin (WSP) (A), chelate-soluble pectin (CSP) (B) and sodium carbonate-soluble pectin (C) in pericarp of harvested longan fruit during storage at 28°C. The asterisks indicate significant difference between control and *P. longanae*-inoculated fruit (* $P < 0.05$, ** $P < 0.01$). ○, control; ●, *P. longanae*-inoculation treatment.

notably correlate to better pericarp structural strength (Huang et al., 1999).

The data acquired from this work indicate that *P. longanae*-inoculated longans had a faster increase in pericarp WSP than the control longans (**Figure 3A**). *P. longanae*-inoculated

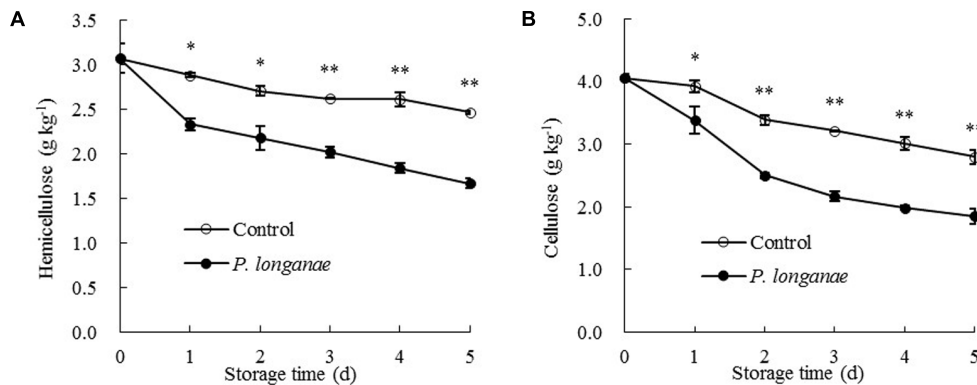


FIGURE 4 | Effects of *P. longanae* infection on hemicellulose (A) and cellulose (B) in pericarp of harvested longan fruit during storage at 28°C. The asterisks indicate significant difference between control and *P. longanae*-inoculated fruit (* $P < 0.05$, ** $P < 0.01$). ○, control; ●, *P. longanae*-inoculation treatment.

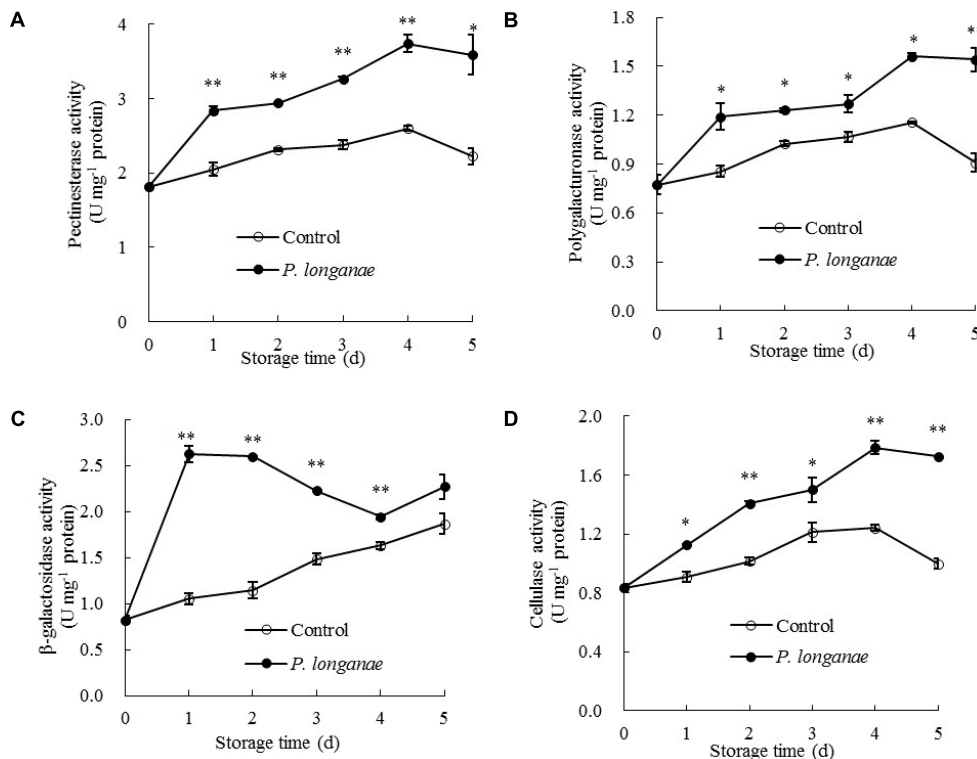


FIGURE 5 | Effects of *P. longanae* infection on activities of pectinesterase (A), polygalacturonase (B), β-galactosidase (C), and cellulase (D) in pericarp of harvested longan fruit during storage at 28°C. The asterisks indicate significant difference between control and *P. longanae*-inoculated fruit (* $P < 0.05$, ** $P < 0.01$). ○, control; ●, *P. longanae*-inoculation treatment.

longans also had faster reduction in pericarp CSP contents (Figure 3B), NSP (Figure 3C), hemicellulose (Figure 4A), and cellulose (Figure 4B) than the control longans. Furthermore, fruit disease index (y) shows negative correlations with CSP content (x) ($y = 1.6142 - 8.7271x$, $r = -0.971$, $P < 0.01$), NSP content (x) ($y = 1.1252 - 2.9018x$, $r = -0.962$, $P < 0.01$), hemicellulose (x) ($y = 1.0903 - 2.584x$, $r = -0.916$, $P < 0.05$) and cellulose (x) ($y = 1.58 - 0.4145x$, $r = -0.956$, $P < 0.01$) in pericarp of *P. longanae*-inoculated longan fruit during storage.

However, a positive correlation between fruit disease index (y) and WSP content (x) ($y = -0.5308 + 8.3717x$, $r = 0.972$, $P < 0.01$) in pericarp of *P. longanae*-inoculated longan fruit was observed. In short, *P. longanae*-inoculation treatment accelerated the degradation of the cell wall components including CSP, NSP, hemicellulose, and cellulose in longans pericarp cell wall and middle lamella; however, the degraded cell wall components like WSP was elevated. Therefore, the mechanical strength of the cell wall of longan pericarp was decreased during disease

development. Cell wall disassembly of longan pericarp may facilitate further pathogen invasion and dissemination.

Changes in Cell Wall Degrading Enzymes

To further explain the change of cell wall components during disease development, changes in CWDEs were measured. PE and PG activities in pericarp of control fruit rose gradually toward the maximum on day 4 and decreased afterwards (**Figures 5A,B**). The PE and PG activities in pericarp of *P. longanae*-inoculated longans followed a similar trend as the control longans but had significantly ($P < 0.05$) higher activities (**Figures 5A,B**). It has been reported that the softening of pericarp tissues were associated with the changes in pectic substances, which could be attributed to the action of PE and PG (Liu et al., 2006). Specifically, PE can remove the methoxyl groups and catalyze the decomposition of galacturonic acid polymer to polygalacturonic acid, which enables PG to hydrolyze 1, 4- α -D-galacturonic bond of polygalacturonic acid to generate galacturonic acid (Liu et al., 2006; Lin et al., 2007; Rugkong et al., 2010; Wei et al., 2010). The degradation of pectic substances by the joint action of PE and PG can destroy the structure of middle lamella and decrease the mechanical strength of cell wall (Deng et al., 2005; Liu et al., 2006). In the present work, PE and PG activities increased significantly after inoculation treatment, which promoted the depolymerization and dissolution of pectin.

As indicated in **Figure 5C**, β -galactosidase activity in pericarp of *P. longanae*-inoculated longans exhibited a sharp increase on the first day of storage, then changed mildly on the second storage day, followed by a quick decline from days 2 to 4, and a rapid increase on day 5. However, the β -galactosidase activity in pericarp of the control longans increased steadily with progressing storage time, with significantly ($P < 0.01$) lower level in contrast to that of *P. longanae*-inoculated fruit from day 1 to day 4 (**Figure 5C**). β -galactosidase also plays a key role in the depolymerization and dissolution of pectic substances in fruits. It can hydrolyze β -1, 4-galactan bonds and separate galactosyl residues from pectin side chains, which may trigger some adverse reactions such as the production of ethylene and stress reaction, and thus further accelerate the disruption of cell wall structure (Liu et al., 2006; Lin et al., 2007; Wei et al., 2010; Chen et al., 2017a,b). The results of this study suggest that higher levels of β -galactosidase activity in inoculated fruits during storage contributed to the degradation of pectin polysaccharides.

Cellulose activity increased gradually in both control and *P. longanae*-inoculated longans during storage days 1–4 and then decreased (**Figure 5D**). After 5 days of storage, *P. longanae*-inoculated longans showed 72.5% higher value of pericarp

cellulose activity as compared with the control longans. Cellulase is a multi-enzyme system including endo-1, 4- β -D-glucanase, exo-1, 4- β -D-glucanase, and β -1, 4-glucosidase (Lin et al., 2007). Cellulase could cause the degradation of cellulose and xyloglucan in cell wall structure, which resulted in pericarp tissue loosening and fruit softening (Deng et al., 2005; Liu et al., 2006; Zhou et al., 2011; Bu et al., 2013; Chen et al., 2017a,b). In this study, the enhanced activity of cellulase due to the *P. longanae*-inoculation treatment correlated well with cellulose degradation (**Figure 4B**) in pericarp of longan fruit during storage.

CONCLUSION

In summary, as compared with the control, fruit inoculated with *P. longanae* could lead to significantly higher fruit disease index, increased activity of CWDEs (e.g., PE, PG, β -galactosidase and cellulase), and lower levels of CWM and cell wall components (such as CSP, NSP, hemicelluloses, and cellulose) in pericarp of harvested longan fruit. These results indicate that *P. longanae* infection can accelerate the cell wall degradation of longan pericarp during disease development by promoting CWDEs activities, which decreased the mechanical strength of the cell walls, resulting in longan pericarp tissue softening, and eventually leading to fruit decay.

AUTHOR CONTRIBUTIONS

YC and HL designed the research. SZ, JZS, YL, and HW conducted the experiments and analyzed the data. YC and SZ wrote the manuscript. HL revised the manuscript. ML and JS edited English language of the manuscript. All authors approved the submission and publication of the manuscript.

FUNDING

This work was supported by the National Natural Science Foundation of China (Grant Nos. 31772035, 31671914, and 31171776), the Natural Science Foundation of Fujian Province of China (Grant No. 2017J01429), the Construction Projects of Top University at Fujian Agriculture and Forestry University of China (Grant No. 612014042), the Science Fund for Distinguished Young Scholars at Fujian Province of China (Grant No. KL16036A), and the Science Fund for Distinguished Young Scholars at Fujian Agriculture and Forestry University of China (Grant No. XJQ201512).

REFERENCES

- Aghdam, M. S., and Fard, J. R. (2017). Melatonin treatment attenuates postharvest decay and maintains nutritional quality of strawberry fruits (*Fragaria × ananassa* cv. Selva) by enhancing GABA shunt activity. *Food Chem.* 221, 1650–1657. doi: 10.1016/j.foodchem.2016.10.123
- Al-Hindi, R. R., Al-Najada, A. R., and Mohamed, S. A. (2011). Isolation and identification of some fruit spoilage fungi: screening of plant cell wall degrading enzymes. *Afr. J. Microbiol. Res.* 5, 443–448. doi: 10.5897/AJMR.10.896
- Andrews, P. K., and Li, S. L. (1995). Cell wall hydrolytic enzyme activity development of nonclimacteric sweet cherry (*Prunus avium* L.) fruit. *J. Hortic. Sci.* 70, 561–567. doi: 10.1080/14620316.1995.11515327
- Bradford, M. M. (1976). A rapid and sensitive method for the quantitation of microgram quantities of protein utilizing the principle of protein-dye binding. *Anal. Biochem.* 72, 248–254. doi: 10.1016/0003-2697(76)90527-3

- Bu, J. W., Yu, Y. C., Aisikaer, G., and Ying, T. J. (2013). Postharvest UV-C irradiation inhibits the production of ethylene and the activity of cell wall-degrading enzymes during softening of tomato (*Lycopersicon esculentum* L.) fruit. *Postharvest Biol. Technol.* 86, 337–345. doi: 10.1016/j.postharvbio.2013.07.026
- Chen, Y. H., Hung, Y. C., Chen, M. Y., and Lin, H. T. (2017a). Effects of acidic electrolyzed oxidizing water on retarding cell wall degradation and delaying softening of blueberries during postharvest storage. *LWT Food Sci. Technol.* 84, 650–657. doi: 10.1016/j.lwt.2017.06.011
- Chen, Y. H., Sun, J. Z., Lin, H. T., Hung, Y. C., Zhang, S., Lin, Y. F., et al. (2017b). Paper-based 1-MCP treatment suppresses cell wall metabolism and delays softening of Huanghua pears during storage. *J. Sci. Food Agric.* 97, 2547–2552. doi: 10.1002/jsfa.8072
- Chen, Y. H., Lin, H. T., Jiang, Y. M., Zhang, S., Lin, Y. F., and Wang, Z. H. (2014). *Phomopsis longanae* Chi-induced pericarp browning and disease development of harvested longan fruit in association with energy status. *Postharvest Biol. Technol.* 93, 24–28. doi: 10.1016/j.postharvbio.2014.02.003
- Chen, Y. H., Lin, H. T., Lin, Y. F., Zhang, J. N., and Zhao, Y. F. (2011a). Effects of *Phomopsis longanae* Chi infection on browning and active oxygen metabolism in pericarp of harvested longan fruits. *Sci. Agric. Sin.* 44, 4858–4866. doi: 10.3864/j.issn.0578-1752.2011.23.012
- Chen, Y. H., Lin, H. T., Lin, Y. F., Zhao, Y. F., and Zhang, J. N. (2011b). Effects of *Phomopsis longanae* Chi infection on lipoxygenase activity and fatty acid constituents of membrane lipids in pericarp of harvested longan fruits. *J. Trop. Subtrop. Bot.* 19, 260–266. doi: 10.3969/j.issn.1005-3395.2011.03.011
- Deng, Y., Wu, Y., and Li, Y. F. (2005). Changes in firmness, cell wall composition and cell wall hydrolases of grapes stored in high oxygen atmospheres. *Food Res. Int.* 38, 769–776. doi: 10.1016/j.foodres.2005.03.003
- Duan, X. W., Cheng, G. P., Yang, E., Yi, C., Ruenroengklin, N., Lu, W. J., et al. (2008). Modification of pectin polysaccharides during ripening of postharvest banana fruit. *Food Chem.* 111, 144–149. doi: 10.1016/j.foodchem.2008.03.049
- Duan, X. W., Zhang, H. Y., Zhang, D. D., Sheng, J. F., Lin, H. T., and Jiang, Y. M. (2011). Role of hydroxyl radical in modification of cell wall polysaccharides and aril breakdown during senescence of harvested longan fruit. *Food Chem.* 128, 203–207. doi: 10.1016/j.foodchem.2011.03.031
- Gharbi, Y., Alkher, H., Triki, M. A., Barkallah, M., Emna, B., Trabelsi, R., et al. (2015). Comparative expression of genes controlling cell wall-degrading enzymes in *Verticillium dahliae* isolates from olive, potato and sunflower. *Physiol. Mol. Plant Pathol.* 91, 56–65. doi: 10.1016/j.pmpp.2015.05.006
- Huang, X. M., Wang, H. C., Gao, F. F., and Huang, H. B. (1999). A comparative study of the pericarp of litchi cultivars susceptible and resistant to fruit cracking. *J. Hortic. Sci. Biotechnol.* 74, 351–354. doi: 10.1080/14620316.1999.11511120
- Kang, Z., and Buchenauer, H. (2000). Ultrastructural and cytochemical studies on cellulose, xylan and pectin degradation in wheat spikes infected by *Fusarium culmorum*. *J. Phytopathol.* 148, 263–275. doi: 10.1046/j.1439-0434.2000.00489.x
- Kikot, G. E., Hours, R. A., and Alconada, T. M. (2009). Contribution of cell wall degrading enzymes to pathogenesis of *Fusarium graminearum*: a review. *J. Basic Microb.* 49, 231–241. doi: 10.1002/jobm.20080231
- Kubicek, C. P., Starr, T. L., and Glass, N. L. (2014). Plant cell wall-degrading enzymes and their secretion in plant-pathogenic fungi. *Annu. Rev. Phytopathol.* 52, 427–451. doi: 10.1146/annurev-phyto-102313-045831
- Lalaoui, F., Halama, P., Dumortier, V., and Paul, B. (2000). Cell wall-degrading enzymes produced in vitro by isolates of *Phaeosphaeria nodorum* differing in aggressiveness. *Plant Pathol.* 49, 727–733. doi: 10.1046/j.1365-3059.2000.00491.x
- Li, J. K., Lei, H. H., Song, H. M., Lai, T. F., Xu, X. B., and Shi, X. Q. (2017). 1-methylcyclopropene (1-MCP) suppressed postharvest blue mold of apple fruit by inhibiting the growth of *Penicillium expansum*. *Postharvest Biol. Technol.* 125, 59–64. doi: 10.1016/j.postharvbio.2016.11.005
- Li, M., Gao, Z. Y., Hu, M. J., Zhou, S., Yang, D. P., Yang, B., et al. (2012). Pathogenicity of cell wall degrading enzymes produced by *Botryodiplodia theobromae* Pat. against mangoes. *Agric. Biotechnol.* 1, 18–21.
- Lin, H. T., Zhao, Y. F., and Xi, Y. F. (2007). Changes in cell wall components and cell wall-degrading enzyme activities of postharvest longan fruit during aril breakdown. *J. Plant Physiol. Mol. Biol.* 33, 137–145. doi: 10.3321/j.issn:1671-3877.2007.02.007
- Lin, Y. F., Chen, M. Y., Lin, H. T., Hung, Y. C., Lin, Y. X., Chen, Y. H., et al. (2017a). DNP and ATP induced alteration in disease development of *Phomopsis longanae* Chi-inoculated longan fruit by acting on energy status and reactive oxygen species production-scavenging system. *Food Chem.* 228, 497–505. doi: 10.1016/j.foodchem.2017.02.045
- Lin, Y. F., Lin, Y. X., Lin, H. T., Chen, Y. H., Wang, H., and Shi, J. (2018). Application of propyl gallate alleviates pericarp browning in harvested longan fruit by modulating metabolisms of respiration and energy. *Food Chem.* 240, 863–869. doi: 10.1016/j.foodchem.2017.07.118
- Lin, Y. F., Lin, Y. X., Lin, H. T., Ritenour, M. A., Shi, J., Zhang, S., et al. (2017b). Hydrogen peroxide-induced pericarp browning of harvested longan fruit in association with energy metabolism. *Food Chem.* 225, 31–36. doi: 10.1016/j.foodchem.2016.12.088
- Lin, Y. F., Lin, Y. X., Lin, H. T., Shi, J., Chen, Y. H., and Wang, H. (2017c). Inhibitory effects of propyl gallate on membrane lipids metabolism and its relation to increasing storability of harvested longan fruit. *Food Chem.* 217, 133–138. doi: 10.1016/j.foodchem.2016.08.065
- Liu, X. D., Wu, Z. X., Han, D. M., Chen, W. X., and Su, M. X. (2006). Changes of the cell-wall metabolism enzymes of pericarp of longan under Storage. *Chin. J. Trop. Crops* 2, 24–28. doi: 10.3969/j.issn.1000-2561.2006.02.005
- Ramos, A. M., Gally, M., Szapiro, G., Itzcovich, T., Carabajal, M., and Levin, L. (2016). In vitro growth and cell wall degrading enzyme production by Argentinean isolates of *Macrophomina phaseolina*, the causative agent of charcoal rot in corn. *Rev. Argent. Microbiol.* 48, 267–273. doi: 10.1016/j.ram.2016.06.002
- Rugkong, A., Rose, J. K. C., Lee, S. J., Giovannoni, J. J., O'Neill, M. A., and Watkins, C. B. (2010). Cell wall metabolism in cold-stored tomato fruit. *Postharvest Biol. Technol.* 57, 106–113. doi: 10.1016/j.postharvbio.2010.03.004
- Sun, J. Z., Lin, H. T., Zhang, S., Lin, Y. F., Wang, H., Lin, M. S., et al. (2018). The roles of ROS production-scavenging system in *Lasiodiplodia theobromae* (Pat.) Griff. & Maubl.-induced pericarp browning and disease development of harvested longan fruit. *Food Chem.* 247, 16–22. doi: 10.1016/j.foodchem.2017.12.017
- Tian, C. M., Zhao, P., and Cao, Z. M. (2009). Role of cell wall degrading enzymes in the interaction of poplar and *Melampsora larici-populina* Kleb. *Front. For. China* 4:111. doi: 10.1007/s11461-009-0006-6
- Vorwerk, S., Somerville, S., and Somerville, C. (2004). The role of plant cell wall polysaccharide composition in disease resistance. *Trends Plant Sci.* 4, 203–209. doi: 10.1016/j.tplants.2004.02.005
- Wang, L., Jin, P., Wang, J., Jiang, L. L., Shan, T. M., and Zheng, Y. H. (2015). Effect of β -aminobutyric acid on cell wall modification and senescence in sweet cherry during storage at 20°C. *Food Chem.* 175, 471–477. doi: 10.1016/j.foodchem.2014.12.011
- Wei, J. M., Ma, F. W., Shi, S. G., Qi, X. D., Zhu, X. Q., and Yuan, J. W. (2010). Changes and postharvest regulation of activity and gene expression of enzymes related to cell wall degradation in ripening apple fruit. *Postharvest Biol. Technol.* 56, 147–154. doi: 10.1016/j.postharvbio.2009.12.003
- Yao, H. J., and Tian, S. P. (2005). Effects of pre- and post-harvest application of salicylic acid or methyl jasmonate on inducing disease resistance of sweet cherry fruit in storage. *Postharvest Biol. Technol.* 35, 253–262. doi: 10.1016/j.postharvbio.2004.09.001
- Zhang, S., Lin, H. T., Lin, Y. F., Lin, Y. X., Hung, Y. C., Chen, Y. H., et al. (2017). Energy status regulates disease development and respiratory metabolism of *Lasiodiplodia theobromae* (Pat.) Griff. & Maubl.-infected

- longan fruit. *Food Chem.* 231, 238–246. doi: 10.1016/j.foodchem.2017.03.132
- Zhang, S., Lin, Y. Z., Lin, H. T., Lin, Y. X., Chen, Y. H., Wang, H., et al. (2018). *Lasioidiplodia theobromae* (Pat.) Griff. & Maubl.-induced disease development and pericarp browning of harvested longan fruit in association with membrane lipids metabolism. *Food Chem.* 244, 93–101. doi: 10.1016/j.foodchem.2017.10.020
- Zhou, R., Li, Y. F., Yan, L. P., and Xie, J. (2011). Effect of edible coatings on enzymes, cell-membrane integrity, and cell-wall constituents in relation to brittleness and firmness of Huanghua pears (*Pyrus pyrifolia* Nakai, cv. Huanghua) during storage. *Food Chem.* 124, 569–575. doi: 10.1016/j.foodchem.2010.06.075

Conflict of Interest Statement: The authors declare that the research was conducted in the absence of any commercial or financial relationships that could be construed as a potential conflict of interest.

Copyright © 2018 Chen, Zhang, Lin, Sun, Lin, Wang, Lin and Shi. This is an open-access article distributed under the terms of the Creative Commons Attribution License (CC BY). The use, distribution or reproduction in other forums is permitted, provided the original author(s) and the copyright owner are credited and that the original publication in this journal is cited, in accordance with accepted academic practice. No use, distribution or reproduction is permitted which does not comply with these terms.



Perillaldehyde Controls Postharvest Black Rot Caused by *Ceratocystis fimbriata* in Sweet Potatoes

Man Zhang^{1†}, Man Liu^{1†}, Shenyuan Pan¹, Chao Pan¹, Yongxin Li^{1*} and Jun Tian^{1,2*}

¹ College of Life Science, Jiangsu Normal University, Xuzhou, China, ² Beijing Advanced Innovation Center for Food Nutrition and Human Health, Beijing Technology and Business University, Beijing, China

OPEN ACCESS

Edited by:

Hongyin Zhang,
Jiangsu University, China

Reviewed by:

Kaifang Zeng,
Southwest University, China
Gianfranco Romanazzi,
Università Politecnica delle Marche,
Italy

*Correspondence:

Yongxin Li
lyxycg@hotmail.com
Jun Tian
tj-085@163.com

[†]These authors have contributed
equally to this work.

Specialty section:

This article was submitted to
Food Microbiology,
a section of the journal
Frontiers in Microbiology

Received: 29 January 2018

Accepted: 08 May 2018

Published: 25 May 2018

Citation:

Zhang M, Liu M, Pan S, Pan C, Li Y
and Tian J (2018) Perillaldehyde
Controls Postharvest Black Rot
Caused by *Ceratocystis fimbriata*
in Sweet Potatoes.
Front. Microbiol. 9:1102.
doi: 10.3389/fmicb.2018.01102

Black rot caused by *Ceratocystis fimbriata* is the most damaging postharvest disease among sweet potatoes. Black rot can be controlled by synthetic fungicides, but these synthetic fungicides also have several negative effects. Perillaldehyde (PAE), a major component of the herb perilla, is an effective and eco-friendly method of controlling this disease. The antifungal activity of PAE on the mycelial growth in *C. fimbriata* was evaluated *in vitro*. Sweet potatoes at the postharvest stage were surfaced-disinfected with 75% ethanol. Artificially created wounds were inoculated with a *C. fimbriata* cell suspension, and then, the PAE was spontaneously volatilized inside the residual airspace of the containers at 28°C. Samples were collected at 0, 3, 6, 9, 12, 15, 18, and 21 days from each group, and the tissues around the wounds of the sweet potatoes were collected using a sterilized knife and then homogenized to determine their defense-related enzyme activity and quality parameters. *In vitro* assays showed that the mycelial growth of *C. fimbriata* was inhibited by PAE in a dose-dependent manner. An *in vivo* test demonstrated that 25, 50, and 100 μ l/l PAE doses, when applied to sweet potatoes inoculated with *C. fimbriata*, could remarkably lower lesion diameter as compared to the control. Even though the storage time was prolonged, PAE vapor treatment still drastically inhibited sweet potato decay during storage at 28°C. These PAE vapor treatments also enhanced the activities of superoxide dismutase (SOD), catalase (CAT), ascorbate peroxidase (APX), peroxidase (POD), polyphenol oxidase (PPO), and phenylalanine ammonia-lyase (PAL). These treatments remarkably decreased weight loss rates and had minor effects on other fruit quality parameters, such as anthocyanin content and vitamin C content. In our study, the results suggested that the effects of PAE on postharvest sweet potatoes may be attributed to the maintenance of enzymatic activity and fruit quality. In sum, PAE may be a promising approach to controlling *C. fimbriata* in sweet potatoes.

Keywords: *Perilla*, postharvest disease, antifungal, enzyme activity, fruit quality

INTRODUCTION

Ceratocystis fimbriata is a pathogenic fungus that causes lethal wilt-type diseases in a broad range of economically important plants (Ferreira et al., 2017). *C. fimbriata* on sweet potatoes [*Ipomoea batatas* (L.) Lam.] was first reported in China, where there were substantial losses due to black rot on stored roots (Muramoto et al., 2012). A widely distributed strain of *C. fimbriata* has been

reported to cause black rot in sweet potatoes and severe deterioration during postharvest storage (Baker et al., 2003; Engelbrecht and Harrington, 2005). Postharvest diseases of crops and fruits cause major losses, and these diseases are primarily controlled via the application of synthetic fungicides. However, in recent years, the resistance of *C. fimbriata* to conventional synthetic fungicides has drastically increased due to the fact that the widespread, long-term agricultural use of synthetic fungicides has caused some major postharvest pathogens to develop resistance against them (Vilaplana et al., 2017). Also, there is a current trend toward safer and more eco-friendly fungicides for the control of postharvest decay (Sharma et al., 2009). Hence, the development of more effective and healthy antifungals is of paramount importance.

Essential oils (EOs) have been used for 1000s of years in food preservation pharmaceuticals and alternative medicine and have attracted interest due to their relative safety, volatility, broad acceptance by consumers, and eco-friendliness (Prabuseenivasan et al., 2006; Tzortzakakis and Economakis, 2007; Liu et al., 2016; Servili et al., 2017). Numerous studies have reported antifungal effects on the part of various EOs used to control deterioration in postharvest fruits and vegetables (Soylu et al., 2010; Fan et al., 2014; Elshafie et al., 2015; Guerra et al., 2015). Perillaldehyde (PAE), a major constituent of essential oil, is found most abundantly in the herb perilla (*Perilla frutescens*, Labiatae), which has been widely used as a medicinal agent (Hobbs et al., 2016). PAE is a safe flavoring additive in foods and a safe ingredient in perfume (Wang et al., 2008). PAE exhibits antioxidant, antidepressant, and other biological properties and also shows antimicrobial activity against *Candida albicans*, *Aspergillus flavus*, *A. niger*, and other microbes (McGeady et al., 2002; Tian et al., 2015a, 2016, 2017). In addition, it can also be developed into a natural preservative to control postharvest fungal decay in table grapes and cherry tomatoes (Tian et al., 2015a,b).

However, information on the effect of PAE on the postharvest activity of defense-related enzymes and fruit quality in crops is lacking. More importantly, the purpose of our study is to investigate the postharvest application of PAE as a novel strategy for the control of postharvest diseases in sweet potatoes. Therefore, in this study, we aimed to evaluate the antifungal activity of PAE against *C. fimbriata* through *in vitro* and *in vivo* experiments and to determine the influences of PAE on the defense-related activity of several enzymes, including superoxide dismutase (SOD), catalase (CAT), ascorbate peroxidase (APX), peroxidase (POD), polyphenol oxidase (PPO), and phenylalanine ammonialyase (PAL), in sweet potatoes, as well as on certain fruit quality parameters, such as weight loss, anthocyanin content, and vitamin C content.

MATERIALS AND METHODS

Medicament, Pathogen, and Plant Materials

The PAE was prepared as a stock solution in 0.1% (v/v) Tween 80. The isolates of *C. fimbriata* (voucher specimen

number CF1.01127) used in this work were obtained from spoiled sweet potatoes (*Ipomoea batatas* Lam. cv. Sushu 8) in a greenhouse at Xuzhou Academy of Agricultural Sciences and then identified via morphological and molecular biology techniques. They were preserved on potato dextrose agar (PDA) that contained an infusion of 200 g/l potatoes, 20 g/l glucose, and 20 g/l agar at 28°C. The spores from a 7-day-old culture were suspended in 0.1% (v/v) Tween 80 and adjusted to 10^6 spores/ml using a hemacytometer. Sweet potatoes were harvested and removed from a commercial greenhouse around Jiangsu Normal University and transported to the laboratory within 2 h. Healthy sweet potatoes of uniform size and maturation were chosen for the experiments.

In Vitro Assay

The inhibition of mycelial growth was analyzed using a modified version of the method of Soylyu et al. (2006) and Shao et al. (2013). Glass Petri dishes (90 mm × 20 mm, with 80 ml air spaces after the addition of 20 ml of agar media) were filled with 20 ml of PDA, and a mycelial disk (6 mm in diameter) was placed in the center of each plate. Next, the appropriate amount of oil (final concentrations of 25, 50, and 100 µl/l PAE) was added onto the inner surface of each Petri dish lid, and the dishes were quickly covered. Two perpendicular diameters (in cm) of the colony zone were measured with calipers. Each treatment contained three replicates, and the experiment was repeated three times.

Treatment and Storage of Sweet Potatoes

Sweet potatoes at the postharvest stage were surfaced-disinfected with 75% ethanol and then artificially wounded once to a depth of 10 or 5 mm in diameter. A suspension of *C. fimbriata* at 10^6 spore/ml (20 µl) was inoculated into each wound. After drying, the inoculated sweet potatoes were randomly distributed into four groups (a control and three PAE vapor treatments). The control groups did not receive PAE.

During the PAE vapor treatments, 25, 50, and 100 µl PAE were placed in 1 l polystyrene containers with snap-on lids to allow for natural evaporation (Tian et al., 2011). The vapor concentration was the ratio of the volumes of the PAE and the containers (µl/l). Hence, the PAE vapor concentrations used in the experiment were 25, 50, and 100 µl/l air.

In Vivo Assay

The treatment and storage methods were the same as those detailed in the Section ‘Treatment and Storage of Sweet Potatoes.’ For the treated groups, each sweet potato was placed into a 1 l container. Based on our preliminary experiments, 25, 50, or 100 µl/l PAE were placed in a small beaker and then in the sealed container. The PAE was spontaneously volatilized inside the residual airspace of the containers at 28°C for 21 days. Lesion diameter was expressed as the mean width and length of the areas of decay (Shao et al., 2013). Each treatment involved three replications, and the entire experiment was conducted in triplicate.

Effects of *C. fimbriata* on Defense-Related Enzyme Activity in Sweet Potatoes

To evaluate the elicitation of active defense responses via PAE vapor treatments, tissue samples surrounding each wound in the fruit were collected at 0, 3, 6, 9, 12, 15, 18, and 21 days in each group.

All enzyme extraction procedures were conducted at 4°C. The tissues around the wounds of the sweet potatoes were collected using a sterilized knife and then homogenized to determine their defense-related enzyme activity. The extracts were then homogenized and centrifuged at $12,000 \times g$ for 30 min at 4°C. The supernatant was used for the enzyme assay.

Superoxide dismutase was extracted using a modification of the method used by Liu et al. (2005), Vatter et al. (2005), and Li et al. (2017) and determined via nitro-blue tetrazolium (NBT) reaction. Five g of fresh sample (homogenized sweet potatoes) were ground with 5 ml of 0.1 M sodium phosphate buffer (pH 7.8). The absorbance at 560 nm was recorded.

Catalase was extracted using a slight modification of the protocol used by Cao et al. (2008). Homogenized sweet potatoes (5 g) were ground with 5 ml of 0.1 M sodium phosphate buffer (pH 7.5). CAT activity was determined by adding 0.1 ml of the enzyme preparation to 2.9 ml of 20 mM hydrogen peroxide (H_2O_2), which acted as the substrate. One unit was defined as the change in 0.01 absorbance units per minute at 240 nm, as determined with a UV-visible spectrophotometer.

For the POD extraction, fresh sample (5 g of homogenized sweet potatoes) was ground with 5 ml of 0.1 M sodium acetate buffer (pH 5.5) containing 4% polyvinylpyrrolidone (PVPP) (m/v), 1 mM polyethylene glycol (PEG) (m/v), and 1% Triton X-100 (v/v). POD activity was determined via the method of Shao et al. (2013). Enzyme activity was defined as the increase in absorbance, and one unit was defined as the change in absorbance units per minute at 420 nm, as determined with a UV-visible spectrophotometer.

Five gram of homogenized sweet potatoes were ground with 5 ml of 0.1 M potassium phosphate buffer (pH 7.5) for APX extraction (Cao et al., 2008; Li et al., 2016). APX activity was determined by adding 0.1 ml of the enzyme preparation to 2.6 ml of potassium phosphate buffer containing 0.1 mM EDTA and 0.5 mM AsA, as well as adding 0.3 ml of H_2O_2 , which acted as the substrate. Enzyme activity was defined as the decrease in absorbance, and one unit was defined as the change in 0.01 absorbance units per minute at 290 nm as determined with a UV-visible spectrophotometer.

Polyphenol oxidase extraction and activity determination were carried out according to the method of Shao et al. (2013), with slight modifications. Briefly, 5 g of fresh sample were ground with 5 ml of 0.1 M sodium acetate buffer (pH 5.5) containing 4% PVPP (m/v), 1 mM PEG (m/v), and 1% Triton X-100 (v/v). Enzyme activity was defined as the increase in absorbance, and one unit was defined as the change in 0.1 absorbance units per minute at 420 nm, as measured with a UV-visible spectrophotometer.

Phenylalanine ammonia-lyase was extracted with 0.1 M brax buffer at a pH of 8.8, which contained 40 g/l PVPP (m/v), 2 mM EDTA (m/v), and 5 mM β -mercaptoethanol (v/v). PAL activity was determined according to the method of Assis et al. (2001) and Zeng et al. (2006). One unit was defined as the change in 0.01 absorbance units per hour at 290 nm, as measured with a UV-visible spectrophotometer.

Determination of Fruit Quality Parameters

Non-inoculated sweet potatoes were randomly distributed into a control and three PAE vapor treatment groups. The method of PAE vapor treatment was described in the Section 'Treatment and Storage of Sweet Potatoes.' After treatment, these fruits were released from the PAE vapor and stored at 28°C for 21 days to investigate changes in quality parameters.

At harvest, the fruits were evaluated by taking the following measurements: weight loss, anthocyanin content, and ascorbic acid content. Tissues around the wound of the sweet potatoes were collected using a sterilized knife and then homogenized to determine their anthocyanin content and ascorbic acid content.

Weight loss was expressed as a percentage of total weight. On each day of storage, sweet potatoes from each treatment were weighed, and then, the weight loss percentage was calculated with respect to the initial weight of the sweet potatoes. The results were obtained from three replicates.

Anthocyanin content was measured as described by Mirdehghan and Rahimi (2016). Five gram of homogenized sweet potatoes were centrifuged at 10,000 rpm. Then, hydrochloric acid-potassium chloride (pH = 1) and acetate (pH = 4.5) buffers were used to dilute the supernatants. The absorbance was measured with a UV-Vis spectrophotometer at 520 and 700 nm in two buffers at pH 1 and 4.5, respectively. All concentrations were measured in three replicates, and each experiment was performed three times.

Ascorbic acid content (vitamin C) was measured via titrimetric methods (Kim and Yook, 2009). The method of measuring ascorbic acid utilized 2,6-dichlorophenol indophenol dye. The reduction of this dye by ascorbic acid is specific. Five g of homogenized sweet potatoes were mixed with 100 ml of a mixture of metaphosphoric and acetic acids (30 g of metaphosphoric acid and 80 ml of acetic acid were diluted to 1 l with distilled water). The sample acid mixture (10 ml) was titrated with indophenol (250 mg of sodium carbonate and 250 mg of indophenol were massed up to 1 l of distilled water). Three replicates were conducted for each parameter, and the entire experiment was performed three times.

Statistical Analysis

The data were analyzed via a one-way analysis of variance (ANOVA), followed by Duncan's multiple-range tests at $p < 0.05$ (SPSS Statistics 17.0 Inc.). In the statistical analysis of the randomized complete block design, each treatment involved three replications, and the entire experiment was conducted in triplicate.

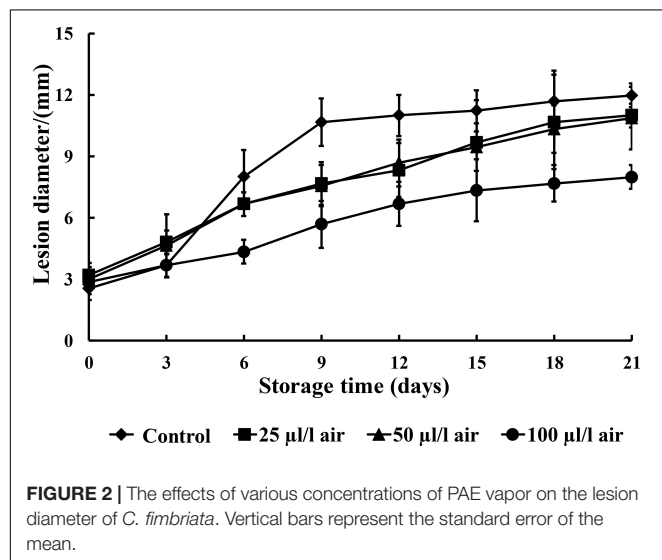
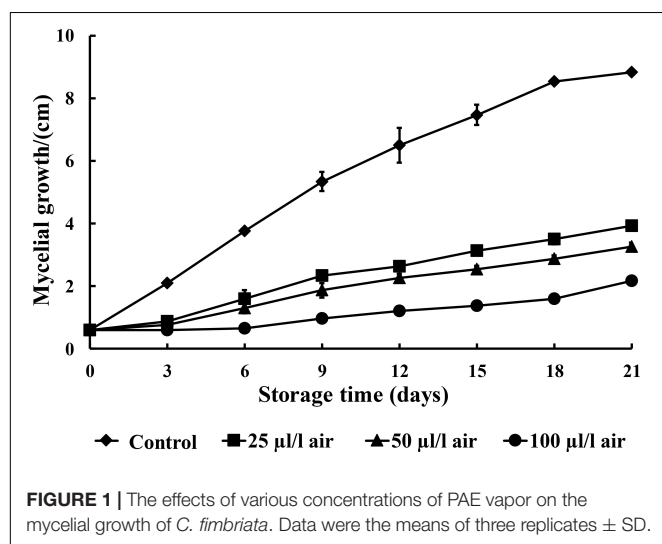
RESULTS

Evaluation of *in Vitro* Antifungal Activity

PAE at 25, 50, and 100 $\mu\text{l/l}$ can effectively inhibit the mycelial growth of *C. fimbriata* in PDA medium over 21 days of incubation. In our study, PAE showed a notable antifungal effect on *C. fimbriata* (Figure 1). The inhibitory efficacy was enhanced as the PAE concentration increased. The mycelial growth of *C. fimbriata* was moderately inhibited by PAE at a low concentration (25 $\mu\text{l/l}$). In contrast, 100 $\mu\text{l/l}$ of PAE induced the 100% inhibition of the mycelial growth of *C. fimbriata* for up to 3 days of culture, and the differences between the various PAE concentrations were statistically significant ($p < 0.05$).

Evaluation of *in Vivo* Antifungal Activity

Figure 2 illustrates that all concentrations of PAE reduced the severity of black rot to some extent as compared to the control



during the entire storage period. The 100 $\mu\text{l/l}$ PAE concentration group showed significant reductions in lesion diameter from the 6th day onward after inoculation ($p < 0.05$).

Effect of PAE Vapor Treatment on Defense-Related Enzyme Activities

In general, the SOD activity levels of sweet potatoes treated with PAE and the control showed increasing trends, except on the 9th and 18th days after inoculation. There was also a noticeable increase on the 21st day of postharvest storage (Figure 3A). The activity levels of SOD in sweet potatoes treated with 100 $\mu\text{l/l}$ PAE were significant higher than those of the control on the 12th and 21st days after inoculation ($p < 0.05$).

Figure 3B shows the effect of PAE at different concentrations on CAT activity levels in sweet potatoes inoculated with *C. fimbriata*. In general, the CAT activity levels of all samples decreased sharply during storage, with the PAE-treated sweet potatoes having higher levels of activity as compared to the control.

As demonstrated in Figure 3C, the patterns of change in POD activity in the control group and two of the treatment groups (PAE with 25 and 50 $\mu\text{l/l}$) were similar during storage. Overall, the POD activity levels of all groups generally increased over the entire period, and a notable decrease in POD activity levels in the PAE-treated sweet potatoes was observed at the 21st day post-inoculation. In addition, during the entire storage period, all groups that received PAE vapor treatment showed no significant differences as compared to the control, except on the 15th day ($p < 0.05$).

In terms of APX activity, in general, the PAE vapor treatments led to higher APX activity levels than those seen in the control over the entire incubation period (Figure 3D). APX activity levels in all four groups showed a noticeable decrease from the 3rd to the 9th day and then remained steady after this timepoint. Furthermore, the group fumigated with PAE at 100 $\mu\text{l/l}$ showed significantly higher APX activity as compared with the control, except on the 12th, 15th, and 18th days ($p < 0.05$).

Figure 3E shows the fluctuations in PPO activity levels, which increased at the 9th day and then decreased in a relatively unstable way during the remaining days. The PPO activity levels of all groups generally went up, and PPO activity in the sweet potatoes given PAE vapor treatments undulated steadily during post-inoculation storage. Meanwhile, in the control group, PPO activity underwent a sharp fluctuation. The PPO activity level was remarkable lower in PAE-treated fruits than in non-treated sweet potatoes, and no significant differences occurred after the 15th day of storage ($p < 0.05$).

Regarding the PAL activity levels of all four groups, Figure 3F shows a generally increasing trend with slight fluctuations before the 15th day. In the PAE-treated groups, except for the 25 $\mu\text{l/l}$ PAE group, PAL exhibited significantly higher activity levels than in the control group at 3 days postharvest ($p < 0.05$).

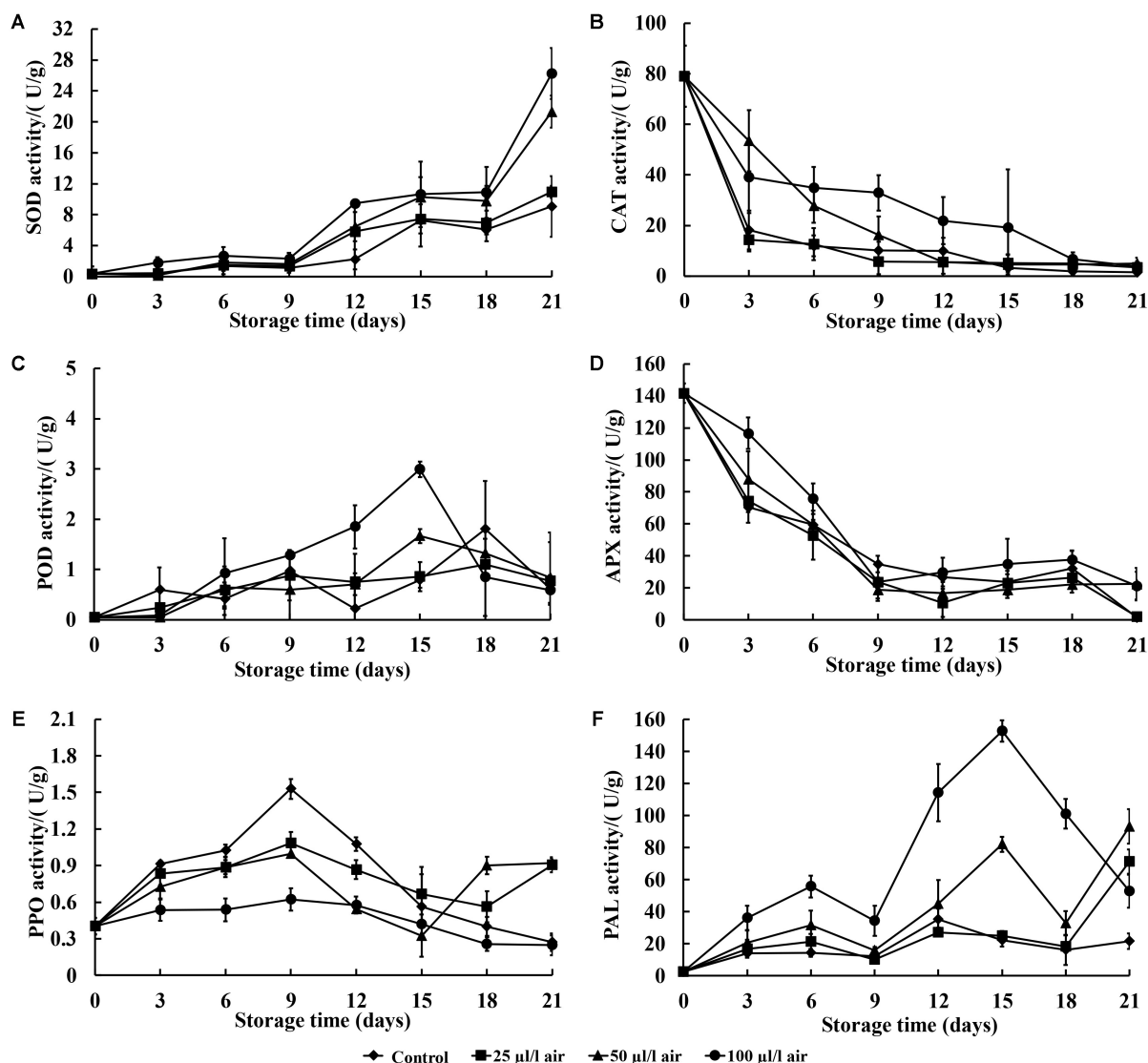


FIGURE 3 | Effect of PAE vapor treatment on SOD (A), CAT (C), APX (B), POD (D), PPO (E), and PAL (F) activity levels in sweet potatoes during storage. Values are means \pm SD. Vertical bars represent standard errors of the means.

Effects of PAE Vapor on Fruit Quality Parameters

It is apparent from **Figure 4A** that the weight loss in the sweet potatoes increased markedly as the storage period advanced. Among the various PAE concentrations, sweet potatoes fumigated with 100 µl/l PAE exhibited substantially less weight loss during the 21 days of storage as compared to the other treatments. In addition, after the 12th day of storage, the PAE-treated groups showed a significant decrease in weight loss rates as compared to the control ($p < 0.05$).

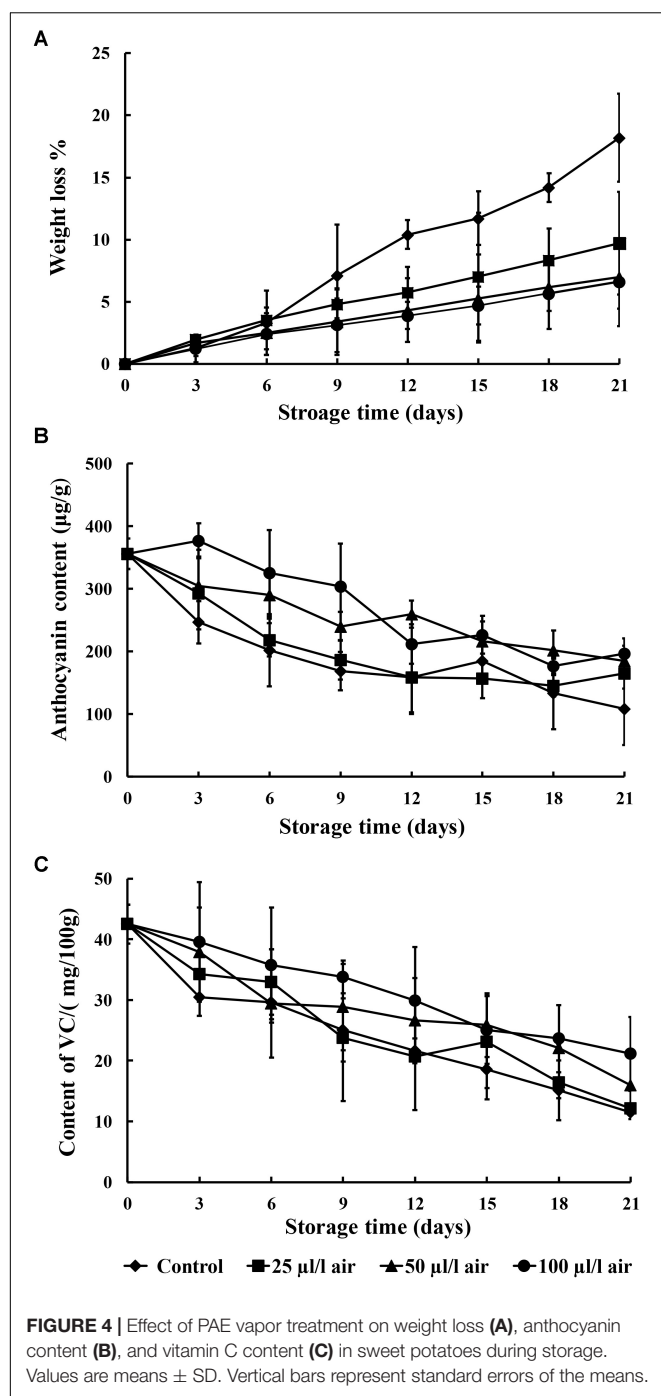
In our work, the anthocyanin content of the sweet potatoes was shown to decline during the entire storage period. In the control group, it decreased relatively quickly, whereas in the three PAE-treated groups, it decreased gradually over the entire storage period (**Figure 4B**). In addition, the anthocyanin content was

higher in sweet potatoes treated with all concentrations of PAE than in the non-treated group.

As shown in **Figure 4C**, the vitamin C content of sweet potatoes fumigated with 25, 50, and 100 µl/l PAE and the control underwent slight variation. The values for the control were significantly reduced as compared to all the treatments, especially samples fumigated with 100 µl/l PAE, at the 21st day of storage. During the entire storage period, sweet potatoes fumigated with 25, 50, and 100 µl/l PAE had higher vitamin C content than the control ($p < 0.05$).

DISCUSSION

The postharvest decay of fruits and vegetables causes considerable losses during storage, and 20–25% of harvested



fruits and vegetables are decayed by pathogens during the postharvest period (Sharma et al., 2009). The application of synthetic fungicides for the control of pathogenic fungi is a standard commercial practice worldwide; however, because of the increasing awareness of chemical compounds that are potentially harmful to human health and the environment, interest in natural methods of maintaining postharvest quality and controlling diseases in plants is increasing (Sharma et al., 2009). Essential oils, as biologically active agents, represent rich

potential sources of alternative and environmentally acceptable compounds for disease management (Servili et al., 2017). PAE, a major constituent of essential oil, is “generally regarded as safe” (GRAS) by the United States Food and Drug Administration (Hobbs et al., 2016) and could be developed into a natural preservative for controlling the infection of sweet potatoes by spoilage fungi.

In our study, the antifungal activities of PAE vapor on fungal mycelial growth were assessed. PAE vapor treatment can remarkably reduce the mycelial growth of *C. fimbriata* *in vitro*. Thus, these *in vitro* results confirm the effectiveness of PAE as an antifungal agent against *C. fimbriata* and reveal that *C. fimbriata* is sensitive to PAE vapor in a dose-dependent manner. To further provide proof-of-concept that PAE vapor is active against black rot caused by the pathogenic fungus *C. fimbriata*, we conducted *in vivo* investigations to assess its efficacy as a natural preservative for the control of decay in sweet potatoes. In this *in vivo* experiment, the PAE vapor treatments also alleviated black rot in artificially infected sweet potatoes.

The activation of defense-related enzymes in fruit is considered to be important in conferring resistance against postharvest diseases (Tian et al., 2006; Wang et al., 2014). One of the most prominent plant defense responses is an oxidative burst, or an accumulation of reactive oxygen species (ROS) (Foyer and Noctor, 2011; Zheng et al., 2017). The generation of ROS serves as a signal that activates additional plant defense reactions (Perumal et al., 2017). Antioxidant and ROS-scavenging systems can effectively help to protect plants from free radicals and stabilize these free radicals (Cao et al., 2008). Generally, ROS are controlled by an array of antioxidant enzymes, such as SOD, CAT, and APX (Deng et al., 2015). They are considered the key enzymes in host defense reactions against pathogenic infections (Zhang et al., 2011; Ma et al., 2013). As the first line of defense against the damages caused by oxygen radicals, SOD is a metalloprotein that catalyzes the dismutation of O_2^- into molecular oxygen and H_2O_2 , while CAT converts H_2O_2 into oxygen and water (Sellamuthu et al., 2013). Therefore, the increased antioxidant enzyme activity levels (SOD, CAT, and APX) in the PAE-vapor-treated sweet potatoes can protect the cell membrane structure and function of the sweet potato tissue by inhibiting the accumulation of reactive oxygen species, resulting in less oxidative stress and damage to the sweet potatoes and thereby contributing to the fruit tissue's resistance against *C. fimbriata*.

In addition to SOD, CAT, and APX activity levels, POD, PAL, and PPO activity levels also play an important role in inducing resistance in fruits (Tian et al., 2006; Yang et al., 2017). POD activity produces the oxidative power needed for the cross-linking of proteins and phenylpropanoid radicals, resulting in the reinforcement of cell walls against fungal penetration (Yao and Tian, 2005). Previous researchers have also suggested that POD is related to enhanced disease resistance in plants (Mohammadi and Kazemi, 2002; Qin et al., 2003; Zhang et al., 2011). PAL is a key enzyme involved in the first step of propane metabolism, which is related to the plant defense system (Dixon et al., 2002; Yao and Tian, 2005; Liu et al., 2016). Also, PAL directly participates in the synthesis of active metabolites associated with plant protection

and the local resistance process, including phenols and lignin (Cao et al., 2008). In our study, we confirmed significantly enhanced PAL activity in response to PAE vapor treatment. PPO is a copper enzyme that can catalyze several reactions leading to the formation of quinones. Quinone synthesis is one of the first responses to fungal attack or wounding (Cindi et al., 2016). In this study, PAE vapor treatment was found to alter PPO activity during incubation, which may result in enhanced pathogen resistance in sweet potatoes. Thus, it seems that these effects could collectively contribute to the development of disease resistance against *C. fimbriata*.

During the postharvest storage of sweet potatoes, changes related to quality, such as the weight loss rate, anthocyanin content, and vitamin C content, were generally observed. The weight loss rate is an important fruit quality parameter during storage (Castillo et al., 2014; Tao et al., 2014). Weight loss is associated with the absence of the protective epidermal layer and waxes, resulting in the deterioration of quality (Toivonen and Brummell, 2008). Our results indicate that PAE can maintain high-quality postharvest sweet potatoes. Anthocyanins, as water-soluble pigments, occur in fruits and vegetables and play important roles in protecting plants against various biotic and abiotic stresses (Mirdehghan and Rahimi, 2016). Our study suggests that PAE vapor can enhance anthocyanin accumulation. Vitamin C is the water-soluble vitamin that is most sensitive to irradiation, and it is also highly sensitive to various modes of degradation (Kilcast, 1994). PAE vapor treatment led to fruits with higher ascorbic acid content at harvest and during postharvest storage. Thus, postharvest PAE vapor treatment can improve the quality and storability of harvested sweet potatoes.

CONCLUSION

The aim of this study was to determine the effectiveness of PAE in controlling postharvest decay in sweet potatoes. PAE vapor significantly reduced *C. fimbriata*, the main pathogen affecting postharvest sweet potatoes, both *in vitro* and *in vivo*. PAE vapor

inhibited artificially inoculated black rot caused by *C. fimbriata* and helped maintain the weight loss rate, anthocyanin content, and vitamin C content in postharvest sweet potatoes, which suggests that PAE could be a potential method of enhancing anthocyanin and vitamin C accumulation and maintaining high-quality postharvest sweet potatoes. In addition, PAE vapor treatment may enhance the resistance of postharvest sweet potatoes to *C. fimbriata* through several defense-related enzymes (SOD, CAT, APX, POD, PPO, and PAL). Taken together, the ability of PAE to reduce decay in postharvest sweet potatoes may be associated with the elicitation of the host defense response. These results suggest that the mode of action of PAE appears to occur both via direct interaction with the fungus itself and via defensive responses in the fruit tissue. Hence, the postharvest application of PAE is a promising strategy for the control of postharvest diseases in sweet potatoes. In addition, further experiments are required to investigate the influence of PAE on global transcriptional changes in sweet potatoes using RNA-Seq technology.

AUTHOR CONTRIBUTIONS

JT and YL designed the experiments. MZ and ML performed the experiments. CP and SP analyzed the data. MZ and ML drafted the manuscript. All authors read and approved the final manuscript.

FUNDING

This study was funded by the National Natural Science Foundation of China (31671944), the Six Talent Peaks Project of Jiangsu Province (SWYY-026), the Qing Lan Project of Jiangsu Province, the Natural Science Foundation by Xuzhou City (KC17053), the Industry-University-Academy Prospective Joint Research Project of Jiangsu Province (BY2016028-01), and the PAPD of Jiangsu Higher Education Institutions.

REFERENCES

- Assis, J. S., Maldonado, R., Munoz, T., Escribano, M. I., and Merodio, C. (2001). Effect of high carbon dioxide concentration on PAL activity and phenolic contents in ripening cherimoya fruit. *Postharvest Biol. Technol.* 23, 33–39. doi: 10.1016/S0925-5214(01)00100-4
- Baker, C. J., Harrington, T. C., Krauss, U., and Alfenas, A. C. (2003). Genetic variability and host specialization in the Latin American clade of *Ceratocystis fimbriata*. *Phytopathology* 93, 1274–1284. doi: 10.1094/Phyto.2003.93.10.1274
- Cao, S. F., Zheng, Y. H., Yang, Z. F., Tang, S. S., Jin, P., Wang, K. T., et al. (2008). Effect of methyl jasmonate on the inhibition of *Colletotrichum acutatum* infection in loquat fruit and the possible mechanisms. *Postharvest Biol. Technol.* 49, 301–307. doi: 10.1016/j.postharvbio.2007.12.007
- Castillo, S., Perez-Alfonso, C. O., Martinez-Romero, D., Guillen, F., Serrano, M., and Valero, D. (2014). The essential oils thymol and carvacrol applied in the packing lines avoid lemon spoilage and maintain quality during storage. *Food Control* 35, 132–136. doi: 10.1016/j.foodcont.2013.06.052
- Cindi, M. D., Soundy, P., Romanazzi, G., and Sivakumar, D. (2016). Different defense responses and brown rot control in two *Prunus persica* cultivars to essential oil vapours after storage. *Postharvest Biol. Technol.* 119, 9–17. doi: 10.1016/j.postharvbio.2016.04.007
- Deng, L. L., Zeng, K. F., Zhou, Y. H., and Huang, Y. (2015). Effects of postharvest oligochitosan treatment on anthracnose disease in citrus (*Citrus sinensis* L. Osbeck) fruit. *Eur. Food Res. Technol.* 240, 795–804. doi: 10.1007/s00217-014-2385-7
- Dixon, R. A., Achnine, L., Kota, P., Liu, C. J., Reddy, M. S., and Wang, L. J. (2002). The phenylpropanoid pathway and plant defence - a genomics perspective. *Mol. Plant Pathol.* 3, 371–390. doi: 10.1046/j.1364-3703.2002.00131.x
- Elshafie, H. S., Mancini, E., Camele, I., De Martino, L., and De Feo, V. (2015). In vivo antifungal activity of two essential oils from Mediterranean plants against postharvest brown rot disease of peach fruit. *Ind. Crop Prod.* 66, 11–15. doi: 10.1016/j.indcrop.2014.12.031
- Engelbrecht, C. J., and Harrington, T. C. (2005). Intersterility, morphology and taxonomy of *Ceratocystis fimbriata* on sweet potato, cacao and sycamore. *Mycologia* 97, 57–69. doi: 10.3852/mycologia.97.1.57
- Fan, F., Tao, N. G., Jia, L., and He, X. L. (2014). Use of citral incorporated in postharvest wax of citrus fruit as a botanical fungicide against *Penicillium digitatum*. *Postharvest Biol. Technol.* 90, 52–55. doi: 10.1016/j.postharvbio.2013.12.005

- Ferreira, M. A., Harrington, T. C., Piveta, G., and Alfenas, A. C. (2017). Genetic variability suggests that three populations of *Ceratocystis fimbriata* are responsible for the Ceratocystis wilt epidemic on kiwifruit in Brazil. *Trop. Plant Pathol.* 42, 86–95. doi: 10.1007/s40858-017-0131-y
- Foyer, C. H., and Noctor, G. (2011). Ascorbate and glutathione: the heart of the redox hub. *Plant Physiol.* 155, 2–18. doi: 10.1104/pp.110.167569
- Guerra, I. C. D., de Oliveira, P. D. L., de Souza Pontes, A. L., Lucio, A. S. S. C., Tavares, J. F., Barbosa-Filho, J. M., et al. (2015). Coatings comprising chitosan and *Mentha piperita* L. or *Mentha x villosa* Huds essential oils to prevent common postharvest mold infections and maintain the quality of cherry tomato fruit. *Int. J. Food Microbiol.* 214, 168–178. doi: 10.1016/j.ijfoodmicro.2015.08.009
- Hobbs, C. A., Taylor, S. V., Beevers, C., Lloyd, M., Bowen, R., Lillford, L., et al. (2016). Genotoxicity assessment of the flavouring agent, perillaldehyde. *Food Chem. Toxicol.* 97, 232–242. doi: 10.1016/j.fct.2016.08.029
- Kilcast, D. (1994). Effect of irradiation on vitamins. *Food Chem.* 49, 157–164. doi: 10.1016/0308-8146(94)90152-X
- Kim, K. H., and Yook, H. S. (2009). Effect of gamma irradiation on quality of kiwifruit (*Actinidia deliciosa* var. *deliciosa* cv. Hayward). *Radiat. Phys. Chem.* 78, 414–421. doi: 10.1016/j.radphyschem.2009.03.007
- Li, J., Bao, X. L., Xu, Y. C., Zhang, M., Cai, Q. W., Li, L. P., et al. (2017). Hypobaric storage reduced core browning of Yali pear fruits. *Sci. Hortic.* 225, 547–552. doi: 10.1016/j.scienta.2017.07.031
- Li, J., Yan, J. Q., Ritenour, M. A., Wang, J. F., Cao, J. K., and Jiang, W. B. (2016). Effects of 1-methylcyclopropene on the physiological response of Yali pears to bruise damage. *Sci. Hortic.* 200, 137–142. doi: 10.1016/j.scienta.2016.01.018
- Liu, H. X., Jiang, W. B., Bi, Y., and Luo, Y. B. (2005). Postharvest BTH treatment induces resistance of peach (*Prunus persica* L. cv. Jiubao) fruit to infection by *Penicillium expansum* and enhances activity of fruit defense mechanisms. *Postharvest Biol. Technol.* 35, 263–269. doi: 10.1016/j.postharvbio.2004.08.006
- Liu, S. M., Shao, X. F., Wei, Y. Z., Li, Y. H., Xu, F., and Wang, H. F. (2016). *Solidago canadensis* L. essential oil vapor effectively inhibits *Botrytis cinerea* growth and preserves postharvest quality of strawberry as a food model system. *Front. Microbiol.* 7:1179. doi: 10.3389/fmicb.2016.01179
- Ma, Z. X., Yang, L. Y., Yan, H. X., Kennedy, J. F., and Meng, X. H. (2013). Chitosan and oligochitosan enhance the resistance of peach fruit to brown rot. *Carbohydr. Polym.* 94, 272–277. doi: 10.1016/j.carbpol.2013.01.012
- McGeady, P., Wansley, D. L., and Logan, D. A. (2002). Carvone and perillaldehyde interfere with the serum-induced formation of filamentous structures in *Candida albicans* at substantially lower concentrations than those causing significant inhibition of growth. *J. Nat. Prod.* 65, 953–955. doi: 10.1021/np010621l
- Mirdehghan, S. H., and Rahimi, S. (2016). Pre-harvest application of polyamines enhances antioxidants and table grape (*Vitis vinifera* L.) quality during postharvest period. *Food Chem.* 196, 1040–1047. doi: 10.1016/j.foodchem.2015.10.038
- Mohammadi, M., and Kazemi, H. (2002). Changes in peroxidase and polyphenol oxidase activities in susceptible and resistant wheat heads inoculated with *Fusarium graminearum* and induced resistance. *Plant Sci.* 162, 491–498. doi: 10.1016/S0168-9452(01)00538-6
- Muramoto, N., Tanaka, T., Shimamura, T., Mitsukawa, N., Hori, E., Koda, K., et al. (2012). Transgenic sweet potato expressing thionin from barley gives resistance to black rot disease caused by *Ceratocystis fimbriata* in leaves and storage roots. *Plant Cell Rep.* 31, 987–997. doi: 10.1007/s00299-011-1217-5
- Perumal, A. B., Sellamuthu, P. S., Nambiar, R. B., and Sadiku, E. R. (2017). Effects of essential oil vapour treatment on the postharvest disease control and different defence responses in two mango (*Mangifera indica* L.) cultivars. *Food Bioprocess Technol.* 10, 1131–1141. doi: 10.1007/s11947-017-1891-6
- Prabuseenivasan, S., Jayakumar, M., and Ignacimuthu, S. (2006). In vitro antibacterial activity of some plant essential oils. *BMC Complement. Altern. Med.* 6:39. doi: 10.1186/1472-6882-6-39
- Qin, G. Z., Tian, S. P., Xu, Y., and Wan, Y. K. (2003). Enhancement of biocontrol efficacy of antagonistic yeasts by salicylic acid in sweet cherry fruit. *Physiol. Mol. Plant Pathol.* 62, 147–154. doi: 10.1016/S0885-5765(03)00046-8
- Sellamuthu, P. S., Sivakumar, D., Soundy, P., and Korsten, L. (2013). Essential oil vapours suppress the development of anthracnose and enhance defence related and antioxidant enzyme activities in avocado fruit. *Postharvest Biol. Technol.* 81, 66–72. doi: 10.1016/j.postharvbio.2013.02.007
- Servili, A., Feliziani, E., and Romanazzi, G. (2017). Exposure to volatiles of essential oils alone or under hypobaric treatment to control postharvest gray mold of table grapes. *Postharvest Biol. Technol.* 133, 36–40. doi: 10.1016/j.postharvbio.2017.06.007
- Shao, X. F., Wang, H. F., Xu, F., and Cheng, S. (2013). Effects and possible mechanisms of tea tree oil vapor treatment on the main disease in postharvest strawberry fruit. *Postharvest Biol. Technol.* 77, 94–101. doi: 10.1016/j.postharvbio.2012.11.010
- Sharma, R. R., Singh, D., and Singh, R. (2009). Biological control of postharvest diseases of fruits and vegetables by microbial antagonists: a review. *Biol. Control* 50, 205–221. doi: 10.1016/j.biocontrol.2009.05.001
- Soylu, E. M., Kurt, S., and Soylu, S. (2010). In vitro and in vivo antifungal activities of the essential oils of various plants against tomato grey mould disease agent *Botrytis cinerea*. *Int. J. Food Microbiol.* 143, 183–189. doi: 10.1016/j.ijfoodmicro.2010.08.015
- Soylu, E. M., Soylu, S., and Kurt, S. (2006). Antimicrobial activities of the essential oils of various plants against tomato late blight disease agent *Phytophthora infestans*. *Mycopathologia* 161, 119–128. doi: 10.1007/s11046-005-0206-z
- Tao, N. G., Fan, F., Jia, L., and Zhang, M. L. (2014). Octanal incorporated in postharvest wax of *Satsuma mandarin* fruit as a botanical fungicide against *Penicillium digitatum*. *Food Control* 45, 56–61. doi: 10.1016/j.foodcont.2014.04.025
- Tian, H., Qu, S., Wang, Y. Z., Lu, Z. Q., Zhang, M., Gan, Y. Y., et al. (2017). Calcium and oxidative stress mediate perillaldehyde-induced apoptosis in *Candida albicans*. *Appl. Microbiol. Biotechnol.* 101, 3335–3345. doi: 10.1007/s00253-017-8146-3
- Tian, J., Ban, X. Q., Zeng, H., He, J. S., Huang, B., and Wang, Y. W. (2011). Chemical composition and antifungal activity of essential oil from *Cicuta virosa* L. var. *latisecta* Celak. *Int. J. Food Microbiol.* 145, 464–470. doi: 10.1016/j.ijfoodmicro.2011.01.023
- Tian, J., Wang, Y. Z., Lu, Z. Q., Sun, C. H., Zhang, M., Zhu, A. H., et al. (2016). Perillaldehyde, a promising antifungal agent used in food preservation, triggers apoptosis through a metacaspase-dependent pathway in *Aspergillus flavus*. *J. Agric. Food Chem.* 64, 7404–7413. doi: 10.1021/acs.jafc.6b03546
- Tian, J., Wang, Y. Z., Zeng, H., Li, Z. Y., Zhang, P., Tessema, A., et al. (2015a). Efficacy and possible mechanisms of perillaldehyde in control of *Aspergillus niger* causing grape decay. *Int. J. Food Microbiol.* 202, 27–34. doi: 10.1016/j.ijfoodmicro.2015.02.022
- Tian, J., Zeng, X. B., Lu, A. J., Zhu, A. H., Peng, X., and Wang, Y. W. (2015b). Perillaldehyde, a potential preservative agent in foods: assessment of antifungal activity against microbial spoilage of cherry tomatoes. *LWT Food Sci. Technol.* 60, 63–70. doi: 10.1016/j.lwt.2014.08.014
- Tian, S. P., Wan, Y. K., Qin, G. Z., and Xu, Y. (2006). Induction of defense responses against *Alternaria* rot by different elicitors in harvested pear fruit. *Appl. Microbiol. Biot.* 70, 729–734. doi: 10.1007/s00253-005-0125-4
- Toivonen, P. M. A., and Brummell, D. A. (2008). Biochemical bases of appearance and texture changes in fresh-cut fruit and vegetables. *Postharvest Biol. Technol.* 48, 1–14. doi: 10.1016/j.postharvbio.2007.09.004
- Tzortzakakis, N. G., and Economakis, C. D. (2007). Antifungal activity of lemongrass (*Cymbopogon citratus* L.) essential oil against key postharvest pathogens. *Innov. Food Sci. Emerg.* 8, 253–258. doi: 10.1016/j.ifset.2007.01.002
- Vattem, D. A., Randhir, R., and Shetty, K. (2005). Cranberry phenolics-mediated elicitation of antioxidant enzyme response in fava bean (*Vicia faba*) sprouts. *J. Food Biochem.* 29, 41–70. doi: 10.1111/j.1745-4514.2005.00007.x
- Vilaplana, R., Paez, D., and Valencia-Chamorro, S. (2017). Control of black rot caused by *Alternaria alternata* in yellow pitahaya (*Selenicereus megalanthus*) through hot water dips. *LWT Food Sci. Technol.* 82, 162–169. doi: 10.1016/j.lwt.2017.04.042
- Wang, C. Y., Wang, S. Y., and Chen, C. (2008). Increasing antioxidant activity and reducing decay of blueberries by essential oils. *J. Agric. Food Chem.* 56, 3587–3592. doi: 10.1021/jf7037696
- Wang, K. T., Jin, P., Han, L., Shang, H. T., Tang, S. S., Rui, H. J., et al. (2014). Methyl jasmonate induces resistance against *Penicillium citrinum* in Chinese bayberry by priming of defense responses. *Postharvest Biol. Technol.* 98, 90–97. doi: 10.1016/j.postharvbio.2014.07.009

- Yang, J. L., Sun, C., Zhang, Y. Y., Fu, D., Zheng, X. D., and Yu, T. (2017). Induced resistance in tomato fruit by gamma-aminobutyric acid for the control of alternaria rot caused by *Alternaria alternata*. *Food Chem.* 221, 1014–1020. doi: 10.1016/j.foodchem.2016.11.061
- Yao, H. J., and Tian, S. P. (2005). Effects of pre- and post-harvest application of salicylic acid or methyl jasmonate on inducing disease resistance of sweet cherry fruit in storage. *Postharvest Biol. Technol.* 35, 253–262. doi: 10.1016/j.postharvbio.2004.09.001
- Zeng, K. F., Cao, J. K., and Jiang, W. B. (2006). Enhancing disease resistance in harvested mango (*Mangifera indica* L. cv. 'Matisu') fruit by salicylic acid. *J. Sci. Food Agric.* 86, 694–698. doi: 10.1002/jsfa.2397
- Zhang, C. F., Wang, J. M., Zhang, J. G., Hou, C. J., and Wang, G. L. (2011). Effects of beta-aminobutyric acid on control of postharvest blue mould of apple fruit and its possible mechanisms of action. *Postharvest Biol. Technol.* 61, 145–151. doi: 10.1016/j.postharvbio.2011.02.008
- Zheng, F. L., Zheng, W. W., Li, L. M., Pan, S. M., Liu, M. C., Zhang, W. W., et al. (2017). Chitosan controls postharvest decay and elicits defense response in kiwifruit. *Food Bioprocess Technol.* 10, 1937–1945. doi: 10.1007/s11947-017-1957-5
- Conflict of Interest Statement:** The authors declare that the research was conducted in the absence of any commercial or financial relationships that could be construed as a potential conflict of interest.
- Copyright © 2018 Zhang, Liu, Pan, Pan, Li and Tian. This is an open-access article distributed under the terms of the Creative Commons Attribution License (CC BY). The use, distribution or reproduction in other forums is permitted, provided the original author(s) and the copyright owner are credited and that the original publication in this journal is cited, in accordance with accepted academic practice. No use, distribution or reproduction is permitted which does not comply with these terms.



Fungal Gene Mutation Analysis Elucidating Photoselective Enhancement of UV-C Disinfection Efficiency Toward Spoilage Agents on Fruit Surface

Pinkuan Zhu*, Qianwen Li, Sepideh M. Azad, Yu Qi, Yiwen Wang, Yina Jiang and Ling Xu*

School of Life Sciences, East China Normal University, Shanghai, China

OPEN ACCESS

Edited by:

Boqiang Li,
Institute of Botany (CAS), China

Reviewed by:

Zhanquan Zhang,
Chinese Academy of Sciences, China
Ernesto P. Benito,
Universidad de Salamanca, Spain

*Correspondence:

Pinkuan Zhu
pkzhu@bio.ecnu.edu.cn
Ling Xu
lxu@bio.ecnu.edu.cn

Specialty section:

This article was submitted to
Food Microbiology,
a section of the journal
Frontiers in Microbiology

Received: 30 March 2018

Accepted: 14 May 2018

Published: 12 June 2018

Citation:

Zhu P, Li Q, Azad SM, Qi Y, Wang Y,
Jiang Y and Xu L (2018) Fungal
Gene Mutation Analysis Elucidating
Photoselective Enhancement of UV-C
Disinfection Efficiency Toward
Spoilage Agents on Fruit Surface.
Front. Microbiol. 9:1141.
doi: 10.3389/fmicb.2018.01141

Short-wave ultraviolet (UV-C) treatment represents a potent, clean and safe substitute to chemical sanitizers for fresh fruit preservation. However, the dosage requirement for microbial disinfection may have negative effects on fruit quality. In this study, UV-C was found to be more efficient in killing spores of *Botrytis cinerea* in dark and red light conditions when compared to white and blue light. Loss of the blue light receptor gene *Bcwcl1*, a homolog of *wc-1* in *Neurospora crassa*, led to hypersensitivity to UV-C in all light conditions tested. The expression of *Bcuve1* and *Bcphr1*, which encode UV-damage endonuclease and photolyase, respectively, were strongly induced by white and blue light in a *Bcwcl1*-dependent manner. Gene mutation analyses of *Bcuve1* and *Bcphr1* indicated that they synergistically contribute to survival after UV-C treatment. *In vivo* assays showed that UV-C (1.0 kJ/m²) abolished decay in drop-inoculated fruit only if the UV-C treatment was followed by a dark period or red light, while in contrast, typical decay appeared on UV-C irradiated fruits exposed to white or blue light. In summary, blue light enhances UV-C resistance in *B. cinerea* by inducing expression of the UV damage repair-related enzymes, while the efficiency of UV-C application for fruit surface disinfection can be enhanced in dark or red light conditions; these principles seem to be well conserved among postharvest fungal pathogens.

Keywords: ultraviolet-C, fungal pathogen, photoreceptor, postharvest decay, *Botrytis cinerea*

INTRODUCTION

Fresh fruits and vegetables are rich in moisture and nutrients, and thus susceptible to postharvest decays caused by microbial contamination and proliferation, especially pathogenic fungi (Sperber et al., 2009). Chemical sanitizers are commonly used for disinfection of the harvested crops. However, the long-term use of chemical fungicides frequently poses the risk of fungicide resistance in pathogens. More importantly, pesticide residue in fresh crops is an increasing health concern among consumers. To address these issues, developing alternative methods to synthetic fungicides for disease management purpose is in urgent need (Romanazzi et al., 2012, 2016).

Ultraviolet-C (UV-C, 200–280 nm) offers interesting possibilities for postharvest disease management as a safe alternative to conventional chemical fungicides. Although the UV-C portion

of the cosmic rays is almost completely absorbed by the outer space atmosphere and is hardly observed in nature on the earth's surface, UV-C radiation can be created by artificial lamps, and usually causes two distinct effects on fresh fruits and vegetables: one is the elicitation of disease resistance and quality improvement in fresh crops, while the other is reduction of microbial population due to its direct germicidal effect (Urban et al., 2016). The former effect on host crops is often defined as hormesis, that is, stimulation of favorable responses in plants exposed to low or sublethal doses of an agent such as a physical stressor (Luckey, 1982). It has been recognized that UV-C light at low hormetic doses reduced the postharvest decay of a wide range of crops (Luckey, 1982), although these beneficial effects depend on the dose and timing of UV-C exposure, the fruit or vegetable species and cultivars, and the exposed area (Allende and Artés, 2003; Vicente et al., 2005; Costa et al., 2006; Pombo et al., 2011; Topcu et al., 2015). UV-C can cause DNA damage, and is thus used as a sterilizing agent for air, water and food (Bintsis et al., 2000). However, the host hormesis-inducing and microbe-disinfecting effects of UV-C on fresh crops are somewhat incompatible: the disease resistance elicitation effect can be achieved only when the UV-C dosage is restricted to certain sublethal dosages, while the microbe-disinfecting effect can be produced by increasing UV-C dosage. Accordingly, UV-C treatment of fruits and vegetables needs to be optimized tactically to obtain a desirable balance between the beneficial changes in host plants along with efficient disinfection against pathogens (Urban et al., 2016). To address this issue, it is important to understand the regulation mechanisms of UV-C resistance in fungal pathogens, which still remains to be elucidated.

It is known that UV-C inhibits microbial growth mainly by inducing the formation of pyrimidine dimers that alter the DNA helix and block microbial cell replication (Bintsis et al., 2000). However, microorganisms can protect themselves against UV radiation by repairing damaged DNA (Sinha and Hader, 2002). Proteins such as DNA photolyases have been found in a variety of species and can restore the UV-damaged bases back to their original undamaged states (Bluhm and Dunkle, 2008; Brettel and Byrdin, 2010). Additionally, the UV-damage endonuclease (UVDE) can directly recognize and cleave damaged DNA, which is followed by lesion removal, gap-filling, and ligation reactions (Bowman et al., 1994; Freyer et al., 1995; Yajima et al., 1995). Therefore, the UV-C dosages for fungicidal purposes must be relatively high, usually ranging from 0.5 to 20 kJ/m² (Bintsis et al., 2000).

Fungi can also sense visible light to promote tolerance against harmful UV radiation (Fuller et al., 2015). This has been validated in several fungi by functional studies on the orthologs of White collar complex (WCC), the blue light receptor of *Neurospora crassa*. These proteins can act both as photosensors as well as transcription factors to regulate the expression of light responsive genes (Ballario et al., 1996; Crosthwaite et al., 1997; Liu et al., 2003). DNA repair enzymes, including photolyases and UVDE, were shown to be induced by light via the conserved WCC signaling pathway in several fungal species, including *Cryptococcus neoformans*, *Phycomyces blakesleeanus*, and *Ustilago maydis* (Verma and Idnurm, 2013; Tagua et al., 2015;

Brych et al., 2016). The light regulation of UV-C resistance in fungi implies that ultraviolet disinfection efficiency can be adjusted by orchestrating photic conditions.

Botrytis cinerea is the gray mold pathogen that causes enormous economic damage to fruits and vegetables, both in field and during postharvest procedures (Fillinger and Elad, 2016). The infection cycle of this pathogen usually starts with the attachment of conidia to the plant surface, followed by infection and rapid hyphal spreading inside the plant tissue leading to host collapse (Fillinger and Elad, 2016). *B. cinerea* shows varied developmental responses to different wavelengths of the light spectrum. The conserved WCC homologs of *B. cinerea* mediate transcriptional responses to the blue light spectrum and inhibit its conidiation. Furthermore, WCC is required for coping with excessive light, oxidative stress, and to achieve full virulence to host plants (Canessa et al., 2013). Recently, cryptochrome/photolyase homologs, BcCRY1 and BcCRY2, were characterized in *B. cinerea*, revealing that BcCRY1 acts as the major photolyase in photoprotection, whereas BcCRY2 acts as a cryptochrome with signaling function in regulating repression of conidiation (Cohrs and Schumacher, 2017). However, the mechanism of photoselective regulation of UV resistance in *B. cinerea* has not been fully elucidated yet.

The present study aims to reveal the mechanism of regulation of UV-C resistance in the fungal fruit spoilage agents. Using *B. cinerea* as a representative model, we find that blue light and *Bcwc11* are required for activating the expression of the UV-damage endonuclease and photolyase genes, *Bcuve1* and *Bcphr1* (or *Bccry1* in an earlier report, Cohrs and Schumacher, 2017), respectively. Gene mutation analysis revealed that *Bcuve1* and *Bcphr1* are synergistically responsible for coping with UV-C induced damage in *B. cinerea*. More importantly, since blue light is the specific spectrum that supports DNA-damage repair activities in fungi, UV-C treatment followed by dark or red-light conditions was thus found to enhance microbe-killing efficiency thereby facilitating fruit spoilage management.

MATERIALS AND METHODS

Fungal Strains and Culture

The reference strain B05.10 of *Botrytis cinerea* was designated as wild type for genetic modification. The other pathogenic fungi were originally isolated from fruits and vegetables (Table 1). Potato dextrose agar (PDA) was used to maintain the fungal cultures at their indicated optimum temperatures. Conidia of each fungal species were collected by flooding the sporulated colonies with sterilized water, followed by filtration through four layers of cheesecloth and centrifugation at 4500 rpm. The concentration of the resulting conidial suspension was measured by a hemacytometer.

Visible and UV-C Light Treatment

White, blue, and red visible light spectra were produced by a light-emitting diode (LED, Qiding Photo Electronic, Shanghai, China). The parameters of each light spectrum are listed in Table 2. Light intensities were fixed at 20 $\mu\text{mol m}^{-2} \text{s}^{-1}$, as

TABLE 1 | Fungal species and growth temperature.

Species	Host origin	Temperature
<i>Botrytis cinerea</i>	Grape	25°C
<i>Alternaria alternata</i>	Broccoli	25°C
<i>Colletotrichum gloeosporioides</i>	Mango	28°C
<i>Penicillium digitatum</i>	Navel orange	25°C

TABLE 2 | Parameters of light.

Light color	Peak λ	Dominant λ	Average λ	$\Delta\lambda$ peak
White	460.0	468.5	544.0	27.0
Blue	470.0	472.4	470.0	25.9
Red	675.0	663.3	674.0	24.3

λ , wavelength (nm).

measured by Quantum Light Meter (Spectrum Technologies, United States), and achieved by manually adjusting the power control switch of the LED devices. For dark treatment, samples were kept in a light-proof plastic box and incubated at a temperature similar to the light-treated ones. HL-2000 cross-linker lamps (UVP, United States) were used for UV-C radiation (254 nm) treatment. The UV-C dosage was recorded as either $\mu\text{J}/\text{cm}^2$ or kJ/m^2 .

Generation of Gene Deletion Mutant

Protoplast transformation mediated homologous recombination strategy was adopted to generate knock out mutants of target genes according to the previous method (Chung and Lee, 2015). 1 kb of the 5' and 3' untranslated regions (UTRs) of target genes were amplified from the DNA of the wild type strain, and selective marker genes, hygromycin (*hyg*) or nourseothricin resistant (*nat*) cassette, were PCR amplified from the plasmid pCambia1300 or pNR2, respectively. Overlap PCR was then performed to fuse the 5'- and 3'-UTRs with the selective marker genes, resulting in 5' UTR-*hyg* (or *nat*) - 3' UTR constructs for protoplast transformation. Diagnostic PCR was performed to identify bonafide targeted disruption mutants among the emerged transformants as indicated in **Supplementary Figure S1**. The gene disruption mutants were further verified by Southern blot hybridization according to the protocol recommended in the DIG high prime DNA labeling and detection starter Kit II (Roche, Mannheim, Germany).

Construction of *Bcuve1*-GFP Fusion Expression Strain and Fluorescent Microscopy

The expression vector pNDN-OGG (Schumacher, 2012) carrying nourseothricin resistance (*NAT*) and *GFP* expression cassettes was digested with *Nco*I. The wild type *Bcuve1* was amplified without the stop codon using the primers P45/46 (**Supplementary Table S1**) that are equipped with 22-bp overlaps corresponding to the sequences in the destination vector for the Gibson assembly-based cloning using the Hieff Clone™ Plus Multi One Step Cloning Kit (YEASEN, China). The resulted clones were identified by PCR diagnosis, and

the positive ones were further confirmed for correctness by sequencing. The correct vector named pNDN-OGG-*Bcuve1* carrying *Bcuve1* upstream of the *GFP* gene was linearized by *Sac*II digestion and transformed into $\Delta bcuve1$. The fungal transformation was selected by nourseothricin (50 $\mu\text{g}/\text{ml}$). The positive resistant transformants were purified by series of single spore culture, and the $\Delta bcuve1$ -*Bcuve1*-GFP strain was obtained for UV-C sensitivity and microscopy analysis. Fluorescence and light microscopy was performed with a Zeiss Axio Imager Z2 microscope. Differential interference microscopy (DIC) was used for bright field images. GFP fluorescence was examined using excitation BP 470/40 and emission BP 525/50, DAPI staining with the excitation G 365 and emission BP 445/50. DIC, GFP, and DAPI images were merged via ImageJ soft ware.

Gene Expression Analysis

Aliquots (200 μl) of conidial suspensions (10^6 conidia/ml) were inoculated on cellophane-overlaid PDA and incubated at 25°C in dark for 24 h. Samples were subsequently divided into four groups each and placed under different light conditions (white, blue, red light, and darkness). After incubating for 1 h, mycelium samples (about 0.1 g) from each of the groups were harvested using cell scrapers in the dark, transferred into 2 ml Eppendorf tubes, and immediately frozen in liquid nitrogen. For total RNA extraction, each sample was submerged in 1 ml Trizol reagent (Invitrogen, Carlsbad, CA, United States), and homogenized by shaking along with four steel balls (2 mm diameter) at 70 Hz and 4°C for 3 min on a TissueLyser (Jingxin Industrial, Shanghai, China). The resulting suspensions were extracted with chloroform according to the manufacturer's instructions supplied with Trizol. One microgram of each RNA sample was used as a template for reverse transcription using the Prime Script™ RT reagent Kit (Perfect Real Time) (TakaRa Biotechnology, Co., Dalian, China). Real-time PCR amplifications were conducted in a CFX96™ Real-Time System (BIO-BAD, Inc., United States) using TakaRa SYBR Premix Ex Taq (TakaRa Biotechnology). Relative quantifications of the real-time PCR amplifications were performed with the following parameters, initial preheating at 95°C for 30 s followed by 39 cycles at 95°C for 5 s and 60°C for 30 s. The β -tubulin gene was analyzed as an internal reference. Experiments were repeated three times for each sample. The primers used in this study are listed in **Supplementary Table S1**. The gene expression levels were calculated using the $2^{-\Delta\Delta C_t}$ method (Livak and Schmittgen, 2001). All experiments were repeated three times.

UV-C Sensitivity Assays

To evaluate fungal UV-C sensitivity, 200 μl of conidial suspensions (5×10^3 conidia/ml) were evenly inoculated on individual PDA surfaces using a cell spreader and subjected to UV-C irradiation, with dosages ranging from 0.6 to 1.2 kJ/m^2 . The samples were immediately incubated at 25°C for 2 h under white, blue, red light and dark conditions. Subsequently, all samples were continuously incubated in the dark for 2 days. Samples that were not subjected to UV-C treatment were used as reference controls. Fungal colonies arising on the plate were counted and survival rates were calculated by dividing the colony

numbers on UV-C treated plates with those on non-UV-C treated ones.

To visualize the effect of visible light on fungal UV-C sensitivity, 5 μ l of conidial suspension (10^6 conidia/ml) was dropped on cellophane overlaid with water agar. After UV-C radiation, the samples were similarly treated for 2 h under different light and dark conditions, and then incubated in the dark for another 22 h. Conidial germination of each sample was finally examined under a light microscope. Five replicates were conducted for all experiments.

Fruit Inoculation Assay

Wild type spores of *B. cinerea* were suspended in sterilized 1% sugar solution, and the concentration was adjusted to 10^6 conidia/ml. Table grapes were purchased from the local super market. Healthy berries with uniform size and maturity stage were selected for this assay. Before inoculation, the fruits were submerged in 0.5% sodium hypochlorite solution for 3 min to eliminate possible contaminating microorganisms on the surface of grape berries, followed by rinsing thrice with sterilized water. The fruits were then artificially wound-inoculated with 10 μ l spore suspension at a site on the equatorial line of each grape berry. The fruits were then exposed to 1 kJ/m² UV-C, and divided into four groups, each including 30 berries, and transferred to dark, white, blue, and red lights to incubate at 25°C for 2 h. Subsequently, all samples were placed in continuous dark, and 4 days later the disease symptoms were photographed, and the decay areas were measured via ImageJ software.

Statistical Analysis

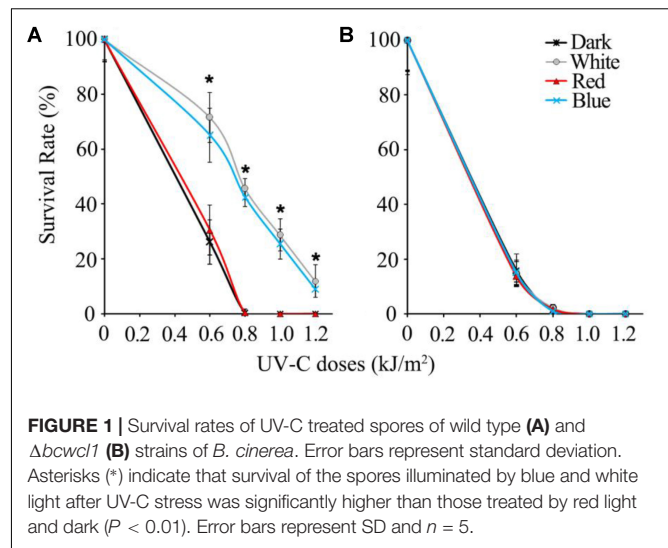
The experiments in this study were repeated three times. The data obtained were analyzed by ANOVA followed by Duncan's multiple range tests ($p < 0.01$) for means comparison with the use of SPSS 17.0.

RESULTS

Blue Light Is Specifically Required for Inducing UV-C Resistance in a *Bcwc1*-Dependent Manner

In the UV-C sensitivity assay, wild type spores of *B. cinerea* were completely killed by 0.8 kJ/m² UV-C in dark and 2 h red light-treated groups, while the spores exposed to white and blue light survived by more than 40%. Even when the UV-C dose reached 1.2 kJ/m², the wild type spores illuminated in white and blue light maintained an approximately 10% survival rate (Figure 1A). Eventually, we confirmed that the blue light spectrum (but not the red light) is specifically effective in enhancing *B. cinerea* spore survivability after UV-C irradiation.

Since blue light is known to be sensed by fungi via the WCC photoreceptors, the WC-1 homolog gene in *B. cinerea*, *Bcwc1* (Canessa et al., 2013), was disrupted by replacing the open reading frame with the hygromycin resistance cassette via homologous recombination. $\Delta bcwc1$ mutant strains were confirmed by genomic PCR, and showed enhanced melanization



and sporulation in contrast to the wild type strain (data not shown). These phenotypes were in agreement with a previous report in which WC-1 was shown to negatively regulate spore formation and melanin biosynthesis (Canessa et al., 2013). One representative $\Delta bcwc1$ strain was thus used for the UV-C sensitivity assay. The results showed that neither blue nor white light could increase survivability of the mutant after UV-C radiation. The survival rates of the $\Delta bcwc1$ mutant dropped down to almost 0% in all the treatment groups when the UV-C dosage was above 0.8 kJ/m² (Figure 1B). Taken together, we conclude that photoinduction of UV-C resistance in *B. cinerea* is specifically caused by the blue light spectrum via signaling through the light receptor encoded by *Bcwc1*.

Expression of DNA Damage Repair Related Genes Is Regulated by Light via *Bcwc1*

Since white collar 1 can function as both blue light receptor and transcription factor (Canessa et al., 2013), it is assumed that certain downstream genes regulated by this protein could be responsible for photo responsive phenotypes. Based on the transcriptomic data (Schumacher et al., 2014), two genes expected to contribute to DNA damage repair in *B. cinerea* were obtained: *Bcuve1* (Bcin01g08960) encoding the protein homologous to the UV damage endonuclease Uve1 of *Schizosaccharomyces pombe* (GenBank: CAA19577.1), and *Bcphr1* (Bcin05g08060, or *Bccry1* in Cohrs and Schumacher, 2017) encoding the homolog of photolyase/cryptochrome of *Neurospora crassa* (GenBank: KHE81232.1). The deduced protein domains of these two gene products are presented in Figure 2A. The expression of *Bcuve1* and *Bcphr1* was analyzed via quantitative RT-PCR. The results showed that white and blue light treatments strongly induced the expression of *Bcuve1* and *Bcphr1* in the wild type, but not in the $\Delta bcwc1$ mutant strain. However, red light exposure did not change the expression of these two genes in both WT and $\Delta bcwc1$ strains (Figure 2B). Taken together, these results indicate that blue light signaling

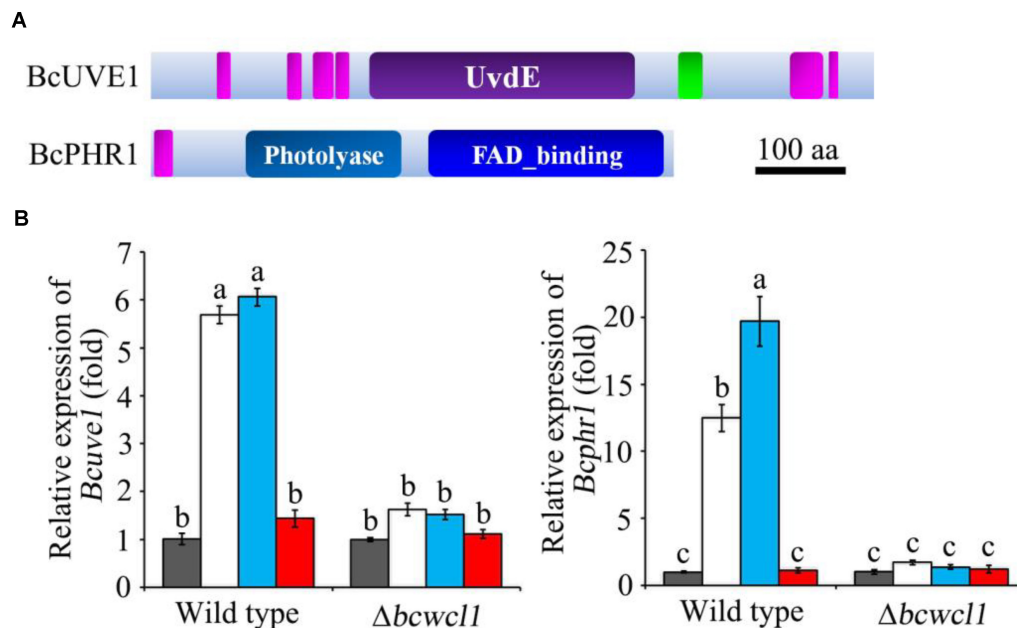


FIGURE 2 | Expression analysis of DNA damage repair related genes. **(A)** The Ensembl Fungi IDs of *Bcuve1* and *Bcphr1* are Bcin01g08960.1 and Bcin05g08060.1, respectively. According to SMART analysis, the BcUVE1 protein contains a UV damage endonuclease domain (UvdE), and BcPHR1 contains a DNA_photolyase domain and a FAD_binding domain. The pink rectangles represent regions of low complexity, and the green one represents the coiled-coil region. The scale bar indicates a length of 100 amino acids. **(B)** Comparison of *Bcuve1* and *Bcphr1* expression levels between the wild type and $\Delta bcwcl1$ strains under different light conditions. Columns represent dark, white, blue, and red light exposure from left to right. Histograms marked with different characters are statistically different ($p < 0.01$). Error bars represent SD and $n = 3$.

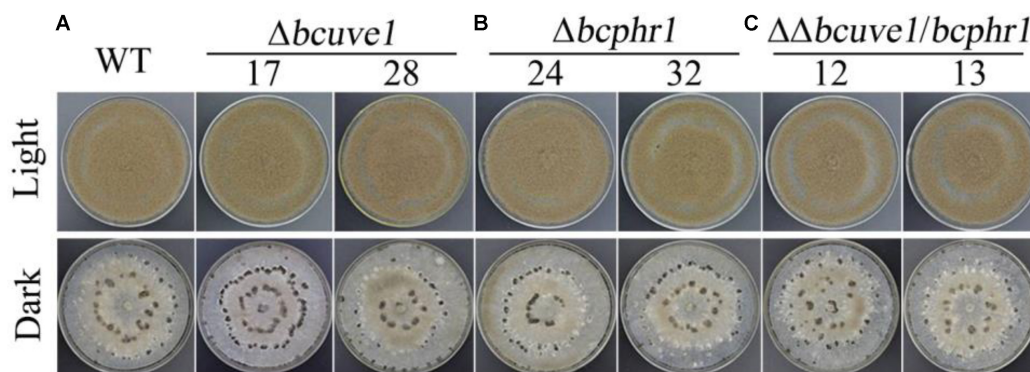


FIGURE 3 | The three mutant strains, **(A)** $\Delta bcuve1$, **(B)** $\Delta bcphr1$, and **(C)** $\Delta\Delta bcuve1/bcphr1$, formed similar sporulation colonies (1 week in light) and sclerotia (2 weeks in dark) on PDA.

via the WC-1 homolog activates both endonuclease excision and photolyase pathways in *B. cinerea*.

Bcuve1* and *Bcphr1* Synergistically Contribute to UV-C Resistance in *B. cinerea

To confirm the roles of *Bcuve1* and *Bcphr1* in *B. cinerea*, single and double mutant strains were created via protoplast transformation and homologous recombination mediated gene replacement. Genomic PCR analysis and Southern blot

confirmed mutation of the targeted locus in the colonies recovered (**Supplementary Figure S1**). The resulting mutants, $\Delta bcuve1$, $\Delta bcphr1$, and $\Delta\Delta bcuve1/bcphr1$, showed growth rates, sporulation, sclerotial development (**Figure 3** and **Table 3**), and virulence equivalent to the wild type strain when tested on grape berries (**Figure 4**), indicating that neither *Bcuve1* nor *Bcphr1* is involved in regulating the vegetative growth, development, and host-invasion processes.

In the UV-C sensitivity assay, the $\Delta bcuve1$ mutant showed significantly reduced survival rates when compared to the wild type strain. However, blue and white lights were still

TABLE 3 | Comparison of colony growth, sporulation, and sclerotia formation.

Genotypes of fungal strains	Growth rate (mm/day)		Sporulation (× 10 ⁷ /dish)	Sclerotia (No./dish)
	Dark	Light		
WT	28.57 ± 0.2	28.48 ± 0.17	5.1 ± 0.15	167.6 ± 5.24
Δ <i>bcuve1</i> -17	28.16 ± 0.18	28.36 ± 0.21	4.67 ± 0.13	163.83 ± 4.06
Δ <i>bcuve1</i> -28	28.13 ± 0.31	28.06 ± 0.31	5.05 ± 0.11	61.83 ± 3.7
Δ <i>bcphr1</i> -24	27.98 ± 0.37	28.16 ± 0.41	5.06 ± 0.12	162.6 ± 5.04
Δ <i>bcphr1</i> -32	28.5 ± 0.23	28.45 ± 0.19	4.92 ± 0.14	163.4 ± 1.72
Δ <i>bcuve1</i> / <i>bcphr1</i> -12	28.23 ± 0.46	28.89 ± 0.39	5.04 ± 0.11	161.6 ± 4.76
Δ <i>bcuve1</i> / <i>bcphr1</i> -13	28.8 ± 0.27	27.95 ± 0.43	4.76 ± 0.1	164.5 ± 3.96

Data in this table were measured from cultures grown in CM medium. Sporulation and sclerotia formation were tested with 1 week old cultures in constant light and 2 week old cultures in constant dark, respectively.

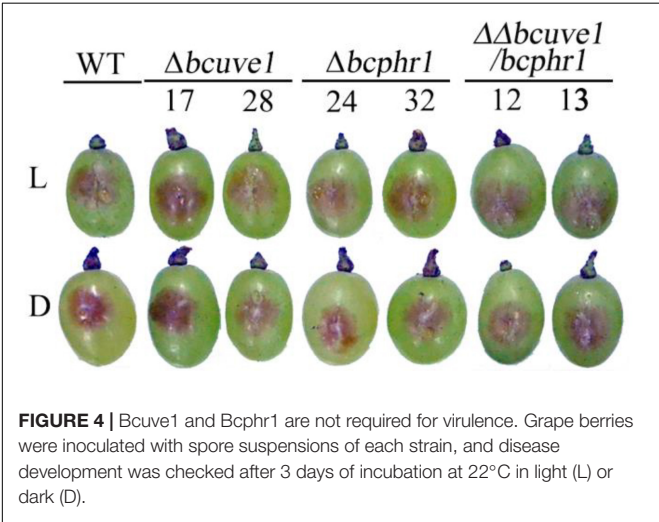


FIGURE 4 | *Bcuve1* and *Bcphr1* are not required for virulence. Grape berries were inoculated with spore suspensions of each strain, and disease development was checked after 3 days of incubation at 22°C in light (L) or dark (D).

capable of enhancing UV-C tolerance of the *Δbcuve1* mutant when the dosage was 0.6 kJ/m² (Figure 5). On the other hand, the *Δbcphr1* mutant was relatively more tolerant to UV-C than *Δbcuve1*, although *Δbcphr1* still showed significantly reduced survival rate under UV-C stress when compared to the wild type. Visible light treatment after UV-C radiation did not alter the survivability of *Δbcphr1* (Figure 5). Moreover, the double mutant, *ΔΔbcuve1/bcphr1*, combined the patterns of the two single mutants, showing similar sensitivity to UV-C as the *Δbcuve1* mutant in dark, and no change in survival rate as the *Δbcphr1* mutant when treated with white light after UV-C treatment (Figure 5). These data together indicate that BcUVE1 and BcPHR1 play synergistic roles in UV-C damage repair in *B. cinerea*.

Since UV radiation can stimulate organisms to generate reactive oxygen species (ROS), which can also cause DNA damage, we additionally tested the sensitivity of each strain to ROS stress upon treatment with hydrogen peroxide (H₂O₂). The results demonstrated that all the strains, i.e., *Δbcuve1*, *Δbcphr1*, *ΔΔbcuve1/bcphr1* and WT, showed decreased survivability with increasing H₂O₂ concentration in the medium, however, no significant difference in susceptibility

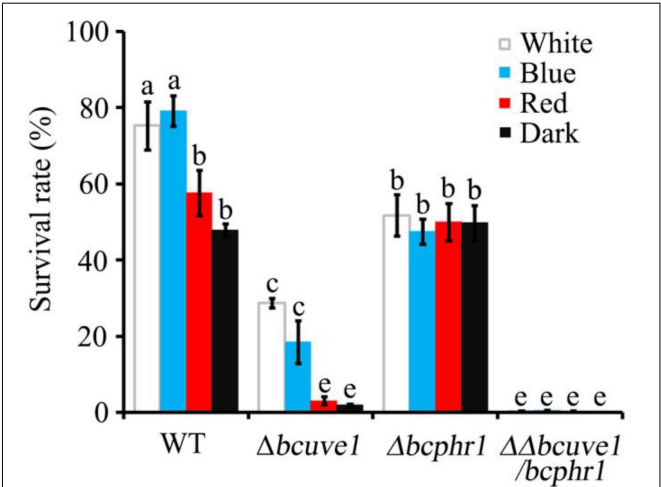
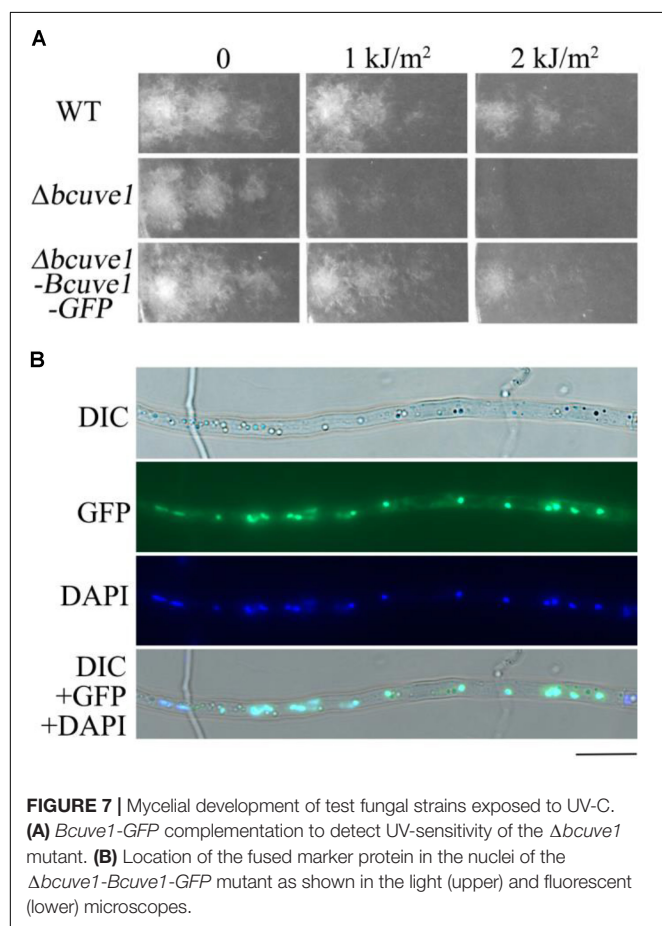
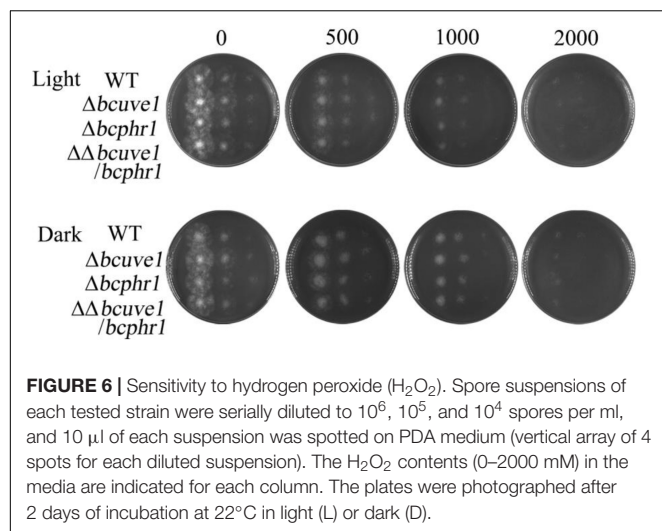


FIGURE 5 | The three mutant strains, *Δbcuve1*, *Δbcphr1*, and *ΔΔbcuve1/bcphr1*, showed differentially altered sensitivities to UV-C (0.6 kJ/m²) when influenced with visible light qualities. Bars marked with non-identical characters are significantly different (*P* < 0.01). Error bars represent SD and *n* = 5.

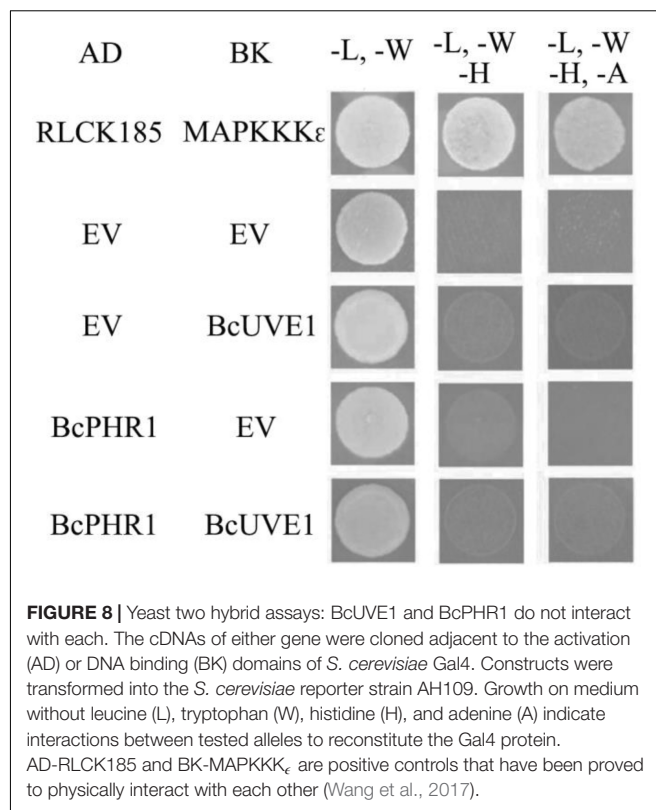
to H₂O₂ was observed between the mutants and wild type (Figure 6).

Role of BcUVE1 in UV-Damage Repair Is Confirmed by Genetic Complementation and Subcellular Localization

In order to confirm that the UV-tolerance deficiency of *Δbcuve1* mutant is due to disruption of the *Bcuve1* gene, wild type *Bcuve1* was tagged with *GFP* at the 3' end and transformed into *Δbcuve1* to produce the complementation mutant strain *Δbcuve1-Bcuve1-GFP*. UV sensitivity assays showed that survival of *Δbcuve1-Bcuve1-GFP* was similar to the WT (Figure 7A). Since the UV-endonuclease is supposed to be involved in DNA damage repair, we determined the subcellular localization patterns of BcUVE1 by tracking the constitutively expressing GFP fusion proteins in the *Δbcuve1-Bcuve1-GFP* strain. As expected, the fused protein BcUVE1-GFP was found in the nuclei (Figure 7B).



Additionally, yeast two hybrid experiments indicated that BcUVE1 and BcPHR1 do not interact with each other (Figure 8), even though BcPHR1 (or named as BcCRY1 earlier) is also localized in nuclei (Cohrs and Schumacher, 2017), and both BcUVE1 and BcPHR1 are involved in UV-damage repair.

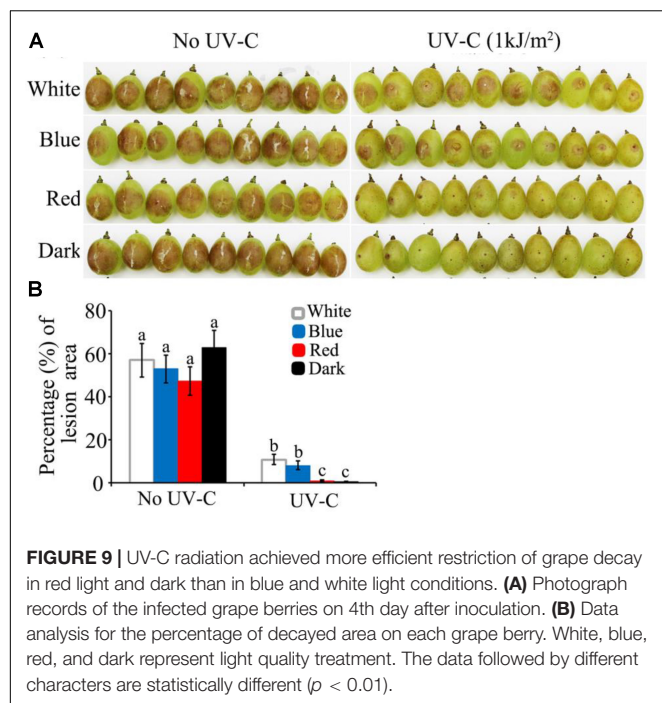


Fungicidal Efficiency of UV-C on Fruits Is Enhanced in Red Light and Dark Conditions but Not in Blue or White Light Conditions

The above study demonstrated that *B. cinerea* is more susceptible to UV-C stress in dark and red light than in blue and white light. These findings enabled us to make an association between the process of light-regulated UV damage repair mechanism and UV-C application for plant disease control, especially at the postharvest stage. The present assay indicated that artificial inoculation of wild type *B. cinerea* spores on grape berries would fail to cause decay symptoms if the UV-C (1 kJ/m²) treatment was followed by dark or red light (Figure 9). In contrast, exposure to blue and white light caused the UV-C treated samples to finally develop typical soft decay (Figure 9). Consequently, the *in vitro* and *in vivo* assays suggest that more satisfactory results of UV-C application for postharvest disease management can be expected if the UV-C damage repair activities of the fungal pathogens are suppressed.

Visible Light Qualities Show Similar Effects on UV-C Sensitivity of Common Postharvest Fungal Pathogens

The regulatory mechanisms of UV-C resistance uncovered here are expected to be valid even in other pathogenic fungi. In this study, we additionally tested the UV-C sensitivity of other important postharvest fungal pathogens: *Alternaria alternata*,



Penicillium digitatum, and *Colletotrichum gloeosporioides*. The results suggest that all of the fungi tested were killed much more easily by relatively lower dosages (less than 1 kJ/m^2) of UV-C in red light and dark conditions, while the spores exposed to blue and white light could survive from higher UV-C dosages (Figure 10).

DISCUSSION

Spoilage decay due to contamination by pathogenic fungi is one of the main causes of abundant postharvest losses of fresh fruits and vegetables. UV-C is an alternative to fungicides for control of postharvest diseases, due to its dual roles of inducing defense in plants and causing surface disinfection of the pathogenic microbes. Induced resistance to postharvest pathogens by UV-C was shown in a wide range of crops (Ben-Yehoshua et al., 1992; Mercier et al., 1993; Charles et al., 2008a,b). However, decontamination of the fruit surface by UV-C could still be interesting from a practical standpoint, as the irradiated tissues would be subject to less inoculum pressure in addition to being more disease resistant. Thus, the present work has been focused on the pathogen rather than the host.

From an evolutionary perspective, the presence of light may signal the upcoming threat of genotoxic ultraviolet radiation to microbes in the natural environment and thus activate UV-damage repair activities (Fuller et al., 2015). Therefore, our study attempted to address the knowledge gap of light-regulation mechanisms of UV-C tolerance in phytopathogenic fungi, and lay the foundation to optimize UV-C treatment parameters for better disinfection efficiency on fresh crop surfaces.

Through quantitative UV-C sensitivity assays with the model species *B. cinerea*, we found that the spores of this fungus incubated in red light and dark are more sensitive to UV-C than those incubated in white and blue light conditions. This phenomenon implies that the blue light spectrum is capable of inducing UV-C resistance in *B. cinerea*. Since the WCC proteins are known to be conserved blue light receptors in the fungal kingdom, we further investigated the role of the key component of the WCC, BcWCL1 of *B. cinerea*, in UV-C resistance. A *Bcwl1* deletion mutant showed substantially reduced UV-C resistance under any light conditions, confirming that the blue light receptor system of *B. cinerea* indeed regulates UV-C resistance. This is in accordance with the reports that WC-1 homologs are pivotal for environmental UV stress tolerance in several other fungal species (Idnurm and Heitman, 2005; Ruiz-Roldan et al., 2008; Kim et al., 2014).

The photoreceptor WCC can serve both signal input (LOV domain) and output (Zn-finger transcription factor domain) functions. Photo induction of DNA repair enzymes represents one of the downstream signaling targets of WCC (Fuller et al., 2015). Photoreactivating enzymes such as photolyases are induced by light via WCC homologues in the ascomycetes *Neurospora crassa*, *Aspergillus fumigatus* (Fuller et al., 2013), *Aspergillus nidulans* (Ruger-Herreros et al., 2011), *Fusarium oxysporum*, (Ruiz-Roldan et al., 2008) and *Cercospora zeae-maydis* (Bluhm and Dunkle, 2008; Kim et al., 2011), as well in as the basidiomycete *Ustilago maydis* (Brych et al., 2016). In these fungi, photolyases are recognized as the major enzymes responsible for UV damage repair. Visible light likely plays dual roles in enhancing photolyase-dependent UV resistance in fungi, one being the induction of expression of photolyase genes via WCC signaling, while the other being energy provision to support photoreactivation activity of the photolyases (Fuller et al., 2015). In *B. cinerea*, there are two cryptochrome/photolyase homologs, BcCRY1 and BcCRY2, but only BcCRY1 was found to act as the major photolyase in photoprotection (Cohrs and Schumacher, 2017), which we therefore re-named as BcPHR1. We confirmed that the expression of *Bcphr1* was induced by white and blue light in a *Bcwl1*-dependent manner, and the deletion mutant $\Delta bcphr1$ showed increased UV-sensitivity when compared with WT as measured by quantitative spore survivability assay. However, $\Delta bcphr1$ was found to be relatively more resistant to UV-C than $\Delta bcwl1$, implying that *Bcphr1* is not the only member of the WCC downstream targets responsible for UV-damage repair.

Actually, as shown in the light-induced transcriptome data (Schumacher et al., 2014), *Bcuve1* represents another candidate for repairing UV-induced damages. This gene encodes a protein that is homologous to UVDE in fission yeast *Schizosaccharomyces pombe*, in which UVDE is essential for excision repair of UV induced DNA damage (Bowman et al., 1994; Freyer et al., 1995; Yajima et al., 1995). Additionally, Uve1, the UVDE homolog in the basidiomycetes *C. neoformans*, is a direct target of WCC signaling and required for UV resistance (Verma and Idnurm, 2013). As shown in our study, expression of *Bcuve1* is also enhanced by blue and white light in a *Bcwl1*-dependent manner, and the deletion mutant $\Delta bcuve1$ is more sensitive to UV-C

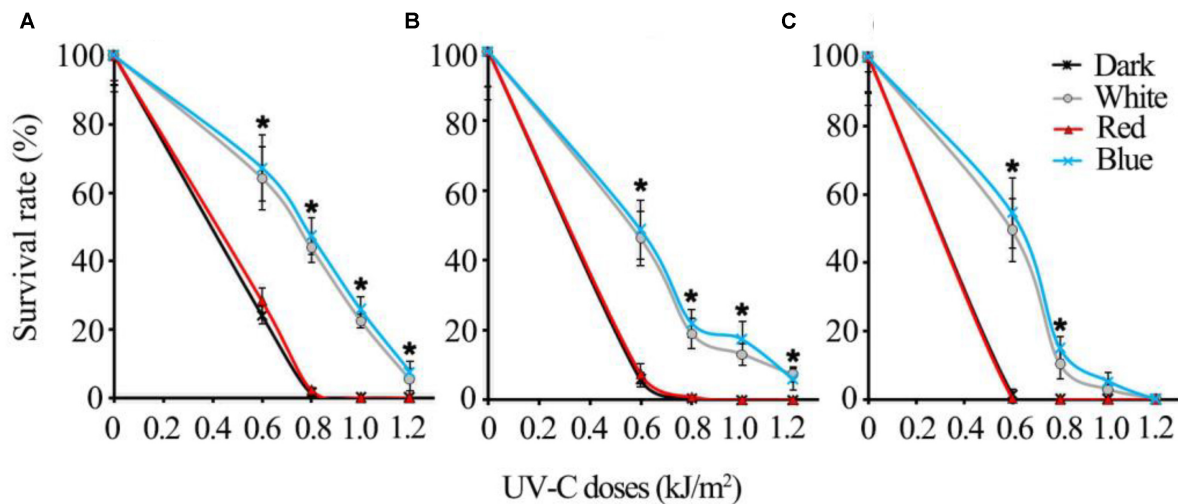


FIGURE 10 | The UV-C sensitivity of three common postharvest fungal pathogens is regulated similarly by different visible light qualities **(A)** *Alternaria alternata*; **(B)** *Penicillium digitatum*; **(C)** *Colletotrichum gloeosporioides*. Asterisks (*) indicate that survival of spores illuminated by blue and white light after UV-C stress was significantly higher than those treated by red light and dark ($P < 0.01$). Error bars represent SD and $n = 5$.

than WT. However, white and blue light still moderately elevated survival rate of $\Delta bcu1$ spores after UV-C treatment, which is most probably due to the presence of functional *Bcphr1* in this mutant. This hypothesis was confirmed by analysis of the double mutant $\Delta \Delta bcu1/bcphr1$, which showed almost similar deficiency of UV-C tolerance as the $\Delta bcw1$ mutant to any kind of light conditions. Taken together, WCC mediated blue light signaling in *B. cinerea* can activate both UV-endonuclease and photolyase to synergistically repair damages caused by UV-C radiation.

The major damage caused by UV-C to organisms is DNA lesions. Thus, subcellular localization of each DNA damage repair enzyme is indicative of its functional preference on either the nuclear or cytoplasmic (the mitochondrion) genomes. BcCRY1 (or BcPHR1 in this paper) was shown to solely localize in the nuclei (Cohrs and Schumacher, 2017). Interestingly, this study found that the UV-endonuclease BcUVE1 also accumulated in the nuclei as shown by analysis of the GFP tagged allele. Thus, these two DNA damage repairing enzymes are regulated by blue light signaling in *B. cinerea*, and are presumably responsible for removing UV-induced lesions in the nuclear genome. However, yeast-two-hybrid assays demonstrated that BcPHR1 and BcUVE1 did not interact with each other, further implying that these two enzymes mediated two independent DNA repair pathways. In addition, the spores of the $\Delta bcu1$ strain were more sensitive to UV-C than those of $\Delta bcphr1$. This phenotype could possibly be explained by the different DNA damage precursors they repair. It is well known that the major DNA lesions induced by UV-C are cyclobutane pyrimidine dimers (CPD) (Watanabe et al., 2006), and other minor lesions are pyrimidine pyrimidone photoproducts (6-4PP) and some diverse rare DNA photoproducts (Stapleton, 1992). BcPHR1 (or BcCRY1) is phylogenetically recognized as belonging to the CPD photolyase group (Cohrs and Schumacher, 2017), and therefore

its target precursors may be limited to CPD lesions. On the other hand, UV-endonuclease was originally discovered in *S. pombe* to be able to recognize both CPD and 6-4PP and initiate their excision repair (Bowman et al., 1994; Freyer et al., 1995; Yajima et al., 1995), even though CPD and 6-4PP differ significantly with respect to the structural distortions that they induce in the DNA duplex. The homolog of UV-endonuclease in *B. cinerea*, BcUVE1, is probably more versatile than the photolyase BcPHR1 in its DNA damage repair capability.

White collar complex of *B. cinerea* were found to be involved in tolerance to ROS (Canessa et al., 2013), which can also cause DNA damage and affect virulence. However, the test of sensitivity against hydrogen peroxide demonstrated that neither *Bcu1* nor *Bcphr1* was involved in detoxification of ROS stress. Besides, the deletion mutants did not show any notable defects in vegetative growth, sporulation, sclerotial formation, or virulence, suggesting that BcUVE1 and BcPHR1 specifically cope with UV stress in *B. cinerea*.

As discussed earlier, UV-C could be used as a potential agent for sanitization of fresh fruit and vegetable surfaces (Nigro et al., 1998). However, the efficacy of UV-C is dependent on the resistance of target microorganisms against UV-C light (Syamaladevi et al., 2013). Based on our study, it can be deduced that the germicidal effect of UV-C on fungal pathogens can be attenuated by exposure to visible light, especially the blue light spectrum, largely due to induction of DNA damage repair enzymes (BcUVE1 and BcPHR1) by light. So, these findings may theoretically verify the rationality of an earlier practical study reporting that dark period following UV-C treatment enhances killing of *Botrytis cinerea* conidia and controls gray mold of strawberries better in green houses (Janisiewicz et al., 2016). Furthermore, we expanded this photosensitive enhancement of UV-C disinfection into postharvest disease management. Consequently, UV-C application for postharvest

disease management can be more effective if the UV-C damage repair activities of the fungal pathogens are suppressed by either dark or red light conditions. Additionally, the UV-C sensitivities of several common fungal pathogens behaved similarly under different light conditions. These phenomena can be explained by the fact that the WCC homologs are widely conserved blue light receptors in the fungal kingdom (Fuller et al., 2015), with the UV damage repair systems being one of their common regulation targets (Idnurm and Heitman, 2005; Verma and Idnurm, 2013; Schumacher et al., 2014; Wu et al., 2014; Brych et al., 2016). As a result, common postharvest pathogenic fungi can be efficiently killed by relatively less amounts of UV-C by following the principles stated in this study. Based on the phenomena and their underlying mechanisms discovered in this study, a shelf device equipped with UV-C inside and a red monochromatic filter on the screen is proposed to be beneficial for better disease management of fresh postharvest crops (**Supplementary Figure S2**).

Although UV-C is directly germicidal to microbial agents of postharvest diseases, its application for conservation purpose of fresh fruit and vegetables is also largely influenced by its effect on physiological modifications of the commodities. The possibility of injuries to crops by higher UV-C doses could even cause an increase in the susceptibility of fruits to postharvest decays (Stevens et al., 1996). We achieved enhancement of UV-C disinfection efficiency on the pathogen with limited dosages that are significantly less than those being commonly used to irradiate fresh crops. Subsequently, future efforts should be focused on selecting proper UV-C parameters to obtain beneficial effects without causing detrimental changes on quality attributes.

AUTHOR CONTRIBUTIONS

PZ and LX designed the experiments. QL, SA, YQ, YW, and PZ performed the experiments. QL, SA, YQ, PZ, YJ, and LX analyzed

and interpreted the data. QL, SA, PZ, and LX wrote the paper with insight from all the authors.

FUNDING

This work was financially supported by the grant of National Key Research and Development Program of China (2016YFD0400105), National Natural Science Foundation of China (Nos. 31571902 and 31501536), and Science and Technology Commission of Shanghai Municipality (15YF1403300).

SUPPLEMENTARY MATERIAL

The Supplementary Material for this article can be found online at: <https://www.frontiersin.org/articles/10.3389/fmicb.2018.01141/full#supplementary-material>

FIGURE S1 | Strategies for deletion of *Bcuve1* and *Bcphr1*. **(A)** Schematic illustration of the homologous recombination strategy to replace the 5' end of the target gene with hygromycin B (*hph*) or nourseothricin (*Nat*) resistance cassette as selective markers. **(B)** Diagnostic PCR analysis for integration of the replacement fragment with genomic DNA. As demonstrated in **(A)**, primer pairs P_{TF} - P_{TR} and P_{MF} - P_{MR} were used to test the presence or absence of target genes (*Bcuve1* or *Bcphr1*) and selection markers (*hph* or *Nat*), respectively; the primer pairs P_{T5F} - $P_{MR'}$ and $P_{MF'}$ - P_{T3R} were used to verify the correctness of integration sites at the 5'-UTR and 3'-UTR regions respectively. **(C)** Southern blot analysis of the WT, $\Delta bcuve1$ and $\Delta bcphr1$ strains. Genomic DNAs were digested with *HindIII*; the probes targeting the selection markers are indicated in **(A)**. A single band of expected size in each mutant verified authentic homologous recombination events, and ruled out the possibility of multicopy insertion of the selection markers. **(D)** Reverse transcript-PCR confirmed the absence of expression of *Bcuve1* and *Bcphr1* in the respective mutants. The constitutively expressed gene β -tubulin was used as a reference.

FIGURE S2 | Shelf device equipped with UV-C inside and a monochromatic filter on the screen for fresh crop preservation and display.

TABLE S1 | Primers used in this study.

REFERENCES

- Allende, A., and Artés, F. (2003). UV-C radiation as a novel technique for keeping quality of fresh processed 'Lollo Rosso' lettuce. *Food Res. Int.* 36, 739–746. doi: 10.1016/S0963-9969(03)00054-1
- Ballario, P., Vittorioso, P., Magrelli, A., Talora, C., Cabibbo, A., and Macino, G. (1996). White collar-1, a central regulator of blue light responses in *Neurospora*, is a zinc finger protein. *EMBO J.* 15, 1650–1657.
- Ben-Yehoshua, S., Rodov, V., Kim, J. J., and Carmeli, S. (1992). Preformed and induced antifungal materials of citrus fruits in relation to the enhancement of decay resistance by heat and ultraviolet treatments. *J. Agr. Food Chem.* 40, 1217–1221. doi: 10.1021/jf00019a029
- Bintsis, T., Litopoulou-Tzanetaki, E., and Robinson, R. K. (2000). Existing and potential applications of ultraviolet light in the food industry – a critical review. *J. Sci. Food Agr.* 80, 637–645. doi: 10.1002/(SICI)1097-0010(20000501)80:6
- Bluhm, B. H., and Dunkle, L. D. (2008). *PHL1* of *Cercospora zaeae-maydis* encodes a member of the photolyase/cryptochrome family involved in UV protection and fungal development. *Fungal Genet. Biol.* 45, 1364–1372. doi: 10.1016/j.fgb.2008.07.005
- Bowman, K. K., Sidik, K., Smith, C. A., Taylor, J. S., Doetsch, P. W., and Freyer, G. A. (1994). A new ATP-independent DNA endonuclease from *Schizosaccharomyces pombe* that recognizes cyclobutane pyrimidine dimers and 6-4 photoproducts. *Nucleic Acids Res.* 22, 3026–3032. doi: 10.1093/nar/22.15.3026
- Brettel, K., and Byrdin, M. (2010). Reaction mechanisms of DNA photolyase. *Curr. Opin. Struct. Biol.* 20, 693–701. doi: 10.1016/j.sbi.2010.07.003
- Brych, A., Mascarenhas, J., Jaeger, E., Charkiewicz, E., Pokorný, R., Bolker, M., et al. (2016). White collar 1-induced photolyase expression contributes to UV-tolerance of *Ustilago maydis*. *Microbiologyopen* 5, 224–243. doi: 10.1002/mbo3.322
- Canessa, P., Schumacher, J., Hevia, M. A., Tudzynski, P., and Larrondo, L. F. (2013). Assessing the effects of light on differentiation and virulence of the plant pathogen *Botrytis cinerea*: characterization of the White Collar Complex. *PLoS One* 8:e84223. doi: 10.1371/journal.pone.0084223
- Charles, M. T., Goulet, A., and Arul, J. (2008a). Physiological basis of UV-C induced resistance to *Botrytis cinerea* in tomato fruit: IV. Biochemical modification of structural barriers. *Postharvest Biol. Tec.* 47, 41–53. doi: 10.1016/j.postharvbio.2007.05.019
- Charles, M. T., Mercier, J., Makhoul, J., and Arul, J. (2008b). Physiological basis of UV-C-induced resistance to *Botrytis cinerea* in tomato fruit: I. Role of pre- and post-challenge accumulation of the phytoalexin-rishitin. *Postharvest Biol. Tec.* 47, 10–20. doi: 10.1016/j.postharvbio.2007.05.013
- Chung, K. R., and Lee, M. H. (2015). "Split-marker-mediated transformation and targeted gene disruption in filamentous fungi," in *Genetic Transformation*

- Systems in Fungi, Fungal Biology*, Vol. 2, eds M. van den Berg, and K. Maruthachalam (Cham: Springer).
- Cohrs, K. C., and Schumacher, J. (2017). The two cryptochrome/photolyase family proteins fulfill distinct roles in DNA photorepair and regulation of conidiation in the gray mold fungus *Botrytis cinerea*. *Appl. Environ. Microb.* 83, e812–e817. doi: 10.1128/AEM.00812-17
- Costa, L., Vicente, A. R., Civello, P. M., Chaves, A. R., and Martínez, G. A. (2006). UV-C treatment delays postharvest senescence in broccoli florets. *Postharvest Biol. Tec.* 39, 204–210. doi: 10.1016/j.postharvbio.2005.10.012
- Crosthwaite, S. K., Dunlap, J. C., and Loros, J. J. (1997). *Neurospora wc-1* and *wc-2*: transcription, photoresponses, and the origins of circadian rhythmicity. *Science* 276, 763–769. doi: 10.1126/science.276.5313.763
- Fillinger, S., and Elad, Y. (2016). *Botrytis – the Fungus, the Pathogen and its Management in Agricultural Systems*. New York, NY: Springer International Publishing. doi: 10.1007/978-3-319-23371-0
- Freyer, G. A., Davey, S., Ferrer, J. V., Martin, A. M., Beach, D., and Doetsch, P. W. (1995). An alternative eukaryotic DNA excision repair pathway. *Mol. Cell. Biol.* 15, 4572–4577. doi: 10.1128/MCB.15.8.4572
- Fuller, K. K., Loros, J. J., and Dunlap, J. C. (2015). Fungal photobiology: visible light as a signal for stress, space and time. *Curr. Genet.* 61, 275–288. doi: 10.1007/s00294-014-0451-0
- Fuller, K. K., Ringelberg, C. S., Loros, J. J., and Dunlap, J. C. (2013). The fungal pathogen *Aspergillus fumigatus* regulates growth, metabolism, and stress resistance in response to light. *mBio* 4, e142–e113. doi: 10.1128/mBio.00142-13
- Idnurm, A., and Heitman, J. (2005). Light controls growth and development via a conserved pathway in the fungal kingdom. *PLoS Biol.* 3:e95. doi: 10.1371/journal.pbio.0030095
- Janisiewicz, W. J., Takeda, F., Glenn, D. M., Camp, M. J., and Jurick, W. N. (2016). Dark period following UV-C treatment enhances killing of *Botrytis cinerea* conidia and controls gray mold of strawberries. *Phytopathology* 106, 386–394. doi: 10.1094/PHYTO-09-15-0240-R
- Kim, H., Ridenour, J. B., Dunkle, L. D., and Bluhm, B. H. (2011). Regulation of stomatal tropism and infection by light in *Cercospora zeae-maydis*: evidence for coordinated host/pathogen responses to photoperiod? *PLoS Pathog* 7:e1002113. doi: 10.1371/journal.ppat.1002113
- Kim, H., Son, H., and Lee, Y. W. (2014). Effects of light on secondary metabolism and fungal development of *Fusarium graminearum*. *J. Appl. Microbiol.* 116, 380–389. doi: 10.1111/jam.12381
- Liu, Y., He, Q., and Cheng, P. (2003). Photoreception in *Neurospora*: a tale of two White Collar proteins. *Cell. Mol. Life Sci.* 60, 2131–2138. doi: 10.1007/s00018-003-3109-5
- Livak, K. J., and Schmittgen, T. D. (2001). Analysis of relative gene expression data using real-time quantitative PCR and the 2^{-ΔΔC_T} method. *Methods* 25, 402–408. doi: 10.1006/meth.2001.1262
- Luckey, T. D. (1982). *Hormesis with Ionizing Radiation*. Boca Raton, FL: CRC Press, 222.
- Mercier, J., Arul, J., and Julien, C. (1993). Effect of UV-C on phytoalexin accumulation and resistance to *Botrytis cinerea* in stored carrots. *J. Phytopathol.* 139, 17–25.
- Nigro, F., Ippolito, A., and Lima, G. (1998). Use of UV-C light to reduce *Botrytis* storage rot of table grapes. *Postharvest Biol. Tec.* 13, 171–181. doi: 10.1016/S0925-5214(98)00009-X
- Pombo, M. A., Rosli, H. G., Martínez, G. A., and Civello, P. M. (2011). UV-C treatment affects the expression and activity of defense genes in strawberry fruit (*Fragaria × ananassa* Duch.). *Postharvest Biol. Tec.* 59, 94–102. doi: 10.1016/j.postharvbio.2010.08.003
- Romanazzi, G., Lichter, A., Gabler, F. M., and Smilanick, J. L. (2012). Recent advances on the use of natural and safe alternatives to conventional methods to control postharvest gray mold of table grapes. *Postharvest Biol. Tec.* 63, 141–147. doi: 10.1016/j.postharvbio.2011.06.013
- Romanazzi, G., Smilanick, J. L., Feliziani, E., and Droby, S. (2016). Integrated management of postharvest gray mold on fruit crops. *Postharvest Biol. Tec.* 113, 69–76. doi: 10.1016/j.postharvbio.2015.11.003
- Ruger-Herreros, C., Rodríguez-Romero, J., Fernández-Barranco, R., Olmedo, M., Fischer, R., Corrochano, L. M., et al. (2011). Regulation of conidiation by light in *Aspergillus nidulans*. *Genetics* 188, 809–822. doi: 10.1534/genetics.111.130096
- Ruiz-Roldan, M. C., Garre, V., Guarro, J., Marine, M., and Roncero, M. I. (2008). Role of the white collar 1 photoreceptor in carotenogenesis, UV resistance, hydrophobicity, and virulence of *Fusarium oxysporum*. *Eukaryot. Cell* 7, 1227–1230. doi: 10.1128/EC.00072-08
- Schumacher, J. (2012). Tools for *Botrytis cinerea*: new expression vectors make the gray mold fungus more accessible to cell biology approaches. *Fungal Genet. Biol.* 49, 483–497. doi: 10.1016/j.fgb.2012.03.005
- Schumacher, J., Simon, A., Cohrs, K. C., Viaud, M., and Tudzynski, P. (2014). The transcription factor BcLTF1 regulates virulence and light responses in the necrotrophic plant pathogen *Botrytis cinerea*. *PLoS Genet.* 10:e1004040. doi: 10.1371/journal.pgen.1004040
- Sinha, R. P., and Hader, D. P. (2002). UV-induced DNA damage and repair: a review. *Photochem. Photobiol. Sci.* 1, 225–236. doi: 10.1039/b201230h
- Sperber, W. H., Doyle, M. P., Barth, M., Hankinson, T. R., Zhuang, H., and Breidt, F. (2009). *Microbiological Spoilage of Fruits and Vegetables*. eds W. H. Sperber, and M. P. Doyle (New York: Springer), 135–183.
- Stapleton, A. E. (1992). Ultraviolet radiation and plants: burning questions. *Plant Cell* 4, 1353–1358. doi: 10.1105/tpc.4.11.1353
- Stevens, C., Wilson, C. L., Lu, J. Y., Khan, V. A., Chaltz, E., Droby, S., et al. (1996). Plant hormesis induced by ultraviolet light-C for controlling postharvest diseases of tree fruits. *Crop Prot.* 15, 129–134. doi: 10.1016/0261-2194(95)00082-8
- Syamaladevi, R. M., Lu, X., Sablani, S. S., Insan, S. K., Adhikari, A., Killinger, K., et al. (2013). Inactivation of *Escherichia coli* population on fruit surfaces using Ultraviolet-C light: influence of fruit surface characteristics. *Food Bioprocess Tech.* 6, 2959–2973. doi: 10.1007/s11947-012-0989-0
- Tagua, V. G., Pausch, M., Eckel, M., Gutierrez, G., Miralles-Duran, A., Sanz, C., et al. (2015). Fungal cryptochrome with DNA repair activity reveals an early stage in cryptochrome evolution. *Proc. Natl. Acad. Sci. U.S.A.* 112, 15130–15135. doi: 10.1073/pnas.1514637112
- Topcu, Y., Dogan, A., Kasimoglu, Z., Sahin-Nadeem, H., Polat, E., and Erkan, M. (2015). The effects of UV radiation during the vegetative period on antioxidant compounds and postharvest quality of broccoli (*Brassica oleracea* L.). *Plant Physiol. Bioch.* 93, 56–65. doi: 10.1016/j.plaphy.2015.02.016
- Urban, L., Charles, F., de Miranda, M. R., and Aarrouf, J. (2016). Understanding the physiological effects of UV-C light and exploiting its agronomic potential before and after harvest. *Plant Physiol. Biochem.* 105, 1–11. doi: 10.1016/j.plaphy.2016.04.004
- Verma, S., and Idnurm, A. (2013). The Uve1 endonuclease is regulated by the white collar complex to protect *Cryptococcus neoformans* from UV damage. *PLoS Genet.* 9:e1003769. doi: 10.1371/journal.pgen.1003769
- Vicente, A. R., Pineda, C., Lemoine, L., Civello, P. M., Martínez, G. A., and Chaves, A. R. (2005). UV-C treatments reduce decay, retain quality and alleviate chilling injury in pepper. *Postharvest Biol. Tec.* 35, 69–78. doi: 10.1016/j.postharvbio.2004.06.001
- Wang, C., Wang, G., Zhang, C., Zhu, P., Dai, H., Yu, N., et al. (2017). OsCERK1-mediated chitin perception and immune signaling requires receptor-like cytoplasmic kinase 185 to activate an MAPK cascade in rice. *Mol. Plant* 10, 619–633. doi: 10.1016/j.molp.2017.01.006
- Watanabe, K., Yamada, N., and Takeuchi, Y. (2006). Oxidative DNA damage in cucumber cotyledons irradiated with ultraviolet light. *J. Plant Res.* 119, 239–246. doi: 10.1007/s10265-006-0266-2
- Wu, C., Yang, F., Smith, K. M., Peterson, M., Dekhang, R., Zhang, Y., et al. (2014). Genome-wide characterization of light-regulated genes in *Neurospora crassa*. *G3 (Bethesda)* 4, 1731–1745. doi: 10.1534/g3.114.012617
- Yajima, H., Takao, M., Yasuhira, S., Zhao, J. H., Ishii, C., Inoue, H., et al. (1995). A eukaryotic gene encoding an endonuclease that specifically repairs DNA damaged by ultraviolet light. *EMBO J.* 14, 2393–2399.

Conflict of Interest Statement: The authors declare that the research was conducted in the absence of any commercial or financial relationships that could be construed as a potential conflict of interest.

The reviewer ZZ and handling Editor declared their shared affiliation.

Copyright © 2018 Zhu, Li, Azad, Qi, Wang, Jiang and Xu. This is an open-access article distributed under the terms of the Creative Commons Attribution License (CC BY). The use, distribution or reproduction in other forums is permitted, provided the original author(s) and the copyright owner are credited and that the original publication in this journal is cited, in accordance with accepted academic practice. No use, distribution or reproduction is permitted which does not comply with these terms.



Efficacy and Mechanism of Cinnamon Essential Oil on Inhibition of *Colletotrichum acutatum* Isolated From 'Hongyang' Kiwifruit

Jingliu He¹, Dingtao Wu¹, Qing Zhang¹, Hong Chen¹, Hongyi Li¹, Qiaohong Han¹, Xingyue Lai¹, Hong Wang¹, Yingxue Wu¹, Jiagen Yuan¹, Hongming Dong² and Wen Qin^{1*}

¹ Sichuan Key Laboratory of Fruit and Vegetable Postharvest Physiology, College of Food Science, Sichuan Agricultural University, Ya'an, China, ² Faculty of Agricultural, Life & Environmental Sciences, University of Alberta, Edmonton, AB, Canada

OPEN ACCESS

Edited by:

Nengguo Tao,
Xiangtan University, China

Reviewed by:

Birinchi Kumar Sarma,
Banaras Hindu University, India
Balasubramanian Natesan,
Universidade Nova de Lisboa,
Portugal

*Correspondence:

Wen Qin
qinwen@sicau.edu.cn

Specialty section:

This article was submitted to
Food Microbiology,
a section of the journal
Frontiers in Microbiology

Received: 01 February 2018

Accepted: 28 May 2018

Published: 18 June 2018

Citation:

He J, Wu D, Zhang Q, Chen H, Li H,
Han Q, Lai X, Wang H, Wu Y, Yuan J,
Dong H and Qin W (2018) Efficacy
and Mechanism of Cinnamon
Essential Oil on Inhibition
of *Colletotrichum acutatum* Isolated
From 'Hongyang' Kiwifruit.
Front. Microbiol. 9:1288.
doi: 10.3389/fmicb.2018.01288

In this study, one of the dominant pathogens, which caused postharvest diseases such as anthracnose, was isolated from decayed 'Hongyang' kiwifruit. It was identified as *Colletotrichum acutatum* by its morphological characteristics and standard internal transcribed spacer ribosomal DNA sequence. Further, the efficacy and possible mechanism of cinnamon essential oil on inhibition of *C. acutatum* were investigated. Results showed that *C. acutatum* was dose-dependently inhibited by cinnamon essential oil. Meanwhile, the mycelial growth and spore germination of *C. acutatum* were completely inhibited at the concentrations of 0.200 $\mu\text{L/mL}$ and 0.175 $\mu\text{L/mL}$ (v/v), respectively. Indeed, both minimal inhibitory and minimum fungicidal concentrations of cinnamon essential oil were measured as 0.200 $\mu\text{L/mL}$. Additionally, the possible antifungal mechanism of cinnamon essential oil on *C. acutatum* was demonstrated. Results showed that the cinnamon essential oil could destroy the cell membrane integrity of *C. acutatum*, and the structure of cell membrane was changed. Indeed, the cell cytoplasm including soluble protein, sugar, and nucleic acid was released, which significantly changed the extracellular conductivity. Results suggested that the cinnamon essential oil exerted great potential to be used as a natural and efficient preservative for kiwifruit postharvest storage, which were helpful for the better understanding of the efficacy and mechanism of cinnamon essential oil on inhibition of pathogens isolated from decayed 'Hongyang' kiwifruit.

Keywords: kiwifruit, *Colletotrichum acutatum*, pathogens, cinnamon essential oil, antifungal mechanism

INTRODUCTION

'Hongyang' kiwifruit (*Actinidia chinensis*) is the first international red-fleshed cultivar in Sichuan of China. Due to its unique flavor and abundant nutrients, such as high levels of vitamin C, anthocyanins, dietary fiber, and amino acids, 'Hongyang' kiwifruit has interested consumers (Lin et al., 2017). China is the leading kiwifruit producing country, and the average level of production topped the list in 2013–2016 (44.5% of the world production). Kiwifruit is infected by different fungi associated with fruit diseases. For instance, gray mold, caused by *Botrytis cinerea*, is one the important postharvest diseases of kiwifruit (Williamson et al., 2007); Blue mold, caused by *Penicillium expansum*, can also cause decay in harvested kiwifruit, although it is not as prevalent as gray mold (Neri et al., 2010). Especially, the anthracnose of kiwifruit is severe, which can infect

leaves, canes, and fruits, resulting in significantly economic losses during storage. However, at present, relevant studies on anthracnose of kiwifruit have seldom been reported.

The use of chemically synthetic preservative in controlling food spoilage and pathogenic fungus has been a controversial topic (Tian et al., 2014). The artificially chemical compounds are considered as chronic and reproductive toxicants causing respiratory diseases or other health risks (Fleming-Jones and Smith, 2003). In this case, natural preservatives such as essential oil (EO) have been extensively used due to its biodegradable and antimicrobial properties. EO contains a variety of substances called 'phytochemicals', which belong to natural components in plants (Pratt, 1992). The phytochemical preparations with dual functionalities in preventing lipid oxidation and antimicrobial properties have tremendous potential for extending shelf life of food products (Singh et al., 2007; Fadli et al., 2012). Generally, EO possesses high volatility. When EO is applied as a vapor, less oil is used. Further, the residues of EO on the product are minimized, and there will be less of a problem with tainting (Szczerbanik et al., 2007). It may be more appropriate to use EO in their vapor phase for postharvest applications (Concha et al., 1998; Zollo et al., 1998). Cinnamon (*Cinnamomum zeylanicum* or *Cinnamomum verum*), rich in EO, belongs to Lauraceae family comprising about 250 species and usually distributes in India, China, Sri Lanka, and Australia (Prasad et al., 2009). Cinnamon essential oil (CEO) is a promising food preservative for the inhibition of foodborne pathogens and spoilage microorganisms (Tian et al., 2012). Our previous studies have shown that CEO have good efficacy on preservation of 'Hongyang' kiwifruit. Moreover, 'Hongyang' kiwifruit fumigated with 0.4 $\mu\text{L/mL}$ of CEO could be stored at $(4 \pm 1)^\circ\text{C}$ with relative humidity of 90–95% for 120 days (He et al., 2015). CEO has been demonstrated as a strong and broad range of inhibition for bacteria, fungi and yeast (Chao et al., 2000; Manso et al., 2015). Our previous studies have demonstrated that CEO have good inhibitory effects against *Botryosphaeria parva* *in vitro*, and can reduce soft rot on 'Hongyang' kiwifruit *in vivo* (He et al., 2015). Antifungal activity of CEO against *C. acutatum* isolated from strawberry anthracnose was investigated (Duduk et al., 2015). Cell plasma membrane (PM) is the action site invaded by antifungal substances, such as silicon and chlorine dioxide (Wei et al., 2008; Liu et al., 2010). For fungi, the integrity of PM plays a crucial role in maintaining cell constituents being important to viability, such as sugar, protein and nucleic acid. The soluble sugar, soluble protein and nucleic acid are the basic and functional components in the cell. The PM is damaged, and the intracellular components can be leaked (Wei et al., 2008; Kim et al., 2009; Liu et al., 2010). The antifungal activity of EO was strongly associated with its compositions, such as monoterpene phenols, especially thymol, carvacrol, and eugenol (Barrera-Necha et al., 2008). The antifungal mechanism of EO is speculated to induce membrane disruption by their lipophilic compounds (Cowan, 1999). The low-molecular-weight and highly lipophilic components of EO pass easily through cell membranes and cause disruption to the fungal cell organization (Chao et al., 2005; Shukla et al., 2012). Therefore, in this study, the dominant pathogens, which caused postharvest diseases such as anthracnose in 'Hongyang' kiwifruit, was firstly isolated

and identified. Further, the antifungal activity and the possible antifungal mechanism of CEO against *C. acutatum* isolated from decayed 'Hongyang' kiwifruit were investigated.

MATERIALS AND METHODS

Materials and Chemicals

Fresh 'Hongyang' kiwifruits grown in Ya'an country, Sichuan Province, China, were harvested from orchards. The spoiled kiwifruits were utilized for the isolation of pathogens in Sichuan Agricultural University of China. Potato dextrose agar (PDA) (Beijing AoBoXing bio-tech Co. Ltd., Beijing, China) was used as the culture media. The fungal DNA was extracted using a commercial kit (Eppendorf, Holstein City, Germany), following the manufacturer's instructions. Whatman No. 1 filter paper disks (Solarbio, Shanghai, China) were cut ($\varnothing = 5\text{ mm}$) using a hole-puncher. The crude cinnamon essential oil (CEO, Ji'an Guoguang flavor Co. Ltd., Jiangxi, China) was obtained by hydrodistillation from cinnamon bark, and the composition of the CEO used in this study was given in Table 1.

Isolation and Identification of Pathogens

According to the tissue separation method (Jogee et al., 2017), the surface of the spoiled 'Hongyang' kiwifruits was washed with sterile double-distilled water (SDW), and disinfested in 75% ethanol for 30 s and in 1% sodium hypochlorite for 30 s, and then rinsed three times in SDW. Then, pieces of kiwifruit sarcocarp about 4 mm^2 were excised from diseased berries with a sterile scalpel from the marginal area between the diseased and healthy tissue. The pieces were incubated on PDA. After isolation, the purified fungi were cultivated on PDA. After incubation at 25°C for 7 days, colonial morphology including micromorphological features, viz., color of colony on both of dorsal and ventral sides, growth diameter and texture of colony, and some microscopic features like mycelial size and conidial shape were measured. The isolated pathogen was assayed its pathogenicity in 'Hongyang' kiwifruit. Further, the pathogen was isolated again from diseased kiwifruits using the above tissue separation method. Finally, the pathogen was subcultivated on PDA and stored at 4°C for consequent identification. The isolated pathogen was coded as WQ1. The pathogen was deposited in Agricultural Culture Collection of China, and the accession number was ACCC 39342.

TABLE 1 | Chemical compositions of CEO.

No.	Components	RT (S)	RI	PA (%)
1	Benzaldehyde	6.998	750	2.68 ± 0.04
2	<i>trans</i> -Cinnamaldehyde	15.945	1567	86.16 ± 0.10
3	<i>trans</i> -Cinnamic acid	20.829	1093	6.75 ± 0.12
4	Others non-identified			<5.00

Phytochemical analysis was conducted by using GC-MS, and data were the mean ($\pm\text{SD}$) of three independent analysis. RT, Retention time; RI, Linear retention index to *n*-alkane C8 - C40 on silica capillary column; % PA, Percentages of the relative areas (%), the data were obtained from the integration of the peaks identified in the spectra by a selective mass detector.

The isolate was grown on potato dextrose broth (PDB) with 140 r/min at 25°C for 5 days. The genomic DNA of mycelia was extracted by kit (Eppendorf, Holstein City, Germany). The internal transcribed spacer (ITS) regions and the small subunit (ITS1-5.8S-ITS2) of the rDNA genes were amplified using the primer set ITS1 (5'-TCCGTAGGTGAACCTGCGG-3') and ITS4 (5'-TCCTCCGCTTATTGATATGC-3') (Zhao et al., 2010). Primers were synthesized by Shanghai Sangon Biological Engineering Technology & Services Co., Ltd (Shanghai, China). PCR amplification was carried out in aqueous volumes of 25 µL. The reactions contained 0.5 µL template DNA (30 ng), 0.5 µL (10 µmol/L) of each primer, 5 × PCR buffer (with MgCl₂) 2.5 µL, 0.5 µL dNTP (2.5 mmol/L), 0.5 µL Taq polymerase (2.5 U/µL) and 20 µL ddH₂O. PCR reactions were performed on a ABI 2720 thermal cycler (Applied Biosystems, Foster City, CA, United States). Thermal cycling was carried out using an initial denaturation step at 98°C for 3 min, followed by 30 cycles of denaturation at 98°C for 25 s, annealing at 55°C for 25 s and extension at 72°C for 60 s. Cycling was completed by a final elongation step at 72°C for 10 min. PCR products were purified using PCR purification kit (Shanghai Sangon Biological Engineering Technology & Services Co., Ltd, Shanghai, China). Sequencing was performed with an ABI 3730XL automated sequencer (Applied Biosystems, Foster City, CA, United States). Further, the sequence was analyzed and determined to search for similar sequences from the Basic Local Alignment Search Tool (BLAST) software¹ algorithm at National Center for Biotechnology Information (NCBI). To construct the relevant phylogenetic tree, MEGA 5.02 software was employed (Saitou and Nei, 1987; Tamura et al., 2007).

Analysis of Antifungal Activity of Cinnamon Essential Oil Against Mycelial Growth and Spore Germination

The inhibitory effect of CEO on mycelial growth was determined using filter paper method with minor modifications (Liu et al., 2010). Briefly, the mycelia disks (Ø = 5 mm) of *C. acutatum*, cut from the edge of 7 days actively growing cultures on PDA, were placed upside down on the center of the inner side of the plate lid with 20 mL of PDA. The sterile filter paper (Ø = 5 mm) was added with different amounts of CEO (4.5, 6.0, 7.5, 9.0, 10.5, 12.0, and 13.5 µL). The filter paper containing CEO were placed on the center of the bottom of the petri dishes to obtain final concentrations of 0.075, 0.100, 0.125, 0.150, 0.175, 0.200, and 0.225 µL/mL of air (v/v). PDA plates without CEO were used as negative controls. Each plate was sealed with Parafilm® (Top Group Co. Ltd., Chengdu, China) to prevent leakage of CEO vapor and incubated in the dark at 25°C until the growth in the control plates (without treatment) reached the edge of the plates. The plates were incubated in inverted position. Each treatment was replicated thrice and the experiment was repeated thrice. The inhibition radius around the oil disk (colony-free perimeter) was measured using a digital vernier caliper (Mitutoyo, Kawasaki, Japan). Mycelia growth (cm) was recorded and the percentage

inhibition (PI) was determined after comparison with the control (Pandey et al., 1982; Trabelsi et al., 2016). The minimal inhibitory concentration (MIC) was defined as the lowest concentration of CEO at which the growth of microorganism was inhibited (Rasooli and Abyaneh, 2004). The fungus treated with the MIC of CEO was sub-cultivated on treatment-free PDA at 25°C for 2 days to determine whether the inhibition was reversible. The minimal fungicidal concentration (MFC) was regarded as the lowest concentration in which the growth of any fungal colony was prevented on PDA (Irobi and Daramola, 1993).

$$PI(\%) = (dc - dt)/dc \times 100$$

where dt is the average diameter of colony after treatment by CEO, and dc is the average diameter of colony used for control.

The inhibitory effect of CEO on spore germination and germ tube elongation of *C. acutatum* was determined using a vapor contact method proposed from previous study with minor modifications (Liu et al., 2007). To stimulate sporulation, *C. acutatum* was grown on PDA in the dark at 25°C. Spores were harvested from 7 days old cultures with 10 mL of SDW and softly scraping the colonies with a sterile L-shaped glass rod. Spore suspension was filtered through sterile paper to remove mycelial fragments. Hundred microliter of spore suspension of 10⁸ CFU/mL was plated on the inner side of petri dishes (Ø = 90 mm) with 20 mL of PDA. The same CEO concentrations used in the mycelial growth assay were examined. Each plate was incubated in the dark at 25°C for 1 days. In the end, germinal spores were observed using a light microscope (Olympus CX 31, Olympus Co., Tokyo, Japan) at 400× magnification. Each slide was fixed in lactophenol cotton blue. Results were expressed in terms of the percentage of spore germination inhibition by comparing control and treated plates (Trabelsi et al., 2016; Ribes et al., 2017).

$$\text{Spore germination inhibition (\%)} = (sc - st)/sc \times 100$$

where sc and st are the average numbers of spores germinated in control plates and treated plates, respectively.

Observations of Fungal Morphology and Ultrastructure

The action mechanism of CEO was determined using transmission electron microscopy (TEM) according to a previous study with minor modifications (Bozzola and Russell, 1999). Seven-day-old *C. acutatum* exposed to 0, MFC and 2MFC of CEO were cultivated in the dark at 25°C for 2 days. The mycelia was harvested from PDA with 10 mL of SDW and softly scraping the colonies with a sterile L-shaped glass rod. The mycelium suspension was centrifuged at 7000 g for 15 min to obtain mycelia. The small segments measuring 5 × 5 mm were excised at the margin of the mycelium colony. Then, the segments were promptly placed in vials containing 2.5% glutaraldehyde in 0.1 mol/L phosphate buffer saline (PBS) (pH 7.2) at 4°C and fixed overnight. The fixed samples were rinsed with the same buffer three times for 10 min. Afterward, the

¹<http://blast.ncbi.nlm.nih.gov>

samples were dehydrated in a graded series of ethanol (70, 80, 90, 95, and 100%, v/v) for 20 min in each alcohol dilution. The last step was performed for 30 min thrice. The dehydrated specimens were then embedded and polymerized in Spurr's resin at 65°C for 72 h. Ultrathin sections (approximately 50 nm in thickness) were hand trimmed with a diamond knife using an MT-X Ultratome for TEM observations (H-600, Hitachi Co. Ltd., Tokyo, Japan).

Membrane integrity was determined using fluorescent microscope (FSM) according to a previous study with minor modifications (Liu et al., 2010). *C. acutatum* was treated with the MFC of CEO as described previously. PDA plates without CEO were served as negative controls. Mycelia were collected after incubation for 0, 1, 2, 3, 4, 5, and 6 days in the dark at 25°C, and washed with cold PBS (0.05 mol/L, pH 7.0) to remove residual medium, respectively. Mycelia were then fixed by cold ethanol (70%, v/v) at 4°C for 1 h. After removal of ethanol, and the mycelia were washed twice with PBS. Then the mycelia were stained with 50 µg/mL propidium iodide for 20 min at 4°C in the dark. Mycelia were collected by centrifugation (4000 × g for 10 min), and washed twice with PBS to remove residual dye. Samples were observed with the E200 Nikon Eclipse microscope (Nikon Co., Tokyo, Japan). Fields of view from each cover slip were chosen randomly, and each treatment was replicated thrice and the experiment was repeated thrice. The number of spores in bright-field was defined as the total number, and membrane integrity (MI) was calculated as:

$$\text{MI (\%)} = \left[1 - \left(\frac{\text{number of stained spores}}{\text{number of total spores}} \right) \right] \times 100$$

Effects of Cinnamon Essential Oil on Ergosterol Content in Plasma Membrane

The ergosterol content was determined using a previously described method with minor modifications (Tian et al., 2012). The same treatment used in the mycelial growth assay was examined. After incubation, mycelia were harvested and washed with 10 mL of SDW. A 5 mL of mixed solution (20 mL of methanol, 5 mL of ethanol and 2.0 g of potassium hydroxide) was added to each sample. After 2 min of vortex using TS-1 Eddy oscillator (Kylin-Bell Lab Instruments Co., Ltd., Shanghai, China), the mixed solution was incubated at 85°C for 4 h. Sterols were extracted from each sample by adding a mixture of 2 mL of SDW and 5 mL of *n*-heptane. Then, the mixture was sufficiently mixed by vortex for 2 min allowing the layers to separate for 1 h at room temperature. The *n*-heptane layer was analyzed by UV-1800 PC spectrophotometer at 230 and 282 nm (Shanghai AoXi Science Instrument Co. Ltd, Shanghai, China). The presence of ergosterol (at 282 nm) and the sterol intermediate 24(28) dehydroergosterol (at 230 nm) in the *n*-heptane layer led to a characteristic curve. The content of ergosterol was calculated as a percentage of the wet weight based on the absorbance and wet weight of the initial pellet. It was calculated as the follow equation,

$$\% \text{ ergosterol} = \frac{\frac{A_{282}}{290}}{\text{wet weight}} - \frac{\frac{A_{230}}{518}}{\text{wet weight}}$$

where 290 and 518 are the *E* values (in percentages per cm) determined for crystalline ergosterol and 24(28) dehydroergosterol, respectively.

Effects of Cinnamon Essential Oil on Intracellular Protein, Sugar, and Nucleic Acid Leakage

The effects of CEO on intracellular leakage were determined using a extracellular conductivity method with minor modifications (Tao et al., 2014). Initially, the mycelia disks (Ø = 5 mm) were placed upside down on the center of Petri dishes with 20 mL of PDA and incubated in the dark at 25°C until the growth reached the edge of the plates. Then, the sterile filter paper was added with the MFC of CEO, and PDA plates without CEO were served as negative controls. Mycelia were collected after incubation for 0, 1, 2, 3, 4, 5, and 6 days in the dark at 25°C, and washed with 15 mL of SDW. The supernatants were collected after centrifugation. The extracellular conductivity at each time point was carried out using a DDS-11A conductivity meter (Shanghai Precision Scientific Instrument Co. Ltd, Shanghai, China) and expressed as µS/cm. Each treatment was replicated thrice and the experiment was repeated thrice.

The intracellular protein, sugar and nucleic acid leakage of mycelia were determined by a spectrophotometry method with minor modification (Fleissner and Glass, 2007). Briefly, *C. acutatum* was treated with the MFC of CEO as described above. PDA plates without CEO were served as negative controls. Mycelia were collected after incubation for 0, 1, 2, 3, 4, 5, and 6 days, and washed with 15 mL of SDW. The mycelium suspension was centrifuged at 4000 × g for 10 min to obtain mycelium, and the filtrate was collected for the determination of the leakage of intracellular content by the assays of total soluble protein, total soluble sugar, and nucleic acid. The content of soluble protein was determined with bovine serum albumin (Solarbio, Shanghai, China) as standard (Bradford, 1976). The content of soluble sugar was estimated by the phenol-sulfuric acid method using glucose (Solarbio, Shanghai, China) as standard (Dubois et al., 1956). The protein or sugar leakage was expressed as g/kg wet weight of mycelia. To determine the concentration of the released nucleic acid, 1 mL of supernatant was used to measure the absorbance at 260 nm with a UV-1800 PC spectrophotometer (Shanghai AoXi Science Instrument Co. Ltd, Shanghai, China) (Zhang et al., 2016). Each treatment was replicated thrice and the experiment was repeated thrice.

Statistical Analysis

Results were expressed as means ± standard deviation (SD) of three independent repeated experiments, as the interaction between treatment and experiment variables was not significant. Statistically significant differences between mean values were analyzed with one-way analysis of variance (ANOVA) and Duncan's multiple range tests using SPSS 19.0 (IBM, New York, NY, United States). Differences at *p* < 0.05 were considered as statistically significant.

RESULTS

Isolation and Identification of *C. acutatum*

The kiwifruit infected by anthracnose appeared on round spots from brown to dark brown launched from center, whose surface was depression, dried-up, and severe dehydration, while the tissue obviously turned into soft (Figure 1A). The pathogenic sarcocarp turned from green into pale yellow. Subsequently, the

whole fruit was rotten (Figure 1B). The colony of pathogen was circular on PDA after 7-day incubation, and its texture was soft and villous, as well as the color was pink (Figure 1C). The aerial mycelia grew radially from the center to the surrounding area. Mycelia were hyaline and septate (Figure 1D). The ellipsoidal spores produced the pale pink spore heaps, while the spore was single, colorless, and hyaline, diameter of $13.1\text{--}18.6 \times 3.0\text{--}4.0 \mu\text{m}$ (Figure 1E). The germinal spore was spheroidal and the diameter of the germinal spore was

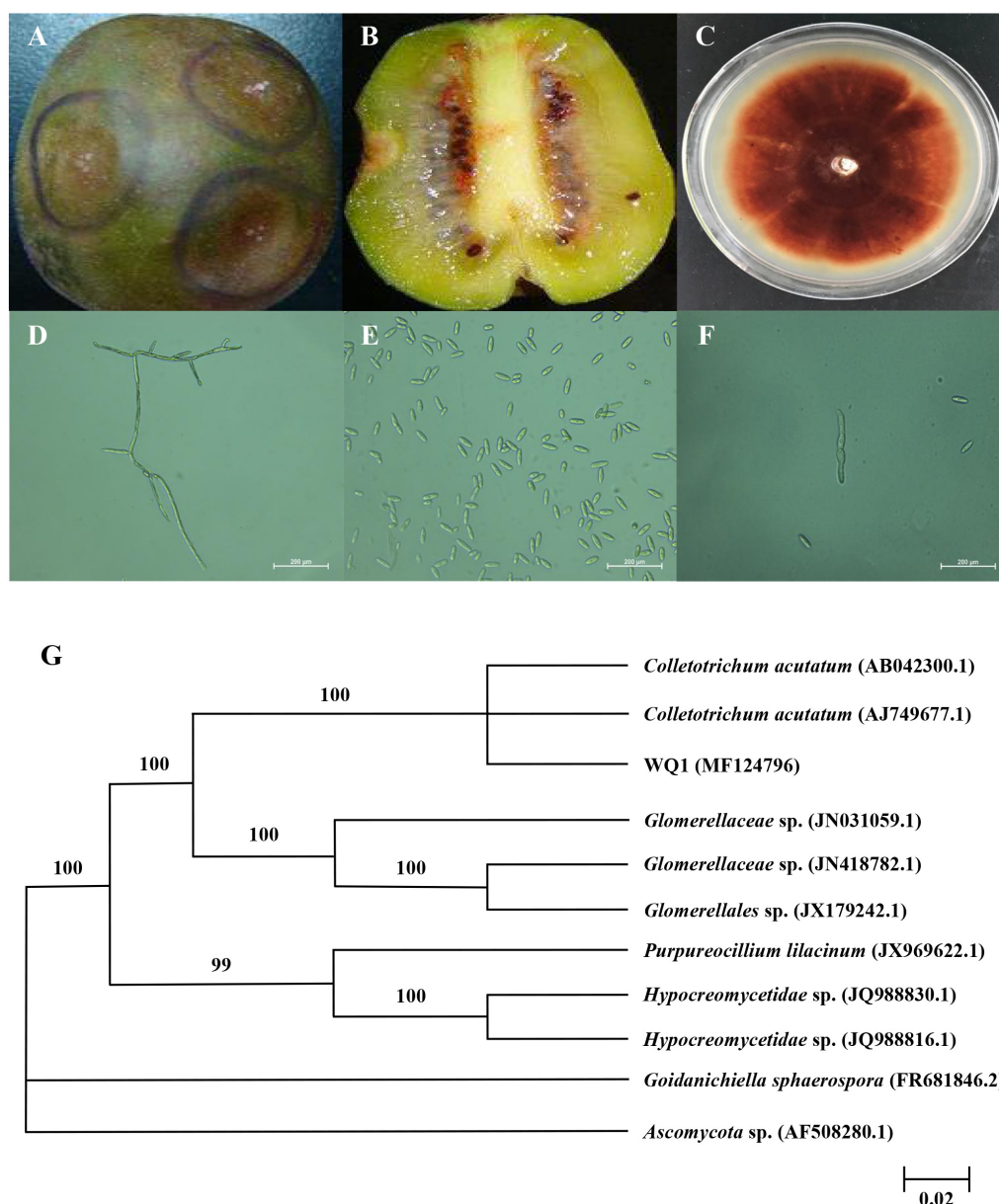


FIGURE 1 | Symptoms of kiwifruit anthracnose (A,B), and cultural (C) and morphological (D–F) characteristics of isolated pathogen, as well as its phylogenetic tree (G). (A) Symptoms on the surface of diseased kiwifruit; (B) Symptoms inside of diseased kiwifruit; (C) Colonies of pathogen cultured for 7 days at 25°C; (D) Mycelia of pathogen and 400× magnification; (E) Spores of pathogen and 400× magnification; (F) Germinal spores and 400× magnification; (G) Phylogenetic analysis of DNA sequences obtained from fragments of the ITS rDNA from the isolate along with the reference sequences from NCBI. The analysis was conducted using neighbor joining method. The scale bar represents 0.02% substitutions of nucleotide.

11.0–15.0 × 2.0–3.0 μm (**Figure 1F**). Thus it could be considered as *Colletotrichum* sp. It was verified that the isolated pathogen could cause the kiwifruit anthracnose through pathogenicity test. The colonial morphology and some microscopic features of the isolated pathogen were accordance with previous observations.

To further identify the isolated pathogen, the ITS1-5.8S-ITS2 region of isolate was sequenced. The PCR product was 531 bp. The obtained sequence was submitted to GenBank, and the accession number was MF 124796. The ITS sequence was preliminarily analyzed and submitted to GenBank as closest to those of *Colletotrichum* sp. For the identification purposes, the sequence was compared to those available in the NCBI database using the BLAST. Furthermore, the homology sequences were analyzed with MEGA 5.02 software to construct phylogenetic tree by the neighbor-joining method (**Figure 1G**). Confidence values above 50% obtained from a 1,000-replicate bootstrap analysis were shown at the branch nodes. Bootstrap values from neighbor-joining method were determined. *Goidanichiella sphaerospora* (FR 681846.2) and *Ascomycota* sp. (AF 508280.1) were used as the out group. The isolated pathogen had higher similar sequences of *C. acutatum* than any other reference taxa. In the neighbor-joining tree, the anthrax pathogen and other three reference taxa including *Glomerellaceae* sp., *Purpureocillium lilacinum* and *Hypocreomycetidae* sp. formed a clade with 100% bootstrap support. In this clade, the reference taxon, *C. acutatum* (AB 042300.1) and *C. acutatum* (AJ 749677.1) also clustered together with it, meanwhile they were same species. The result of similarity comparisons of the ITS1-5.8S-ITS2 region sequence revealed that isolated pathogen had the highest nucleotide similarities with *C. acutatum*.

Effect of CEO on *C. acutatum* in Vitro

We evaluated the antifungal activity of CEO *in vitro* against *C. acutatum*. The antifungal activity was mainly determined by inhibition of mycelial growth and spore germination of *C. acutatum*. The mycelial growth of *C. acutatum* was sensitive to CEO (**Figure 2A**). The mycelial growth of *C. acutatum* (CEO-treated group) was reduced during incubation compared with the untreated group, with the greater inhibitory at the higher concentration ($p < 0.05$). The mycelial growth of *C. acutatum* was completely inhibited by CEO at the concentration of 0.2 μL/mL. The efficacies of CEO on the spore germination of *C. acutatum* were shown in **Figure 2B**. The different concentrations of CEO had a significant inhibitory effect on spore germination (**Figure 2B**, $p < 0.05$). Observations showed an inhibition on the spore germination of *C. acutatum* within the range of 0.075–0.150 μL/mL. Results indicated that the spore germination was reduced with the increasing CEO concentrations. CEO could completely inhibit the spore germination at the concentration of 0.175 μL/mL. In summary, the CEO completely prevented the mycelial growth and spore germination of *C. acutatum* at concentrations of 0.2 μL/mL and 0.175 μL/mL, respectively. Further, the MIC and MFC values of CEO against *C. acutatum* were presented in **Table 2**. The MIC of CEO was 0.200 μL/mL. The MFC of CEO was

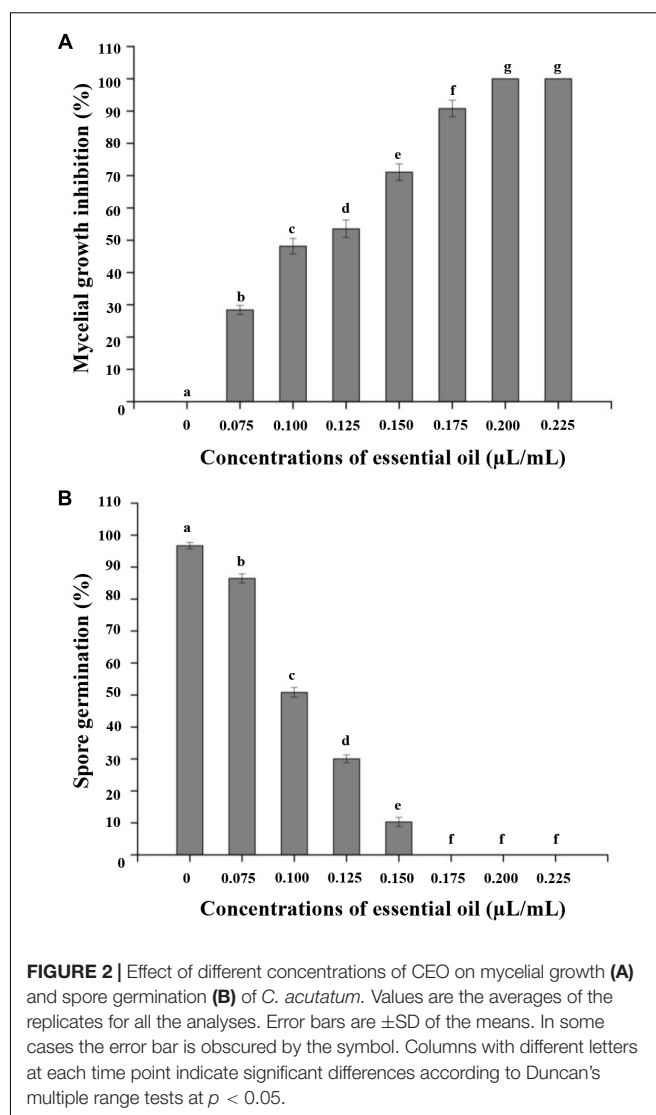


FIGURE 2 | Effect of different concentrations of CEO on mycelial growth (A) and spore germination (B) of *C. acutatum*. Values are the averages of the replicates for all the analyses. Error bars are \pm SD of the means. In some cases the error bar is obscured by the symbol. Columns with different letters at each time point indicate significant differences according to Duncan's multiple range tests at $p < 0.05$.

TABLE 2 | MIC and MFC of CEO against *C. acutatum*.

Concentration of CEO (μL/mL)	MIC	MFC
0	++++	++++
0.075	+++	+++
0.100	+++	+++
0.125	++	++
0.150	++	++
0.175	+	+
0.200	–	–
0.225	–	–

Growth of *C. acutatum* in the presence of CEO. Medium used: PDA. Inoculating in dark at 25°C. Growth: +++++, very good; +++, good; ++, fair; +, little; –, no growth. Values are mean ($n = 3$).

found to be equal to the corresponding MIC results. CEO showed the good fungistatic and fungicidal activity against *C. acutatum*.

Effects of CEO on Morphology and Ultrastructure of *C. acutatum*

Transmission electron microscopy could intuitively reflect the morphological alterations of the cell wall (CW), cell membrane (CM) and cytoplasm. The growth inhibition of *C. acutatum*

induced with different concentrations of CEO for 2 days was found to be well correlated with morphological changes of fungi exposed to control, MFC and 2MFC of CEO. The morphological changes of untreated and treated fungal cell were shown in **Figure 3**. In the control samples, the cells were dense appearance

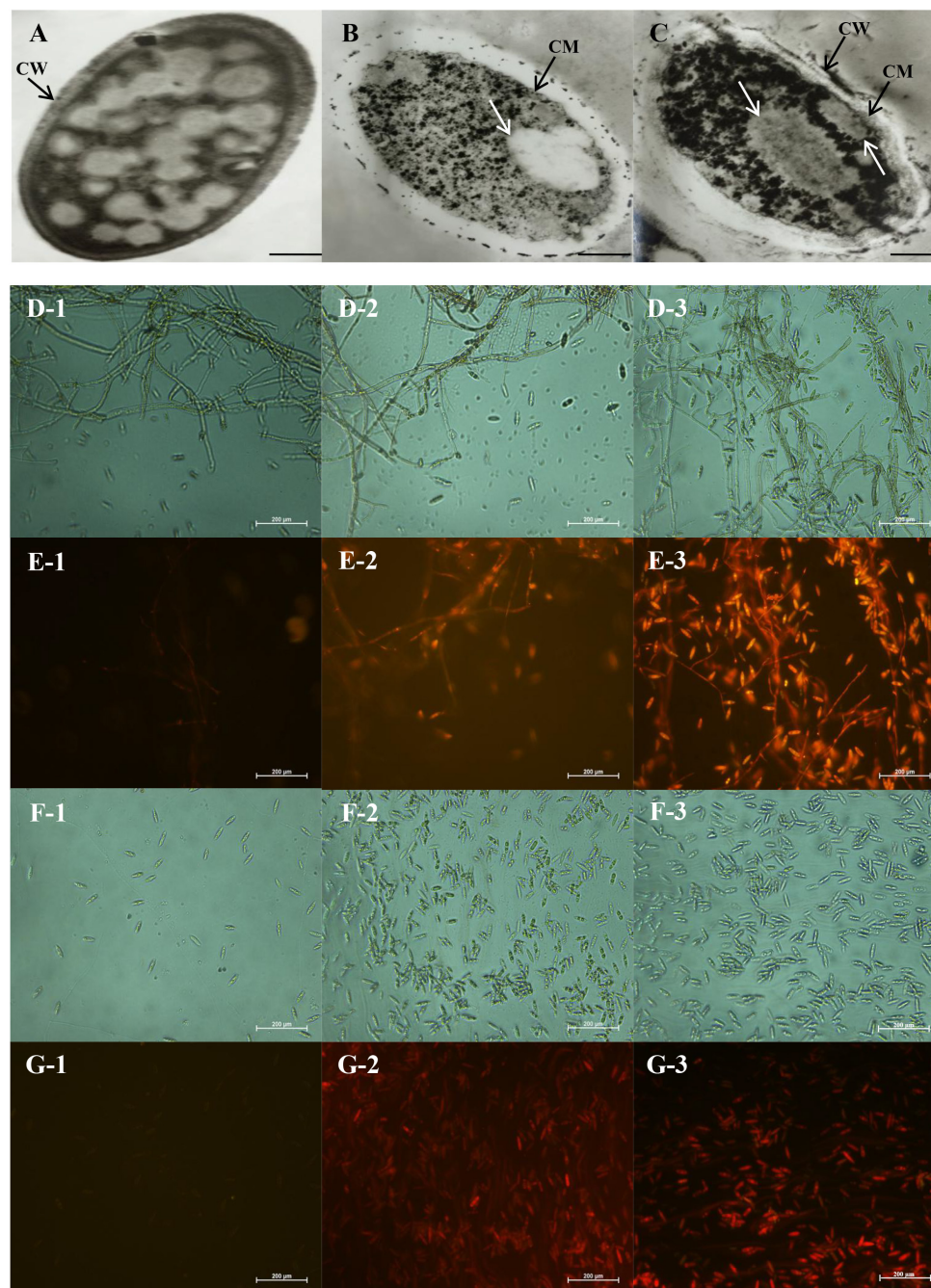


FIGURE 3 | Transmission electron microscopy (A–C) and fluorescence microscopy images (D–G) of antifungal effect of CEO against *C. acutatum*. (A) Healthy mycelia with control, the magnitudes of 15000 \times ; (B) Mycelia treated with the MFC of CEO; (C) Mycelia treated with the 2MFC of CEO; (D1–D3) Bright field of mycelia in microscopy after 0, 3, and 6 days of incubation, in the magnitudes of 400 \times ; (E1–E3) Propidium iodide of mycelia in microscopy after 0, 3, and 6 days of incubation; (F1–F3) Bright field of spores in microscopy after 0, 3, and 6 days of incubation; (G1–G3) Propidium iodide of spores in microscopy after 0, 3, and 6 days of incubation.

(Figure 3A). Results showed that the CW was uniform and thoroughly surrounded by an intact fibrillar layer for untreated fungi. Indeed, the CM was unfolded and uniform in shape (Figure 3A). All organelles had a normal appearance, and were clearly observed. In treated fungi, the destroyed cell structures were marked in CW and organelles (Figures 3B,C). The major disruption was the endomembrane system, containing the CM and membranous organelles. *C. acutatum* was treated with the MFC of CEO, the CW was deformed (Figure 3B). The fibrillar layers gradually lost their constitutions, becoming thinner and eventually detaching from the CW (Figure 3B). The fibrillar layers were hardly observed when the cells were treated with CEO of 2MFC (Figure 3C). The CM of *C. acutatum* treated with CEO lost its linear structure, becoming rough and villous with invaginations of vesicles. The CM was ruptured and detached from the cytoplasm (Figures 3B,C). After treatment with CEO, most organelles were indistinct and many structures were unidentifiable (Figures 3B,C). The intracellular organization was noticeably disrupted with uneven distribution, showing cytoplasmic condensation and absent (Figures 3B,C). Moreover, the damage in the intracellular organization was more severe with the increasing concentration of CEO (Figures 3B,C).

The results of staining *C. acutatum* mycelia and spores with propidium iodide were presented in Figures 3D–G. The cells are intact, which cannot be stained by propidium iodide. The mycelia treated without CEO could not be stained by propidium iodide (Figure 3E-1), and the cell structure was integral and clear (Figure 3D-1). The propidium iodide penetrated mycelia treated with CEO after 3 and 6 days (Figures 3E-2,E-3), and the cell structure was indistinct (Figures 3D-2,D-3). The damage of PM of mycelia was positively correlated with treatment time of CEO. The changes of spores treated with CEO were similar to that of mycelia (Figure 3E,G). The propidium iodide penetrated spores treated with CEO, showing that the membrane integrity has been compromised. In summary, the permeation to propidium iodide indicated that the CEO was responsible for a fungicidal effect, resulting in extensive damage to the plasmatic membrane between mycelia and spores (Figures 3D–G). MI of *C. acutatum* spores declined obviously with the increase of incubation time on PDA containing MFC of CEO (Figure 4A). However, MI stayed at a relatively high level for spores incubated in PDA without CEO (Figure 4A). Moreover, results showed that the damage of the plasmatic membrane of spores was markedly more severe than the membrane of mycelia, which were in accordance with the above mentioned result that the spore germination was more sensitive to CEO treatment than that of mycelial growth (Figures 3D–G).

Effects of CEO on Ergosterol Content, and Intracellular Protein, Sugar, and Nucleic Acid Leakage

Figure 4B showed the effects of different concentrations of CEO on the ergosterol content of the PM in *C. acutatum* compared with the control. Results indicated that the total ergosterol content was reduced with the increasing of CEO

concentrations. The production of ergosterol decreased at the CEO concentrations of 0, 0.075, 0.100, 0.125, 0.150, and 0.175 $\mu\text{L/mL}$, presenting a value of 0.5885, 0.4954, 0.3750, 0.2514, 0.1412, and 0.0863%, respectively. The cells treated with CEO showed inhibition rate of 15.81, 36.28, 57.28, 76.01, and 85.34% to ergosterol compared with the control, respectively. Further, the exposure of *C. acutatum* to different concentrations of CEO caused various levels of extracellular conductivity. The extracellular conductivity in *C. acutatum* suspension was increased with exposure time and the concentrations of CEO (Figure 4C). All CEO treated *C. acutatum* showed higher electric conductivity than the control. Moreover, the electric conductivity increased rapidly in respond to increasing levels of CEO during the first 4 days (Figure 4C). After that, the growth tended to slow down. After 4 days, the extracellular conductivity of suspensions with CEO (512 $\mu\text{S/cm}$ and 526 $\mu\text{S/cm}$) remained at the same level, but the values CEO treated cells were significantly higher ($p < 0.05$) than the control (211 $\mu\text{S/cm}$ and 223 $\mu\text{S/cm}$) (Figure 4C). Additionally, the leakage of protein, sugar, and nucleic acid could be considered as important indicators of CM damage. *C. acutatum* cells were treated with the MFC of CEO, and the amounts of released protein, sugar, and nucleic acid were investigated. The results showed that *C. acutatum* cells treated with CEO accumulated more protein, sugar, and nucleic acid than the untreated group (Figures 4D–F). In this study, protein, sugar, and nucleic acid leakages can be detected in time-dependent tests. In time-dependent killing, protein, sugar and nucleic acid leakages were initially sluggish, and the leakages increased with treatment duration (Figures 4D–F). At the first 4 days, proteins and sugar leaked markedly in treatment, and the leakage increased slowly after 4 days (Figures 4D,E). However, the leakage of protein and sugar stayed at a very low level for control (Figures 4D,E). Hence, the leakages of treatment groups were significantly higher than that of control. At the first 4 days, the absorbance value for nucleic acid (OD 260 nm) of *C. acutatum* increased significantly ($p < 0.05$) from 0.018 to 0.048 (control), and from 0.013 to 1.269 (CEO treatment group), respectively (Figure 4F). After 4 days, the value of OD 260 nm was followed by a steady state, which clearly indicated that the CM integrity of *C. acutatum* had been compromised after exposure to CEO, which could consequently lead to cell death.

DISCUSSION

The isolated pathogen was inoculated in the surface-sterilized and healthy kiwifruit. The results showed that the sample was attacked after inoculating 24 h at 25°C because of brown dots on the surface of fruit. Then the lesion rapidly expanded and showed drying shrinkage and depression on the 5th day. The color of pericarp turned to dim and pink, and then sticky particulates on pathogenic sites, which were the conidial heaps. Finally, as the decay spread out, the whole of fruit was brown rot and even dried. According to the morphological and molecular identification, the pathogen from 'Hongyang' kiwifruit was further determined as *C. acutatum*. Previous studies found that *C. musae* occurring anthracnose could cause the development of black circular/

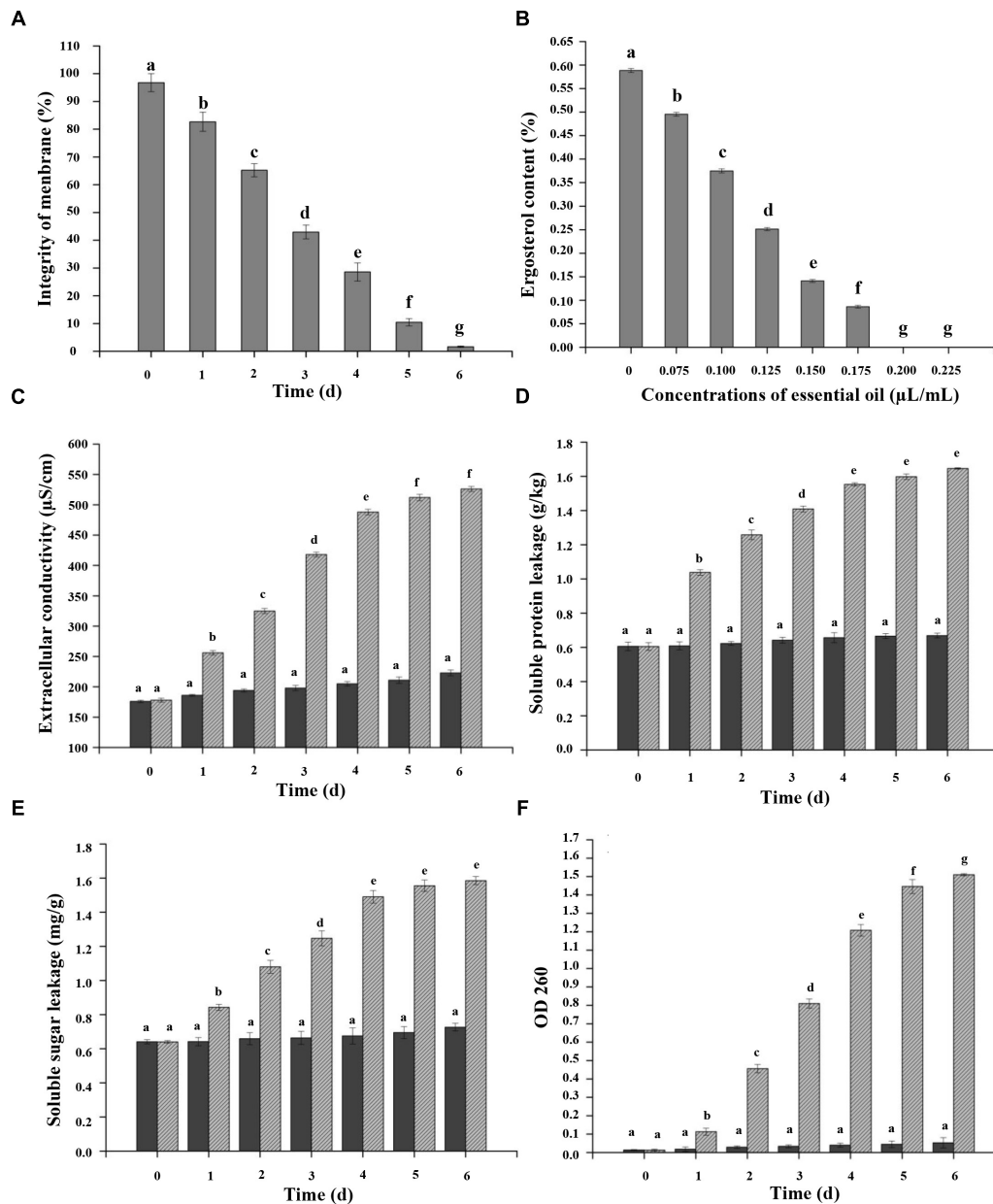


FIGURE 4 | Effects of CEO on percentage of plasma membrane integrity (A), ergosterol content (B), extracellular conductivity (C), and protein (D), sugar (E), and nucleic acid (F) leakage of *C. acutatum*. (A) Percentage of plasma membrane integrity of *C. acutatum* spores, *C. acutatum* was cultured in PDA containing CEO or in PDA without CEO as the control at 25°C; (B) Ergosterol contents of *C. acutatum* on PDA containing different concentrations of CEO at 25°C were assayed; (C) Cellular leakage from fungal tissues was determined 0–6 days after incubation with the CEO. Mycelia were cultured in PDA containing CEO or in SDW without EO as the control at 25°C. Samples for the leakage were measured for 6 days; (D) Soluble protein leakage of *C. acutatum*; (E) Soluble sugar leakage of *C. acutatum*; (F) Nucleic acid leakage of *C. acutatum*. Values are the averages of the replicates for all the analyses. Error bars are \pm SD of the means. In some cases the error bar is obscured by the symbol. Columns with different letters at each time point indicate significant differences according to Duncan's multiple range tests at $p < 0.05$.

lenticular spots during ripening in banana (Barrera-Necha et al., 2008). So far, to best of our knowledge, there were no reports on *C. acutatum* from 'Hongyang' kiwifruit.

Essential oil showed a superior antimicrobial activity that the growth of tested organisms was inhibited more efficiently by gaseous contact than by solution contact (Inouye et al., 2003; Oonmetta-Aree et al., 2006). Therefore, in this study,

the antifungal activity of CEO was carried out with its volatile substances, and the antifungal effect was good. The results showed that CEO exhibited antifungal activity against *C. acutatum* as a volatile *in vitro*. Both MIC and MFC of CEO were 0.200 μ L/mL. These results confirmed other findings on antifungal activity of CEO against several fungal pathogens including *Aspergillus flavus*, *Penicillium expansum*,

Zygosaccharomyces rouxii and *Zygosaccharomyces bailii* *in vitro* (Manso et al., 2015; Ribeiro-Santos et al., 2017; Ribes et al., 2017). CEO had a strong antifungal effect against *Aspergillus flavus*, with a MIC of 0.05–0.10 mg/mL, and a MFC of 0.05–0.20 mg/mL (Manso et al., 2013). The MIC of CEO against *Aspergillus flavus* strains and *Aspergillus oryzae* were 0.125 μ L/mL and 0.250 μ L/mL, respectively (Kocevski et al., 2013). CEO could effectively inhibit the growth of *Botryosphaeria parva* in the dilution method, and both MIC and MFC of CEO were 0.078 μ L/mL (He et al., 2015). Volatiles of CEO obviously affected appressorium formation, while in control treatment germinal spores formed one or more appressoria. Results showed that inhibitory activity of CEO was significantly correlated with the concentration of CEO. In present study, the spore germination was more sensitive to CEO treatment than mycelial growth, which was in accordance with previous studies (Duduk et al., 2015). CEO had a fungistatic effect against mycelial growth of *C. acutatum* isolated from strawberry anthracnose at 0.667 μ L/mL. Meanwhile, CEO completely prevented the spore germination and appressorium formation at 0.00153 μ L/mL (Duduk et al., 2015). In addition, CEO strengthens its merits as a post-harvest fungicide against food-borne pathogens. Moreover, the MIC and MFC of CEO against *Colletotrichum* sp. were lower than those of some earlier reported EO viz., *Thymus vulgaris* L. (Zambonelli et al., 1996), clove [*Syzygium aromaticum* (L.)] (Ranasinghe et al., 2002) and tea tree oil (Szczerbanik et al., 2007). These results indicated that CEO had high potential of economic exploitation.

The potential mechanisms underlying the antifungal activity of plant essential oils are not fully understood, but a number of possible mechanisms have been proposed. The results of TEM indicated that the CEO destroyed not only the CW, but also the PM, by interacting with the structures of cytoplasmic organelles in comparison with untreated samples. The degree of damage had dose-effect relationship, and that destructiveness of 2MFC was stronger than MFC. The CEO showed antifungal activity against *C. acutatum* causing cellular damages and irreversible morphological changes. Previous studies revealed morphological alterations in *Aspergillus flavus* by TEM observations (Nogueira et al., 2010). Results showed that a marked disruption of membranes of major organelles such as nuclei, mitochondria and endoplasmic reticulum, indicated that *Ageratum conyzoides* EO passed not only through the CW, but also through the PM and then interacted with membranous structures of the cytoplasmic organelles. Studies also reported irreversible damage to CW, CM and organelles of *Aspergillus flavus* by *Cinnamomum jensenianum* essential oil (CJEO) (Tian et al., 2012). In the CJEO-treated hyphae, the fibrillar layers had gradually lost their integrity, becoming thinner, and eventually failing to deposit on the CW. In addition, the mitochondria suffered a severe disruption of the internal structure with complete lysis. Indeed, studies demonstrated that the TTO could destruct for organelles of *Botrytis cinerea* by TEM observation (Yu et al., 2015). The PM appears to be the main target of the EO according to TEM data. Furthermore, FMS observation showed that the propidium iodide could permeate CM into intracellular cytoplasm while cells were destroyed. Then CEO was responsible for a fungicidal

effect, resulting in extensive lesion to the plasmatic membrane, either from a direct effect or as a secondary result of metabolic impairment. Results showed that CEO could be used as a fungicide to damage membrane integrity.

In order to confirm the CEO targets in the PM, the amount of ergosterol was assessed. Ergosterol is the major sterol component of the fungal CM, helping to maintain cell function and integrity (Vale-Silva et al., 2010). It is a sterol with a CM specific of fungi and microalgae with the advantage of indicating only viable biomass, since it is quickly degraded after the cell's death (Gutarowska and Zakowska, 2009). The correlation between ergosterol and biomass of several fungal species has been confirmed (Khan et al., 2010; Silva et al., 2010). Previous studies suggested that the PM was the main target of EOs against fungi, and that the oil caused dose-dependent reduction in ergosterol quantity (Tian et al., 2012; Yu et al., 2015). Our results supported a model in which cellular membranes were the primary targets for CEO with different concentrations.

The lipophilicity of EOs enable them to preferentially part from an aqueous phase into membrane structures of the fungi, resulting in expansion of membrane, and then increase of membrane fluidity and permeability, disturbance of membrane-embedded proteins and soluble sugars, and other cellular contents. The electric conductivity was examined to express the changes of CM permeability. Our results showed that the extracellular conductivity rose with the increasing of CEO concentration and treatment time. The results clearly indicated that there was a leakage of electrolytes due to the disruption of cell permeability caused by CEO. Excessive electrolyte loss would cause the death of *C. acutatum*. This slight increase for control might be due to regular fungal cytolysis and death, just as Diao et al. (2014) and Zhang et al. (2016). The integrity of the cytoplasmic membrane is a critical factor to fungal growth. Analyzing the leakage of cell constituents could therefore give further insight into the mechanism of antifungal action. The ability of CEO to disturb the integrity of the PM of fungal cells was also assessed by measuring the protein, sugar, and nucleic acid released in cell suspensions. Results showed that the leakage increased with the extension of treatment time.

The antifungal property of EO may be contributed to its major components. 1, 8-cineole (56%) was the major component in *Callistemon lanceolatus* (Sm.). Sweet essential oil, which showed great inhibitor effect against fungi (Shukla et al., 2012). (*E*)-cinnamaldehyde was found as the major component in cinnamon leaf volatile oil, which possessed crucial inhibitory activity (Singh et al., 2007). The compositions of CEO are greatly influenced by the species, part of plant used, geographic origin, time of harvest, stage of development, age of plants and extraction method (Lee et al., 2005). Twenty components in CEO extracted from bark was identified, and twenty-one components of CEO extracted from leaf was identified. The major components of bark EO are methyl cinnamate (81.87%), linalool (3.90%) and α -pinene (2.41%). The major components of leaf volatile oil are linalool (67.60%), methyl cinnamate (17.32%) and α -pinene (2.74%) (Malsawmtluangi et al., 2016). Previous studies have validated that the major components of CEO are *trans*-cinnamaldehyde

or cinnamaldehyde (Goñi et al., 2009), which were consistent with our results (Table 1). Furthermore, the content of *trans*-cinnamaldehyde (86.16%) in our study was much higher than that of previous studies (Lv et al., 2011; Li et al., 2013). It remains to be further defined whether major components are the main antifungal composition.

CONCLUSION

Results demonstrated that the major pathogen from 'Hongyang' kiwifruit causing to anthracnose was *C. acutatum*. The inhibition of CEO against *C. acutatum* attributed to the reducing of fungal growth and spore germination. CEO could penetrate CW, and pass through the PM, and then interact with the membranous structures of cytoplasmic organelles. Moreover, the major components of CEO such as cinnamaldehyde could

be used as a natural fungistat. The antifungal mechanism of cinnamaldehyde requires further investigations.

AUTHOR CONTRIBUTIONS

JH, WQ, and DW designed the study. JH, HL, QH, XL, HW, YW, and JY performed the experiments. JH drafted the work. JH, DW, QZ, HC, and HD wrote and revised the manuscript. JH, WQ, and DW revised the final version to be published.

FUNDING

This work was supported by the Scientific Research Fund Project of Science and Technology Department of Sichuan Province (Grant Nos. 2016NZ0105, 2017NZ0039, and 2018NZ0010).

REFERENCES

- Barrera-Necha, L. L., Bautista-Baños, S., Flores-Moctezuma, H. E., and Estudillo, A. R. (2008). Efficacy of essential oils on the conidial germination, growth of *Colletotrichum gloeosporioides* (Penz.) Penz. and Sacc and control of postharvest diseases in Papaya (*Carica papaya* L.). *Plant Pathol.* 7, 174–178. doi: 10.3923/ppj.2008.174.178
- Bozzola, J. J., and Russell, L. D. (1999). *Electron Microscopy: Principles and Techniques for Biologists*. Boston, MA: Jones and Bartlett Publishers.
- Bradford, M. M. (1976). A rapid and sensitive method for the quantitation of microgram quantities of protein using the principle of protein dye binding. *Anal. Biochem.* 72, 248–254. doi: 10.1006/abio.1976.9999
- Chao, L. K., Hua, K. F., Hsu, H. Y., Cheng, S. S., Liu, J. Y., and Chang, S. T. (2005). Study on the antiinflammatory activity of essential oil from leaves of *Cinnamomum osmophloeum*. *J. Agric. Food Chem.* 53, 7274–7278. doi: 10.1021/jf051151u
- Chao, S. C., Young, D. G., and Oberg, C. J. (2000). Screening for inhibitory activity of essential oils on selected bacteria, fungi and viruses. *J. Essent. Oil Res.* 12, 639–649. doi: 10.1080/10412905.2000.9712177
- Concha, J. M., Moore, L. S., and Holloway, W. J. (1998). Antifungal activity of *Melaleuca alternifolia* (tea-tree) oil against various pathogenic organisms. *J. Am. Podiatr. Med. Assoc.* 88, 489–492. doi: 10.7547/87507315-88-10-489
- Cowan, M. M. (1999). Plant products as antimicrobial agents. *Clin. Microbiol. Rev.* 12, 564–582.
- Diao, W. R., Hu, Q. P., Zhang, H., and Xu, J. G. (2014). Chemical composition, antibacterial activity and mechanism of action of essential oil from seeds of fennel (*Foeniculum vulgare* Mill.). *Food Control* 35, 109–116. doi: 10.1016/j.foodcont.2013.06.056
- Dubois, M., Gilles, K. A., Hamilton, J. K., Rebers, P. A., and Smith, F. (1956). Colorimetric method for determination of sugars and related substances. *Anal. Chem.* 28, 350–356. doi: 10.1021/ac60111a017
- Duduk, N., Markovic, T., Vasic, M., Duduk, B., Vico, I., and Obradovic, A. (2015). Antifungal activity of three essential oils against *Colletotrichum acutatum*, the causal agent of strawberry anthracnose. *J. Essent. Oil Bear. Plants* 18, 529–537. doi: 10.1080/0972060X.2015.1004120
- Fadli, M., Saad, A., Sayadi, S., Chevalier, J., Mezrioui, N. E., Pagès, J. M., et al. (2012). Antibacterial activity of *Thymus maroccanus* and *Thymus broussonetii* essential oils against nosocomial infection - bacteria and their synergistic potential with antibiotics. *Phytomedicine* 19, 464–471. doi: 10.1016/j.phymed.2011.12.003
- Fleissner, A., and Glass, N. L. (2007). SO, a protein involved in hyphal fusion in *Neurospora crassa*, localizes to septal plugs. *Eukaryot. Cell* 6, 84–94. doi: 10.1128/EC.00268-06
- Fleming-Jones, M. E., and Smith, R. E. (2003). Volatile organic compounds in foods: a five year study. *J. Agric. Food Chem.* 51, 8120–8127. doi: 10.1021/jf0303159
- Goñi, P., López, P., Sánchez, C., Gómez-Lus, R., Becerril, R., and Nerín, C. (2009). Antimicrobial activity in the vapour phase of a combination of cinnamon and clove essential oils. *Food Chem.* 116, 982–989. doi: 10.1016/j.foodchem.2009.03.058
- Gutarowska, B., and Zakowska, Z. (2009). Mathematical models of mycelium growth and ergosterol synthesis in stationary mould culture. *Lett. Appl. Microbiol.* 48, 605–610. doi: 10.1111/j.1472-765X.2009.02577.x
- He, J. L., Liu, J., Du, X. Q., Ye, X. Y., Chen, Q. Y., Qin, W., et al. (2015). Preservation of 'Red Sun' kiwifruit fumigated with plant essential oil during cold storage'. *Sci. Technol. Food Ind.* 36, 320–326.
- Inouye, S., Abe, S., Yamaguchi, H., and Asakura, M. (2003). Comparative study of antimicrobial and cytotoxic effects of selected essential oils by gaseous and solution contacts. *Int. J. Aromather.* 13, 33–41. doi: 10.1016/S0962-4562(03)00057-2
- Irobi, O. N., and Daramola, S. O. (1993). Antifungal activities of crude extracts of *Mitracarpus villosus* (Rubiaceae). *J. Ethnopharmacol.* 40, 137–140. doi: 10.1016/0378-8741(93)90059-E
- Jogee, P. S., Ingle, A., and Rai, M. (2017). Isolation and identification of toxigenic fungi from infected peanuts and efficacy of silver nanoparticles against them. *Food Control* 71, 143–151. doi: 10.1016/j.foodcont.2016.06.036
- Khan, A., Ahmad, A., Akhtar, F., Yousuf, S., Xess, I., Khan, L. A., et al. (2010). Ocimum sanctum essential oil and its active principles exert their antifungal activity by disrupting ergosterol biosynthesis and membrane integrity. *Res. Microbiol.* 161, 816–823. doi: 10.1016/j.resmic.2010.09.008
- Kim, K. J., Sung, W. S., Suh, B. K., Moon, S. K., Choi, J. S., Kim, J. G., et al. (2009). Antifungal activity and mode of action of silver nanoparticles on *Candida albicans*. *Biomaterials* 22, 235–242. doi: 10.1007/s10534-008-9159-2
- Kocevski, D., Du, M. Y., Kan, J. Q., Jing, C. J., Lačnanin, I., and Pavlović, H. (2013). Antifungal effect of *Allium tuberosum*, *Cinnamomum cassia*, and *Pogostemon cablin* essential oils and their components against population of *Aspergillus* species. *J. Food Sci.* 78, 731–737. doi: 10.1111/1750-3841.12118
- Lee, H. C., Cheng, S. S., and Chang, S. T. (2005). Antifungal property of the essential oils and their constituents from *Cinnamomum osmophloeum* leaf against tree pathogenic fungi. *J. Sci. Food Agric.* 85, 2047–2053. doi: 10.1002/jsfa.2216
- Li, Y., Kong, D., and Wu, H. (2013). Analysis and evaluation of essential oil components of cinnamon barks using GC-MS and FTIR spectroscopy. *Ind. Crop. Prod.* 41, 269–278. doi: 10.1016/j.indcrop.2012.04.056
- Lin, M. M., Fang, J. B., Qi, X. J., Li, Y. K., Chen, J. Y., Sun, L. M., et al. (2017). iTRAQ-based quantitative proteomic analysis reveals alterations in the metabolism of *Actinidia arguta*. *Sci. Rep.* 7:5670. doi: 10.1038/s41598-017-06074-6
- Liu, J., Tian, S. P., Meng, X. H., and Xu, Y. (2007). Effects of chitosan on control of postharvest diseases and physiological responses of tomato fruit. *Postharvest Biol. Technol.* 44, 300–306. doi: 10.1016/j.postharvbio.2006.12.019

- Liu, J., Zong, Y. Y., Qin, G. Z., Li, B. Q., and Tian, S. P. (2010). Plasma membrane damage contributes to antifungal activity of silicon against *Penicillium digitatum*. *Curr. Microbiol.* 61, 274–279. doi: 10.1007/s00284-010-9607-4
- Lv, F., Liang, H., Yuan, Q. P., and Li, C. F. (2011). In vitro antimicrobial effects and mechanism of action of selected plant essential oil combinations against four food-related microorganisms. *Food Res. Int.* 44, 3057–3064. doi: 10.1016/j.foodres.2011.07.030
- Malsawmtluangi, L., Nautiyal, B. P., Hazarika, T., Chauhan, R. S., and Tava, A. (2016). Essential oil composition of bark and leaves of *Cinnamomum verum* Bertch. & Presl from Mizoram, North East India. *J. Essent. Oil Res.* 28, 551–556. doi: 10.1080/10412905.2016.1167131
- Manso, S., Becerril, R., Nerin, C., and Gómez-Lus, R. (2015). Influence of pH and temperature variations on vapor phase action of an antifungal food packaging against five mold strains. *Food Control* 47, 20–26. doi: 10.1016/j.foodcont.2014.06.014
- Manso, S., Cacho-Nerin, F., Becerril, R., and Nerin, C. (2013). Combined analytical and microbiological tools to study the effect on *Aspergillus flavus* of cinnamon essential oil contained in food packaging. *Food Control* 30, 370–378. doi: 10.1016/j.foodcont.2012.07.018
- Neri, F., Donati, I., Veronesi, F., Mazzoni, D., and Mari, M. (2010). Evaluation of *Penicillium expansum* isolates for aggressiveness, growth and patulin accumulation in usual and less common fruit hosts. *Int. J. Food Microbiol.* 143, 109–117. doi: 10.1016/j.ijfoodmicro.2010.08.002
- Nogueira, J. H., Gonzalez, E., Galletti, S. R., Facanali, R., Marques, M. O., and Felício, J. D. (2010). Ageratum conyzoides essential oil as aflatoxin suppressor of *Aspergillus flavus*. *Int. J. Food Microbiol.* 137, 55–60. doi: 10.1016/j.ijfoodmicro.2009.10.017
- Oonmetta-Aree, J., Suzuki, T., Gasaluck, P., and Eumkeb, G. (2006). Antimicrobial properties and action of galangal (*Alpinia galanga* Linn.) on *Staphylococcus aureus*. *LWT Food Sci. Technol.* 39, 1214–1220. doi: 10.1016/j.lwt.2005.06.015
- Pandey, D. K., Tripathi, N. N., Tripathi, R. D., and Dixit, S. N. (1982). Fungitoxic and phytotoxic properties of the essential oil of *Hyptis suaveolens*. *J. Plant Dis. Prot.* 89, 344–349.
- Prasad, K. N., Yang, B., Dong, X. H., Jiang, G. X., Zhang, H. Y., Xie, H. H., et al. (2009). Flavonoid contents and antioxidant activities from *Cinnamomum* species. *Innov. Food Sci. Emerg.* 10, 627–632. doi: 10.1016/j.ifset.2009.05.009
- Pratt, D. E. (1992). "Natural antioxidants from plant material," in *Phenolic Compounds in Food and Their Effects on Health*, eds I. M. T. Huang, C. T. Ho, and C. Y. Lee (Washington, DC: American Chemical Society), 54–72. doi: 10.1021/bk-1992-0507.ch005
- Ranasinghe, L., Jayawardena, B., and Abeywickrama, K. (2002). Fungicidal activity of essential oils of *Cinnamomum zeylanicum* (L.) and *Syzygium aromaticum* (L.) Merr et L.M. Perry against crown rot and anthracnose pathogens isolated from banana. *Lett. Appl. Microbiol.* 35, 208–211. doi: 10.1046/j.1472-765X.2002.01165.x
- Rasooli, I., and Abyaneh, M. R. (2004). Inhibitory effects of Thyme oils on growth and aflatoxin production by *Aspergillus parasiticus*. *Food Control* 15, 479–483. doi: 10.1016/j.foodcont.2003.07.002
- Ribeiro-Santos, R., Andrade, M., de Melo, N. R., dos Santos, F. R., de Araújo Neves, I., de Carvalho, M. G., et al. (2017). Biological activities and major components determination in essential oils intended for a biodegradable food packaging. *Ind. Crop. Prod.* 97, 201–210. doi: 10.1016/j.indcrop.2016.12.006
- Ribes, S., Fuentes, A., Talens, P., and Barat, J. M. (2017). Application of cinnamon bark emulsions to protect strawberry jam from fungi. *LWT Food Sci. Technol.* 78, 265–272. doi: 10.1016/j.lwt.2016.12.047
- Saitou, N., and Nei, M. (1987). The neighbor-joining method: a new method for reconstructing phylogenetic trees. *Mol. Biol. Evol.* 4, 406–425. doi: 10.1093/oxfordjournals.molbev.a040454
- Shukla, R., Singh, P., Prakash, B., and Dubey, N. K. (2012). Antifungal, aflatoxin inhibition and antioxidant activity of *Callistemon lanceolatus* (Sm.) Sweet essential oil and its major component 1,8-cineole against fungal isolates from chickpea seeds. *Food Control* 25, 27–33. doi: 10.1016/j.foodcont.2011.10.010
- Silva, R. R., Corso, C. R., and Matheus, D. R. (2010). Effect of culture conditions on the biomass determination by ergosterol of *Lentinus crinitus* and *Psilocybe castanella*. *World J. Microbiol. Biotechnol.* 26, 841–846. doi: 10.1007/s11274-009-0241-x
- Singh, G., Maurya, S., Delampasona, M. P., and Catalan, C. A. (2007). A comparison of chemical, antioxidant and antimicrobial studies of cinnamon leaf and bark volatile oils, oleoresins and their constituents. *Food Chem. Toxicol.* 45, 1650–1661. doi: 10.1016/j.fct.2007.02.031
- Szczerbanik, M., Jobling, J., Morris, S., and Holford, P. (2007). Essential oil vapours control some common postharvest fungal pathogens. *Aust. J. Exp. Agric.* 47, 103–109. doi: 10.1071/EA05236
- Tamura, K., Dudley, J., Nei, M., and Kumar, S. (2007). MEGA4, a molecular evolutionary genetic analysis MEGA software version 4.0. *Mol. Biol. Evol.* 24, 1596–1599. doi: 10.1093/molbev/msm092
- Tao, N. G., Jia, L., and Zhou, H. E. (2014). Anti-fungal activity of *Citrus reticulata* Blanco essential oil against *Penicillium italicum* and *Penicillium digitatum*. *Food Chem.* 153, 265–271. doi: 10.1016/j.foodchem.2013.12.070
- Tian, J., Huang, B., Luo, X. L., Zeng, H., Ban, X. Q., He, J. S., et al. (2012). The control of *Aspergillus flavus* with *Cinnamomum jensenianum* Hand.-Mazz essential oil and its potential use as a food preservative. *Food Chem.* 130, 520–527. doi: 10.1016/j.foodchem.2011.07.061
- Tian, J., Zeng, X. B., Feng, Z. Z., Miao, X. M., Peng, X., and Wang, Y. W. (2014). *Zanthoxylum molle* Rehd. essential oil as a potential natural preservative in management of *Aspergillus flavus*. *Ind. Crop. Prod.* 60, 151–159. doi: 10.1016/j.indcrop.2014.05.045
- Trabelsi, D., Hamdane, A. M., Said, M. B., and Abdrrabba, M. (2016). Chemical composition and antifungal activity of essential oils from flowers, leaves and peels of Tunisian *Citrus aurantium* against *Penicillium digitatum* and *Penicillium italicum*. *J. Essent. Oil Bear. Plants* 19, 1660–1674. doi: 10.1080/0972060X.2016.1141069
- Vale-Silva, L. A., Gonçalves, M. J., Cavaleiro, C., Salgueiro, L., and Pinto, E. (2010). Antifungal activity of the essential oil of *Thymus x viciosoi* against *Candida*, *Cryptococcus*, *Aspergillus* and dermatophyte species. *Planta Med.* 76, 882–888. doi: 10.1055/s-0029-1240799
- Wei, M. K., Wu, Q. P., Huang, Q., Wu, J. L., and Zhang, J. M. (2008). Plasma membrane damage to *Candida albicans* caused by chlorine dioxide (ClO₂). *Lett. Appl. Microbiol.* 47, 67–73. doi: 10.1111/j.1472-765X.2008.02387.x
- Williamson, B., Tudzynski, B., Tudzynski, P., and van Kan, J. A. (2007). Botrytis cinerea: the cause of grey mould disease. *Mol. Plant Pathol.* 8, 561–580. doi: 10.1111/j.1364-3703.2007.00417.x
- Yu, D., Wang, J., Shao, X., Xu, F., and Wang, H. (2015). Antifungal modes of action of tea tree oil and its two characteristic components against *Botrytis cinerea*. *J. Appl. Microbiol.* 119, 1253–1262. doi: 10.1111/jam.12939
- Zambonelli, A., D'Aulerio, A. Z., Bianchi, A., and Albasini, A. (1996). Effects of essential oils on phytopathogenic fungi in vitro. *J. Phytopathol.* 144, 491–494. doi: 10.1111/j.1439-0434.1996.tb00330.x
- Zhang, Y. B., Liu, X. Y., Wang, Y. F., Jiang, P. P., and Quek, S. Y. (2016). Antibacterial activity and mechanism of cinnamon essential oil against *Escherichia coli* and *Staphylococcus aureus*. *Food Control* 59, 282–289. doi: 10.1016/j.foodcont.2015.05.032
- Zhao, J. J., Zeng, J. S., de Hoog, G. S., Attili-Angelis, D., and Prenafeta-Boldú, F. X. (2010). Isolation and identification of black yeasts by enrichment on atmospheres of monoaromatic hydrocarbons. *Microb. Ecol.* 60, 149–156. doi: 10.1007/s00248-010-9651-4
- Zollo, P. H. A., Biyiti, L., Tchoumboungang, F., Menut, C., Lamaty, G., and Bouchet, P. (1998). Aromatic plants of tropical central Africa. Part XXXII. Chemical composition and antifungal activity of thirteen essential oils from aromatic plants of Cameroon. *Flavour Fragr. J.* 13, 107–114. doi: 10.1002/(SICI)1

Conflict of Interest Statement: The authors declare that the research was conducted in the absence of any commercial or financial relationships that could be construed as a potential conflict of interest.

Copyright © 2018 He, Wu, Zhang, Chen, Li, Han, Lai, Wang, Wu, Yuan, Dong and Qin. This is an open-access article distributed under the terms of the Creative Commons Attribution License (CC BY). The use, distribution or reproduction in other forums is permitted, provided the original author(s) and the copyright owner are credited and that the original publication in this journal is cited, in accordance with accepted academic practice. No use, distribution or reproduction is permitted which does not comply with these terms.



Phomopsis longanae Chi-Induced Disease Development and Pericarp Browning of Harvested Longan Fruit in Association With Energy Metabolism

Yihui Chen¹, Hetong Lin^{1*}, Shen Zhang¹, Junzheng Sun¹, Yifen Lin¹, Hui Wang¹, Mengshi Lin² and John Shi³

¹ Institute of Postharvest Technology of Agricultural Products, College of Food Science, Fujian Agriculture and Forestry University, Fuzhou, China, ² Food Science Program, Division of Food System and Bioengineering, University of Missouri, Columbia, MO, United States, ³ Guelph Food Research Center, Agriculture and Agri-Food Canada, Guelph, ON, Canada

OPEN ACCESS

Edited by:

Hongyin Zhang,
Jiangsu University, China

Reviewed by:

Jinhe Bai,
U.S. Horticultural Research
Laboratory, United States
Zisheng Luo,
Zhejiang University, China

*Correspondence:

Hetong Lin
hetonglin@126.com;
hetonglin@163.com

Specialty section:

This article was submitted to
Food Microbiology,
a section of the journal
Frontiers in Microbiology

Received: 25 March 2018

Accepted: 11 June 2018

Published: 03 July 2018

Citation:

Chen Y, Lin H, Zhang S, Sun J, Lin Y,
Wang H, Lin M and Shi J (2018)
Phomopsis longanae Chi-Induced
Disease Development and Pericarp
Browning of Harvested Longan Fruit
in Association With Energy
Metabolism. *Front. Microbiol.* 9:1454.
doi: 10.3389/fmicb.2018.01454

Longan fruit is a popular subtropical fruit with a relatively short shelf life at room temperature mainly due to pericarp browning and fungal infection. This study aimed to investigate the infection of *Phomopsis longanae* Chi in longan fruit and its effects on the storability and shelf life of longan fruit. The relationship between the energy metabolism of harvested longan fruit and disease development and pericarp browning was elucidated. Results show that *P. longanae*-inoculation accelerated the deterioration of longan fruit and caused pericarp browning. It also led to the energy deficit in pericarp of longan fruit, which was reflected as lower contents of ATP and ADP, higher AMP content, and lower energy charge as compared to the control samples. Additionally, *P. longanae*-infection reduced the activities of H⁺-ATPase, Ca²⁺-ATPase, and Mg²⁺-ATPase in plasma, vacuolar, and mitochondrial membranes during the storage period. The results demonstrate that *P. longanae*-infection led to disease development and pericarp browning in harvested longan fruit, which were due to the infection-induced energy deficit and low ATPase activity that caused disorders of ion transport and distribution, and damaged the structure and function of vacuole, mitochondria, and eventually the whole cells of fruit tissues.

Keywords: longan (*Dimocarpus longan* Lour.) fruit, *Phomopsis longanae* Chi, disease development, pericarp browning, energy metabolism, ATP content, energy charge, ATPase

INTRODUCTION

Longan is a popular subtropical fruit with a short shelf life at room temperature mainly due to pericarp browning and fungal infection (Holcroft et al., 2005; Chen et al., 2014; Zhang et al., 2017, 2018). Growing evidence suggests that the fruit tissue browning and loss of disease resistance are related to physiological disorders commonly caused by various stresses that can induce functional and structural damages of cellular membrane system (Yi et al., 2010; Jin et al., 2014; Li et al., 2017; Pan et al., 2017). Pathogenic infection, among various stress conditions, is a critical factor that can damage cell membrane in different ways such as creating energy deficit, oxidative burst, and

alterations of membrane lipid compositions (Chen et al., 2014; Lin et al., 2017a; Sun et al., 2018; Zhang et al., 2018).

Membranes of plasma and organelles like vacuole and mitochondria are key components that contribute to cell integrity and prevent fruit tissue browning and disease development (Luo et al., 2012; Wang et al., 2016; Li D. et al., 2016; Lin Y.F. et al., 2016; Lin et al., 2017b, c, 2018). Plasma membrane is crucial for both cellular homeostasis and communications in extracellular environment (Olsen et al., 2009; Li D. et al., 2016). Whereas, vacuole and its membrane take part in regulating osmotic pressure, maintaining the homeostasis, and keeping internal phenolics from oxidase in cytoplasm which otherwise can lead to enzymatic browning (Holcroft et al., 2005; Anil et al., 2008; Lin et al., 2013, 2014, 2015, 2017b). Additionally, mitochondria play a foremost role in ATP production and thereby supply energy for normal life activities (Olsen et al., 2009; Lin et al., 2018), and the enzymes responsible for electron transfer and ATP synthesis are located on the inner membrane of mitochondria (Lin et al., 2017b, 2018). However, the regular function of the cell and these organelles depends on transmembrane transport of ions, in which active transport serves as an essential pathway with proton electrochemical potential gradient as a driving force (Morsomme and Boutry, 2000; Kasamo, 2003). Moreover, this driving force of transporting certain ions relies on energy from corresponding adenosine triphosphatase (ATPase) catalyzing ATP hydrolysis (Falhof et al., 2016). Previous literature indicated that hydrogen peroxide treatment could promote longan pericarp browning via decreasing the levels of ATP content and energy charge, and reducing activities of H^+ -ATPase, Ca^{2+} -ATPase and Mg^{2+} -ATPase in mitochondria, and damaging mitochondrial structure (Lin Y.X. et al., 2016; Lin et al., 2017b). In contrast, propyl gallate-retarded browning development in pericarp of harvested longans was resulted from retaining higher levels of ATP content and energy charge, as well as higher activities of mitochondrial ATPase (Lin et al., 2018). Furthermore, it was found that the acibenzolar-S-methyl treatment promoted the activities of Ca^{2+} -ATPase and H^+ -ATPase in pear fruit, which enhanced its disease resistance against blue mold induced by *Penicillium expansum*-inoculation (Ge et al., 2017). Thus, the pathogenic infection-induced tissue browning and the reduction of disease resistance on longan fruit might be related to the damage of biomembranes via influencing energy status and ATPase activity.

Phomopsis longanae Chi is a major pathogenic fungus of harvested longan fruit in Southern China (Chen et al., 2014). Previous studies have shown that inoculation with pathogenic fungi on harvested longan fruit could lead to severe pericarp browning and disease development, which might be in association with elevated cell membrane permeability and lowered energy level (Chen et al., 2014; Zhang et al., 2017). However, more information is needed regarding changes in energy status and their damage to cellular membrane via affecting ATPase activity in pathogen-infected longan fruit. Therefore, the main goals of this work were to study the effects of the *P. longanae* infection on ATP, ADP, AMP, energy charge, and activities of H^+ -ATPase, Ca^{2+} -ATPase, and Mg^{2+} -ATPase in plasma, vacuolar, and mitochondrial membranes in pericarp of longan fruit, and investigate the effects of *P. longanae* infection on the disease

development, pericarp browning, and the biomembrane damage of harvested longan fruit from a perspective of the changes in energy level and ATPase.

MATERIALS AND METHODS

Materials and Treatments

Phomopsis longanae culturing and the preparation of spore suspension were conducted according to Chen et al. (2014). The concentration of spore suspension was diluted to 1×10^4 spores mL^{-1} and used for inoculation.

"Fuyan" longan (*Dimocarpus longan* Lour. cv. Fuyan) fruit at commercial maturity were handpicked from a longan orchard (Quanzhou, Fujian, China). The harvested fruit were carefully packed and transported to a research laboratory in Fujian Agriculture and Forestry University within 3 h and stored at 4°C. Fruit in uniform maturity and size were selected for the experiment and any rotten or damaged fruit were excluded.

The fruit were washed with a sodium hypochlorite solution (0.5%) for 10 s to eliminate surface microorganisms, followed by being washed with sterile distilled water. The fruit samples were then air-dried. A total of 150 fruits were used for the analysis on harvest day (day 0). Another 3,000 longans were randomly divided into two groups (1,500 fruits each) for the following treatments: one group of 1,500 fruits was immersed in sterile deionised water for 5 min and defined as the control group, and the other group of 1,500 fruits was immersed in the *P. longanae* spore solution of 1×10^4 spores mL^{-1} for 5 min. All fruits were then air dried and packed in a polyethylene bag with a thickness of 0.015 mm. Each bag contained 50 longan fruits and 30 bags were used for each treatment. The samples were then stored at 28°C with a relative humidity of 90%. For each treatment, three bags of fruit (total 150 longan fruits) were randomly selected on a daily basis during the storage period and used for the assessments of longan fruit. All the evaluations were conducted in triplicate.

Assessments of the Index of Fruit Disease and Pericarp Browning

Longan fruit disease and pericarp browning were assessed based on our previous study (Chen et al., 2014). The lesion proportion on fruit surface of 50 individual longan fruits was measured and defined to five disease scales. The total browning area on inner pericarp of 50 selected longan fruits was measured and defined to six scales. The calculations of pericarp browning index and fruit disease index were performed based on the method of Chen et al. (2014).

Measurement of ATP, ADP, and AMP and Energy Charge

The content of ATP, ADP, and AMP, and the energy charge were determined with 5 g of pericarp tissue from 10 longan fruits based on a previous study (Chen et al., 2014), using a high-performance liquid chromatography (HPLC, LC-2030C, Shimadzu Corporation, Kyoto, Japan) equipped

with an ultraviolet detector and a Megres™ C18 column (4.6×250 mm). Energy charge was calculated by $(\text{ATP} + 1/2 \text{ADP})/(\text{ATP} + \text{ADP} + \text{AMP})$.

Assay of ATPase Activity

The activities of ATPase were measured following the methods of Lin et al. (2017b). Three enzymes (H^+ -ATPase, Ca^{2+} -ATPase, and Mg^{2+} -ATPase) from plasma membrane, vacuolar membrane and mitochondrial membrane were extracted respectively, from 1 g of pericarp tissue from 10 longan fruits. One unit of ATPase activity was considered as 1 μmol phosphorus released per minute at 660 nm. Bradford (1976) method was used to determine the protein content. The ATPase activity was expressed as U mg^{-1} protein.

Statistical Analyses

All experiments were repeated three times and data were acquired. The values in figures were expressed in the format of the mean values and standard errors. Analysis of variance (ANOVA) was used to analyze the data using the software (SPSS version 17.0). Student's *t*-test was used to compare the mean values of the data set. A *P*-value of less than or equal to 0.05 or 0.01 was considered statistically significant.

RESULTS

Effects of *P. longanae* Infection on Indices of Fruit Disease and Pericarp Browning of Harvested Longan Fruit

Figure 1A shows that the disease index of harvested longan fruit increased with extending storage time. The disease lesions on *P. longanae*-inoculated longans developed quickly with white mycelia growing on the exocarp. By day 5 of the storage, the fruit disease index was 0.91, and the whole longan pericarp was covered with white lesions made of hypha. However, fruit disease index in control longans went up slowly (day 5 = 0.4). Further comparison shows that fruit disease index of *P. longanae*-inoculated longans were significantly ($P < 0.01$) higher as compared to the control samples during the storage period.

Figure 1B indicates that the pericarp browning index increased gradually in the first 2 days of storage, and then increased rapidly in the following days for both control samples and inoculated longans. The results of statistical analysis demonstrate that the browning index of *P. longanae*-inoculated longans were significantly ($P < 0.01$) higher than that of the control samples for the same storage time.

Effects of *P. longanae* Infection on the Content of ATP, ADP, AMP, and Energy Charge in Pericarp of Harvested Longan Fruit

As shown in Figure 2A, the ATP content in longans pericarp went down with increasing storage time. After 1 day of storage, the pericarp ATP content of *P. longanae*-inoculated longans

displayed a drastic decrease from $29.2 \mu\text{g g}^{-1}$ (day 1) to $19.9 \mu\text{g g}^{-1}$ (day 5), while that of the control samples decreased slowly during the same storage period. On day 5 of the storage, the pericarp ATP content of control longans was 1.4 times higher than that of *P. longanae*-inoculated longans. Statistical analysis suggests that there was significant ($P < 0.01$) lower ATP content in the pericarp of *P. longanae*-inoculated longans than that of control fruit during storage day 1 to day 5.

Figure 2B illustrates that the ADP content in longans pericarp declined rapidly with increasing storage time. *P. longanae*-inoculated longans displayed lower content of pericarp ADP than the control longans during the whole storage period. After 5 days of storage, the ADP content in the pericarp of *P. longanae*-inoculated longans decreased from 10.85 to $2.52 \mu\text{g g}^{-1}$, while that of the control longans was at a value of $5.12 \mu\text{g g}^{-1}$. Statistical analysis indicates that there was significant ($P < 0.01$) lower pericarp ADP content in pericarp of *P. longanae*-inoculated longans from day 1 to day 5 of storage as compared to the control samples.

As shown in Figure 2C, the AMP content in pericarp of the control longans increased gradually in the whole storage period. Whereas, for the *P. longanae*-inoculated longans, it displayed a rapid rise during storage day 0 to day 1, changed slightly on storage day 2, followed by an increase from day 2 to day 5 of the storage. Further comparison reveals that the AMP content in pericarp of *P. longanae*-inoculated longans was significantly ($P < 0.01$) higher than that of control samples from the storage day 1 to day 5.

As displayed in Figure 2D, the energy charge in control longans decreased slowly as the storage time progressed, while that of the *P. longanae*-inoculated longans decreased much more quickly than the control longans. Further comparison shows that *P. longanae*-inoculated longan pericarp had significant ($P < 0.05$) lower energy charge than the control samples during storage period.

Effects of *P. longanae* Infection on H^+ -ATPase Activities in Membranes of Plasma, Vacuole and Mitochondria in Pericarp of Harvested Longan Fruit

Figure 3A illustrates that the H^+ -ATPase activity in plasma membrane of the control longans pericarp grew slightly in the first 2 days of the storage and then decreased; while in the *P. longanae*-inoculated longans fruit, it displayed a quick decrease during the first 4 days, followed with a sharp decline from the fourth to the fifth day. Further comparison shows that the plasma membrane H^+ -ATPase activity in pericarp of *P. longanae*-inoculated longans was significantly ($P < 0.01$) lower than that of the control samples during the whole storage period.

As shown in Figure 3B, H^+ -ATPase activity in vacuolar membrane of control longan pericarp increased quickly on the first day of storage, and then diminished gradually from the first day to day 5 of the storage. However, H^+ -ATPase activity in vacuolar membrane of *P. longanae*-inoculated longan pericarp exhibited a sharp decrease during storage. Further comparison demonstrates that the vacuolar membrane H^+ -ATPase activity

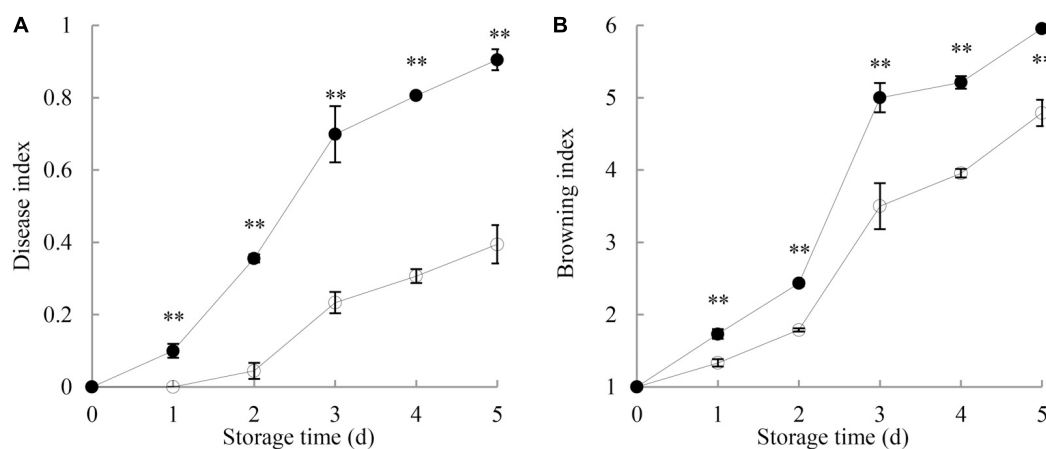


FIGURE 1 | Effects of *P. longanae* infection on fruit disease index (A) and pericarp browning index (B) of harvested longan fruit during storage at 28°C. The asterisks indicate significant difference between control and *P. longanae*-inoculated fruit (** $P < 0.01$). ○, control; ●, *P. longanae*-inoculation treatment.

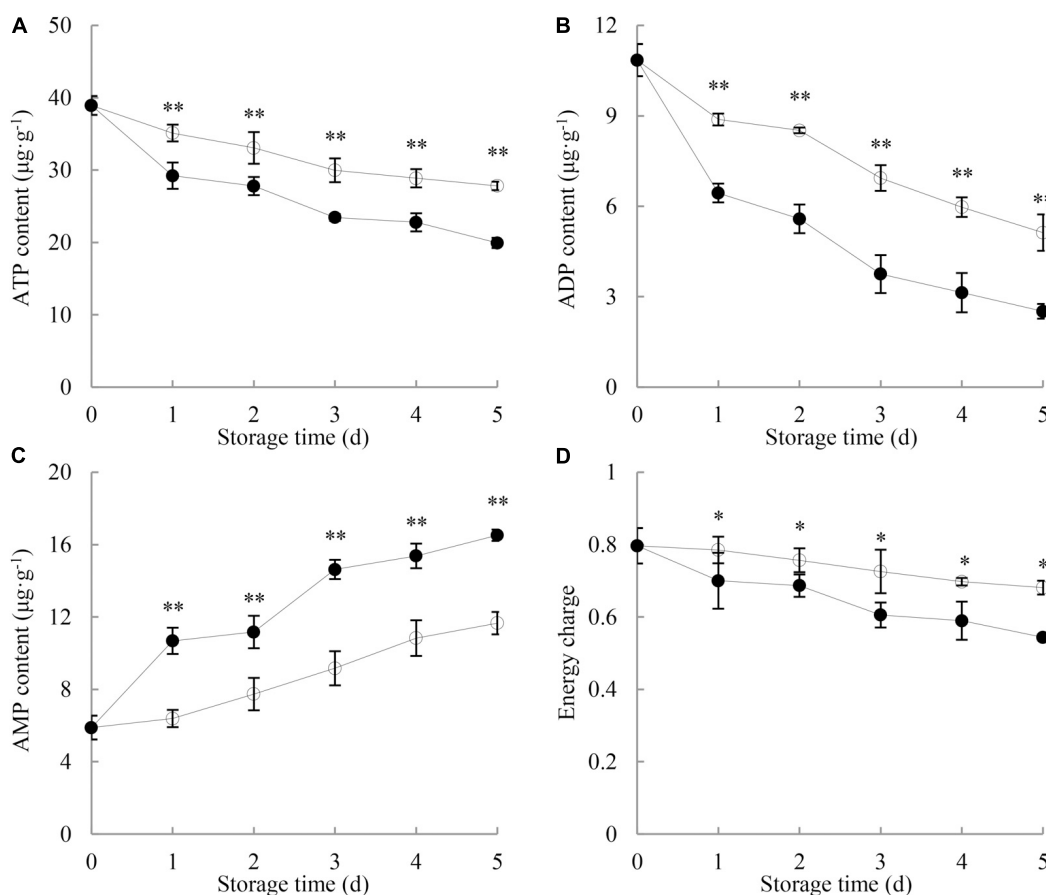


FIGURE 2 | Effects of *P. longanae* infection on ATP (A), ADP (B), and AMP (C) contents and energy charge (D) in pericarp of harvested longan fruit during storage at 28°C. The asterisks indicate significant difference between control and *P. longanae*-inoculated fruit (* $P < 0.05$, ** $P < 0.01$). ○, control; ●, *P. longanae*-inoculation treatment.

in pericarp of *P. longanae*-inoculated longans was significantly ($P < 0.01$) lower as compared with the control group in the whole storage period.

As shown in **Figure 3C**, H^+ -ATPase activity in mitochondrial membrane of control longan pericarp went up rapidly on the first day, then decreased slightly on the second day, and continued

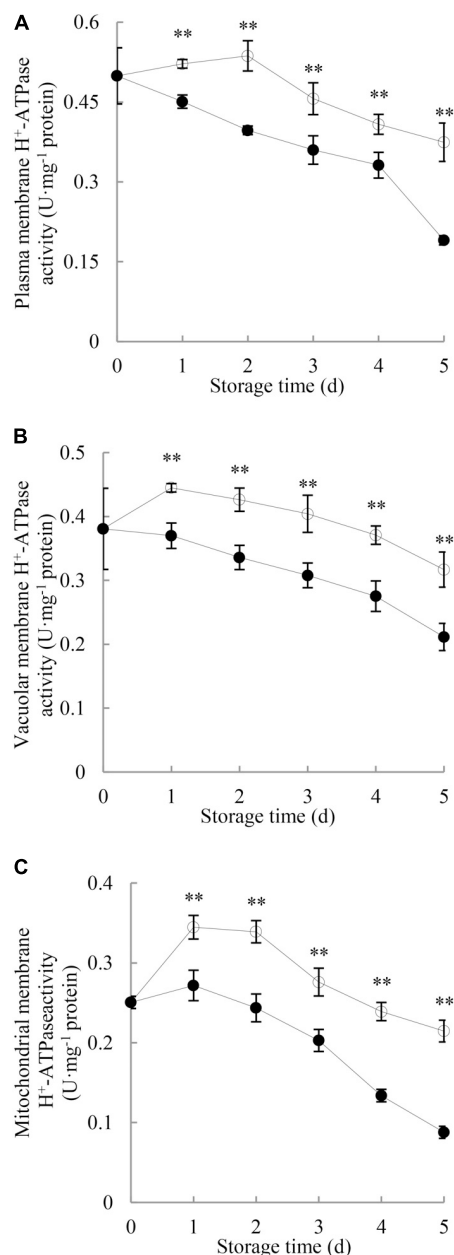


FIGURE 3 | Effects of *P. longanae* infection on activities of H⁺-ATPase in membranes of plasma (A), vacuole (B), and mitochondria (C) in pericarp of harvested longan fruit during storage at 28°C. The asterisks indicate significant difference between control and *P. longanae*-inoculated fruit (***P* < 0.01). ○, control; ●, *P. longanae*-inoculation treatment.

to drop rapidly to the last storage day. Whereas, the H⁺-ATPase activity in mitochondrial membrane of *P. longanae*-inoculated longan pericarp exhibited a mild increase on the first day of storage, and then diminished rapidly in the following days. Further statistical comparison indicates that H⁺-ATPase activity in mitochondrial membrane of pericarp of *P. longanae*-inoculated longans was significantly (*P* < 0.01) lower than that of the control samples from the first to the last day of storage.

Effects of *P. longanae* Infection on Ca²⁺-ATPase Activities in Membranes of Plasma, Vacuole and Mitochondria in Pericarp of Harvested Longan Fruit

As shown in Figure 4A, Ca²⁺-ATPase activity in plasma membrane of the control longan pericarp increased to a small degree during the first 2 days and then decreased gradually, while it declined as storage time progressed in the *P. longanae*-inoculated longan pericarp. Statistical analysis indicates that there were significant (*P* < 0.01) differences in the plasma membrane Ca²⁺-ATPase activities between the pericarp of *P. longanae*-inoculated and control fruit from day 2 to day 5.

As shown in Figure 4B, Ca²⁺-ATPase activity in vacuolar membrane of control longan pericarp increased from 0.37 U mg⁻¹ protein on day 0 of storage to a maximum value of 0.51 U mg⁻¹ protein on storage day 2, but then declined gradually to 0.38 U mg⁻¹ protein on storage day 5. Whereas, the *P. longanae*-inoculated longans showed a slow increase in the Ca²⁺-ATPase activity in vacuolar membrane in the first day of the storage period and then decreased. Statistical comparison suggests that there was significantly (*P* < 0.01) lower Ca²⁺-ATPase activity in vacuolar membrane of pericarp of the *P. longanae*-inoculated longans than that of the control samples during day 1 to day 5 of the storage.

The Ca²⁺-ATPase activity in mitochondrial membrane in longans pericarp (Figure 4C) followed a similar trend as Ca²⁺-ATPase activity in plasma membrane (Figure 4A), and the mitochondria membrane Ca²⁺-ATPase activity in pericarp of *P. longanae*-inoculated longans were notably (*P* < 0.01) lower than that of the control longans during the last 3 days of storage.

Effects of *P. longanae* Infection on Mg²⁺-ATPase Activities in the Membrane of Plasma, Vacuole and Mitochondria in Pericarp of Harvested Longan Fruit

As shown in Figure 5, changes in Mg²⁺-ATPase activity in the membranes of plasma, vacuole and mitochondria of pericarp during the entire period of storage were observed. The Mg²⁺-ATPase activity in membranes of plasma, vacuole and mitochondria of the pericarp of the control longans rose rapidly toward a maximum on day 2 and then declined. *P. longanae*-inoculated longans showed significant (*P* < 0.01) lower pericarp Mg²⁺-ATPase activity during the whole storage period than that of the control longans.

DISCUSSION

The Role of Energy Deficit in *P. longanae*-Induced Pericarp Browning and Disease Development of Harvested Longan Fruit

ATP generated from mitochondria is the most important energy source for life activities (Pan et al., 2017). In plant cells, ATP is used for the synthesis of fatty acids, phospholipids, and

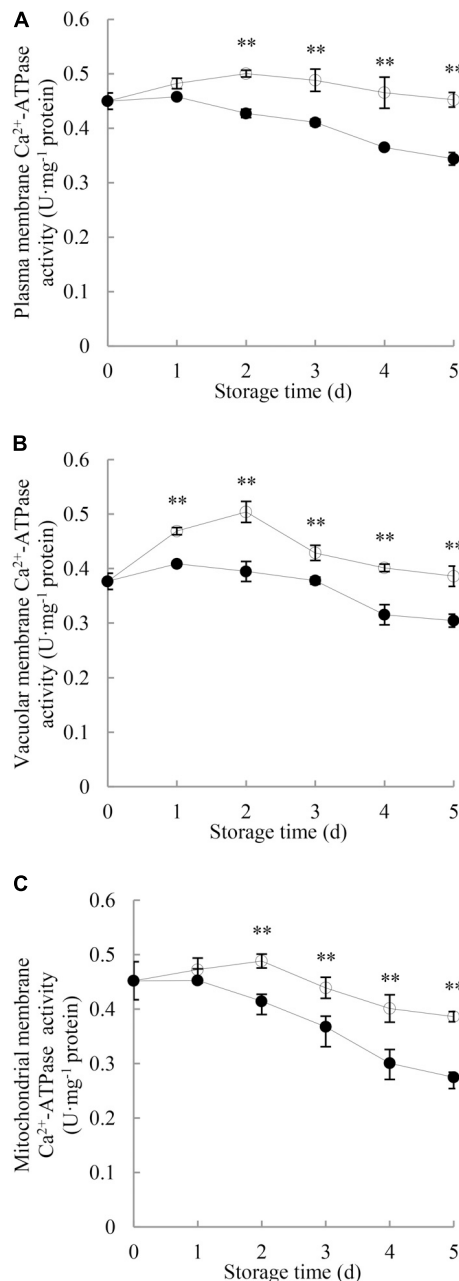


FIGURE 4 | Effects of *P. longanae* infection on activities of Ca^{2+} -ATPase in membranes of plasma (A), vacuole (B), and mitochondria (C) in pericarp of harvested longan fruit during storage at 28°C. The asterisks indicate significant difference between control and *P. longanae*-inoculated fruit (** $P < 0.01$). ○, control; ●, *P. longanae*-inoculation treatment.

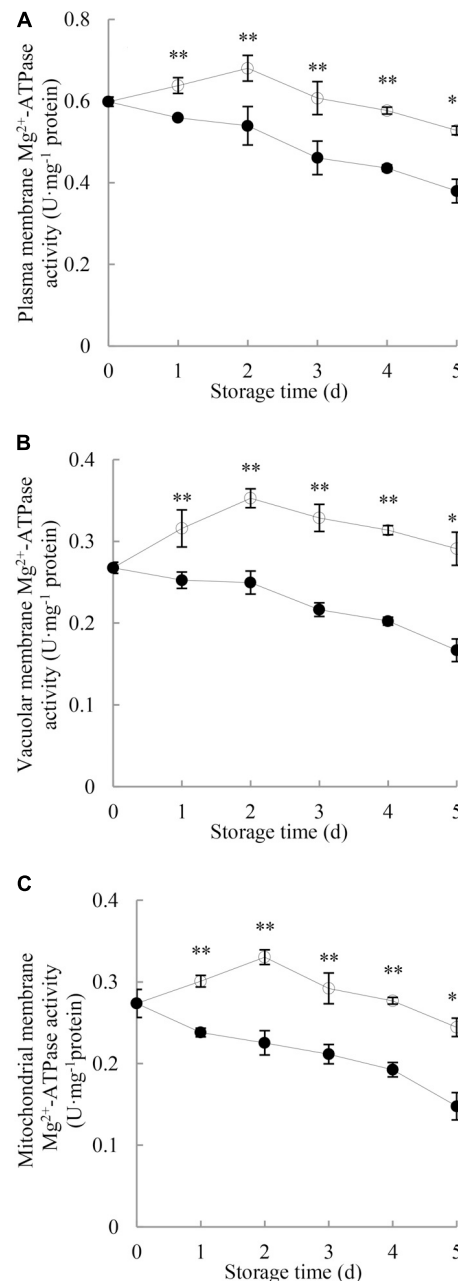


FIGURE 5 | Effects of *P. longanae* infection on activities of Mg^{2+} -ATPase in membranes of plasma (A), vacuole (B), and mitochondria (C) in pericarp of harvested longan fruit during storage at 28°C. The asterisks indicate significant difference between control and *P. longanae*-inoculated fruit (** $P < 0.01$). ○, control; ●, *P. longanae*-inoculation treatment.

proteins on membranes of the cell and organelles such as vacuole and mitochondria to help sustain their structure and regular function (Jin et al., 2014; Zhou et al., 2014). However, ATP synthesis and energy level of fruit can be reduced by postharvest stress conditions like pathogen infection via altering respiration pathway and inducing excessive accumulation of reactive oxygen species (ROS), which can weaken mitochondria

and result in energy deficit (Yi et al., 2008; Chen et al., 2014; Zhang et al., 2017). Recent studies indicated that the energy deficit was a critical factor leading to the damage of cellular membranes including decompartmentalization that conducted to enzymatic browning (Duan et al., 2004; Jiang et al., 2004; Jin et al., 2014; Lin Y.X. et al., 2016; Lin et al., 2017b). Other than membrane damage, insufficient

energy supply may give rise to the reduction of disease resistance by inactivating defensive responses like the synthesis of pathogenesis-related protein (Qu et al., 2008; Yi et al., 2009; Chen et al., 2014). Zhang et al. (2017, 2018) reported that *Lasiodiplodia theobromae*-infection could reduce the energy charge and damage the membrane structure in pericarp of inoculated longan fruit while aggravate disease progress and pericarp browning. Besides, exogenous ATP supply was beneficial for keeping membrane integrity to decrease pericarp browning and disease development of litchi and longan fruit (Song et al., 2006; Yi et al., 2008, 2009; Chen et al., 2015; Lin et al., 2017a).

The data acquired from this work indicate that *P. longanae*-inoculated longans showed drastic increase in the indices of pericarp browning and fruit disease with notably higher values as compared to the control samples during 5 days of storage (Figure 1). In the meanwhile, the energy charge and content of ATP and ADP in the pericarp of *P. longanae*-inoculated samples decreased quickly and were much lower than those of the control fruit (Figures 2A,B,D). The pericarp AMP content of inoculated longans exhibited an uptrend at relative higher levels with contrast to the control fruit throughout the storage period (Figure 2C). Correlation analysis suggests that there was an obvious inverse correlation between fruit disease index and both pericarp ATP content ($r = -0.919$, $P < 0.01$) and energy charge ($r = -0.963$, $P < 0.01$) in longans inoculated with *P. longanae*. The correlation analysis also denotes that the pericarp browning index were in an inverse correlation with ATP content ($r = -0.917$, $P < 0.05$) and energy charge ($r = -0.968$, $P < 0.01$) in pericarp of *P. longanae*-inoculated longans, respectively. However, the pericarp AMP content of inoculated longans was positively correlated with either fruit disease index ($r = 0.952$, $P < 0.01$) or pericarp browning index ($r = 0.955$, $P < 0.01$). These results provide convincing evidence that accelerated disease development and pericarp browning of inoculated longan fruit is closely associated with the infection-induced energy deficit. These findings were in agreement with our previous study (Chen et al., 2014).

The Role of ATPase in *P. longanae*-Induced Pericarp Browning and Disease Development of Harvested Longan Fruit

ATPase like H^+ -ATPase, Ca^{2+} -ATPase, and Mg^{2+} -ATPase take vital roles in botanic cellular homeostasis and physiological metabolisms as they are located in the membranes of cell and organelles such as mitochondria and vacuole, and catalyze ATP hydrolysis for transmembrane transport of corresponding ions and signal transmission (Elmore and Coaker, 2011; Wang et al., 2015; Liu et al., 2016; Falhof et al., 2016; Pan et al., 2017). The distribution of H^+ not only affects cellular pH value, but also is the key part of transmembrane electrochemical gradient and electrodynamic potential, which have great influence on various kinds of physiological activities, especially on the respiratory chain and ATP synthesis (Morsomme and Boutry, 2000; Olsen

et al., 2009; Falhof et al., 2016; Li P.Y. et al., 2016; Li et al., 2017). Ca^{2+} acts as the second-messenger in signals transmission, while transport and distribution disorders of Ca^{2+} might cause structural damage of cellular membranes and metabolic dysregulation (Muchhal et al., 1997; Li et al., 2017; Pan et al., 2017). In addition, Mg^{2+} acts as a cofactor in respiratory and energy metabolisms in fruit cells, and its disorder will conduce to peroxidation and oxidative stress (Tewari et al., 2006; Nozadze et al., 2015). Besides, balanced Ca^{2+} and Mg^{2+} distribution and transport are beneficial for keeping cellular osmotic pressure, which contributes to cell structural integrity (Wang et al., 2008; Li et al., 2017). Thus, the regular activity of ATPase can maintain the dynamic equilibrium of these ions and transmembrane electrochemical gradient to support the homeostasis and integrity of botanic cell, as well as physiological activities relating to disease-resistant responses (Wang et al., 2015; Lin et al., 2017b, 2018). However, the dysfunction of ATPase may break the endo-cellular homeostasis and damage plasma, vacuolar, and mitochondrial membranes, and thereby cause energy deficit and integrity loss, result in tissue browning and weakened disease resistance (Morsomme and Boutry, 2000; Anil et al., 2008; Jin et al., 2014; Shi et al., 2015; Li et al., 2017; Pan et al., 2017). Furthermore, the change in ATPase activity of harvested fruit might be associated with energy status and pathogenic stress. Wang et al. (2008) reported that the depletion of ATP was associated with pathogen infection in the *Phylospora piricola* Nose-inoculated “Ya” pear fruit, and the activity of Ca^{2+} -ATPase in pulp of inoculated pears declined and the decline rate was faster than the control (Wang et al., 2008). Treatment with nitric oxide maintained higher activities of Ca^{2+} -ATPase in harvested peach fruit during storage, which was in association with the inhibition on disease development of *Monilinia fructicola*-inoculated fruit (Shi et al., 2015).

This study shows that compared with the control longan fruit, the H^+ -ATPase, Ca^{2+} -ATPase, Mg^{2+} -ATPase activities in *P. longanae*-inoculated longan fruit were lower and reduced continually during the storage (Figures 3–5), as the indices of fruit disease and pericarp browning kept increasing with higher values (Figure 1) and the pericarp ATP content and energy charge declined gradually to lower levels (Figures 2A,D). The results indicate that the accelerated pericarp browning and loss of disease resistance of longan fruit during storage could be attributed to energy deficit and inactivity of ATPase. The low H^+ -ATPase activity caused by infection and energy deficit could induce cellular pH value turbulence to threaten homeostasis. Besides, it could also lower ATP synthesis in turn via reducing the proton electrochemical gradient, which was in accordance with the decrease in ATP content in pericarp of *P. longanae*-inoculated fruit as illustrated in Figure 2A. Furthermore, the energy deficit and decreased activities of Ca^{2+} -ATPase and Mg^{2+} -ATPase led to incapability of pumping out redundant Ca^{2+} and Mg^{2+} from cytoplasm or transferring them to vacuole and mitochondria. This contributed to the disequilibrium of Ca^{2+} and Mg^{2+} distribution either in cytoplasm or between endo-cellular

and extracellular environment, resulting in disturbed calcium messenger system, respiratory metabolism, and transmembrane osmotic pressure. These disorders aggravated the energy deficit and the homeostasis by damaging the structure of vacuole, mitochondria, and the whole cell, which jointly conducted to the pericarp browning and loss of disease resistance of *P. longanae*-inoculated longan fruit.

CONCLUSION

In summary, this work demonstrate that *P. longanae*-inoculation could reduce the ATP and ADP content, but increase AMP content, and thereby lower the energy charge, cause energy deficit in pericarp of *P. longanae*-infected longans. Consequently, the activities of H^+ -ATPase, Ca^{2+} -ATPase, and Mg^{2+} -ATPase in the membrane of plasma, vacuole, and mitochondria decreased, which aggravated the structural and functional damage of cellular biomembrane system and energy deficit, leading to disease development and pericarp browning of *P. longanae* -infected longan fruit.

REFERENCES

- Anil, V. S., Rajkumar, P., Kumar, P., and Mathew, M. K. (2008). A Plant Ca^{2+} pump, ACA2, relieves salt hypersensitivity in yeast. *J. Biol. Chem.* 283, 3497–3506. doi: 10.1074/jbc.M700766200
- Bradford, M. M. (1976). A rapid and sensitive method for the quantitation of microgram quantities of protein utilizing the principle of protein-dye binding. *Anal. Biochem.* 72, 248–254. doi: 10.1016/0003-2697(76)90527-3
- Chen, M. Y., Lin, H. T., Zhang, S., Lin, Y. F., Chen, Y. H., and Lin, Y. X. (2015). Effects of adenosine triphosphate (ATP) treatment on postharvest physiology, quality and storage behavior of longan fruit. *Food Bioprocess Technol.* 8, 971–982. doi: 10.1007/s11947-014-1462-z
- Chen, Y. H., Lin, H. T., Jiang, Y. M., Zhang, S., Lin, Y. F., and Wang, Z. H. (2014). *Phomopsis longanae* Chi-induced pericarp browning and disease development of harvested longan fruit in association with energy status. *Postharvest Biol. Technol.* 93, 24–28. doi: 10.1016/j.postharvbio.2014.02.003
- Duan, X. W., Jiang, Y. M., Su, X. G., Liu, H., Li, Y. B., Zhang, Z. Q., et al. (2004). Role of pure oxygen treatment in browning of litchi fruit after harvest. *Plant Sci.* 167, 665–668. doi: 10.1016/j.plantsci.2004.05.009
- Elmore, J. M., and Coaker, G. (2011). The role of the plasma membrane H^+ -ATPase in plant-microbe interactions. *Mol. Plant.* 4, 416–427. doi: 10.1093/mp/ssf083
- Falhof, J., Pedersen, J. T., Fuglsang, A. T., and Palmgren, M. (2016). Plasma membrane H^+ -ATPase regulation in the center of plant physiology. *Mol. Plant.* 9, 323–337. doi: 10.1016/j.molp.2015.11.002
- Ge, Y. H., Wei, M. L., Li, C. Y., Chen, Y. R., Lv, J. Y., and Li, J. R. (2017). Effect of acibenzolar-S-methyl on energy metabolism and blue mould of nanguo pear fruit. *Sci. Hortic.* 225, 221–225. doi: 10.1016/j.scienta.2017.07.012
- Holcroft, D. M., Lin, H. T., and Ketsa, S. (2005). "Harvesting and storage," in *Litchi and Longan: Botany, Production and Uses*, eds C. M. Menzel and G. K. Waite (Wallingford: CAB International), 273–295. doi: 10.1079/9780851996967.0273
- Jiang, Y. M., Duan, X. W., Joyce, D., Zhang, Z. Q., and Li, J. R. (2004). Advances in understanding of enzymatic browning in harvested litchi fruit. *Food Chem.* 88, 443–446. doi: 10.1016/j.foodchem.2004.02.004
- Jin, P., Zhu, H., Wang, L., Shan, T. M., and Zheng, Y. H. (2014). Oxalic acid alleviates chilling injury in peach fruit by regulating energy metabolism and fatty acid contents. *Food Chem.* 161, 87–93. doi: 10.1016/j.foodchem.2014.03.103
- Kasamo, K. (2003). Regulation of plasma membrane H^+ -ATPase activity by the membrane environment. *J. Plant Res.* 116, 517–523. doi: 10.1007/s10265-003-0112-8
- Li, D., Li, L., Ge, Z. W., Limwachiranon, J., Ban, Z. J., Yang, D. M., et al. (2017). Effects of hydrogen sulfide on yellowing and energy metabolism in broccoli. *Postharvest Biol. Technol.* 129, 136–142. doi: 10.1016/j.postharvbio.2017.03.017
- Li, D., Limwachiranon, J., Li, L., Du, R. X., and Luo, Z. S. (2016). Involvement of energy metabolism to chilling tolerance induced by hydrogen sulfide in cold-stored banana fruit. *Food Chem.* 208, 272–278. doi: 10.1016/j.foodchem.2016.03.113
- Li, P. Y., Yin, F., Song, L. J., and Zheng, X. L. (2016). Alleviation of chilling injury in tomato fruit by exogenous application of oxalic acid. *Food Chem.* 202, 125–132. doi: 10.1016/j.foodchem.2016.01.142
- Lin, Y. F., Hu, Y. H., Lin, H. T., Liu, X., Chen, Y. H., Zhang, S., et al. (2013). Inhibitory effects of propyl gallate on tyrosinase and its application in controlling pericarp browning of harvested longan fruits. *J. Agric. Food Chem.* 61, 2889–2895. doi: 10.1021/jf305481h
- Lin, Y. F., Chen, M. Y., Lin, H. T., Hung, Y. C., Lin, Y. X., Chen, Y. H., et al. (2017a). DNP and ATP induced alteration in disease development of *Phomopsis longanae* Chi-inoculated longan fruit by acting on energy status and reactive oxygen species production-scavenging system. *Food Chem.* 228, 497–505. doi: 10.1016/j.foodchem.2017.02.045
- Lin, Y. F., Lin, H. T., Lin, Y. X., Zhang, S., Chen, Y. H., and Jiang, X. J. (2016). The roles of metabolism of membrane lipids and phenolics in hydrogen peroxide-induced pericarp browning of harvested longan fruit. *Postharvest Biol. Technol.* 111, 53–61. doi: 10.1016/j.postharvbio.2015.07.030
- Lin, Y. F., Lin, H. T., Zhang, S., Chen, Y. H., Chen, M. Y., and Lin, Y. X. (2014). The role of active oxygen metabolism in hydrogen peroxide-induced pericarp browning of harvested longan fruit. *Postharvest Biol. Technol.* 96, 42–48. doi: 10.1016/j.postharvbio.2014.05.001
- Lin, Y. F., Lin, Y. X., Lin, H. T., Chen, Y. H., Wang, H., and Shi, J. (2018). Application of propyl gallate alleviates pericarp browning in harvested longan fruit by modulating metabolisms of respiration and energy. *Food Chem.* 240, 863–869. doi: 10.1016/j.foodchem.2017.07.118
- Lin, Y. F., Lin, Y. X., Lin, H. T., Ritenour, M. A., Shi, J., Zhang, S., et al. (2017b). Hydrogen peroxide-induced pericarp browning of harvested longan fruit in association with energy metabolism. *Food Chem.* 225, 31–36. doi: 10.1016/j.foodchem.2016.12.088
- Lin, Y. F., Lin, Y. X., Lin, H. T., Shi, J., Chen, Y. H., and Wang, H. (2017c). Inhibitory effects of propyl gallate on membrane lipids metabolism and its

AUTHOR CONTRIBUTIONS

YC and HL designed the research. SZ, JS, YL, and HW conducted the experiments and analyzed the data. YC and SZ wrote the manuscript. HL revised the manuscript. ML and JS edited English language of the manuscript. All authors have approved the submission and publication of the manuscript.

FUNDING

This work was supported by the National Natural Science Foundation of China (Grant Nos. 31772035, 31671914, and 31171776), the Natural Science Foundation of Fujian Province of China (Grant No. 2017J01429), the Construction Projects of Top University at Fujian Agriculture and Forestry University of China (Grant No. 612014042), the Science Fund for Distinguished Young Scholars at Fujian Province University of China (Grant No. KLa16036A), and the Science Fund for Distinguished Young Scholars at Fujian Agriculture and Forestry University of China (Grant No. XJQ201512).

- relation to increasing storability of harvested longan fruit. *Food Chem.* 217, 133–138. doi: 10.1016/j.foodchem.2016.08.065
- Lin, Y. F., Lin, Y. X., Lin, H. T., Zhang, S., Chen, Y. H., and Shi, J. (2015). Inhibitory effects of propyl gallate on browning and its relationship to active oxygen metabolism in pericarp of harvested longan fruit. *LWT Food Sci. Technol.* 60, 1122–1128. doi: 10.1016/j.lwt.2014.10.008
- Lin, Y. X., Lin, Y. F., Chen, Y. H., Wang, H., Shi, J., and Lin, H. T. (2016). Hydrogen peroxide induced changes in energy status and respiration metabolism of harvested longan fruit in relation to pericarp browning. *J. Agric. Food Chem.* 64, 4627–4632. doi: 10.1021/acs.jafc.6b01430
- Liu, Z. L., Li, L., Luo, Z. S., Zeng, F. F., Jiang, L., and Tang, K. C. (2016). Effect of brassinolide on energy status and proline metabolism in postharvest bamboo shoot during chilling stress. *Postharvest Biol. Technol.* 111, 240–246. doi: 10.1016/j.postharvbio.2015.09.016
- Luo, Z. S., Wu, X., Xie, Y., and Chen, C. (2012). Alleviation of chilling injury and browning of postharvest bamboo shoot by salicylic acid treatment. *Food Chem.* 131, 456–461. doi: 10.1016/j.foodchem.2011.09.007
- Morsomme, P., and Boutry, M. (2000). The plant plasma membrane H^+ -ATPase: structure, function and regulation. *Biochim. Biophys. Acta.* 1465, 1–16. doi: 10.1016/S0005-2736(00)00128-0
- Muchhal, U. S., Liu, C. M., and Raghothama, K. G. (1997). Ca^{2+} -ATPase is expressed differentially in phosphate-starved roots of tomato. *Physiol. Plant.* 101, 540–544. doi: 10.1111/j.1399-3054.1997.tb01035.x
- Nozadze, E., Arutinova, N., Tsakadze, L., Shiozhvili, L., Leladze, M., Dzenladze, S., et al. (2015). Molecular mechanism of Mg-ATPase activity. *J. Membr. Biol.* 248, 295–300. doi: 10.1007/s00232-014-9769-2
- Olsen, L. F., Andersen, A. Z., Lunding, A., Brasen, J. C., and Poulsen, A. K. (2009). Regulation of glycolytic oscillations by mitochondrial and plasma membrane H^+ -ATPases. *Biophys. J.* 96, 3850–3861. doi: 10.1016/j.bpj.2009.02.026
- Pan, Y. G., Yuan, M. Q., Zhang, W. M., and Zhang, Z. K. (2017). Effect of low temperatures on chilling injury in relation to energy status in papaya fruit during storage. *Postharvest Biol. Technol.* 125, 181–187. doi: 10.1016/j.postharvbio.2016.11.016
- Qu, H. X., Yi, C., and Jiang, Y. M. (2008). Loss of pathogen resistance by harvested horticultural crops. *Stewart Postharvest Rev.* 4, 1–4. doi: 10.2212/spr.2008.2.4
- Shi, J. Y., Liu, N., Gu, R. X., Zhu, L. Q., Zhang, C., Wang, Q. G., et al. (2015). Signals induced by exogenous nitric oxide and their role in controlling brown rot disease caused by *Monilinia fructicola* in postharvest peach fruit. *J. Gen. Plant Pathol.* 81, 68–76. doi: 10.1007/s10327-014-0562-y
- Song, L. L., Jiang, Y. M., Gao, H. Y., Li, C. T., Liu, H., You, Y. L., et al. (2006). Effects of adenosine triphosphate on browning and quality of harvested litchi fruit. *Am. J. Food Technol.* 1, 173–178. doi: 10.3923/ajft.2006.173.178
- Sun, J. Z., Lin, H. T., Zhang, S., Lin, Y. F., Wang, H., Lin, M. S., et al. (2018). The roles of ROS production-scavenging system in *Lasiodiplodia theobromae* (Pat.) Griff. & Maubl.-induced pericarp browning and disease development of harvested longan fruit. *Food Chem.* 247, 16–22. doi: 10.1016/j.foodchem.2017.12.017
- Tewari, R. K., Kumar, P., and Sharma, P. N. (2006). Magnesium deficiency induced oxidative stress and antioxidant responses in mulberry plants. *Sci. Hortic.* 108, 7–14. doi: 10.1016/j.scienta.2005.12.006
- Wang, Y. N., Wang, G. X., Liang, L. S., and Zhao, X. F. (2008). Effects of low temperature and pathogen stress during storage periods on pear fruit pulp ATP contents, H^+ -ATPase and Ca^{2+} -ATPase activity. *Sci. Silvae Sin.* 44, 72–76. doi: 10.3321/j.issn:1001-7488.2008.12.013
- Wang, Y. S., Luo, Z. S., Khan, Z. U., Mao, L. C., and Ying, T. J. (2015). Effect of nitric oxide on energy metabolism in postharvest banana fruit in response to chilling stress. *Postharvest Biol. Technol.* 108, 21–27. doi: 10.1016/j.postharvbio.2015.05.007
- Wang, Y. S., Luo, Z. S., Mao, L. C., and Ying, T. J. (2016). Contribution of polyamines metabolism and GABA shunt to chilling tolerance induced by nitric oxide in cold-stored banana fruit. *Food Chem.* 197, 333–339. doi: 10.1016/j.foodchem.2015.10.118
- Yi, C., Jiang, Y. M., Shi, J., Qu, H. X., Duan, X. W., Yang, B., et al. (2009). Effect of adenosine triphosphate on changes of fatty acids in harvested litchi fruit infected by *Peronophythora litchii*. *Postharvest Biol. Technol.* 54, 159–164. doi: 10.1016/j.postharvbio.2009.06.008
- Yi, C., Jiang, Y. M., Shi, J., Qu, H. X., Xue, S., Duan, X. W., et al. (2010). ATP-regulation of antioxidant properties and phenolics in litchi fruit during browning and pathogen infection process. *Food Chem.* 118, 42–47. doi: 10.1016/j.foodchem.2009.04.074
- Yi, C., Qu, H. X., Jiang, Y. M., Shi, J., Duan, X. W., Joyce, D. C., et al. (2008). ATP-induced changes in energy status and membrane integrity of harvested litchi fruit and its relation to pathogen resistance. *J. Phytopathol.* 156, 365–371. doi: 10.1111/j.1439-0434.2007.01371.x
- Zhang, S., Lin, H. T., Lin, Y. F., Lin, Y. X., Hung, Y. C., Chen, Y. H., et al. (2017). Energy status regulates disease development and respiratory metabolism of *Lasiodiplodia theobromae* (Pat.) Griff. & Maubl.-infected longan fruit. *Food Chem.* 231, 238–246. doi: 10.1016/j.foodchem.2017.03.132
- Zhang, S., Lin, Y. Z., Lin, H. T., Lin, Y. X., Chen, Y. H., Wang, H., et al. (2018). *Lasiodiplodia theobromae* (Pat.) Griff. & Maubl.-induced disease development and pericarp browning of harvested longan fruit in association with membrane lipids metabolism. *Food Chem.* 244, 93–101. doi: 10.1016/j.foodchem.2017.10.020
- Zhou, Q., Zhang, C. L., Cheng, S. C., Wei, B. D., Liu, X. J., and Ji, S. J. (2014). Changes in energy metabolism accompanying pitting in blueberries stored at low temperature. *Food Chem.* 164, 493–501. doi: 10.1016/j.foodchem.2014.05.063

Conflict of Interest Statement: The authors declare that the research was conducted in the absence of any commercial or financial relationships that could be construed as a potential conflict of interest.

Copyright © 2018 Chen, Lin, Zhang, Sun, Lin, Wang, Lin and Shi. This is an open-access article distributed under the terms of the Creative Commons Attribution License (CC BY). The use, distribution or reproduction in other forums is permitted, provided the original author(s) and the copyright owner(s) are credited and that the original publication in this journal is cited, in accordance with accepted academic practice. No use, distribution or reproduction is permitted which does not comply with these terms.



Effect of β -Aminobutyric Acid on Disease Resistance Against *Rhizopus* Rot in Harvested Peaches

Jing Wang¹, Shifeng Cao², Lei Wang³, Xiaoli Wang⁴, Peng Jin¹ and Yonghua Zheng^{1*}

¹ College of Food Science and Technology, Nanjing Agricultural University, Nanjing, China, ² College of Biological and Environmental Sciences, Zhejiang Wanli University, Ningbo, China, ³ College of Agriculture, Liaocheng University, Liaocheng, China, ⁴ School of Life Science and Food Engineering, Huaiyin Institute of Technology, Huai'an, China

OPEN ACCESS

Edited by:

Hongyin Zhang,
Jiangsu University, China

Reviewed by:

Hetong Lin,
Fujian Agriculture and Forestry
University, China
Carlos R. Figueroa,
University of Talca, Chile

*Correspondence:

Yonghua Zheng
zhengyh@njau.edu.cn

Specialty section:

This article was submitted to
Food Microbiology,
a section of the journal
Frontiers in Microbiology

Received: 31 March 2018

Accepted: 18 June 2018

Published: 10 July 2018

Citation:

Wang J, Cao S, Wang L, Wang X,
Jin P and Zheng Y (2018) Effect
of β -Aminobutyric Acid on Disease
Resistance Against *Rhizopus* Rot
in Harvested Peaches.
Front. Microbiol. 9:1505.
doi: 10.3389/fmicb.2018.01505

The effect of β -aminobutyric acid (BABA) on *Rhizopus* rot produced by *Rhizopus stolonifer* in harvested peaches and the possible action modes were investigated. Treatment with 50 mmol L⁻¹ of BABA resulted in significantly lower lesion diameter and disease incidence compared with the control. The activities of defense-related enzymes chitinase and β -1,3-glucanase were notably enhanced by this treatment. Meanwhile, BABA treatment also increased lignin accumulation and maintained higher energy status in peaches by enhancing activities of enzymes in the phenylpropanoid and energy metabolism pathways. Semiquantitative reverse transcription PCR results indicated that the transcription of four defense-related genes was substantially and rapidly enhanced only in that BABA-treated fruit upon inoculation with the pathogen. Thus, our results demonstrated that BABA was effective on controlling *Rhizopus* rot by inducing disease resistance, which includes the increase in gene transcription and activity of defense-related enzymes, the enhancement of cell wall strength, and the maintenance of high energy status in *Prunus persica* fruit. Moreover, the disease resistance induced by BABA was demonstrated through priming model rather than direct induction.

Keywords: *Prunus persica* fruit, β -aminobutyric acid, *Rhizopus stolonifer*, induced resistance, energy status

INTRODUCTION

Peaches [*Prunus persica* (L.) Batsch] suffer a short shelf life at room temperature after harvest, due to their rapid ripening and high susceptibility to pathogens, including *Rhizopus stolonifer* Ehrenb.: Fr., *Monilinia* spp., *Botrytis cinerea* Pers.: Er., and *Penicillium expansum* Link (Usall et al., 2015). Among these diseases, it is reported that *Rhizopus* rot caused by *R. stolonifer* is the most destructive disease in post-harvest stone fruit including peaches in China (Fan and Tian, 2000). In order to enhance disease resistance and extend shelf life of peaches, a number of physical or chemical treatments such as methyl jasmonate (MeJA; Jin et al., 2009), heat (Liu et al., 2012), high oxygen (Wang et al., 2005), and benzo-(1,2,3)-thiadiazole-7-carbothioic acid *S*-methyl ester (BTH; Liu et al., 2005; Cao et al., 2011) have been explored.

In general, energy plays an important role in maintaining membrane integrity, which is essential to plant cells. When plants are suffered from extreme or sustained energy deficiency, membrane damage cannot be repaired, and cells, tissues, or entire plants subsequently will die (De Block et al., 2005). It is well known that biotic and abiotic stresses result in great energy depletion, which is associated with the reduction of disease resistance (Jiang et al., 2007; Yi et al., 2010; Chen et al., 2014). Therefore, maintaining a high-energy status is essential in disease resistance.

It has been reported that the application of exogenous adenosine triphosphate (ATP) improved the energy status of litchi fruit and suppressed disease development caused by *Peronophythora litchii* (Yi et al., 2008). Cao et al. (2014) also found that the maintenance of ATP content was an important mechanism by which MeJA treatment induced disease resistance in post-harvest loquat fruit.

Defense priming in plants was first noted in 1933 and was initially termed as “sensitization” (Chester, 1933). Recently, priming is considered as a common phenomenon that plants do not exhibit any detectable defense responses after treatment with a priming inducing agent; however, a faster and stronger activation of defense responses is initiated only after they have been subjected to a subsequent stress (Conrath et al., 2002, 2006; Conrath, 2011). Recent studies showed that elicitors such as *Bacillus cereus* AR156 (Wang et al., 2013b; Wang X.L. et al., 2014) and MeJA (Wang et al., 2015; Saavedra et al., 2017) primed disease resistance in post-harvest fruits, thereby resulting in faster and stronger defense responses against pathogens. The small molecule β -aminobutyric acid (BABA), which is considered as a potential chemical inducer of disease resistance, has been investigated for many years (Thevenet et al., 2017). Previous reports demonstrated that the application of BABA treatment induced local or systemic resistance against various plant pathogens (Justyna and Ewa, 2013; Thevenet et al., 2017). Moreover, it has been shown that BABA can induce disease resistance and suppress disease incidence in a number of post-harvest fruits. For instance, BABA treatment induced disease resistance and reduced blue mold rot caused by *P. expansum* in grapefruit (Porat et al., 2003) and apples (Quaglia et al., 2011; Zhang et al., 2011), and the anthracnose rot caused by *Colletotrichum gloeosporioides* in mangoes (Zhang et al., 2013). However, no study has evaluated the efficacy of BABA against *Rhizopus* rot in peaches. In addition, it is unclear whether priming is a common phenomenon in BABA-induced resistance. Thus, our aims were to assess the effect of BABA on controlling *Rhizopus* rot caused by *R. stolonifer* in peaches after harvest and to investigate possible mechanistic models involved in disease resistance.

MATERIALS AND METHODS

Pathogen

Rhizopus stolonifer was purified from infected peaches and cultured at 26°C on potato dextrose agar (PDA) medium for 2 weeks. The petri dishes were flushed with sterile distilled water with Tween 80 (0.05%) to collect *R. stolonifer* spores, and adjust the suspension to 1×10^5 spores per milliliter with water described above. The spore suspension was maintained at 4°C for no more than 2 h prior to use.

Plant Material and Treatments

Peaches [*P. persica* (L.) Batsch cv. Baifeng] were picked in a commercial garden (latitude 32°02'N; longitude 118°51'E) in Nanjing, Jiangsu province, at the firm-mature stage (Fernández-Trujillo et al., 1998) and transported to the laboratory within

2 h. In the laboratory, fruit free of wounds and rot were selected for homogeneous size, color, and maturity stage and divided randomly into four groups for four treatments: Mock, BABA, Inoculation, and BABA + Inoculation. The fruit was sterilized with 70% ethanol around the fruit equator and air-dried for 1 h prior to wounding.

Each peach was punched on two sides around the equatorial section with a sterilized nail to create two uniform wounds (2 mm wide and 4 mm deep). For the Mock and Inoculation groups, 30 μ L of sterile distilled water was injected into each hole. For the BABA and BABA + Inoculation groups, the fruit were injected with 30 μ L of 50 mmol L⁻¹ BABA (Sigma, St. Louis, MO, United States). This specific concentration was chosen according to our preliminary experiment, which indicated that 50 mmol L⁻¹ BABA was the most effective concentration comparing to the ones at 5 and 100 mmol L⁻¹. The fruit were air-dried and placed in 330 mm \times 220 mm \times 60 mm plastic containers at 20°C. Six hours later, the Inoculation and BABA + Inoculation groups were challenge-inoculated with 15 μ L of a *R. stolonifer* spore suspension (1×10^5 spores per mL) in each wound. All peaches then were stored at 20°C for 60 h to allow for disease development. Three replicates of 48 fruit each were used per treatment, and eight fruit from each replicate were used at each time point for different analyses.

To investigate the efficacy of BABA on controlling *Rhizopus* rot caused by *R. stolonifer* infection in harvested peaches and its relation to disease resistance induction by BABA, disease incidence, and lesion diameter on each fruit wound were observed at 12, 24, 36, 48, and 60 h post inoculation in the Inoculation and BABA + Inoculation groups. Meanwhile, fruit flesh tissue from these two groups was collected within 10 mm around decay area by freezing in liquid nitrogen and storing at -20°C for lignin content, energy status, and enzyme assays.

For further revealing whether the BABA induced disease resistance against *Rhizopus* rot is associated with priming of defense responses in peaches, fruit samples from all the four groups were collected at 3, 6, 12, and 24 h post inoculation within 10 mm around decay area in pathogen challenged fruit (Inoculation and BABA + Inoculation) or equal position of healthy area in pathogen-free fruit (Mock and BABA) at the equator of peach fruit. Semiquantitative reverse transcription PCR (RT-PCR) was used to analyze the expression patterns of the four defense-related genes β -1,3-glucanase (*GNS*), chitinase (*CHI*), non-expressor of pathogenesis-related protein1 (*NPR1-like*), and pathogenesis-related protein (*PR-like*).

Evaluation of Decay

Eight fruit from each triplicate were used for decay evaluation at each time point. Fruit with a visibly diseased area more than 1 mm wide around the wound were considered decayed. Lesion diameter was measured using a vernier caliper. Disease incidence was determined according to the following formula:

$$\text{Disease incidence (\%)} = \frac{\text{decayed fruits}}{\text{total fruits}} \times 100\%$$

Enzyme Assays

A crude enzyme extracted from 1 g of frozen flesh tissue with 50 mmol L⁻¹ of sodium acetate buffer for detecting β -1,3-glucanase (GLU) and chitinase (CHI) activities was prepared. GLU and CHI activity was determined referred to the procedure of Abeles et al. (1971). One unit of GLU activity was expressed as the increase in absorbance of 0.001 at 540 nm. One unit of CHI activity was expressed by the production of 1 mg glucose per minute.

Phenylalanine ammonia lyase (PAL) activity was evaluated according to Cheng and Breen (1991) with some modification. One unit of PAL activity is defined as the quantity of enzyme that causes a 0.01 increase in absorbance at 290 nm in 1 h. 4-Coumaryl CoA ligase (4CL) activity was assayed as the protocol of Knobloch and Hahlbrock (1977). The activity of 4CL is determined as the quantity of enzyme that resulted in a 0.01 increase in absorbance per minute. Cinnamate 4-hydroxy (C4H) activity was evaluated as the protocol of Lamb and Rubery (1975). We measured 4-hydroxy-*trans*-cinnamic acid production by the absorbance at 340 nm compared to a reference extract containing *trans*-cinnamic acid that was measured using the same procedure.

Five grams of fruit flesh was homogenized with 10 mL Tris-HCl buffer (pH 7.5) and filtered with four-layer nylon gauze. The homogenate was centrifuged at 4,000 g for 10 min at 4°C, and the supernatant was centrifuged at 12,000 g for 10 min at 4°C. The ultimate supernatant was crude mitochondria enzyme extract that was used for measurement of activities of enzymes related to energy metabolism. ATPases activity was assayed by determining inorganic phosphorus product by the catalytic of ATP reaction to adenosine diphosphate (ADP) as the method of Jin et al. (2013). For H⁺-ATPase activity assay, 1.0 mL reaction system was 30 mmol L⁻¹ Tris-HCl (pH 8.0) containing 3 mmol L⁻¹ Mg₂SO₄, 0.1 mmol L⁻¹ Na₃VO₄, 50 mmol L⁻¹ NaNO₃, 50 mmol L⁻¹ KCl, and 0.1 mmol L⁻¹ ammonium nitrate. Enzyme crude extract (0.05 mL) and 0.1 mL ATP-Tris was added into the mixture to start the reaction and incubated at 37°C water bath for 20 min. The reaction was terminated by 0.1 mL 55% TCA. Ca²⁺-ATPase activity assay method was similar to H⁺-ATPase. In this sense, 3 mmol L⁻¹ Mg₂SO₄ was replaced by 3 mmol L⁻¹ Ca(NO₃)₂. Ca²⁺-ATPase activity was expressed by dispersion activity with and without Ca(NO₃)₂. One unit of

H⁺-ATPase and Ca²⁺-ATPase activities were expressed by the release of phosphorus per minute.

Cytochrome *c* oxidase (CCO) and succinate dehydrogenase (SDH) activity was measured referred to the procedure of Ackrell et al. (1984) with modifications. A total of 2.8 mL potassium phosphate buffer (0.2 mol L⁻¹, pH 7.4) containing 0.2 mol L⁻¹ sodium succinate and 0.9 mmol L⁻¹ 2,6-dichlorophenolindophenol sodium salt was incubated at 30°C for 5 min. Enzyme extract (0.1 mL) and phenazine methosulfate (0.1 mL) were added to the reaction systems successively. Absorption was detected at 600 nm. One unit of SDH activity was defined as an increase of 0.01 per minute and expressed as U mg⁻¹ protein. For CCO activity measurement, 0.2 mL enzyme extract was added with 0.02 mL 0.04% (w/v) cytochrome *c* and 2 mL ultrapure water. The whole system was bathed at 37°C water for 2 min. Then, 0.5 mL 0.4% (w/v) dimethyl-*p*-phenylenediamine was added to the mixture and the absorption was determined at 510 nm. One unit of CCO activity was defined as an increase of 0.01 per min and expressed as U mg⁻¹ protein.

Measurement of Lignin Content

Lignin content was quantified gravimetrically as the protocol of Femenia et al. (1998) with little modification. Ten grams of tissue were ground with 10 mL of distilled water and homogenized in 20 mL of concentrated sulfuric acid overnight. The mixture was then diluted to 250 mL and boiled for 2.5 h. The homogenate was filtered with hot water (90°C) until the effluent was not acidic. The remaining sediment was dried at 105°C to a constant mass. The mass was noted and expressed as a percentage.

Determination of ATP, ADP, and AMP Contents and Energy Charge

Adenosine triphosphate, ADP, and adenosine monophosphate (AMP) were quantified using the protocol of Liu et al. (2006). Two grams of frozen flesh was homogenized with 6.0 mL perchloric acid and centrifuged at 12,000 g for 15 min. The supernatant was filtered by 0.45- μ m filter membrane. A 20- μ L sample was taken for HPLC analysis. A mixture of ATP, ADP, and AMP was injected onto the HPLC as an external standard solution under the same conditions. The energy charge was equivalent as the function according to Pradet and Raymond (1983).

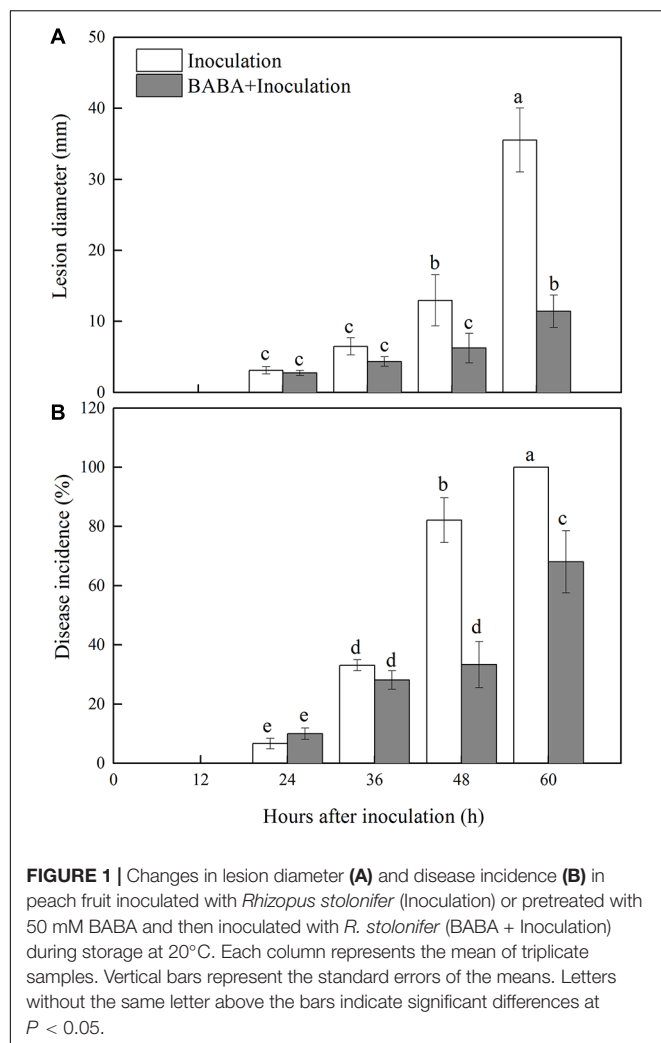
$$\text{Energy charge} = \frac{\text{ATP} + \frac{1}{2} \text{ADP}}{\text{ATP} + \text{AMP} + \text{ADP}}$$

Determination of Defense-Related Gene Expression by Semiquantitative RT-PCR

Fruit flesh tissue was collected from peaches in Mock, BABA, Inoculation, and BABA + Inoculation groups at 3, 6, 12, and 24 h after inoculation. For each replicate at different sampling time, 4 g of frozen flesh tissue was powdered in liquid nitrogen to get total RNA according to the method of cetyltrimethyl ammonium bromide (Chang et al., 1993). Total RNA (100 ng) was reverse-transcribed with HisScript® 1st Strand cDNA Synthesis Kit (Vazyme, Jiangsu, China). Short and conserved segments of *GNS*

TABLE 1 | Primers used in this assay for semiquantitative RT-PCR.

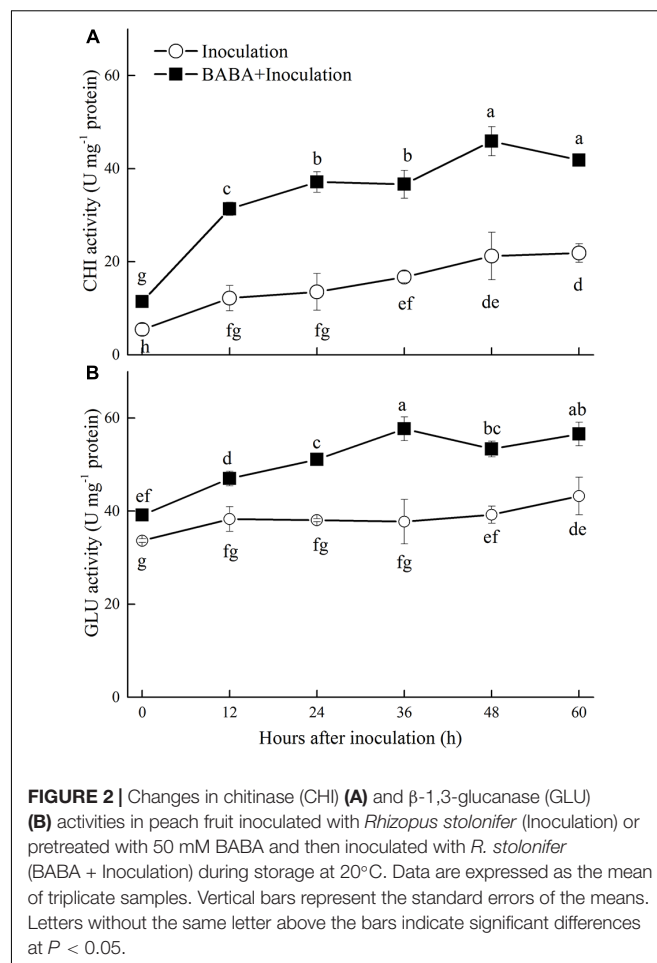
Genes	Primer sequence (5'→3')	Product length (bp)
<i>GNS</i>	Forward: ATTTCTCTTGCTGGTCTTG	528
	Reverse: CTCTGGGGTCTTTCTATTCT	
<i>CHI</i>	Forward: GTGGAAAGCAATAGGGGAG	244
	Reverse: TTCCAGCCCTTACCACAT	
<i>PR-like</i>	Forward: ATCAACTGGGACTTGCGTACT	317
	Reverse: TAGTCGCCACAGTCAACAAAG	
<i>NPR1-like</i>	Forward: GACCCAAACATGCCAGCAGTG	375
	Reverse: ATCCTTCGGCCTTGTCACCT	
<i>18S-rRNA</i>	Forward: ATGGCCGTTCTTAGTTGGTG	356
	Reverse: GTACAAAGGCGAGGGACGTA	



(Genebank: U49454.1), *CHI* (Genebank: AF206635.1), *NPR1-like* (Genebank: DQ149935.1), and *PR-like* (Genebank: AF362989.1, known as pathogen-related protein class 4) were cloned with 2 × Taq Master Mix kit (Vazyme, Jiangsu, China) using specific degenerate primers obtained from the SBS Genetech Co., Ltd. (Beijing, China). Semiquantitative RT-PCR was conducted as previously reported (Wang et al., 2013b). Independent 35 cycles were performed using 1 µl of cDNA samples to make sure linear amplification. The cycling conditions were conducted as the following program: 94°C – 5 min (1 cycle); 94°C – 30 s, 55°C – 30 s, and 72°C – 60 s/kb (35 cycles); 72°C – 7 min (1 cycle). *18S-rRNA* (Genebank: L28749.1) was set as the housekeeping gene for reference. Primers used in semiquantitative RT-PCR were shown in Table 1.

Statistical Analysis

All values were shown as the means ± standard error (SE) of triplicate assays. Two-way analysis of variance (ANOVA) was conducted with SPSS version 17.0 (SPSS Inc., Chicago, IL, United States) to evaluate the effects of treatment and storage



time. Duncan's multiple range tests were used to separate mean with $P < 0.05$ (regarded as significant).

RESULTS

Effects of BABA on Controlling *Rhizopus* Rot in Peaches

Decay symptoms resulting from *R. stolonifer* appeared in Inoculation and BABA + Inoculation peaches after 24 h post-inoculation. However, the lesion diameter and disease incidence of *Rhizopus* rot in BABA + Inoculation peaches were significantly ($P < 0.05$) lower than inoculation group from 36 to 60 h at 20°C (Figure 1). BABA treatment lowered lesion diameter and disease incidence by 67.88 and 31.94%, respectively, at 60 h post-inoculation compared with those in the Inoculation group (Figure 1).

Effects of BABA Treatment on Chitinase and β-1,3-Glucanase Activities in Peaches

Chitinase and GLU are important enzymes for the catalytic hydrolysis of fungal cell walls. As shown in Figure 2, the activities

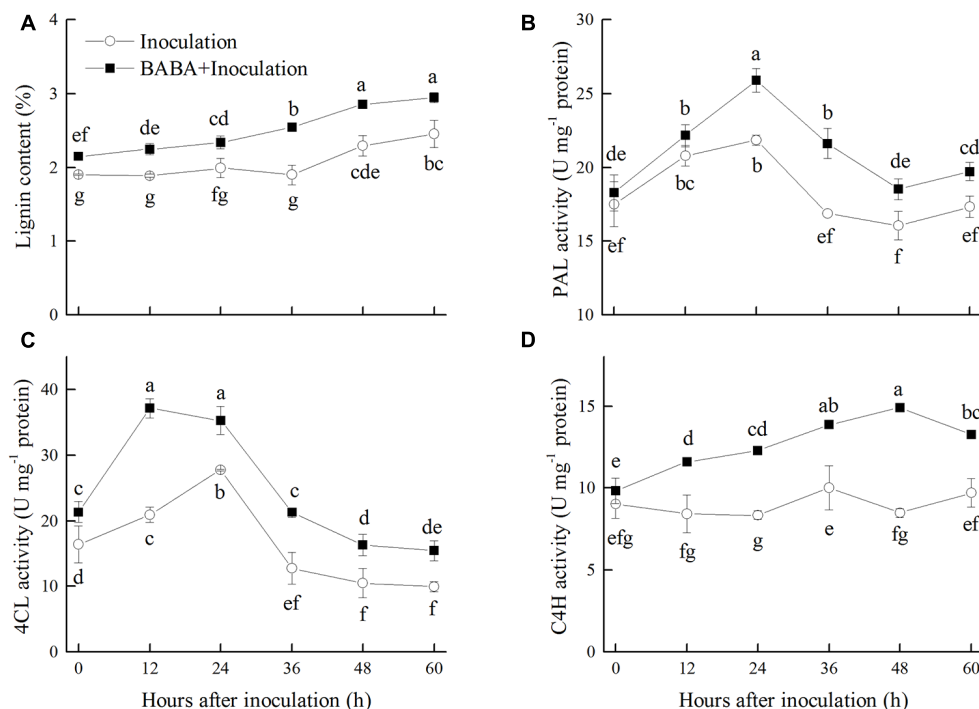


FIGURE 3 | Changes in lignin content (A), activities of phenylalanine ammonia lyase (PAL) (B), 4-coumaryl CoA ligase (4CL) (C), and cinnamate 4-hydroxy (C4H) (D) in peach fruit inoculated with *Rhizopus stolonifer* (Inoculation) or pretreated with 50 mM BABA and then inoculated with *R. stolonifer* (BABA + Inoculation) during storage at 20°C. Data are expressed as the mean of triplicate samples. Vertical bars represent the standard errors of the means. Letters without the same letter above the bars indicate significant differences at $P < 0.05$.

of both enzymes increased during storage. BABA treatment induced and maintained significantly ($P < 0.05$) higher activities of these two enzymes than the untreated fruit.

Effects of BABA Treatment on Lignin Content and Related Enzymes in Post-harvest Peaches

Lignin content in peaches accumulated gradually during storage at 20°C, which was significantly induced by BABA treatment. Lignin content in the BABA treatment group was 16.67% higher than that in the control fruit after 60 h of storage (Figure 3A). PAL, 4CL, and C4H, the key enzymes responsible for the first steps of lignin biosynthesis in the phenylpropanoid pathway, were induced by BABA treatment during the storage. The activities of PAL, 4CL, and C4H were 13.77, 55.31, and 36.50% higher than the control group, respectively, at the end of the storage (Figures 3B–D).

Effects of BABA Treatment on Energy Status in Peaches

Adenosine triphosphate content in peaches exhibited a gradually decreasing trend, whereas ADP content was maintained at a stable level in peaches inoculated with *R. stolonifer* (Figures 4A,B). Significantly ($P < 0.05$) higher levels of ATP were observed in BABA-treated peaches in comparison with the control group with the exception at 36 h. Meanwhile,

ADP level showed the similar change as ATP level. ADP content accumulated at the initial storage time after BABA treatment and showed significantly ($P < 0.05$) higher levels at 36 and 48 h than that in control peaches. BABA treatment significantly ($P < 0.05$) limited the increase of AMP content during storage (Figure 4C). The energy charge in peaches declined over time during storage. However, the values of the energy charge in BABA-treated peaches were significantly ($P < 0.05$) higher compared to those in untreated fruit (Figure 4D).

Effects of BABA Treatment on Ca²⁺-ATPase, H⁺-ATPase, SDH, and CCO Activities in Peaches

Activities of Ca²⁺-ATPase and H⁺-ATPase in peaches of Inoculation group increased slightly and peaked at 36 and 24 h, respectively, and then decreased during storage. BABA treatment stimulated the enhancement of Ca²⁺-ATPase and H⁺-ATPase activities, and kept them at significantly ($P < 0.05$) higher levels compared with the non-BABA-treated fruit over the entire storage period (Figures 5A,C). CCO activity increased at the first 24 h and then decreased gradually during the remaining storage time. The activity of CCO was significantly ($P < 0.05$) induced by BABA treatment within the whole storage (Figure 5B). As shown in Figure 5D, SDH activity increased during the first 48 and 24 h in the Inoculation and BABA + Inoculation groups, respectively,

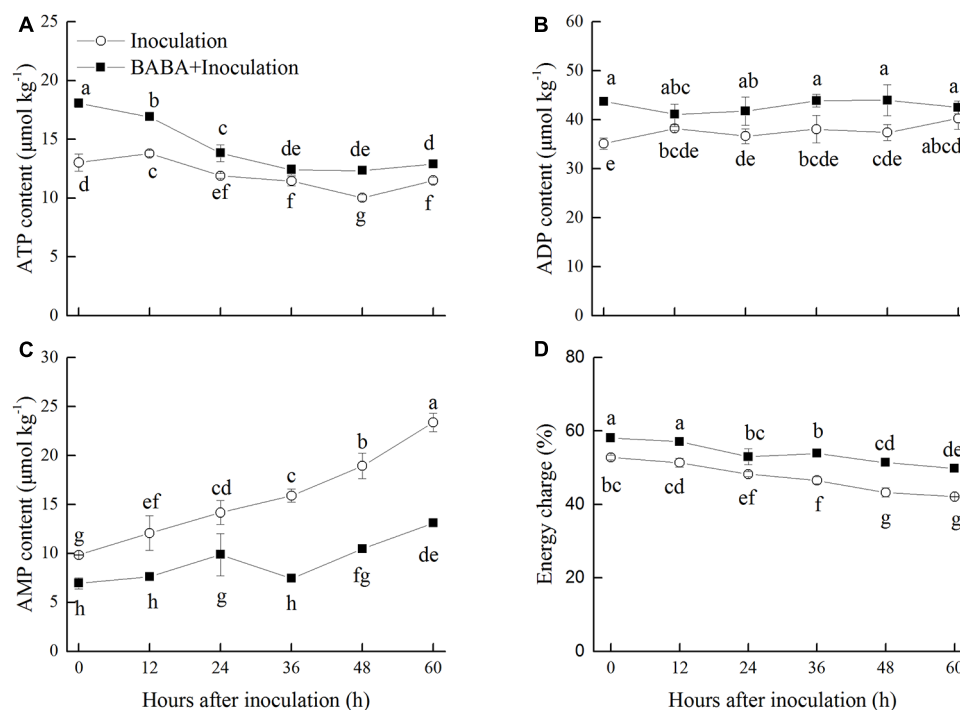


FIGURE 4 | Changes in contents of adenosine triphosphate (ATP, **A**), adenosine diphosphate (ADP, **B**), adenosine monophosphate (AMP, **C**), and energy charge (**D**) in peach fruit inoculated with *Rhizopus stolonifer* (Inoculation) or pretreated with 50 mM BABA and then inoculated with *R. stolonifer* (BABA + Inoculation) during storage at 20°C. Data are expressed as the mean of triplicate samples. Vertical bars represent the standard errors of the means. Letters without the same letter above the bars indicate significant differences at $P < 0.05$.

and decreased afterwards. Significantly higher SDH activity was observed in BABA-treated peaches ($P < 0.05$).

Effects of BABA Treatment and *R. stolonifer* Inoculation on the Expression of Defense-Related Genes in Peach Fruit

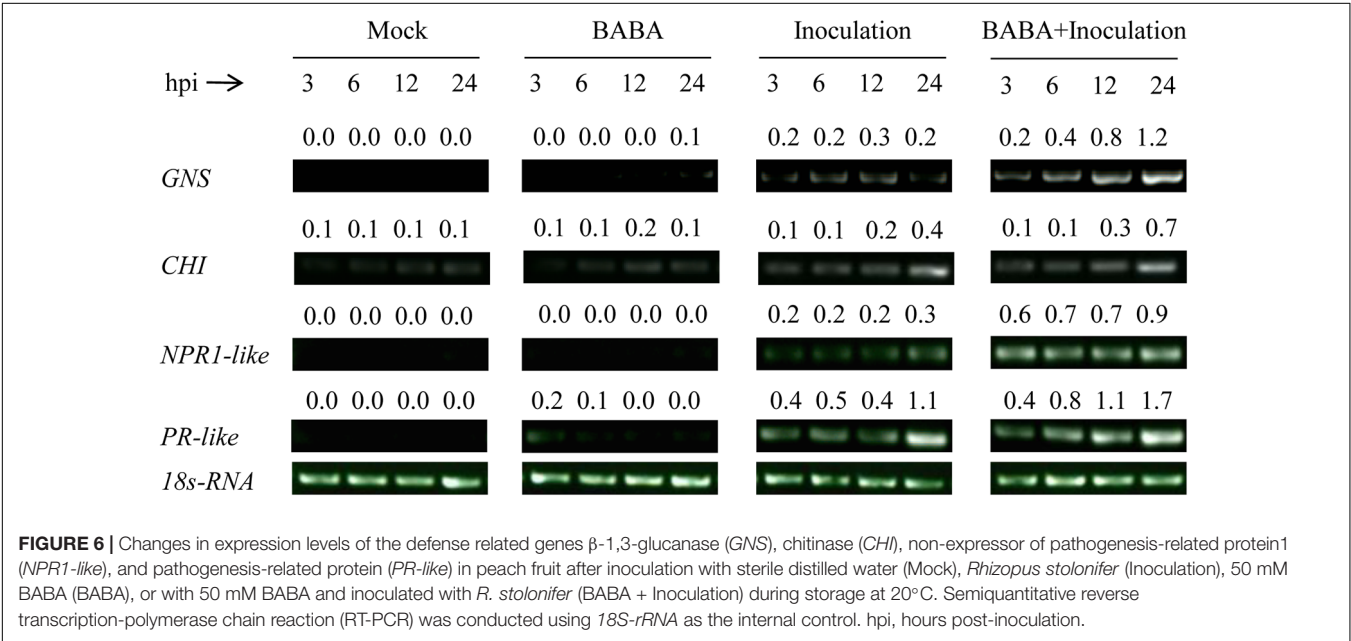
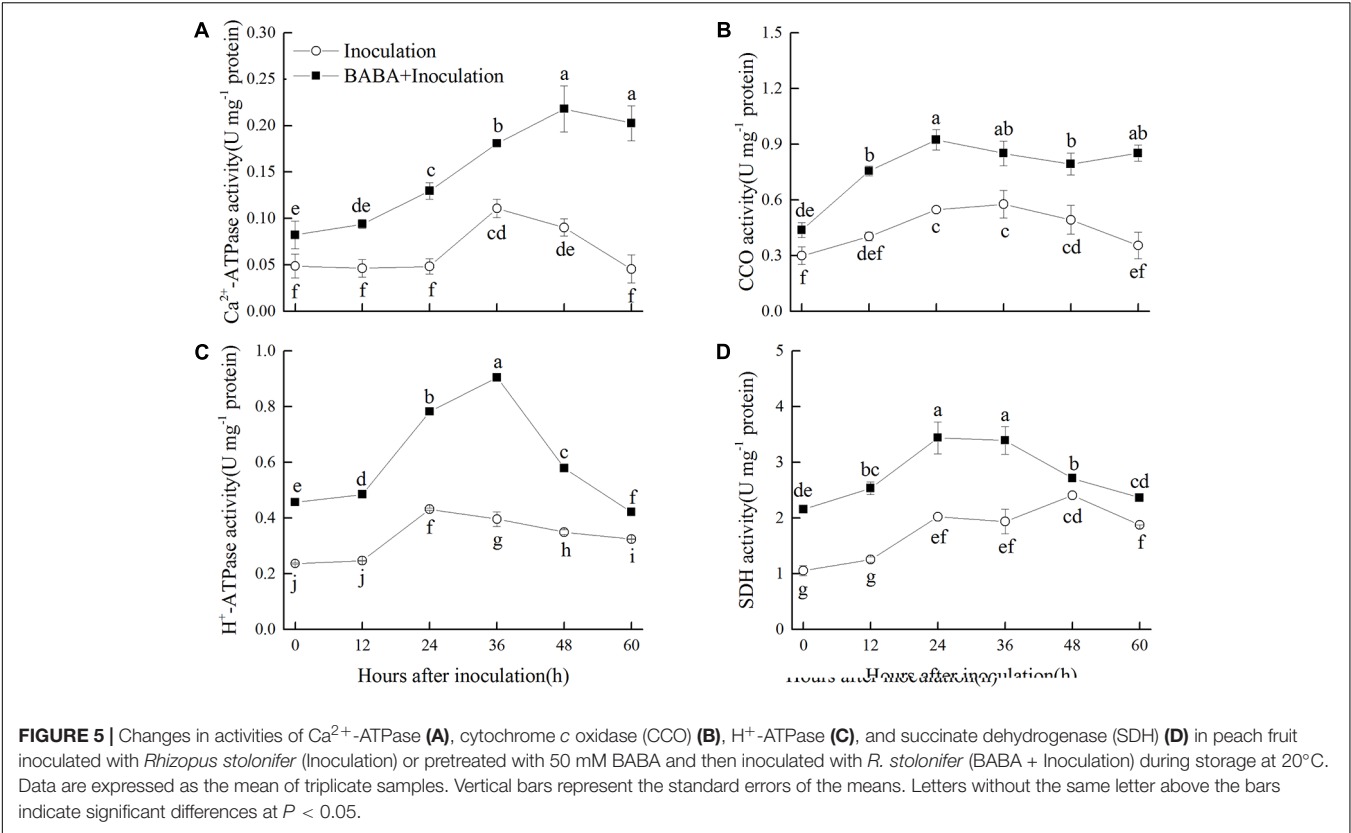
The transcription of the four defense-related genes *GNS*, *CHI*, *NPR1-like*, and *PR-like* remained at a very low level in peach fruit only treated with BABA or sterile distilled water (Mock), while the transcription was slightly increased in fruit only inoculated with *R. stolonifer*. However, the transcription of the four genes in peaches both treated with BABA and inoculated with *R. stolonifer* was significantly enhanced and kept at higher level during storage compared with the other three treatments (**Figure 6**), which indicated BABA treatment induced higher expression of the four defense related genes in peaches upon inoculation with the pathogen of *R. stolonifer*.

DISCUSSION

Our study found that BABA treatment markedly reduced the development of *Rhizopus* rot in peaches during storage at 20°C, which suggested that disease resistance in peaches was enhanced by BABA. CHI and GLU are the crucial enzymes that degrade

the cell walls of pathogens. Increased transcript accumulation of genes encoding these two enzymes and enhancement of enzyme activities have been extensively observed in the induction of disease resistance in post-harvest fruits (Cao et al., 2011; Liu et al., 2012; Wang et al., 2013a,b; Saavedra et al., 2017). Zhang et al. (2011) revealed that BABA treatment induced a remarkable enhancement in CHI and GLU activities in apples against blue mold decay. In the present study, BABA treatment significantly increased the gene transcription and activity of these two enzymes and inhibited *Rhizopus* rot in peaches, which suggested that the control of the disease by BABA was resulted from the induction of these two defense-related enzymes.

Lignin biosynthesis and lignification of cell wall play an important role in plant defense against pathogen invasion (Bhuiyan et al., 2009). PAL, C4H, and 4CL are three key enzymes responsible for the first steps of lignin biosynthesis in the phenylpropanoid pathway (Ferrer et al., 2008). The accumulation of gene transcripts for these three enzymes or the increase in their activities in response to elicitors has been observed in different harvested fruits. For example, Wang et al. (2015) reported the inhibition of decay development in sweet cherries by MeJA treatment was associated with the increased accumulation of PAL transcripts. Hershkovitz et al. (2012) found that the biocontrol agent *Metschnikowia fructicola* increased the abundance of plant defensive compounds via increasing expression of the genes encoding PAL and



4CL in grapes. In addition, acibenzolar-S-methyl treatment induced the increase of PAL, C4H, and 4CL activities and thereby activated the phenylpropanoid pathway and prevented pathogenic invasion in muskmelon (Liu et al., 2014). In our present study, BABA treatment significantly increased PAL, C4H, and 4CL activities and consequently promoted the accumulation of lignin, which could contribute to the delay of *Rhizopus* rot development.

Energy status is a fundamental feature of ripening and senescence in harvested horticultural crops (Jiang et al., 2007). As a non-specific response in the host, the enhancement of ATP content plays a vital role in disease defense (Yi et al., 2010).

Along with less disease development, higher energy status in post-harvest fruit will contribute to the production of natural compounds related to defense such as phytoalexins, and the enhancement of *PR-like* activity (Yi et al., 2010). Thus, the exogenous application of inducers that improve energy status may be an effective way to inhibit post-harvest diseases. Yi et al. (2010) reported that exogenous ATP treatment improved the energy status of harvested litchi fruit and inhibited disease development caused by *P. litchii*. The disease resistance in loquat fruit induced by MeJA was also found to be related to higher ATP content (Cao et al., 2014). Therefore, in our present study, the maintenance of high ATP level and energy charge with BABA treatment was crucial to disease resistance induction in peaches inoculated with *R. stolonifera*.

Adenosine triphosphate, ADP, and AMP contents are relevant to the enzymes activities in energetic metabolism pathways, involving Ca^{2+} -ATPase, H^{+} -ATPase, SDH, and CCO. Ca^{2+} -ATPase is responsible for maintaining low cytoplasmic Ca^{2+} , which is necessary for cellular balance (Palmgren and Harper, 1999). H^{+} -ATPase produces a chemiosmotic H^{+} -gradient and establishes a pH gradient around the plant plasma membrane, playing an important role in energy metabolism (Palmgren and Harper, 1999). SDH generates ATP by catalyzing succinate oxidized to fumarate, while CCO is the ultimate decisive enzyme in the respiratory electron transport system (Millar et al., 1995). All of these enzymes are essential for energy supply and maintenance of normal mitochondrial function. It has been demonstrated that alleviation of chilling injury in post-harvest fruit is relevant to increase of energy metabolism enzymes activities. Jin et al. (2013, 2014) discovered that MeJA or oxalic acid reduced chilling injury of peaches during cold storage by enhancing the activities of ATPases, SDH, and CCO. In our present study, we showed that BABA treatment maintained higher activities of Ca^{2+} -ATPase, H^{+} -ATPase, SDH, and CCO and thereby a higher energy status was observed in treated peaches compared to control fruit which plays a crucial role in inducing disease resistance.

Plant immunity consists of induced systemic resistance (ISR) and systemic acquired resistance (SAR). For a long time, it has been assumed that protection by induced disease resistance is based on direct activation of defense responses. Recently, priming is considered as a mechanism that is common to different types of induced disease resistance in plants, based on studies on field crops and model plants (Conrath, 2011). More recent studies have demonstrated that priming might also be a common phenomenon of induced disease resistance in post-harvest fruits. For examples, *B. cereus* AR156 induced disease resistance against *Rhizopus* rot in peach fruit and anthracnose rot in loquat fruit by priming of defense responses (Wang et al., 2013b; Wang X.L. et al., 2014). MeJA primed disease resistance against *Penicillium citrinum* in Chinese bayberries (Wang K.T. et al., 2014), *P. expansum* in sweet cherry fruit (Wang et al., 2015), and *B. cinerea* in table grapes and strawberries (Jiang et al., 2015; Saavedra et al., 2017). Yu et al. (2014) found that γ -aminobutyric acid induced disease resistance against *P. expansum* in pear fruit through priming of defense responses. In line with these

results, our present study showed the transcription of the defense-related genes in peach fruit was not induced by BABA treatment alone, only in fruit that were both treated with BABA and inoculated with *R. stolonifera* was a significant increase in these genes expression observed. Therefore, our results indicated that BABA induced disease resistance against *R. stolonifera* via priming.

Non-expressor of pathogenesis-related protein1 is a key regulator in plant immune system which activates the expression of PR genes (Kinkema et al., 2000). Luna et al. (2014) found that BABA primed disease resistance against the pathogens *Hyaloperonospora arabidopsidis* and *Pseudomonas syringae* pv. *tomato* DC3000 in *Arabidopsis* plants for up to 4 weeks after the treatment. This long-lasting priming was controlled by NPR1 and associated with priming of SA-inducible genes. In this study, BABA primed for augmented expression of defense-related genes including *NPR1-like* and enhanced disease resistance against *R. stolonifera* in peach fruit. However, the role of NPR1 on regulating the expression of PR genes in BABA-induced priming defense in harvested fruits needs further investigation.

CONCLUSION

Our study indicated that BABA treatment primed induction of the resistance response to control *Rhizopus* rot development in post-harvest peaches by enhancing the expression of defense-related genes. BABA also induced activities of enzymes involved in lignin biosynthesis and energy metabolism pathways and thereby maintaining the strength of the cell wall and energy status in harvested peaches, which contributes to increase the disease resistance against *Rhizopus* rot.

AUTHOR CONTRIBUTIONS

JW and YZ conceived and designed the experiments. JW, LW, and XW performed gene expression and enzyme activity assays. JW and SC carried out ATP, ADP, AMP, lignin content, and analyzed the data. PJ and YZ contributed to reagents, materials, and analysis tools. JW, SC, PJ, LW, XW, and YZ participated in writing the manuscript. All the authors read and approved the final manuscript.

FUNDING

This study was supported by National Natural Science Foundation of China (No. 31672209), the Fundamental Research Funds for the Central Universities of China (KYZ201420), and Natural Science Foundation of Jiangsu Province (BK20131073).

ACKNOWLEDGMENTS

We thank Dr. Kaituo Wang of Chongqing Three Gorges University for the critical revision of this manuscript.

REFERENCES

- Abeles, F. B., Bosshart, R. P., Forrence, L. E., and Habig, W. H. (1971). Preparation and purification of glucanase and chitinase from bean leaves. *Plant Physiol.* 47, 129–134. doi: 10.1104/pp.47.1.129
- Ackrell, B. A., Maguire, J. J., and Dallman, P. R., Kearney, E. B. (1984). Effect of iron deficiency on succinate- and NADH-ubiquinone oxidoreductases in skeletal muscle mitochondria. *J. Biol. Chem.* 259, 10053–10059.
- Bhuiyan, N. H., Selvaraj, G., Wei, Y. D., and King, J. (2009). Role of lignification in plant defense. *Plant Signal. Behav.* 4, 158–159. doi: 10.4161/psb.4.2.7688
- De Block, M., Verduyn, C., De Brouwer, D., and Cornelissen, M. (2005). Poly(ADP-ribose) polymerase in plants affects energy homeostasis, cell death and stress tolerance. *Plant J.* 41, 95–106. doi: 10.1111/j.1365-3113.2004.02277.x
- Cao, S. F., Cai, Y. T., Yang, Z. F., Joyce, D. C., and Zheng, Y. H. (2014). Effect of MeJA treatment on polyamine, energy status and anthracnose rot of loquat fruit. *Food Chem.* 145, 86–89. doi: 10.1016/j.foodchem.2013.08.019
- Cao, S. F., Yang, Z. F., Hu, Z. C., and Zheng, Y. H. (2011). The effects of the combination of *Pichia membranefaciens* and BTH on controlling of blue mould decay caused by *Penicillium expansum* in peach fruit. *Food Chem.* 124, 991–996. doi: 10.1016/j.foodchem.2010.07.041
- Chang, S. J., Puryear, J., and Cairney, J. (1993). A simple and efficient method for isolating RNA from pine trees. *Plant Mol. Biol. Rep.* 11, 113–116. doi: 10.1007/BF02670468
- Cheng, G. W., and Breen P. J. (1991). Activity of phenylalanine ammonia-lyase (PAL) and concentrations of anthocyanins and phenolics in developing strawberry fruit. *J. Am. Soc. Hortic. Sci.* 116, 865–869.
- Chen, Y. H., Lin, H. T., Jiang, Y. M., Zhang, S., Lin, Y. F., and Wang, Z. H. (2014). Phomopsis longanae Chi-induced pericarp browning and disease development of harvested longan fruit in association with energy status. *Postharvest Biol. Technol.* 93, 24–28. doi: 10.1016/j.postharvbio.2014.02.003
- Chester, K. S. (1933). The problem of acquired physiological immunity in plants. *Q. Rev. Biol.* 8, 275–324. doi: 10.1086/394440
- Conrath, U. (2011). Molecular aspects of defence priming. *Trends Plant Sci.* 16, 524–531. doi: 10.1016/j.tplants.2011.06.004
- Conrath, U., Beckers, G. J. M., Flors, V., García-Agustín, P., Jakab, G., Mauch, F., et al. (2006). Priming: getting ready for battle. *Mol. Plant Microbe Interact.* 19, 1062–1071. doi: 10.1094/MPMI-19-1062
- Conrath, U., Pieterse, C. M. J., and Mauch-Mani, B. (2002). Priming in plant-pathogen interactions. *Trends Plant Sci.* 7, 210–216. doi: 10.1016/S1360-1385(02)02244-6
- Fan, Q., and Tian, S. P. (2000). Postharvest biological control of *Rhizopus* rot of nectarine fruits by *Pichia membranefaciens*. *Plant Dis.* 84, 1212–1216. doi: 10.1094/PDIS.2000.84.11.1212
- Femenia, A., Garcia-Conesa, M., Simal, S., and Rosselló, C. (1998). Characterisation of the cell walls of loquat (*Eriobotrya japonica* L.) fruit tissues. *Carbohydr. Polym.* 35, 169–177. doi: 10.1016/S0144-8617(97)00240-3
- Fernández-Trujillo, J. P., MartíNez, J. A., and Artés, F. (1998). Modified atmosphere packaging affects the incidence of cold storage disorders and keeps 'flat' peach quality. *Food Res. Int.* 31, 571–579. doi: 10.1016/S0963-9969(99)00030-7
- Ferrer, J. L., Austin, M. B., Stewart, C., and Noel, J. P. (2008). Structure and function of enzymes involved in the biosynthesis of phenylpropanoids. *Plant Physiol. Biochem.* 46, 356–370. doi: 10.1016/j.plaphy.2007.12.009
- Herschkovitz, V., Ben-Dayana, C., Raphael, G., Pasmanik-Chor, M., Liu, J., Belausov, E., et al. (2012). Global changes in gene expression of grapefruit peel tissue in response to the yeast biocontrol agent *Metschnikowia fructicola*. *Mol. Plant Pathol.* 13, 338–349. doi: 10.1111/j.1364-3703.2011.00750.x
- Jiang, L. L., Jin, P., Wang, L., Yu, X., Wang, H. Y., and Zheng, Y. H. (2015). Methyl jasmonate primes defense responses against *Botrytis cinerea* and reduces disease development in harvested table grapes. *Sci. Hortic.* 192, 218–223. doi: 10.1016/j.scienta.2015.06.015
- Jiang, Y. M., Jiang, Y. L., Qu, H. X., Duan, X. W., Luo, Y. B., and Jiang, W. B. (2007). Energy aspects in ripening and senescence of harvested horticultural crops. *Stewart Postharvest Rev.* 3, 1–5.
- Jin, P., Zheng, Y. H., Tang, S. S., Rui, H. J., and Wang, C. Y. (2009). Enhancing disease resistance in peach fruit with methyl jasmonate. *J. Sci. Food. Agric.* 89, 802–808. doi: 10.1002/jsfa.3516
- Jin, P., Zhu, H., Wang, J., Chen, J. J., Wang, X. L., and Zheng, Y. H. (2013). Effect of methyl jasmonate on energy metabolism in peach fruit during chilling stress. *J. Sci. Food Agric.* 93, 1827–1832. doi: 10.1002/jsfa.5973
- Jin, P., Zhu, H., Wang, L., Shan, T. M., and Zheng, Y. H. (2014). Oxalic acid alleviates chilling injury in peach fruit by regulating energy metabolism and fatty acid contents. *Food Chem.* 161, 87–93. doi: 10.1016/j.foodchem.2014.03.103
- Justyna, P., and Ewa, K. (2013). Induction of resistance against pathogens by β -aminobutyric acid. *Acta Physiol. Plant.* 35, 1735–1748. doi: 10.1007/s11738-013-1215-z
- Kinkema, M., and Fan, W. H., Dong, X. N. (2000). Nuclear localization of NPR1 is required for activation of PR gene expression. *Plant Cell* 12, 2339–2350. doi: 10.1105/tpc.12.12.2339
- Knobloch, K. H., and Hahlbrock, K. (1977). 4-coumarate: coA ligase from cell suspension cultures of *Petroselinum hortense* hoffm: partial purification, substrate specificity, and further properties. *Arch. Biochem. Biophys.* 184, 237–248. doi: 10.1016/0003-9861(77)90347-2
- Lamb, C. J., and Rubery, P. H. (1975). A spectrophotometric assay for trans-cinnamic acid 4-hydroxylase activity. *Anal. Biochem.* 68, 554–561. doi: 10.1016/0003-2697(75)90651-X
- Liu, H., Jiang, Y. M., Luo, Y. B., and Jiang, W. B. (2006). A simple and rapid determination of ATP, ADP and AMP concentrations in pericarp tissue of litchi fruit by high performance liquid chromatography. *Food Technol. Biotech.* 44, 531–534.
- Liu, H. X., Jiang, W. B., Bi, Y., and Luo, Y. B. (2005). Postharvest BTH treatment induces resistance of peach (*Prunus persica* L. cv. Jiubao) fruit to infection by *Penicillium expansum* and enhances activity of fruit defense mechanisms. *Postharvest Biol. Technol.* 35, 263–269. doi: 10.1016/j.postharvbio.2004.08.006
- Liu, J., Sui, Y., Wisniewski, M., Droby, S., Tian, S. P., Norelli, J., et al. (2012). Effect of heat treatment on inhibition of *Monilinia fructicola* and induction of disease resistance in peach fruit. *Postharvest Biol. Technol.* 65, 61–68. doi: 10.1016/j.postharvbio.2011.11.002
- Liu, Y. Y., Ge, Y. H., Bi, Y., Li, C. Y., Deng, H. W., Hu, L. G., et al. (2014). Effect of postharvest acibenzolar-S-methyl dipping on phenylpropanoid pathway metabolism in muskmelon (*Cucumis melo* L.) fruits. *Sci. Hortic.* 168, 113–119. doi: 10.1016/j.scienta.2014.01.030
- Luna, E., López, A., Kooiman, J., and Ton, J. (2014). Role of NPR1 and KYP in long-lasting induced resistance by β -aminobutyric acid. *Front. Plant Sci.* 5:184. doi: 10.3389/fpls.2014.00184
- Millar, A. H., Atkin, O. K., Lambers, H., Wiskich, J. T., and Day, D. A. (1995). A critique of the use of inhibitors to estimate partitioning of electrons between mitochondrial respiratory pathways in plants. *Physiol. Plant.* 95, 523–532. doi: 10.1111/j.1399-3054.1995.tb05518.x
- Palmgren, M. G., and Harper, J. F. (1999). Pumping with plant P-type ATPases. *J. Exp. Bot.* 50, 883–893. doi: 10.1093/jxb/50.Special_Issue.883
- Porat, R., Vinokur, V., Weiss, B., Cohen, L., Daus, A., Goldschmidt, E. E., et al. (2003). Induction of resistance to *Penicillium digitatum* in grapefruit by β -aminobutyric acid. *Eur. J. Plant Pathol.* 109, 901–907. doi: 10.1023/B:EJPP.0000003624.28975.45
- Pradet, A., and Raymond, P. (1983). Adenine nucleotide ratios and adenylate energy charge in energy metabolism. *Annu. Rev. Plant Phys.* 34, 199–224. doi: 10.1146/annurev.pp.34.060183.001215
- Quaglia, M., Ederli, L., Pasqualini, S., and Zizzerini, A. (2011). Biological control agents and chemical inducers of resistance for postharvest control of *Penicillium expansum* link. On apple fruit. *Postharvest Biol. Technol.* 59, 307–315. doi: 10.1016/j.postharvbio.2010.09.007
- Saavedra, G. M., Sanfuentes, E., Figueroa, P. M., and Figueroa, C. R. (2017). Independent preharvest applications of methyl jasmonate and chitosan elicit differential upregulation of defense-related genes with reduced incidence of gray mold decay during postharvest storage of fragaria chiloensis fruit. *Int. J. Mol. Sci.* 18:1420. doi: 10.3390/ijms18071420
- Thevenet, D., Pastor, V., Baccelli, I., Balmer, A., Vallat, A., Neier, R., et al. (2017). The priming molecule β -aminobutyric acid is naturally present in plants and is induced by stress. *New Phytol.* 213, 552–559. doi: 10.1111/nph.14298
- Usall, J., Casals, C., Sisquella, M., Palou, L., and De Cal, A. (2015). Alternative technologies to control postharvest diseases of stone fruits. *Stewart Postharvest Rev.* 11, 1–6.

- Wang, K. T., Jin, P., Han, L., Shang, H. T., Tang, S. S., Rui, H. J., et al. (2014). Methyl jasmonate induces resistance against *Penicillium citrinum* in Chinese bayberry by priming of defense responses. *Postharvest Biol. Technol.* 98, 90–97. doi: 10.1016/j.postharvbio.2014.07.009
- Wang, L., Jin, P., Wang, J., Jiang, L. L., Shan, T. M., and Zheng, Y. H. (2015). Methyl jasmonate primed defense responses against *Penicillium expansum* in sweet cherry fruit. *Plant Mol. Biol. Rep.* 33, 1461–1471. doi: 10.1007/s11105-014-0844-8
- Wang, X. L., Wang, J., Jin, P., and Zheng, Y. H. (2013a). Investigating the efficacy of *Bacillus subtilis* SM21 on controlling *Rhizopus* rot in peach fruit. *Int. J. Food Microbiol.* 164, 141–147. doi: 10.1016/j.ijfoodmicro.2013.04.010
- Wang, X. L., Xu, F., Wang, J., Jin, P., and Zheng, Y. H. (2013b). *Bacillus cereus* AR156 induces resistance against *Rhizopus* rot through priming of defense responses in peach fruit. *Food Chem.* 136, 400–406. doi: 10.1016/j.foodchem.2012.09.032
- Wang, X. L., Wang, L., Wang, J., Jin, P., Liu, H. X., and Zheng, Y. H. (2014). *Bacillus cereus* AR156-induced resistance to *Colletotrichum acutatum* is associated with priming of defense responses in loquat fruit. *PLoS One* 9:e112494. doi: 10.1371/journal.pone.0112494
- Wang, Y. S., Tian, S. P., and Xu, Y. (2005). Effects of high oxygen concentration on pro- and anti-oxidant enzymes in peach fruits during postharvest periods. *Food Chem.* 91, 99–104. doi: 10.1016/j.foodchem.2004.05.053
- Yi, C., Jiang, Y. M., Shi, J., Qu, H. X., Xue, S., Duan, X. W., et al. (2010). ATP-regulation of antioxidant properties and phenolics in litchi fruit during browning and pathogen infection process. *Food Chem.* 118, 42–47. doi: 10.1016/j.foodchem.2009.04.074
- Yi, C., Qu, H. X., Jiang, Y. M., Shi, J., Duan, X. W., Joyce, D. C., et al. (2008). ATP-induced changes in energy status and membrane integrity of harvested litchi fruit and its relation to pathogen resistance. *J. Phytopathol.* 156, 365–371. doi: 10.1111/j.1439-0434.2007.01371.x
- Yu, C., Zeng, L. Z., Sheng, K., Chen, F. X., Zhou, T., Zheng, X. D., et al. (2014). γ -aminobutyric acid induces resistance against *Penicillium expansum* by priming of defence responses in pear fruit. *Food Chem.* 159, 29–37. doi: 10.1016/j.foodchem.2014.03.011
- Zhang, C. F., Wang, J. M., Zhang, J. G., Hou, C. J., and Wang, G. L. (2011). Effects of β -aminobutyric acid on control of postharvest blue mould of apple fruit and its possible mechanisms of action. *Postharvest Biol. Technol.* 61, 145–151. doi: 10.1016/j.postharvbio.2011.02.008
- Zhang, Z. K., Yang, D. P., Yang, B., Gao, Z. Y., Li, M., Jiang, Y. M., et al. (2013). β -aminobutyric acid induces resistance of mango fruit to postharvest anthracnose caused by *Colletotrichum gloeosporioides* and enhances activity of fruit defense mechanisms. *Sci. Hortic.* 160, 78–84. doi: 10.1016/j.scienta.2013.05.023

Conflict of Interest Statement: The authors declare that the research was conducted in the absence of any commercial or financial relationships that could be construed as a potential conflict of interest.

Copyright © 2018 Wang, Cao, Wang, Wang, Jin and Zheng. This is an open-access article distributed under the terms of the Creative Commons Attribution License (CC BY). The use, distribution or reproduction in other forums is permitted, provided the original author(s) and the copyright owner(s) are credited and that the original publication in this journal is cited, in accordance with accepted academic practice. No use, distribution or reproduction is permitted which does not comply with these terms.



Control of Citrus Post-harvest Green Molds, Blue Molds, and Sour Rot by the Cecropin A-Melittin Hybrid Peptide BP21

Wenjun Wang¹, Sha Liu¹, Lili Deng^{1,2}, Jian Ming^{1,2}, Shixiang Yao^{1,2} and Kaifang Zeng^{1,2*}

¹ College of Food Science, Southwest University, Chongqing, China, ² Research Center of Food Storage & Logistics, Southwest University, Chongqing, China

OPEN ACCESS

Edited by:

Hongyin Zhang,
Jiangsu University, China

Reviewed by:

Jon Y. Takemoto,
Utah State University, United States
Prabuddha Dey,
Rutgers University – The State
University of New Jersey,
United States
Hai-Lei Wei,
Chinese Academy of Agricultural
Sciences, China

*Correspondence:

Kaifang Zeng
zengkafang@hotmail.com

Specialty section:

This article was submitted to
Food Microbiology,
a section of the journal
Frontiers in Microbiology

Received: 05 June 2018

Accepted: 25 September 2018

Published: 10 October 2018

Citation:

Wang W, Liu S, Deng L, Ming J,
Yao S and Zeng K (2018) Control
of Citrus Post-harvest Green Molds,
Blue Molds, and Sour Rot by
the Cecropin A-Melittin Hybrid
Peptide BP21.
Front. Microbiol. 9:2455.
doi: 10.3389/fmicb.2018.02455

In this study, the activity of the cecropin A-melittin hybrid peptide BP21 (Ac-FKLFFKKILKVL-NH₂) in controlling of citrus post-harvest green and blue molds and sour rot and its involved mechanism was studied. The minimum inhibitory concentrations of BP21 against *Penicillium digitatum*, *Penicillium italicum*, and *Geotrichum candidum* were 8, 8, and 4 $\mu\text{mol L}^{-1}$, respectively. BP21 could inhibit the growth of mycelia, the scanning electron microscopy results clearly showed that the mycelia treated with BP21 shrank, formed a rough surface, became distorted and collapsed. Fluorescent staining with SYTOX Green (SG) indicated that BP21 could disintegrate membranes. Membrane permeability parameters, including extracellular conductivity, the leakage of potassium ions, and the release of cellular constituents, visibly increased as the BP21 concentration increased. Gross and irreversible damage to the cytoplasm and membranes was observed. There was a positive correlation between hemolytic activity and the concentration of BP21. These results suggest peptide BP21 could be used to control citrus post-harvest diseases.

Keywords: peptide BP21, post-harvest, citrus fruit, diseases control, mode of action

INTRODUCTION

Green mold, blue mold, and sour rot caused by *Penicillium digitatum*, *Penicillium italicum*, and *Geotrichum candidum* (syn. *Geotrichum citri-aurantii*) are the most serious post-harvest fungal diseases. Sour rot cannot be inhibited by imazalil and thiabendazole, which are effective chemical fungicides against green mold and blue mold (Droby et al., 2002; Ismail and Zhang, 2004). The application of chemical fungicides has been restricted due to the concerns about pesticide residues, environmental pollution and pathogens resistance. It is urgent to search for effective, ecofriendly methods of diseases control to replace or reduce the use of harmful chemical fungicides (Schirra et al., 2011; Romanazzi et al., 2017).

Antimicrobial peptides (AMPs) as novel antibiotics are widely studied, it has been proposed their use to fight phytopathogens in agriculture, animal husbandry, post-harvest conservation, and the food industry (Jenssen et al., 2006; Keymanesh et al., 2009; Ciociola et al., 2016). The application of peptides in the control of fruit and vegetable diseases is gaining attention. An increasing number of AMPs have been shown to control fruit and vegetable diseases. In previous research, PAF56 (GHRKKWFW) was shown to effectively control of fungi infection in citrus

fruits (Wang et al., 2018). There are likely many AMPs yet to be discovered that can effectively control fruit and vegetable diseases.

Cecropins were first discovered in the hemolymph of the giant silk moth *Hyalophora cecropia* (Andreu et al., 1983), and they are some of the best known cationic AMPs, representing a family of highly basic α -helical peptides. In particular, Cecropin A displays powerful lytic activity against bacteria but has no cytotoxic effects against eukaryotic cells. However, because many fruit and vegetable diseases are caused by fungi, certain natural AMPs should be modified with new sequences that confer improved antimicrobial and therapeutic properties (Chicharro et al., 2001; Alberola et al., 2004). In particular, certain peptides from the CECMEL11 library (LIPPSO-CIDSAV, University of Girona, Girona, Spain), which is composed of *de novo* designed and synthetically produced cecropin A-melittin hybrid linear undecapeptides, have been derived from the peptide Pep3 (WKLFKKILKVL-NH₂) and evaluated for *Stemphylium vesicarium* infection control in pears (Badosa et al., 2009). For example, BP15 (KKLFKKILKVL-NH₂) inhibited *S. vesicarium* growth, produced morphological alterations to germ tubes and induced cell membrane disruption (Ferre et al., 2006; Puig et al., 2014, 2016). BP15 also could control the infection caused by *P. digitatum* on citrus fruit (Muñoz et al., 2007). In addition, BP21 (Ac-FKLFKKILKVL-NH₂) was designed to inhibit the plant pathogenic fungi *Fusarium oxysporum*, *Aspergillus niger*, *Rhizopus stolonifer*, and *Penicillium expansum*. It has been shown that BP21 can effectively inhibit *P. expansum* *in vitro* and control the post-harvest decay caused by *P. expansum* in apples (Badosa et al., 2009). *Penicillium* species that affect the post-harvest of fruits further highlight the need to develop AMPs. We predicted that BP21 could control post-harvest diseases on citrus fruit as well. Cecropin A, melittin and their hybrids have been widely studied for their antibacterial mode of action (Makovitzki et al., 2007; Ferre et al., 2009), but the mechanisms that underlie their interactions with plant pathogenic filamentous fungi are still unclear.

The aim of the present study was to investigate the effects of the peptide BP21 in inhibiting *P. digitatum*, *P. italicum*, and *G. candidum* *in vitro* and *in vivo*, and the mode of action of BP21 was studied.

MATERIALS AND METHODS

Antifungal Peptide and Fungal Strains

Peptide BP21 (FKLFKKILKVL) was synthesized at >90% purity from GenScript Corporation (Nanjing, China) by solid-phase methods using *N*-(9-fluorenyl) methoxycarbonyl (Fmoc) chemistry. BP21 was acetylated at the N terminus (Ac) and amidated at the C terminus (NH₂). Stock solutions of peptides were prepared at 1 m mol L⁻¹ in sterile ultrapure water and stored at -40°C.

The fungi (*P. digitatum*, *P. italicum*, and *G. candidum*) used in this work were obtained from spoiled citrus fruits and identified. They were cultured on potato dextrose agar (PDA) that contained an infusion of 200 g L⁻¹ potatoes, 20 g L⁻¹ glucose, and 20 g L⁻¹

agar at 25°C. The spores from a 7-day-old culture were collected, filtered, and adjusted to the suitable concentration with the aid of a hemacytometer (Jeong et al., 2016).

Effects of the Fungal Growth *in vitro*

The fungicidal activities of the peptide BP21 was determined by dose-response curves as previously described (López-García et al., 2002; Wang et al., 2018). BP21 was added to a final concentration of 0.25, 0.5, 1, 2, 4, 8, 16, 32, 64 μ M, respectively. In all experiments, three replicates were prepared for each treatment. The growth of the fungi was determined by measuring OD₆₀₀ using a Multiskan Spectrum microplate spectrophotometer (BioTek Instruments, Inc., United States) at 48 h after mixing with BP21. The minimum inhibitory concentration (MIC) of the peptide BP21 for three fungi was defined as the peptide BP21 concentration that completely inhibited growth in all the experiments carried out.

Scanning Electron Microscopy (SEM)

To determine the effect of BP21 on the mycelia morphology of the three fungi, a scanning electron microscopic (SEM) study was performed. The mycelia from 2-day-old culture were collected, washed, and then resuspended in sterilized distilled water. BP21 (10 or 100 μ mol L⁻¹) was mixed into the suspensions for 48 h, and controls without BP21 were tested similarly. The mycelia were collected and placed in vials containing 3.0% (v/v) glutaraldehyde in 0.05 mol L⁻¹ phosphate buffered saline (pH 6.8) at 4°C. The mycelia were kept in this solution for 48 h for fixation and then washed with 0.05 mol L⁻¹ phosphate buffered saline two times. The samples were dehydrated in an ethanol series (30, 50, 70, 85 and 95%, v/v) for 10 min in each alcohol dilution, ending with absolute ethanol twice. Then, the ethanol was replaced with tertiary butyl alcohol. After dehydration, the samples were dried with carbon dioxide. Finally, the specimens were sputter-coated with gold in an ion coater for 2 min. All samples were viewed in a JEOL JSM-6510LV SEM (JEOL, Tokyo,

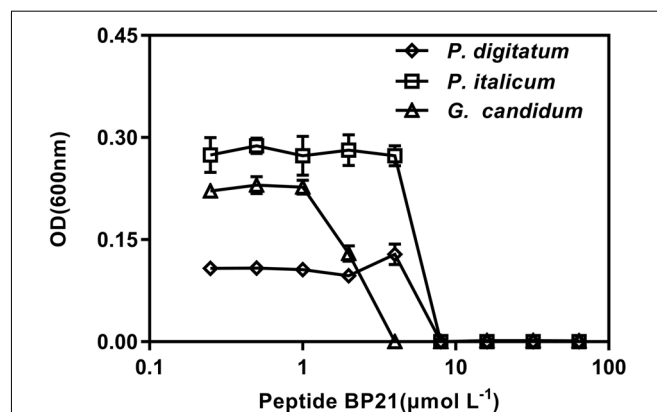


FIGURE 1 | Dose-response curves of the growth inhibition of *Penicillium digitatum*, *Penicillium italicum*, and *Geotrichum candidum* by BP21 *in vitro*. The data shown are the mean values of the OD measurements at each peptide concentration after 48 h of incubation for *P. digitatum*, *P. italicum*, and *G. candidum*. Vertical bars indicate the standard error of the means.

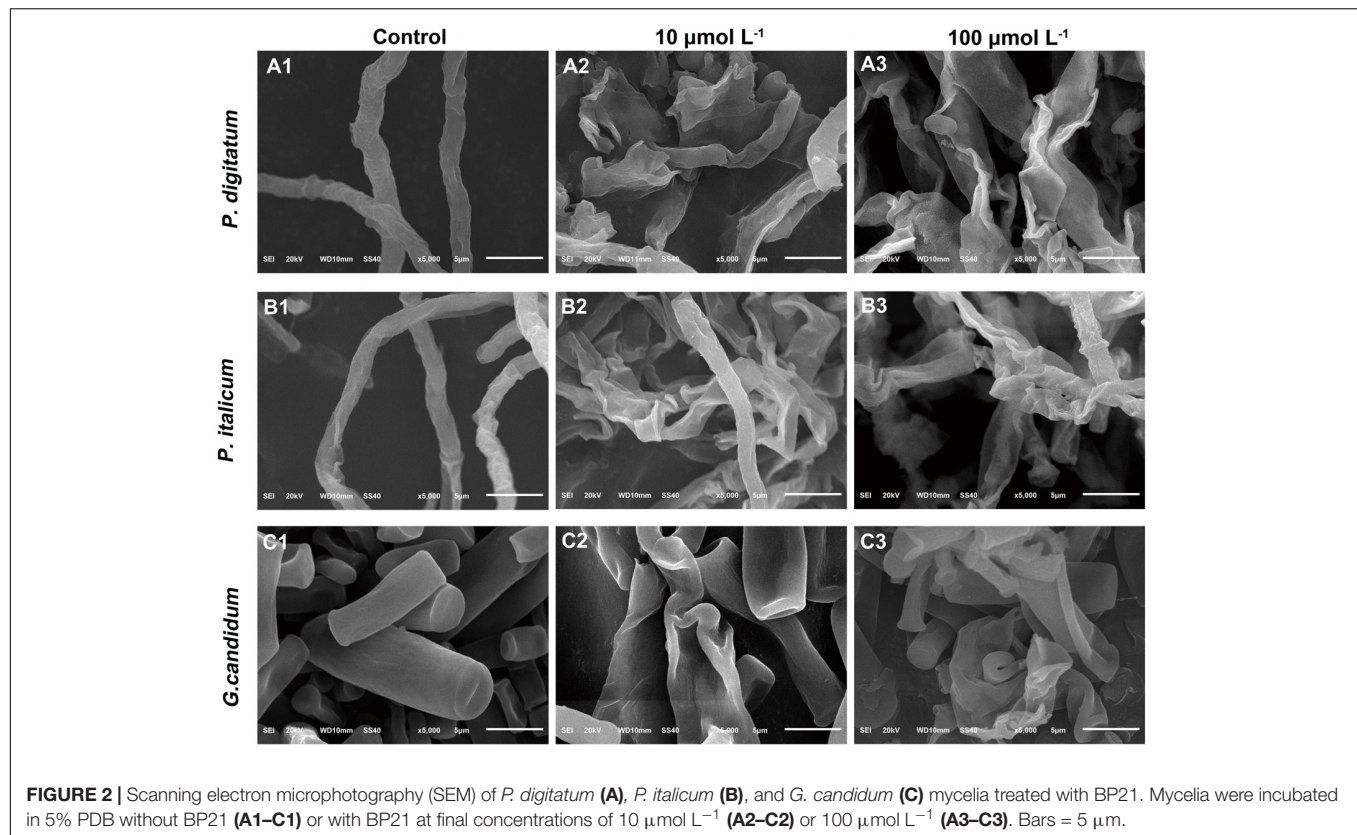


FIGURE 2 | Scanning electron microphotography (SEM) of *P. digitatum* (A), *P. italicum* (B), and *G. candidum* (C) mycelia treated with BP21. Mycelia were incubated in 5% PDB without BP21 (A1–C1) or with BP21 at final concentrations of 10 $\mu\text{mol L}^{-1}$ (A2–C2) or 100 $\mu\text{mol L}^{-1}$ (A3–C3). Bars = 5 μm .

Japan) operating at 25 kV at 5000 \times magnification (Tao et al., 2014).

Fluorescence Microscopy

The mode of action of BP21 with the mycelia was characterized by the fluorescent dye SYTOX Green (SG) (Molecular Probes; Invitrogen, Corp, Carlsbad, CA, United States) as described previously (Puig et al., 2016; Wang et al., 2018). BP21 was used to each treatment groups to reach a final concentration of 10 or 100 $\mu\text{mol L}^{-1}$. After incubation with BP21, the fungal suspensions were stained with SG. Fluorescence was examined and photographed with an Eclipse TS100 epifluorescence microscope (Nikon Corporation, Japan) with FITC filter sets. Simultaneous brightfield images were captured as well.

Measurement of Extracellular Conductivity, K^+ Efflux and Release of Cellular Constituents

BP21 was used to each treatment groups to reach a final concentration of 10 or 100 $\mu\text{mol L}^{-1}$. The extracellular conductivity of mycelia by using a DDS-307A conductivity meter (INESA, Shanghai, China) according to a previously described method (Wang et al., 2018), and controls without BP21 were tested similarly. Then, a previously described method was used to determine the amount of the potassium ions (Bajpai et al., 2013; Tao et al., 2014). The concentration of free potassium ions in the suspensions of *P. digitatum*, *P. italicum*, and *G. candidum*

mycelia was measured at 0, 3, 6, 9, 12, 24, and 48 h of treatment. The extracellular potassium concentration were determined in the supernatant using flame atomic absorption spectroscopy (Shimadzu AA6300, Japan).

The release of cellular constituents into the supernatant was measured according to a method described previously (Paul et al., 2011) with minor modifications. The release of cellular constituents into the supernatant was measured using a wavelength of 260 nm from a Multiskan Spectrum microplate spectrophotometer. Fungi was incubated in an environmental shaking incubator for 48 h, then the mycelia were collected and washed three times with phosphate buffered saline (pH 7.0) and resuspended in buffered saline. BP21 (10 or 100 $\mu\text{mol L}^{-1}$) was added to the suspensions, and controls without BP21 were tested similarly. The results were expressed in terms of the optical density of absorption at 260 nm at 0, 3, 6, 9, 12, 24, and 48 h of treatment.

Fruit Decay Tests

Experiments were carried out on freshly harvested navel oranges [*Citrus sinensis* (L.) Osbeck]. Fruit were harvested from a local orchard (Beibei, Chongqing). A previously described method was used in this experiment (Wang et al., 2018). Briefly, the fruit were surface-disinfected for 2 min in 2% sodium hypochlorite solution, washed and allowed to air dry. Citrus fruit were wounded (3 mm wide and 4 mm deep) by making punctures at two sites around the equator. The inocula contained 10^4 CFU mL^{-1} spores and peptide BP21 at 8 $\mu\text{mol L}^{-1}$ in water.

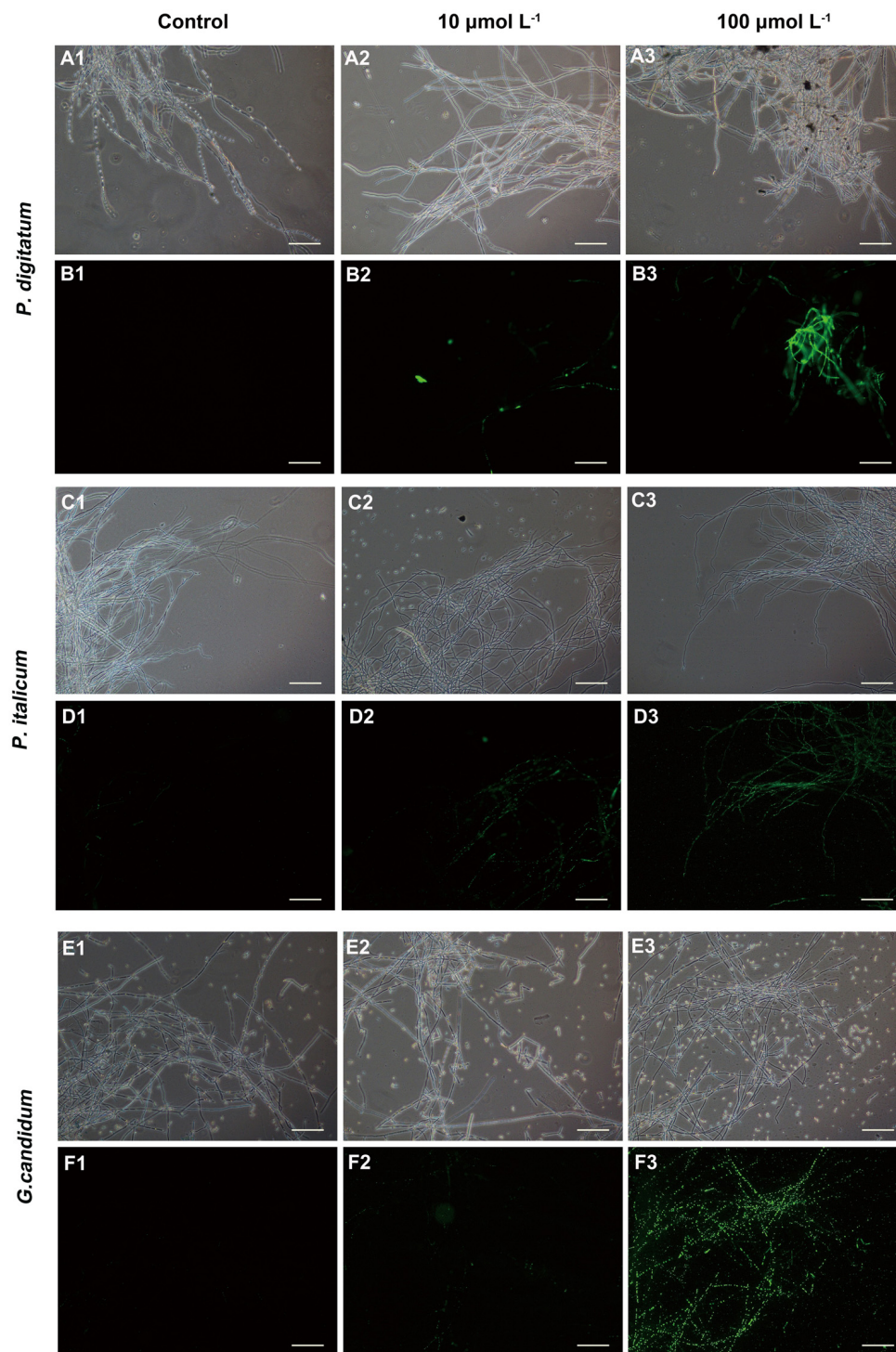


FIGURE 3 | Fluorescence microscopy analysis of *P. digitatum* (A,B), *P. italicum* (C,D), and *G. candidum* (E,F) mycelia treated with BP21. Mycelia were incubated in 5% PDB without BP21 (A1–F1) or with BP21 at final concentrations of 10 $\mu\text{mol L}^{-1}$ (A2–F2) or 100 $\mu\text{mol L}^{-1}$ (A3–F3). Bars = 100 μm .

As described in Section “Results,” two different times (A: 0 h; B: 16 h) of incubation of conidia with BP21 prior to inoculation were evaluated. Citrus fruit inoculated with conidia alone as the controls. The disease incidence (DI) and the lesion diameter

(LD) was assessed daily. Three replicates (15 fruits per replicate, 2 wounds per fruit) were prepared for each treatment. The mean values \pm SD of the DI and LD for each treatment were calculated.

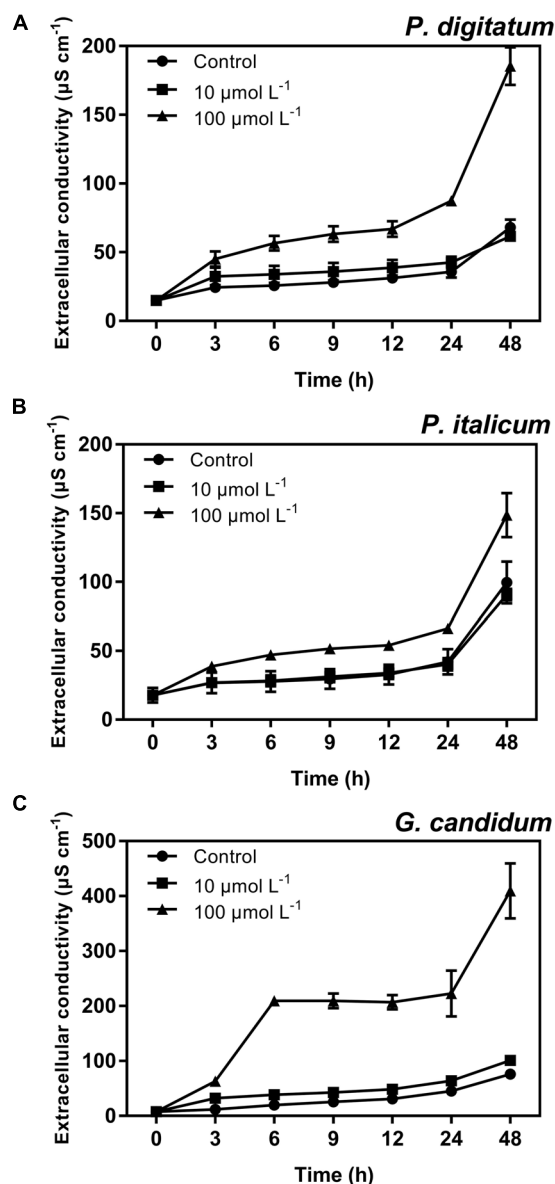


FIGURE 4 | Extracellular conductivity of *P. digitatum* (A), *P. italicum* (B), and *G. candidum* (C) mycelia treated with BP21. Mycelia were incubated in 10 or 100 $\mu\text{mol L}^{-1}$ or without BP21 (control) solutions. Vertical bars indicate the standard error of the means.

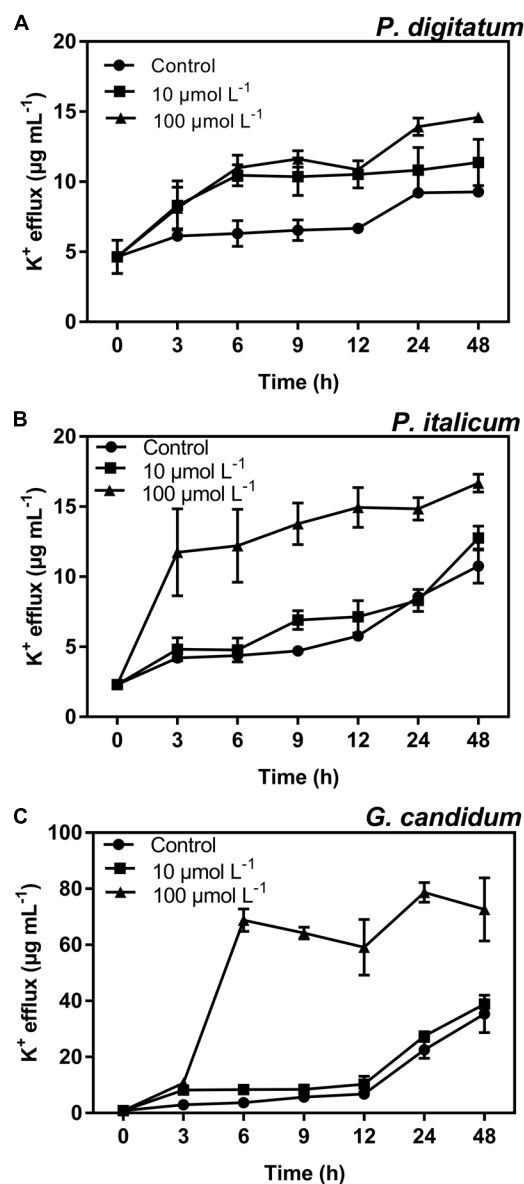


FIGURE 5 | K^+ efflux of *P. digitatum* (A), *P. italicum* (B), and *G. candidum* (C) mycelia treated with BP21. Mycelia were incubated in 10 or 100 $\mu\text{mol L}^{-1}$ or without BP21 (control) solutions. Vertical bars indicate the standard error of the means.

Hemolytic Activity of BP21

The hemolytic test was carried out by using 2% erythrocyte suspension, which was prepared from human blood according to the previous description (Muñoz et al., 2006) with partial modifications. No hemolysis and 100% hemolysis were determined for controls with normal saline (NS) and 0.1% Triton X-100, respectively. The AMPs BP21 (The final concentration was 8, 16, 32, or 64 $\mu\text{mol L}^{-1}$) was mixed with 2% red blood cells and incubated at 37°C for 1 h. After diluted 600 times, commercial Prochloraz was mixed with erythrocyte suspension. The samples were centrifuged at

1,000 $\times g$ for 5 min, and the supernatant was transferred to 96-well plates. Release of hemoglobin was determined by OD₅₄₀, and the data were measured by a Multiskan Spectrum microplate spectrophotometer. The hemolytic activity of peptide was calculated as the percentage of total hemoglobin released compared with that released by incubation with 0.1% Triton X-100.

Statistical Analysis

In the statistical analysis of the randomized complete block design, each treatment involved three replications, and the

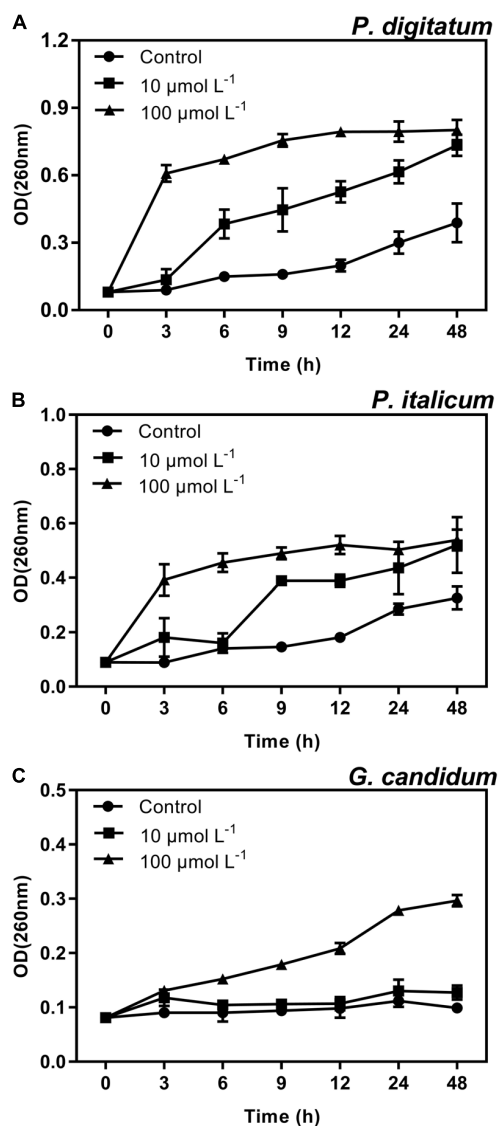


FIGURE 6 | Release of cellular constituents of *P. digitatum* (A), *P. italicum* (B), and *G. candidum* (C) mycelia treated with BP21. Mycelia were mixed with peptide BP21 at 10 or 100 µmol L⁻¹ or without BP21 (control) in phosphate buffered saline. Vertical bars indicate the standard error of the means.

entire experiment was conducted in triplicate. The data were analyzed via a one-way analysis of variance (ANOVA), followed by Duncan's multiple-range tests at $p < 0.05$ (SPSS Statistics 22.0, Inc.).

RESULTS

Growth Inhibition of the Fungi by BP21 *in vitro*

The *in vitro* growth inhibition activities of the peptide BP21 were tested (Figure 1). The peptide BP21 showed the best inhibitory activity toward these three fungi. The MIC of BP21

against *P. digitatum*, *P. italicum*, and *G. candidum* was 8, 8, and 4 µmol L⁻¹, respectively.

Effect of BP21 on Morphological Alterations of Fungal Mycelia Analyzed Using Scanning Electron Microscopy (SEM)

A SEM analysis was carried out to further visualize the effect of BP21 on the morphology of *P. digitatum*, *P. italicum*, and *G. candidum* mycelia, compared to control group (Figure 2). The control fungus without BP21 exhibited a regular and smooth surface (Figures 2A1,B1,C1). In contrast, *P. digitatum*, *P. italicum*, and *G. candidum* mycelia treated with BP21 (10 and 100 µmol L⁻¹) exhibited considerable changes in hyphal morphology. The mycelia treated with BP21 appeared to be severely collapsed due to leak. Mycelia became deformed, shrunken, and distorted (Figures 2A2,B2,C2,A3,B3,C3). Increasing concentrations of BP21 resulted in more serious damage.

Effect of BP21 on the Permeation of Fungal Mycelia Analyzed Using Fluorescence Microscopy

We used fluorescence microscopy and fluorescent dye SG to observe the mode of action of the mycelia with the peptide BP21. In controls in which mycelia was incubated with the SG probe without pretreatment with peptide BP21 (0 µmol L⁻¹), no appreciable SG green fluorescent signal was discerned by using fluorescence microscopy (Figures 3B1,D1,F1). Mycelia exhibited slight discontinuous green fluorescence at 10 µmol L⁻¹ BP21 (Figures 3B2,D2,F2). At this high BP21 concentration (100 µmol L⁻¹), SG green fluorescence staining was very intense all along the *P. digitatum* and *P. italicum* mycelia (Figures 3B3,D3). *G. candidum* mycelia exposed to BP21 at 100 µmol L⁻¹ exhibited discontinuous green fluorescent (Figure 3F3).

The Effect of BP21 on Extracellular Conductivity of Fungal Mycelia

Further antibacterial mode of action of peptide BP21 against the fungi was confirmed using the assay for the extracellular conductance (Figure 4). In this assay, the conductivity of all test groups increased gradually with increased treatment duration. The extracellular conductance sharply increased in the high-concentration (100 µmol L⁻¹) BP21 treatment group ($p < 0.05$). According to the results, the peptide BP21 could increase the extracellular conductivity of *P. digitatum*, *P. italicum*, and *G. candidum*.

Effect of BP21 on K⁺ Efflux of Fungal Mycelia

Potassium ions (K⁺) were found to leak from mycelia incubated with BP21 (Figure 5). BP21 significantly induced the release of K⁺, as the K⁺ efflux of the high-concentration (100 µmol L⁻¹) BP21 treatment group was significantly higher ($p < 0.05$) than

TABLE 1 | Effects of BP21 on the fungal infection of citrus fruits.

Pathogen	Days	DI (%)			LD (mm)		
		Control	A	B	Control	A	B
<i>P. digitatum</i>	3	70.00 ± 10.00 a	6.67 ± 5.77 b	0.00 ± 0.00 b	18.57 ± 2.23 a	1.30 ± 1.17 b	0.00 ± 0.00 b
	4	100.00 ± 0.00 a	73.33 ± 11.55 b	3.33 ± 5.77 c	60.43 ± 3.61 a	25.75 ± 9.07 b	1.42 ± 2.45 c
	5	100.00 ± 0.00 a	86.67 ± 5.77 b	3.33 ± 5.77 c	95.15 ± 2.75 a	58.28 ± 8.62 b	2.67 ± 4.62 c
<i>P. italicum</i>	4	30.00 ± 17.32 a	16.67 ± 5.77 b	0.00 ± 0.00 c	5.32 ± 1.50 a	2.92 ± 0.88 b	0.00 ± 0.00 c
	5	79.17 ± 8.78 a	70.00 ± 10.00 a	0.00 ± 0.00 b	20.04 ± 0.83 a	13.82 ± 0.36 b	0.00 ± 0.00 c
	6	93.33 ± 11.55 a	86.67 ± 11.55 a	3.33 ± 5.77 b	33.24 ± 3.35 a	26.00 ± 0.98 b	0.25 ± 0.43 c
<i>G. candidum</i>	8	13.33 ± 15.28 a	0.00 ± 0.00 b	0.00 ± 0.00 b	3.43 ± 3.45 a	0.00 ± 0.00 b	0.00 ± 0.00 b
	10	16.67 ± 11.55 a	0.00 ± 0.00 b	0.00 ± 0.00 b	6.80 ± 2.22 a	0.00 ± 0.00 b	0.00 ± 0.00 b
	12	16.67 ± 11.55 a	0.00 ± 0.00 b	0.00 ± 0.00 b	9.81 ± 4.29 a	0.00 ± 0.00 b	0.00 ± 0.00 b

Fruits were inoculated with conidia alone as control. Conidia were mixed with 8 $\mu\text{mol L}^{-1}$ BP21 and either immediately inoculated (A) or incubated for 16 h prior to inoculation (B). Values are mean \pm SD. The letters 'a,' 'b,' and 'c' indicate significant differences at the 0.05 level. The analysis was conducted using the data from the same pathogen on the same day.

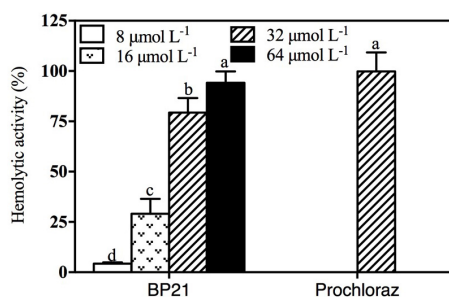


FIGURE 7 | Hemolytic activity of BP21. Release of hemoglobin was determined by the value of OD₅₄₀. The hemolytic activity is given as the mean \pm SD of the percentage of human erythrocyte hemolysis. Values followed by different letters are significantly different according to Duncan's multiple range test at $P < 0.05$.

that of the control. Incubation with 10 $\mu\text{mol L}^{-1}$ BP21 did not result in a K^+ release significantly different from that of the control mycelia for *P. italicum* and *G. candidum* mycelia, but this concentration of BP21 did induce the release of K^+ from *P. digitatum* mycelia. Moreover, *G. candidum* mycelia incubated with 100 $\mu\text{mol L}^{-1}$ BP21 displayed significantly increased K^+ release compared to the 10 $\mu\text{mol L}^{-1}$ BP21 treatment group and the control group.

Effect of BP21 on the Release of Cellular Constituents of Fungal Mycelia

Another strategy for determining the mode of action of BP21 against these three filamentous phytopathogenic was to analyze the release of 260 nm absorbing materials from the treated mycelia of *P. digitatum*, *P. italicum*, and *G. candidum*. The OD₂₆₀ value of the culture filtrates of *P. digitatum*, *P. italicum*, and *G. candidum* mycelia exposed to BP21 revealed an increasing release of cellular constituents with respect to exposure time (Figure 6). However, the OD₂₆₀ values of untreated (control) mycelia of *P. digitatum* and *P. italicum* increased slowly, and only slight changes in the OD₂₆₀ value of the untreated (control)

mycelia of *G. candidum* were observed. This finding directly confirms the release of cellular constituents from *P. digitatum*, *P. italicum*, and *G. candidum* treated with BP21.

Effect of BP21 on *P. digitatum*, *P. italicum*, and *G. candidum* Infections on Citrus Fruit

The inhibitory activity of the peptide BP21 against *P. digitatum*, *P. italicum*, and *G. candidum* infection was evaluated. The results showed that BP21 (treatment groups A and B) significantly inhibited citrus fruit diseases at 8 $\mu\text{mol L}^{-1}$ compared to the non-treated controls ($p < 0.05$) (Table 1). Treatment B resulted in the most effective control of the three fungi growth on citrus fruit, wherein the growth of green mold and blue mold was reduced by 90% or more. Treatment A was more effective than the control treatment, but it was not as beneficial as treatment B. It turned out that the antifungal activity of BP21 increased along with time of incubation. In addition, BP21 completely controlled the *G. candidum* infection on citrus fruit, the LD and DI % were 0 (A and B). This could be indicated that BP21 could also control infection *in vivo*.

Hemolytic Activity of BP21

Toxicity of different concentrations of BP21 to eukaryotic cells was determined by lysing human red blood cells (erythrocytes) (Figure 7). Prochloraz showed very high hemolytic activity, about 99.8%. Low concentration of BP21 showed low hemolysis, the hemolysis activity of BP21 at 8 $\mu\text{mol L}^{-1}$ was 4.30%. However, the higher the concentration, the higher the hemolysis activity.

DISCUSSION

Blue mold and green mold are the primary post-harvest pathogen of citrus, and there is little effective control measures for sour rot; sour rot could be controlled by low-temperature environment, but chilling injury still causes major bottlenecks (Mercier and Smilanick, 2005). Therefore, exploration of effective methods for controlling these diseases have become urgently needed.

Currently, the post-harvest application of short synthetic AMPs is an attractive alternative to fungicides (López-García et al., 2002).

In the present study, BP21 was shown to effectively inhibit the growth of *P. digitatum*, *P. italicum*, and *G. candidum* *in vitro*. When the concentration of BP21 was 8 $\mu\text{mol L}^{-1}$, these fungi could not grow (Figure 1). The results of the SEM analysis clearly showed the difference between the treated and untreated fungi mycelia. The mycelia treated with BP21 became shrunken, collapsed, distorted, and formed a rough surface (Figure 2). This effect on the cell membranes of pathogens is similar to the effect of several essential oils (Helal et al., 2007; Bajpai et al., 2013) and citral (Tao et al., 2014). The effect may be attributed to the leakage of intracellular constituents. The cell membrane plays an important role in cell life activities, and cell membrane breakage causes the leakage of small molecular substances and ions. SG signals showed that BP21 could change the membrane permeability (Figure 3). The SG signals were more strong at higher concentration groups than at lower concentration groups. The increase in BP21 concentration resulted in a concomitant increase in the damage to the cell membrane. This mode is very similar to many of the cationic AMPs, such as some PAFs (Harries et al., 2013; López-García et al., 2015) and tetralipopeptides (Makovitzki et al., 2006), their mode of action involves permeation and disintegration of membranes. Membrane permeability parameters, including extracellular conductivity (Figure 4), leakage of potassium ions (Figure 5), and release of cellular constituents (Figure 6), were used to indicate gross and irreversible damage to the cytoplasmic and membranes (Bajpai et al., 2013). These parameters visibly increased as the concentration of BP21 increased. Although, hemolytic activity was positively correlated with the concentration of BP21 (Figure 7). After systematic toxicity evaluation in future research, BP21 could also be used at lower concentrations or be modified to reduce its hemolysis.

The peptide BP21 was shown to effectively control of *P. digitatum*, *P. italicum*, and *G. candidum* infection in citrus fruits *in vivo* (Table 1). Conidia were incubated with BP21 at a single concentration (8 $\mu\text{mol L}^{-1}$) for 0 h (treatment A) or 16 h (treatment B) before inoculation. Treatment B resulted in the

best performance of control of fungi infect and growth on fruits. Treatment A was more effective than the control treatment, but it was not as effective as treatment B. Obviously, in treatment B, the BP21 had more time to interact with the conidia, thus resulting in better disease control. This finding suggests that BP21 could be applied in production by soaking the fruits in a BP21 solution for a short duration. More research on the most effective method is warranted.

CONCLUSION

The results of this study have shown that BP21 could effectively control infectious fungal diseases of citrus fruits, and it underlines the potential utility of BP21 as a novel broad-spectrum fungicide against pathogens of citrus as well. The major challenge of the widespread use of peptides for food and agriculture is to meet the requirement of a low production cost. Therefore, it is necessary to find or design peptides with no or little toxicity that control bacteria and fungi even when applied at low concentrations.

AUTHOR CONTRIBUTIONS

KZ conceived and supervised the project. WW and SL designed the experiments and performed most of the experiments. WW analyzed the data and wrote the manuscript. LD, SY, and JM gave advice and edited the manuscript. All authors read and approved the final manuscript.

FUNDING

This research was supported by the Technology Innovation Fund of Chongqing (Grant No. cstc2016shms-ztx80005), the Key Project in Applied Technology of Chongqing Science and Technology Commission (Grant No. cstc2017shms-xdny80058), and the Fundamental Research Funds for the Central Universities (Grant No. XDJK2017D132).

REFERENCES

- Alberola, J., Rodriguez, A., Francino, O., Roura, X., Rivas, L., and Andreu, D. (2004). Safety and efficacy of antimicrobial peptides against naturally acquired leishmaniasis. *Antimicrob. Agents Chemother.* 48, 641–643. doi: 10.1128/AAC.48.2.641-643.2004
- Andreu, D., Merrifield, R. B., Steiner, H., and Boman, H. G. (1983). Solid-phase synthesis of cecropin A and related peptides. *Proc. Natl. Acad. Sci. U.S.A.* 80, 6475–6479. doi: 10.1073/pnas.80.21.6475
- Badosa, E., Ferré, R., Francés, J., Bardají, E., Feliu, L., Planas, M., et al. (2009). Sporidicidal activity of synthetic antifungal undecapeptides and control of *Penicillium* rot of apples. *Appl. Environ. Microbiol.* 75, 5563–5569. doi: 10.1128/AEM.00711-09
- Bajpai, V. K., Sharma, A., and Baek, K. H. (2013). Antibacterial mode of action of *Cudrania tricuspidata* fruit essential oil, affecting membrane permeability and surface characteristics of food-borne pathogens. *Food Control* 32, 582–590. doi: 10.1016/j.foodcont.2013.01.032
- Chicharro, C., Granata, C., Lozano, R., Andreu, D., and Rivas, L. (2001). N-terminal fatty acid substitution increases the leishmanicidal activity of CA (1-7) M (2-9), a cecropin-melittin hybrid peptide. *Antimicrob. Agents Chemother.* 45, 2441–2449. doi: 10.1128/AAC.45.9.2441-2449.2001
- Ciociola, T., Giovati, L., Conti, S., Magliani, W., Santinoli, C., and Polonelli, L. (2016). Natural and synthetic peptides with antifungal activity. *Future Med. Chem.* 8, 1413–1433. doi: 10.4155/fmc-2016-0035
- Droby, S., Vinoku, V., Weiss, B., Cohen, L., Daus, A., Goldschmidt, E. E., et al. (2002). Induction of resistance to *Penicillium digitatum* in grapefruit by the yeast biocontrol agent *Candida oleophila*. *Phytopathology* 92, 393–399. doi: 10.1094/PHYTO.2002.92.4.393
- Ferre, R., Badosa, E., Feliu, L., Planas, M., Montesinos, E., and Bardají, E. (2006). Inhibition of plant-pathogenic bacteria by short synthetic cecropin A-melittin hybrid peptides. *Appl. Environ. Microbiol.* 72, 3302–3308. doi: 10.1128/AEM.72.5.3302-3308.2006
- Ferre, R., Melo, M. N., Correia, A. D., Feliu, L., Bardají, E., Planas, M., et al. (2009). Synergistic effects of the membrane actions of cecropin-melittin antimicrobial hybrid peptide BP100. *Biophys. J.* 96, 1815–1827. doi: 10.1016/j.bpj.2008.11.053
- Harries, E., Carmona, L., Muñoz, A., Ibeas, J. I., Read, N. D., Gandía, M., et al. (2013). Genes involved in protein glycosylation determine the activity and cell

- internalization of the antifungal peptide PAF26 in *Saccharomyces cerevisiae*. *Fungal Genet. Biol.* 58, 105–115. doi: 10.1016/j.fgb.2013.08.004
- Helal, G. A., Sarhan, M. M., Abu Shahla, A. N. K., and Abou El-Khair, E. K. (2007). Effects of *Cymbopogon citratus* L. essential oil on the growth, morphogenesis and aflatoxin production of *Aspergillus flavus* ML2-strain. *J. Basic Microbiol.* 47, 5–15. doi: 10.1002/jobm.200610137
- Ismail, M., and Zhang, J. (2004). Post-harvest citrus diseases and their control. *Outlooks Pest Manage.* 15, 29–35. doi: 10.1564/15feb12
- Jenssen, H., Hamill, P., and Hancock, R. E. (2006). Peptide antimicrobial agents. *Clin. Microbiol. Rev.* 19, 491–511. doi: 10.1128/CMR.00056-05
- Jeong, R. D., Chu, E. H., Lee, G. W., Cho, C., and Park, H. J. (2016). Inhibitory effect of gamma irradiation and its application for control of postharvest green mold decay of Satsuma mandarins. *Int. J. Food Microbiol.* 234, 1–8. doi: 10.1016/j.jfoodmicro.2016.06.026
- Keymanesh, K., Soltani, S., and Sardari, S. (2009). Application of antimicrobial peptides in agriculture and food industry. *World J. Microbiol. Biotechnol.* 25, 933–944. doi: 10.1007/s11274-009-9984-7
- López-García, B., Harries, E., Carmona, L., Campos-Soriano, L., López, J. J., Manzanares, P., et al. (2015). Concatemerization increases the inhibitory activity of short, cell-penetrating, cationic and tryptophan-rich antifungal peptides. *Appl. Microbiol. Biotechnol.* 99, 8011–8021. doi: 10.1007/s00253-015-6541-1
- López-García, B., Pérez-Payá, E., and Marcos, J. F. (2002). Identification of novel hexapeptides bioactive against phytopathogenic fungi through screening of a synthetic peptide combinatorial library. *Appl. Environ. Microbiol.* 68, 2453–2460. doi: 10.1128/AEM.68.5.2453-2460.2002
- Makovitzki, A., Avrahami, D., and Shai, Y. (2006). Ultrashort antibacterial and antifungal lipopeptides. *Proc. Natl. Acad. Sci. U.S.A.* 103, 15997–16002. doi: 10.1073/pnas.0606129103
- Makovitzki, A., Viterbo, A., Brotman, Y., Chet, I., and Shai, Y. (2007). Inhibition of fungal and bacterial plant pathogens in vitro and in planta with ultrashort cationic lipopeptides. *Appl. Environ. Microbiol.* 73, 6629–6636. doi: 10.1128/AEM.01334-07
- Mercier, J., and Smilanick, J. L. (2005). Control of green mold and sour rot of stored lemon by biofumigation with *Muscodor albus*. *Biol. Control* 32, 401–407. doi: 10.1016/j.biocontrol.2004.12.002
- Muñoz, A., López-García, B., and Marcos, J. F. (2006). Studies on the mode of action of the antifungal hexapeptide PAF26. *Antimicrob. Agents Chemother.* 50, 3847–3855. doi: 10.1128/AAC.00650-06
- Muñoz, A., López-García, B., and Marcos, J. F. (2007). Comparative study of antimicrobial peptides to control citrus postharvest decay caused by *Penicillium digitatum*. *J. Agric. Food Chem.* 55, 8170–8176. doi: 10.1021/jf0718143
- Paul, S., Dubey, R. C., Maheswari, D. K., and Kang, S. C. (2011). *Trachyspermum ammi* (L.) fruit essential oil influencing on membrane permeability and surface characteristics in inhibiting food-borne pathogens. *Food Control* 22, 725–731. doi: 10.1016/j.foodcont.2010.11.003
- Puig, M., Moragrega, C., Ruz, L., Calderón, C. E., Cazorla, F. M., Montesinos, E., et al. (2016). Interaction of antifungal peptide BP15 with *Stemphylium vesicarium*, the causal agent of brown spot of pear. *Fungal Biol.* 120, 61–71. doi: 10.1016/j.funbio.2015.10.007
- Puig, M., Moragrega, C., Ruz, L., Montesinos, E., and Llorente, I. (2014). Postinfection activity of synthetic antimicrobial peptides against *Stemphylium vesicarium* in pear. *Phytopathology* 104, 1192–1200. doi: 10.1094/PHYTO-02-14-0036-R
- Romanazzi, G., Feliziani, E., Baños, S. B., and Sivakumar, D. (2017). Shelf life extension of fresh fruit and vegetables by chitosan treatment. *Crit. Rev. Food Sci. Nutr.* 57, 579–601. doi: 10.1080/10408398.2014.900474
- Schirra, M., D'Aquino, S., Cabras, P., and Angioni, A. (2011). Control of postharvest diseases of fruit by heat and fungicides: efficacy, residue levels, and residue persistence. A review. *J. Agric. Food Chem.* 59, 8531–8542. doi: 10.1021/jf201899t
- Tao, N., OuYang, Q., and Jia, L. (2014). Citral inhibits mycelial growth of *Penicillium italicum* by a membrane damage mechanism. *Food Control* 41, 116–121. doi: 10.1016/j.foodcont.2014.01.010
- Wang, W., Deng, L., Yao, S., and Zeng, K. (2018). Control of green and blue mold and sour rot in citrus fruits by the cationic antimicrobial peptide PAF56. *Postharvest Biol. Technol.* 136, 132–138. doi: 10.1016/j.postharvbio.2017.10.015

Conflict of Interest Statement: The authors declare that the research was conducted in the absence of any commercial or financial relationships that could be construed as a potential conflict of interest.

Copyright © 2018 Wang, Liu, Deng, Ming, Yao and Zeng. This is an open-access article distributed under the terms of the Creative Commons Attribution License (CC BY). The use, distribution or reproduction in other forums is permitted, provided the original author(s) and the copyright owner(s) are credited and that the original publication in this journal is cited, in accordance with accepted academic practice. No use, distribution or reproduction is permitted which does not comply with these terms.



Phomopsis longanae Chi-Induced Change in ROS Metabolism and Its Relation to Pericarp Browning and Disease Development of Harvested Longan Fruit

Hui Wang¹, Yihui Chen¹, Hetong Lin^{1*}, Junzheng Sun¹, Yifen Lin¹ and Mengshi Lin²

¹ Institute of Postharvest Technology of Agricultural Products, College of Food Science, Fujian Agriculture and Forestry University, Fuzhou, China, ² Food Science Program, Division of Food Systems and Bioengineering, University of Missouri, Columbia, MO, United States

OPEN ACCESS

Edited by:

Hongyin Zhang,
Jiangsu University, China

Reviewed by:

Jinhe Bai,
U.S. Horticultural Research
Laboratory, United States
Zisheng Luo,
Zhejiang University, China

*Correspondence:

Hetong Lin
hetonglin@126.com;
hetonglin@163.com

Specialty section:

This article was submitted to
Food Microbiology,
a section of the journal
Frontiers in Microbiology

Received: 30 June 2018

Accepted: 26 September 2018

Published: 16 October 2018

Citation:

Wang H, Chen Y, Lin H, Sun J, Lin Y
and Lin M (2018) *Phomopsis*
longanae Chi-Induced Change
in ROS Metabolism and Its Relation
to Pericarp Browning and Disease
Development of Harvested Longan
Fruit. *Front. Microbiol.* 9:2466.
doi: 10.3389/fmicb.2018.02466

Phomopsis longanae Chi is a major pathogenic fungus that infects harvested longan fruit. This study aimed to investigate the effects of *P. longanae* on reactive oxygen species (ROS) metabolism and its relation to the pericarp browning and disease development of harvested longan fruit during storage at 28°C and 90% relative humidity. Results showed that compared to the control longans, *P. longanae*-inoculated longans displayed higher indexes of pericarp browning and fruit disease, higher $O_2^{\cdot-}$ generation rate, higher accumulation of malondialdehyde (MDA), lower contents of glutathione (GSH) and ascorbic acid (AsA), lower 1,1-diphenyl-2-picrylhydrazyl (DPPH) radical scavenging ability and reducing power in pericarp. In addition, *P. longanae*-infected longans exhibited higher activities of superoxide dismutase (SOD), catalase (CAT), and ascorbate peroxidase (APX) in the first 2 days of storage, and lower activities of SOD, CAT, and APX during storage day 2–5 than those in the control longans. These findings indicated that pericarp browning and disease development of *P. longanae*-infected longan fruit might be the result of the reducing ROS scavenging ability and the increasing $O_2^{\cdot-}$ generation rate, which might lead to the peroxidation of membrane lipid, the loss of compartmentalization in longan pericarp cells, and subsequently cause polyphenol oxidase (PPO) and peroxidase (POD) to contact with phenolic substrates which result in enzymatic browning of longan pericarp, as well as cause the decrease of disease resistance to *P. longanae* and stimulate disease development of harvested longan fruit.

Keywords: longan fruit, disease development, pericarp browning, reactive oxygen species (ROS), ROS metabolism, ROS scavenging ability, *Phomopsis longanae* Chi

INTRODUCTION

Longan (*Dimocarpus longan* Lour.) is a popular tropical fruit famous for its appealing flavor and abundant nutritional ingredients (Lin et al., 2001; Chen et al., 2015). However, harvested longan fruits deteriorate rapidly due to water loss, injury, energy deficiency, pathogen infection, or damage caused by reactive oxygen, resulting in pericarp browning, decline of fruit quality and rot (Holcroft et al., 2005). Pericarp browning is a vital factor affecting edible quality and commercial value of postharvest longan fruits seriously (Jiang et al., 2002).

There are abundant phenolic compounds in longan pericarp tissue (Prasad et al., 2009; Yang et al., 2011). Researches indicated that pericarp browning of postharvest longan fruit was mainly due to the formation of browning substances resulting from enzymatic browning (Wang et al., 2015; Lin et al., 2017b).

Reactive oxygen species (ROS), such as superoxide anion ($O_2^{\cdot-}$) and hydrogen peroxide (H_2O_2), was reported to cause pericarp browning of fruits (Shah et al., 2017). Overaccumulation of ROS could lead to peroxidation of membrane lipid, loss of compartmentalization of cells and organelles, and formation of browning substances when peroxidase (POD) and polyphenol oxidase (PPO) contact with phenols (Lin Y.F. et al., 2016; Lin et al., 2017a; Sun et al., 2018). There are active oxygen-scavenging enzymes including catalase (CAT), superoxide dismutase (SOD), and ascorbate peroxidase (APX) (Jiang et al., 2015; Luo et al., 2015; Xu et al., 2017; Chen et al., 2019). Moreover, plant cells contain non-enzymatic endogenous antioxidant substances, including glutathione (GSH) and ascorbic acid (AsA) (Sun et al., 2018).

Fungal infection is a main problem in quality keeping for harvested longan fruits (Chen et al., 2014; Zhang et al., 2017, 2018). *Phomopsis longanae* Chi is a major fungus infecting postharvest longans (Chen et al., 2014, 2018b). *P. longanae*-inoculation could induce disease development and pericarp browning of postharvest longans (Chen et al., 2018a). However, there is no comprehensive understanding about the mechanisms of disease development and pericarp browning of postharvest longans induced by *P. longanae*.

This study aimed to analyze effects of *P. longanae*-inoculation on production rate of $O_2^{\cdot-}$, content of malondialdehyde (MDA) (resulting from oxidative damage of membrane lipids), activities of CAT, SOD, and APX, levels of GSH and AsA, reducing power and 1,1-diphenyl-2-picrylhydrazyl (DPPH) radical scavenging ability, and to explore mechanisms of pericarp browning and disease development of postharvest longans induced by *P. longanae*-infection.

MATERIALS AND METHODS

Materials and Treatments

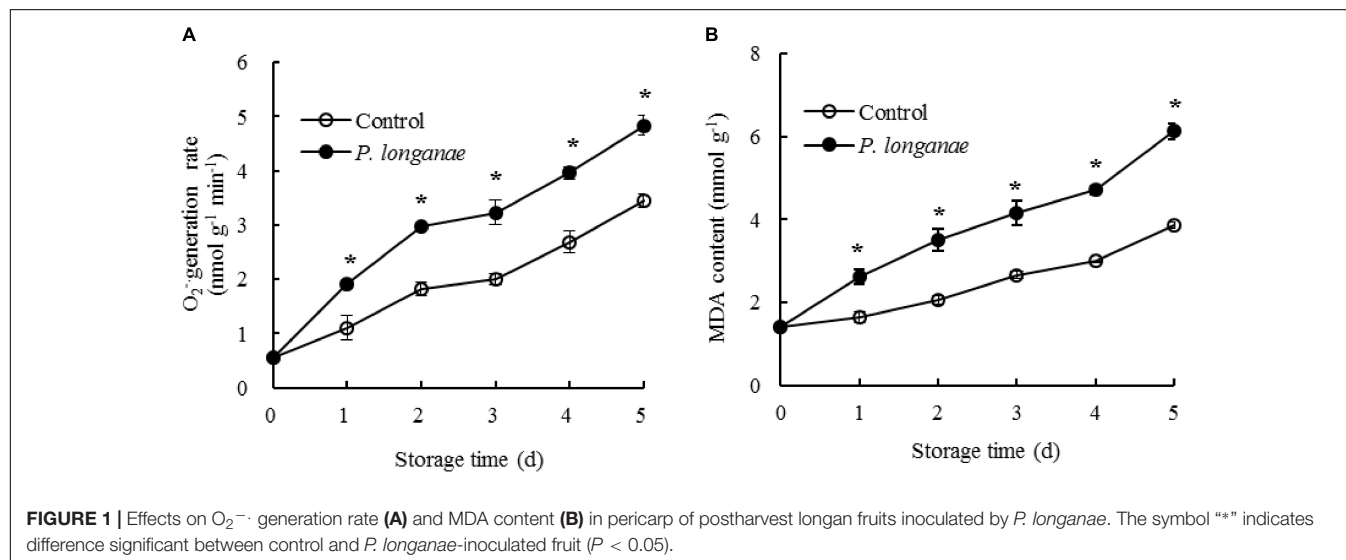
The spore suspension of *P. longanae* with the concentration of $\times 10^4$ spores mL^{-1} was prepared according to Chen et al. (2014).

Longan (*Dimocarpus longan* Lour. cv. Fuyan) fruits at commercial maturity were harvested from an orchard in Quanzhou, Fujian, China, thereafter carried back by a refrigerated truck to our laboratory in less than 3 h.

Fruits were selected with absence of injury or diseases, and uniform size, color and maturity. and absence of injury, blemishes, insect pests or diseases. Fruits were surface-sterilized by dipped in 0.5% NaClO for 10 s, thereafter were air dried. Then 30,150 longans were used for experiment. Among them, 150 fruits were selected for used for analysis on the harvest day (day 0). The rest 3,000 longans were divided into a control group (1,500 longans) and a *P. longanae*-inoculated group (1,500 longans). Longans in control group were dipped in sterile deionized water for 5 min, while longans in another group used for inoculation were treated by *P. longanae* spore suspension instead of sterile deionized water for 5 min. After air-dried, all the treated fruits were packed (50 fruits/bag) in polyethylene bags (0.015-mm-thick). Each treatment contains 30 bags. Then the fruits were stored under the same storage condition of 28°C and 90% relative humidity. 150 fruits (3 bags) from each treatment were randomly selected at each storage day to determine the physiological and biochemical indexes and their relations to longan pericarp browning and disease development caused by *P. longanae* (Chen et al., 2018a).

$O_2^{\cdot-}$ Generation Rate and MDA Content

One gram of pericarp tissue from 10 longans was used for analysis of $O_2^{\cdot-}$ the generation rate according to previously reported method (Lin et al., 2014). The $O_2^{\cdot-}$ generating rate was represented as $nmol\ g^{-1}\ min^{-1}$.



One gram of pericarp tissue from 10 longans was used for measurement of MDA content according to previously reported method (Lin et al., 2014). The MDA content was represented as mmol g^{-1} .

Activities of SOD, CAT, and APX

The activities of SOD, CAT, and APX, and the protein content were determined using one gram of pericarp from 10 longans, respectively, referring to previously reported method (Sun et al., 2018). Activities of these enzymes were represented as U mg^{-1} protein.

Contents of GSH and AsA

One gram of pericarp tissue from 10 longans was used to measure contents of GSH and AsA, respectively, according to previously reported method (Sun et al., 2018). The contents of GSH and AsA were represented as mg kg^{-1} .

DPPH Radical Scavenging Activity and Reducing Power

One gram of pericarp tissue from 10 longans was used to measure DPPH radical scavenging activity and reducing power, respectively, with previously reported method (Sun et al., 2018). The DPPH radical scavenging ability and reducing power were represented as % and g kg^{-1} , respectively.

Statistical Analysis

All experiments were repeated for three times. Data were represented in form of means \pm standard error. Statistical analyses were performed for analyzing the data by SPSS Statistics (version 17.0). Statistical differences were assessed with a significant level when P -value less than 0.05.

RESULTS

Effects of *P. longanae* Infection on $\text{O}_2^{\cdot-}$ Generation Rate and MDA Content in Pericarp of Harvested Longan Fruit

The generation rate of $\text{O}_2^{\cdot-}$ in pericarp tissue of the control longan fruits rose rapidly within 0–2 days, then a slow increase from 2 to 3 days, thereafter a quick increase during 3–5 days of storage (Figure 1A). The $\text{O}_2^{\cdot-}$ generation rate in *P. longanae*-inoculated longan fruits showed a trend similar as the control longans. Moreover, the $\text{O}_2^{\cdot-}$ generation rate was higher ($P < 0.05$) in postharvest longans inoculated by *P. longanae* compared to the control longans during 1–5 days of storage.

The content of MDA in pericarp tissue of the control longan fruits presented a gradual rise in storage days 0–5 (Figure 1B). While the content of MDA in postharvest longans inoculated by *P. longanae* showed a rapid rise from 0 day of storage. For example, the MDA content of *P. longanae*-inoculated longan fruits increased about 4-fold from storage day 0 to day 5. Statistical comparison suggested that the MDA content in postharvest longans inoculated by *P. longanae* was higher

($P < 0.05$) compared to the control longan fruits during 1–5 days of storage.

Effects of *P. longanae* Infection on Activities of SOD, CAT, and APX in Pericarp of Harvested Longan Fruit

The SOD activity changed little during 0–1 day of storage, and thereafter declined rapidly in pericarp tissue of the control longan

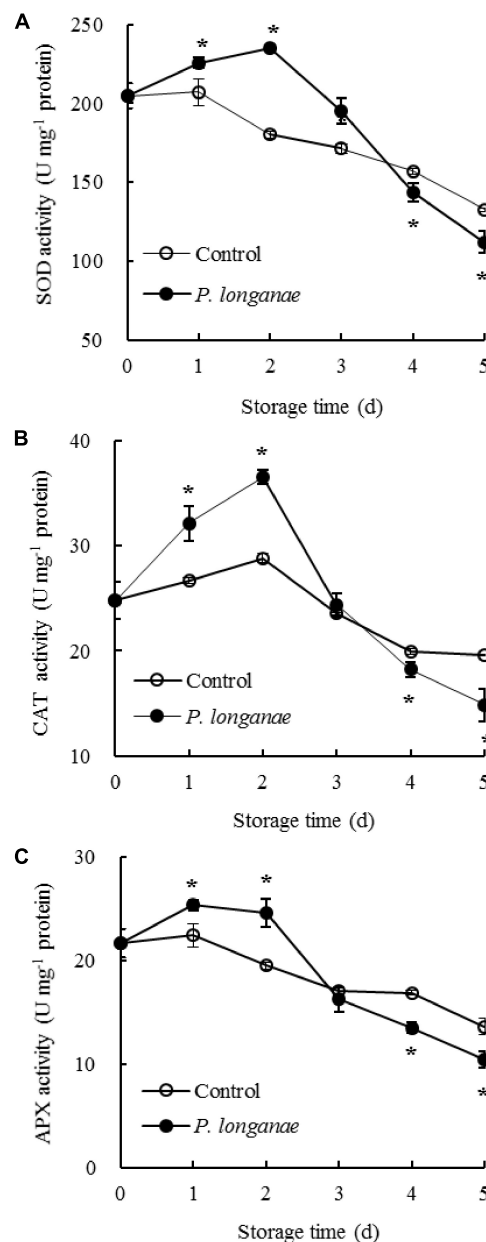


FIGURE 2 | Effects on activities of SOD (A), CAT (B), and APX (C) in pericarp of postharvest longans inoculated by *P. longanae*. The symbol “*” indicates difference significant between control and *P. longanae*-inoculated fruit ($P < 0.05$).

fruits (**Figure 2A**). While SOD activity increased within 0–2 days of storage, thereafter decreased quickly in longans inoculated by *P. longanae*. Compared to control longans, the *P. longanae*-inoculation treated longans showed a higher ($P < 0.05$) and a lower ($P < 0.05$) SOD activity during 1–3 and 4–5 days, respectively.

The CAT activity in the control longan pericarp tissue rose slightly during the first 0–2 days, then declined rapidly after 2 days of storage (**Figure 2B**). Whereas, the CAT activity showed a dramatic rise in the first 0–2 days of storage and declined sharply thereafter in *P. longanae*-inoculated longans. Further comparison showed CAT activity was higher ($P < 0.05$) in pericarp tissue of postharvest longans inoculated by *P. longanae* within 0–2 days of storage, and lower ($P < 0.05$) on the storage day 5 compared to the control longans.

Figure 2C showed that in control longan pericarp tissue the APX activity changed little within 0–1 day, followed by a reduction from 1 to 5 days. However, the APX activity in *P. longanae*-inoculated longan fruits showed a noticeably rise during 0–1 day, and changed little during 1–2 days, then declined rapidly during 2–5 days. Furthermore, in pericarp tissue of longans inoculated by *P. longanae*, APX activity was higher ($P < 0.05$) within the first 2 days, and lower ($P < 0.05$) during 4–5 days of storage compared to control longans.

Effects of *P. longanae* Infection on Contents of GSH and AsA in Pericarp of Harvested Longan Fruit

Contents of GSH and AsA reduced rapidly as storage time prolonging in pericarp tissue of the control longan fruit

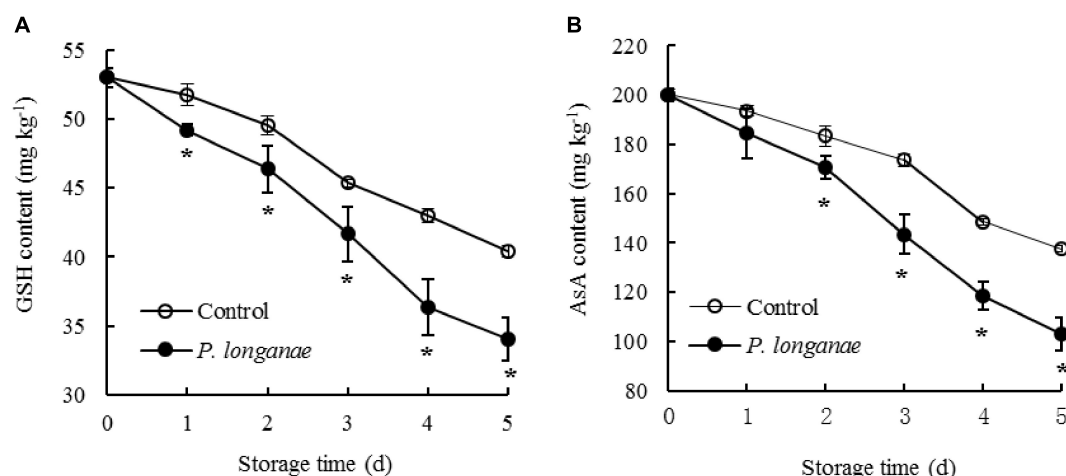


FIGURE 3 | Effects on contents of GSH (**A**) and AsA (**B**) in pericarp of postharvest longans inoculated by *P. longanae*. The symbol “*” indicates difference significant between control and *P. longanae*-inoculated fruit ($P < 0.05$).

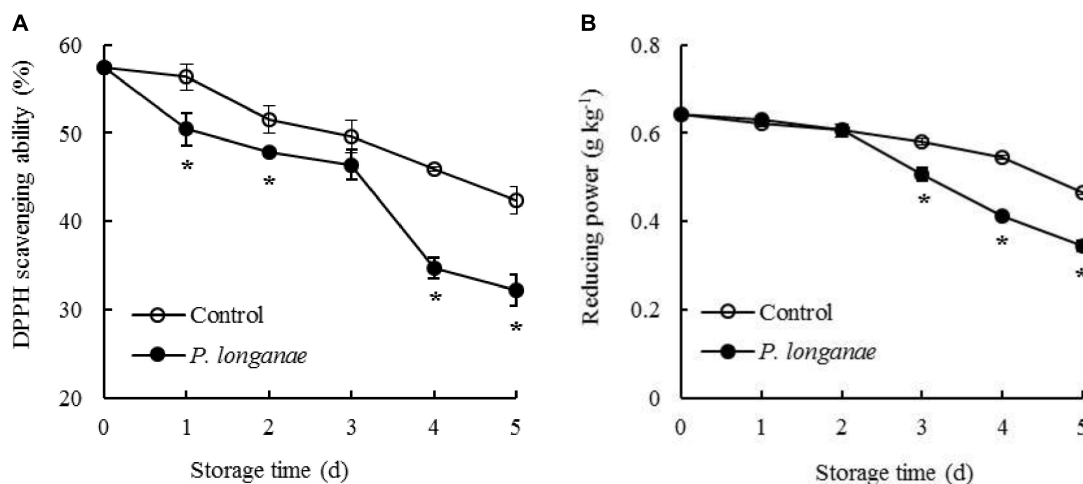


FIGURE 4 | Effects on DPPH radical scavenging ability (**A**) and reducing power (**B**) of postharvest longans inoculated by *P. longanae*. The symbol “*” indicates difference significant between control and *P. longanae*-inoculated fruit ($P < 0.05$).

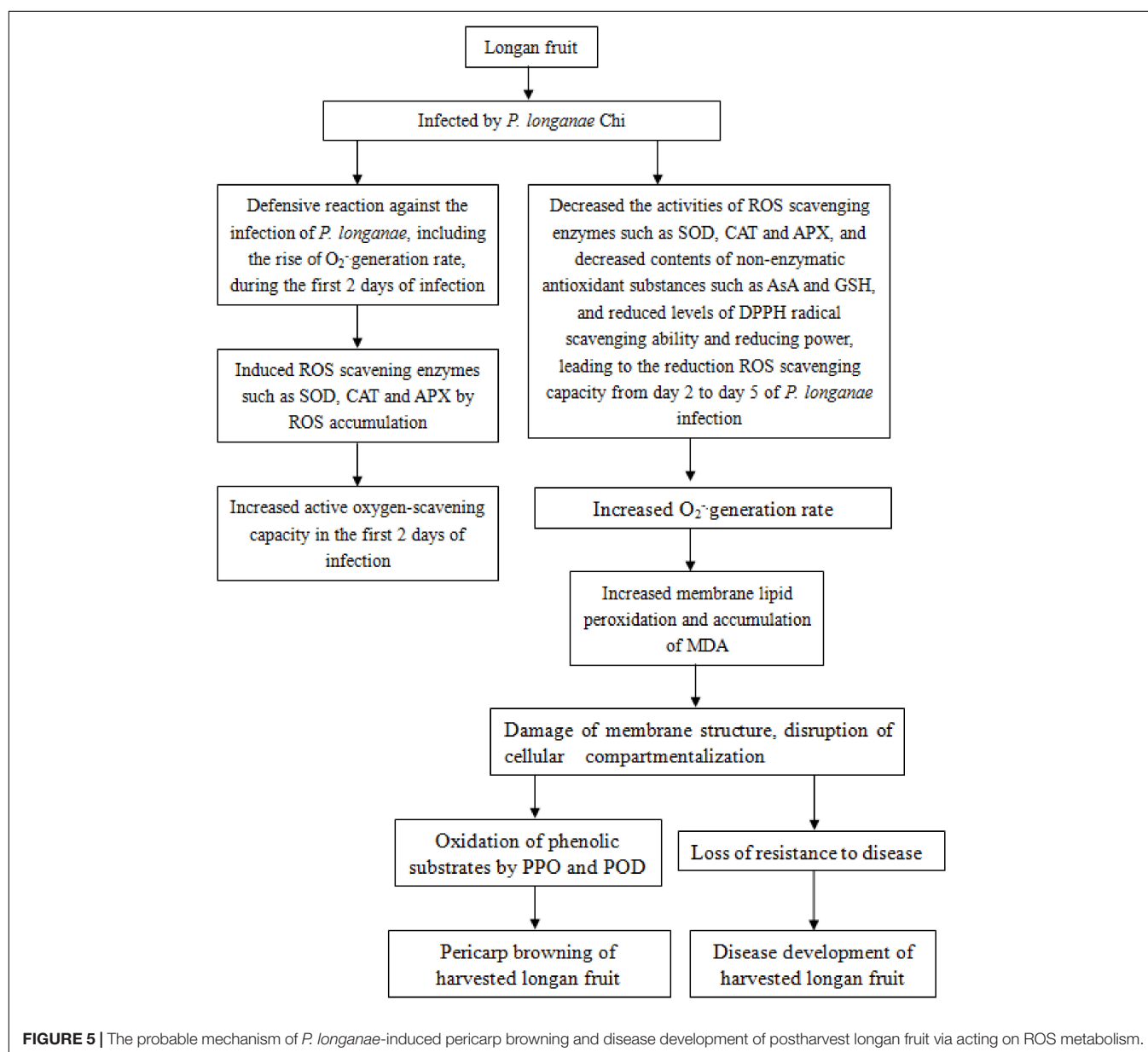
(Figure 3). Compared to control longan fruit, *P. longanae*-inoculated longans displayed faster decline of contents of GSH and AsA from 0 to 5 days. Moreover, the contents of GSH and ASA were lower ($P < 0.05$) in longans inoculated by *P. longanae* compared to the control longans during 2–5 days of storage.

Effects of *P. longanae* Infection on DPPH Radical Scavenging Ability and Reducing Power in Pericarp of Harvested Longan Fruit

The DPPH radical scavenging ability in control longan pericarp tissue exhibited a slightly decrease from 0 to 1 day, followed by a faster decreased from 1 to 5 days of storage

(Figure 4A). Whereas, the DPPH radical scavenging ability in longans inoculated by *P. longanae* exhibited a rapid decline from 0 d, thereafter a decrease during 1–3 days, a sharp reduction during 3–4 days, then a fast decline during 4–5 days. Furthermore, there was a lower ($P < 0.05$) DPPH radical scavenging ability in longans inoculated by *P. longanae* compared to the control longans within 1–5 days except storage day 3.

The reducing power decreased slowly within 0–4 days in pericarp tissue of the control longan fruits, thereafter declined rapidly from 4 to 5 days of storage (Figure 4B). While the reducing power in longans inoculated by *P. longanae* decreased slightly during 0–2 days, then declined remarkably from 4.06 g kg^{-1} on storage day 3 to 2.76 g kg^{-1} on day 5. Compared to the control longans, the



P. longanae-inoculation treated longan fruits showed a lower ($P < 0.05$) reducing power in pericarp tissue during 3–5 days of storage.

DISCUSSION

Longan fruit is prone to turn to pericarp browning and diseased after harvest, which results in a decline in fruit quality and commercial value, and is the main limitation of its long-time storage and long-distant transport (Sun et al., 2018). Pathogen infection is a major reason accounting for disease and pericarp browning of postharvest longans (Chen et al., 2014). Disease development and pericarp browning of postharvest longans was thought to be related to reactive oxygen metabolism disorder and accumulation of ROS (Chomkitichai et al., 2014; Lin Y.X. et al., 2016). It has been reported that H_2O_2 and $O_2^{\cdot-}$ accumulated during the process of disease and pericarp browning development in harvested longans (Lin et al., 2017a). Chen et al. (2018a) reported that compared to the control longans, *P. longanae*-inoculated longans displayed higher indexes of pericarp browning and fruit disease. In present work, results showed that *P. longanae*-infection induced the rise of $O_2^{\cdot-}$ generation rate (Figure 1A). During 0–2 days of storage, the rise of $O_2^{\cdot-}$ generation rate might be related with the defensive reaction against the infection of *P. longanae* (Sun et al., 2018). MDA is a product resulting from oxidative damage of membrane lipids (Wang et al., 2013, 2014, 2015). In this study, the content of MDA accumulated as storage time prolonging (Figure 1B). However, *P. longanae*-infection enhanced the accumulation of MDA, indicating that the biomembrane system was seriously damaged in *P. longanae*-inoculated longan fruit.

In plant cells, there are ROS scavenging enzymes playing crucial roles in protecting cells from oxidative stress (Blokina et al., 2003; Luo et al., 2015; Xu et al., 2017; Chen et al., 2019). SOD can catalyze two $O_2^{\cdot-}$ to H_2O_2 and O_2 (Duan et al., 2007). Both CAT and APX could catalyze H_2O_2 to H_2O and O_2 (Yi et al., 2010). Under normal circumstances, the ROS is in a dynamic equilibrium between generation and scavenging. However, when the equilibrium is broken under stress conditions, ROS would be accumulated (Yi et al., 2008; Sun et al., 2018). The increase of ROS account for membrane lipid peroxidation and cellular compartmentalization lost, leading to the disease increase and enzymatic browning resulting from oxidation of phenolic substrates by PPO and POD (Sun et al., 2010; Lin et al., 2013, 2017c, 2018; Jiang et al., 2018). It has been reported that the enhanced activities of CAT, SOD, and APX might be caused by pathogen infection in early infection stage to scavenge excessed ROS in harvested longans (Lin et al., 2015). Whereas, the activities of CAT, SOD, and APX decreased with prolonged storage time, leading to the increase of $O_2^{\cdot-}$ content, peroxidation of membrane lipid and increased browning of harvested longans (Sun et al., 2018).

In present study, activities of SOD, CAT, and APX showed rise within 0–2 days in *P. longanae*-inoculated longans (Figure 2). Meanwhile, the generation rate of $O_2^{\cdot-}$ increase quickly (Figure 1A). Thus, the enhanced activities of SOD, CAT, and APX

when $O_2^{\cdot-}$ generation rate rise in early stage (0–2 days of storage) of *P. longanae*-infection might be a defense to reduce contents of ROS. Besides, in longans infected by *P. longanae* activities of CAT, SOD, and APX decreased rapidly during 2–5 days of storage while the $O_2^{\cdot-}$ generation rate still exhibited a trend of increase. This indicated that the equilibrium between ROS scavenging enzymes and ROS was broken during 2–5 days of storage, resulting in the rise of $O_2^{\cdot-}$ generation rate, membrane lipid peroxidation, and accumulation of MDA.

In addition, non-enzymatic antioxidant substances, including GSH and AsA, exist in fruit tissues, playing important roles in ROS elimination (Jiang et al., 2015, 2018). AsA and GSH participate in the reaction of catalyzing H_2O_2 to H_2O by APX (Lin et al., 2017a). Our results presented that contents of GSH and AsA decreased quickly in longans inoculated by *P. longanae* and showed a lower ($P < 0.05$) compared with the control longan fruits during 2–5 days of storage (Figure 3). It can be inferred that *P. longanae*-infection induced decrease of GSH and AsA contents in pericarp tissue of postharvest longan fruits, which might account for the increase of $O_2^{\cdot-}$ generation rate during storage.

Besides, there is another free radical-scavenging system for inhibiting lipid peroxidation (Sun et al., 2018). The reducing power and DPPH radical scavenging activity were generally tested to analysis the antioxidant activity (Sun et al., 2007; Lin et al., 2017a). The browning in pathogen infected fruit pericarp tissue was thought to be correlated with the reduced reducing power and the decline of DPPH radical scavenging activity (Sun et al., 2018). In this research, the *P. longanae*-inoculated longans showed lower reducing power and DPPH radical scavenging ability compared to control longans in late storage period (4–5 days). Meanwhile, the $O_2^{\cdot-}$ generation rate (Figure 1A), pericarp browning developed faster in *P. longanae*-inoculated longan compared with control longans (Chen et al., 2018a). This suggested that the rising $O_2^{\cdot-}$ generation rate and browning index of *P. longanae*-inoculated longans might due to the reduced antioxidant activity.

CONCLUSION

In conclusion, the disruption of reactive oxygen scavenging system by *P. longanae* inoculation might be a vital reason causing pericarp browning accelerated and disease increased of postharvest longan fruits. The increasing $O_2^{\cdot-}$ generation rate and content of MDA in longans infected by *P. longanae* might be the result of the decreased ROS scavenging enzyme activities, the reduced the contents of non-enzymatic antioxidant substances, the declined reducing power, and the lowered DPPH radical scavenging ability, which leads to the peroxidation of membrane lipid, the loss of compartmentalization in longan pericarp cells, and subsequently cause PPO and POD to contact with phenolic substrates, in turn, result in enzymatic browning of longan pericarp, as well as cause the decrease of disease resistance to *P. longanae* and stimulate disease development of harvested longan fruit. The probable mechanism of *P. longanae*-induced pericarp browning and disease development of postharvest

longan fruit via acting on ROS metabolism was demonstrated in **Figure 5**.

AUTHOR CONTRIBUTIONS

HW and YC performed the experiments. HL designed the research. JS and YL conducted the experiments and analyzed the data. HW and YC wrote the manuscript. HL revised the manuscript. ML edited English language of the manuscript. All authors have approved the submission and publication of the manuscript.

REFERENCES

- Bloknina, O., Virolainen, E., and Fagerstedt, K. V. (2003). Antioxidants, oxidative damage and oxygen deprivation stress: a review. *Ann. Bot.* 91, 179–194. doi: 10.1093/aob/mcf118
- Chen, M. Y., Lin, H. T., Zhang, S., Lin, Y. F., Chen, Y. H., and Lin, Y. X. (2015). Effects of adenosine triphosphate (ATP) treatment on postharvest physiology, quality and storage behavior of longan fruit. *Food Bioproc. Technol.* 8, 971–982. doi: 10.1007/s11947-014-1462-z
- Chen, Y., Lin, H., Jiang, Y., Zhang, S., Lin, Y., and Wang, Z. (2014). *Phomopsis longanae* Chi-induced pericarp browning and disease development of harvested longan fruit in association with energy status. *Postharvest Biol. Technol.* 93, 24–28. doi: 10.1016/j.postharvbio.2014.02.003
- Chen, Y. H., Hung, Y. C., Chen, M. Y., Lin, M. S., and Lin, H. T. (2019). Enhanced storability of blueberries by acidic electrolyzed oxidizing water application may be mediated by regulating ROS metabolism. *Food Chem.* 270, 229–235. doi: 10.1016/j.foodchem.2018.07.095
- Chen, Y. H., Lin, H. T., Zhang, S., Sun, J. Z., Lin, Y. F., Wang, H., et al. (2018a). *Phomopsis longanae* Chi-induced disease development and pericarp browning of harvested longan fruit in association with energy metabolism. *Front. Microbiol.* 9:1454. doi: 10.3389/fmicb.2018.01454
- Chen, Y. H., Zhang, S., Lin, H. T., Sun, J. Z., Lin, Y. F., Wang, H., et al. (2018b). *Phomopsis longanae* Chi-induced changes in activities of cell wall-degrading enzymes and contents of cell wall components in pericarp of harvested longan fruit and its relation to disease development. *Front. Microbiol.* 9:1051. doi: 10.3389/fmicb.2018.01051
- Chomkitichai, W., Faiyue, B., Rachtanapun, P., Uthabutra, J., and Saengnil, K. (2014). Enhancement of the antioxidant defense system of post-harvested 'Daw' longan fruit by chlorine dioxide fumigation. *Sci. Hortic.* 178, 138–144. doi: 10.1016/j.scienta.2014.08.016
- Duan, X. W., Su, X. G., You, Y. L., Qu, H. X., Li, Y. B., and Jiang, Y. M. (2007). Effect of nitric oxide on pericarp browning of harvested longan fruit in relation to phenolic metabolism. *Food Chem.* 104, 571–576. doi: 10.1016/j.foodchem.2006.12.007
- Holcroft, D. M., Lin, H. T., and Ketsa, S. (2005). "Harvesting and storage," in *Litchi and longan: Botany, Production and Uses*, eds C. M. Menzel and G. K. Waite (Wallingford: CAB International), 273–295. doi: 10.1079/9780851996967.0273
- Jiang, T. J., Luo, Z. S., and Ying, T. J. (2015). Fumigation with essential oils improves sensory quality and enhanced antioxidant ability of shiitake mushroom (*Lentinus edodes*). *Food Chem.* 172, 692–698. doi: 10.1016/j.foodchem.2014.09.130
- Jiang, X. J., Lin, H. T., Lin, M. S., Chen, Y. H., Wang, H., Lin, Y. X., et al. (2018). A novel chitosan formulation treatment induces disease resistance of harvested litchi fruit to *Peronophythora litchii* in association with ROS metabolism. *Food Chem.* 266, 299–308. doi: 10.1016/j.foodchem.2018.01.095
- Jiang, Y. M., Zhang, Z. Q., Joyce, D. C., and Ketsa, S. (2002). Postharvest biology and handling of longan fruit (*Dimocarpus longan* Lour.). *Postharvest Biol. Technol.* 26, 241–252. doi: 10.1016/S0925-5214(02)00047-9
- Lin, H. T., Chen, S. J., Chen, J. Q., and Hong, Q. Z. (2001). Current situation and advances in post-harvest storage and transportation technologies of longan fruit. *Acta Hortic.* 558, 343–351. doi: 10.17660/ActaHortic.2001.558.56
- Lin, Y. F., Chen, M. Y., Lin, H. T., Hung, Y. C., Lin, Y. X., Chen, Y. H., et al. (2017a). DNP and ATP induced alteration in disease development of *Phomopsis longanae* Chi inoculated longan fruit by acting on energy status and reactive oxygen species production-scavenging system. *Food Chem.* 228, 497–505. doi: 10.1016/j.foodchem.2017.02.045
- Lin, Y. F., Lin, Y. X., Lin, H. T., Ritenour, M. A., Shi, J., Zhang, S., et al. (2017b). Hydrogen peroxide-induced pericarp browning of harvested longan fruit in association with energy metabolism. *Food Chem.* 225, 31–36. doi: 10.1016/j.foodchem.2016.12.088
- Lin, Y. F., Lin, Y. X., Lin, H. T., Shi, J., Chen, Y. H., and Wang, H. (2017c). Inhibitory effects of propyl gallate on membrane lipids metabolism and its relation to increasing storability of harvested longan fruit. *Food Chem.* 217, 133–138. doi: 10.1016/j.foodchem.2016.08.065
- Lin, Y. F., Hu, Y. H., Lin, H. T., Liu, X., Chen, Y. H., Zhang, S., et al. (2013). Inhibitory effects of propyl gallate on tyrosinase and its application in controlling pericarp browning of harvested longan longans. *J. Agric. Food Chem.* 61, 2889–2895. doi: 10.1021/jf305481h
- Lin, Y. F., Lin, H. T., Lin, Y. X., Zhang, S., Chen, Y. H., and Jiang, X. J. (2016). The roles of metabolism of membrane lipids and phenolics in hydrogen peroxide-induced pericarp browning of harvested longan fruit. *Postharvest Biol. Technol.* 111, 53–61. doi: 10.1016/j.postharvbio.2015.07.030
- Lin, Y. F., Lin, H. T., Zhang, S., Chen, Y. H., Chen, M. Y., and Lin, Y. X. (2014). The role of active oxygen metabolism in hydrogen peroxide-induced pericarp browning of harvested longan fruit. *Postharvest Biol. Technol.* 96, 42–48. doi: 10.1016/j.postharvbio.2014.05.001
- Lin, Y. F., Lin, Y. X., Lin, H. T., Chen, Y. H., Wang, H., and Shi, J. (2018). Application of propyl gallate alleviates pericarp browning in harvested longan fruit by modulating metabolisms of respiration and energy. *Food Chem.* 240, 863–869. doi: 10.1016/j.foodchem.2017.07.118
- Lin, Y. F., Lin, Y. X., Lin, H. T., Zhang, S., Chen, Y. H., and Shi, J. (2015). Inhibitory effects of propyl gallate on browning and its relationship to active oxygen metabolism in pericarp of harvested longan fruit. *LWT Food Sci. Technol.* 60, 1122–1128. doi: 10.1016/j.lwt.2014.10.008
- Lin, Y. X., Lin, Y. F., Chen, Y. H., Wang, H., Shi, J., and Lin, H. T. (2016). Hydrogen peroxide induced changes in energy status and respiration metabolism of harvested longan fruit in relation to pericarp browning. *J. Agric. Food Chem.* 64, 4627–4632. doi: 10.1016/j.foodchem.2016.12.088
- Luo, Z. S., Li, D. D., Du, R. X., Mou, W. S., and Mao, L. C. (2015). Hydrogen sulfide alleviates chilling injury of banana fruit by enhanced antioxidant capacity and proline content. *Sci. Hortic.* 183, 144–151. doi: 10.1016/j.scienta.2014.12.021
- Prasad, K. N., Hao, J., Shi, J., Liu, T., Li, J., Wei, X. Y., et al. (2009). Antioxidant and anticancer activities of high pressure-assisted extract of longan (*Dimocarpus longan* Lour) fruit pericarp. *Innov. Food Sci. Emerg.* 10, 413–419. doi: 10.1016/j.ifset.2009.04.003
- Shah, H. M. S., Khan, A. S., and Ali, S. (2017). Pre-storage kojic acid application delays pericarp browning and maintains antioxidant activities of litchi fruit. *Postharvest Biol. Technol.* 132, 154–161. doi: 10.1016/j.postharvbio.2017.06.004
- Sun, J., Lin, H., Zhang, S., Lin, Y., Wang, H., Lin, M., et al. (2018). The roles of ROS production-scavenging system in *Lasiodiplodia theobromae* (Pat.) Griff. & Maubl.-induced pericarp browning and disease development of harvested longan fruit. *Food Chem.* 247, 16–22. doi: 10.1016/j.foodchem.2017.12.017

FUNDING

This work was supported by the National Natural Science Foundation of China (Grant Nos. 31671914, 31171776, and 31772035), the Natural Science Foundation of Fujian Province of China (Grant No. 2017J01429), the National Science Fund for Distinguished Young Scholars at Fujian Province University of China (Grant No. KLa16036A), and the Science Fund for Distinguished Young Scholars at Fujian Agriculture and Forestry University of China (Grant No. XJQ201512).

- Sun, J., Shi, J., Jiang, Y. M., Xue, S. J., and Wei, X. Y. (2007). Identification of two polyphenolic compounds with antioxidant activities in *longan* pericarp tissues. *J. Agric. Food Chem.* 55, 5864–5868. doi: 10.1021/jf070839z
- Sun, J., Zhang, Z., Xu, L. X., Li, Z. C., Wang, Z. X., and Li, C. B. (2010). Comparison on characterization of *longan* (*Dimocarpus longan* Lour) polyphenoloxidase using endogenous and exogenous substrates. *J. Agric. Food Chem.* 58, 10195–10201. doi: 10.1021/jf101639d
- Wang, H., Zhi, W., Qu, H. X., Lin, H. T., and Jiang, Y. M. (2015). Application of α -aminoisobutyric acid and β -aminoisobutyric acid inhibits pericarp browning of harvested *longan* fruit. *Chem. Cent. J.* 9:54. doi: 10.1186/s13065-015-0124-1
- Wang, Y. S., Luo, Z. S., Du, R. X., Liu, Y., Ying, T. J., and Mao, L. C. (2013). Effect of nitric oxide on antioxidative response and proline metabolism in banana during cold storage. *J. Agric. Food Chem.* 61, 8880–8887. doi: 10.1021/jf401447y
- Wang, Y. S., Luo, Z. S., Huang, X. D., Yang, K. L., and Gao, S. J. (2014). Effect of exogenous γ -aminobutyric acid (GABA) treatment on chilling injury and antioxidant capacity in banana. *Sci. Hortic.* 168, 132–137. doi: 10.1016/j.scienta.2014.01.022
- Xu, Y. Q., Luo, Z. S., Charles, M. T., Rolland, D., and Roussel, D. (2017). Pre-harvest UV-C irradiation triggers VOCs accumulation with alteration of antioxidant enzymes and phytohormones in strawberry leaves. *J. Plant Physiol.* 218, 265–274. doi: 10.1016/j.jplph.2017.09.002
- Yang, B., Jiang, Y., Shi, J., Chen, F., and Ashraf, M. (2011). Extraction and pharmacological properties of bioactive compounds from *longan* (*Dimocarpus longan* Lour.) fruit—a review. *Food Res. Int.* 44, 1837–1842. doi: 10.1016/j.foodres.2010.10.019
- Yi, C., Jiang, Y. M., Shi, J., Qu, H. X., Xue, S., Duan, X. W., et al. (2010). ATP regulation of antioxidant properties and phenolics in litchi fruit during browning and pathogen infection process. *Food Chem.* 118, 42–47. doi: 10.1016/j.foodchem.2009.04.074
- Yi, C., Qu, H. X., Jiang, Y. M., Shi, J., Duan, X. W., Joyce, D. C., et al. (2008). ATP induced changes in energy status and membrane integrity of harvested litchi fruit and its relation to pathogen resistance. *J. Phytopathol.* 156, 365–371. doi: 10.1111/j.1439-0434.2007.01371.x
- Zhang, S., Lin, H. T., Lin, Y. F., Lin, Y. X., Hung, Y. C., Chen, Y. H., et al. (2017). Energy status regulates disease development and respiratory metabolism of *Lasiodiplodia theobromae* (Pat.) Griff. & Maubl.-infected *longan* fruit. *Food Chem.* 231, 238–246. doi: 10.1016/j.foodchem.2017.03.132
- Zhang, S., Lin, Y. Z., Lin, H. T., Lin, Y. X., Chen, Y. H., Wang, H., et al. (2018). *Lasiodiplodia theobromae* (Pat.) Griff. & Maubl.-induced disease development and pericarp browning of harvested *longan* fruit in association with membrane lipids metabolism. *Food Chem.* 244, 93–101. doi: 10.1016/j.foodchem.2017.10.020

Conflict of Interest Statement: The authors declare that the research was conducted in the absence of any commercial or financial relationships that could be construed as a potential conflict of interest.

Copyright © 2018 Wang, Chen, Lin, Sun, Lin and Lin. This is an open-access article distributed under the terms of the Creative Commons Attribution License (CC BY). The use, distribution or reproduction in other forums is permitted, provided the original author(s) and the copyright owner(s) are credited and that the original publication in this journal is cited, in accordance with accepted academic practice. No use, distribution or reproduction is permitted which does not comply with these terms.



Antifungal Activity and Action Mechanism of Ginger Oleoresin Against *Pestalotiopsis microspora* Isolated From Chinese Olive Fruits

Tuanwei Chen¹, Ju Lu¹, Binbin Kang², Mengshi Lin³, Lijie Ding¹, Lingyan Zhang¹, Guoying Chen⁴, Shaojun Chen¹ and Hetong Lin^{1*}

¹ College of Food Science, Fujian Agriculture and Forestry University, Fuzhou, China, ² Fujian Bio-Engineering Professional Technology Institute, Fuzhou, China, ³ Food Science Program, Division of Food System & Bioengineering, University of Missouri, Columbia, MO, United States, ⁴ U.S. Department of Agriculture, Agricultural Research Service, Eastern Regional Research Center, Wyndmoor, PA, United States

OPEN ACCESS

Edited by:

Nengguo Tao,
Xiangtan University, China

Reviewed by:

Masoomah Shams-Ghahfarokhi,
Tarbiat Modares University, Iran
Zhanquan Zhang,
Key Laboratory of Plant Resources,
Institute of Botany (CAS), China

*Correspondence:

Hetong Lin
hetonglin@126.com;
hetonglin@163.com

Specialty section:

This article was submitted to
Food Microbiology,
a section of the journal
Frontiers in Microbiology

Received: 30 June 2018

Accepted: 10 October 2018

Published: 30 October 2018

Citation:

Chen T, Lu J, Kang B, Lin M, Ding L, Zhang L, Chen G, Chen S and Lin H (2018) Antifungal Activity and Action Mechanism of Ginger Oleoresin Against *Pestalotiopsis microspora* Isolated From Chinese Olive Fruits. *Front. Microbiol.* 9:2583. doi: 10.3389/fmicb.2018.02583

Pestalotiopsis microspora (*P. microspora*) is one of dominant pathogenic fungi causing rotten disease in harvested Chinese olive (*Canarium album* Lour.) fruits. The purposes of this study were to evaluate the antifungal activities of ginger oleoresin (GO) against *P. microspora* and to illuminate the underlying action mechanisms. The *in vitro* assays indicate that GO exhibited strong antifungal activity against mycelial growth of *P. microspore*, and with 50%-inhibition concentration (EC_{50}) and 90%-inhibition concentration (EC_{90}) at 2.04 μ L GO and 8.87 μ L GO per mL propylene glycol, respectively, while the minimal inhibitory concentration (MIC) and minimal fungicidal concentration were at 10 μ L GO and 30 μ L GO per mL propylene glycol, respectively. Spore germination of *P. microspora* was inhibited by GO in a dose-dependent manner, and with 100% inhibition rate at the concentration of 8 μ L GO per mL propylene glycol. Compared to the control, the cellular membrane permeability of *P. microspora* increased due to severe leakage of intercellular electrolytes, soluble proteins, and total sugars with the treatments (EC_{50} , EC_{90}) by GO during incubation. In addition, analysis of fatty acid contents and compositions in cellular membrane by GC-MS indicated that GO could significantly promote the degradation or peroxidation of unsaturated fatty acids in *P. microspore*, resulting in the enhancement of membrane fluidity. Moreover, observations of microstructure further showed the damage to plasma membrane and morphology of *P. microspora* caused by GO, which resulted in distortion, sunken and shriveled spores and mycelia of the pathogen. Furthermore, *in vivo* assay confirmed that over 3 MIC GO treatments remarkably suppressed disease development in *P. microspore* inoculated-Chinese olive fruit. These results demonstrate that owing to its strong antifungal activity, GO can be used as a promising antifungal agent to inhibit the growth of pathogenic fungi in Chinese olives.

Keywords: Chinese olive (*Canarium album* Lour.), fruit, pathogenic fungi, *Pestalotiopsis microspora*, ginger oleoresin, antifungal activity, action mechanism

INTRODUCTION

Chinese olive (*Canarium album* (Lour.) Raeusch), a widely consumed subtropical fruit, is endemic to southeast China. It has a fusiform drupe and is in yellowish green similar to Mediterranean olive (*Olea europaea* L.), but has a relatively low oil content (Zhan et al., 2015). Matured Chinese olive fruits are usually consumed fresh or processed by the food industry to beverages, candy, and other products that conserve high nutritional values. They possess great pharmacological functions such as detoxification and inhibition against bacteria, virus, inflammation, and oxidation (He et al., 2008; Kuo et al., 2015; Chang et al., 2017; Lin et al., 2017). However, unfortunately, putrefaction can develop due to pathogenic infections in the harvested fresh fruits of Chinese olive, which may result in considerable quality losses and a shorter shelf life. A long list of pathogens has been reported causing postharvest infectious diseases of Chinese olive fruits, including *Pestalotiopsis microspora*, *Fusarium oxysporum* Schlecht., *Monochaetia karstenii* (Sacc & Syd.) Sutton, *Pestalotiopsis eriobotrya folia* (Guba) Chen et Chao, *Glomerella cingulata* (Stonem.) Spauld. Et Schrenk, *Colletotrichum gloeosporioides* Penz., *Botryodiplodia theobromae* Pat., *Penicillium* sp., and *Phytophthora palmivora* (Butl.) Butler (Chen et al., 2015, 2016a,b). Our previous studies demonstrated that *P. microspora* is a dominant pathogenic fungus that can make fruits rot (Chen et al., 2016b).

To date, traditional chemical fungicides such as prochloraz, thiophanate methyl, and carbendazol have been extensively used to combat infectious diseases in postharvest Chinese olive fruits. However, pesticide residues in fruits can lead to harmful effects on human health and the development of fungicide resistance in pathogens. Hence, there remains a need to develop safer, more effective and eco-friendly alternative fungicides that cause minimal damage to the environment and human health.

The use of botanical fungicides was considered a viable and better alternative approach for the control of pathogenic fungi because effective control of a variety of rot pathogens in diverse foods have been reported (Nanasombat and Wimuttigol, 2011; Jayasena and Jo, 2013; Bag and Chattopadhyay, 2015; Chaemsanit et al., 2018). For example, ginger oleoresin (GO), a complex mixture extracted from ginger (*Zingiber officinale* Roscoe), is rich in gingerols and shogaols. Some previous studies showed that GO had good capability of inhibiting the growth of certain types of fungi, such as *Aspergillus* species, *Fusarium moniliforme*, *Fusarium verticillioides*, *Rhizoctonia solani*, *Cryptococcus Neoformans*, *Candida albicans*, and *Penicillium* spp. (Singh et al., 2008; Yamamoto-Ribeiro et al., 2013; Bellik, 2014; Ashraf et al., 2017; Varakumar et al., 2017). However, to the best of our knowledge, little information is available on the antifungal activity and the mode of action of GO against *P. microspora* in Chinese olives. Thus, this study aimed to verify a hypothesis that GO is a potent antifungal agent against *P. microspora* in Chinese olives.

The main goal of this study was to investigate the effects of GO *in vitro* on the growth of *P. microspora* in Chinese olives. In addition, the changes of structures and components

of cell membrane were also evaluated to elucidate the possible antifungal mechanism of GO. Moreover, antifungal effects of the GO treatment on the *in vivo* disease development of *P. microspora* in Chinese olive fruits were also evaluated.

MATERIALS AND METHODS

Preparation of *P. microspora* Spore Suspension

Pestalotiopsis microspora (GL-3) was isolated from Chinese olive (*Canarium album* Lour. cv. Changying) fruit via tissue isolation and identified using the methods of morphology, molecular biology, and phylogenetic analysis as described by Chen et al. (2016a). *P. microspora* (GL-3) was preserved at Institute of Postharvest Technology of Agricultural Products, College of Food Science, Fujian Agriculture and Forestry University, Fuzhou, China.

The preparation of *P. microspora* spore suspension was based on the method of Chen et al. (2016b). Briefly, *P. microspora* was inoculated in autoclaved potato dextrose agar (PDA) medium for activation, and then transferred to oat bran medium (OB, contains 60 g oat flour, 60 g rice bran flour, 20 g sugar, and 20 g agar per liter) for inoculation for 7 d at 28°C. The plates were then washed with sterile 0.9% of NaCl and the solutions were transferred into sterile conical bottles and gently shaken to release spores. Finally, the spore suspensions were filtered through multilayers of sterile gauze to remove mycelial fragments, and adjusted to 1×10^6 spores mL^{-1} with the aid of a hemocytometer.

Determination of Mycelial Growth Inhibition by GO

The measurement of the mycelial growth of *P. microspora* was conducted by two perpendicular directions method (Zhang et al., 2012). GO, which contains 25% (m/v) gingerols, was purchased from Yanyi Bio., Co., Ltd., Shanghai, China. Different concentrations of GO with 2, 4, 6, 8, 10, and 12 μL per mL propylene glycol were prepared, and added to autoclaved liquid PDA mediums, respectively, then cooled to obtain solid PDA medium with different concentrations of GO. PDA mediums containing 0 μL GO per mL propylene glycol served as the controls. A mycelial colony (5 mm in diameter) was cut from the edge of 5 d-old *P. microspora* colony and placed upside down on the center of the plate with fungi in contact with the growth medium. Cultures were incubated at 28°C for 5 d prior to measurement of the mycelial growth diameter (mm) of *P. microspora* in two perpendicular directions. The inhibitory rate of mycelial growth was calculated with the following formula:

$$IR_{\text{mg}} = \frac{(d_c - d_t)}{d_c - 5} \times 100\%$$

where IR_{mg} was the inhibitory rate of mycelial growth, %;

d_c and d_t were average diameter (mm) of mycelial colonies of the control and the GO treatment, respectively;

5 was the diameter (mm) of original mycelial colony.

In addition, the effective concentration for a 50% reduction (EC_{50}) and 90% reduction (EC_{90}) of mycelial growth was calculated according to the growth curves of the relationship between the GO concentration (μL per mL propylene glycol) and IR_{mg} (%).

Determination of Spore Germination Inhibition Activity

Spore germination of *P. microspora* was detected with minor modifications as described by Pane et al. (2016). A volume of 20 μL of spore suspension containing 1×10^6 spores mL^{-1} was incorporated into PDA mediums with 100 μL various concentrations of GO at 0, 2, 4, 6, 8, 10, and 12 μL per mL propylene glycol, respectively, and then cultured at 28°C for 7 h. The spore germination was observed by microscopy. The germination was determined when the length of a germ tube exceeded half of the small-end diameter of the spore, and at least 200 spores were examined in each visual field before determination. Spore germination rate was expressed as percentage of the germinated spores to the total calculated spores, and the inhibitory rate of spore germination was calculated by the following formula:

$$IR_{\text{sg}} = 1 - \frac{IR_t}{IR_c} \times 100\%,$$

where IR_{sg} was the inhibitory rate of spore germination, %;

IR_t and IR_c were represented as the inhibitory rate of spore germination at control and at GO treatment, respectively.

Each replicate consisted of three observations, and three replicates were performed for each treatment.

Determination of the MIC and MFC

The minimal inhibitory concentration (MIC) and minimal fungicidal concentration (MFC) for *P. microspora* were determined by broth dilution method (Shukla et al., 2009). 20 μL spore suspension containing 1×10^6 spores mL^{-1} was incorporated into PDA media with different concentrations of GO at 5, 10, 15, 20, 25, 30, and 35 μL per mL propylene glycol, respectively, and then cultured at 28°C for 7 d. MIC is the lowest concentration which did not support visible fungus. Mycelia from the plates showing no growth were sub-cultured on treatment-free PDA plates to determine if the inhibition was reversible. The lowest concentration at which no growth occurred was defined as MFC.

Observation of Morphological Structures of Mycelia

The mycelial sample preparation for mycelia observation was based on a modified method of Tian et al. (2012). An aliquot of 1 mL spore suspension (1×10^6 spores mL^{-1}) was added to autoclave PDA medium containing GO at 0, EC_{50} and EC_{90} . After 7 d incubation at 28°C , 10 mL fungal suspension was centrifuged at $10\,000\text{ r min}^{-1}$ for 15 min at 4°C , the supernatant

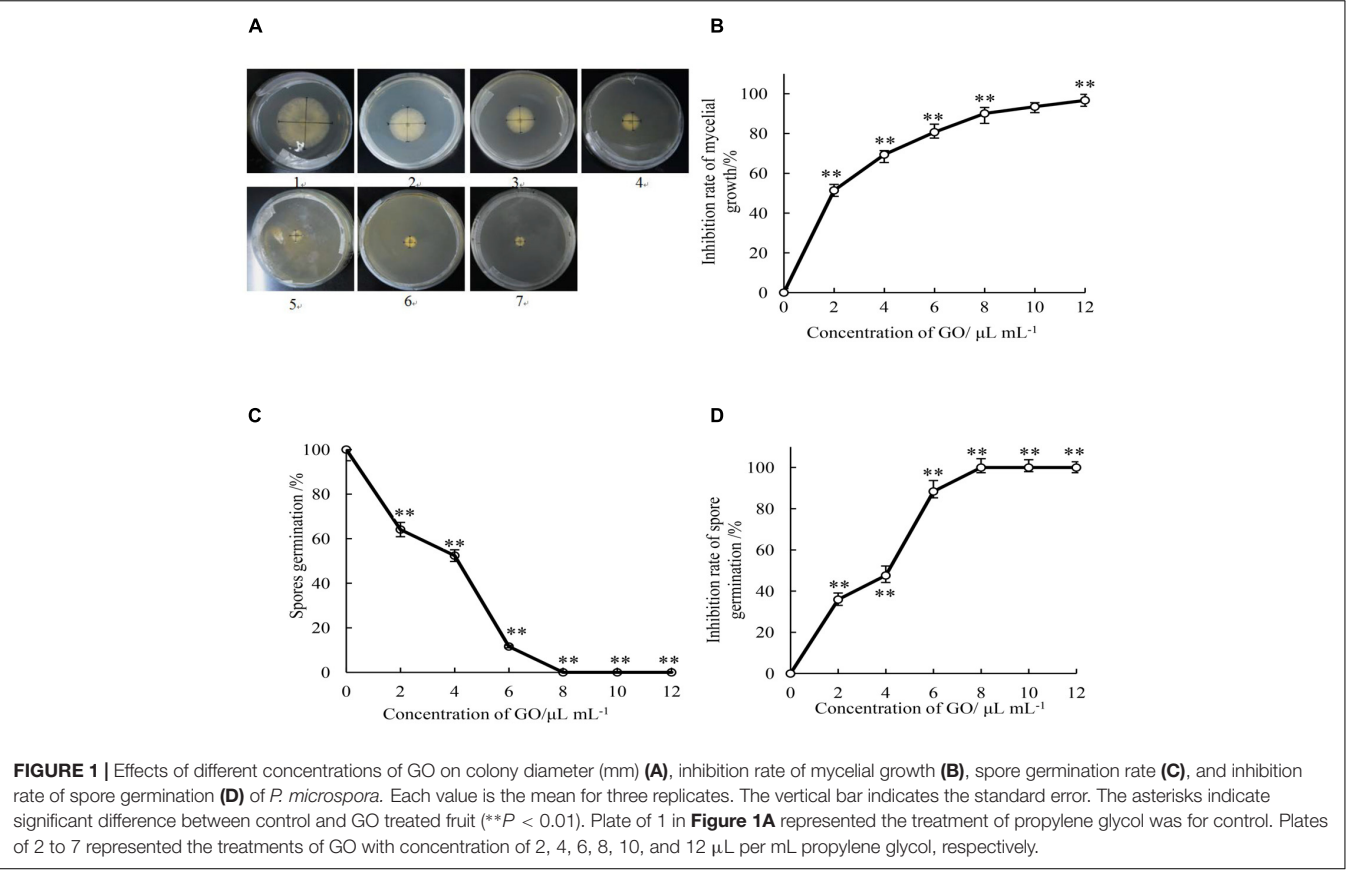
was discarded, and the precipitate was washed three times with sterile distilled water for microscopic observation.

The microstructural images of the as-prepared mycelia samples were observed using scanning electron microscopy (SEM) equipped with a JSM-6380LA microscope (JEOL, Japan) at an accelerating voltage of 15 KV. The mycelial samples were firstly fixed with 3–4% (v/v) glutaraldehyde at room temperature for 4–6 h and then washed five times with 100 m mol L^{-1} phosphate buffer (PBS, pH 7.0), post-fixed with 1% osmium tetroxide for 1.5 h. After washing with the same buffer twice, the specimens were dehydrated in a graded ethanol series (30, 50, 70, 80, 90, and 100%) for three times for 15 min in each series. Finally, the samples were dried in vacuum dryer (DZF6020, JingHong, Shanghai, China), then gold-coated and examined by SEM.

Measurement of Cellular Leakage

The leakage of electrolytes of *P. microspora* was measured according to the method of Tian et al. (2015) with minor modifications. A volume of 1 mL spore suspension (1×10^6 spores mL^{-1}) was added into 100 mL autoclave potato dextrose broth (PDB) medium, follow by incubation at 28°C for 3 d, then the fungal cells were centrifuged at $10\,000\text{ r min}^{-1}$ for 15 min at 4°C to obtain the supernatant. The extracellular conductivities ($\mu\text{S cm}^{-1}$) of *P. microspora* cells supernatant were determined continuously using a DDS-307 electric conductivity meter (Jingke Scientific Instrument, Shanghai, China) after treatments with different GO concentration at 0, EC_{50} and EC_{90} for 0, 60, 120, 180, 240, and 300 min. Finally, the relative conductivity was used to reflect the cellular leakage of pathogen, which was calculated and expressed as the percentage of conductivity in treatment with GO as the control.

The leakage of the intracellular soluble proteins, total sugars and nuclein from mycelium of *P. microspora* was assayed according to the method of Li et al. (2018). A volume of 1 mL spore suspension containing 1×10^6 spores mL^{-1} was cultured on 100 mL PDB medium for 5 d at 28°C and mycelium were harvested. The mycelium was collected and lyophilized (FDU-1200, EYELA, Tokyo, Japan) after being washed three time with sterile distilled water. Subsequently, 1.0 mg lyophilized mycelium were re-suspended in 0.1 mol L^{-1} PBS (pH 7.0) containing the addition of various GO concentration at 0, EC_{50} and EC_{90} and incubated at 28°C . Then, the fungal suspension was centrifuged at $12\,000\text{ r min}^{-1}$ for 5 min after 2, 4, and 6 h incubation and the supernatant was collected for determination of the leakage of intracellular soluble proteins, total sugars, and nuclein. The total sugars content of mycelia of *P. microspora* was determined by anthrone-sulfuric acid method (Moshayedi et al., 2013) using glucose as the standard. Soluble protein content was determined according to the Bradford assay (Bradford, 1976) with bovine serum albumin as the standard. The leakage from cellular membrane was measured according to the absorbance at 260 nm ($OD_{260\text{ nm}}$) by ultraviolet visible adsorption spectrometry (UV-1750, Shimadzu, Japan) using fungal suspension with only PBS as the control.



Assay of Fatty Acid Composition in Cell Membrane

The change of fatty acid contents and compositions in cell membrane of *P. microspora* was analyzed by GC-MS (Tridion-9, Torion, United States). Preparation of fatty-acid methyl ester in cell membrane was performed according to Hazzit et al. (2006) with minor modifications. Aliquots of 20–30 mg mycelia were weighed into a 5 mL centrifuge tube, 1.0 mL of NaOH-MetOH, and 2.0 mL of HCl-methanol were added and kept in boiling water bath for 30 min, and then cooled to room temperature using ice bath. Next, the mixture was extracted with 1.25 mL hexane/ether (2:1, v/v) and allowed to stand at room temperature for 15 min for stratification. The organic phase was transferred to another tube and 3.0 mL of NaOH and few drops of saturated NaCl solution was added. The tubes were sealed and shaken back and forth for 10 min. Finally, 1 mL of organic phase was pipetted for GC-MS quantification of fatty acid. The indexes of unsaturated fatty acid were calculated and expressed as the percentage of contents of unsaturated fatty acid to contents of saturated fatty acid.

Antifungal Activity *in vivo*

Healthy and uniform maturity “Changying” Chinese olives were obtained from an olive orchard in Fuzhou, Fujian, China. Antifungal experiment *in vivo* was conducted by injury inoculation with some minor modifications (Li et al.,

TABLE 1 | Results of minimal inhibitory concentration (MIC) and minimal fungicidal concentration (MFC) of GO for *P. microspora*.

Concentration of GO/ $\mu\text{L mL}^{-1}$	Mycelial growth for 2 days	Mycelial growth for 7 days	MIC/ $\mu\text{L mL}^{-1}$	MFC/ $\mu\text{L mL}^{-1}$
0	+	+	10	30
5	+	+		
10	–	+		
15	–	+		
20	–	+		
25	–	+		
30	–	–		
35	–	–		

“+”: presence of mycellia growth; “–”, absence of mycellia growth.

2018). Firstly, fruits were surface-sterilized using 2% sodium hypochlorite solution (Sinopharm, Beijing, China) for 2 min and rinsed twice with sterilized distilled water, then air-dried. Next, the fruits were artificially injured using a sterilized hole punch to make a 5 mm \times 3 mm (diameter \times depth) wound on the surface, in which 15 μL freshly prepared spore suspension (1×10^6 spores mL^{-1}) was inoculated, follow by addition of 20 μL of GO with the concentration of 1, 2, 3, and 4 MIC. Finally, the treated fruits were incubated at 28°C and 95% relative humidity (RH) for 6 d. Fruit not treated with GO was used as the control. The lesion diameter (in mm) of fruit was measured using a vernier caliper every another day.

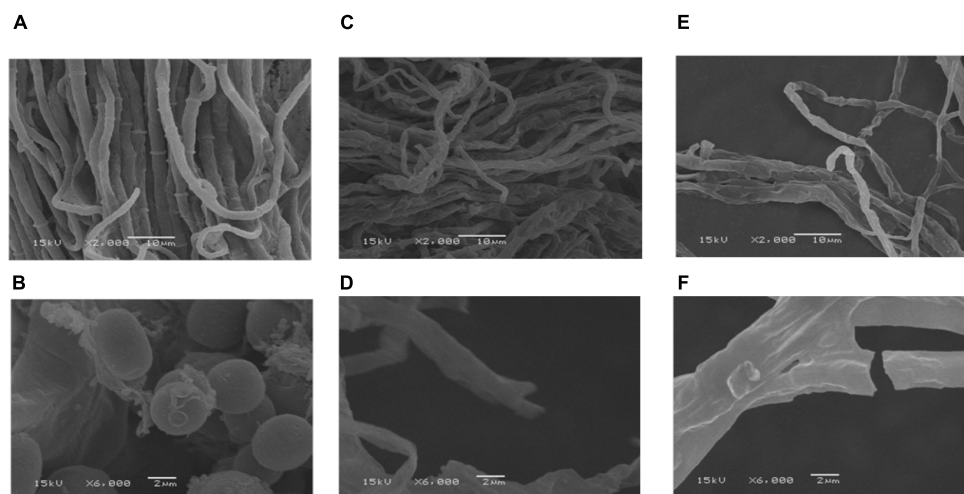


FIGURE 2 | Scanning electron microscopy images with the bars at 2 μm and 10 μm of mycelia of *P. microspora* exposure to 0 (A,B), EC_{50} (C,D) and EC_{90} (E,F) of GO.

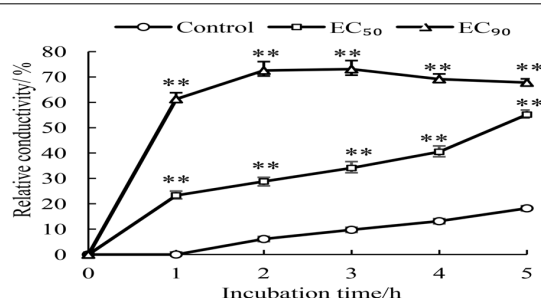


FIGURE 3 | Effects of different concentrations of GO on extracellular conductivity of *P. microspora*. Each value is the mean for three replicates. The vertical bar indicates the standard error. The asterisks indicate significant difference between control and GO treated fruit (** $P < 0.01$).

Statistical Analysis

All experiments were repeated three times and data were acquired. The values in figures were expressed as the means and standard errors. Analysis of variance (ANOVA) was used to analyze the data using the software (SPSS version 17.0). Student's *t*-test was used to compare the mean values of the data set. A p -value ≤ 0.05 or 0.01 was considered statistically significant.

RESULTS AND DISCUSSION

Effect of GO on Inhibition Activity of *P. microspora* Mycelial Growth

As shown in Figure 1A, the increase of the colony diameter of mycelial growth was comparatively slower in all treatments with GO than in the control medium during 5 d incubation period. Mycelial growth of *P. microspora* was significantly ($p < 0.05$) inhibited by GO in a concentration-dependent

manner, the higher the concentration, the higher the inhibition rate (Figure 1B). Furthermore, the EC_{50} ($2.04 \mu\text{L mL}^{-1}$) and EC_{90} ($8.87 \mu\text{L mL}^{-1}$) of mycelial growth by the GO treatment was calculated according to the regression analysis ($y = 2.0093x + 4.3759$, $r = 0.986$), which indicated that *P. microspora* was inhibited effectively at low concentration.

Effect of GO on Inhibition Activity of *P. microspora* Spore Germination

The spore germination rate of GO treatments with the concentration of 0, 2, 4, 6, 8, 10, and 12 μL per mL propylene glycol were determined after 7 h incubation (Figure 1C). Spore germination of *P. microspora* was significantly ($p < 0.01$) inhibited by various concentration of GO treatments. The spore germination rate reached 100% in the control after incubation for 7 h, it was inhibited by 35.9, 47.6, and 88.4% by GO concentration of 2, 4, and 6 μL per mL propylene glycol. Complete inhibition (100%) was achieved at GO concentrations beyond 8 μL per mL propylene glycol (Figure 1D).

Determination of MIC and MFC

Based on the observation of mycelial growth on the PDA medium with GO treatments at 0, 5, 10, 15, 20, 25, 30, and 35 μL per mL propylene glycol during 7 d incubation period, the MIC and MFC values of GO treatment against mycelial growth of *P. microspora* were measured to be 10 and 30 μL per mL propylene glycol, respectively (Table 1).

Effect of GO on Mycelial Morphology of *P. microspora*

Morphological observations by SEM exhibited that the control sample of *P. microspora* had smooth, uniform and vigorous mycelia (Figure 2A), with distinctive intercellular septa and broom-like structures with beaded conidium at the top (Figure 2B). However, the mycelia appeared evidently

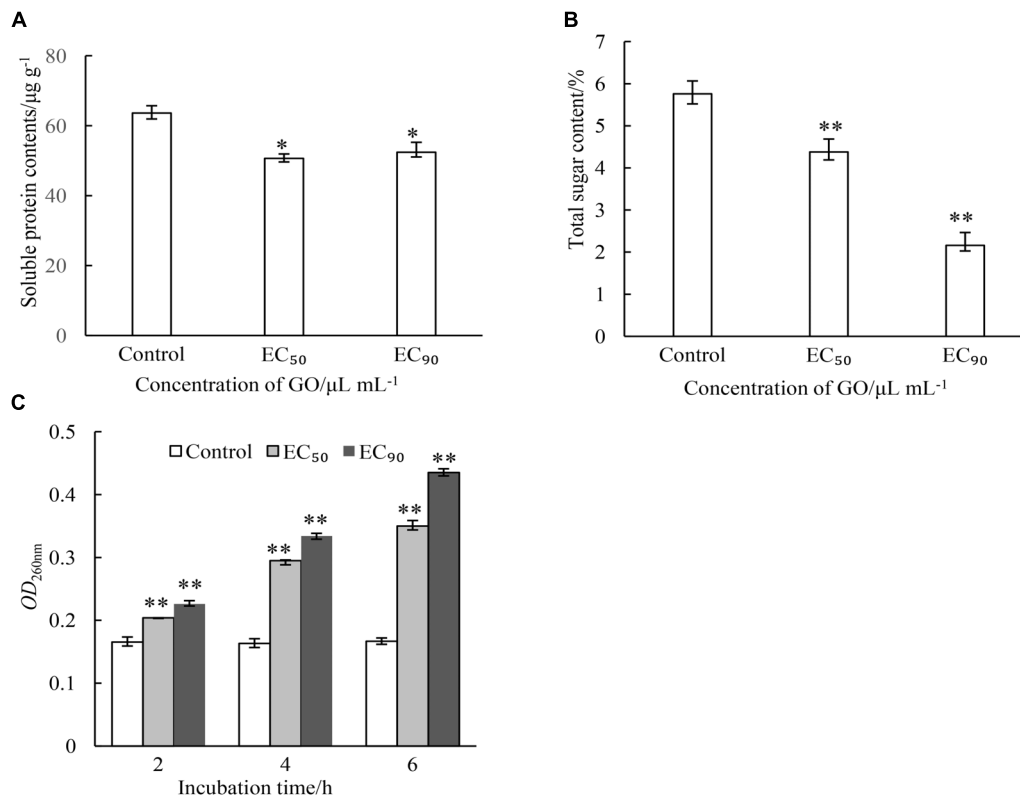


FIGURE 4 | Effects of different concentrations of GO on leakage of proteins (A), leakage of total sugars (B) and leakage of nuclein (C) of *P. microspora*. Each value is the mean for three replicates. The vertical bar indicates the standard error. The asterisks indicate significant difference between control and GO treated fruit (** $P < 0.01$, * $P < 0.05$).

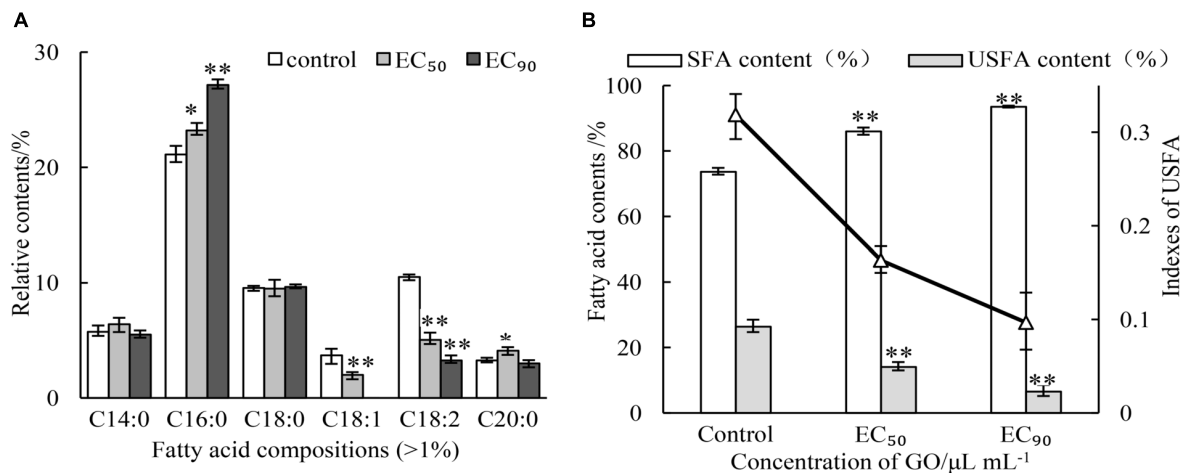


FIGURE 5 | Effects of different concentrations of GO on fatty acid compositions (A) and indexes of unsaturated fatty acid (B). Each value is the mean for three replicates. The vertical bar indicates the standard error. The asterisks indicate significant difference between control and GO treated fruit (** $P < 0.01$, * $P < 0.05$).

disordered, rough and sunken after exposure to $2.04 \mu\text{L mL}^{-1}$ (EC₅₀) GO (Figure 2C); meanwhile, the intercellular septa disappeared and no conidium were observed in the structure (Figure 2D). Furthermore, the mycelia of *P. microspora* treated with $8.87 \mu\text{L mL}^{-1}$ propylene glycol (EC₉₀) were greatly

distorted, intertwined and crimped (Figure 2E), which caused irregular constriction even disruption (Figure 2F). Therefore, the evidence from SEM observation indicated that the treatments with GO caused distortion, sunken and serious damage to the morphology of the mycelial and effectively inhibited its growth

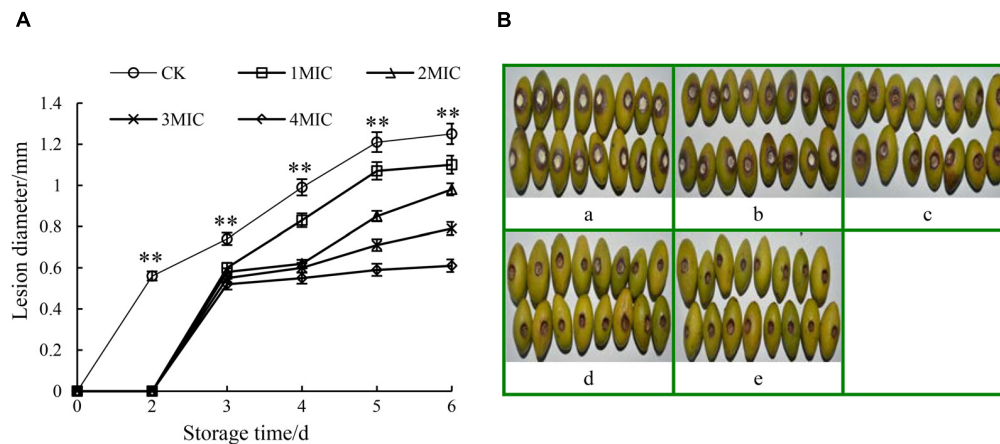


FIGURE 6 | Effects of GO treatments on the lesion diameter (A) and lesion development (B) of *P. microspora*-infected Chinese olive fruits. Each value is the mean for three replicates. The vertical bar indicates the standard error. Photograph of a in **Figure 6B** represented the treatment of propylene glycol for control. Photographs of b to e represented the treatments of GO with concentration of 1 MIC, 2 MIC, 3 MIC, 4 MIC, respectively. The vertical bar indicates the standard error. The asterisks indicate significant difference between control and GO treated fruit (** $P < 0.01$).

due to the serious destruction of integrity of mycelial structure that interfered physiological metabolism.

Effect of GO on Membrane Permeability of *P. microspora*

Changes of membrane permeability were considered as an indicator of damage of cell membrane structure (Li et al., 2018). The membrane permeability increased when the normal cells were destroyed, which caused variation of conductivity due to imbalance of intracellular and extracellular electrolytes. In general, the more serious the cell membrane damage, the higher the conductivity. So, the relative conductivities of mycelia treated for 1–5 h by GO were detected. As shown in **Figure 3**, the relative conductivity slowly increased overtime (0–5 h) in the control, which could be attributed to the autolysis of normal cell. However, the relative conductivities of the mycelia treated with GO exhibited obvious increase comparing to the control, especially, which reached highest value after 2 h and maintained at higher level by GO treatment with EC_{90} than that of EC_{50} . In short, GO treatment accelerated the leakage of electrolytes in *P. microspora*, resulting in the great increase of membrane permeability.

Effect of GO on Cellular Leakage of *P. microspora*

Intracellular substances are essential material bases for the growth and reproduction of microorganisms. This study evaluated the effects of GO on the contents of cellular substances including protein, total sugar and nuclein in mycelia of *P. microspora*. As demonstrated in **Figure 4**, GO treatments caused different degrees of leakage of the substances via cell membrane of *P. microspora* in the control. The content of protein in mycelia was not substantially affected by the concentration of GO, but significantly different ($p < 0.05$) from the control (**Figure 4A**). The contents of total sugar in mycelia decreased

dramatically ($p < 0.01$) from $5.76 \mu\text{g g}^{-1}$ without GO to 4.38% and 2.16% with GO at EC_{50} and EC_{90} , respectively (**Figure 4B**). Simultaneously, the longer the treating time, the greater the release of nuclein from mycelia, the absorbance of mycelial supernatant ($OD_{260\text{nm}}$) increased dramatically to a value 2.45-fold, which is higher than that of the control after 5 h inoculation (**Figure 4C**). These results aligned with the morphological observations in this study.

Effect of GO on Fatty Acid Composition of Membrane Lipids in *P. microspora*

As the main components of membrane, the contents and compositions of fatty acids affect the stability of membrane. The impacts of GO on fatty acid composition of membrane lipids were analyzed by GC-MS. The results were presented in **Figure 5A**. Six main kinds of fatty acids were found, including palmitic acid, linoleic acid, octadecanoic acid, tetradecanoic acid, oleic acid, eicosanoic acid in the normal cell of *P. microspora* after 3 d of incubation (control), where saturated fatty acids and unsaturated fatty acid were account for 73.63 and 26.37%, respectively. Nevertheless, the saturated fatty acids increased by treating with GO, but the opposite was true for unsaturated fatty acids. In particular, the oleic acid was not detected after treatment with GO at EC_{90} . The changes of fatty acid composition (**Figure 5B**) also caused sharp decline of indexes of unsaturated fatty acid (IUFA) from 0.3186 (control) to 0.1632 (EC_{50}), and 0.0697 (EC_{90}). These findings indicate that GO could significantly promote the degradation or peroxidation of unsaturated fatty acids in *P. microspora*, resulting in enhancement of membrane fluidity.

Antifungal Effect of GO on Disease Development in Chinese Olive Fruits

Compared to the control, the disease development of harvested Chinese olive fruit wounded-inoculated with *P. microspora* was

remarkably suppressed ($p < 0.01$) by the treatments with GO (Figure 6). As shown in Figure 6A, the lesion diameter of *P. microspora*-infected Chinese olive fruits treated with GO was smaller than that of the control group (CK). The extension rate of lesion zone slowed down with the increase in the GO concentration, while no obvious increase was observed when the GO concentration exceeded 3 MIC. Meanwhile, the lesion zone of the fruits was accompanied by orange halo, pitted pericarp and covered with a large number of gray-white mycelia at the end of storage period, however, no mycelia growth and the lesion dried quickly on fruits when treated with concentration of 3 and 4 MIC GO (Figure 6B). Based on the above results, the optimal inhibitory concentration of GO for *P. microspora* infected Chinese olive fruits was 3 MIC.

CONCLUSION

Ginger oleoresin effectively inhibited *in vitro* mycelial growth and spore germination of *P. microspora*, and exerted antifungal activity *via* membrane-targeted mechanism with alteration of membrane permeability, collapse of membrane integrity, and membrane lipid peroxidation. The GO treatments destroyed the morphology of the mycelia increasing the leakage of intercellular electrolytes, proteins, sugars, and nuclein of *P. microspora*, leading to lethal effects on the pathogen. Moreover, the GO treatments remarkably suppressed disease development

in harvested Chinese olive fruit wounded-inoculated with *P. microspora*. In summary, GO could be a potentially effective alternative to the traditional fungicides against the postharvest pathogenic fungi of fruits and vegetables.

AUTHOR CONTRIBUTIONS

TC, SC, and HL conceived and designed the research. TC, BK, LD, and JL carried out the experiments and analyzed the data. TC, BK, and LZ wrote the manuscript. GC and ML edited the English language of the manuscript. HL and SC supervised the research. All authors discussed the results, provided critical feedback and contributed to the final manuscript.

FUNDING

This work was supported by the National Natural Science Foundation of China (Grant Nos. 31871860 and 31201441), the Natural Science Foundation of Fujian Province of China (Grant Nos. 2012J05054 and C94015), the Key Technology R&D Program of Fujian Province of China (Grant No. 2015N0002), the Project of Finance Department of Fujian Province in China (Grant Nos. KLe16H01A and KLe16002A), and the Science and Technology Innovation Program of Fujian Agriculture and Forestry University of China (Grant No. CXZX2016093).

REFERENCES

- Ashraf, S. A., Al-Shammari, E., Hussain, T., Tajuddin, S., and Panda, B. P. (2017). In-vitro antimicrobial activity and identification of bioactive components using GC-MS of commercially available essential oils in Saudi Arabia. *J. Food Sci. Technol.* 54, 3948–3958. doi: 10.1007/s13197-017-2859-2
- Bag, A., and Chattopadhyay, R. R. (2015). Evaluation of synergistic antibacterial and antioxidant efficacy of essential oils of spices and herbs in combination. *PLoS One* 10:e0131321. doi: 10.1371/journal.pone.0131321
- Bellik, Y. (2014). Total antioxidant activity and antimicrobial potency of the essential oil and oleoresin of *Zingiber officinale* roscove. *Asian Pac. J. Trop. Dis.* 4, 40–44. doi: 10.1016/S2222-1808(14)60311-X
- Bradford, M. M. (1976). A rapid and sensitive method for the quantitation of microgram quantities of protein utilizing the principle of protein-dye binding. *Anal. Biochem.* 72, 248–254. doi: 10.1016/0003-2697(76)90527-3
- Chaemsanit, S., Matan, N., and Matan, N. (2018). Effect of peppermint oil on the shelf-life of dragon fruit during storage. *Food Control* 90, 172–179. doi: 10.1016/j.foodcont.2018.03.001
- Chang, Q., Su, M. H., Chen, Q. X., Zeng, B. Y., Li, H. H., and Wang, W. (2017). Physicochemical properties and antioxidant capacity of Chinese Olive (*Canarium album* L.) cultivars. *J. Food Sci.* 82, 1369–1377. doi: 10.1111/1750-3841.13740
- Chen, N. Q., Chen, Y. H., Lin, H. T., Lin, Y. F., and Wang, H. (2016a). Isolation and identification of the pathogen causing fruit rot in harvested Chinese olives. *Modern Food Sci. Technol.* 32, 138–142. doi: 10.13982/j.mfst.1673-9078.2016.10.022
- Chen, N. Q., Lin, H. T., Chen, Y. H., Lin, Y. F., and Wang, H. (2016b). Biological characteristics of *Pestalotiopsis microspora*. *Storage Process* 16, 5–10. doi: 10.3969/j.issn.1009-6221.2016.03.002
- Chen, N. Q., Liu, Y. M., Lin, H. T., Kong, X. J., Lin, Y. F., and Chen, Y. H. (2015). Advances in post-harvest disease and storage technology of Chinese olive fruit. *Packag. Food Mach.* 33, 49–53.
- Hazzit, M., Baaliouamer, A., Faleiro, M. L., and Miguel, M. G. (2006). Composition of the essential oils of thymus and origanum species from algeria and their antioxidant and antimicrobial activities. *J. Agric. Food Chem.* 54, 6314–6321. doi: 10.1021/jf0606104
- He, Z., Xia, W., Liu, Q., and Chen, J. (2008). Identification of a new phenolic compound from Chinese olive (*Canarium album* L.) fruit. *Eur. Food Res. Technol.* 228, 339–343. doi: 10.1007/s00217-008-0939-2
- Jayasena, D. D., and Jo, C. (2013). Potential application of essential oils as natural antioxidants in meat and meat products: a review. *Food Rev. Int.* 30, 71–90. doi: 10.1080/87559129.2013.853776
- Kuo, C. T., Liu, T. H., Hsu, T. H., Lin, F. Y., and Chen, H. Y. (2015). Antioxidant and antiglycation properties of different solvent extracts from Chinese olive (*Canarium album* L.) fruit. *Asian Pac. J. Trop. Med.* 8, 1013–1021. doi: 10.1016/j.apjtm.2015.11.013
- Li, W., Yuan, S., Sun, J., Li, Q., Jiang, W., and Cao, J. (2018). Ethyl p-coumarate exerts antifungal activity in vitro and in vivo against fruit *Alternaria alternata* via membrane-targeted mechanism. *Int. J. Food Microbiol.* 278, 26–35. doi: 10.1016/j.ijfoodmicro.2018.04.024
- Lin, S. L., Chi, W. W., Hu, J. M., Pan, Q., Zheng, B. D., and Zeng, S. X. (2017). Sensory and nutritional properties of Chinese olive pomace based high fibre biscuit. *Emir. J. Food Agric.* 29, 495–501. doi: 10.9755/efja.2016-12-1908
- Moshayedi, S., Shahraz, F., Schaffner, D. W., Khanlarkhani, A., Shojaei-Aliabadi, S., Shahnia, M., et al. (2013). In vitro control of enterococcus faecalis by zataria multiflora boiss, origanum vulgare l. and mentha pulegium essential oils. *J. Food Safety* 33, 327–332. doi: 10.1111/jfs.12056
- Nanasombat, S., and Wuttigol, P. (2011). Antimicrobial and antioxidant activity of spice essential oils. *Food Sci. Biotechnol.* 20, 45–53. doi: 10.1007/s10068-011-0007-8
- Pane, C., Fratianni, F., Parisi, M., Nazzaro, F., and Zaccardelli, M. (2016). Control of alternaria post-harvest infections on cherry tomato fruits by wild pepper phenolic-rich extracts. *Crop Prot.* 84, 81–87. doi: 10.1016/j.cropro.2016.02.015
- Shukla, R., Kumar, A., Singh, P., and Dubey, N. K. (2009). Efficacy of Lippia alba (Mill.) N.E. *Int. J. Food Microbiol.* 135, 165–170. doi: 10.1016/j.ijfoodmicro.2009.08.002
- Singh, G., Kapoor, I. P., Singh, P., de Heluani, C. S., de Lampasona, M. P., and Catalan, C. A. (2008). Chemistry, antioxidant and antimicrobial investigations

- on essential oil and oleoresins of *Zingiber officinale*. *Food Chem. Toxicol.* 46, 3295–3302. doi: 10.1016/j.fct.2008.07.017
- Tian, J., Huang, B., Luo, X. L., Zeng, H., Ban, X. Q., He, J. S., et al. (2012). The control of *Aspergillus flavus* with cinnamomum jensenianum Hand-Mazz essential oil and its potential use as a food preservative. *Food Chem.* 130, 520–527. doi: 10.1016/j.foodchem.2011.07.061
- Tian, J., Wang, Y. Z., Zeng, H., Li, Z. Y., Zhang, P., Tessema, A., et al. (2015). Efficacy and possible mechanisms of perillaldehyde in control of *Aspergillus niger* causing grape decay. *Int. J. Food Microbiol.* 202, 27–34. doi: 10.1016/j.ijfoodmicro.2015.02.022
- Varakumar, S., Umesh, K. V., and Singhal, R. S. (2017). Enhanced extraction of oleoresin from ginger (*Zingiber officinale*) rhizome powder using enzyme-assisted three phase partitioning. *Food Chem.* 216, 27–36. doi: 10.1016/j.foodchem.2016.07.180
- Yamamoto-Ribeiro, M. M., Grespan, R., Kohiyama, C. Y., Ferreira, F. D., Mossini, S. A., Silva, E. L., et al. (2013). Effect of *Zingiber officinale* essential oil on *Fusarium verticillioides* and fumonisin production. *Food Chem.* 141, 3147–3152. doi: 10.1016/j.foodchem.2013.05.144
- Zhan, M. M., Cheng, Z. Z., Su, G. C., Wang, A. Y., Chen, H. P., Shan, Z., et al. (2015). Genetic relationships analysis of olive cultivars grown in China. *Genet. Mol. Res.* 14, 5958–5969. doi: 10.4238/2015.June.1.13
- Zhang, C. Q., Liu, Y. H., Wu, H. M., Xu, B. C., Sun, P. L., and Xu, Z. H. (2012). Baseline sensitivity of *Pestalotiopsis microspora*, which causes black spot disease on Chinese hickory (*Carya cathayensis*), to pyraclostrobin. *Crop Prot.* 42, 256–259. doi: 10.1016/j.cropro.2012.07.018

Conflict of Interest Statement: The authors declare that the research was conducted in the absence of any commercial or financial relationships that could be construed as a potential conflict of interest.

Copyright © 2018 Chen, Lu, Kang, Lin, Ding, Zhang, Chen, Chen and Lin. This is an open-access article distributed under the terms of the Creative Commons Attribution License (CC BY). The use, distribution or reproduction in other forums is permitted, provided the original author(s) and the copyright owner(s) are credited and that the original publication in this journal is cited, in accordance with accepted academic practice. No use, distribution or reproduction is permitted which does not comply with these terms.



Selection Pressure Pathways and Mechanisms of Resistance to the Demethylation Inhibitor-Difenoconazole in *Penicillium expansum*

Emran Md Ali and Achour Amiri*

Department of Plant Pathology, Tree Fruit Research and Extension Center, Washington State University, Wenatchee, WA, United States

OPEN ACCESS

Edited by:

Hongyin Zhang,
Jiangsu University, China

Reviewed by:

Bartolome Moya Canellas,
University of Florida, United States
Hetong Lin,
Fujian Agriculture and Forestry
University, China

*Correspondence:

Achour Amiri
a.amiri@wsu.edu

Specialty section:

This article was submitted to
Food Microbiology,
a section of the journal
Frontiers in Microbiology

Received: 29 June 2018

Accepted: 27 September 2018

Published: 31 October 2018

Citation:

Ali EM and Amiri A (2018)
Selection Pressure Pathways
and Mechanisms of Resistance to the
Demethylation
Inhibitor-Difenoconazole in *Penicillium*
expansum. *Front. Microbiol.* 9:2472.
doi: 10.3389/fmicb.2018.02472

Penicillium expansum causes blue mold, the most economically important postharvest disease of pome fruit worldwide. Beside sanitation practices, the disease is managed through fungicide applications at harvest. Difenoconazole (DIF) is a new demethylation inhibitor (DMI) fungicide registered recently to manage postharvest diseases of pome fruit. Herein, we evaluated the sensitivity of 130 *P. expansum* baseline isolates never exposed to DIF and determined the effective concentration (EC₅₀) necessary to inhibit 50% germination, germ tube length, and mycelial growth. The respective mean EC₅₀ values of 0.32, 0.26, and 0.18 µg/ml indicate a high sensitivity of *P. expansum* baseline isolates to DIF. We also found full and extended control efficacy *in vivo* after 6 months of storage at 1°C. We conducted a risk assessment for DIF-resistance development using ultraviolet excitation combined with or without DIF-selection pressure to generate and characterize lab mutants. Fifteen DIF-resistant mutants were selected and showed EC₅₀ values of 0.92 to 1.4 µg/ml and 1.7 to 3.8 µg/ml without and with a DIF selection pressure, respectively. Resistance to DIF was stable *in vitro* over a 10-week period without selection pressure. Alignment of the full *CYP51* gene sequences from the three wild-type and 15 mutant isolates revealed a tyrosine to phenylalanine mutation at codon 126 (Y126F) in all of the 15 mutants but not in the wild-type parental isolates. Resistance factors increased 5 to 15-fold in the mutants compared to the wild-type-isolates. DIF-resistant mutants also displayed enhanced *CYP51* expression by 2 to 14-fold and was positively correlated with the EC₅₀ values ($R^2 = 0.8264$). Cross resistance between DIF and fludioxonil, the mixing-partner in the commercial product, was not observed. Our findings suggest *P. expansum* resistance to DIF is likely to emerge in commercial packinghouse when used frequently. Future studies will determine whether resistance to DIF is qualitative or quantitative which will be determinant in the speed at which resistance will develop and spread in commercial packinghouses and to develop appropriate strategies to extend the lifespan of this new fungicide.

Keywords: demethylation inhibitors, blue mold, *CYP51*, postharvest, fludioxonil, overexpression

INTRODUCTION

The extended storage of apple fruit for up to 12 months in low temperatures and controlled atmospheres (low O₂ and high CO₂ concentrations) makes them prone to infections by several fungal pathogens. *Penicillium expansum* is an ascomycete fungus causing blue mold, a major postharvest disease of apple and pear fruit worldwide (Amiri and Bompeix, 2005a; Morales et al., 2007; Jurick et al., 2011). In recent surveys in Washington State, blue mold accounted for nearly 50% of total decay caused on apple postharvest (Amiri and Ali, 2016). *Penicillium expansum* is a typical airborne and wound pathogen with short life cycles and copious asexual conidial production which are responsible for pome fruit infections in storage rooms (Sanderson and Spotts, 1995; Amiri and Bompeix, 2005a). Spores of *P. expansum* seldom infect fruit in orchards (Amiri and Bompeix, 2005a) but can be abundant on storage bins and in storage rooms if appropriate sanitation practices are not implemented at the beginning of the season (Spotts and Cervantes, 1993; Sanderson and Spotts, 1995; Amiri and Bompeix, 2005a). Primary infections, resulting from residual inoculum, may start on fresh wounds or punctures caused at harvest or during postharvest handling (Rosenberger et al., 1991; Amiri and Bompeix, 2005b). Thereafter, inoculum can quickly build up inside storage rooms to cause multiple secondary infections (Amiri and Bompeix, 2005a).

There is no known host resistance to *P. expansum* in current commercial apple cultivars. Therefore, besides some sanitation practices at packing facilities and other biological or physical methods with moderate efficacy, management of *P. expansum* and other postharvest pathogens is mainly achieved using single-site synthetic fungicides. The number of molecules registered postharvest has been limited to three, i.e., thiabendazole (TBZ) registered four decades ago, pyrimethanil (PYR) and fludioxonil (FDL) registered 15 years ago. *P. expansum* is considered a “high risk” fungus for fungicide resistance development. Thus, resistance to TBZ, linked to several mutations in the β -tubulin gene, has been reported widely from numerous production regions worldwide (Rosenberger et al., 1991; Errampalli et al., 2006; Malandrakis et al., 2013; Yin and Xiao, 2013). Resistance to PYR has emerged in recent years in the U.S. Pacific Northwest and Mid-Atlantic regions but remains at relatively low frequencies (Jurick et al., 2017; Caiazzo et al., 2014; Yan et al., 2014; Amiri et al., 2018). Lately, low levels of resistance or reduced sensitivity to FDL have been sporadically found in some U.S. apple packinghouses (Gaskins et al., 2015; Amiri et al., 2017). The emergence of resistance to PYR and FDL and the relatively lower FDL efficacy against *Neofabraea* spp. (Amiri, unpublished data) suggest registration of new fungicides with different modes of action than the current three postharvest fungicides is necessary to maintain effective disease control.

Difenoconazole (1-[2-[2-chloro-4-(4-chloro-phenoxy)-phenyl]-4-methyl[1,3]-dioxolan-2-ylmethyl]-1H-1,2,4-triazole) (**Supplementary Figure S1**), a new demethylation inhibitor (DMI) fungicide, was registered in 2016 for postharvest use in pome fruit. It is pre-mixed with FDL and commercially available as AcademyTM (Syngenta Crop Protection). Difenoconazole

(DIF) has a systemic activity and broad-spectrum antifungal potency as shown recently (Hof, 2001; Fonseka and Gudmestad, 2016; Bartholomäus et al., 2017; Dang et al., 2017; Jurick et al., 2017; Koehler and Shew, 2018; Ali et al., 2018). DMIs, such as DIF, target the sterol 14 α -Demethylase Cytochrome P450 (CYP51), an essential component of fungal membrane sterols required for a proper membrane functioning (Rodriguez et al., 1985; Joseph-Horne and Hollomon, 1997). Although classified as “medium risk,” resistance to DMIs has been reported in several fungal pathogens (Golembiewski et al., 1995; Erickson and Wilcox, 1997; Schnabel and Jones, 2001; Fraaije et al., 2007; Omrane et al., 2015), i.e., in *Penicillium digitatum* from citrus fruit (Eckert and Ogawa, 1988; Bus et al., 1991; Hamamoto et al., 2001a; Ghosop et al., 2007; Sun et al., 2011). Resistance to the DMIs in *P. digitatum* and other micro-organisms has been linked to single amino-acid alterations in the target site (Délye et al., 1997; Favre et al., 1999; Diaz-Guerra et al., 2003; Leroux et al., 2007; Wang et al., 2015; Pereira et al., 2017), increased energy dependent fungicide efflux mechanisms (Nakaune et al., 1998; Reimann and Deising, 2005), or overexpression of the CYP51 gene (Van Den Brink et al., 1996; Hamamoto et al., 2001a; Schnabel and Jones, 2001; Sun et al., 2013). A mechanism involving both amino-acid alterations with overexpression of the CYP51 gene has been suggested to cause DMI resistance in some other fungi (Mellado et al., 2007; Snelders et al., 2008; Mair et al., 2016; Lichtemberg et al., 2017).

The widespread resistance of *P. expansum* to two of the three existing postharvest fungicides and the fact that DIF will be premixed with FDL for which some tolerance has already been reported suggest a thorough risk assessment is needed before DIF becomes widely used. Herein, we evaluated the sensitivity of a baseline wild-type *P. expansum* population to DIF, determined impact of storage conditions on fungicide potency, and evaluated the risk and mechanisms of resistance development to DIF in lab mutants of *P. expansum*. We show that DIF would be a useful tool to include in future management programs but strategies are needed to extend its lifespan.

MATERIALS AND METHODS

Cultivation and Characterization of *P. expansum* Baseline Isolates

A total of 130 *P. expansum* isolates, never exposed to difenoconazole (DIF), collected in 2004 and 2005 were used to determine the baseline sensitivity. These isolates were single-spored and stored in 20% glycerol at -80°C at the WSU-TFREC pathology laboratory. Isolates were identified to the species level based on the β -tubulin gene using the PE-Chang5'-F and PE-Tub-R2 primer pair (**Supplementary Table S1**) developed in this study and based on a previous work published by Sholberg et al. (2005). Prior to each experiment, the isolates were grown on potato dextrose agar (PDA) at 22°C for 5 to 7 days or until profuse sporulation was observed. Three wild-type isolates, Pe3175, Pe3136, and Pe3334, were used for mutant selection as described below.

Fungicides

Formulated difenoconazole (DIF, Thesis, Syngenta Crop Protection, Greensboro, NC, United States), fludioxonil (Scholar SC, Syngenta), and fludioxonil + difenoconazole (Academy, Syngenta) were used in this study. For *in vitro* bioassay, stock solutions of 1,000 µg/ml of the active ingredients were made in sterile distilled water and stored in the dark at 4°C for no more than 21 days. Preliminary tests showed no negative effect of sensitivity levels of fungicide stocks prepared and stored as described above (data not shown). DIF was used to determine the baseline sensitivity of the 130 baseline isolates and selected mutants, whereas fludioxonil (FDL) was used to determine cross-sensitivity with DIF in mutant isolates. For *in vivo* assays, the formulated products were used following the label rate or as otherwise described.

Determination of Baseline Sensitivity to Difenoconazole

The sensitivity of 130 baseline isolates to DIF was determined *in vitro* using mycelial growth, spore germination, and germ tube inhibition assays on 1% malt extract agar (MEA) medium. Molten autoclaved MEA was cooled to 50°C and DIF was added from the stock to obtain final concentrations of 0.0, 0.05, 0.1, 0.5, 5.0, and 10.0 µg/ml and poured into 60-mm Petri plates. Spores were harvested from 7-day-old plates by transferring dry spores with a sterile plastic loop to a 2-ml tube containing 1 ml of sterile deionized water with 0.05% Tween 20. The spore concentrations were determined with a hemacytometer and adjusted to 10⁵ spores/ml. A 10 µl-droplet was plated onto the center of a DFC-amended and non-amended MEA plates, which were incubated for 6 days at 20°C before measuring the colony diameter. The spore germination inhibition assay was conducted on MEA as described for mycelial growth except that spore germination was measured microscopically after 16 h incubation at 20°C. A conidium was considered germinated when the germ tube length was at least twice the conidium diameter. The germ tube length of 10 conidia per plate was measured using the reticle ruler and used to assess sensitivity based on germ tube length inhibition. For each bioassay, trials were conducted in quadruplicates and repeated twice.

Generation and Characterization of DIF-Resistant Mutants

Mutants Generation

Three *P. expansum* wild-type isolates, Pe3175, Pe3136, and Pe3334, were used as parental isolates to generate fungicide-resistant mutants using ultraviolet (UV) light excitation as described by Li and Xiao (2008) with some modifications. For each isolate, a 100 µl-aliquot of a spore suspension at 3.7×10^7 conidia per ml was spread onto PDA media amended with 10 µg/ml DIF. Five replicate-plates were used for each of the three isolates and the plates were incubated at 20°C for 5 h in the dark before exposition to UV light (plates 27 cm from the UV light at 253.7 nm) for 30 s followed by a 7-day-incubation in the dark at 20°C. Growing colonies, including from the non-UV exposed WT parental isolates, were transferred twice on PDA amended

with DIF at 10 µg/ml and incubated for 6 days for each transfer. Thereafter, colonies were grown and transferred twice on DIF-free PDA and incubated at 20°C. No growth was observed on the WT isolates grown on PDA with 10 µg/ml after 12 days of incubation (data not shown).

Evaluation of Resistance of Mutants to DIF and Its Stability With and Without Selection Pressure

Five colonies were selected from each wild-type parent and the total of 15 mutants were characterized for their sensitivity to DIF using a mycelial growth assay as described above for the baseline isolates. The stability of resistance to DIF was evaluated without and with DIF selection pressure. Nine isolates, i.e., three WT-isolates Pe3136, Pe3175, and Pe3334 and three mutants selected from each of them, were used. A 10-µl droplet of a spore suspension (10⁴ spores/ml) of each isolate was transferred to fresh free-DIF MEA plates (three replicates/isolates) to test for stability in absence of selection pressure or onto MEA plates amended with DIF at 2.5 µg/ml to test with selection pressure. Isolates were incubated for 1 week at 20°C, then transferred weekly on DIF-free or DIF-amended plates for seven additional successive weeks. After 8 weeks, the EC₅₀ values were determined based on a mycelial growth inhibition assay and compared with the initial EC₅₀ values of the WT and the mutant isolates.

Virulence on Apple Fruit and Efficacy of DIF to Control Resistant Mutants

Organic cv. Fuji apples harvested at commercial maturity from an experimental orchard in East Wenatchee, Washington, were surface-disinfected for 3 min in 0.8% sodium hypochlorite, rinsed twice with sterile water and air-dried. Fruits were punctured twice near the stem-end area with a sterile needle (1.5 mm diameter, 3 mm deep), dipped for 30 s in a suspension of formulated DIF (Thesis, Syngenta) at label rate of 0.26 mg/L, allowed to dry at 4°C for 12, 24, 48, and 96 h then inoculated with a 25-µl droplet of spore suspension (5×10^4 spores/ml) on each wound. Control fruit were wounded and dipped in sterile water. The three WT-baseline isolates, Pe3334 (EC₅₀ = 0.13 µg/ml), Pe3136 (EC₅₀ = 0.21 µg/ml), and Pe3175 (EC₅₀ = 0.29 µg/ml), and nine lab DIF-mutants that had EC₅₀ values ranging from 0.6 to 3.7 µg/ml were used for inoculation. Eight replicate fruit in duplicate were used for each isolate and fungicide combination and the trials were conducted twice. Inoculated fruit (two reps of four fruit each per each treatment) were incubated in separate sterile boxes in saturated growth chambers at 0°C and a regular atmosphere. Disease incidence and severity were determined relative to untreated control fruit monthly up to 6 months of storage.

Cross-Sensitivity With Fludioxonil and Efficacy of Academy™ to Control DIF-Resistant Mutants

Difenoconazole is pre-mixed with fludioxonil (FDL) and registered as Academy™ for commercial use. Therefore, we verified that the DIF-lab mutants were not resistant to FDL. The three parental wild-type isolates, Pe3136, Pe3175, Pe3334, and the 15 DIF-resistant mutants selected were tested on PDA amended with FDL at 0, 0.001, 0.01, 0.1, 1.0, and 10.0 µg/ml.

Sensitivity tests were conducted based on a mycelial growth assay as described above for the baseline isolates. Three replicate plates were used for each isolate and fungicide concentration and the experiment was repeated twice.

A detached fruit assay was conducted to evaluate the efficacy of the mixture DIF + FDL (Academy™, Syngenta) to control DIF-resistant mutants. Organic Fuji apples were prepared as described above for virulence assay and treated preventively with Academy at 1.25 ml/L (0.26 mg DIF/L), then inoculated 4 h later with spore suspensions at 5×10^4 spores/ml of the parental wild-type isolate Pe3175 and two of its mutants. The number of replicate fruit, storage conditions and assessments of disease incidence and severity were conducted similarly to virulence assays above.

Amplification and Sequencing of the *PeCYP51* Gene

DNA of the three WT parental isolates and 15 mutants, i.e., 5 mutants from each WT isolate, was extracted from DIF-free 14 day-old-PDA plates using the FastDNA Kit (MP Biomedicals, Solon, OH, United States) according to the supplier's instructions. The quantity and purity of DNA was measured with a NanoDrop Spectrophotometer (ND-1000, NanoDrop Technology, Wilmington, DE, United States). Three sets of primers were developed (Supplementary Table S1) based on the sequences of *CYP51* in GenBank accession numbers XM016737741 and NW015971309 (Supplementary Figure S2) and used to amplify 1751 bp of the *P. expansum CYP51* (*PeCYP51*) gene. The primer pair CYP51-S2F/CYP51-S2R, developed based on the GenBank accession XM016737741, was used to amplify a 567 bp fragment of the coding region. The two other sets of primers were developed to amplify

parts of the *CYP51* and the flanking regions based on the GenBank accession NW015971309. The primer set CYP51-S5'F/CYP51-S1R was used to amplify an 811 bp fragment including 137 bp upstream of the 5' end of *CYP51* whereas the set CYP51-S3F/CYP51-S3'R was used to amplify an 884 bp fragment including 129 bp downstream the 3' end of the *CYP51* gene through conventional PCR. Fungal DNA (100 ng) was used as a template for PCR reactions which were run in 30 cycles of 94°C (30 s), 55°C (60 s), and 72°C (60 s) in a Bio-Rad T1000 thermocycler using EconoTaq® plus green 2× master mix (Lucigen, Middleton, WI, United States) following a protocol suggested by supplier. All PCR products were analyzed by electrophoresis on a 1% agarose gel, purified using a PCR purification kit (Qiagen, Valencia, CA, United States), and Sanger-sequenced at Retrogen, Inc. (San Diego, CA, United States). Sequences from the three fragments of the gene were concatenated and a multiple alignment was constructed using BioEdit Version 7.2.5 (Hall, 1999) to determine nucleotide and amino acid changes.

RNA Extraction and Quantitative Expression of the *PeCYP51* Gene

Total RNA was isolated from DIF-free 14-day-old PDA plates using a ZR Fungal/Bacterial RNA MiniPrep Kit (Zymo Research, Irvine, CA, United States) according to the supplier's instructions. All RNA was analyzed for quantity and quality spectroscopically on 1% TBE agarose gel. After extraction, 1 µg of total RNA from each sample was treated with DNase and single strand cDNA was synthesized using the Bio-Rad iScript™ gDNA Clear cDNA Synthesis Kit (Bio-Rad Inc., Hercules, CA, United States). All samples were DNase-treated

TABLE 1 | Virulence of wild-type and mutants of *Penicillium expansum* on detached Fuji apples and *in vivo* control efficacy of preventive difenoconazole applications.

Blue mold incidence (%) and lesion diameter (mm) on fruit treated or not with DFC								
Isolate	UV-C treatment ^a				8-Weeks selection pressure ^b			
	Mean EC ₅₀	Incidence ^d	Lesion diameter (mm)		Mean EC ₅₀	Incidence	Lesion diameter (mm)	
			DFC ⁻ C	DFC ⁺			DFC ⁻	DFC ⁺
Pe3334-WT (0.13) ^e	...	0.0*	55.8	0.0*	...	0.0*	39.5	0.0*
Pe3334-M1	1.3	75.0	54.5	18.5	1.7	100	36.8	14.5
Pe3334-M2	1.4	75.0	49.5	11.5	1.8	100	38.3	14.8
Pe3334-M3	1.4	100.0	52.5	7.5*	1.9	100	38.8	15.3
Pe3136-WT (0.21)	...	0.0*	53.8	0.0*	...	0.0*	40.3	0.0*
Pe3136-M1	1.3	75.0	53.8	22.5	1.9	100	37.3	16.5
Pe3136-M2	1.2	75.0	52.3	15.8	1.7	100	38.5	17.0
Pe3136-M3	1.3	75.0	51.8	18.3	1.9	100	39.8	17.8
Pe3175-WT (0.29)	...	0.0*	55.8	0.0*	...	0.0*	40.8	0.0*
Pe3175-M1	2.5	100.0	52.5	34.3	3.7	100	39.3	18.3
Pe3175-M2	2.5	75.0	49.5	21.8	3.7	100	39.8	17.3
Pe3175-M3	2.4	75.0	54.5	23.8	3.6	100	38.8	16.8

^{a,b}Indicate mutants selected after UV excitation and UV + 8 weeks of selection pressure on difenoconazole (DIF)-amended MEA, respectively. ^c- and + indicate virulence (lesion diameter in mm) on untreated (control) and DIF-treated fruit, respectively. ^dBlue mold incidence expressed as the number of infected fruit relative to the total number of fruit inoculated after 6 months of storage at 1°C. ^eNumbers in brackets indicate effective concentration to inhibit 50% growth (EC₅₀ in µg/ml) of the wild-type (WT) isolates. Values within the same column followed by an asterisk are statistically different from the other values based on an ANOVA test and Student's *t*-test at *P* ≤ 0.05.

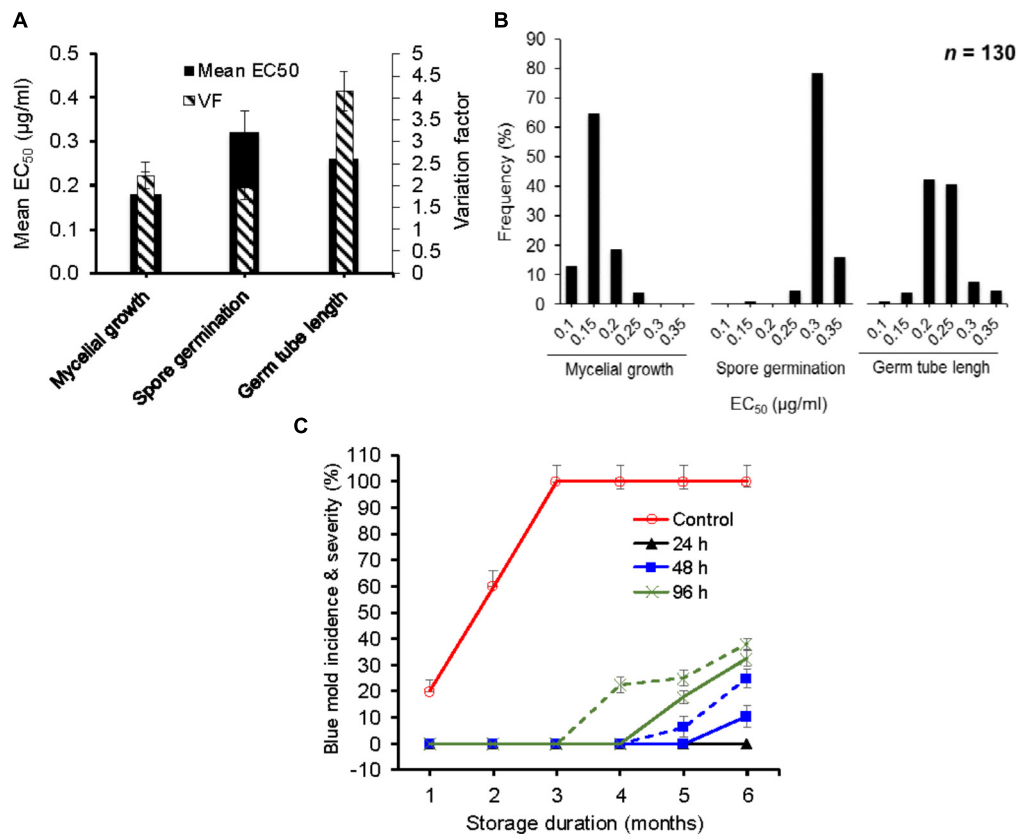


FIGURE 1 | *In vitro* and *in vivo* efficacy of difenoconazole against baseline isolates of *Penicillium expansum*. **(A)** Mean effective concentration of difenoconazole for 50% growth, germination and germ tube elongation inhibition (EC₅₀) and variation factor (VF, highest EC₅₀/lowest EC₅₀) of 130 baseline isolates of *P. expansum*. **(B)** Frequency distribution of respective EC₅₀ values among 130 baseline isolates of *P. expansum*. **(C)** Temporal change in blue mold incidence (continuous lines) and severity (dashed lines) on detached apple fruit treated preventively with 0.26 mg/L of difenoconazole and inoculated with WT-isolates of *P. expansum* 24, 48, and 96 h post-treatment at 1°C and regular atmosphere. Data are the mean incidences from 3 WT-isolates (data were merged after no significance difference was observed between the isolates) and 58 fruit across two experimental runs. Data from the 12-h post-treatment inoculation are not shown because no disease was seen.

and cDNA synthesized in a single run with one batch of reagents and stored at -80°C . All quantitative (qPCR) reactions were run on a CFX96™ Real-Time PCR Detection System using SsoAdvanced™ Universal SYBR® Green Supermix (Bio-Rad Inc., Hercules, CA, United States) in a 10 μl -reaction volume containing 5 μl of SYBR Green Supermix (antibody-mediated hot-start Sso7d fusion polymerase, 50 mM Na⁺, 1.5 mM Mg²⁺, 1.2 mM dNTPs, and 250 nM annealing oligo), 0.3 μl of 1000 nM of each forward (cyp51A-F/ β -actin-F) and reverse primers (cyp51A-R/ β -actin-R) (Table 1), and 2 μl (10 pg) of cDNA and 2.4 μl of PCR grade water. The recommended thermal cycling protocol for SsoAdvanced™ SYBR Green was used at an annealing/extension temperature of 60°C , and a melt curve analysis was included. The CFX Maestro™ Software¹ was used to analyze all qPCR data. The $2^{-\Delta\Delta\text{Ct}}$ equation (Livak and Schmittgen, 2001) was used to calculate the relative gene expression using the β -actin as a reference control gene. *CYP51* expression

data presented herein are averages of nine values for each isolate across three separate experimental runs. The “sample maximization” experimental set-up for multi-plate qPCR studies was used to minimize technical variation between samples (Helleman et al., 2007).

Statistical Analysis

Data from the two independent runs of *in vitro* and *in vivo* experiments were averaged when no statistical difference was observed between the two runs. Difenoconazole *in vitro* sensitivity data, expressed as percent inhibition relative to the control, were computed and log-transformed to calculate effective concentrations to inhibit 50% growth or germination (EC₅₀). Variation factors (VF) were calculated as the highest EC₅₀ value by the lowest EC₅₀ value within the baseline population, whereas the resistance factors (RF) for DIF-mutants were calculated as their EC₅₀ value by the EC₅₀ value of the parental WT-isolate. Virulence *in vivo* bioassay data were used to calculate disease incidence and severity. Gene expression was expressed as the ratio between *CYP51*

¹ www.bio-rad.com

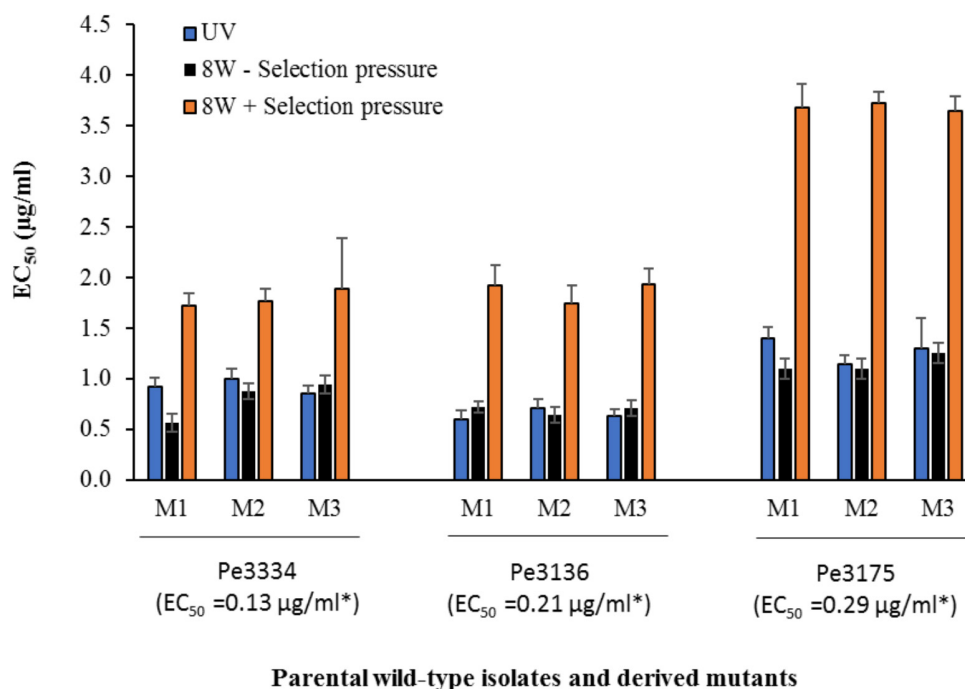


FIGURE 2 | Mean effective concentration for 50% growth inhibition values (EC₅₀) of difenoconazole for DIF-resistant mutants selected following UV excitation of Pe3334, Pe3136, and Pe3175 *P. expansum* isolates or after 8 weeks of adaptation on MEA amended with DIF at 2.5 µg/ml (+ selection pressure, orange bars) or without (– selection pressure, black bars) at 22°C. Asterisks indicates the EC₅₀ values of each parental WT-isolate. Data are the mean of 12 values across two experimental runs for each mutant.

and β -actin genes. Data were subjected to ANOVA analyses and mean separations using Student *t*-test at $P < 0.05$ in SAS software (Version 9.2, SAS Institute Inc., Cary, NC, United States).

RESULTS

In vitro and *in vivo* Sensitivities of *P. expansum* Baseline Isolates to Difenoconazole

The mean EC₅₀ values (\pm SD) for difenoconazole (DIF) determined for mycelial growth, spore germination and germ tube length inhibition were 0.17 ± 0.03 , 0.32 ± 0.02 , and 0.26 ± 0.06 µg/ml, respectively (Figure 1A). The EC₅₀ values ranged from 0.13 to 0.29 µg/ml based on mycelial growth and from 0.19 to 0.37 µg/ml for spore germination inhibition and from 0.14 to 0.58 µg/ml for germ tube length inhibition (Figure 1B). The VF were 2.23, 1.95, and 4.14 µg/ml, respectively. The frequency distribution of EC₅₀ values for germ tube length and mycelial growth were the closest to a unimodal distribution with a right-hand tail (Figure 1B), contrary to spore germination, which had a left-hand tail.

The EC₅₀ value of the *P. expansum* WT-isolates did not affect the efficacy of DIF *in vivo* since the three isolates Pe3175 (EC₅₀ = 0.13 µg/ml), Pe3334 (EC₅₀ = 0.21 µg/ml), and Pe3175 (EC₅₀ = 0.29 µg/ml) resulted in similar incidence and severity

on detached fruit treated by the label rate of DIF. Therefore, data of the three isolates were averaged and presented in Figure 1C. The wild-type isolates were fully controlled on detached fruit for up to 6 months of storage at 0°C when DIF was applied 12 to 24 h pre-inoculation and for up to 4 months when DIF was applied preventively 48 or 96 h pre-inoculation (Figure 1C). After 6 months of storage, the blue mold incidence was 25 and 38% on fruit inoculated 48 and 96 h pre-inoculation, respectively, and similar severity trend was observed.

Characterizations of DIF-Resistant Mutants

Resistance Levels, Stability, Cross-Resistance With FDL and Efficacy of DIF *in vivo*

In total, 15 *P. expansum* mutants generated through UV excitation were tested for sensitivity to DIF using a mycelial growth inhibition assay to determine variation in their EC₅₀ values compared to the parental wild-type (WT) isolates. The mutants selected from the parental WT isolates Pe3334 (EC₅₀ = 0.13 µg/ml) and Pe3136 (EC₅₀ = 0.21 µg/ml) had EC₅₀ values ranging from 1.1 to 1.4 and respective RF ranging from 5.7 to 10.6, whereas the mutants selected from the parental isolate Pe3175 (EC₅₀ = 0.29 µg/ml) had EC₅₀ values ranging from 2.1 to 2.5 (Table 1) and RFs from 7.7 to 8.8. After 8 weekly transfers on MEA supplemented with DIF at 2.5 µg/ml (selection pressure), the EC₅₀ values of the mutants ranged from 1.6 to 1.9 µg/ml for the mutants selected from the Pe3334 and Pe3136 WT isolates

and from 3.3 to 3.7 $\mu\text{g/ml}$ for the mutants selected from the parental isolate Pe3175 (**Figure 2**). RF values relative to the WT isolates ranged from 8 to 13 and increased by 1 to 1.5-fold relative to the first mutants transfer (data not shown). After 10 weekly transfers on DIF-free MEA (no selection pressure), the EC_{50} values of DIF-resistant mutants decreased by 0.04 to 0.36 $\mu\text{g/ml}$ for 6 mutants out of nine tested while EC_{50} increased in three mutants. However, EC_{50} values were not significantly different from the first transfer and remained within the resistance range (**Figure 2**).

All the nine mutants originating from UV excitation caused blue mold on detached apple fruit and they were as virulent (lesion diameter) as the parental WT isolates (**Table 1**). While the three WT isolates were fully controlled by a preventive DIF application after 6 months of storage at 1°C (**Table 1**), the fungicide failed to control the nine selected mutants as the blue mold incidence ranged from 75 to 100% (**Table 1** and **Figure 3**). The UV mutants adapted on 2.5 $\mu\text{g/ml}$ of DIF for 8 weeks caused 100% blue mold incidence and their virulence (lesion diameter) was not significantly reduced compared to same isolate at the first transfer (**Table 1** and **Figure 3**).

The WT isolates Pe3334, Pe3136, and Pe3175 had an EC_{50} of 0.04, 0.04, and 0.05 $\mu\text{g/ml}$ for fludioxonil (FDL), respectively (data not shown). The EC_{50} values of the DIF-mutants for FDL were similar to those of the WT isolates and ranged from 0.04 to 0.06 $\mu\text{g/ml}$. There was a moderate positive correlation ($R^2 = 0.4257$) between EC_{50} values of FDL and DIF for DIF-mutants adapted for 8 weeks on DIF at 2.5 $\mu\text{g/ml}$ compared to the original UV mutants ($R^2 = 0.3567$) (**Figure 4A**). DIF (Thesis) alone controlled the WT isolate Pe3175 but failed to control its

two mutants M1 and M2, whereas FDL (pre-mixed with DIF) in AcademyTM, applied preventively, fully controlled the WT isolate and its DIF-mutants after 6 months of storage at 1°C (**Figure 4B**).

Sequence Analysis and Expression of the *PeCYP51* Gene

The sequencing of full *PeCYP51* gene of *P. expansum* yielded a sequence with a length of 1751 bp with three introns of 68, 69, and 63 bp, respectively, and coded for 516 amino acids (**Figure 5A** and **Supplementary Figure S2**). A blast of the amino acid sequence of the WT isolate Pe3175 revealed 100, 96, 92, and 67% identity with *P. expansum*, *P. italicum*, *P. digitatum*, and *Aspergillus fumigatus* accession numbers XP106598797, KGO74727, XP014532172, and ARS45267, respectively. The alignments of nucleotide and amino-acid sequences of the GenBank reference accession number XM016737741, the sensitive WT parental isolates, and the resulting DIF-mutants is shown in **Figure 5B**. A single polymorphism from A to T at nucleotide 445 resulted in an amino-acid substitution from tyrosine to phenylalanine at codon 126 (Y126F) of the *PeCYP51* gene was detected in all mutants regardless of their EC_{50} value and was absent in all WT isolates (**Figure 5B** and **Supplementary Figure S2**). The *CYP51* sequence from the Pe3175 WT-isolates and of its mutants (M1) were submitted to GenBank under the accession numbers MH507024 and MH507025, respectively.

We evaluated the *CYP51* gene expression in 3 parental and 5 mutant isolates not challenged with DIF prior to RNA extraction. The relative expression (RE) of the *CYP51* gene

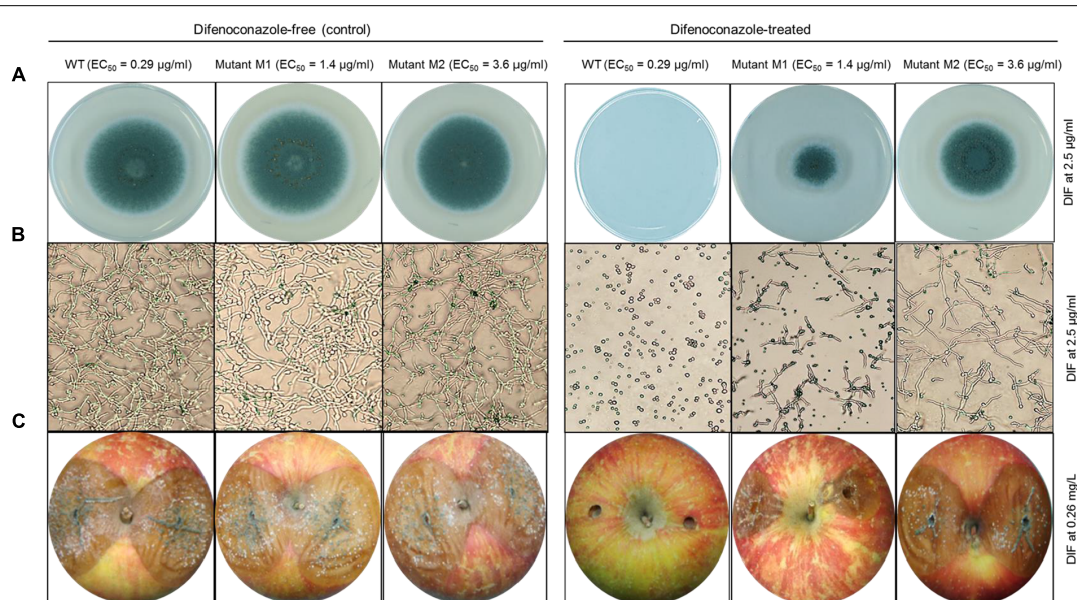
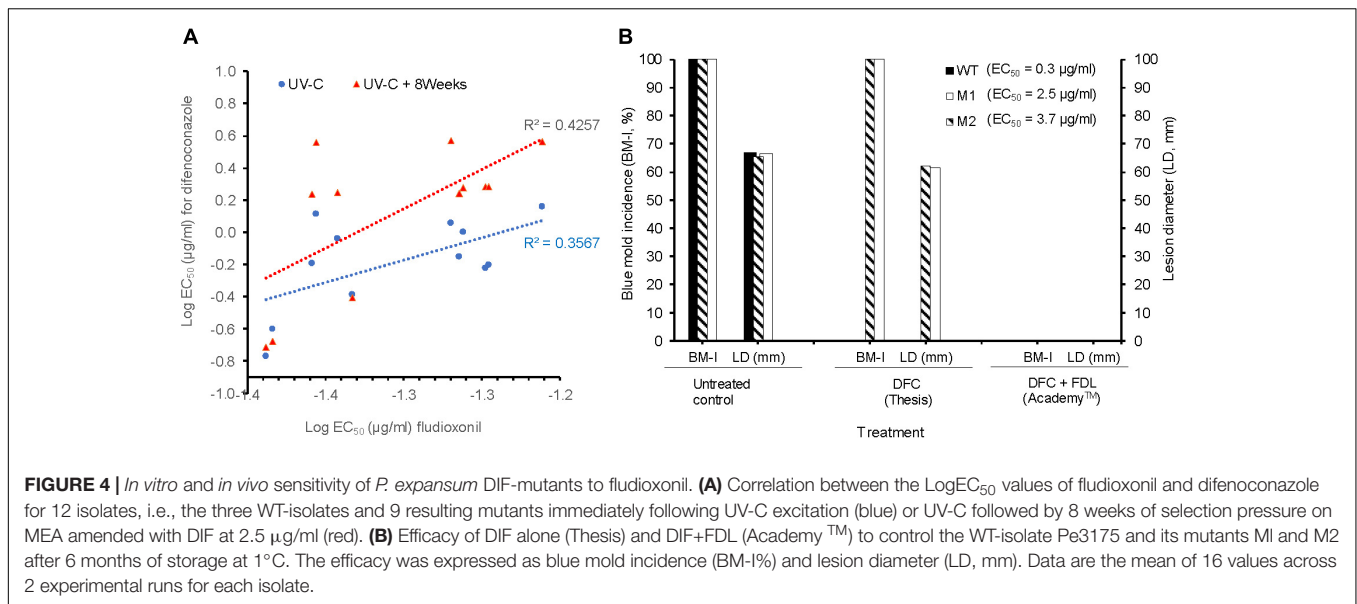


FIGURE 3 | *In vitro* and *in vivo* efficacy of difenoconazole against *P. expansum* wild-type and DIF-mutants. **(A)** Mycelial growth and **(B)** germination of the *P. expansum* Pe3175 WT-isolate, mutant M1 (generated from UV-C treatment) and mutant M2 (UV-C + 8 weeks adaptation on DIF at 2.5 $\mu\text{g/ml}$) on DIF-free MEA (left, control) or on MEA amended with DIF at 2.5 $\mu\text{g/ml}$ (right) after 24 h and 7 days incubation at 22°C for spore germination and mycelial growth, respectively. **(C)** Blue mold lesion diameter caused by Pe3175 WT and its respective mutants M1 and M2 on Fuji apples treated or not (control) with 0.26 mg/L DIF and incubated at 1°C for 6 months.



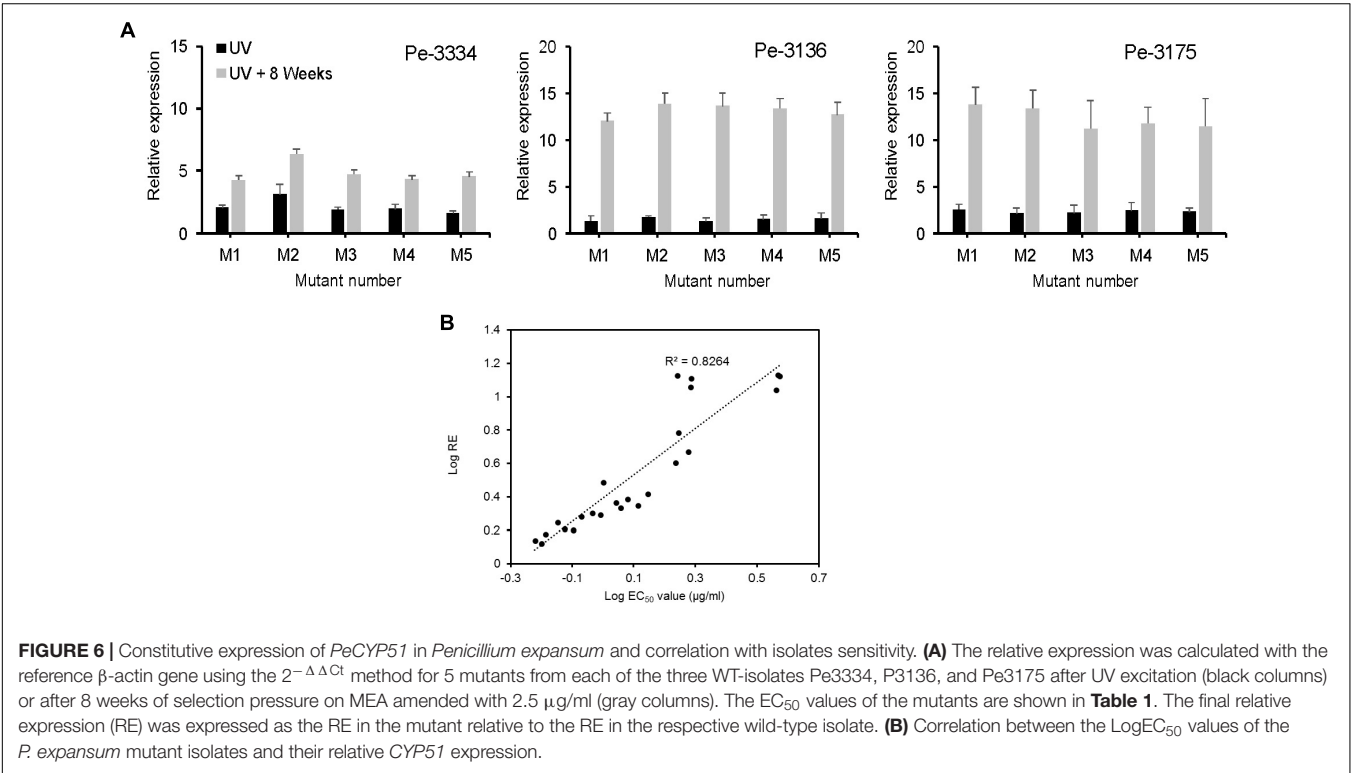
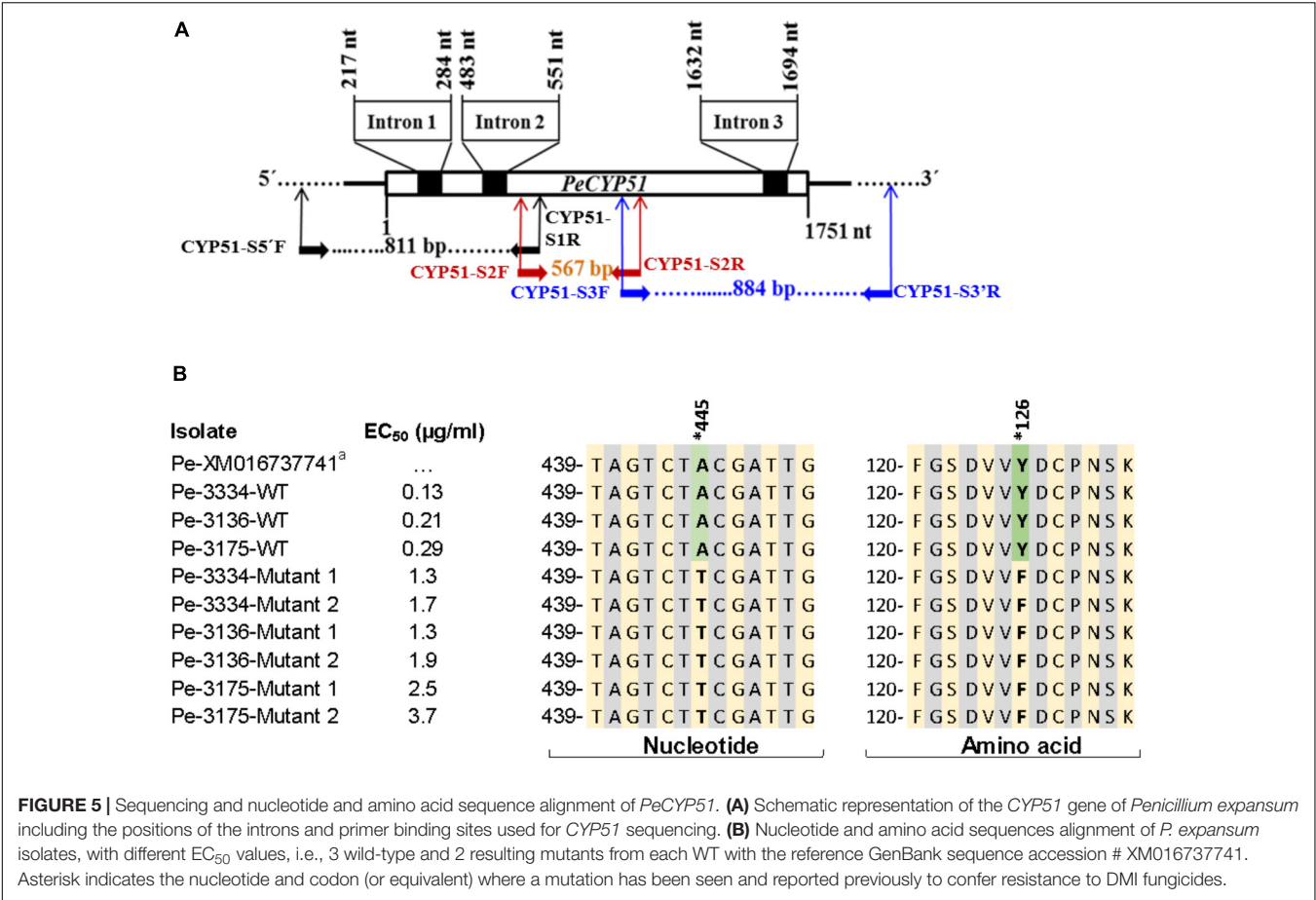
increased 2 to 3 folds in UV-mutants and 4 to 14 fold in mutants adapted for 8 weeks DIF at 2.5 µg/ml (Figure 6A). The *CYP51*-RE was positively and significantly correlated ($R^2 = 0.8264$) with the EC₅₀ values of the isolates (Figure 6B). The mutants resulting from the Pe-3334 WT-isolate (EC₅₀ = 0.21 µg/ml) had a lower *CYP51* RE compared to the mutants from the two other isolates after UV excitation or adaptation on DIF (Figure 6A).

DISCUSSION

Demethylation inhibitors have been used for years to control *P. digitatum* and *P. italicum* and other citrus pathogens. However, difenoconazole (DIF) is the first DMI registered for managing *P. expansum* and other postharvest diseases of pome fruit. The baseline *P. expansum* population was highly sensitive to DIF, as shown by the low EC₅₀ values (<0.5 µg/ml) for all growth stages, i.e., germination, germ tube elongation, and mycelial growth, *in vitro* as well by the ability of DIF to fully control blue mold infections on apple fruits for at least 6 months in cold storage. High control efficacy of DIF has been reported in several ascomycetes such as *Phacidiopycnis* spp., *Venturia inaequalis*, *Colletotrichum* spp., *Marssonina coronaria*, *Alternaria* spp., and *Fusarium* spp. (Munkvold and O'Mara, 2002; Villani et al., 2015; Fonseka and Gudmestad, 2016; Cao et al., 2017; Dang et al., 2017; Ali et al., 2018) and the basidiomycete *Rhizoctonia solani* (Bartholomäus et al., 2017). Given the widespread occurrence of resistance to two of the three current postharvest fungicides and the stringent limitations to new postharvest fungicides registration, DIF could be a valuable additional tool to manage blue mold of pome fruit in the years to come if used appropriately and if its efficacy against other major postharvest diseases is proven.

Our data suggest a risk for *P. expansum* to develop resistance to DIF in packinghouses where it is expected to be part of regular management programs. This suggests it should be rotated with other fungicides, to extend its lifespan. The selection and characterization of *P. expansum* mutants in this study will be valuable to estimate the risk and the speed of DIF resistance development and will serve as a reference for future DIF resistance monitoring in exposed populations. Mutants with an EC₅₀ value >0.8 µg/ml were not controlled by the DIF label rate on detached fruit, and we, therefore, suggest a dose of 1.0 µg/ml and above as a potential discriminatory dose for future DIF resistance monitoring. Fitness penalties have been linked with resistance to other DMIs in multiple pathogens such as *Monilinia fructicola*, *Aspergillus nidulans*, and *Colletotrichum truncatum* (Van Tuyl, 1977; Chen et al., 2012; Zhang et al., 2017) but not in *P. digitatum* (Nakaune et al., 2002). We did not investigate the fitness of the DIF-*P. expansum* mutants, but the latter were as virulent at the parental wild-type isolates on apple fruit in the absence of a DIF selection pressure (Table 1). Moreover, although the level of resistance to DIF in the mutants slightly decreased over a 10-week period in the absence of a selection pressure *in vitro*, the EC₅₀ values remained within the resistance range. Given that *P. expansum* is considered among the group of fungi with a "high risk" for fungicide resistance development, field resistance is likely to occur and persist in packinghouses if rational practices are not implemented immediately upon registration.

The mixture of DIF with fludioxonil as Academy™ should be effective in controlling DIF-resistant populations of *P. expansum* if/when they emerge in commercial packinghouses. Indeed, no cross-resistance was observed between FDL and DIF and the EC₅₀ values (≤ 0.06 µg/ml) of the DIF-mutants for FDL were not different from those of the parental isolates. There was a correlation with *in vivo* susceptibility as the label rate of Academy™ fully controlled the DIF-resistant mutants on apple



fruit after 6 months of storage (Figure 4B). However, because of a slightly stronger positive correlation (Figure 4A) observed between the EC₅₀ values of FDL and DIF under a DIF-continuous selection pressure, further investigations are needed to ensure that mechanisms of resistance in *P. expansum* do not select for dual-resistant populations as it has been reported recently in the closely related species *P. digitatum* (Wang et al., 2014).

We present evidence that resistance to DMIs in *P. expansum* is likely caused by variation in the amino acid sequence and overexpression of the *PeCYP51* gene, although other mechanisms cannot be completely excluded. The Tyr-Phe mutation found at codon 126 of *P. expansum* is well known for its role in resistance to DMIs as an equivalent mutation at codon 136 of *Erysiphe necator* (Délye et al., 1997, 1998; Frenkel et al., 2015), *Blumeria graminis* (Wyand and Brown, 2005), and *Parastagonospora nodorum* (Pereira et al., 2017) was reported to confer resistance to different DMIs. Other amino acid substitutions at different codons have also been reported to cause DMI resistance in several other plant pathogens (Leroux et al., 2007; Wang et al., 2015; Mair et al., 2016; Lichtemberg et al., 2017; Pereira et al., 2017). The Y126F substitution was present in all DIF mutants with an EC₅₀ value >1.0 µg/ml and no other mutation was detected in mutants with higher EC₅₀ values (>3 µg/ml) after 8 weeks of selection pressure which suggest a major role of this alteration in conferring resistance to the DMI fungicides in *P. expansum*. If a single point mutation is proven to be the major driving factor of resistance to DIF and other DMIs in *P. expansum*, resistance can be expected to emerge and build-up quickly once DIF is used frequently in the packinghouses.

The Y126F alteration is located in the conserved substrate binding domain of the *CYP51* gene (van Nestelrooy et al., 1996) and a mutation in this region could affect mRNA stability and heme structure of *CYP51* which can decrease the affinity of DMIs as reported in *Candida albicans* (Kelly et al., 1999). The reduced affinity due to smaller amounts fungicide docking to the binding site prevents complete control. The significant 12 to 14-fold increase in the expression of the *CYP51* gene without DIF induction prior to total RNA extraction in mutants of the second generation (selection pressure) suggests a role of *CYP51* overexpression in DMI resistance in *P. expansum*. In the closely related species *P. italicum* and *P. digitatum*, several mechanisms of resistance to DMIs have been elucidated. Thus, the expression of the *P. italicum*-*CYP51* gene by heterologous combination in *Aspergillus niger* was 2 to 5-fold higher in a resistant transformant compared to a wild-type isolate, but whether a change in the amino-acid sequence has occurred was not investigated (van Nestelrooy et al., 1996). In the citrus green mold-causal species *P. digitatum*, resistance to DMIs has been linked to the *ABC* and *CYP51* genes. *Penicillium* multidrug resistance (*PMR1* and *PMR5*) genes encoding an ATP-binding cassette were suggested to play a role in *P. digitatum* resistance to the DMIs (Nakaune et al., 1998, 2002; Sun et al., 2013) although the role of *PMR1* was not clearly evidenced by Hamamoto et al. (2001b). Moreover, a 199 bp transposon insert in the promoter region of the *CYP51* gene of *P. digitatum* DMI-resistant isolates increased its expression 7.5 to 13.6-fold (Ghosoph et al., 2007;

Sun et al., 2011), similar to the overexpression levels seen in *P. expansum* mutants in this study. Recently, a role of major facilitator superfamily transporters (MFS) has been hypothesized as potential mechanisms of DMI-resistance in *P. digitatum* (Wu et al., 2016). Worrisomely, some of the above mechanisms reported in *P. digitatum* were also found to confer multidrug (MDR) resistance (Nakaune et al., 2002; Sun et al., 2011). The 100 bp sequenced upstream and downstream the *CYP51* of *P. expansum* did not reveal any mutations in the DIF-mutants (data not shown). Research investigation is ongoing to explore additional potential mutations and study a potential role of the above or other mechanisms in DMI or MDR resistance of *P. expansum* populations in commercial packinghouses. This information will be critical to clearly assess the expected risk for resistance emergence in this pome fruit-*Penicillium* pathosystem and develop appropriate management strategies.

In summary, we conducted a risk assessment study to evaluate the efficacy and risk associated with the introduction of a new DMI in the pome fruit-postharvest system. We showed a high and lasting control efficacy of difenoconazole alone or in combination with fludioxonil. However, resistance to DIF seems likely to emerge in *P. expansum* packinghouse populations for which resistance levels and speed of selection will depend on the actual mechanism(s) of resistance and the selection pressure through usage frequency.

AUTHOR CONTRIBUTIONS

AA designed the project and supervised the work. EA performed the experiments and analyzed the data. All authors participated in writing and editing the manuscript.

FUNDING

This work was supported by a Washington Tree Fruit Research Commission (WTFRC) Grant no. AP-16-105. PPNS # 0766, Department of Plant Pathology, College of Agricultural, Human, and Natural Resource Sciences, Agricultural Research Center, Hatch Project No. WNP0555, Washington State University, Pullman, WA, United States.

ACKNOWLEDGMENTS

The authors thank Laxmi K. Pandit, WSU-TFREC for technical assistance and the WTFRC for funding.

SUPPLEMENTARY MATERIAL

The Supplementary Material for this article can be found online at: <https://www.frontiersin.org/articles/10.3389/fmicb.2018.02472/full#supplementary-material>

REFERENCES

- Ali, E. M., Pandit, L. K., Mulvaney, K. A., and Amiri, A. (2018). Sensitivity of *Phacidiopycnis* spp. isolates from pome fruit to six pre- and postharvest fungicides. *Plant Dis.* 102, 533–539.
- Amiri, A., and Ali, E. M. (2016). *Prevalence of Storage Decays of Apple: Lessons from the 2016 Statewide Survey*. Available at: <http://treefruit.wsu.edu/news/prevalence-of-storage-decays-of-apple-lessons-from-the-2016-statewide-survey/>
- Amiri, A., Ali, E. M., De Angelis, D. R., Mulvaney, K. A., and Pandit, L. K. (2018). "Prevalence and distribution of *Penicillium expansum* and *Botrytis cinerea* in apple packinghouses across Washington State and their sensitivity to the postharvest fungicide-pyrimethanil," in *Proceedings of IV International Symposium on Postharvest Pathology*, Skukuza.
- Amiri, A., Mulvaney, K. A., and Pandit, L. K. (2017). First report of *Penicillium expansum* isolates with low levels of resistance to fludioxonil from commercial apple packinghouses in Washington State. *Plant Dis.* 101, 835–835. doi: 10.1094/PDIS-09-16-1353-PDN
- Amiri, A., and Bompeix, G. (2005a). Diversity and population dynamics of *Penicillium* spp. on apples in pre- and postharvest environments: consequences for decay development. *Plant Pathol.* 54, 74–81. doi: 10.1111/j.1365-3059.2005.01112.x
- Amiri, A., and Bompeix, G. (2005b). Micro-wound detection on apple and pear fruit surfaces using sulfur dioxide. *Postharvest Biol. Technol.* 36, 51–59. doi: 10.1016/j.postharvbio.2004.10.010
- Bartholomäus, A., Mittler, S., Märkländer, B., and Varrelmann, M. (2017). Control of *Rhizoctonia solani* in sugar beet and effect of fungicide application and plant cultivar on inoculum potential in the soil. *Plant Dis.* 101, 941–947. doi: 10.1094/PDIS-09-16-1221-RE
- Bus, V., Bongers, A., and Risse, L. (1991). Occurrence of *Penicillium digitatum* and *P. italicum* resistant to benomyl, thiabendazole and imazalil on citrus fruit from different geographic origins. *Plant Dis.* 75, 1098–1100. doi: 10.1094/PD-75-1098
- Caiazzo, R., Kim, Y., and Xiao, C. (2014). Occurrence and phenotypes of pyrimethanil resistance in *Penicillium expansum* from apple in Washington state. *Plant Dis.* 98, 924–928. doi: 10.1094/PDIS-07-13-0721-RE
- Cao, X., Xu, X., Che, H., West, H. S., and Luo, D. (2017). Distribution and fungicide sensitivity of *Colletotrichum* species complexes from rubber tree in Hainan. *China Plant Dis.* 101, 1774–1780. doi: 10.1094/PDIS-03-17-0352-RE
- Chen, F. P., Fan, J. R., Zhou, T., Liu, X. L., Liu, J. L., and Schnabel, G. (2012). Baseline sensitivity of *Monilinia fructicola* from China to the DMI fungicide SYP-Z048 and analysis of DMI-resistant mutants. *Plant Dis.* 96, 416–422. doi: 10.1094/PDIS-06-11-0495
- Dang, J., Gleason, M., Niu, C., Liu, X., Guo, Y., Zhang, R., et al. (2017). Effects of fungicides and spray application interval on controlling Marssonina blotch of apple in the Loess Plateau Region of China. *Plant Dis.* 101, 568–575. doi: 10.1094/PDIS-04-16-0464-RE
- Délye, C., Bousset, L., and Corio-Costet, M. F. (1998). PCR cloning and detection of point mutations in the eburicol 14 alpha-demethylase (CYP51) gene from *Erysiphe graminis* f. sp. hordei, a "recalcitrant" fungus. *Curr. Genet.* 34, 399–403. doi: 10.1007/s002940050413
- Délye, C., Laigret, F., and Corio-Costet, M.-F. (1997). A mutation in the 14 alpha-demethylase gene of *Uncinula necator* that correlates with resistance to a sterol biosynthesis inhibitor. *Appl. Environ. Microbiol.* 63, 2966–2970.
- Diaz-Guerra, T., Mellado, E., Cuenca-Estrella, M., and Rodriguez-Tudela, J. (2003). A point mutation in the 14 α -sterol demethylase gene cyp51A contributes to itraconazole resistance in *Aspergillus fumigatus*. *Antimicrob. Agents Chemother.* 47, 1120–1124. doi: 10.1128/AAC.47.3.1120-1124.2003
- Eckert, J. W., and Ogawa, J. M. (1988). The chemical control of postharvest diseases: deciduous fruits, berries, vegetables and root/tuber crops. *Ann. Rev. Phytopathol.* 26, 433–469. doi: 10.1146/annurev.py.26.090188.002245
- Erickson, E. O., and Wilcox, W. F. (1997). Distributions of sensitivities to three sterol demethylation inhibitor fungicides among populations of *Uncinula necator* sensitive and resistant to triadimefon. *Phytopathology* 87, 784–791. doi: 10.1094/PHYTO.1997.87.8.784
- Errampalli, D., Brubacher, N. R., and DeEll, J. R. (2006). Sensitivity of *Penicillium expansum* to diphenylamine and thiabendazole and postharvest control of blue mold with fludioxonil in 'McIntosh' apples. *Postharvest Biol. Technol.* 39, 101–107. doi: 10.1016/j.postharvbio.2005.09.008
- Favre, B., Didmon, M., and Ryder, N. S. (1999). Multiple amino acid substitutions in lanosterol 14 α -demethylase contribute to azole resistance in *Candida albicans*. *Microbiology* 145, 2715–2725. doi: 10.1099/00221287-145-10-2715
- Fonseka, D., and Gudmestad, N. (2016). Spatial and temporal sensitivity of Alternaria species associated with potato foliar diseases to demethylation inhibiting and anilino-pyrimidine fungicides. *Plant Dis.* 100, 1848–1857. doi: 10.1094/PDIS-01-16-0116-RE
- Fraaije, B., Cools, H., Kim, S. H., Motteram, J., Clark, W., and Lucas, J. (2007). A novel substitution I381V in the sterol 14 α -demethylase (CYP51) of *Mycosphaerella graminicola* is differentially selected by azole fungicides. *Mol. Plant Pathol.* 8, 245–254. doi: 10.1111/j.1364-3703.2007.00388.x
- Frenkel, O., Cadle-Davidson, L., Wilcox, W. F., and Milgroom, M. G. (2015). Mechanisms of resistance to an azole fungicide in the grapevine powdery mildew fungus *Erysiphe necator*. *Phytopathology* 105, 370–377. doi: 10.1094/PHYTO-07-14-0202-R
- Gaskins, V. L., Vico, I., Yu, J., and Yurick, W. M. (2015). First report of *Penicillium expansum* isolates with reduced sensitivity to fludioxonil from a commercial packinghouse in Pennsylvania. *Plant Dis.* 99:1182. doi: 10.1094/PDIS-11-14-1161-PDN
- Ghosh, J. M., Schmidt, L. S., Margosan, D. A., and Smilanick, J. L. (2007). Imazalil resistance linked to a unique insertion sequence in the PdCYP51 promoter region of *Penicillium digitatum*. *Postharvest Biol. Technol.* 44, 9–18. doi: 10.1016/j.postharvbio.2006.11.008
- Golembiewski, R., Vargas, J., Jones, A., and Detweiler, A. (1995). Detection of demethylation inhibitor (DMI) resistance in *Sclerotinia homoeocarpa* populations. *Plant Dis.* 79, 491–493. doi: 10.1094/PD-79-0491
- Hall, T. A. (1999). BioEdit. A user-friendly biological sequence alignment editor and analysis program for windows 95/98/NT. *Nucleic Acids Symp. Ser.* 41, 95–98.
- Hamamoto, H., Hasegawa, K., Nakaune, R., Lee, Y. J., Makizumi, Y., Akutsu, K., et al. (2001a). Tandem repeat of a transcriptional enhancer upstream of the sterol 14 α -demethylase gene (CYP51) in *Penicillium digitatum*. *Appl. Environ. Microbiol.* 66, 3421–3426. doi: 10.1128/AEM.66.8.3421-3426.2000
- Hamamoto, H., Nawata, O., Hasegawa, K., Nakaune, R., Lee, Y. J., Makizumi, Y., et al. (2001b). The role of the ABC transporter gene PMR1 in demethylation inhibitor resistance in *Penicillium digitatum*. *Pest Biochem. Physiol.* 70, 19–26. doi: 10.1006/pest.2000.2530
- Hellemans, J., Mortier, G., De Paepe, A., Speleman, F., and Vandesompele, J. (2007). qBase relative quantification framework and software for management and automated analysis of real-time quantitative PCR data. *Genome Biol.* 8:R19. doi: 10.1186/gb-2007-8-2-r19
- Hof, H. (2001). Critical annotations to the use of azole antifungals for plant protection. *Antimicrob. Agents Chemother.* 45, 2987–2990. doi: 10.1128/AAC.45.11.2987-2990.2001
- Joseph-Horne, T., and Hollomon, D. W. (1997). Molecular mechanisms of azole resistance in fungi. *FEMS Microbiol. Lett.* 149, 141–149. doi: 10.1111/j.1574-6968.1997.tb10321.x
- Jurick, W. M., Janisiewicz, W. J., Saftner, R. A., Vico, I., Gaskins, V. L., Park, E., et al. (2011). Identification of wild apple germplasm (*Malus* spp.) accessions with resistance to the postharvest decay pathogens *Penicillium expansum* and *Colletotrichum acutatum*. *Plant Breed.* 130, 481–486. doi: 10.1111/j.1439-0523.2011.01849.x
- Jurick, W. M., Macarasin, O., Gaskins, V. L., Park, E., Yu, J., Janisiewicz, W., et al. (2017). Characterization of postharvest fungicide-resistant *Botrytis cinerea* isolates from commercially stored apple fruit. *Phytopathology* 107, 362–368. doi: 10.1094/PHYTO-07-16-0250-R

- Kelly, S. L., Lamb, D. C., Loeffler, J., Einsele, H., and Kelly, D. E. (1999). The G464S amino acid substitution in *Candida albicans* sterol 14 alpha-demethylase causes fluconazole resistance in the clinic through reduced affinity. *Biochem. Biophys. Res. Commun.* 262, 174–179. doi: 10.1006/bbrc.1999.1136
- Koehler, A., and Shew, H. (2018). Field efficacy and baseline sensitivity of *Septoria steviae* to fungicides used for managing *Septoria* leaf spot of stevia. *Crop Prot.* 109, 95–101. doi: 10.1016/j.cropro.2018.03.006
- Leroux, P., Albertini, C., Gautier, A., Gredt, M., and Walker, A.-S. (2007). Mutations in the CYP51 gene correlated with changes in sensitivity to sterol 14 α -demethylation inhibitors in field isolates of *Mycosphaerella graminicola*. *Pest Manag. Sci.* 63, 688–698. doi: 10.1002/ps.1390
- Li, H. X., and Xiao, C. L. (2008). Resistance to fludioxonil-resistant and pyrimethanil-resistant phenotypes of *Penicillium expansum* from apple. *Phytopathology* 98, 427–435. doi: 10.1094/PHYTO-98-4-0427
- Lichtemberg, P. S. F., Luo, Y., Morales, R. G., Muehlmann-Fischer, J. M., Michailides, T. J., and May De Mio, L. L. (2017). The point mutation g461s in the mfcyp51 gene is associated with tebuconazole resistance in *Monilinia fructicola* populations in Brazil. *Phytopathology* 107, 1507–1514. doi: 10.1094/PHYTO-02-17-0050-R
- Livak, K. J., and Schmittgen, T. D. (2001). Analysis of relative gene expression data using real-time quantitative PCR and the 2(T)(-Delta Delta C) method. *Methods* 25, 402–408. doi: 10.1006/meth.2001.1262
- Mair, W. J., Deng, W., Mullins, J. G. L., West, S., Wang, P., Besharat, N., et al. (2016). demethylase inhibitor fungicide resistance in *Pyrenophora teres* f. sp. *teres* associated with target site modification and inducible overexpression of *Cyp51*. *Front. Microbiol.* 7:1279. doi: 10.3389/fmicb.2016.01279
- Malandrakis, A. A., Markoglou, A. N., Konstantinou, S., Doukas, E. G., Kalampokis, J. F., and Karaoglanidis, G. S. (2013). Molecular characterization, fitness and mycotoxin production of benzimidazole-resistant isolates of *Penicillium expansum*. *Int. J. Food Microbiol.* 162, 237–244. doi: 10.1016/j.ijfoodmicro.2013.01.014
- Mellado, E., Garcia-Effron, G., Alcazar-Fuoli, L., Melchers, W., Verweij, P., Cuenca-Estrella, M., et al. (2007). A new *Aspergillus fumigatus* resistance mechanism conferring in vitro cross-resistance to azole antifungals involves a combination of CYP51A alterations. *Antimicrob. Agents Chemother.* 51, 1897–1904. doi: 10.1128/AAC.01092-06
- Morales, H., Marín, S., Rovira, A., Ramos, A. J., and Sanchis, V. (2007). Patulin accumulation in apples by *Penicillium expansum* during postharvest stages. *Acc. Appl. Microbiol.* 44, 30–35. doi: 10.1111/j.1472-765X.2006.02035.x
- Munkvold, G. P., and O'Mara, J. K. (2002). Laboratory and growth chamber evaluation of fungicidal seed treatments for maize seedling blight caused by *Fusarium* species. *Plant Dis.* 86, 143–150. doi: 10.1094/PDIS.2002.86.2.143
- Nakaune, R., Adachi, K., Nawata, O., Tomiyama, M., Akutsu, K., and Hibi, T. (1998). A novel ATP-binding cassette transporter involved in multidrug resistance in the phytopathogenic fungus *Penicillium digitatum*. *Appl. Environ. Microbiol.* 64, 3983–3988.
- Nakaune, R., Hamamoto, H., Imada, J., Akutsu, K., and Hibi, T. (2002). A novel ABC transporter gene. *Mol. Genet. Genomics* 267, 179–185. doi: 10.1007/s00438-002-0649-6
- Omrane, S., Sghyer, H., Audéon, C., Lanen, C., Duplaix, C., Walker, A. S., et al. (2015). Fungicide efflux and the MgMFS1 transporter contribute to the multidrug resistance phenotype in *Zymoseptoria tritici* field isolates. *Environ. Microbiol.* 17, 2805–2823. doi: 10.1111/1462-2920.12781
- Pereira, D. A. S., McDonald, B. A., and Brunner, P. C. (2017). Mutations in the CYP51 gene reduce DMI sensitivity in *Parastagonospora nodorum* populations in Europe and China. *Pest Manag. Sci.* 73, 1503–1510. doi: 10.1002/ps.4486
- Reimann, S., and Deising, H. B. (2005). Inhibition of efflux transporter-mediated fungicide resistance in *Pyrenophora tritici-repentis* by a derivative of 4'-hydroxyflavone and enhancement of fungicide activity. *Appl. Environ. Microbiol.* 71, 3269–3275. doi: 10.1128/AEM.71.6.3269-3275.2005
- Rodriguez, R. J., Low, C., Bottema, C. D. K., and Parks, L. W. (1985). Multiple functions for sterols in *Saccharomyces cerevisiae*. *Biochim. Biophys. Acta* 837, 336–343. doi: 10.1016/0005-2760(85)90057-8
- Rosenberger, D., Wicklow, D., Korjagin, V., and Rondinaro, S. (1991). Pathogenicity and benzimidazole resistance in *Penicillium* species recovered from flotation tanks in apple packinghouses. *Plant Dis.* 75, 712–715. doi: 10.1094/PD-75-0712
- Sanderson, P., and Spotts, R. (1995). Postharvest decay of winter pear and apple fruit caused by species of *Penicillium*. *Phytopathology* 85, 103–110. doi: 10.1094/Phyto-85-103
- Schnabel, G., and Jones, A. L. (2001). The 14 α -Demethylase (CYP51A1) gene is overexpressed in *Venturia inaequalis* strains resistant to myclobutanil. *Phytopathology* 91, 102–110. doi: 10.1094/PHYTO.2001.91.1.102
- Sholberg, P. L., Harlton, C., Haag, P., Levesque, C. A., O'Gorman, D., and Seifert, K. (2005). Benzimidazole and diphenylamine sensitivity and identity of *Penicillium* spp. that cause postharvest blue mold of apples using beta-tubulin gene sequences. *Postharvest Biol. Technol.* 36, 41–49. doi: 10.1094/PD-89-1143
- Snelders, E., van der Lee, H. A. L., Kuijpers, J., Rijs, A. J. M. M., Varga, J., Samson, R. A., et al. (2008). Emergence of azole resistance in *Aspergillus fumigatus* and spread of a single resistance mechanism. *PLoS Med.* 5:e219. doi: 10.1371/journal.pmed.0050219
- Spotts, R., and Cervantes, L. (1993). Filtration to remove spores of *Penicillium expansum* from water in pome fruit packinghouses. *Tree Fruit Postharvest J.* 4, 16–18.
- Sun, X., Ruan, R., Lin, L., Zhu, C., Zhang, T., Wang, M., et al. (2013). Genome wide investigation into DNA elements and ABC transporters involved in imazalil resistance in *Penicillium digitatum*. *FEMS Microbiol. Lett.* 348, 11–18. doi: 10.1111/1574-6968.12235
- Sun, X., Wang, J., Feng, D., Ma, Z., and Li, H. (2011). *PdCYP51B*, a new putative sterol 14 α -demethylase gene of *Penicillium digitatum* involved in resistance to imazalil and other fungicides inhibiting ergosterol synthesis. *Appl. Microbiol. Biotechnol.* 91:1107. doi: 10.1007/s00253-011-3355-7
- Van Den Brink, H. J. M., Van Nistelrooy, H. J. G. M., De Waard, M. A., Van Den Honde, C. A. M. J. J., and Van Gorcom, R. F. M. (1996). Increased resistance to 14 α -demethylase inhibitors (DMIs) in *Aspergillus niger* by coexpression of the *Penicillium italicum* eburicol 14 α -demethylase (*cyp51*) and the *A. niger* cytochrome P450 reductase (*cprA*) genes. *J. Biotechnol.* 49, 13–18. doi: 10.1016/0168-1656(96)01403-4
- van Nestelrooy, J. G. M., van den Brink, J. M., van Kan, J. A. L., van Gorcom, R. F. M., and de Waard, M. A. (1996). Isolation and molecular characterization of the gene encoding eburicol 14 α -demethylase (*CYP51*) from *Penicillium italicum*. *Mol. Gen. Genet.* 250, 725–733.
- Van Tuyl, J. M. (1977). Genetics of fungal resistance to systemic fungicides. *Mededelingen Landbouwhogeschool Wageningen* 77, 1–136.
- Villani, S. M., Biggs, A. R., Cooley, D. R., Raes, J. J., and Cox, K. D. (2015). Prevalence of myclobutanil resistance and difenoconazole insensitivity in populations of *Venturia inaequalis*. *Plant Dis.* 99, 1526–1536. doi: 10.1094/PDIS-01-15-0002-RE
- Wang, F., Lin, Y., Yin, W.-X., Peng, Y.-L., Schnabel, G., Huang, J.-B., et al. (2015). The Y137H mutation of VvCYP51 gene confers the reduced sensitivity to tebuconazole in *Villosiclava virens*. *Sci. Rep.* 5:17575. doi: 10.1038/srep17575
- Wang, M., Chen, C., Zhu, C., Sun, X., Ruan, R., and Li, H. (2014). Os2 MAP kinase-mediated osmotic stress tolerance in *Penicillium digitatum* is associated with its positive regulation on glycerol synthesis and negative regulation on ergosterol synthesis. *Microbiol. Res.* 169, 511–521. doi: 10.1016/j.micres.2013.12.004
- Wu, Z., Wang, S., Yuan, Y., Zhang, T., Liu, J., and Liu, D. (2016). A novel major facilitator superfamily transporter in *Penicillium digitatum* (PdMFS2) is required for prochloraz resistance, conidiation and full virulence. *Biotechnol. Lett.* 38, 1349–1357. doi: 10.1007/s10529-016-2113-4
- Wyand, R. A., and Brown, J. K. M. (2005). Sequence variation in the CYP51 gene of *Blumeria graminis* associated with resistance to sterol demethylase inhibiting fungicides. *Fungal Genet. Biol.* 42, 726–735. doi: 10.1016/j.fgb.2005.04.007
- Yan, H. J., Gaskins, V. L., Vico, I., Luo, Y. G., and Jurick, W. M. (2014). First report of *Penicillium expansum* isolates resistant to pyrimethanil

- from stored apple fruit in Pennsylvania. *Plant Dis.* 98, 1004–1004. doi: 10.1094/PDIS-12-13-1214-PDN
- Yin, Y. N., and Xiao, C. L. (2013). Molecular characterization and a multiplex allele-specific PCR method for detection of thiabendazole resistance in *Penicillium expansum* from apple. *Eur. J. Plant Pathol.* 136, 703–713. doi: 10.1007/s10658-013-0199-2
- Zhang, C., Diao, Y., Wang, W., Hao, J., Imran, M., Duan, H. X., et al. (2017). Assessing the risk for resistance and elucidating the genetics of *Colletotrichum truncatum* that is only sensitive to some DMI fungicides. *Front. Microbiol.* 8:1779. doi: 10.3389/fmicb.2017.01779

Conflict of Interest Statement: The authors declare that the research was conducted in the absence of any commercial or financial relationships that could be construed as a potential conflict of interest.

Copyright © 2018 Ali and Amiri. This is an open-access article distributed under the terms of the Creative Commons Attribution License (CC BY). The use, distribution or reproduction in other forums is permitted, provided the original author(s) and the copyright owner(s) are credited and that the original publication in this journal is cited, in accordance with accepted academic practice. No use, distribution or reproduction is permitted which does not comply with these terms.



Assessment of Detoxification Efficacy of Irradiation on Zearalenone Mycotoxin in Various Fruit Juices by Response Surface Methodology and Elucidation of Its *in-vitro* Toxicity

Naveen Kumar Kalagatur^{1*}, Jalarama Reddy Kamasani² and Venkataramana Mudili^{1*}

¹ Toxicology and Immunology Division, DRDO-BU-Centre for Life Sciences, Bharathiar University, Coimbatore, India, ² Freeze Drying and Processing Technology Division, Defence Food Research Laboratory, Mysore, India

OPEN ACCESS

Edited by:

Boqiang Li,
Institute of Botany (CAS), China

Reviewed by:

Carlos Augusto Fernandes Oliveira,
University of São Paulo, Brazil
Yueju Zhao,
Institute of Food Science and
Technology (CAAS), China

*Correspondence:

Naveen Kumar Kalagatur
knaveenkumar.kalagatur@yahoo.co.in
Venkataramana Mudili
ramana.micro@gmail.com

Specialty section:

This article was submitted to
Food Microbiology,
a section of the journal
Frontiers in Microbiology

Received: 12 June 2018

Accepted: 15 November 2018

Published: 30 November 2018

Citation:

Kalagatur NK, Kamasani JR and
Mudili V (2018) Assessment of
Detoxification Efficacy of Irradiation on
Zearalenone Mycotoxin in Various
Fruit Juices by Response Surface
Methodology and Elucidation of Its
in-vitro Toxicity.
Front. Microbiol. 9:2937.
doi: 10.3389/fmicb.2018.02937

Fruits are vital portion of healthy diet owed to rich source of vitamins, minerals, and dietary fibers, which are highly favorable in keeping individual fit. Unfortunately, these days, one-third of fruits were infested with fungi and their toxic metabolites called mycotoxins, which is most annoying and pose significant health risk. Therefore, there is a need to suggest appropriate mitigation strategies to overcome the mycotoxins contamination in fruits. In the present study, detoxification efficiency of irradiation on zearalenone (ZEA) mycotoxin was investigated in distilled water and fruit juices (orange, pineapple, and tomato) applying statistical program response surface methodology (RSM). The independent factors were distinct doses of irradiation and ZEA, and response factor was a percentage of ZEA reduction in content. A central composite design (CCD) consists of 13 experiments were planned applying software program Design expert with distinct doses of irradiation (up to 10 kGy) and ZEA (1–5 µg). The results revealed that independent factors had a positive significant effect on the response factor. The analysis of variance (ANOVA) was followed to fit a proper statistical model and suggested that quadratic model was appropriate. The optimized model concluded that doses of irradiation and ZEA were the determinant factors for detoxification of ZEA in fruit juices. Further, toxicological safety of irradiation mediated detoxified ZEA was assessed in the cell line model by determining the cell viability (MTT and live/dead cell assays), intracellular reactive oxygen species (ROS), mitochondrial membrane potential (MMP), nuclear damage, and caspase-3 activity. The higher level of live cells and MMP, lower extent of intracellular ROS molecules and caspase-3, and intact nuclear material were noticed in cells treated with irradiation mediated detoxified ZEA related to non-detoxified ZEA. The results confirmed that toxicity of ZEA was decreased with irradiation treatment and detoxification of ZEA by irradiation is safe. The study concluded that irradiation could be a potential post-harvest food processing technique for detoxification of ZEA mycotoxin in fruit juices. However, irradiation of fruit juices with high dose of 10 kGy has minimally altered the quality of fruit juices.

Keywords: mycotoxins, zearalenone, detoxification, irradiation, response surface methodology, toxicological assessment

INTRODUCTION

Fungi plays a substantial role in spoilage of agricultural commodities and produces a variety of toxic secondary metabolites called mycotoxins that are harmful to humans and farm animals (Andersen and Thrane, 2006; Van Egmond et al., 2007; Mudili et al., 2014; Venkataramana et al., 2014; Muthulakshmi et al., 2018). The fungal infestations primarily commence at pre-harvesting and post-harvesting times owed to inappropriate agronomic practices (Neme and Mohammed, 2017). The Food and Agricultural Organization (FAO) have estimated that almost one-fourth of agricultural commodities are contaminated with fungi and mycotoxins worldwide (Bryla et al., 2016). The fungi predominantly infest cereals, and its by-products (Aldred et al., 2004; Mudili et al., 2014). However, over last few decades, researchers have ascertained that fruits were as well substantially contaminated with fungi and mycotoxins and pose health at risk (Barkai-Golan and Paster, 2011; Juan et al., 2017; Škrbić et al., 2017; Zheng et al., 2017; De Berardis et al., 2018; Sandoval-Contreras et al., 2018). Mycotoxins can persevere in fruits even once the fungi have been eradicated and could diffuse into healthy portion of fruits (Taniwaki et al., 1992; Restani, 2008).

The chief mycotoxigenic fungi that infest fruits are *Aspergillus*, *Alternaria*, and *Penicillium* and mycotoxins produced by them are aflatoxins, ochratoxins, patulin, and alternaria (Barkai-Golan and Paster, 2011). Though, some surveys were published that *Fusarium* spp. and its mycotoxins, explicitly zearalenone (ZEA) mycotoxin is occasionally accountable for contamination of fruits (Zinedine et al., 2007). Foremost, Chakrabarti and Ghosal (1986) have reported the contamination of *F. verticillioides* and ZEA in banana fruit at pre-harvesting and post-harvesting sessions and found that contamination of ZEA was quite high (0.8–1 mg/g of fruit). Following, Blumenthal-Yonassi et al. (1988) have assessed the ZEA production by *Fusarium equiseti* strains in fruits and noticed 0.05, 3.5, 0.2, and 0.05 mg/40 g in tomato, avocado, melon, and banana, respectively. Further, Bilgrami et al. (1990) have isolated *Fusarium* species from cereals, fruits, and vegetables, and noticed that 6.8% of *Fusarium* isolates were capable to produce ZEA in the moist-rice medium under laboratory conditions. In another study, Jime and Mateo (1997) have isolated a range of *Fusarium* species, including *Fusarium graminearum* and *F. equiseti* from banana fruits and unveiled its competence to produce ZEA under laboratory conditions. The *F. graminearum* and *F. equiseti* have produced 520 and 488 µg/g, and 45 and 40 µg/g of ZEA in corn and rice cultures, respectively (Jime and Mateo, 1997). Similarly, Sharma et al. (1998) have isolated the toxigenic *F. verticillioides* from stored fruit *Buchanania lanzan* Spreng. (Chironji) of family Anacardiaceae native to India and observed 1–2 µg of ZEA production in broth culture. Recently, Alghuthaymi and Bahkali (2015) have assessed the toxigenic profiles of *Fusarium* species isolated from banana fruits and noticed potent producers of ZEA mycotoxin, including *F. chlamydosporum*, *F. circinatum*, *F. semitectum*, *F. solani*, *F. thapsinum*, and *F. proliferatum* and detected a maximum production of 0.912 µg/mL of ZEA in the

rice culture medium under laboratory conditions. Likewise, *F. oxysporum* is one of the typical fungal contaminants of orange, pineapple, and tomato juices and could produce ZEA (Milano and López, 1991; Corbo et al., 2010; Bevilacqua et al., 2012, 2013). These scenarios have confirmed that ZEA is one of the noticeable contaminants of fruits and poses a serious threat to humans.

The ZEA is heat resilient, color, and odorless, and only know potent estrogenic mycotoxin. Many researchers have well-established the toxic effects of ZEA in cell line models and reported the involvement of caspase-3 and caspase-9-dependent mitochondrial signaling pathways in inducing the apoptotic and necrotic death of cells (Zhu et al., 2012; Venkataramana et al., 2014; Kalagatur et al., 2017). The ZEA primarily elevates the intracellular ROS and lipid peroxidation, and incites phosphorylation of histone H3, aberrations of chromosome and exchange of sister chromatid and instabilities in the mitotic index, DNA fragments and adduct formation, micronuclei development, inhibits DNA and RNA syntheses, and finally affects the cell viability (Kouadio et al., 2005; Gao et al., 2013). The International Agency for Research on Cancer (IARC) has evaluated the genotoxic and carcinogenic effects of ZEA under *in-vitro* conditions and recommended under Group 3 carcinogens (IARC, 1993). In view of the taxological effects, many nations and regulatory bodies, i.e., European Union (EU), World Health Organization (WHO), and Food and Agriculture Organization (FAO) have recommended stringent regulations and management practices to lower ZEA levels in food and feed matrices (European Commission, 2006; JECFA, 2011; Kalagatur et al., 2015).

In the contemporary concern, physical process, especially γ -radiation has attained great demand due to its prompt and robust action (Karlovsky et al., 2016; Kalagatur et al., 2018b,c). The γ -radiation is the shorter wavelength of electromagnetic radiation and offers high penetrating power of above 100 keV. The irradiation processing improves the microbiological safety and prolongs the shelf life of food without much substantially change in physical, chemical, and nutritional properties (Calado et al., 2014; Kalawate and Mehetre, 2015; Choi and Lim, 2016). Furthermore, WHO and FAO of the United Nations have specified that irradiation of some niche products and markets up to dosage rate of 25 kGy is safe and endorsed as appropriate decontamination technique in agriculture and food industry (FAO/IAEA/WHO, 1999).

Best of our knowledge, detoxification efficacy of irradiation on ZEA in fruit juices has not been reported, and this is the first attempt. In the present study, detoxification efficiency of irradiation on ZEA was established in distilled water, and fruit juice of orange, pineapple, and tomato by response surface methodology (RSM). Furthermore, toxicological safety of irradiation mediated detoxified ZEA was assessed in the cell line model by determining cell viability (MTT and live/dead cell assays), intracellular ROS, MMP, nuclear damage, and caspase-3 activity.

MATERIALS AND METHODS

Chemicals and Reagents

Standard ZEA (HPLC grade, 99% pure), caspase-3 assay kit, rhodamine 123, 4',6-diamidino-2-phenylindole (DAPI), dichloro-dihydro-fluorescein diacetate (DCFH-DA), and [3-(4,5-dimethylthiazol-2-yl)-2,5-diphenyltetrazolium bromide] (MTT) were received from Sigma-Aldrich (Bengaluru, India). The live/dead cell assay kit was from Invitrogen Molecular Probes (Bengaluru, India). The Dulbecco's phosphate-buffered saline pH 7.4 (DPBS), antibiotic solution (streptomycin and penicillin), fetal bovine serum (FBS), Dulbecco's modified Eagle's medium (DMEM), and plasticware were obtained from HiMedia (Mumbai, India). Acetonitrile, methanol, dimethyl sulfoxide (DMSO), distilled water, and other chemicals of superior grade were bought from Merck Millipore Corporation (Bengaluru, India).

Preparation of Fruit Juices

A fresh orange, pineapple, and tomato were obtained from the regional agricultural market of Mysuru, Karnataka state, India, and washed rigorously with distilled water. The endocarp of orange, fine pieces of pineapple and tomato were squeezed and attained the juice. Further, debris was separated from juice by filtering through 0.45 μm syringe filter and clear juice were used in detoxification studies.

Detoxification of ZEA by Irradiation

Design of Experiment

The detoxification efficiency of irradiation on ZEA was assessed in distilled water and clear fruit juice of orange, pineapple, and tomato accomplishing the statistical program RSM. A central composite design (CCD) consists of 13 experiments were planned with distinctive doses of irradiation (up to 10 kGy) and ZEA (1 to 5 μg) applying software program Design-Expert trial version 10 (State-Ease, Minnesota, USA) (Atkinson and Donev, 1992; Whitcomb and Anderson, 2004; Anderson and Whitcomb, 2016; Kalagatur et al., 2018a). The type, unit, range, coded levels, mean, and standard deviation of independent variables are shown in **Supplementary Table 1**. The response factor was a percentage of ZEA reduction in distilled water and fruit juices after exposing to irradiation. The optimized design intended for the study was generated by polynomial regression analysis.

Irradiation Process

The stock solution of ZEA (1 mg/mL) was prepared in acetonitrile and further different test concentrations of ZEA was made in 1 mL of distilled water and clear fruit juice of orange, pineapple, and tomato (1–5 $\mu\text{g/mL}$) following CCD as shown in **Table 1** and subjected to irradiation. Cobalt 60 was a source of γ -rays and irradiation was carried out at 35°C with a dosage rate of 5.57 kGy per hour under Gamma irradiation chamber-5000. The Ceric-cerous standard dosimeter that fixed on top and surface bottom of the sample was used to measure the absorbed dose of γ -radiation. The uniformity of irradiation dose ($D_{\text{max}}/D_{\text{min}}$) was maintained at 1.01 (Reddy et al., 2015).

Quantification of ZEA by HPLC

Following irradiation treatments, quantification of ZEA was carried out using HPLC system (Shimadzu, Kyoto, Japan) as per methodology of Kumar et al. (2016) and HPLC conditions are provided in **Supplementary Table 2**. The quantification of ZEA was deducted from the calibrated curve of standard ZEA. For constructing calibration curve, different dilutions of ZEA were made in water (100 ng–1 $\mu\text{g/mL}$) from stock solution of ZEA (1 mg/mL in acetonitrile) and 25 μL was injection into HPLC. The calibration curve was constructed with area of peak vs concentration of ZEA. The precise of the calibration curve was judged by linear regression analysis. The attained regression curve has shown decent linearity with a coefficient of determination (R^2) of 0.9932. The limit of detection (LOD) was the signal-noise ratio of 3 and limit of quantification (LOQ) was the signal-noise ratio of 10. The LOD and LOQ were noticed as 22 and 86 ng/mL, respectively. The percentage of recovery of technique was 96.58 for 1 $\mu\text{g/mL}$ of ZEA. The accuracy of the technique for inter-day was expressed by Relative Standard Deviation (RSD%) and it was 7.31%.

The percentage of ZEA reduction (response factor) in irradiated test samples was deducted from the formula,

$$\text{ZEA reduction (\%)} = \frac{Z_{\text{PI}} - Z_{\text{AI}}}{Z_{\text{PI}}} \times 100$$

Where, Z_{PI} was a concentration of ZEA prior irradiation and Z_{AI} was a concentration of ZEA after irradiation.

Optimization of Design

The regression analysis of the response factor (percentage of ZEA reduction) was assessed by the second-order polynomial equation. The design was optimized by considering variables of polynomial regression at $p < 0.05$. Furthermore, precision of the optimized model was approved by asserting the coefficient of determination (R^2). In conclusion, accuracy of the optimized design was assessed by normal plot residuals, Box-Cox, actual vs. predicted, and 3-D response plots (Anderson and Whitcomb, 2016). The second-order polynomial equation applied for the analysis of variables as follows,

$$Y = \beta_0 + \sum_{i=1}^n \beta_i x_i + \sum_{i=1}^n \beta_{ii} x_i^2 + \sum_{i \neq j=1}^n \beta_{ij} x_i x_j$$

Where, “0” represents suitable response value at center point of the model. The linear, quadratic, cross-product terms of the model were symbolized by i , ii , and ij , respectively. The total number of independent variables in the model were symbolized by alphabetical letter “n.”

In-vitro Toxicological Examination of Detoxified ZEA

The conclusive aim for the study was to assess the toxicological safety of irradiation mediated detoxified ZEA. The toxic effects of irradiation mediated detoxified ZEA was appraised by comparing with non-detoxified ZEA in *in-vitro* cell line model by determination of cell viability (MTT and live/dead cell), intracellular ROS, MMP, nuclear damage, and caspase-3 activity.

TABLE 1 | Central composite design (CCD) for evaluation of detoxification efficiency of irradiation on zearalenone (ZEA) in distilled water and fruit juice of orange, pineapple, and tomato.

Run order	Independent factors		Response factor (percentage of ZEA reduction)			
	A: Conc. of ZEA (μg)	B: Dose of irradiation (kGy)	Distilled water	Orange juice	Pineapple juice	Tomato juice
1	4.41 (+1)	1.46 (−1)	11.73 \pm 0.22 ^a	10.99 \pm 0.40 ^a	10.05 \pm 0.32 ^a	11.46 \pm 0.26 ^a
2	1.58 (−1)	8.53 (+1)	83.71 \pm 2.09 ^b	82.63 \pm 1.17 ^b	81.97 \pm 1.89 ^b	81.59 \pm 1.93 ^b
3	4.41 (1)	8.53 (+1)	52.09 \pm 1.36 ^c	50.42 \pm 0.91 ^c	51.71 \pm 0.94 ^c	52.81 \pm 0.80 ^c
4	3.00 (0)	5.00 (0)	46.92 \pm 0.85 ^d	44.35 \pm 0.97 ^d	43.60 \pm 0.66 ^d	45.08 \pm 0.88 ^d
5	1.58 (−1)	1.46 (−1)	27.46 \pm 0.71 ^e	26.88 \pm 0.39 ^e	25.92 \pm 0.41 ^e	26.37 \pm 0.56 ^e
6	5.00 (+ α)	5.00 (0)	34.07 \pm 0.78 ^f	33.29 \pm 0.64 ^f	32.16 \pm 0.83 ^f	33.64 \pm 0.80 ^f
7	3.00 (0)	5.00 (0)	47.02 \pm 0.92 ^{dg}	46.09 \pm 0.70 ^{dg}	45.39 \pm 0.82 ^{dg}	45.11 \pm 0.67 ^{dg}
8	3.00 (0)	10.00 (+ α)	71.05 \pm 0.81 ^h	69.47 \pm 1.14 ^h	70.54 \pm 0.89 ^h	70.53 \pm 1.45 ^h
9	3.00 (0)	5.00 (0)	41.89 \pm 0.69 ^{dgi}	41.70 \pm 0.47 ^{dgi}	40.83 \pm 0.63 ^{dgi}	40.12 \pm 0.81 ^{dgi}
10	3.00 (0)	5.00 (0)	43.55 \pm 0.77 ^{dgij}	43.38 \pm 0.41 ^{dgij}	42.62 \pm 0.65 ^{dgij}	42.07 \pm 0.82 ^{dgij}
11	1.00 (− α)	5.00 (0)	72.51 \pm 0.84 ^k	70.02 \pm 1.01 ^k	68.37 \pm 1.77 ^k	69.19 \pm 0.94 ^k
12	3.00 (0)	5.00 (0)	43.11 \pm 0.29 ^{dgjil}	41.20 \pm 0.50 ^{dgjil}	40.59 \pm 0.43 ^{dgjil}	42.30 \pm 0.61 ^{dgjil}
13	3.00 (0)	0.00 (− α)	0.00 ^m	0.00 ^m	0.00 ^m	0.00 ^m

The statistical analysis was executed by Tukey's multiple comparison test and the columns with different alphabetic letters were statistically significant ($p < 0.05$) in respective study.

Cell Culture and Maintenance

The macrophage cell line (RAW 264.7) of *Mus musculus* was obtained from the National Center for Cell Science, India (NCCS). The cells were maintained in moisturized incubator at 5% CO₂ and 37°C. The growth media for cell line was DMEM completed with 10% FBS, 50 mU/mL of penicillin, and 50 $\mu\text{g}/\text{mL}$ of streptomycin. The cells were grown-up in 75 cm² flasks and confluent cells have employed in the further experiments.

Experimental Design

In the present study, test samples of ZEA (3 $\mu\text{g}/\text{mL}$ prepared in distilled water) were distinctly subjected to detoxification with 5 and 10 kGy of irradiation. The test sample not treated with irradiation was considered as non-detoxified ZEA. Following, test samples were dried out by lyophilization and suspended in 100 μL of DMEM devoid of FBS and used for *in-vitro* toxicological analysis. The exposure of test samples to cells was categorized into following groups. Group A: Cells were treated alone with 100 μL of DMEM devoid of FBS (control). Group B: Cells were treated with non-detoxified ZEA (3 μg) in 100 μL of DMEM devoid of FBS. Group C: Cells were treated with detoxified ZEA (3 μg) of 5 kGy irradiated in 100 μL of DMEM devoid of FBS. Group D: Cells were treated with detoxified ZEA (3 μg) of 10 kGy irradiated in 100 μL of DMEM devoid of FBS.

Cell Culture Treatment

Approximately, 5×10^3 cells were seeded in 96-well cell culture plates and allowed to adhere for 12 h. The cells were treated with different experimental groups as aforementioned in “experimental design” and incubated for 12 h. The volume of the media in all experimental groups was maintained as 100 $\mu\text{L}/\text{well}$. Following, plates were separately employed for various toxicological assessments, i.e., cell viability (MTT and live/dead cell), intracellular ROS, MMP, nuclear staining, and caspase-3 assays.

MTT assay

Following, treatments and incubation as detailed in section “Cell culture treatment.” The cells were washed for twice with DPBS and treated with 100 μL of MTT reagent (5 mg/mL in DPBS) for 4 h (Venkataramana et al., 2014). Following, MTT solution was replaced with 100 μL of DMSO to liquefy the formazan crystals for 30 min and optical density was measured at 570 nm using a multiplate reader (Synergy H1, BioTek, USA). The cell viability was determined in percentage with respect to control sample (100%).

Live/dead cell assay

Following, treatments and incubation as detailed in section “Cell culture treatment.” The cells were washed with DPBS for two times and stained with dyes (2 μM of calcein AM and 4 μM of ethidium homodimer-1) of live/dead cell assay kit as per directions from the manufacturer (Haugland et al., 1994). Subsequently, cells were washed with DPBS and fluorescence images were captured under green fluorescent protein (GFP) and red fluorescent protein (RFP) filters using an inverted fluorescence microscope (EVOS, Life Technologies, USA). The optical density was measured at excitation and emission of 485 and 530 nm for calcein AM, and 530 nm and 645 nm for ethidium homodimer-1, respectively using a multimode plate reader (Synergy H1, BioTek, USA) and the percentage of live and dead cells were calculated as per methodology of Garcia-Recio et al. (2015). The results were expressed with respect to control sample (100%).

Analysis of intracellular ROS molecules

Following, treatments and incubation as detailed in section “Cell culture treatment.” The cells were washed with DPBS for twice and stained with 5 μM of DCFH-DA for 5 min. Subsequently, cells were subjected to DPBS wash and optical density was measured at excitation of 495 nm and emission of

550 nm using a multiplate reader (Synergy H1, BioTek, USA). The fluorescent images were captured under GFP filter using an inverted fluorescence microscope (EVOS, Life Technologies, USA). The results were expressed as a percentage of intracellular ROS release with respect to the control (Venkataramana et al., 2014).

Analysis of mitochondrial membrane potential (MMP)

Following, treatments and incubation as detailed in section “Cell culture treatment.” The cells were washed with DPBS for twice and stained with rhodamine 123 (5 μ M) in DPBS for 15 min and again washed with DPBS. The fluorescent images were captured under GFP filter using an inverted fluorescence microscope (EVOS, Life Technologies, USA). Also, optical density was measured at excitation and emission of 511 and 534 nm, respectively using a multiplate reader (Synergy H1, BioTek, USA) and results of test samples were expressed with respect to the control (Venkataramana et al., 2014).

Analysis of nuclear damage

Following, treatments and incubation as detailed in section “Cell culture treatment.” The cells were subjected to wash for twice with DPBS and stained with 5 μ M of DAPI for 15 min. Next, cells were again washed with DPBS and fluorescent images were captured under DAPI filter using an inverted fluorescence microscope (EVOS, Life Technologies, USA).

Analysis of caspase-3 activity

Following, treatments and incubation as detailed in section “Cell culture treatment.” The cells were washed with DPBS for twice and exposed to reagents of caspase-3 kit and optical density was recorded at an excitation of 360 nm and emission of 460 nm using a multiplate reader (Synergy H1, BioTek, USA) following the directions from the manufacturer (Riss et al., 2016). The quantification of caspase-3 activity was determined from a standard of the fluorescent molecule 7-amino-4-methyl coumarin (AMC) release as per instructions of kit. The results were expressed in percentage of caspase-3 release with respect to the control (Lozano et al., 2009).

Quality Assessment of Fruit Juices Treated With Irradiation

A quantity of 10 mL fresh juice of orange, pineapple, and tomato were treated with different doses of irradiation, i.e., 2.5, 5, 7.5, and 10 kGy. The juice sample not treated with irradiation was referred as control. Following, quality of fruit juices of control and test samples were evaluated by sensory (appearance, aroma, consistency, and taste), pH, acidity, total soluble solids, total phenolic and flavonoid content, and total antioxidant activity.

Sensory Evaluation

The sensory evaluation was carried out by 13 semi-trained panelists on the 9-point hedonic scale (1: Extremely poor. 2: Very poor. 3: Poor. 4: Fair above poor. 5: Fair. 6: Good above fair. 7: Good. 8: Very good. 9: Excellent) as per Murray et al. (2001). Further, over-all acceptability of fruit juices was also carried out by 13 semi-trained panelists on 9-point hedonic scale (1:

Dislike extremely. 2: Dislike very much. 3: Dislike moderately. 4: Dislike slightly. 5: Neither like nor dislike. 6: Like slightly. 7: Like moderately. 8: Like very much. 9: Like extremely) as per Murray et al. (2001).

Determination of Acidity and pH

The pH of the samples was determined using an Orion Expandable Ion Analyzer EA 940 pH meter (Expotech, USA). The total titratable acidity of the samples was measured following official methods of analysis of AOAC International 1996 and expressed as % citric acid. The total soluble solids in terms of °Brix was determined using a Carl Zeiss 844976 Jena refractometer as per official methods of analysis of AOAC International 1996.

Estimation of Total Phenolic Content

The total phenolic content of fruit juice was estimated by Folin-Ciocalteu assay. Briefly, 0.5 mL of fruit juice was diluted with distilled water by three times and blended with 0.5 mL of 7.5% sodium carbonate solution and 0.25 mL of Folin-Ciocalteu reagent. The obtained mixture was incubated at $27 \pm 2^\circ\text{C}$ for 30 min in the dark and absorbance was recorded at 765 nm using multimode plate reader (Synergy H1, BioTek, USA). Gallic acid was used as the reference and obtained results was stated as mg of gallic acid equivalents per mL (mg GAE/mL).

Estimation of Total Flavonoid Content

The total flavonoid content in fruit juice was determined by aluminum chloride colorimetric method. Briefly, 0.5 mL of juice was added to 70 μ L of sodium nitrite solution (5%) and incubated for 5 min at $27 \pm 2^\circ\text{C}$. Subsequently, mixture was blended with 0.5 mL of sodium hydroxide (1 M), 0.15 mL of aluminum chloride (10%), and 1.3 mL of deionized water and incubated for 5 min at $27 \pm 2^\circ\text{C}$. Following, absorbance was measured at 415 nm using a multimode plate reader (Synergy H1, BioTek, USA). Catechin was used as reference and results were expressed as mg of catechin equivalents per mL (mg CE/mL).

Determination of Total Antioxidant Activity

The total antioxidant activity of fruit juice was determined by DPPH radical scavenging assay. Briefly, 100 μ L of fruit juice was blended with 3 mL of 4% DPPH methanolic solution. The mixture was incubated at $27 \pm 2^\circ\text{C}$ for 20 min in the dark and absorbance was measured at 517 nm using multimode plate reader (Synergy H1, BioTek, USA). The DPPH methanolic solution not blended with fruit juice was conceded as blank. The total antioxidant activity of the test sample was calculated using following formula,

$$\text{DPPH (\% inhibition)} = \frac{(Ab_b - Ab_t)}{Ab_b} \times 100$$

Where, Ab_b and Ab_t were absorbance of blank and test samples, respectively.

Statistical Analysis

The experiments were set up independently for six times, and results were expressed as mean \pm standard deviation. The

CCD and actual and predicted analysis of RSM, and *in-vitro* toxicological data were analyzed by one-way ANOVA following the Tukey's multiple comparison test using GraphPad Prism trial version 7 software application and value of $p < 0.05$ was considered statistically significant. Though, quality assessment of irradiated fruit juices was compared with control by Dunnett's test using GraphPad Prism trial version 7 software application and $p < 0.05$ was considered as statistically significant.

RESULTS AND DISCUSSION

Detoxification of ZEA by Irradiation

Knowledge on the detoxification efficiency of irradiation for mycotoxins is insufficient, and most of the studies in the literature were addressed on aflatoxins (Calado et al., 2014). Till a date, no study was focused upon the application of irradiation for detoxification of standard ZEA (HPLC grade, 99% pure) in liquid food matrices, and this is the first report. Though, (Hooshmand and Klopfenstein, 1995) and (Aziz et al., 1997) have reported the detoxification action of irradiation on ZEA in solid food matrices (maize, wheat, and soybean). In these studies, detoxification competence of irradiation on ZEA was unclear and toxic effects of detoxified ZEA was not assessed. Henceforth, present study was focused on to establish detoxification efficiency of irradiation on standard ZEA in distilled water and fruit juice of orange, pineapple, and tomato by RSM statistical program. Also, toxic effects of detoxified ZEA was assessed under *in-vitro* studies by comparing with non-detoxified ZEA.

In the present study, RSM method was applied to assess the interface among the two independent variables (ZEA and γ -radiation) on the percentage of ZEA reduction (response factor) in distilled water and fruit juices. The design with variables (different dosage of ZEA and γ -radiation) and actual responses (% of ZEA reduction) is shown in **Table 1**. The attained CCD results were analyzed by second order polynomial equation to fit appropriate response surface design.

The analysis of variance (ANOVA) was designated to fit suitable statistical model between independent variables and response factor, and to assess the model statistics for the optimization process. A quadratic model was highly applicable for all the responses and ANOVA results are presented in **Supplementary Tables 3–6**. All attained models were presented larger F -value and smaller p -value. On the other hand, lack of fit of attained designs was not significant. The goodness of the designs was estimated from the coefficient of determination (R^2). The obtained R^2 -value of 0.9953 (distilled water), 0.9969 (orange juice), 0.9969 (pineapple juice), and 0.9960 (tomato juice) concluded that 99.53, 99.69, 99.69, and 99.60% of variations in the study possibly will be explained by design models of distilled water, orange, pineapple, and tomato fruit juices, respectively (**Supplementary Table 7**). Likewise, predictable R^2 -value was much closer to the adjusted R^2 -value in all the responses, and attained differences were quite in agreement (**Supplementary Table 7**). Moreover, adequate precision was higher than 4.0 in all responses and which concluded that attained design has an adequate signal and comfortable to navigate in the design space. The coefficient of independent

variables in terms of coded factors for second order regression equation for responses was obtained as,

Percentage of ZEA reduction in distilled water

$$= +44.50 - 12.71 *A + 24.64 *B - 3.97 *A *B + 4.23 *A^2 - 4.65 *B^2$$

Percentage of ZEA reduction in orange juice

$$= +43.34 - 12.51 *A + 24.18 *B - 4.08 *A *B + 4.04 *A^2 - 4.42 *B^2$$

Percentage of ZEA reduction in pineapple juice

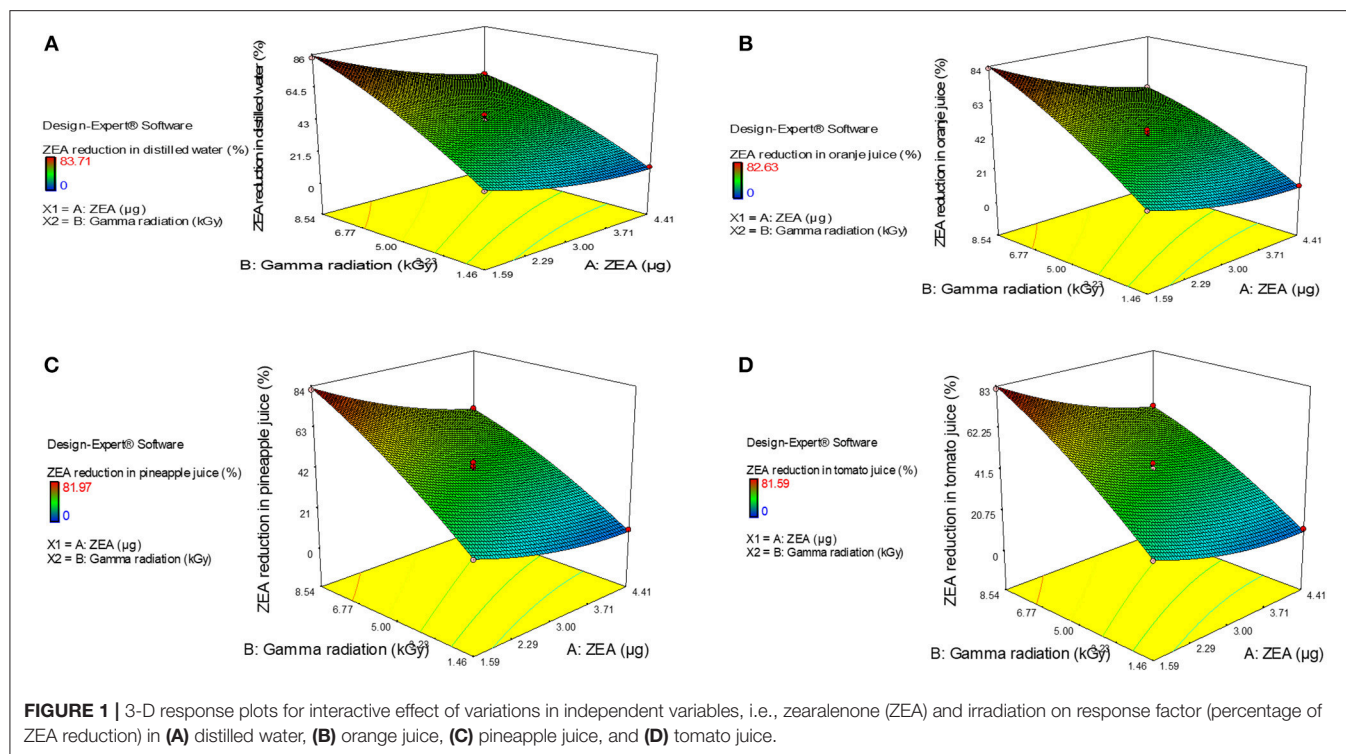
$$= +42.61 - 12.17 *A + 24.68 *B - 3.60 *A *B + 3.74 *A^2 - 3.76 *B^2$$

Percentage of ZEA reduction in tomato juice

$$= +42.94 - 11.75 *A + 24.54 *B - 3.47 *A *B + 4.17 *A^2 - 3.91 *B^2$$

Furthermore, normal plot residuals, Box-Cox, and actual vs. predicted plots were considered to evaluate the accuracy of optimized design. The external studentized residuals were closely distributed and followed the normal plot residuals (**Supplementary Figure 1**), which showed that residuals were in linear behavior and the attained design was accurate (Anderson and Whitcomb, 2016). The Box-Cox plots of responses were considered to determine the most appropriate power law transformation. In the obtained design, best recommend transform (λ) were noticed for all responses (**Supplementary Figure 2**). The obtained λ -value was close to the current value of 1 for none and, which indicated that responses were followed Box-Cox power transform and attained design was accurate. In **Supplementary Figure 3**, obtained data points of actual were close to predicted and generated decent R^2 -value for all responses. Finally, fitted second-order polynomial equation was expressed in 3D-surface plots in **Figure 1** to represent the interactive effect of variations in independent variables on responses. These figures have revealed that levels of ZEA have more impression trailed by altered doses of irradiation. Thus, diagnostic plots were concluded that optimized design well-appropriate and significant. Finally, the predicted values of the design were verified with actual values of optimized design to conclude the appropriateness of the design. The actual values of the experiment were in agreement with predicted values of the study (**Table 2**).

As we have noticed, ZEA in an aqueous solution can be effectively detoxified by irradiation and it is mostly mediated by the reactive species that are produced from radiolysis of water. The radiolysis of water by irradiation is a quick process, which takes only about 10^{-6} s and generates positive-charged water radicals (H_2O^+) and negative-charged free electrons (e^-). Furthermore, series of cross-combination and recombination reactions between H_2O^+ and e^- leads to the formation of highly reactive species, i.e., e^-_{aq} , H^\bullet , H_2 , HO^\bullet , OH^- , HO_2^\bullet , H_3O^+ , and H_2O_2 (Le Caër, 2011). These highly reactive molecules formed as a result of radiolysis of water could attack and cleave the hydrogen, methyl, and hydroxyl molecules of ZEA and thus



degrade the ZEA (Shier et al., 2001). The present study has proven the detoxification efficiency of the irradiation process on ZEA in aqueous solution of water, and fruit juice of orange, pineapple, and tomato. However, further research is needed on extraction, purification, and structural elucidation of radiolytic products of ZEA to reveal the precise process of ZEA detoxification.

In-vitro Toxicological Analysis of Detoxified ZEA

The concluding study was commenced to know the toxicological safety of irradiation mediated detoxified ZEA, and it was assessed in RAW 264.7 cells by determining the cell viability, intracellular ROS molecules, MMP, nuclear damage, and caspase-3 activity.

The cell viability was assessed by two methods, i.e., MTT and live/dead dual staining assays. MTT assay is one of the widely used cell viability techniques in *in-vitro* studies and, which assess the cell viability based on metabolic activity of NAD(P)H-dependent oxidoreductase enzymes of cell (Fotakis and Timbrell, 2006; Venkataramana et al., 2014). The other cell viability technique, live/dead cell assay is dual staining technique comprising of calcein AM and ethidium homodimer-1 dyes. The calcein AM enter through the cell membrane and gets converted into fluorescent calcein by ubiquitous intracellular esterases of live cells and emits green fluorescence in live cells at an excitation and emission of 495 and 515 nm, respectively. Whereas, ethidium homodimer-1 enters through the damaged membrane of dead cells and strongly binds to nuclear material and produces red fluorescence in dead cells at an excitation of 495 nm and emission of 635 nm. The ethidium homodimer-1 is

not a membrane permeable and excluded by membrane intact of live cells (Haugland et al., 1994; Kalagatur et al., 2017). In the present study, toxic effect of non-detoxified and irradiation mediated detoxified ZEA on cell viability was determined with respect to control. The MTT and live/dead cell assays concluded that cell viability was significantly ($p < 0.05$) decreased on treatment of non-detoxified ZEA (3 μg) related to control. While, cell viability was significantly ($p < 0.05$) high in cells treated with 5 and 10 kGy irradiation mediated detoxified ZEA (3 μg) related to non-detoxified ZEA (3 μg). In MTT assay, 14.10 ± 1.69 , 64.05 ± 4.21 , and $86.22 \pm 2.73\%$ of viable cells were observed in non-detoxified ZEA (3 μg), 5 kGy irradiation mediated detoxified ZEA (3 μg), and 10 kGy irradiation mediated detoxified ZEA (3 μg), respectively (Table 3). These results were well-supported by live/dead dual staining assay. The images of control cells, cells treated with non-detoxified ZEA (3 μg), and cells treated with 5 and 10 kGy irradiation mediated detoxified ZEA (3 μg) are shown in Supplementary Figure 4. The number of green fluorescent cells (live cells) in cells treated with non-detoxified ZEA (3 μg) was significantly less ($p < 0.05$) compared to control, and it was noticed as $11.29 \pm 1.08\%$ (Table 3). Whereas, 65.29 ± 3.37 and $89.67 \pm 3.51\%$ of live cells were observed in cells treated with irradiation mediated detoxified ZEA (3 μg) of 5 and 10 kGy, respectively (Table 3). A hundred percentage of live cells was not determined in irradiation mediated detoxified ZEA with respect to control, and this may be due to presence minute amount of non-detoxified ZEA. The percentage of ZEA reduction in 3 μg of ZEA was $41.89 \pm 0.69\%$ – $47.02 \pm 0.92\%$ and $71.05 \pm 0.81\%$ at 5 and 10 kGy of irradiation, respectively and complete reduction of ZEA was not observed (Table 1). Therefore, 100% of live cells

TABLE 2 | Assessment of proposed predicted values of design with actual values of study.

S. No	Independent factors		Responses (percentage of ZEA reduction in distilled water, and fruit juice of orange, pineapple, and tomato)							
	A: ZEA (μ g)	B: Irradiation (kGy)	Predicted				Actual			
			Distilled water	Orange juice	Pineapple juice	Tomato juice	Distilled water	Orange juice	Pineapple juice	Tomato juice
1	1.6	6.0	69.12 \pm 1.11	67.49 \pm 0.88	66.19 \pm 0.89	66.43 \pm 1.01	68.58 \pm 1.72 ^a	66.09 \pm 1.80 ^a	68.16 \pm 0.93 ^a	68.07 \pm 0.31 ^a
2	2	6.1	63.71 \pm 0.95	62.22 \pm 0.75	61.21 \pm 0.76	61.36 \pm 0.86	62.07 \pm 0.81 ^b	61.44 \pm 0.66 ^b	63.18 \pm 0.81 ^b	60.32 \pm 1.16 ^b
3	3	6.3	52.91 \pm 0.91	51.62 \pm 0.72	51.16 \pm 0.74	51.41 \pm 0.83	51.02 \pm 0.79 ^c	52.72 \pm 1.02 ^c	50.90 \pm 0.93 ^c	49.67 \pm 0.82 ^c
4	1.6	8.5	84.95 \pm 1.63	83.28 \pm 1.28	82.59 \pm 1.31	82.51 \pm 1.47	87.39 \pm 1.04 ^d	82.41 \pm 0.79 ^d	83.80 \pm 1.07 ^d	79.30 \pm 0.93 ^d
5	2	8.5	78.21 \pm 1.33	76.66 \pm 1.03	76.35 \pm 1.07	76.21 \pm 1.20	75.08 \pm 1.66 ^e	72.29 \pm 1.19 ^e	74.48 \pm 1.03 ^e	72.16 \pm 1.02 ^e
6	3	8.5	64.32 \pm 1.07	62.94 \pm 0.85	63.36 \pm 0.86	63.40 \pm 0.97	67.54 \pm 0.92 ^{af}	64.10 \pm 1.32 ^{af}	61.19 \pm 0.77 ^{bf}	60.08 \pm 1.28 ^{bf}

The statistical analysis was executed by Tukey's multiple comparison test and the columns with different alphabetic letters were statistically significant ($p < 0.05$) in respective study.

were not observed in cells treated with 5 and 10 kGy irradiation mediated detoxified ZEA. The study concluded that irradiation mediated detoxified ZEA was less toxic and safe compared to non-detoxified ZEA.

Previous reports of Venkataramana et al. (2014), Kalagatur et al. (2017), Muthulakshmi et al. (2018), and Zheng et al. (2018) have revealed that ZEA induces the cell death through oxidative stress by generation of intracellular ROS molecules. The effect non-detoxified and irradiation mediated detoxified ZEA on generation of ROS molecules was determined by DCFH-DA staining. The DCFH-DA converts to non-fluorescent molecules through a deacetylation process over action of cellular esterases. Furthermore, oxidize to fluorescent 2',7'-dichlorofluorescein molecules by intracellular ROS. The intensity of fluorescence is directly proportional to amount of ROS generated. In the present study, fluorescent images of control cells, cells treated with non-detoxified ZEA (3 μ g), and cells treated with 5 and 10 kGy irradiation mediated detoxified ZEA (3 μ g) are shown in **Supplementary Figure 5**. The fluorescence intensity and percentage of intracellular ROS molecules was high in cells treated with non-detoxified ZEA (3 μ g) compared to control and observed as $321.6 \pm 6.97\%$ ($p < 0.05$). Another hand, cells treated with detoxified ZEA (3 μ g) of 5 and 10 kGy irradiated have produced $173.9 \pm 8.43\%$ and $128.7 \pm 5.17\%$ of intracellular ROS molecules, respectively ($p < 0.05$) and the perceived fluorescence intensity was less compared to non-detoxified ZEA (3 μ g) (**Supplementary Figure 5** and **Table 3**). The small amount of intracellular ROS molecules was detected in cells treated with irradiation mediated detoxified ZEA due to presence of a smaller amount of non-detoxified ZEA. The results concluded that irradiation mediated detoxified ZEA has less capability to produce intracellular ROS molecules compared to non-detoxified ZEA and therefore, irradiation mediated detoxified ZEA was much safer compared to non-detoxified ZEA.

Also, earlier reports of Zhu et al. (2012), Venkataramana et al. (2014), and Kalagatur et al. (2017) have demonstrated that ZEA cause toxicity in cells by depletion of MMP levels. The effect of non-detoxified ZEA and irradiation mediated detoxified ZEA on MMP level was determined by rhodamine 123. The rhodamine 123 is a cell permeable dye and produce fluorescence by an appropriated act of metabolically active mitochondria at an excitation and emission of 511 and 534 nm, respectively and, which is used to consider as an indicator for MMP. The depletion in MMP could halt ATP synthesis and trigger death by an apoptosis process (Hussain et al., 2005). In the present study, MMP levels in cells were depleted on exposure of non-detoxified ZEA (3 μ g) compared to control and noticed as $22.82 \pm 2.98\%$. Remarkably, MMP levels were significantly high in cells treated with irradiation mediated detoxified ZEA compared to non-detoxified ZEA, and it was determined as $60.47 \pm 3.70\%$ and $81.90 \pm 3.31\%$ in cells treated with 5 and 10 kGy irradiation mediated detoxified ZEA (3 μ g), respectively (**Table 3**). Correspondingly, fluorescent images of MMP analysis are shown in **Supplementary Figure 6**. A low fluorescence intensity was noticed in cells treated with non-detoxified ZEA (3 μ g) due to depletion of MMP levels compared to control cells. Moreover, high intensity of fluorescence was

perceived in cells treated with 5 and 10 kGy irradiation mediated detoxified ZEA (3 μ g) related to non-detoxified ZEA (3 μ g).

Many *in-vitro* studies have demonstrated that ZEA induces the cell death through an apoptosis process by introducing nuclear damage and elevating the activity of caspase-3 (Zhu et al., 2012; Venkataramana et al., 2014; Wang et al., 2014; Tatay et al., 2016; Kalagatur et al., 2017; Zheng et al., 2018). The DAPI staining is relied upon the principle that intact DNA holds a well-organized association with protein matrix of nucleus and appears round and intact in a center of the cell. While, cells on exposure to toxic substances produce fragmented and disrupted nuclear material as a result intact DNA assembly with protein matrix at a center of cell tends to lose and could be noticed by bright fluorescent intensity and leakage of nuclear material from cell, which is a hallmark of apoptosis (Venkataramana et al., 2014). In the present study, DAPI fluorescent images of control cells, cells treated with non-detoxified ZEA (3 μ g), and cells treated with 5 and 10 kGy irradiation mediated detoxified ZEA (3 μ g) are shown in **Supplementary Figure 7**. The nuclear damage, i.e., bright fluorescent and leaky nuclei were noticed in cells treated with non-detoxified ZEA (3 μ g), and the

nuclear damage were much less perceived in cells treated with 5 and 10 kGy irradiation mediated detoxified ZEA (3 μ g). To conclude, effect of non-detoxified ZEA and irradiation mediated detoxified ZEA on apoptosis was assessed by measuring caspase-3 activity. The caspase-3 is a member of caspase family and its successive activation of caspases plays a vital role in the accomplishment of cellular apoptosis (Chen et al., 1998; Porter and Jänicke, 1999). In the present study, the caspase-3 activity was high in non-detoxified ZEA (3 μ g) compared to control (100%) and noticed as $226.4 \pm 14.17\%$ ($p < 0.05$). Whereas, cells exposed with detoxified ZEA (3 μ g) of 5 and 10 kGy irradiated have exhibited 162.1 ± 5.65 and $114.2 \pm 6.78\%$ of caspase-3 activity, respectively (**Table 3**). The study showed that caspase-3 activity was less elevated in irradiation mediated detoxified ZEA compared to non-detoxified ZEA. The slight activity of caspase-3 was determined in irradiation mediated detoxified ZEA due to the presence of smaller amounts of non-detoxified ZEA. The results were in accordance with the analysis of cell viability, intracellular ROS molecules, MMP, and nuclear damage. The outcome from the study clearly evidenced that detoxification of ZEA using irradiation produce non-toxic by-products, and this

TABLE 3 | Assessment of *in-vitro* toxicity of irradiation mediated detoxified ZEA and non-detoxified ZEA in RAW 264.7 cells for 12 h.

Group	Test sample	Cell viability (%)		ROS (%)	MMP (%)	Caspase-3 (%)
		MTT	Live/dead			
A	Control cells in 100 μ L of DMEM devoid of FBS	100 ^a	100 ^a	100 ^a	100 ^a	100 ^a
B	Cells treated with non-detoxified ZEA (3 μ g) in 100 μ L of DMEM devoid of FBS	14.10 ± 1.69^b	11.29 ± 1.08^b	321.6 ± 6.97^b	22.82 ± 2.98^b	226.4 ± 14.17^b
C	Cells treated with detoxified ZEA (3 μ g) of 5 kGy irradiated in 100 μ L of DMEM devoid of FBS	64.05 ± 4.21^c	65.29 ± 3.37^c	173.9 ± 8.43^c	60.47 ± 3.70^c	162.1 ± 5.65^c
D	Cells treated with detoxified ZEA (3 μ g) of 10 kGy irradiated in 100 μ L of DMEM devoid of FBS	86.22 ± 2.73^d	89.67 ± 3.51^d	128.7 ± 5.17^d	81.90 ± 3.31^d	114.2 ± 6.78^d

The statistical analysis was executed by Tukey's multiple comparison test and the columns with different alphabetic letters were statistically significant ($p < 0.05$) in respective study.

TABLE 4 | Quality assessment of orange fruit juice treated with different doses of irradiation.

Quality parameter	Irradiation dose				
	0 kGy (Control)	2.5 kGy	5 kGy	7.5 kGy	10 kGy
1. Sensory attributes					
A. Appearance [©]	7.75 ± 0.16	$7.65 \pm 0.32^{\#}$	$7.34 \pm 0.28^{\#}$	$6.97 \pm 0.14^{\#}$	$6.50 \pm 0.21^*$
B. Aroma [©]	8.31 ± 0.23	$8.23 \pm 0.37^{\#}$	$7.84 \pm 0.31^{\#}$	$7.15 \pm 0.12^{\#}$	$6.20 \pm 0.24^*$
C. Consistency [©]	7.59 ± 0.18	$7.55 \pm 0.15^{\#}$	$7.52 \pm 0.26^{\#}$	$7.48 \pm 0.11^{\#}$	$7.14 \pm 0.19^{\#}$
D. Taste [©]	8.18 ± 0.41	$7.84 \pm 0.24^{\#}$	$7.51 \pm 0.33^{\#}$	$6.73 \pm 0.16^{\#}$	$6.07 \pm 0.30^*$
E. Overall acceptability [§]	8.08 ± 0.27	$7.8 \pm 0.19^{\#}$	$7.51 \pm 0.22^{\#}$	$6.94 \pm 0.38^{\#}$	$6.57 \pm 0.21^*$
2. Total soluble solids ([°] Brix)	12.50 ± 0.79	$12.4 \pm 0.84^{\#}$	$12.6 \pm 0.69^{\#}$	$12.5 \pm 0.31^{\#}$	$12.6 \pm 0.55^{\#}$
3. Acidity (% citric acid)	0.62 ± 0.04	$0.62 \pm 0.06^{\#}$	$0.63 \pm 0.02^{\#}$	$0.65 \pm 0.06^{\#}$	$0.68 \pm 0.04^{\#}$
4. pH	3.78 ± 0.14	$3.78 \pm 0.27^{\#}$	$3.77 \pm 0.26^{\#}$	$3.75 \pm 0.11^{\#}$	$3.14 \pm 0.14^{\#}$
5. Total phenolic content (mg GAE/mL)	0.89 ± 0.07	$0.83 \pm 0.07^{\#}$	$0.76 \pm 0.05^{\#}$	$0.71 \pm 0.04^{\#}$	$0.67 \pm 0.05^{\#}$
6. Total flavonoid content (mg CE/mL)	0.51 ± 0.02	$0.49 \pm 0.03^{\#}$	$0.44 \pm 0.04^{\#}$	$0.43 \pm 0.07^{\#}$	$0.32 \pm 0.01^*$
7. Total antioxidant activity (% inhibition of DPPH radical)	31.65 ± 1.18	$30.44 \pm 0.94^{\#}$	$28.91 \pm 0.77^{\#}$	$27.1 \pm 0.59^{\#}$	$26.05 \pm 1.01^*$

Quality assessment of irradiated fruit juices was compared with control by Dunnett's test applying software GraphPad Prism trial version 7. The $p < 0.05$ was considered as statistically significant and represented as *. Whereas, $p > 0.05$ was considered as statistically not significant and represented as #.

©1: Extremely poor. 2: Very poor. 3: Poor. 4: Fair above poor. 5: Fair. 6: Good above fair. 7: Good. 8: Very good. 9: Excellent.

§ 1: Dislike extremely. 2: Dislike very much. 3: Dislike moderately. 4: Dislike slightly. 5: Neither like nor dislike. 6: Like slightly. 7: Like moderately. 8: Like very much. 9: Like extremely.

TABLE 5 | Quality assessment of pineapple fruit juice treated with different doses of irradiation.

Quality parameter	Irradiation dose				
	0 kGy (Control)	2.5 kGy	5 kGy	7.5 kGy	10 kGy
1. Sensory attributes					
A. Appearance [®]	8.11 ± 0.49	8.05 ± 0.26 [#]	7.81 ± 0.33 [#]	7.59 ± 0.25 [#]	7.12 ± 0.27 [*]
B. Aroma [®]	8.56 ± 0.27	8.25 ± 0.18 [#]	7.9 ± 0.27 [#]	7.32 ± 0.31 [#]	6.91 ± 0.22 [*]
C. Consistency [®]	7.60 ± 0.14	7.5 ± 0.29 [#]	7.35 ± 0.12 [#]	7.22 ± 0.16 [#]	7.00 ± 0.24 [#]
D. Taste [®]	8.60 ± 0.38	8.25 ± 0.20 [#]	8.07 ± 0.27 [#]	7.82 ± 0.31 [#]	7.24 ± 0.23 [*]
E. Overall acceptability [§]	8.71 ± 0.46	8.33 ± 0.41 [#]	8.01 ± 0.29 [#]	7.44 ± 0.37 [#]	6.82 ± 0.22 [*]
2. Total soluble solids (°Brix)	14.8 ± 0.39	14.8 ± 0.64 [#]	14.9 ± 0.41 [#]	14.8 ± 0.27 [#]	15.1 ± 0.83 [#]
3. Acidity (% citric acid)	0.51 ± 0.02	0.52 ± 0.05 [#]	0.54 ± 0.04 [#]	0.55 ± 0.02 [#]	0.57 ± 0.04 [#]
4. pH	3.95 ± 0.17	3.93 ± 0.18 [#]	3.90 ± 0.22 [#]	3.90 ± 0.16 [#]	3.88 ± 0.18 [#]
5. Total phenolic content (mg GAE/mL)	0.76 ± 0.07	0.72 ± 0.06 [#]	0.62 ± 0.04 [#]	0.59 ± 0.03 [#]	0.55 ± 0.06 [*]
6. Total flavonoid content (mg CE/mL)	0.37 ± 0.04	0.36 ± 0.08 [#]	0.34 ± 0.04 [#]	0.31 ± 0.07 [#]	0.18 ± 0.00 [*]
7. Total antioxidant activity (% inhibition of DPPH radical)	22.59 ± 0.84	22.1 ± 1.09 [#]	20.15 ± 0.69 [#]	19.48 ± 0.91 [#]	18.22 ± 0.58 [*]

Quality assessment of irradiated fruit juices was compared with control by Dunnett's test applying software GraphPad Prism trial version 7. The $p < 0.05$ was considered as statistically significant and represented as *. Whereas, $p > 0.05$ was considered as statistically not significant and represented as #.

©1: Extremely poor. 2: Very poor. 3: Poor. 4: Fair above poor. 5: Fair. 6: Good above fair. 7: Good. 8: Very good. 9: Excellent.

§1: Dislike extremely. 2: Dislike very much. 3: Dislike moderately. 4: Dislike slightly. 5: Neither like nor dislike. 6: Like slightly. 7: Like moderately. 8: Like very much. 9: Like extremely.

TABLE 6 | Quality assessment of tomato juice treated with different doses of irradiation.

Quality parameter	Irradiation dose				
	0 kGy (Control)	2.5 kGy	5 kGy	7.5 kGy	10 kGy
1. Sensory attributes					
A. Appearance [®]	7.21 ± 0.29	7.02 ± 0.14 [#]	6.87 ± 0.35 [#]	6.51 ± 0.41 [#]	6.31 ± 0.22 [*]
B. Aroma [®]	7.82 ± 0.34	7.60 ± 0.16 [#]	7.25 ± 0.11 [#]	6.88 ± 0.26 [#]	6.52 ± 0.19 [*]
C. Consistency [®]	7.50 ± 0.29	7.45 ± 0.11 [#]	7.38 ± 0.19 [#]	7.24 ± 0.19 [#]	7.20 ± 0.24 [#]
D. Taste [®]	7.11 ± 0.46	7.00 ± 0.33 [#]	6.80 ± 0.26 [#]	6.42 ± 0.24 [#]	6.00 ± 0.37 [*]
E. Overall acceptability [§]	7.64 ± 0.37	7.52 ± 0.33 [#]	7.01 ± 0.19 [#]	6.72 ± 0.28 [#]	6.31 ± 0.31 [*]
2. Total soluble solids (°Brix)	5.20 ± 0.22	5.16 ± 0.27 [#]	5.21 ± 0.06 [#]	5.32 ± 0.09 [#]	5.30 ± 0.14 [#]
3. Acidity (% citric acid)	0.65 ± 0.03 [#]	0.66 ± 0.05 [#]	0.69 ± 0.03 [#]	0.70 ± 0.02 [#]	0.72 ± 0.04 [#]
4. pH	3.72 ± 0.21 [#]	3.72 ± 0.37 [#]	3.70 ± 0.24 [#]	3.69 ± 0.19 [#]	3.65 ± 0.27 [#]
5. Total phenolic content (mg GAE/mL)	0.81 ± 0.05	0.78 ± 0.02 [#]	0.76 ± 0.03 [#]	0.72 ± 0.04 [#]	0.7 ± 0.02 [*]
6. Total flavonoid content (mg CE/mL)	0.39 ± 0.01	0.38 ± 0.04 [#]	0.36 ± 0.07 [#]	0.34 ± 0.02 [#]	0.18 ± 0.01 [*]
7. Total antioxidant activity (% inhibition of DPPH radical)	29.83 ± 0.89	28.15 ± 0.73 [#]	26.72 ± 1.10 [#]	25.39 ± 0.81 [#]	24.15 ± 0.94 [*]

Quality assessment of irradiated fruit juices was compared with control by Dunnett's test applying software GraphPad Prism trial version 7. The $p < 0.05$ was considered as statistically significant and represented as *. Whereas, $p > 0.05$ was considered as statistically not significant and represented as #.

©1: Extremely poor. 2: Very poor. 3: Poor. 4: Fair above poor. 5: Fair. 6: Good above fair. 7: Good. 8: Very good. 9: Excellent.

§1: Dislike extremely. 2: Dislike very much. 3: Dislike moderately. 4: Dislike slightly. 5: Neither like nor dislike. 6: Like slightly. 7: Like moderately. 8: Like very much. 9: Like extremely.

is the first report. However, further studies should be carried out on identification and purification of radiolytic products of ZEA to propose the detailed toxic feature of detoxified ZEA.

Quality Assessment of Fruit Juices Treated With Irradiation

Effect of different irradiation doses on quality of fruit juice was assessed by considering various parameters, i.e., sensory (appearance, aroma, consistency, and taste), pH, acidity, total soluble solids, total phenolic and flavonoid content, and total antioxidant activity (Tables 4–6).

The sensory evaluation showed that irradiation doses of 2.5, 5, and 7.5 kGy have no significant effect on quality of

fruit juices compared to control. While, 10 kGy of irradiation has produced significant changes in sensory attributes except consistency of fruit juices compared to control. Subsequently, overall acceptability of fruit juices has significant affected at high dose of 10 kGy compared to control. The observed sensory results could be due to production of off-flavor and off-color in the fruit juices during irradiation processing (Yun et al., 2010).

Further, control and irradiation treated fruit juices were analyzed for total soluble solids and results revealed that irrespective of radiation doses, total soluble solids have shown no significant difference related to control. In support of our results, earlier reports of Arjeh et al. (2015) and Naresh et al. (2015) have reported that irradiation dose of 6 and 3 kGy not

produced significant changes in total soluble solids of cherry and mango juices, respectively. On the other hand, acidity and pH were correspondingly increased and decreased in fruit juices upon irradiation and insignificant changes were noticed in fruit juices at all irradiation doses related to control. In support of these results, Youssef et al. (2002) and Harder et al. (2009) have reported a slight rise in acidity and reduction in pH of mango pulp and nectar of kiwi fruits, respectively and concluded that may be due to inactivation of citric acid cleaving enzyme.

Also, total phenolic and flavonoid contents of fruit juices were decreased upon irradiation and significant changes were observed at 10 kGy compared to control. The total phenolic and flavonoid contents were decreased in irradiated fruit juices and it could be due to degradative action of irradiation on phenolic and flavonoid contents (Najafabadi et al., 2017). Likewise, total antioxidant activity of fruit juices was decreased upon irradiation and significant changes were noticed in 10 kGy compared to control. The antioxidant potential of plant derived products mainly depend on its phenolic and flavonoid contents (George et al., 2016; Muniyandi et al., 2017). In this study, total phenolic and flavonoid contents were decreased in irradiated fruit juices compared to control. Therefore, might be antioxidant activity of fruit juices was decreased upon irradiation compared to control.

Overall, study determined that irradiation of fruit juices with high doses minimally alters the quality of fruit juices. However, irradiation enhances the microbiological safety and prolongs the shelf life of food products. Thus, WHO and FAO has specified that irradiation of food products up to 25 kGy are safe and recognized as suitable decontamination technique in agriculture and food industry (FAO/IAEA/WHO, 1999).

CONCLUSION

In the present study, detoxification efficacy of irradiation on ZEA in water and fruit juice was assessed by CCD of RSM statistical program. The independent factors (dose of irradiation and concentration of zearalenone) had a positive significance on the response factor (percentage of ZEA reduction). The RSM study concluded that dose of irradiation and concentration of zearalenone were the determinant factors for detoxification of ZEA. The toxic effects of detoxified ZEA were studied under *in-vitro* conditions. The irradiation mediated detoxified ZEA has exhibited less toxicity compared to non-detoxified ZEA. The results confirmed that the toxicity of ZEA was decreased with irradiation treatment. To reveal the precise process of ZEA detoxification, further research is needed on extraction, purification, and structural elucidation of radiolytic products of ZEA. In conclusion, due to its rapidity and effectiveness on detoxification of ZEA, irradiation could be a potential food processing technique in the agriculture and food industry. However, irradiation of fruit juices with high dose of 10 kGy has minimally altered the quality of fruit juices. Nevertheless, irradiation process should carry out with well-directed standard operating procedures (SOPs) in approved laboratories as per FAO/IAEA/WHO.

AUTHOR CONTRIBUTIONS

NK and VM designed the work. NK, JK, and VM executed the work, analyzed data, and drafted the results. All authors have approved the final version of the manuscript.

ACKNOWLEDGMENTS

NK is thankful to UGC, New Delhi, India for providing the Junior Research Fellowship {File. No: 2-14/2102 (SA-I)} to pursue Ph.D. Also, we are thankful to Director, DFRL, and Joint Director, DRDO-BU-Centre for Life Sciences for their kind support and encouragement.

SUPPLEMENTARY MATERIAL

The Supplementary Material for this article can be found online at: <https://www.frontiersin.org/articles/10.3389/fmicb.2018.02937/full#supplementary-material>

Supplementary Table S1 | Experimental range, levels, mean, and standard deviation of independent variables, i.e. zearalenone (ZEA) and irradiation.

Supplementary Table S2 | HPLC conditions for determination of zearalenone (ZEA).

Supplementary Table S3 | ANOVA for percentage of zearalenone (ZEA) reduction in distilled water.

Supplementary Table S4 | ANOVA for percentage of zearalenone (ZEA) reduction in orange juice.

Supplementary Table S5 | ANOVA for percentage of zearalenone (ZEA) reduction in pineapple juice.

Supplementary Table S6 | ANOVA for percentage of zearalenone (ZEA) reduction in tomato juice.

Supplementary Table S7 | Sequential model and regression coefficients of optimized designs.

Supplementary Figure S1 | Normal plot of residuals for detoxification effect of irradiation on zearalenone (ZEA) in (A) distilled water, (B) orange juice, (C) pineapple juice, and (D) tomato juice.

Supplementary Figure S2 | Box-cox plots for detoxification effect of irradiation on zearalenone (ZEA) in (A) distilled water, (B) orange juice, (C) pineapple juice, and (D) tomato juice.

Supplementary Figure S3 | Actual versus predicted plots for detoxification effect of irradiation on zearalenone (ZEA) in (A) distilled water, (B) orange juice, (C) pineapple juice, and (D) tomato juice.

Supplementary Figure S4 | Assessment of toxic effect of non-detoxified and irradiation mediated detoxified zearalenone (ZEA) on cell viability in RAW 264.7 cells for 12 h by live/dead dual staining technique.

Supplementary Figure S5 | Assessment of effect of non-detoxified and irradiation mediated detoxified zearalenone (ZEA) on generation of intracellular reactive oxygen species (ROS) in RAW 264.7 cells for 12 h by DCFH-DA staining.

Supplementary Figure S6 | Assessment of effect of non-detoxified and irradiation mediated detoxified zearalenone (ZEA) on mitochondrial membrane potential (MMP) in RAW 264.7 cells for 12 h by rhodamine 123 staining.

Supplementary Figure S7 | Assessment of effect of non-detoxified and irradiation mediated detoxified zearalenone (ZEA) on nuclear damage in RAW 264.7 cells for 12 h by DAPI staining.

REFERENCES

- Aldred, D., Magan, N., and Olsen, M. (2004). "The use of HACCP in the control of mycotoxins: the case of cereals," in *Mycotoxins in Food: Detection and Control* (Boca Raton, FL: CRC Press) 139–173. doi: 10.1201/9781439823361.pt2
- Alghuthaymi, M. A., and Bahkali, A. H. (2015). Toxigenic profiles and trinucleotide repeat diversity of *Fusarium* species isolated from banana fruits. *Biotechnol. Biotechnol. Equip.* 29, 324–330. doi: 10.1080/13102818.2014.995519
- Andersen, B., and Thrane, U. (2006). Food-borne fungi in fruit and cereals and their production of mycotoxins. *Adv. Food Mycol.* 137–152. doi: 10.1007/0-387-28391-9_8
- Anderson, M. J., and Whitcomb, P. J. (2016). *DOE Simplified: Practical Tools for Effective Experimentation*. Boca Raton, MA: CRC Press.
- Arjeh, E., Barzegar, M., and Sahari, M. A. (2015). Effects of gamma irradiation on physicochemical properties, antioxidant and microbial activities of sour cherry juice. *Radiat. Phys. Chem.* 114, 18–24. doi: 10.1016/j.radphyschem.2015.05.017
- Association of Office Analytical Chemists (AOAC) (1996). *Official Methods of Analysis, 15th Edn*. Washington, DC: George Banta.
- Atkinson, A. C., and Donev, A. N. (1992). *Optimum Experimental designs*. Oxford: Oxford Science Publications.
- Aziz, N. H., Attia, E. S., and Farag, S. A. (1997). Effect of gamma-irradiation on the natural occurrence of *Fusarium* mycotoxins in wheat, flour and bread. *Mol. Nutr. Food Res.* 41, 34–37.
- Barkai-Golan, R., and Paster, N. (2011). *Mycotoxins in Fruits and Vegetables*. San Diego, CA: Academic Press.
- Bevilacqua, A., Campaniello, D., Sinigaglia, M., Ciccarone, C., and Corbo, M. R. (2012). Sodium-benzoate and citrus extract increase the effect of homogenization towards spores of *Fusarium oxysporum* in pineapple juice. *Food Control* 28, 199–204. doi: 10.1016/j.foodcont.2012.04.038
- Bevilacqua, A., Sinigaglia, M., and Corbo, M. R. (2013). Ultrasound and antimicrobial compounds: a suitable way to control *Fusarium oxysporum* in juices. *Food Bioprocess Technol.* 6, 1153–1163. doi: 10.1007/s11947-012-0782-0
- Bilgrami, K. S., Sahay, S. S., Shrivastava, A. K., and Rahman, M. F. (1990). Incidence of zearalenone, D. O. N., and T-2 toxin producing strains of *Fusarium* sp. on food items. *Proc. Indian Natl. Sci. Acad. B* 56, 223–228.
- Blumenthal-Yonassi, J. I. L. L., Paster, N., and Barkai-Golan, R. (1988). Differences in zearalenone production by *Fusarium equiseti* strains *in vitro* and in fruits. *JSM Mycotoxins* 1988, 232–233. doi: 10.2520/myco1975.1988.1Supplement_232
- Bryła, M., Waśkiewicz, A., Podolska, G., Szymczyk, K., Jedrzejczak, R., Damaziak, K., et al. (2016). Occurrence of 26 mycotoxins in the grain of cereals cultivated in Poland. *Toxins* 8:160. doi: 10.3390/toxins8060160
- Calado, T., Venâncio, A., and Abrunhosa, L. (2014). Irradiation for mold and mycotoxin control: a review. *Comprehens. Rev. Food Sci. Food Saf.* 13, 1049–1061. doi: 10.1111/1541-4337.12095
- Chakrabarti, D. K., and Ghosal (1986). Occurrence of free and conjugated 12, 13-epoxytrichothecenes and zearalenone in banana fruits infected with *Fusarium moniliforme*. *Appl. Environ. Microbiol.* 51, 217–219.
- Chen, Y. C., Lin-Shiau, S. Y., and Lin, J. K. (1998). Involvement of reactive oxygen species and caspase 3 activation in arsenite-induced apoptosis. *J. Cell. Physiol.* 177, 324–333.
- Choi, J. I., and Lim, S. (2016). Inactivation of fungal contaminants on Korean traditional cashbox by gamma irradiation. *Radiat. Phys. Chem.* 118, 70–74. doi: 10.1016/j.radphyschem.2015.05.009
- Corbo, M. R., Bevilacqua, A., Campaniello, D., Ciccarone, C., and Sinigaglia, M. (2010). Use of high pressure homogenization as a mean to control the growth of foodborne moulds in tomato juice. *Food Control* 21, 1507–1511. doi: 10.1016/j.foodcont.2010.04.023
- De Berardis, S., De Paola, E. L., Montevicchi, G., Garbini, D., Masino, F., Antonelli, A., et al. (2018). Determination of four *Alternaria alternata* mycotoxins by QuEChERS approach coupled with liquid chromatography-tandem mass spectrometry in tomato-based and fruit-based products. *Food Res. Int.* 106, 677–685. doi: 10.1016/j.foodres.2018.01.032
- European Commission (2006). Regulation EU "2006 of 19 December 2006 (2006): Setting maximum levels for certain contaminants in foodstuff." *Off. J. Eur. Commission* 1881, 5–24.
- FAO/IAEA/WHO (1999). High-dose irradiation: wholesomeness of food irradiated with doses above 10 kGy. Report of a Joint FAO/IAEA/WHO study group. *World Health Organ. Tech. Rep. Ser.* 890, 1–197.
- Fotakis, G., and Timbrell, J. A. (2006). *In vitro* cytotoxicity assays: comparison of LDH, neutral red, MTT and protein assay in hepatoma cell lines following exposure to cadmium chloride. *Toxicol. Lett.* 160, 171–177. doi: 10.1016/j.toxlet.2005.07.001
- Gao, F., Jiang, L. P., Chen, M., Geng, C. Y., Yang, G., Ji, F., et al. (2013). Genotoxic effects induced by zearalenone in a human embryonic kidney cell line. *Mutat. Res. Genet. Toxicol. Environ. Mutagen.* 755, 6–10. doi: 10.1016/j.mrgentox.2013.04.009
- García-Recio, S., Pastor-Arroyo, E. M., Marín-Aguilera, M., Almendro, V., and Gascón, P. (2015). The transmodulation of HER2 and EGFR by substance P in breast cancer cells requires c-Src and metalloproteinase activation. *PLoS ONE* 10:e0129661. doi: 10.1371/journal.pone.0129661
- George, E., Kasipandi, M., Vekataramana, M., Kumar, K. N., Allen, J. A., Parimelazhagan, T., et al. (2016). *In vitro* anti-oxidant and cytotoxic analysis of *Pogostemon mollis* Benth. *Bangladesh J. Pharmacol.* 11, 148–158. doi: 10.3329/bjpv.v11i1.24157
- Harder, M. N. C., De Toledo, T. C. F., Ferreira, A. C. P., and Arthur, V. (2009). Determination of changes induced by gamma radiation in nectar of kiwi fruit (*Actinidia deliciosa*). *Radiat. Phys. Chem.* 78, 579–582. doi: 10.1016/j.radphyschem.2009.04.012
- Haugland, R. P., MacCoubrey, I. C., and Moore, P. L. (1994). U.S. Patent No. 5,314,805. Washington, DC: U.S. Patent and Trademark Office.
- Hooshmand, H., and Klopfenstein, C. F. (1995). Effects of gamma irradiation on mycotoxin disappearance and amino acid contents of corn, wheat, and soybeans with different moisture contents. *Plant Foods Hum. Nutr.* 47, 227–238. doi: 10.1007/BF01088331
- Hussain, S. M., Hess, K. L., Gearhart, J. M., Geiss, K. T., and Schlager, J. J. (2005). *In vitro* toxicity of nanoparticles in BRL 3A rat liver cells. *Toxicol. In Vitro* 19, 975–983. doi: 10.1016/j.tiv.2005.06.034
- IARC (1993). *Monographs on the Evaluation of Carcinogenic Risks to Humans: Some Naturally Occurring Substances: Food Items and Constituents, Heterocyclic Aromatic Amines and Mycotoxins*. Lyon: International Agency for Research on Cancer, 1–599.
- JECFA (2011). *Evaluation of Certain Food Additives and Contaminants: Seventy-Third [73rd] Report of the Joint FAO/WHO Expert Committee on Food Additives*.
- Jime, M., and Mateo, R. (1997). Determination of mycotoxins produced by *Fusarium* isolates from banana fruits by capillary gas chromatography and high-performance liquid chromatography. *J. Chromatogr. A* 778, 363–372. doi: 10.1016/S0021-9673(97)00328-2
- Juan, C., Mañes, J., Font, G., and Juan-García, A. (2017). Determination of mycotoxins in fruit berry by-products using QuEChERS extraction method. *LWT Food Sci. Technol.* 86, 344–351. doi: 10.1016/j.lwt.2017.08.020
- Kalagatur, N. K., Kamasani, J. R., Mudili, V., Krishna, K., Chauhan, O. P., and Sreepathi, M. H. (2018a). Effect of high pressure processing on growth and mycotoxin production of *Fusarium graminearum* in maize. *Food Biosci.* 21, 53–59. doi: 10.1016/j.fbio.2017.11.005
- Kalagatur, N. K., Karthick, K., Allen, J. A., Nirmal Ghosh, O. S., Chandranayaka, S., Gupta, V. K., et al. (2017). Application of Activated Carbon Derived from Seed Shells of *Jatropha curcas* for Decontamination of Zearalenone Mycotoxin. *Front. Pharmacol.* 8:760. doi: 10.3389/fphar.2017.00760
- Kalagatur, N. K., Mudili, V., Kamasani, J. R., and Siddaiah, C. (2018b). Discrete and combined effects of Ylang-Ylang (*Cananga odorata*) essential oil and gamma irradiation on growth and mycotoxins production by *Fusarium graminearum* in maize. *Food Control* 94, 276–283. doi: 10.1016/j.foodcont.2018.07.030
- Kalagatur, N. K., Mudili, V., Siddaiah, C., Gupta, V. K., Natarajan, G., Sreepathi, M. H., et al. (2015). Antagonistic activity of *Ocimum sanctum* L. essential oil on growth and zearalenone production by *Fusarium graminearum* in maize grains. *Front. Microbiol.* 6:892. doi: 10.3389/fmicb.2015.00892
- Kalagatur, N. K., Reddy, J. K., Nayak, C., Krishna, K., and Gupta, V. K. (2018c). Combinational inhibitory action of *Hedychium spicatum* L. essential oil and γ -radiation on growth rate and mycotoxins content of *Fusarium graminearum* in maize: response surface methodology. *Front. Microbiol.* 9:1511. doi: 10.3389/fmicb.2018.01511

- Kalawate, A., and Mehrete, S. (2015). Isolation and characterization of mold fungi and insects infecting sawmill wood, and their inhibition by gamma radiation. *Radiat. Phys. Chem.* 117, 191–197. doi: 10.1016/j.radphyschem.2015.08.016
- Karlovsky, P., Suman, M., Berthiller, F., De Meester, J., Eisenbrand, G., Perrin, I., et al. (2016). Impact of food processing and detoxification treatments on mycotoxin contamination. *Mycotoxin Res.* 32, 179–205. doi: 10.1007/s12550-016-0257-7
- Kouadio, J. H., Mobio, T. A., Baudrimont, I., Moukha, S., Dano, S. D., and Creppy, E. E. (2005). Comparative study of cytotoxicity and oxidative stress induced by deoxynivalenol, zearalenone or fumonisin B1 in human intestinal cell line Caco-2. *Toxicology* 213, 56–65. doi: 10.1016/j.tox.2005.05.010
- Kumar, K. N., Venkataramana, M., Allen, J. A., Chandranayaka, S., Murali, H. S., and Batra, H. V. (2016). Role of *Curcuma longa* L. essential oil in controlling the growth and zearalenone production of *Fusarium graminearum*. *LWT Food Sci. Technol.* 69, 522–528. doi: 10.1016/j.lwt.2016.02.005
- Le Caër, S. (2011). Water radiolysis: influence of oxide surfaces on H₂ production under ionizing radiation. *Water* 3, 235–253. doi: 10.3390/w3010235
- Lozano, G. M., Bejarano, I., Espino, J., Gonzalez, D., Ortiz, A., Garcia, J. F., et al. (2009). Relationship between caspase activity and apoptotic markers in human sperm in response to hydrogen peroxide and progesterone. *J. Reproduct. Dev.* 55, 615–621. doi: 10.1262/jrd.20250
- Milano, G. D., and López, T. A. (1991). Influence of temperature on zearalenone production by regional strains of *Fusarium graminearum* and *Fusarium oxysporum* in culture. *Int. J. Food Microbiol.* 13, 329–333. doi: 10.1016/0168-1605(91)90092-4
- Mudili, V., Siddai, C. N., Nagesh, M., Garapati, P., Naveen Kumar, K., Murali, H. S., et al. (2014). Mould incidence and mycotoxin contamination in freshly harvested maize kernels originated from India. *J. Sci. Food Agric.* 94, 2674–2683. doi: 10.1002/jsfa.6608
- Muniyandi, K., George, E., Mudili, V., Kalagatur, N. K., Anthuvan, A. J., Krishna, K., et al. (2017). Antioxidant and anticancer activities of *Plectranthus stocksii* Hook. f. leaf and stem extracts. *Agric. Nat. Resour.* 51, 63–73. doi: 10.1016/j.anres.2016.07.007
- Murray, J. M., Delahunty, C. M., and Baxter, I. A. (2001). Descriptive sensory analysis: past, present and future. *Food Res. Int.* 34, 461–471. doi: 10.1016/S0963-9969(01)00070-9
- Muthulakshmi, S., Maharajan, K., Habibi, H. R., Kadirvelu, K., and Venkataramana, M. (2018). Zearalenone induced embryo and neurotoxicity in zebrafish model (*Danio rerio*): role of oxidative stress revealed by a multi biomarker study. *Chemosphere* 198, 111–121. doi: 10.1016/j.chemosphere.2018.01.141
- Najafabadi, N. S., Sahari, M. A., Barzegar, M., and Esfahani, Z. H. (2017). Effect of gamma irradiation on some physicochemical properties and bioactive compounds of jujube (*Ziziphus jujuba* var *vulgaris*) fruit. *Radiat. Phys. Chem.* 130, 62–68. doi: 10.1016/j.radphyschem.2016.07.002
- Naresh, K., Varakumar, S., Variyar, P. S., Sharma, A., and Reddy, O. V. S. (2015). Effect of γ -irradiation on physico-chemical and microbiological properties of mango (*Mangifera indica* L.) juice from eight Indian cultivars. *Food Biosci.* 12, 1–9. doi: 10.1016/j.fbio.2015.06.003
- Neme, K., and Mohammed, A. (2017). Mycotoxin occurrence in grains and the role of postharvest management as a mitigation strategies. A review. *Food Control* 78, 412–425. doi: 10.1016/j.foodcont.2017.03.012
- Porter, A. G., and Jänicke, R. U. (1999). Emerging roles of caspase-3 in apoptosis. *Cell Death Differ.* 6:99. doi: 10.1038/sj.cdd.4400476
- Reddy, K. J., Jayatilakan, K., and Pandey, M. C. (2015). Effect of ionizing radiation on the protein and lipid quality characteristics of mutton kheema treated with rice bran oil and sunflower oil. *Radiat. Phys. Chem.* 117, 217–224. doi: 10.1016/j.radphyschem.2015.09.002
- Restani, P. (2008). “Diffusion of mycotoxins in fruits and vegetables,” in *Mycotoxins in Fruits and Vegetables* (San Diego, CA: Elsevier), 105–114. doi: 10.1016/B978-0-12-374126-4.00005-X
- Riss, T. L., Moravec, R. A., Niles, A. L., Duellman, S., Benink, H. A., Worzella, T. J., et al. (2016). “Cell viability assays.” in *Assay Guidance Manual* (Bethesda, MD: Eli Lilly & Company and the National Center for Advancing Translational Sciences), 262–291.
- Sandoval-Contreras, T., Villarruel-López, A., Torres-Vitela, R., Garciglia-Mercado, C., Gómez-Anduro, G., Velázquez-Lizárraga, A. E., et al. (2018). Mycotoxigenic potential of phytopathogenic moulds isolated from citrus fruits from different states of Mexico. *Qual. Assur. Saf. Crops Foods* 10, 125–136. doi: 10.3920/QAS2016.0890
- Sharma, N., Ghosh, R., and Nigam, M. (1998). Toxigenic fungi associated with stored, fruits of chironji. *Indian Phytopathol.* 51, 284–286.
- Shier, W. T., Shier, A. C., Xie, W., and Mirocha, C. J. (2001). Structure-activity relationships for human estrogenic activity in zearalenone mycotoxins. *Toxicol.* 39, 1435–1438. doi: 10.1016/S0041-0101(00)00259-2
- Škrbić, B., Antić, I., and Cvejanov, J. (2017). Determination of mycotoxins in biscuits, dried fruits and fruit jams: an assessment of human exposure. *Food Addit. Contamin. A* 34, 1012–1025. doi: 10.1080/19440049.2017.1303195
- Taniwaki, M. H., Hoenderboom, C. J. M., De Almeida Vitali, A., and Eiroa, M. N. U. (1992). Migration of patulin in apples. *J. Food Prot.* 55, 902–904. doi: 10.4315/0362-028X-55.11.902
- Tatay, E., Font, G., and Ruiz, M. J. (2016). Cytotoxic effects of zearalenone and its metabolites and antioxidant cell defense in CHO-K1 cells. *Food Chem. Toxicol.* 96, 43–49. doi: 10.1016/j.fct.2016.07.027
- Van Egmond, H. P., Schothorst, R. C., and Jonker, M. A. (2007). Regulations relating to mycotoxins in food. *Anal. Bioanal. Chem.* 389, 147–157. doi: 10.1007/s00216-007-1317-9
- Venkataramana, M., Nayaka, S. C., Anand, T., Rajesh, R., Aiyaz, M., Divakara, S. T., et al. (2014). Zearalenone induced toxicity in SHSY-5Y cells: the role of oxidative stress evidenced by N-acetyl cysteine. *Food Chem. Toxicol.* 65, 335–342. doi: 10.1016/j.fct.2013.12.042
- Wang, Y., Zheng, W., Bian, X., Yuan, Y., Gu, J., Liu, X., et al. (2014). Zearalenone induces apoptosis and cytoprotective autophagy in primary Leydig cells. *Toxicol. Lett.* 226, 182–191. doi: 10.1016/j.toxlet.2014.02.003
- Whitcomb, P. J., and Anderson, M. J. (2004). *RSM Simplified: Optimizing Processes Using Response Surface Methods for Design of Experiments*. CRC Press.
- Youssef, B. M., Asker, A. A., El-Samahy, S. K., and Swailam, H. M. (2002). Combined effect of steaming and gamma irradiation on the quality of mango pulp stored at refrigerated temperature. *Food Res. Int.* 35, 1–13. doi: 10.1016/S0963-9969(00)00153-8
- Yun, H. J., Kim, H. J., Jung, Y. K., Jung, S., Lee, J. W., and Jo, C. R. (2010). Effect of natural ingredients and red wine for manufacturing meat products on radiation sensitivity of pathogens inoculated into ground beef. *Korean J. Food Sci. Anim. Resour.* 30, 819–825. doi: 10.5851/kosfa.2010.30.5.819
- Zheng, W. L., Wang, B. J., Wang, L., Shan, Y. P., Zou, H., Song, R. L., et al. (2018). ROS-mediated cell cycle arrest and apoptosis induced by zearalenone in mouse sertoli cells via ER stress and the ATP/AMPK Pathway. *Toxins* 10:24. doi: 10.3390/toxins10010024
- Zheng, X., Yang, Q., Zhang, X., Apaliya, M. T., Ianiri, G., Zhang, H., et al. (2017). Biocontrol agents increase the specific rate of patulin production by *Penicillium expansum* but Decrease the disease and total patulin contamination of apples. *Front. Microbiol.* 8:1240. doi: 10.3389/fmicb.2017.01240
- Zhu, L., Yuan, H., Guo, C., Lu, Y., Deng, S., Yang, Y., et al. (2012). Zearalenone induces apoptosis and necrosis in porcine granulosa cells via a caspase 3 and caspase 9 dependent mitochondrial signaling pathway. *J. Cell. Physiol.* 227, 1814–1820. doi: 10.1002/jcp.22906
- Zinedine, A., Soriano, J. M., Molto, J. C., and Manes, J. (2007). Review on the toxicity, occurrence, metabolism, detoxification, regulations and intake of zearalenone: an oestrogenic mycotoxin. *Food Chem. Toxicol.* 45, 1–18. doi: 10.1016/j.fct.2006.07.030

Conflict of Interest Statement: The authors declare that the research was conducted in the absence of any commercial or financial relationships that could be construed as a potential conflict of interest.

Copyright © 2018 Kalagatur, Kamasani and Mudili. This is an open-access article distributed under the terms of the Creative Commons Attribution License (CC BY). The use, distribution or reproduction in other forums is permitted, provided the original author(s) and the copyright owner(s) are credited and that the original publication in this journal is cited, in accordance with accepted academic practice. No use, distribution or reproduction is permitted which does not comply with these terms.



Chitosan, a Biopolymer With Triple Action on Postharvest Decay of Fruit and Vegetables: Eliciting, Antimicrobial and Film-Forming Properties

Gianfranco Romanazzi^{1*}, Erica Feliziani¹ and Dharini Sivakumar²

¹ Department of Agricultural, Food and Environmental Sciences, Marche Polytechnic University, Ancona, Italy, ² Department of Crop Sciences, Postharvest Technology Group, Tshwane University of Technology, Pretoria, South Africa

OPEN ACCESS

Edited by:

Boqiang Li,
Institute of Botany (CAS), China

Reviewed by:

Xianghong Meng,
Ocean University of China, China
Hongbing Deng,
Wuhan University, China

*Correspondence:

Gianfranco Romanazzi
g.romanazzi@univpm.it

Specialty section:

This article was submitted to
Food Microbiology,
a section of the journal
Frontiers in Microbiology

Received: 04 July 2018

Accepted: 26 October 2018

Published: 04 December 2018

Citation:

Romanazzi G, Feliziani E and
Sivakumar D (2018) Chitosan,
a Biopolymer With Triple Action on
Postharvest Decay of Fruit
and Vegetables: Eliciting,
Antimicrobial and Film-Forming
Properties. *Front. Microbiol.* 9:2745.
doi: 10.3389/fmicb.2018.02745

Chitosan is a natural biopolymer from crab shells that is known for its biocompatibility, biodegradability, and bioactivity. In human medicine, chitosan is used as a stabilizer for active ingredients in tablets, and is popular in slimming diets. Due to its low toxicity, it was the first basic substance approved by the European Union for plant protection (Reg. EU 2014/563), for both organic agriculture and integrated pest management. When applied to plants, chitosan shows triple activity: (i) elicitation of host defenses; (ii) antimicrobial activity; and (iii) film formation on the treated surface. The eliciting activity of chitosan has been studied since the 1990's, which started with monitoring of enzyme activities linked to defense mechanisms (e.g., chitinase, β -1,3 glucanase, phenylalanine ammonia-lyase) in different fruit (e.g., strawberry, other berries, citrus fruit, table grapes). This continued with investigations with qRT-PCR (Quantitative Real-Time Polymerase Chain Reaction), and more recently, with RNA-Seq. The antimicrobial activity of chitosan against a wide range of plant pathogens has been confirmed through many *in-vitro* and *in-vivo* studies. Once applied to a plant surface (e.g., dipping, spraying), chitosan forms an edible coating, the properties of which (e.g., thickness, viscosity, gas and water permeability) depend on the acid in which it is dissolved. Based on data in literature, we propose that overall, the eliciting represents 30 to 40% of the chitosan activity, its antimicrobial activity 35 to 45%, and its film-forming activity 20 to 30%, in terms of its effectiveness in the control of postharvest decay of fresh fruit. As well as being used alone, chitosan can be applied together with many other alternatives to synthetic fungicides, to boost its eliciting, antimicrobial and film-forming properties, with additive, and at times synergistic, interactions. Several commercial chitosan formulations are available as biopesticides, with their effectiveness due to the integrated combination of these three mechanisms of action of chitosan.

Keywords: antimicrobial activity, biopolymer, coating, induced resistance, natural fungicide

INTRODUCTION

Chitosan is the linear polysaccharide of glucosamine and N-acetylglucosamine units joined by β -1,4-glycosidic links and it is obtained by deacetylation of chitin through exposure to NaOH solutions or to the enzyme chitinase. Chitosan and chitin are naturally occurring polymers. For their biocompatibility and biosafety, their applications are widespread in many industries, such as cosmetology, food, biotechnology, pharmacology, medicine, and agriculture (Ding et al., 2013; Lei et al., 2014). In particular, chitosan has increasing interest in plant protection as a natural fungicide and plant defense booster, and meets the interest of many researchers, that used it to prolong the storage of an array of fruit and vegetables worldwide. Chitosan was the first compound in the list of basic substances approved in the European Union for plant protection purposes (Reg. EU 66 2014/563), for both organic agriculture and integrated pest management. A comprehensive review on the available data on the effectiveness of chitosan was published recently, for its preservation of fruit and vegetables, both alone and in combination with other treatments, and its mechanisms of action (Romanazzi et al., 2017). However, the increasing knowledge of this biopolymer (**Figure 1**) and the fast advances in basic and applied research in this field require a more focused and schematic update based on the last 5 years of investigations (2013–2018). The reader can then focus on specific aspects from the long list of other reviews that have appeared on the subject, among which some have focused on the applications of chitosan to fruit and vegetables (Bautista-Baños et al., 2006; Bautista-Baños et al., 2016; Zhang et al., 2011). When applied to plants, chitosan shows triple activity: (i) elicitation of host defenses; (ii) antimicrobial activity; and (iii) film formation on the treated surface. We will cover the recent information on these issues in the following sections, which is also listed comprehensively in the Tables, with examples of these applications.

EFFECTIVENESS OF CHITOSAN IN THE CONTROL OF POSTHARVEST DECAY OF FRUIT

The potential effectiveness of chitosan as a coating for fresh fruit was first proposed by Muzzarelli (1986). The first *in-vivo* application of chitosan on fruit was in the Josep Arul Laboratory, by Ahmed El Ghaouth, who produced a list of papers through the last decade of the last century. These included El Ghaouth et al. (1992), where they applied chitosan to strawberries and other fruit, both alone and in combinations with other potential biocontrol agents, which then contributed to the develop of some commercial formulations. Following these promising investigations, and with the growing need for alternatives to the use of synthetic fungicides, chitosan use became popular, and it was proposed to be part of a new class of plant protectants (Bautista-Baños et al., 2006). Chitosan coatings have now been applied to numerous temperate and subtropical fruit, both alone and in combination with other treatments (**Tables 1–3**), with generally additive, and in some cases synergistic, effectiveness (Romanazzi et al., 2012).

CHITOSAN ELICITING ACTIVITY

Chitosan is known to elicit plant defences against several classes of pathogens, including fungi, viruses, bacteria and phytoplasma (El Hadrami et al., 2010). Moreover, in some studies, its eliciting activity was reported to be effective on pests (Badawy and Rabea, 2016). Based on our experience, the eliciting activity of chitosan accounts for 30 to 40% of its effectiveness in the control of postharvest decay of fresh fruit (**Figure 2**). The extent of this eliciting activity depends on the reactivity of the fruit tissues, and it is well known that fruit responses to stress decline with ripening (Romanazzi et al., 2016). This eliciting activity of chitosan has been studied since the 1990's, which started with monitoring of

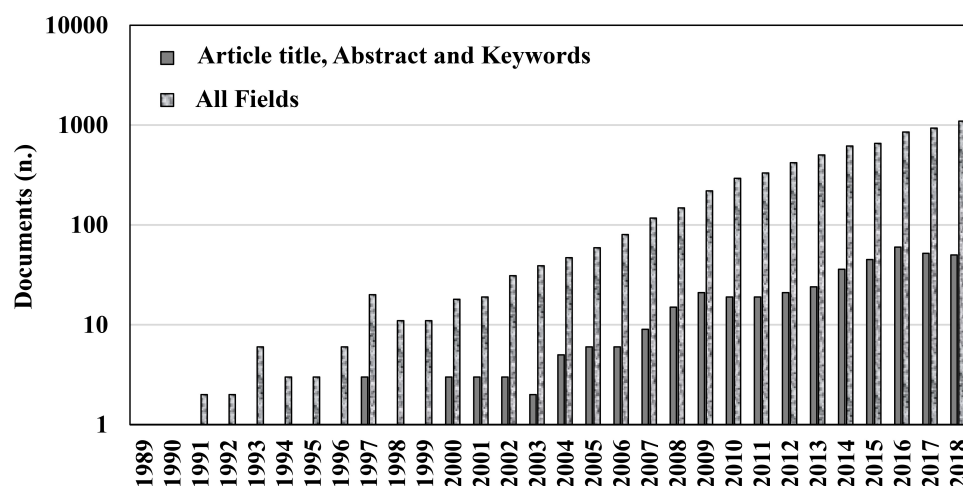


FIGURE 1 | Number of documents available on Scopus through searches with keywords 'chitosan' and 'postharvest' in 'Article title, Abstract, and Keywords' or in 'All fields' published over the last 30 years (accessed on 6 November 2018).

TABLE 1 | Postharvest chitosan treatments with other applications for storage decay of temperate fruit.

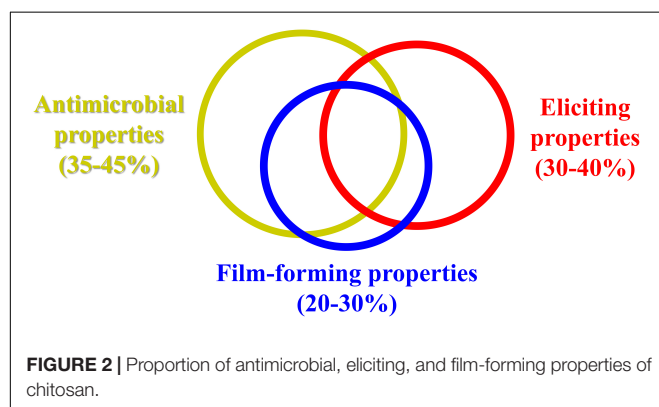
Fruit	Decay agent	Combination with chitosan	Reference
Table grapes	<i>Botrytis cinerea</i>	Salicylic acid	Shen and Yang, 2017
	General decay	Glucose complex	Gao et al., 2013
	<i>Aspergillus niger</i> , <i>Rhizopus stolonifer</i>	–	de Oliveira et al., 2014
	<i>Fusarium oxysporum</i>	–	Irkin and Guldaz, 2014
	General decay	–	Feliziani et al., 2013a
	General decay	Ultraviolet-C	Freitas et al., 2015
	General decay	–	Al-Qurashi and Mohamed, 2015
	<i>Aspergillus niger</i> , <i>Botrytis cinerea</i> , <i>Penicillium expansum</i> , <i>Rhizopus stolonifer</i>	Menta essential oil	Guerra et al., 2016
	<i>Botrytis cinerea</i>	Salvia officinalis essential oil	Kanetis et al., 2017
	<i>Botrytis cinerea</i>	Lavander and thyme essential oil	Sangsuwan et al., 2016
Strawberry	General decay	Poeny extract	Pagliarulo et al., 2016
	<i>Penicillium expansum</i> , <i>Rhizopus stolonifer</i>	Olive oil processing waste	Khalifa et al., 2016
	Total microbial load	Natamycin, nisin, pomegranate, grape seed extract	Duran et al., 2016
	Total microbial load	Quinoa protein-chitosan and quinoa protein-chitosan-sunflower oil	Valenzuela et al., 2015
	Total microbial load	Sodium benzoate and potassium sorbate	Treviño-Garza et al., 2015
	<i>Botrytis cinerea</i>	Zataria multiflora essential oil	Mohammadi et al., 2015
	<i>Rhizopus stolonifer</i>	Cinnamon leaf essential oil containing oleic acid	Perdones et al., 2014
	General decay	–	Benhabiles et al., 2013
	General decay	Geraniol and thymol	Badawy et al., 2017
	General decay	Carboxymethyl cellulose, hydroxypropylmethyl cellulose	Gol et al., 2013
Pear	<i>Botrytis cinerea</i>	Nanosized silver-chitosan composite	Moussa et al., 2013
	General decay	Beeswax	Velickova et al., 2013
	<i>Botryosphaeria</i> sp.	–	Wang et al., 2017
	General decay	Cellulose nanocrystals	Deng et al., 2017
	General decay	Acyated soy protein isolate and stearic acid	Wu et al., 2017
Apple	General decay	Olive waste extracts	Khalifa et al., 2017, 2016
	<i>Penicillium expansum</i>	–	Darolt et al., 2016
	<i>Venturia inaequalis</i>	–	Felipini et al., 2016
	<i>Penicillium expansum</i>	–	Li et al., 2015
	Calyx senescence	V	Deng et al., 2016
Citrus	<i>Penicillium digitatum</i> , <i>Penicillium italicum</i>	Silver nanoparticles	Al-Sheikh and Yehia, 2016
	<i>Colletotrichum gloeosporioides</i>	<i>Pichia membranaefaciens</i>	Zhou et al., 2016
	<i>Penicillium digitatum</i> , <i>Penicillium italicum</i>	Cress and/or pomegranate extracts	Tayel et al., 2016
	<i>Penicillium digitatum</i>	Clove oil	Shao et al., 2015
	<i>Penicillium digitatum</i>	Cyclic lipopeptide antibiotics from <i>Bacillus subtilis</i>	Waewthongrak et al., 2015
	General decay	Carboxymethyl cellulose	Arnon et al., 2014
	Total microbial load	Silver and zinc oxide nanoparticles	Kaur et al., 2017
Peach	<i>Monilinia laxa</i>	Polyethylene terephthalate punnets containing thyme oil and sealed with chitosan/boehmite nanocomposite lidding films	Cindi et al., 2015
	General decay	γ-ray	Elbarbary and Mostafa, 2014
	<i>Monilinia fructicola</i>	–	Ma et al., 2013
	<i>Monilinia laxa</i> , <i>Botrytis cinerea</i> , <i>Rhizopus stolonifer</i>	–	Feliziani et al., 2013b
	General decay	–	Pasquariello et al., 2015
Sweet cherry	–	Hydroxypropyl methylcellulose	Shanmuga Priya et al., 2014
Plum	General decay	Ascorbic acid	Liu et al., 2014

TABLE 2 | Postharvest chitosan treatments with other applications for storage decay of subtropical fruit.

Fruit	Decay agent	Combination with chitosan	Reference
Mango	Anthrachnose (<i>Colletotrichum gloeosporioides</i>)	Spermidine	Jongsri et al., 2017
	Anthrachnose (<i>Colletotrichum gloeosporioides</i>), stem-end rot (<i>L. theobromae</i> strains)	Lactoperoxidase system incorporated chitosan films	Kouakou et al., 2013
	Anthrachnose	<i>Mentha piperita</i> L. essential oil	de Oliveira et al., 2017
	Anthrachnose (<i>Colletotrichum gloeosporioides</i>), stem-end rot (<i>L. theobromae</i> strains)	Lactoperoxidase system incorporated chitosan films	Kouakou et al., 2013
	Anthrachnose	<i>Mentha piperita</i> L. essential oil	de Oliveira et al., 2017
Citrus	Green mold (<i>Penicillium digitatum</i>)	<i>Bacillus subtilis</i> ABS-S14	Waewthongrak et al., 2015
	Anthrachnose (<i>Colletotrichum gloeosporioides</i>)	<i>Pichia membranifaciens</i>	Zhou et al., 2016
Avocado	Anthrachnose (<i>Colletotrichum gloeosporioides</i>)	Thyme oil	Bill et al., 2014
Tomato	<i>Alternaria alternata</i>	Methyl jasmonate	Chen et al., 2014
	<i>Aspergillus niger</i> , <i>Rhizopus stolonifer</i>	Essential oil from <i>Origanum vulgare</i> L	Barreto et al., 2016
Pomegranate	<i>Penicillium</i> spp., <i>Piliidiella granati</i>	Lemongrass film	Munhuweyi et al., 2017

TABLE 3 | Preharvest chitosan treatments with other applications for storage decay of temperate fruit.

Fruit	Decay	Combination with chitosan	Reference
Citrus	<i>Penicillium digitatum</i>	<i>Rhodosporidium paludigenum</i>	Lu et al., 2014
Peach	General decay	Calcium chloride	Gayed et al., 2017
Jujube fruit	<i>Alternaria alternata</i>	–	
Table grapes	<i>Botrytis cinerea</i>	Salicylic acid	Shen and Yang, 2017
	<i>Botrytis cinerea</i>	–	Feliziani et al., 2013a
Strawberry	<i>Botrytis cinerea</i> and <i>Rhizopus stolonifer</i>	–	Romanazzi et al., 2013; Feliziani et al., 2015
	<i>Botrytis cinerea</i>	–	Lopes et al., 2014
	General decay	–	Saavedra et al., 2016
Sweet cherry	<i>Monilinia laxa</i> , <i>Botrytis cinerea</i> , and <i>Rhizopus stolonifer</i>	–	Feliziani et al., 2013a



the activities of enzymes linked to the defense mechanisms (e.g., chitinase) in different fruit (e.g., strawberries) (El Ghaouth et al., 1992). This was followed by investigations on other berries, citrus fruit and table grapes, among others. More recently, tools such as qRT-PCR and in recent years RNA-Seq (RNA-Sequencing) have allowed important information to be gained, first at the level of single gene expression, and then later at the level of global gene expression (Xoca-Orozco et al., 2017). This has provided good understanding of the multiple actions of chitosan applications and how they affect a number of physiological changes in fruit. As an example, the application of chitosan to strawberries at

different times before harvest can affect the expression of a thousand or more genes (Landi et al., 2017). Some examples that have become available in the literature over the last 5 years are listed in Table 4, which deal with the physiological changes that can occur in chitosan-treated fruit, both when the biopolymer is applied alone, and when it is combined with other treatments. The eliciting activity of chitosan is particularly effective toward latent infections, as a more reactive fruit can stop the infection process, through a balance that resembles quorum sensing, which is well known for bacterial infections (Papenfort and Bassler, 2016).

CHITOSAN ANTIMICROBIAL ACTIVITY

Numerous studies on chitosan inhibitory activities toward numerous microorganisms have been carried out since the first report of almost half a century ago (Allan and Hadwiger, 1979). The antimicrobial activities of chitosan against a wide range of plant pathogens have been confirmed by any of *in-vitro* and *in-vivo* studies. The antimicrobial activity of chitosan is one of its main properties, and this depends on the concentration at which it is applied. In the control of postharvest decay of fresh fruit, the antimicrobial activity can account for 35–45% of its effectiveness, as an antifungal barrier on a fruit inhibits the germination of fungal spores and slows down the rate of decay-causing fungi of already infected fruit, both latently and

TABLE 4 | Physiological changes that can occur in fresh fruit after chitosan treatment, alone or in combination with other applications.

Fruit	Physiological change	Combination with chitosan	Reference
Apple	20 genes involved in defence responses, metabolism, signal transduction, transcription factors, protein biosynthesis, cytoskeleton.	–	Li et al., 2015
Peach	Total phenolic, flavonoids, antioxidants, pigments, weight loss	Olive waste extract	Khalifa et al., 2017
	Malondialdehyde content	γ -ray	Elbarbary and Mostafa, 2014
	Catalase, peroxidase, β -1,3-glucanase and chitinase	–	Ma et al., 2013
	Total soluble solids, weight loss, ascorbic acid content	Silver and zinc oxide nanoparticles	Kaur et al., 2017
Plum	Color and fruit firmness	Polyethylene terephthalate punnets containing thyme oil and sealed with chitosan/boehmite nanocomposite lidding films	Cindi et al., 2015
	Fruit firmness, weight loss, total soluble solids, total phenolic content, and titratable acidity	Calcium chloride	Gayed et al., 2017
	Fruit firmness, respiration rate, fruit color, polygalacturonase, superoxide dismutase, peroxidase, catalase, polyphenol oxidase, phenylalanine ammonia lyase and pectin methylesterase activities, superoxide free radicals, malondialdehyde content	Ascorbic acid	Liu et al., 2014
	Malondialdehyde content and superoxide dismutase, catalase, ascorbate peroxidase, polyphenol oxidase, guaiacol peroxidase lipoxigenase activities	–	Pasquariello et al., 2015
Sweet cherry	Over 5000 differently expressed genes	–	Landi et al., 2017
Strawberry	18 defence genes	–	Landi et al., 2014
	Fruit color	–	Feliziani et al., 2015
	Fruit firmness, anthocyanin and total phenol content	–	Saavedra et al., 2016
	Weight loss, titratable acidity, pH, total soluble solids, total phenols, anthocyanin and ascorbic acid content, activity of polygalacturonase, pectin methyl esterase, β -galactosidase and cellulose	Carboxymethyl cellulose, hydroxypropylmethyl cellulose	Gol et al., 2013
	Weight loss	Lavander and thyme essential oil	Sangsuwan et al., 2016
	Titratable acidity, soluble solids content	–	Benhabiles et al., 2013
	pH and soluble solids content	Natamycin, nisin, pomegranate, grape seed extract	Duran et al., 2016
	Weight loss, ascorbic acid	Poeny extract	Paglierulo et al., 2016
	Weight loss, respiration rate, skin and flesh color, firmness, pH, titratable acidity, soluble solids content, reducing sugars content	Beeswax	Velickova et al., 2013
	Weight loss, firmness, color and total soluble solids content	Sodium benzoate, potassium sorbate	Treviño-Garza et al., 2015
Table grapes	Weight losses, total soluble solids and titratable acidity	Olive waste extract	Khalifa et al., 2016
	Allergen-related gene	–	Petriccione et al., 2017
	Phenylalanine ammonia lyase, chitinase, and β -1, 3-glucanase, phenolic compounds, respiration rate, weight loss, total soluble solids, titratable acidity	Salicylic acid	Shen and Yang, 2017
	Total phenols, flavonoids and ascorbic acid content, activities of peroxidase, polyphenoloxidase, polygalacturonase, and xylanase, fruit firmness	–	Al-Qurashi and Mohamed, 2015
	Fruit color	–	Irkin and Guldaz, 2014
	Weight loss, titratable acidity, pH and soluble solids content, resveratrol content	Ultraviolet-C	Freitas et al., 2015
	Weight loss, soluble solids content and titratable acidity	Salvia officinalis essential oil	Kanetis et al., 2017
	Firmness, titratable acidity, soluble solids, color, weight loss	Menta essential oil	Guerra et al., 2016
	Total soluble solids, ascorbic acid content, titratable acidity, weight loss, respiration rate, activities of peroxidase and superoxide dismutase	Glucose complex	Gao et al., 2013
	Titratable acidity, soluble solids, color, firmness	–	de Oliveira et al., 2014
Citrus	Chitinase activity, quercetin, myricetin, and resveratrol content	–	Feliziani et al., 2013b
	Chitinase and phenylalanine ammonia lyase	–	Lu et al., 2014
	640 differentially expressed genes, many involved in secondary metabolism and hormone metabolism pathways	–	Coqueiro et al., 2015
	Fruit firmness, weight loss, total soluble solids	Carboxymethyl cellulose	Arnon et al., 2014
	Peroxidase and phenylalanine ammonia-lyase	Cyclic lipopeptide antibiotics from <i>Bacillus subtilis</i>	Waewthongrak et al., 2015
	Contents of chlorophylls and total carotenoids	–	–
	Phenylalanine ammonia-lyase, β -1,3-glucanase, chitinase	–	–

(Continued)

TABLE 4 | Continued

Fruit	Physiological change	Combination with chitosan	Reference
Jujube	Fruit firmness, cellulase, pectinase	–	Guo et al., 2017
Pear	Total phenolic and flavonoid contents, superoxide dismutase, peroxidase and catalase activities, total antioxidant activity	Calcium chloride	Kou et al., 2014a
	Malic acid-metabolising enzymes and related genes expression	Calcium chloride	Kou et al., 2014b
Mango	Peroxidase (POD) and polyphenol oxidase (PPO) gene expression	–	Gutierrez-Martinez et al., 2017
Kiwifruit	Induced gene expression and increased enzymatic activity of catalase, superoxide dismutase and ascorbate peroxidase	–	Zheng et al., 2017

TABLE 5 | Some chitosan-based commercial products that are available for control of postharvest diseases of fruit and vegetables.

Product trade name	Company (Country)	Formulation	Active ingredient (%)
Chito plant	ChiPro GmbH (Bremen, Germany)	Powder	99.9
Chito plant	ChiPro GmbH (Bremen, Germany)	Liquid	2.5
OII-YS	Venture Innovations (Lafayette, LA, United States)	Liquid	5.8
KaitoSol	Advanced Green Nanotechnologies Sdn Bhd (Cambridge, United Kingdom)	Liquid	12.5
Armour-Zen	Botry-Zen Limited (Dunedin, New Zealand)	Liquid	14.4
Biorend	Bioagro S.A. (Chile)	Liquid	1.25
Kiforce	Alba Milagro (Milan, Italy)	Liquid	6
FreshSeal	BASF Corporation (Mount Olive, NJ, United States)	Liquid	2.5
ChitoClear	Primex ehf (Siglufjörður, Iceland)	Powder	100
Bioshield	Seafresh (Bangkok, Thailand)	Powder	100
Biochikol 020 PC	Gumitex (Lowics, Poland)	Liquid	2
Kadozan	Lytone Enterprise, Inc. (Shanghai Branch, China)	Liquid	2
Kendal cops	Valagro (Atessa, Italy)	Liquid	4
Chitosan 87%	Korea Chengcheng Chemical Company (China)	TC (Technical material)	87
Chitosan 2%	Korea Chengcheng Chemical Company (China)	SLX (Soluble concentrate)	2

actively (**Figure 2**). A standard application rate of chitosan to provide a significant control of postharvest decay of fruit and vegetables can be considered 1%, except for the control of *Penicillia*, where higher concentrations may be needed to provide a good effectiveness. The degree of deacetylation and the molecular weight of chitosan characterize its properties, such as the number of positively charges of amino groups and therefore, its electrostatic interactions with different substrate and organisms at different pH. Chitosan with a higher degree of deacetylation, which has greater numbers of positive charges, would also be expected to have stronger antibacterial activities. On the other hand, numerous studies have generated different results relating to correlations between the chitosan bactericidal activities and its molecular weight (Romanazzi et al., 2017). In addition, there are many differences between the chitosan antifungal and antibacterial activities and several mechanisms relating to these remain still unclear and further researches are needed (Romanazzi et al., 2017).

CHITOSAN FILM-FORMING PROPERTIES

Once applied to a plant surface by dipping or spraying, chitosan can form an edible coating, the properties of which (e.g., thickness, viscosity, gas, and water permeability) greatly depend

on the acid in which the biopolymer is dissolved. The film-forming properties of chitosan account for 20–30% of the chitosan effectiveness in the control of postharvest decay of fruit and vegetables (**Figure 2**). Coating produces a barrier for gas exchanges and reduced respiration, and slows down fruit ripening. Of note, a less ripe fruit is less sensitive to postharvest decay.

TOWARD LARGE-SCALE COMMERCIAL APPLICATIONS

When first used in experimental trials, chitosan needed to be dissolved in an acid (e.g., hydrochloric acid, acetic acid, which were among the most effective ones; see Romanazzi et al., 2009), and then taken to the optimal pH (~5.6). This approach can even take 1–2 days, and it is impractical for use by growers. More recently, several commercial chitosan formulations that can be dissolved in water have become available on the market to be used as biopesticides (**Table 5**). Some of these are formulated as powders, and then the cost of shipping is lower (although still higher compared to most of the commercially available synthetic fungicides), although the chitosan needs to be dissolved in water, in some cases a few hours before its application. This makes chitosan more difficult to use, as the grower wants to use an alternative to synthetic fungicides in

the same way as a commercial compound, such that it should have the same effectiveness. This objective can be achieved with liquid formulations, which have concentrations of 2–15%. In this case, the cost of shipping is higher, as the volumes are larger due to the amounts of water that travel with the chitosan. In tests of three different commercial products, even when used at the same concentration, differential effectiveness was seen (Feliziani et al., 2013a). The higher cost of chitosan treatment compared to standard applications might also induce companies toward the use of low doses (e.g., even well below 0.1%). Based on data in literature, the optimal dose is around 1%, while decreasing the concentration, the effectiveness declines. Furthermore, when the concentration of chitosan is decreased, its effectiveness also declines. However, applications to the plant canopy also need to take in account possible phytotoxic effects, mainly if repeated applications occur. This has been shown for grapevines (Romanazzi et al., 2016a), such that for these purposes a good concentration might be 0.5%. However, under some particular conditions, even low concentrations of chitosan (e.g., 0.02%) in a commercial formulation can be beneficial, such as for the improved storage of litchi (Jiang et al., 2018).

CONCLUDING REMARKS

The effectiveness of chitosan application arises from the integrated combination of its three mechanisms of action. There are increasing consumer requests for fruit and vegetables to be

free from residues of synthetic pesticides, such that the rules defined by the public administration have become more limiting in terms of the active ingredients allowed and the maximum residue limits. Also, large stores compete with each other to further reduce these limits, compared to the legal thresholds (Romanazzi et al., 2016b). These trends make the concept of the application of alternatives to synthetic fungicides more popular, and among these the main one that is already used in human medicine is chitosan, which is particularly welcomed by public opinion. These aspects have promoted further studies based on the multiple actions of chitosan on fruit and vegetables. Therefore, further increases in our knowledge are expected following the widespread practical application of chitosan due to the regulation of its use in agriculture and the interest of companies to promote chitosan-based products, with potential benefits for the growers, the consumers and the environment.

AUTHOR CONTRIBUTIONS

GR proposed the review, collected data on chitosan popularity over time and on commercial products, coordinated the authors, and wrote the article. EF collected papers on effectiveness of chitosan on temperate fruit and on the mechanisms of action in the tables, and helped with the writing. DS collected papers on effectiveness of chitosan on tropical fruit and on the mechanisms of action in the tables, and helped with the writing.

REFERENCES

- Allan, C. R., and Hadwiger, L. A. (1979). The fungicidal effect of chitosan on fungi of varying cell wall composition. *Exp. Mycol.* 3, 285–287. doi: 10.1016/S0147-5975(79)80054-7
- Al-Qurashi, A. D., and Mohamed, S. A. (2015). Postharvest chitosan treatment affects quality, antioxidant capacity, antioxidant compounds and enzymes activities of ‘El-Bayadi’ table grapes after storage. *Sci. Hortic.* 197, 393–398. doi: 10.1016/j.scienta.2015.09.065
- Al-Sheikh, H., and Yehia, R. S. S. (2016). In vitro antifungal efficacy of *Aspergillus niger* ATCC 9642 chitosan-AgNPs composite against post-harvest disease of citrus fruits. *Appl. Biochem. Microbiol.* 52, 413–420. doi: 10.1134/S0003683816040177
- Arnon, H., Zaitsev, Y., Porat, R., and Poverenov, E. (2014). Effects of carboxymethyl cellulose and chitosan bilayer edible coating on postharvest quality of citrus fruit. *Postharv. Biol. Technol.* 87, 21–26. doi: 10.1016/j.postharvbio.2013.08.007
- Badawy, M., and Rabea, I. (2016). “Chitosan and its derivatives as active ingredients against plant pests and diseases,” in *Chitosan in the Preservation of Agricultural Commodities*, eds S. Bautista-Baños, G. Romanazzi, and A. Jiménez-Aparicio (Amsterdam: Elsevier), 179–219. doi: 10.1016/B978-0-12-802735-6.00007-0
- Badawy, M. E. I., Rabea, E. I., El-Nouby, M. A. M., Ismail, R. I. A., and Taktak, N. E. M. (2017). Strawberry shelf life, composition, and enzymes activity in response to edible chitosan coatings. *Int. J. Fruit Sci.* 17, 117–136. doi: 10.1080/15538362.2016.1219290
- Barreto, T., Andrade, S. C., Maciel, J. F., Arcanjo, N. M. O., Madruga, M. S., Meireles, B., et al. (2016). A Chitosan coating containing essential oil from *Origanum vulgare* L. to control postharvest mold infections and keep the quality of cherry tomato fruit. *Front. Microbiol.* 7:1724. doi: 10.3389/fmicb.2016.01724
- Bautista-Baños, S., Hernandez-Lauzardo, A. N., Velazquez-del Valle, M. G., Hernandez-Lopez, M., Ait Barka, E., Bosquez-Molina, E., et al. (2006). Chitosan as a potential natural compound to control pre and postharvest diseases of horticultural commodities. *Crop Prot.* 25, 108–118. doi: 10.1016/j.cropro.2005.03.010
- Bautista-Baños, S., Romanazzi, G., and Jiménez-Aparicio, A. (eds) (2016). *Chitosan in the Preservation of Agricultural Commodities*. Amsterdam: Elsevier.
- Benhabiles, M. S., Drouiche, N., Lounici, H., Paus, A., and Mameri, N. (2013). Effect of shrimp chitosan coatings as affected by chitosan extraction processes on postharvest quality of strawberry. *J. Food Meas. Charact.* 7, 215–221. doi: 10.1007/s11694-013-9159-y
- Bill, M., Sivakumar, D., Korsten, L., and Thompson, A. K. (2014). The efficacy of combined application of edible coating and thyme oil in inducing resistance components in avocado (*Persea americana* Mill.) against anthracnose during post-harvest storage. *Crop Prot.* 64, 159–167. doi: 10.1016/j.cropro.2014.06.015
- Chen, J., Zou, X., Liu, Q., Wang, F., Feng, W., and Wan, N. (2014). Combination effect of chitosan and methyl jasmonate on controlling *Alternaria alternata* and enhancing activity of cherry tomato fruit defence mechanisms. *Crop Prot.* 56, 31–36. doi: 10.1016/j.cropro.2013.10.007
- Cindi, M. D., Shittu, T., Sivakumar, D., and Bautista-Baños, S. (2015). Chitosan boehmite-alumina nanocomposite films and thyme oil vapour control brown rot in peaches (*Prunus persica* L.) during postharvest storage. *Crop Prot.* 72, 127–131. doi: 10.1016/j.cropro.2015.03.011
- Coqueiro, D. S. O., de Souza, A. A., Takita, M. A., Rodrigues, C. M., Kishi, L. T., and Machado, M. A. (2015). Transcriptional profile of sweet orange in response to chitosan and salicylic acid. *BMC Genomics* 16:288. doi: 10.1186/s12864-015-1440-5
- Darolt, J. C., Rocha Neto, A. C., and Di Piero, R. M. (2016). Effects of the protective, curative, and eradication applications of chitosan against *Penicillium expansum* in apples. *Braz. J. Microbiol.* 47, 1014–1019. doi: 10.1016/j.bjm.2016.07.007
- de Oliveira, C. E. V., Magnani, M., de Sales, C. V., de Souza Pontes, A. L., Campos-Takaki, G. M., Stamford, T. C. M., et al. (2014). Effects of post-harvest treatment using chitosan from *Mucor circinelloides* on fungal pathogenicity and quality of table grapes during storage. *Food Microbiol.* 44, 211–219. doi: 10.1016/j.fm.2014.06.007
- de Oliveira, K. Á.R., Berger, L. R. R., de Araújo, S. A., Camara, M. P. S., and de Souza, E. L. (2017). Synergistic mixtures of chitosan and *Mentha piperita* L. essential oil to inhibit Colletorichum species and anthracnose

- development in mango cultivar Tommy Atkins. *Food Microbiol.* 66, 96–103. doi: 10.1016/j.fm.2017.04.012
- Deng, L., Yin, B., Yao, S., Wang, W., and Zeng, K. (2016). Postharvest application of oligochitosan and chitosan reduces calyx alterations of citrus fruit induced by ethephon degreening treatment. *J. Agric. Food Chem.* 64, 7394–7403. doi: 10.1021/acs.jafc.6b02534
- Deng, Z., Jung, J., Simonsen, J., Wang, Y., and Zhao, Y. (2017). Cellulose nanocrystal reinforced chitosan coatings for improving the storability of postharvest pears under both ambient and cold storages. *J. Food Sci.* 82, 453–462. doi: 10.1111/1750-3841.13601
- Ding, F., Nie, Z., Deng, H., Xiao, L., Du, Y., and Shi, X. (2013). Antibacterial hydrogel coating by electrophoretic co-deposition of chitosan/alkynyl chitosan. *Carbohydr. Polym.* 98, 1547–1552. doi: 10.1016/j.carbpol.2013.07.042
- Duran, M., Aday, M. S., Zorba, N. N. D., Temizkan, R., Büyükcın, M. B., and Caner, C. (2016). Potential of antimicrobial active packaging “containing natamycin, nisin, pomegranate and grape seed extract in chitosan coating” to extend shelf life of fresh strawberry. *Food Bioprod. Process.* 98, 354–363. doi: 10.1016/j.fbp.2016.01.007
- El Ghauth, A., Arul, J., Grenier, J., and Asselin, A. (1992). Antifungal activity of chitosan on two postharvest pathogens of strawberry fruits. *Phytopathology* 82, 398–402. doi: 10.1094/Phyto-82-398
- El Hadrami, A., Adam, L. R., El Hadrami, I., and Daayf, F. (2010). Chitosan in plant protection. *Mar. Drugs* 8, 968–987. doi: 10.3390/md8040968
- Elbarbary, A. M., and Mostafa, T. B. (2014). Effect of γ -rays on carboxymethyl chitosan for use as antioxidant and preservative coating for peach fruit. *Carbohydr. Polym.* 104, 109–117. doi: 10.1016/j.carbpol.2014.01.021
- Felipini, R. B., Boneti, J. I., Katsurayama, Y., Neto, A. C. R., Veleirinho, B., Maraschin, M., et al. (2016). Apple scab control and activation of plant defence responses using potassium phosphite and chitosan. *Eur. J. Plant Pathol.* 145, 929–939. doi: 10.1007/s10658-016-0881-2
- Feliziani, E., Landi, L., and Romanazzi, G. (2015). Preharvest treatments with chitosan and other alternatives to conventional fungicides to control postharvest decay of strawberry. *Carbohydr. Polym.* 132, 111–117. doi: 10.1016/j.carbpol.2015.05.078
- Feliziani, E., Romanazzi, G., Margosan, D. A., Mansour, M. F., Smilanick, J. L., Gu, S., et al. (2013a). Preharvest fungicide, potassium sorbate, or chitosan use on quality and storage decay of table grapes. *Plant Dis.* 97, 307–314. doi: 10.1094/pdis-12-11-1043-re
- Feliziani, E., Santini, M., Landi, L., and Romanazzi, G. (2013b). Pre- and postharvest treatment with alternatives to synthetic fungicides to control postharvest decay of sweet cherry. *Postharv. Biol. Technol.* 78, 133–138. doi: 10.1016/j.postharvbio.2012.12.004
- Freitas, P. M., López-Gálvez, F., Tudela, J. A., Gil, M. I., and Allende, A. (2015). Postharvest treatment of table grapes with ultraviolet-C and chitosan coating preserves quality and increases stilbene content. *Postharv. Biol. Technol.* 105, 51–57. doi: 10.1016/j.postharvbio.2015.03.011
- Gao, P., Zhu, Z., and Zhang, P. (2013). Effects of chitosan-glucose complex coating on postharvest quality and shelf life of table grapes. *Carbohydr. Polym.* 95, 371–378. doi: 10.1016/j.carbpol.2013.03.029
- Gayed, A. A. N. A., Shaarawi, S. A. M. A., Elkhishen, M. A., and Elsherbini, N. R. M. (2017). Pre-harvest application of calcium chloride and chitosan on fruit quality and storability of “Early Swelling” peach during cold storage. *Ciência Agrot.* 41, 220–231. doi: 10.1590/1413-70542017412005917
- Gol, N. B., Patel, P. R., and Rao, T. V. R. (2013). Improvement of quality and shelf-life of strawberries with edible coatings enriched with chitosan. *Postharv. Biol. Technol.* 85, 185–195. doi: 10.1016/j.postharvbio.2013.06.008
- Guerra, I. C. D., De Oliveira, P. D. L., Santos, M. M. F., Lúcio, A. S. S. C., Tavares, J. F., Barbosa-Filho, J. M., et al. (2016). The effects of composite coatings containing chitosan and *Mentha (piperita L. or x villosa Huds)* essential oil on postharvest mold occurrence and quality of table grape cv. Isabella. *Innov. Food Sci. Emerg. Technol.* 34, 112–121. doi: 10.1016/j.ifset.2016.01.008
- Guo, H., Xing, Z., Yu, Q., Zhao, Y., and Zhu, E. (2017). Effectiveness of preharvest application of submicron chitosan dispersions for controlling Alternaria rot in postharvest jujube fruit. *J. Phytopathol.* 165, 425–431. doi: 10.1111/jph.12576
- Gutierrez-Martinez, P., Bautista-Baños, S., Berúmen-Varela, S., Ramos-Guerrero, A., and Hernández-Ibañez, A. M. (2017). In vitro response of Colletotrichum to chitosan. Effect on incidence and quality on tropical fruit. Enzymatic expression in mango. *Acta Agron.* 62, 282–289. doi: 10.15446/acag.v66n2.53770
- Irkin, R., and Guldaz, M. (2014). Chitosan coating of red table grapes and fresh-cut honey melons to inhibit *Fusarium oxysporum* growth. *J. Food Process. Preserv.* 38, 1948–1956. doi: 10.1111/jfpp.12170
- Jiang, X., Lin, H., Shi, J., Neethirajan, S., Lin, Y., Chen, Y., et al. (2018). Effects of a novel chitosan formulation treatment on quality attributes and storage behavior of harvested litchi fruit. *Food Chem.* 252, 134–141. doi: 10.1016/j.foodchem.2018.01.095
- Jongsri, P., Rojsithisak, P., Wangsomboondee, T., and Seraypheap, K. (2017). Influence of chitosan coating combined with spermidine on anthracnose disease and qualities of ‘Nam Dok Mai’ mango after harvest. *Sci. Hortic.* 224, 180–187. doi: 10.1016/j.scienta.2017.06.011
- Kanetis, L., Exarchou, V., Charalambous, Z., and Goulas, V. (2017). Edible coating composed of chitosan and *Salvia fruticosa* Mill. extract for the control of grey mould of table grapes. *J. Sci. Food Agric.* 97, 452–460. doi: 10.1002/jsfa.7745
- Kaur, M., Kalia, A., and Thakur, A. (2017). Effect of biodegradable chitosan–rice-starch nanocomposite films on post-harvest quality of stored peach fruit. *Starch* 69:1600208. doi: 10.1002/star.201600208
- Khalifa, I., Barakat, H., El-Mansy, H. A., and Soliman, S. A. (2016). Improving the shelf-life stability of apple and strawberry fruits applying chitosan-incorporated olive oil processing residues coating. *Food Packag. Shelf Life* 9, 10–19. doi: 10.1016/j.fpsl.2016.05.006
- Khalifa, I., Barakat, H., El-Mansy, H. A., and Soliman, S. A. (2017). Preserving apple (*Malus domestica* var. Anna) fruit bioactive substances using olive wastes extract-chitosan film coating. *Inform. Process. Agric.* 4, 90–99. doi: 10.1016/j.inpa.2016.11.001
- Kou, X. H., Guo, W. L., Guo, R. Z., Li, X. Y., and Xue, Z. H. (2014a). Effects of chitosan, calcium chloride, and pullulan coating treatments on antioxidant activity in Pear cv. “Huang guan” during storage. *Food Bioprocess. Technol.* 7, 671–681. doi: 10.1007/s11947-013-1085-9
- Kou, X. H., Wang, S., Zhang, Y., Guo, R. Z., Wu, M. S., Chen, Q., et al. (2014b). Effects of chitosan and calcium chloride treatments on malic acid-metabolizing enzymes and the related gene expression in post-harvest pear cv. “Huang guan.” *Sci. Hortic.* 165, 252–259. doi: 10.1016/j.scienta.2013.10.034
- Kouakou, I. M., Clementine, M., Didier, M., Gérard, L., and Ducamp-Collin, M. N. (2013). Antimicrobial and physical properties of edible chitosan films enhanced by lactoperoxidase system. *Food Hydrocoll.* 30, 576–580. doi: 10.1016/j.foodhyd.2012.07.018
- Landi, L., De Miccolis Angelini, R. M., Pollastro, S., Feliziani, E., Faretra, F., and Romanazzi, G. (2017). Global transcriptome analysis and identification of differentially expressed genes in strawberry after preharvest application of benzothiadiazole and chitosan. *Front. Plant Sci.* 8:235. doi: 10.3389/fpls.2017.00235
- Landi, L., Feliziani, E., and Romanazzi, G. (2014). Expression of defense genes in strawberry fruits treated with different resistance inducers. *J. Agric. Food Chem.* 62, 3047–3056. doi: 10.1021/jf404423x
- Lei, J., Yang, L., Zhan, Y., Wang, Y., Ye, T., Deng, H., et al. (2014). Plasma treated polyethylene terephthalate/polypropylene films assembled with chitosan and various preservatives for antimicrobial food packaging. *Coll. Surf. Biointerfaces* 114, 60–66. doi: 10.1016/j.colsurfb.2013.09.052
- Li, H., Wang, Y., Liu, F., Yang, Y., Wu, Z., Cai, H., et al. (2015). Effects of chitosan on control of postharvest blue mold decay of apple fruit and the possible mechanisms involved. *Sci. Hortic.* 186, 77–83. doi: 10.1016/j.scienta.2015.02.014
- Liu, K., Yuan, C., Chen, Y., Li, H., and Liu, J. (2014). Combined effects of ascorbic acid and chitosan on the quality maintenance and shelf life of plums. *Sci. Hortic.* 176, 45–53. doi: 10.1016/j.scienta.2014.06.027
- Lopes, U. P., Zambolim, L., Costa, H., Pereira, O. L., and Finger, F. L. (2014). Potassium silicate and chitosan application for gray mold management in strawberry during storage. *Crop Prot.* 63, 103–106. doi: 10.1016/j.cropro.2014.05.013
- Lu, L., Liu, Y., Yang, J., Azat, R., Yu, T., and Zheng, X. (2014). Quaternary chitosan oligomers enhance resistance and biocontrol efficacy of *Rhodosporidium paludigenum* to green mold in satsuma orange. *Carbohydr. Polym.* 113, 174–181. doi: 10.1016/j.carbpol.2014.06.077

- Ma, Z., Yang, L., Yan, H., Kennedy, J. F., and Meng, X. (2013). Chitosan and oligochitosan enhance the resistance of peach fruit to brown rot. *Carbohydr. Polym.* 94, 272–277. doi: 10.1016/j.carbpol.2013.01.012
- Mohammadi, A., Hashemi, M., and Hosseini, S. M. (2015). Nanoencapsulation of *Zataria multiflora* essential oil preparation and characterization with enhanced antifungal activity for controlling *Botrytis cinerea*, the causal agent of gray mould disease. *Innov. Food Sci. Emerg. Technol.* 28, 73–80. doi: 10.1016/j.ifset.2014.12.011
- Moussa, S. H., Tayel, A. A., Alsohim, A. S., and Abdallah, R. R. (2013). Botryticidal activity of nanosized silver-chitosan composite and its application for the control of gray mold in strawberry. *J. Food Sci.* 78, 1589–1594. doi: 10.1111/1750-3841.12247
- Munhuweyi, K., Oluwafemi, J. C., Lennox, C. L., van Reenen, A. J., and Opara, L. U. (2017). In vitro and in vivo antifungal activity of chitosan-essential oils against pomegranate fruit pathogens. *Postharv. Biol. Technol.* 129, 9–22. doi: 10.1016/j.postharvbio.2017.03.002
- Muzzarelli, R. A. A. (1986). "Filmogenic properties of chitin/chitosan," in *Chitin in Nature and Technology*, eds R. A. A. Muzzarelli, C. Jeuniaux, and G. W. Gooday (New York, NY: Plenum Press), 389–396. doi: 10.1007/978-1-4613-2167-5_48
- Pagliarulo, C., Sansone, F., Moccia, S., Russo, G. L., Aquino, R. P., Salvatore, P., et al. (2016). Preservation of strawberries with an antifungal edible coating using peony extracts in chitosan. *Food Bioprocess. Technol.* 9, 1951–1960. doi: 10.1007/s11947-016-1779-x
- Papenfort, K., and Bassler, B. L. (2016). Quorum sensing signal–response systems in Gram-negative bacteria. *Nat. Rev. Microbiol.* 14, 576–588. doi: 10.1038/nrmicro.2016.89
- Pasquariello, M. S., Di Patre, D., Mastrobuoni, F., Zampella, L., Scortichini, M., and Petriccione, M. (2015). Influence of postharvest chitosan treatment on enzymatic browning and antioxidant enzyme activity in sweet cherry fruit. *Postharv. Biol. Technol.* 109, 45–56. doi: 10.1016/j.postharvbio.2015.06.007
- Perdones, Á., Vargas, M., Atarés, L., and Chiralt, A. (2014). Physical, antioxidant and antimicrobial properties of chitosan-cinnamon leaf oil films as affected by oleic acid. *Food Hydrocoll.* 36, 256–264. doi: 10.1016/j.foodhyd.2013.10.003
- Petriccione, M., Mastrobuoni, F., Zampella, L., Nobis, E., Capriolo, G., and Scortichini, M. (2017). Effect of chitosan treatment on strawberry allergen-related gene expression during ripening stages. *J. Food Sci. Technol.* 54, 1340–1345. doi: 10.1007/s13197-017-2554-3
- Romanazzi, G., Feliziani, E., Bautista-Baños, S., and Sivakumar, D. (2017). Shelf life extension of fresh fruit and vegetables by chitosan treatment. *Crit. Rev. Food Sci. Nutr.* 57, 579–601. doi: 10.1080/10408398.2014.900474
- Romanazzi, G., Feliziani, E., Santini, M., and Landi, L. (2013). Effectiveness of postharvest treatment with chitosan and other resistance inducers in the control of storage decay of strawberry. *Postharv. Biol. Technol.* 75, 24–27. doi: 10.1016/j.postharvbio.2012.07.007
- Romanazzi, G., Lichter, A., Mlikota Gabler, F., and Smilanick, J. (2012). Recent advances on the use of natural and safe alternatives to conventional methods to control postharvest gray mold of table grapes. *Postharv. Biol. Technol.* 63, 141–147. doi: 10.1016/j.postharvbio.2011.06.013
- Romanazzi, G., Mlikota Gabler, F., Margosan, D. A., Mackey, B. E., and Smilanick, J. L. (2009). Effect of chitosan dissolved in different acids on its ability to control postharvest gray mold of table grape. *Phytopathology* 99, 1028–1036. doi: 10.1094/PHYTO-99-9-1028
- Romanazzi, G., Sanzani, S. M., Bi, Y., Tian, S., Gutierrez-Martinez, P., and Alkan, N. (2016). Induced resistance to control postharvest decay of fruit and vegetables. *Postharv. Biol. Technol.* 122, 82–94. doi: 10.1016/j.postharvbio.2016.08.003
- Romanazzi, G., Mancini, V., Feliziani, E., Servili, A., Endeshaw, S., and Neri, D. (2016a). Impact of alternative fungicides on grape downy mildew control and vine growth and development. *Plant Dis.* 100, 739–748. doi: 10.1094/PDIS-05-15-0564-RE
- Romanazzi, G., Smilanick, J. L., Feliziani, E., and Droby, S. (2016b). Integrated management of postharvest gray mold on fruit crops. *Postharv. Biol. Technol.* 113, 69–76. doi: 10.1016/j.postharvbio.2015.11.003
- Saavedra, G. M., Figueroa, N. E., Poblete, L. A., Cherian, S., and Figueroa, C. R. (2016). Effects of preharvest applications of methyl jasmonate and chitosan on postharvest decay, quality and chemical attributes of *Fragaria chiloensis* fruit. *Food Chem.* 190, 448–453. doi: 10.1016/j.foodchem.2015.05.107
- Sangsuwan, J., Pongsapakworawat, T., Bangmo, P., and Sutthasupa, S. (2016). Effect of chitosan beads incorporated with lavender or red thyme essential oils in inhibiting *Botrytis cinerea* and their application in strawberry packaging system. *Food Sci. Technol.* 74, 14–20. doi: 10.1016/j.lwt.2016.07.021
- Shanmuga Priya, D., Suriyaprabha, R., Yuvakkumar, R., and Rajendran, V. (2014). Chitosan-incorporated different nanocomposite HPMC films for food preservation. *J. Nanopart. Res.* 16:2248. doi: 10.1007/s11051-014-2248-y
- Shao, X., Cao, B., Xu, F., Xie, S., Yu, D., and Wang, H. (2015). Effect of postharvest application of chitosan combined with clove oil against citrus green mold. *Postharv. Biol. Technol.* 99, 37–43. doi: 10.1016/j.postharvbio.2014.07.014
- Shen, Y., and Yang, H. (2017). Effect of preharvest chitosan-g-salicylic acid treatment on postharvest table grape quality, shelf life, and resistance to *Botrytis cinerea*-induced spoilage. *Sci. Hortic.* 224, 367–373. doi: 10.1016/j.scienta.2017.06.046
- Tayel, A. A., Moussa, S. H., Salem, M. F., Mazrou, K. E., and El-Tras, W. F. (2016). Control of citrus molds using bioactive coatings incorporated with fungal chitosan/plant extracts composite. *J. Sci. Food Agric.* 96, 1306–1312. doi: 10.1002/jsfa.7223
- Treviño-Garza, M. Z., García, S., Flores-González, M., del, S., and Arévalo-Niño, K. (2015). Edible active coatings based on pectin, pullulan, and chitosan increase quality and shelf life of strawberries (*Fragaria × ananassa*). *J. Food Sci.* 80, M1823–M1830. doi: 10.1111/1750-3841.12938
- Valenzuela, C., Tapia, C., López, L., Bunge, A., Escalona, V., and Abugoch, L. (2015). Effect of edible quinoa protein-chitosan based films on refrigerated strawberry (*Fragaria × ananassa*) quality. *Electron. J. Biotechnol.* 18, 406–411. doi: 10.1016/j.ejbt.2015.09.001
- Velickova, E., Winkelhausen, E., Kuzmanova, S., Alves, V. D., and Moldão-Martins, M. (2013). Impact of chitosan-beeswax edible coatings on the quality of fresh strawberries (*Fragaria × ananassa* cv Camarosa) under commercial storage conditions. *Food Sci. Technol.* 52, 80–92. doi: 10.1016/j.lwt.2013.02.004
- Waewthongrak, W., Pisuchpen, S., and Leelasuphakul, W. (2015). Effect of *Bacillus subtilis* and chitosan applications on green mould (*Penicillium digitatum* Sacc.) decay in citrus fruit. *Postharv. Biol. Technol.* 99, 44–49. doi: 10.1016/j.postharvbio.2014.07.016
- Wang, Y., Li, B., Zhang, X., Peng, N., Mei, Y., and Liang, Y. (2017). Low molecular weight chitosan is an effective antifungal agent against *Botryosphaeria* sp. and preservative agent for pear (*Pyrus*) fruits. *Int. J. Biol. Macromol.* 95, 1135–1143. doi: 10.1016/j.ijbiomac.2016.10.105
- Wu, T., Dai, S., Cong, X., Liu, R., and Zhang, M. (2017). Succinylated soy protein film coating extended the shelf life of apple fruit. *J. Food Process. Preserv.* 41, 13024–13034. doi: 10.1111/jfpp.13024
- Xoca-Orozco, L. A., Cuellar-Torres, E. A., González-Morales, S., Gutiérrez-Martínez, P., López-García, U., Herrera-Estrella, L., et al. (2017). Transcriptomic analysis of avocado Hass (*Persea americana* Mill) in the interaction system fruit-chitosan- *Colletotrichum*. *Front. Plant Sci.* 8:956. doi: 10.3389/fpls.2017.00956
- Zhang, H., Li, R., and Liu, W. (2011). Effects of chitin and its derivative chitosan on postharvest decay of fruits: a review. *Int. J. Mol. Sci.* 12, 917–934. doi: 10.3390/ijms12020917
- Zheng, W., Li, L., Pan, S., Liu, M., Zhang, W., Liu, H., et al. (2017). Controls postharvest decay and elicits defense response in kiwifruit. *Food Bioprocess. Technol.* 11, 1937–1945. doi: 10.1007/s11947-017-1957-5
- Zhou, Y., Zhang, L., and Zeng, K. (2016). Efficacy of *Pichia membranaefaciens* combined with chitosan against *Colletotrichum gloeosporioides* in citrus fruits and possible modes of action. *Biol. Control* 96, 39–47. doi: 10.1016/j.biocontrol.2016.02.001

Conflict of Interest Statement: The authors declare that the research was conducted in the absence of any commercial or financial relationships that could be construed as a potential conflict of interest.

Copyright © 2018 Romanazzi, Feliziani and Sivakumar. This is an open-access article distributed under the terms of the Creative Commons Attribution License (CC BY). The use, distribution or reproduction in other forums is permitted, provided the original author(s) and the copyright owner(s) are credited and that the original publication in this journal is cited, in accordance with accepted academic practice. No use, distribution or reproduction is permitted which does not comply with these terms.

Advantages of publishing in Frontiers



OPEN ACCESS

Articles are free to read
for greatest visibility
and readership



FAST PUBLICATION

Around 90 days
from submission
to decision



HIGH QUALITY PEER-REVIEW

Rigorous, collaborative,
and constructive
peer-review



TRANSPARENT PEER-REVIEW

Editors and reviewers
acknowledged by name
on published articles

Frontiers

Avenue du Tribunal-Fédéral 34
1005 Lausanne | Switzerland

Visit us: www.frontiersin.org

Contact us: info@frontiersin.org | +41 21 510 17 00



REPRODUCIBILITY OF RESEARCH

Support open data
and methods to enhance
research reproducibility



DIGITAL PUBLISHING

Articles designed
for optimal readership
across devices



FOLLOW US

[@frontiersin](https://twitter.com/frontiersin)



IMPACT METRICS

Advanced article metrics
track visibility across
digital media



EXTENSIVE PROMOTION

Marketing
and promotion
of impactful research



LOOP RESEARCH NETWORK

Our network
increases your
article's readership